frontiers | Research Topics

Insights in extreme microbiology 2022

Edited by
Andreas Teske and Virginia P. Edgcomb

Published in
Frontiers in Microbiology

ISSN 1664-8714
ISBN 978-2-8325-3923-1
DOI 10.3389/978-2-8325-3923-1

About Frontiers

Frontiers is more than just an open access publisher of scholarly articles: it is a pioneering approach to the world of academia, radically improving the way scholarly research is managed. The grand vision of Frontiers is a world where all people have an equal opportunity to seek, share and generate knowledge. Frontiers provides immediate and permanent online open access to all its publications, but this alone is not enough to realize our grand goals.

Frontiers journal series

The Frontiers journal series is a multi-tier and interdisciplinary set of open-access, online journals, promising a paradigm shift from the current review, selection and dissemination processes in academic publishing. All Frontiers journals are driven by researchers for researchers; therefore, they constitute a service to the scholarly community. At the same time, the *Frontiers journal series* operates on a revolutionary invention, the tiered publishing system, initially addressing specific communities of scholars, and gradually climbing up to broader public understanding, thus serving the interests of the lay society, too.

Dedication to quality

Each Frontiers article is a landmark of the highest quality, thanks to genuinely collaborative interactions between authors and review editors, who include some of the world's best academicians. Research must be certified by peers before entering a stream of knowledge that may eventually reach the public - and shape society; therefore, Frontiers only applies the most rigorous and unbiased reviews. Frontiers revolutionizes research publishing by freely delivering the most outstanding research, evaluated with no bias from both the academic and social point of view. By applying the most advanced information technologies, Frontiers is catapulting scholarly publishing into a new generation.

What are Frontiers Research Topics?

Frontiers Research Topics are very popular trademarks of the *Frontiers journals series*: they are collections of at least ten articles, all centered on a particular subject. With their unique mix of varied contributions from Original Research to Review Articles, Frontiers Research Topics unify the most influential researchers, the latest key findings and historical advances in a hot research area.

Find out more on how to host your own Frontiers Research Topic or contribute to one as an author by contacting the Frontiers editorial office: frontiersin.org/about/contact

Insights in extreme microbiology: 2022

Topic editors

Andreas Teske — University of North Carolina at Chapel Hill, United States

Virginia P. Edgcomb — Woods Hole Oceanographic Institution, United States

Citation

Teske, A., Edgcomb, V. P., eds. (2023). *Insights in extreme microbiology: 2022*. Lausanne: Frontiers Media SA. doi: 10.3389/978-2-8325-3923-1

Table of contents

frontiers | Frontiers in Microbiology

TYPE Editorial
PUBLISHED 31 October 2023
DOI 10.3389/fmicb.2023.1324080

OPEN ACCESS

EDITED AND REVIEWED BY
Antonio Ventosa,
Sevilla University, Spain

*CORRESPONDENCE
Andreas P. Teske
✉ teske@email.unc.edu

RECEIVED 18 October 2023
ACCEPTED 23 October 2023
PUBLISHED 31 October 2023

CITATION
Teske AP and Edgcomb VP (2023) Editorial: Insights in extreme microbiology: 2022. *Front. Microbiol.* 14:1324080. doi: 10.3389/fmicb.2023.1324080

Editorial: Insights in extreme microbiology: 2022

Andreas P. Teske[1]* and Virginia P. Edgcomb[2]

[1]Department of Earth, Marine and Environmental Sciences, University of North Carolina at Chapel Hill, Chapel Hill, NC, United States, [2]Department of Geology and Geophysics, Woods Hole Oceanographic Institution, Woods Hole, MA, United States

KEYWORDS

microbiology, insights, Research Topic, microbial community, 2022

Editorial on the Research Topic
Insights in extreme microbiology: 2022

Taking stock of the contributions to the "*Insights in extreme microbiology: 2022*" Research Topic again reveals the extraordinary breadth that exists within the field of Extreme Microbiology.

The strong showing of hydrothermal microbiology in the 2021 Research Topic continues this year. Two papers (Truong et al.; Adam-Beyer et al.), address hydrothermal vent microbiology from distinct biogeochemical/mineralogical and ecosystem angles. Truong et al. examine the formation and composition of pyrite spherules as a potential biomarker for the activity of omnipresent sulfur-reducing Thermococcales spp. at vent sites; and Adam-Beyer et al. examine linkages between microbial communities and particular niches on understudied Indian Ocean mid-ocean ridges, and they demonstrate the key role of hydrogen-oxidizing Epsilonproteobacteria.

Applied environmental research is represented by two papers, a genomic analysis of groundwater microbial communities in a continuous flow-through reactor that respond to phenol pollution (Yavari-Bafghi et al.), and bacterial community changes during artisanal indigo reduction under different (including highly alkaline) environmental conditions (Farjana et al.). These studies serve as helpful reminders that extreme microorganisms and conditions can be found in applied contexts and in traditional practices/procedures, far from well-known and charismatic field sites. First and foremost, microbes "see" and react to the chemistry of their immediate surroundings.

A study of spatially compressed microbial stratification within a cyanobacterial mat (Bourhane et al.), contrasts with an investigation of microbial methane cycling in extensive deep marine subsurface sediments in the Peru Trench (Lever et al.), and shows how biogeochemical gradients—from the micrometer scale in the hypersaline mat to the 100-meter scale in deep-sea sediments—shape the habitat, diversity and activity of microorganisms. Ecosystems with chemical gradients that microorganisms can exploit are particularly instructive, as they demonstrate the feedbacks that exist between changing geochemistry and microbial community structure and activity.

A particular theme from the 2021 Research Topic is continued here, in 2022, which is the pure culture-based physiological study on cesium ion resistance in *Microbacterium* sp. (Ishida et al.) which sheds light on microbial ecophysiology of heavy metal resistance, and its specific mechanisms at the single-cell level.

Finally, we are very happy to announce three creative and timely reviews in the 2022 topic. The first is on experimental simulations of early Earth's microbial activity, and presents strategies to ground-truth inferences on how microbial life has shaped the geochemical evolution of early Earth (Zhao et al.). The second is an introduction to the aeromicrobiome, which is the Earth's outermost microbial biosphere; this survey of a newly emergent research area attracted almost 2,000 views at the time of writing this editorial (Amato et al.). Finally, our most frequently viewed paper in this Research Topic (almost 5,000 views at the time of writing this editorial), is a review on decoding microbial dark matter by new approaches in extremophile cultivation (Schultz et al.). It was a distinct editorial pleasure to guide the gradual development of this review, and to help sharpen its focus.

Readers may be interested to take a look at the geographic origin of the contributions. We have papers from French, Spanish, and German working groups, from a widely dispersed German-American collaboration, from a Chinese group with links to England, from two Japanese labs with highly specific expertise, from an Iranian collaboration that has entrained support from the Iranian diaspora in Sweden, and—in the case of our high-impact authors—from Spanish and Brazilian microbiologists working out of KAUST in Saudi Arabia. Clearly, the old notion that environmental and extreme microbiology thrives best in European countries with a damp, clammy climate, and in midwestern land-grant universities where ruminants and C4-plants have center stage, no longer holds; we see instead emerging global patterns of expertise and authorship. That said, we are looking forward to more representation from Africa and Latin America, which do not suffer from a shortage of extreme microbial ecosystems.

Without further ado, here is the harvest of Extreme Insights for 2022.

Author contributions

AT: Writing—original draft. VE: Writing—review & editing.

Funding

The author(s) declare that no financial support was received for the research, authorship, and/or publication of this article.

Conflict of interest

The authors declare that the research was conducted in the absence of any commercial or financial relationships that could be construed as a potential conflict of interest.

The author(s) declared that they were an editorial board member of Frontiers, at the time of submission. This had no impact on the peer review process and the final decision.

Publisher's note

frontiers | Frontiers in Microbiology

TYPE Review
PUBLISHED 12 January 2023
DOI 10.3389/fmicb.2022.1052831

OPEN ACCESS

EDITED BY
Andreas Teske,
University of North Carolina at Chapel Hill,
United States

REVIEWED BY
Yiran Dong,
China University of Geosciences Wuhan,
China
Andrew Free,
University of Edinburgh,
United Kingdom

*CORRESPONDENCE
Ke-Qing Xiao
✉ k.q.xiao@leeds.ac.uk

SPECIALTY SECTION
This article was submitted to Extreme Microbiology, a section of the journal Frontiers in Microbiology

RECEIVED 24 September 2022
ACCEPTED 16 December 2022
PUBLISHED 12 January 2023

CITATION
Zhao M, Zhao Y, Lin W and Xiao K-Q (2023) An overview of experimental simulations of microbial activity in early Earth. *Front. Microbiol.* 13:1052831. doi: 10.3389/fmicb.2022.1052831

An overview of experimental simulations of microbial activity in early Earth

Mingyu Zhao[1], Yao Zhao[2], Wei Lin[3] and Ke-Qing Xiao[4]*

[1]Key Laboratory of Cenozoic Geology and Environment, Institute of Geology and Geophysics, Chinese Academy of Sciences, Beijing, China, [2]State Key Laboratory of Environmental Criteria and Risk Assessment, Chinese Research Academy of Environmental Sciences, Beijing, China, [3]Key Laboratory of Earth and Planetary Physics, Institute of Geology and Geophysics, Chinese Academy of Sciences, Beijing, China, [4]School of Earth and Environment, University of Leeds, Leeds, United Kingdom

Microbial activity has shaped the evolution of the ocean and atmosphere throughout the Earth history. Thus, experimental simulations of microbial metabolism under the environment conditions of the early Earth can provide vital information regarding biogeochemical cycles and the interaction and coevolution between life and environment, with important implications for extraterrestrial exploration. In this review, we discuss the current scope and knowledge of experimental simulations of microbial activity in environments representative of those of early Earth, with perspectives on future studies. Inclusive experimental simulations involving multiple species, and cultivation experiments with more constraints on environmental conditions similar to early Earth would significantly advance our understanding of the biogeochemical cycles of the geological past.

KEYWORDS

early Earth, microbes, biogeochemical cycles, experimental simulations, interactions

Introduction

Microbes are the main drivers for global biogeochemical cycles throughout the Earth history (e.g., Falkowski et al., 2008). In fact, microbial activity not only sustains the habitable environments of the Earth surface, but also is responsible for the gradual development of an oxygen-rich atmosphere that paved the way for the rise of eukaryotes (e.g., Lyons et al., 2014). Life only existed as single-cell microbes before the appearance of multicellular eukaryotes, perhaps as early as the Mesoproterozoic (e.g., Zhu et al., 2016; Figure 1). Thus, these primitive microbes were important in shaping the biogeochemical cycles as well as the environmental conditions of early Earth.

The environments of Earth surface during the Precambrian (before the Phanerozoic Eon) could be fundamentally different from those of modern times and the Phanerozoic. Firstly, the astronomical conditions of the Precambrian were significantly different from modern conditions. The solar luminosity has steadily increased throughout the history of the Earth, from ~70% of the present value in the Precambrian (e.g., Gough, 1981; Kasting, 1987), according to standard solar evolution theory. The daylength has also

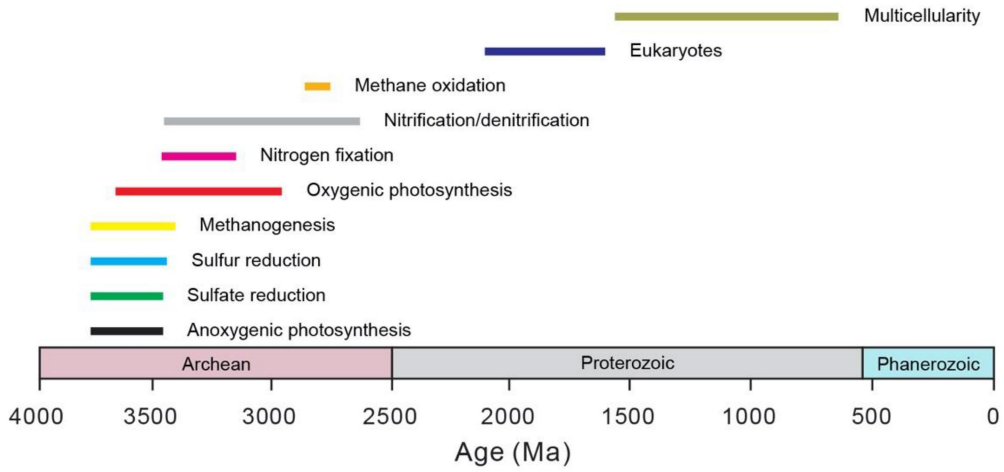

FIGURE 1
Origin of major microbial metabolisms and groups through time. The bars represent the uncertainty in the estimation. The data are mainly from Moore et al. (2017). Note that the microbes before the rise of eukaryotes all belong to prokaryotes. The age for the origin of eukaryotes comes from Knoll et al. (2006). The age for the origin of multicellular eukaryotes comes from Zhu et al. (2016) and the references therein.

increased during geological history due to the change in Earth's rotation rate (e.g., Munk and MacDonald, 1960; Zahnle and Walker, 1987; Williams, 2000; Bartlett and Stevenson, 2016; Figures 2A,B). It is generally accepted that daylength increases with time as the rotation rate of the Earth decreases due to tidal friction (e.g., Munk and MacDonald, 1960). The daylength may have had a long period of stasis at 21 h from ~2,200 to 600 Ma and potentially in prior periods, owing to the resonance between Earth's rotation and the semidiurnal atmospheric thermal tide (Zahnle and Walker, 1987; Bartlett and Stevenson, 2016). In addtion, the oxygen level of the Precambrian atmosphere could have been much lower than the modern level (e.g., Farquhar et al., 2000; Lyons et al., 2014), whereas the pCO_2 and pCH_4 levels of the Precambrian could have been much higher (e.g., Kasting, 1987; Zhao et al., 2018; Catling and Zahnle, 2020; Figures 2C,D). The atmospheric oxygen level was likely lower than 0.001% of the present atmospheric level during the Archean period (e.g., Pavlov and Kasting, 2002; Lyons et al., 2014). The atmospheric oxygen level during the Proterozoic is highly debated, with estimates in the range of <0.1 to 40% (Canfield, 1998; Rye and Holland, 1998; Planavsky et al., 2014, 2020; Canfield et al., 2021). Furthermore, the chemical composition, redox status and *p*H of ocean water (Figure 3) during the Precambrian could have been significantly different from those of today. Ferruginous conditions may have been a predominant state for the Precambrian ocean (e.g., Sperling et al., 2015), while the modern ocean is largely oxic. Seawater calcium, bicarbonate, silica and barium concentrations could have been much higher (Walker, 1977; Halevy and Bachan, 2017; Isson and Planavsky, 2018), but sulfate and carbonate ion concentrations could have been much lower during early Earth (Walker, 1977; Habicht et al., 2002). The concentrations of trace components have also varied with time, mainly due to the change in seawater redox conditions (Moore et al., 2017). Marine pH in early Earth was expected to be much lower than what is found today (Halevy and Bachan, 2017; Isson and Planavsky, 2018), largely because of the high atmospheric pCO_2 during this period. Finally, the flux of ultraviolet (UV) radiation to the Earth surface before the Great Oxidation Event (GOE) at the end of Archean could have been orders of magnitude higher than that of today (e.g., Cockell, 1998; Rettberg et al., 1998), which is due to the rise in atmospheric oxygen and the corresponding production of ozone during the GOE.

As a perfect modern analogue for Precambrian environments is lacking, experimental simulation of microbial activity under artificial Precambrian conditions is an instructive method of investigating the adaptive strategies of microorganisms under the extreme environmental conditions of early Earth (e.g., high UV radiation) as well as the mechanisms, kinetics and evolution of biogeochemical cycles. Moreover, microbial biomineralisation could be one of the main drivers for the formation of unique deposits in the Precambrian, such as banded iron formations (BIFs) and substantial stromatolites. Thus, biomineralisation experiments can provide vital information regarding the mechanism and conditions for the formation of Precambrian chemical sediments. Here, we review recent advances in microbial experiments on these topics, although we acknowledge that well-calibrated ecosystem simulation models, based on predicted physicochemical parameters and expected biogeochemical activities, could also be helpful in simulating Earth's early environments (e.g., Herman and Kump, 2005; Ozaki et al., 2018; Zhao et al., 2018). There are also extensive studies on microbial activities in hydrothermal vents, which have important implications on the origin of life and the early environments of the Earth. These have been reviewed elsewhere (e.g., Martin et al., 2008; Xiao and Yu, 2014; Weiss et al., 2016).

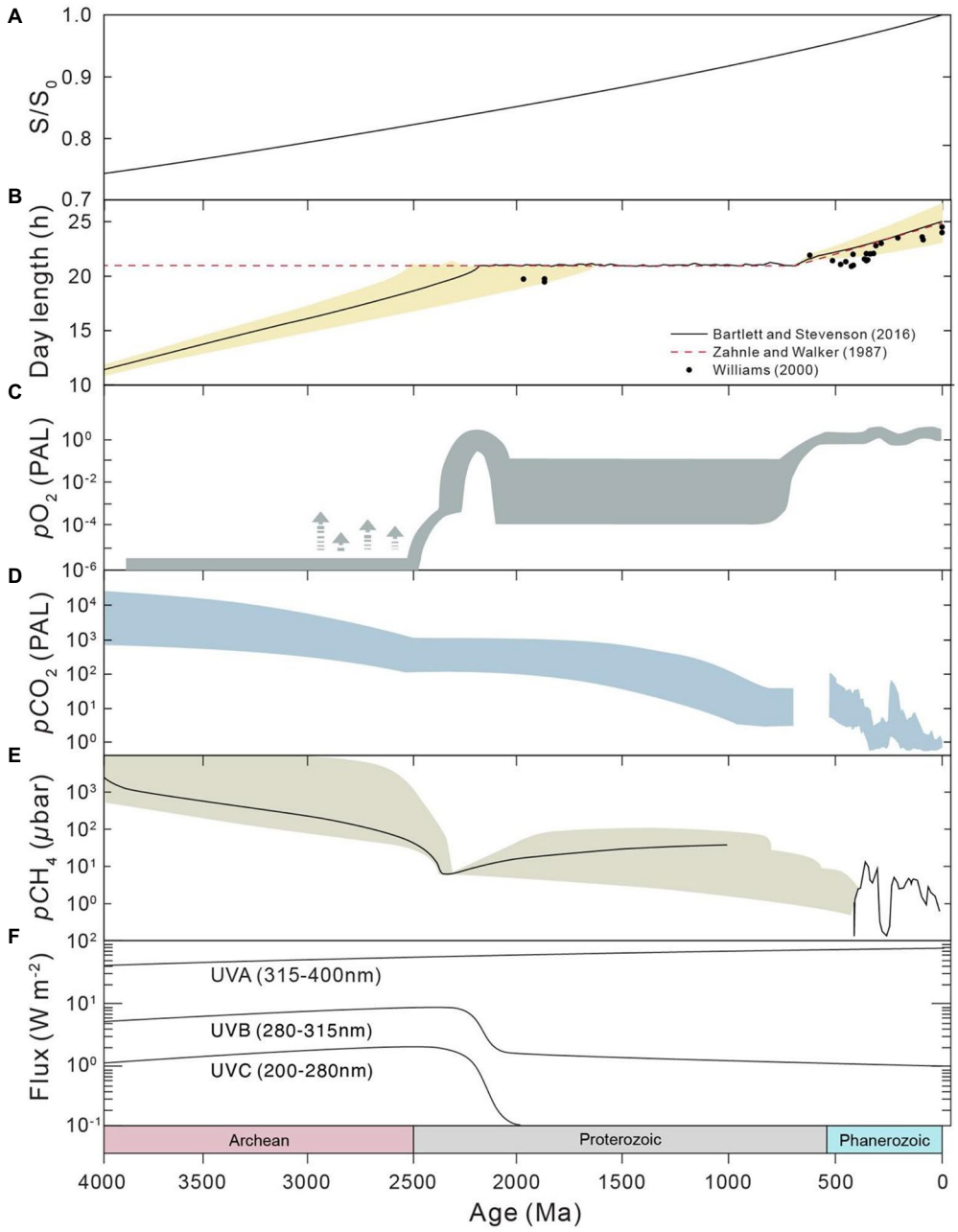

FIGURE 2
Evolution of astronomical conditions and atmospheric composition throughout Earth history. **(A)** Solar luminosity, derived from Kasting (1987). **(B)** Day length. **(C)** Atmospheric pO_2, after Lyons et al. (2014). **(D)** Atmospheric pCO_2. Results of the Precambrian (left) are from Kasting (1987), whereas those of the Phanerozoic (right) are from Royer et al. (2004). **(E)** Atmospheric pCH_4, derived from Catling and Zahnle (2020). **(F)** Ultraviolet (UV) radiation at the ground, modified from Cockell (2000).

Ultraviolet radiation

High levels of UV radiation exist not only in the space environment but also in the early Earth. Thus, studies on the response of microbes upon exposure to UV radiation are important in elucidating the selective pressure and ecology niche of microbes on early Earth (Sagan, 1973; Cockell et al., 2011). In addition, these types of experiments are also important for understanding the potential of the natural transport and spread of microbes between planets and finding microbes that are suitable for food and oxygen production or geoengineering in space exploration (e.g., Olsson-Francis and Cockell, 2010a,b; Cockell et al., 2011). In this section, we focus on the application of UV radiation experiments that have implications for learning about the early Earth biosphere. In the Archean period, microbes resident on the Earth surface might have been exposed to UV

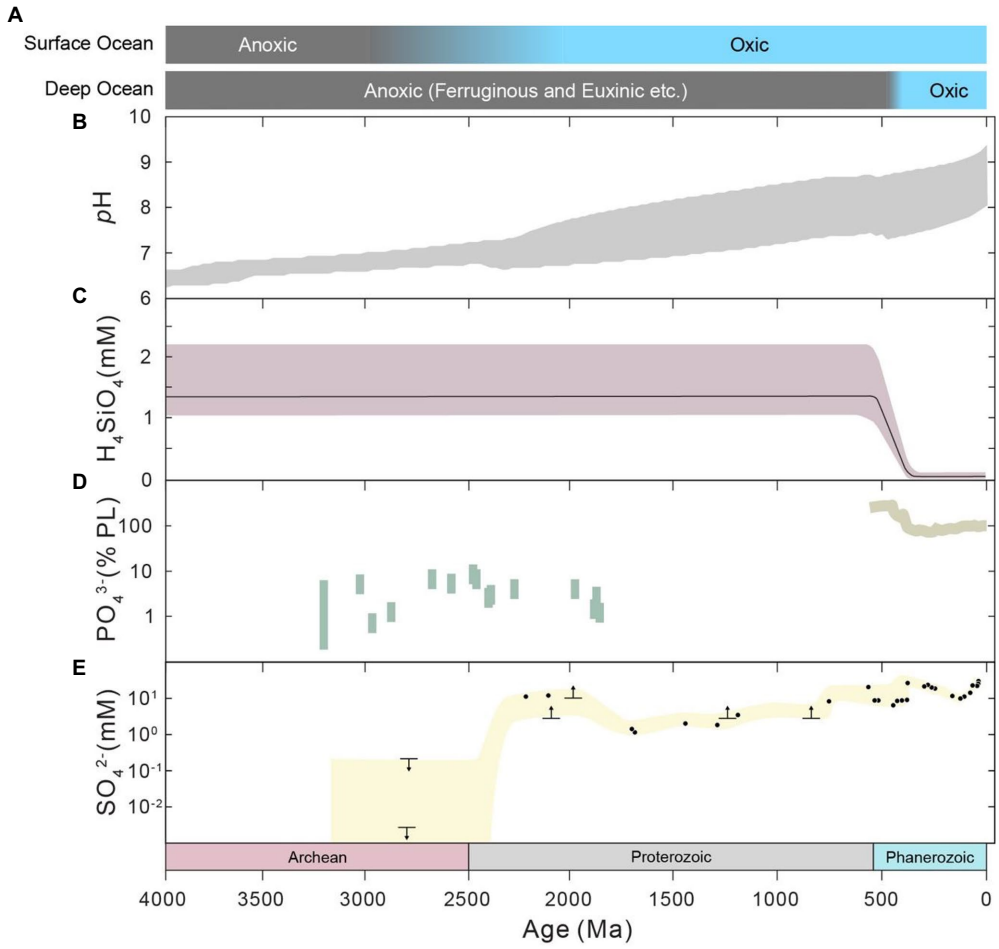

FIGURE 3
Evolution of seawater conditions and composition through Earth history. **(A)** Redox state, after Sperling et al. (2015). **(B)** Marine pH, which is the results within the 95% confidence interval from Halevy and Bachan (2017). **(C)** Marine silica concentration, from Isson and Planavsky (2018). **(D)** Marine dissolved phosphate concentration. Results of the Precambrian (left) are from Bjerrum and Canfield (2002), Konhauser et al. (2007) and Jones et al. (2015), which were constrained by the Fe/P ratios of iron-rich sediments. The results of the Phanerozoic (right) are from the model results of Lenton et al. (2018). **(E)** Marine sulfate concentration, taken from Habicht et al. (2002), Planavsky et al. (2012) and references therein, Crowe et al. (2014) and Blättler et al. (2018).

influx with wavelengths >200 nm, whereas the influx of UV radiation on Earth today is limited to wavelengths >290 nm (Figure 2F, e.g., Rettberg et al., 1998; Cockell, 2000). However, some suggest that the early atmosphere might have been a UV screen (e.g., Sagan, 1973; Kasting, 1993). UV >200 nm radiation could generate more than three orders of magnitude greater damage to DNA (e.g., Rettberg et al., 1998). Such radiation could also cause strong damage to proteins, lipids and pigments (e.g., Tevini, 1993; Cockell, 1998). Although UV radiation is a strong selective pressure for microbes, the presence of physical protection, biological protection, biological adaption and repair ability (Cockell, 1998) might have made UV radiation not a critical limitation to microbes in early Earth (e.g., Pierson et al., 1993). Extensive cultivation experiments under artificial UV conditions of the early Earth have been performed to understand the mechanism for the survival of microbials under high UV radiation, which will be discussed in the following sections.

Physical protection

Various screening methods under high UV radiation have been proposed and experimentally studied (Cockell, 1998), including physical protection and biological protection. A variety of substances were found to have the ability of physical protection, such as water, iron compounds (Pierson et al., 1993; Bishop et al., 2006; Gómez et al., 2007; Gauger et al., 2016), Fe(III)-silica precipitates (Phoenix et al., 2001; Mloszewska et al., 2018), clays (Kugler and Dong, 2019), minerals (Garcia-Pichel and Belnap, 1996), porous rocks (Cockell et al., 2002; Bryce et al., 2015), nitrogenous salts (Margulis et al., 1976), π-electron-containing chromophores (Sagan, 1973; Cockell, 1998), organic compounds (Cleaves and Miller, 1998), silica (Phoenix et al., 2001, 2006) and dead cells (Margulis et al., 1976). Water bodies, such as lakes, rivers and oceans, could also act as an effective shield through the attenuation effect (Sagan, 1973; Margulis et al., 1976). As Fe(II)

and silica were both enriched in Archean ocean water (Maliva et al., 2005; Czaja et al., 2012), understanding the screen effect of Fe(III)-silica precipitates on UV radiation can provide important insight into the microbial ecosystems in the Archean ocean (Mloszewska et al., 2018). The transmission of UV radiation through gels of $FeCl_3$ was measured by Pierson et al. (1993). They found that a 1 mm gel of 0.1% $FeCl_3$ can reduce UV radiation to 1% of its initial intensity. Meanwhile, with respect to radiation used in photosynthesis, 85% of visible radiation and 93% of near infrared (NIR) radiation can pass through the same gels. Such an experiment demonstrates that iron compounds at the surface of mats or dispersed iron compounds in water bodies can protect the underlying microbials from UV radiation. Meanwhile, nanograins of iron (hydro)oxides formed by certain anoxygenic phototrophic Fe(II) oxidisers such as *Rhodopseudomonas palustris* strain TIE-1 and Rhodobacter ferrooxidans strain SW2 can be loosely attached to the cell surfaces and protect the cells from UV radiation (Gauger et al., 2016). Cultivation of cyanobacteria from hot springs in artificial Archean seawater (iron-silica solution) revealed that the formation of iron-enriched silica gels and crusts could efficiently protect the bacteria against UV radiation (Phoenix et al., 2001). Mloszewska et al. (2018) further investigated the protection efficiency of Fe(III)-silica precipitates in Archean ocean water against UV radiation. They found that both Fe(III) and silica can efficiently screen UV radiation. UV-C is attenuated by 18% in Si-only solution, 32% in Fe(III)-only solution and 56–70% in Fe(III)-silica solution. Furthermore, they have used a model to show that UV-C is attenuated by ~80% in Archean seawater analogues with 100 nM Fe(II). However, although their cultivation experiment on planktonic cyanobacteria *Synechococcus* reveals much higher survival rates in Fe(II)-silica media (3%) than in un-supplemented media (0.13%), the high mortality rate (97%) even under the protection of Fe(III)-silica precipitates suggests that the ecology niche of plankton and its primary productivity in the Archean ocean still might have been strongly limited by the UV radiation. Kugler and Dong (2019) examined the protection efficiency of three mica minerals (muscovite, phlogopite and biotite) against UV radiation. They found that biotite has the best ability to screen UV radiation, owing to the Fe(II) content in biotite, which is the highest among the three minerals.

Cyanobacteria mats are likely the most important ecosystem on land during the Archean period (e.g., Planavsky et al., 2021). In this case, due to the shielding effect of water and minerals, the surface of mats can effectively attenuate UV radiation and protect microorganisms from damage from UV fluxes (Garcia-Pichel and Belnap, 1996). Margulis et al. (1976) observed that cells in the interior of a mat can survive after 3 days of continuous UV irradiation, even if the cells on the surface died after minutes. This suggests that the cells in the interior were excellently protected by the surface cells. Nitrogenous salts in solution can also protect microbials due to their strong adsorption ability on UV radiation (Margulis et al., 1976). Cleaves and Miller (1998) have proposed that prebiotic organic polymers such as cyanide polymer and spark discharge polymer in seawater might have acted as efficient UV adsorbers that can protect probiotic organic compounds. In an experiment outside of the International Space Station, it was found that *Chroococcidiopsis* could survive after exposure to UV radiation in space (>110 nm or 200 nm) for 548 days, although other microbes cannot recover from such detrimental exposure (Cockell et al., 2011). Self-shielding due to multiple layers of cells could be an important factor in maintaining the survival of *Chroococcidiopsis* (Cockell et al., 2011). This study suggests that, even under the worst-case scenario of UV exposure, some microorganisms might have had the potential to occupy the land during the Archean period without any protection by physical screening.

Biological protection

Experimental studies on modern microbes have also revealed several biological mechanisms that serve to screen UV radiation, including negative UV phototaxis (Bebout and Garcia-Pichel, 1995), compression of spirals (Wu et al., 2005) as well as the production of pigments and organics for UV screening (Garcia-Pichel et al., 1992, 1993; Ehling-Schulz et al., 1997; Oren, 1997; Sinha and Häder, 2002, Sinha and Häder, 2008). A vertical migration strategy for cyanobacteria was found in both mats and water columns (e.g., Reynolds et al., 1987; Garcia-Pichel et al., 1994). Bebout and Garcia-Pichel (1995) have found that photoautotrophic microbes in the cyanobacteria mat can migrate downward upon the application of UV radiation, which results in a color change in the surface of mats as well as downward displacement of the maximum oxygen layer. Experiments by Garcia-Pichel et al. (1992, 1993) show that extracellular pigment scytonemin from terrestrial cyanobacterium *Chlorogloeopsis* sp. can reduce UV radiation (365 nm) by 70%, whereas mycosporine-like amino acids of terrestrial cyanobacterium *Gloeocapsa* sp. can reduce UV radiation (320 nm) by ~20–30%. Moreover, a variety of biological repair processes, such as photolyase photoreactivation, DNA excision repair, SOS response and post-replication repair, have also been found and well-investigated (e.g., Sutherland, 1981; O'Brian and Houghton, 1982; Owttrim and Coleman, 1989; Friso et al., 1994; Sancar, 1994). Some magnetotactic bacteria can produce intracellular iron nanoparticles, which could have been used for mitigating the stress from UV and free-iron-generated reactive oxygen species (ROS) in early Earth (Lin et al., 2019; Liu et al., 2022). Microbial adaption to high-UV radiation through mutation might have occurred during the early Earth. Studies have showed that microbial populations can evolve under continued UV stress and gradually develop the resistance to UV radiation (Wassmann et al., 2010). For example, Luckiesh and Knowles (1948) revealed that *Escherichia coli* can double their resistance to UV radiation through five times repeated exposure to UV radiation. In a space experiment, Wassmann et al. (2010) found that populations of *Bacillus subtilis* can increase their UV resistance by a factor of

three after approximately 700 generations of periodic UV radiation. It should be noted that ancient microorganisms might have possessed additional unknown protection mechanisms during the early Earth that have now been lost due to evolutionary redundancy under the current exposure conditions. As these could be difficult to re-acquire under short-term evolutionary selection, we may not be able to observe their full potential through experiments on present-day microorganisms.

Biogeochemical cycles

Microbial mats

Microbial mats might have been an important player in global biogeochemical cycles during the early Earth. Microbial mats are microbial ecosystems that consist of vertically distributed layers of pigmented bacteria that can harvest energy from the chemical gradients at the boundary between soils/sediments and water (e.g., Ludwig, 2004). In modern environments, cyanobacteria-dominated mats are restricted in various harsh settings, including hypersaline salterns and deserts (e.g., Bebout et al., 2004; Rodriguez-Caballero et al., 2018). However, before the occurrence of plants and bioturbation during the Phanerozoic, the land and perhaps marginal marine were likely covered mainly by microbial mats (e.g., Dornbos, 2006; Lalonde and Konhauser, 2015), which might have acted as a major source and/or sink for some global biogeochemical components such as CH_4 and O_2. Petrographic and geochemical evidence suggests the occurrence of microbial mats on river systems as early as 3.22 Ga (Homann et al., 2018).

In a landmark study, Hoehler et al. (2001) revealed that modern cyanobacteria mats can release reducing gases such as H_2, CO and CH_4, which would have been important for the biogeochemical cycles during the early Earth. For example, the generation of H_2 might have resulted in an H_2-rich atmosphere and the escape of H_2 to space, which might have been the mechanism for the gradual oxygenation of the atmosphere (Walker, 1977; Hoehler et al., 2001). Moreover, the release of CH_4 might have warmed the climate of the early Earth, a hypothesis that has received much attention in the literature (e.g., Bebout et al., 2004; Kelley et al., 2006; Zhao et al., 2018).

Both cultivation experiments and biogeochemical models have been used to clarify the potential role of microbial mats in the climate of the Precambrian (Bebout et al., 2004; Kelley et al., 2006; Zhao et al., 2018). During the majority of the Precambrian, the Earth was in a clement climate, although the solar luminosity was lower than that in modern times (e.g., Gough, 1981). Microbial mats might have been a solution to this "faint young sun" paradox, as it could release substantial CH_4 under the low atmospheric oxygen level of the Precambrian, which would have warmed Earth's climate. Cultivation experiments were designed to understand the change in methane release in the coastal marine mats under low SO_4^{2-} conditions during the Archean period (Bebout et al., 2004; Kelley et al., 2006). At low SO_4^{2-} (<0.2 mM), methane fluxes increased by 10-fold as sulfate reduction was out-competed by methanogenesis during organic matter remineralisation, but the remineralisation by methanogenesis was still insignificant (0.4%) relative to the total carbon release by mats. However, as has been mentioned in Bebout et al. (2004), the rates of net methane production still showed a linear increase at the end of the experiments, which represents an important caveat that the experiment might have not reached steady state. In another experiment with low SO_4^{2-} concentration (<1 mM), methane production was found to reach as high as 7% of the total carbon degradation (Kelley et al., 2006). Therefore, there is still a large uncertainty in the estimate of the potential contribution of CH_4 from costal marine mats to the climate of early Earth. If 7% of the Archean primary production (~800 Tmol/yr. according to Lalonde and Konhauser, 2015) was transferred to CH_4 in the atmosphere, this would result in a methane flux of ~56 Tmol/yr, which would likely have a large influence on the climate of early Earth (e.g., Zhao et al., 2018). It is worthy to note that there is a large uncertainty in the estimate of the primary productivity of the Archean. While UV radiation may have been harmful to the productivity of early mats, high atmospheric pCO_2 could have been a factor that could significantly elevate the productivity (e.g., Ji et al., 2020).

However, it must be noticed that the Archean period is not only characterised by low seawater SO_4^{2-} but also low atmospheric oxygen. Oxygen in the ocean and atmosphere should have had a big influence on the methane flux of both terrestrial and marine microbial mats at night, due to the existence of aerobic methane oxidation in the mats. Thus, the presence of oxygen might have been a reason for the relatively low methanogenesis rate in the experiment of Bebout et al. (2004). Through a biogeochemical model, it was demonstrated that terrestrial microbial mats could release substantial CH_4 under low atmospheric oxygen during early Earth (Zhao et al., 2018). Considering that the SO_4^{2-} concentrations in terrestrial water bodies such as rivers, lakes and wetlands should be even lower than that of seawater (Zhao et al., 2018), the potential of CH_4 release by terrestrial mats can be higher.

As microbial mats were one of the major ecosystems in early Earth, they have also shaped the long-term evolution of other global biogeochemical cycles, such as those of nitrogen and oxygen. Thomazo et al. (2018) argued that microbial mats such as biological soil crusts (BSCs) could have been an important source of N components such as ammonium and nitrate, which might have played a significant role in the early evolution of the global nitrogen cycle. As revealed by a recent study by Klatt et al. (2021), the net productivity and thus oxygen generation in cyanobacterial mats are positively correlated with the daylength. The authors further proposed that the increase in daylength and thus oxygen generation from microbial mats with time could be one of the reasons for the stepwise oxygenation of the Earth surface. Microbial mats could also have some indirect effect on global biogeochemical cycles. For example, oxygen produced by mats could have generated oxygen oases at the top of the mats, which

could result in the oxidative weathering of sulfur and redox-sensitive trace metals before the rise of atmospheric oxygen (Lalonde and Konhauser, 2015). The oxidative weathering related to microbial mats could be the reason for pre-GOE signals of oxidation (Lalonde and Konhauser, 2015). Note that the oxygen oases at the top of the mats only occurred at daytime during the Precambrian due to photosynthesis, and it would have disappeared during night as the oxygen level of the atmosphere was reduced (e.g., Zhao et al., 2018). This would have resulted in a high CH_4 flux from the mats to the atmosphere during the night.

Environmental forcings for primary productivity

Primary production is one of the main drivers for global biogeochemical cycles. It is therefore important to understand the forcings for primary productivity in early Earth. Several experimental studies have been conducted to investigate the response of primary productivity to Precambrian conditions, such as high seawater Fe(II), high atmospheric pCO_2, and unique ecophysiological mechanisms such as competition for nutrients between oxygenic cyanobacteria and Fe(II)-oxidising anoxygenic photosynthesizers (Swanner et al., 2015; Kamennaya et al., 2018; Ozaki et al., 2019; Herrmann et al., 2021; Szeinbaum et al., 2021). Although extant organisms used in the studies described almost certainly cannot be mapped to those present in ecosystems on the early Earth, we can reasonably assume that their core metabolic pathways and ecological activities had equivalents in those early ecosystems (e.g., Falkowski et al., 2008).

As ferruginous seawater conditions were probably widespread in the Precambrian (e.g., Sperling et al., 2015), it is important to understand the influence of Fe(II)-rich seawater on oxygenic photosynthesis, which elucidates the history of oceanic and atmospheric oxygenation. Through cultivation experiments, Swanner et al. (2015) found that both the growth rates and efficiency of oxygenic photosynthesis of planktonic cyanobacterium *Synechococcus* PCC 7002 decrease under high Fe(II) concentrations (>50 μM). The authors further proposed that Fe(II) toxicity of cyanobacteria under the conditions of Fe(II) upwelling might have decreased the oxygen generation rate in the photo zone in the oceans of early Earth, determining the onset of the GOE.

However, several lines of evidence show that Fe(II) toxicity might have not significantly limited the expansion of cyanobacteria in the early oceans (Ward et al., 2019; Szeinbaum et al., 2021). Firstly, many types of terrestrial cyanobacteria can survive at high Fe(II) concentrations (10–150 μM), which characterised the Archean oceans (Brown et al., 2005; Thompson et al., 2019; Ward et al., 2019). Next, microbial "helpers" such as facultative anaerobic gammaproteobacterial *Shewanella* using an ROS defence strategy, might have partially relieved the toxicity of Fe(II) on cyanobacteria (Szeinbaum et al., 2021). This is because the Fe(II) toxicity of cyanobacteria could be generated by the hydroxyl radicals from the reaction between Fe(II) and ROS formed during photosynthesis (Swanner et al., 2015; Szeinbaum et al., 2021). Finally, experimental setup and strain selection may have a great influence on the conclusion (Herrmann et al., 2021). Previous experiments examining Fe(II) toxicity were performed in a closed system (Swanner et al., 2015). In the cultivation experiments on cyanobacteria *Pseudanabaena* sp. *PCC7367* and *Synechococcus* sp. *PCC7336*, Herrmann et al. (2021) analysed the influence of experimental setup (open vs. closed system) on the observation of Fe(II) toxicity. In their experiments, Fe(II) toxicity was not observed in open-system cultures with continuous gaseous exchange. They further suggested that closed systems are not suitable for simulating the Archean environments, as the varying pCO_2 concentration during the experiment could have a significant impact on the experimental results.

Other than Fe(II) toxicity, the competition of nutrients such as P between oxygenic cyanobacteria and Fe(II)-oxidising anoxygenic photosynthesizers (photoferrotrophs) might also have had an influence on productivity and oxygen release in the early oceans (Ozaki et al., 2019). These photoferrotrophs inhabit at a deeper water depth than oxygenic cyanobacteria, which are located closer to the source of nutrients in the deep ocean water. Photoferrotrophs also undergo high-affinity PO_4^{3-} metabolism. These competitive advantages possessed by photoferrotrophs might have decreased the productivity and oxygen release of oxygenic cyanobacteria, resulting in the delayed oxygenation of the ocean and atmosphere system.

Other studies on biogeochemical cycles

Besides studies on microbial mats and primary productivity, other aspects of global biogeochemical cycles of early Earth have been experimentally investigated, such as the nitrogen cycle (Michiels et al., 2017), biological pumps (Kamennaya et al., 2018) and chemical weathering (Zaharescu et al., 2019). Through an incubation experiment in a modern ferruginous basin, an analogue for the Precambrian ocean, Michiels et al. (2017) reveals that a large fraction (40%) of NO_3^- is reduced to NH_4^+ rather than lost to the atmosphere as N_2. The transformation of NO_3^- to NH_4^+ would promote the retention of N in seawater, further boosting primary productivity. Using a biogeochemical model, Michiels et al. (2017) further suggested that the global primary productivity in the ferruginous ocean might have been limited by P rather than N. The biological pump is an important process in global C and O cycles, as it influences the final retention of C in marine sediments, further impacting the accumulation of O_2 in the atmosphere. It was suggested that the efficiency of the biological pump was low during the early Earth due to the lack of a ballast with a high sinking rate from a predator (Logan et al., 1995). However, it was recently found that the conditions of high pCO_2 in the early Earth can promote the formation of acidic extracellular polysaccharides (EPS; Kamennaya et al., 2018). These EPS can aggregate the dead cells of planktonic cyanobacteria to a ballast, increasing the efficiency of the biological pump.

Mineral formation

Banded iron formation

The sediments of the Precambrian could be different from those found in today's environments. In particular, a substantial number of BIFs with alternating layers of iron minerals and silica were formed in the Precambrian (e.g., Konhauser et al., 2017), in contrast to the lack of such deposits during the Phanerozoic. Both abiotic and biotic models of BIF formation have been proposed and intensely investigated. Many microbial experiments have been performed to investigate the mechanism of BIF formation, which has been reviewed in Posth et al. (2013, 2014) and will only be briefly discussed here.

Two biological processes may have contributed to the original precipitation of iron minerals of BIF. Firstly, Fe(II) can be oxidated to ferric hydroxide by O_2 generated by planktonic bacteria such as cyanobacteria. In this case, ferric hydroxide is the indirect product of the microbial process. Secondly, photoferrotrophy that use Fe(II) as an electron donor can produce Fe(III) (Garrels et al., 1973). The anoxygenic photoautotrophic bacteria used in photoferrotrophy could live below the layer of cyanobacteria. The anoxygenic bacteria thus has a competitive advantage to oxidate Fe(II), as it is closer to the source of Fe(II) in the Precambrian ocean, which is thought to be hydrothermal (e.g., Holland, 1973). Calculations based on the results of microbial experiments suggest that the anoxygenic photoautotrophic bacteria could account for the formation of most, if not all, of the initial iron minerals in BIF (Kappler et al., 2005). Furthermore, microbial processes such as microbial Fe(III) reduction could also contribute to the formation of minerals with Fe(II) such as magnetite and siderite in BIF (e.g., Konhauser et al., 2005; Li et al., 2011; Köehler et al., 2013; Halama et al., 2016; Bauer et al., 2020).

The formation of BIF through photoferrotrophy also requires the separation of biomass from Fe(III) minerals. Their co-precipitation could result in intense respiration in sediment, which could preclude the preservation of Fe(III) in BIF. However, data indicate the richness of Fe(III) in BIF, with an average Fe oxidation state of 2.4–2.6 (Posth et al., 2013; Thompson et al., 2019). A recent experiment suggests that the cell surface of a photoferrotroph could repel iron oxides under silica-rich seawater (Thompson et al., 2019), which can explain the lack of organic matter and the preservation of Fe(III) in BIF. Microbial cultivation experiments were also conducted to more precisely simulate the rate of photoferrotrophy under early Earth conditions. Konhauser et al. (2007) simulated the biological and abiotic oxidation of Fe(II) under disequilibrium water chemistry when Fe(II)-rich hydrothermal fluids mixed with Precambrian seawater that was rich in silica and HCO_3^-. They found that abiotic oxidation of Fe(II) was not quick enough to compete with the precipitation of Fe(II) silicates, whereas photoferrotrophy could induce rapid formation of Fe(III) hydroxide. The presence of silica could increase the oxidation rate of Fe(II) by green-sulfur bacteria *Chlorobium ferrooxidans* KoFox (Gauger et al., 2016). On the other hand, Croal et al. (2009) found that the rate of phototrophic Fe(II) oxidation by purple bacteria *Rhodopseudomonas palustris* and *Rhodobacter* species would not have been significantly influenced by high atmospheric H_2 under the high bicarbonate concentrations of the Archean.

The mechanisms for the formation of alternative bands of iron- and silica-rich minerals in BIF have also been studied through laboratory experiments (Posth et al., 2008; Schad et al., 2019). One possibility is that the iron- and silica-rich bands were formed under different temperatures. Whereas the rate of Fe(III) minerals formed by anoxygenic photoautotrophic bacteria is highest between 20 and 25°C, abiotic silica precipitation occurs at lower temperatures, owing to the decrease in silica solubility with cooling (Posth et al., 2008).

Stromatolites

Stromatolites are layered carbonate formations that were widespread in marine settings before the rise of animals, although they are restricted to limited settings in the modern ocean due to the existence of grazing and burrowing animals (Garrett, 1970; Bosak et al., 2013; Peters et al., 2017). Although the morphology and texture of Precambrian stromatolites could be similar to those of the modern ocean, the processes for the formation of stromatolites may be different due to the evolution of seawater conditions and the potential of changes in stromatolite-forming microbial communities over time (Bosak et al., 2013). For instance, sulfate reduction is believed to stimulate carbonate precipitation in modern stromatolites, as it can increase the dissolved inorganic carbon (DIC) concentration and thus the saturation index of carbonate. However, the DIC concentration of Precambrian seawater could be much higher than that of modern seawater, thus sulfate reduction would not have had much influence on the DIC concentration at the site of stromatolite formation. Through experiments with sulfate-reducing bacteria under artificial Precambrian seawater, Bosak and Newman (2003) revealed that sulfate-reducing bacteria could promote the formation of carbonate in Precambrian stromatolites by modulating carbonate nucleation rather than DIC concentration.

Cyanobacterial photosynthesis is the driver for microbial activity in modern stromatolites (e.g., Riding et al., 1991). However, the first extensive formation of stromatolites occurred at about 3.43 Ga (Allwood et al., 2006), which could be earlier than the occurrence of oxygenic photosynthesis (e.g., Planavsky et al., 2021). Bosak et al. (2007) experimentally evaluated the hypothesis that anoxygenic photosynthesis could build stromatolites. They found that anoxygenic photosynthetic bacteria could simulate the formation of carbonate crusts for stromatolites and thus may have played an important role in the formation of the earliest stromatolites. However, a later study using different species of anoxygenic phototrophic bacteria suggested the existence of a mechanism that impedes the formation of carbonate by anoxygenic phototrophic bacteria (Bundeleva et al., 2012), resulting in low-efficiency carbonate formation by anoxygenic phototrophic bacteria.

Future works

Although microbial cultivation experiment can greatly advance our understanding of the interaction between life and environments during the early Earth, there are several pitfalls to using this method. Firstly, as mentioned above, the environmental conditions of the Precambrian were quite different from those of the modern era in multiple aspects, and the artificial Precambrian environments used in cultivation experiments usually only consider a limited number of environmental factors, which cannot fully simulate the actual processes in the Precambrian. For instance, the primary productivity of the Precambrian could be influenced by various environmental forcings such as UV intensity, solar constant, length of daytime, pCO_2, marine *p*H, temperature, nutrient concentrations, and toxic components such as Fe(II). Thus, more constraints on the Precambrian environmental conditions would certainly be beneficial for further experimental simulation, and the consideration of additional environmental factors during the cultivation experiments would increase the reliability of the conclusions.

Secondly, the microbial species of the Precambrian could be different from those of today. Although it has been suggested that the components of well-adapted ecosystems may remain unchanged if there is no change in the physical-biological environment (e.g., Schopf et al., 2015), the environmental settings of the Precambrian were significantly different from those of modern environments and a perfect modern analogue for Precambrian settings is lacking. Thus, it is not known whether the species used in current cultivation experiments did actually exist during the Precambrian. On the other hand, there are a lot of biological mechanisms in the organisms of the early Earth that have now been lost due to evolutionary redundancy under current environmental conditions. Moreover, there are many species with similar functions and yet there are even more species to be discovered in the modern Earth surface, which adds more complexity to the identification of species that are applicable to the Precambrian. For example, a considerable number of photoferrotrophs in both fresh water and seawater are known today, including green sulfur bacteria, purple sulfur bacteria and purple non-sulfur bacteria (Posth et al., 2014 and the references therein). Knowledge of the first group of microorganisms that has developed certain metabolic pathways such as photoferrotrophs and the time of gene transfer between microbial groups would certainly be helpful in the design of simulation experiments. In this case, biomarkers may provide vital information on the existence of specific groups or even species of microbes in rock records. Other methods such as molecular clock and geochemical tracer, could also be helpful in the identification of certain metabolic pathways or groups of microorganisms on early Earth. Meanwhile, the similarities between the environmental settings of modern strains and those of the Precambrian should be evaluated to identify the applicability of certain species to the Precambrian period.

Thirdly, most simulation experiments are based on isolated / culturable species, whereas it is known that most microorganisms are not yet cultivated (Steen et al., 2019). Meanwhile, the effect of a single species may not be applicable to an entire ecosystem. This is due to the existence of competition and mutualistic symbiosis in the ecosystem (e.g., Ozaki et al., 2019; Szeinbaum et al., 2021), which could significantly alter the adaptability of microorganisms to certain environments. Experimental studies on microbial mats usually include the entire microbial ecosystem. However, other studies of simulated Precambrian environments usually involve only one or a few species (e.g., Konhauser et al., 2007; Gauger et al., 2016; Ozaki et al., 2019; Szeinbaum et al., 2021), partially because of the difficulty in choosing the proper combination of microbial strains to mimic the Precambrian ecosystem, as there is no perfect modern analogue. In this case, omics based methods (e.g., metagenomics, metatranscriptomics and metaproteomics) can be used to target multiple functional groups / species, various metabolic pathways and their activities (Ayala-Muñoz et al., 2022; McCain et al., 2022). These culture-independent studies can provide invaluable information for us to understand the potential of microbial life and how microbes thrived in extreme environments analogous to the early Earth, such as hydrothermal vents, the deep subsurface, and serpentinites, which are not easy to sample and are hard or time-consuming (months to years) to simulate in the lab (Jørgensen and Boetius, 2007; Trembath-Reichert et al., 2017). Interestingly, chemoautotrophy is found to be one of the dominant living strategies in many samples from these environments, either through oxidation of CO, reduced sulfur or H_2 (Fortunato and Huber, 2016; Lecoeuvre et al., 2021; Nobu et al., 2022; Rogers et al., 2022), showing a slow lifestyle and adaption to the limited availability of nutrients and energy. Multi-omics studies not only reveal unknown lineages, metabolic pathways and functions (Hug et al., 2016) but also can help identify new species (Lewis et al., 2020), such as new anaerobic arsenic methylating bacterium (Viacava et al., 2022) or an archaeon at the prokaryote–eukaryote interface (Imachi et al., 2020). Therefore, both culture-dependent and culture-independent methods are needed for future experimental studies of microbial activities in early Earth.

Lastly, the scope of current experimental simulations on the biogeochemical cycles of the early Earth is still limited. Although there are a considerable number of experimental studies simulating the primary productivity of the Archean ocean, experimental simulations on the speed and/or kinetics of other processes in the organic carbon cycle such as oxic weathering, biological pump, and remineralisations in both seawater and sediments, remain limited. Moreover, experimental simulations on the biogeochemical cycle of the other major and trace elements such as N, P and S are also largely lacking. Therefore, further experimental studies on these aspects have the potential to significantly advance our understanding of the biogeochemical cycles of the early Earth and perhaps other extraterrestrial planets that hold life.

Author contributions

MZ and K-QX discussed the idea. MZ wrote the manuscript and revised it together with YZ, WL, and K-QX. All authors contributed to the article and approved the submitted version.

Funding

MZ is funded by the 100 Talents program of the Chinese Academy of Sciences (E251520401).This research project has also received funding from the European Research Council (ERC) under the European Union's Horizon 2020 research and innovation programme (grant agreement no. 725613 MinOrg).

Conflict of interest

The authors declare that the research was conducted in the absence of any commercial or financial relationships that could be construed as a potential conflict of interest.

Publisher's note

All claims expressed in this article are solely those of the authors and do not necessarily represent those of their affiliated organizations, or those of the publisher, the editors and the reviewers. Any product that may be evaluated in this article, or claim that may be made by its manufacturer, is not guaranteed or endorsed by the publisher.

References

Allwood, A., Walter, M., Kamber, B., Marshall, C., and Burch, I. (2006). Stromatolite reef from the early Archaean era of Australia. *Nature* 441, 714–718. doi: 10.1038/nature04764

Ayala-Muñoz, D., Macalady, J. L., Sánchez-España, J., Falagán, C., Couradeau, E., and Burgos, W. D. (2022). Microbial carbon, sulfur, iron, and nitrogen cycling linked to the potential remediation of a meromictic acidic pit lake. *ISME J.* 16, 2666–2679. doi: 10.1038/s41396-022-01320-w

Bartlett, B. C., and Stevenson, D. J. (2016). Analysis of a Precambrian resonance-stabilized day length. *Geophys. Res. Lett.* 43, 5716–5724. doi: 10.1002/2016GL068912

Bauer, K. W., Byrne, J. M., Kenward, P., Simister, R. L., Michiels, C. C., Friese, A., et al. (2020). Magnetite biomineralization in ferruginous waters and early Earth evolution. *Earth Planet. Sci. Lett.* 549:116495. doi: 10.1016/j.epsl.2020.116495

Bebout, B. M., and Garcia-Pichel, F. (1995). UV B-induced vertical migrations of cyanobacteria in a microbial mat. *Applied and Environmental Microbiology* 61, 4215–4222.

Bebout, B. M., Hoehler, T. M., Thamdrup, B. O., Albert, D., Carpenter, S. P., Hogan, M., et al. (2004). Methane production by microbial mats under low sulphate concentrations. *Geobiology* 2, 87–96. doi: 10.1111/j.1472-4677.2004.00024.x

Bishop, J. L., Louris, S. K., Rogoff, D. A., and Rothschild, L. J. (2006). Nanophase iron oxides as a key ultraviolet sunscreen for ancient photosynthetic microbes. *Int. J. Astrobiol.* 5, 1–12. doi: 10.1017/S1473550406002886

Bjerrum, C. J., and Canfield, D. E. (2002). Ocean productivity before about 1.9 Ga ago limited by phosphorus adsorption onto iron oxides. *Nature* 417, 159–162. doi: 10.1038/417159a

Blättler, C. L., Claire, M. W., Prave, A. R., Kirsimäe, K., Higgins, J. A., Medvedev, P. V., et al. (2018). Two-billion-year-old evaporites capture Earth's great oxidation. *Science* 360, 320–323. doi: 10.1126/science.aar2687

Bosak, T., Greene, S. E., and Newman, D. K. (2007). A likely role for anoxygenic photosynthetic microbes in the formation of ancient stromatolites. *Geobiology* 5, 119–126.

Bosak, T., Knoll, A. H., and Petroff, A. P. (2013). The meaning of stromatolites. *Annu. Rev. Earth Planet. Sci.* 41, 21–44. doi: 10.1146/annurev-earth-042711-105327

Bosak, T., and Newman, D. K. (2003). Microbial nucleation of calcium carbonate in the Precambrian. *Geology* 31, 577–580.

Brown, I. I., Mummey, D., and Cooksey, K. E. (2005). A novel cya- nobacterium exhibiting an elevated tolerance for iron. *FEMS Microbiol. Ecol.* 52, 307–314. doi: 10.1016/j.femsec.2004.11.020

Bryce, C. C., Horneck, G., Rabbow, E., Edwards, H. G., and Cockell, C. S. (2015). Impact shocked rocks as protective habitats on an anoxic early earth. *Int. J. Astrobiol.* 14, 115–122. doi: 10.1017/S1473550414000123

Bundeleva, I. A., Shirokova, L. S., Bénézeth, P., Pokrovsky, O. S., Kompantseva, E. I., and Balor, S. (2012). Calcium carbonate precipitation by anoxygenic phototrophic bacteria. *Chem. Geol.* 291, 116–131. doi: 10.1016/j.chemgeo.2011.10.003

Canfield, D. E. (1998). A new model for Proterozoic Ocean chemistry. *Nature* 396, 450–453. doi: 10.1038/24839

Canfield, D. E., van Zuilen, M. A., Nabhan, S., Bjerrum, C. J., Zhang, S., Wang, H., et al. (2021). Petrographic carbon in ancient sediments constrains Proterozoic era atmospheric oxygen levels. *Proc. Natl. Acad. Sci.* 118:e2101544118. doi: 10.1073/pnas.2101544118

Catling, D. C., and Zahnle, K. J. (2020). The Archean atmosphere. *Sci. Adv.* 6:eaax1420. doi: 10.1126/sciadv.aax1420

Cleaves, H. J., and Miller, S. L. (1998). Oceanic protection of prebiotic organic compounds from UV radiation. *Proc. Natl. Acad. Sci.* 95, 7260–7263. doi: 10.1073/pnas.95.13.7260

Cockell, C. S. (1998). Biological effects of high ultraviolet radiation on early earth—a theoretical evaluation. *J. Theor. Biol.* 193, 717–729. doi: 10.1006/jtbi.1998.0738

Cockell, C. S. (2000). The ultraviolet history of the terrestrial planets—implications for biological evolution. *Planet. Space Sci.* 48, 203–214. doi: 10.1016/S0032-0633(99)00087-2

Cockell, C. S., Lee, P., Osinski, G., Horneck, G., and Broady, P. (2002). Impact-induced microbial endolithic habitats. *Meteorit. Planet. Sci.* 37, 1287–1298. doi: 10.1111/j.1945-5100.2002.tb01029.x

Cockell, C. S., Rettberg, P., Rabbow, E., and Olsson-Francis, K. (2011). Exposure of phototrophs to 548 days in low Earth orbit: microbial selection pressures in outer space and on early earth. *ISME J.* 5, 1671–1682. doi: 10.1038/ismej.2011.46

Croal, L. R., Jiao, Y., Kappler, A., and Newman, D. K. (2009). Phototrophic Fe (II) oxidation in an atmosphere of H2: implications for Archean banded iron formations. *Geobiology* 7, 21–24.

Crowe, S. A., Paris, G., Katsev, S., Jones, C., Kim, S. T., Zerkle, A. L., et al. (2014). Sulfate was a trace constituent of Archean seawater. *Science* 346, 735–739. doi: 10.1126/science.1258966

Czaja, A. D., Johnson, C. M., Roden, E. E., Beard, B. L., Voegelin, A. R., Nägler, T. F., et al. (2012). Evidence for free oxygen in the Neoarchean Ocean based on coupled iron–molybdenum isotope fractionation. *Geochim. Cosmochim. Acta* 86, 118–137. doi: 10.1016/j.gca.2012.03.007

Dornbos, S. Q. (2006). Evolutionary palaeoecology of early epifaunal echinoderms: response to increasing bioturbation levels during the Cambrian radiation. *Palaeogeogr. Palaeoclimatol. Palaeoecol.* 237, 225–239. doi: 10.1016/j.palaeo.2005.11.021

Ehling-Schulz, M., Bilger, W., and Scherer, S. (1997). UV-B-induced synthesis of photo- protective pigments and extracellular polysaccharides in the terrestrial cyano- bacterium Nostoc commune. *J. Bacteriol.* 179, 1940–1945. doi: 10.1128/jb.179.6.1940-1945.1997

Falkowski, P. G., Fenchel, T., and Delong, E. F. (2008). The microbial engines that drive Earth's biogeochemical cycles. *Science* 320, 1034–1039. doi: 10.1126/science.1153213

Farquhar, J., Bao, H., and Thiemens, M. (2000). Atmospheric influence of Earth's earliest sulfur cycle. *Science* 289, 756–758. doi: 10.1126/science.289.5480.756

Fortunato, C. S., and Huber, J. A. (2016). Coupled RNA-SIP and metatranscriptomics of active chemolithoautotrophic communities at a deep-sea hydrothermal vent. *ISME J.* 10, 1925–1938. doi: 10.1038/ismej.2015.258

Friso, G., Spetea, C., Giacometti, G. M., Vass, I., and Barbato, R. (1994). Degradation of photosystem II reaction center D1-protein induced by UVB radiation in isolated thylakoids. Identification and characterization of C-and N-terminal breakdown products. *Biochim. Biophys. Acta - Bioenerg.* 1184, 78–84. doi: 10.1016/0005-2728(94)90156-2

Garcia-Pichel, F., and Belnap, J. (1996). Microenvironments and microscale productivity of cyanobacterial desert crusts. *J. Phycol.* 32, 774–782. doi: 10.1111/j.0022-3646.1996.00774.x

Garcia-Pichel, F., Mechling, M., and Castenholz, R. W. (1994). Diel migrations of microorganisms within a benthic, hypersaline mat community. *Appl. Environ. Microbiol.* 60, 1500–1511. doi: 10.1128/aem.60.5.1500-1511.1994

Garcia-Pichel, F., Sherry, N. D., and Castenholz, R. W. (1992). Evidence for an ultraviolet sunscreen role of the extracellular pigment scytonemin in the terrestrial cyanobacterium Chiorogloeopsis sp. *Photochem. Photobiol.* 56, 17–23. doi: 10.1111/j.1751-1097.1992.tb09596.x

Garcia-Pichel, F., Wingard, C. E., and Castenholz, R. W. (1993). Evidence regarding the UV sunscreen role of a mycosporine-like compound in the cyanobacterium Gloeocapsa sp. *Appl. Environ. Microbiol.* 59, 170–176. doi: 10.1128/aem.59.1.170-176.1993

Garrels, R. M., Perry, E. A. Jr., and MacKenzie, F. T. (1973). Genesis of Precambrian iron-formations and the development of atmospheric oxygen. *Econ. Geol.* 68, 1173–1179. doi: 10.2113/gsecongeo.68.7.1173

Garrett, P. (1970). Phanerozoic stromatolites: non- competitive ecologic restriction by grazing and burrowing animals. *Science* 169, 171–173. doi: 10.1126/science.169.3941.171

Gauger, T., Byrne, J. M., Konhauser, K. O., Obst, M., Crowe, S., and Kappler, A. (2016). Influence of organics and silica on Fe(II) oxidation rates and cell–mineral aggregate formation by the green-sulfur Fe(II)-oxidizing bacterium Chlorobium ferrooxidans KoFox–implications for Fe(II) oxidation in ancient oceans. *Earth Planet. Sci. Lett.* 443, 81–89. doi: 10.1016/j.epsl.2016.03.022

Gómez, F., Aguilera, A., and Amils, R. (2007). Soluble ferric iron as an effective protective agent against UV radiation: implications for early life. *Icarus* 191, 352–359. doi: 10.1016/j.icarus.2007.04.008

Gough, D. O. (1981). "Solar interior structure and luminosity variations" in *Physics of Solar Variations*. ed. V. Domingo (Dordrecht: Springer), 21–34.

Habicht, K. S., Gade, M., Thamdrup, B., Berg, P., and Canfield, D. E. (2002). Calibration of sulfate levels in the Archean Ocean. *Science* 298, 2372–2374. doi: 10.1126/science.1078265

Halama, M., Swanner, E. D., Konhauser, K. O., and Kappler, A. (2016). Evaluation of siderite and magnetite formation in BIFs by pressure–temperature experiments of Fe(III) minerals and microbial biomass. *Earth Planet. Sci. Lett.* 450, 243–253. doi: 10.1016/j.epsl.2016.06.032

Halevy, I., and Bachan, A. (2017). The geologic history of seawater pH. *Science* 355, 1069–1071. doi: 10.1126/science.aal4151

Herman, E. K., and Kump, L. R. (2005). Biogeochemistry of microbial mats under Precambrian environmental conditions: a modelling study. *Geobiology* 3, 77–92. doi: 10.1111/j.1472-4669.2005.00048.x

Herrmann, A. J., Sorwat, J., Byrne, J. M., Frankenberg-Dinkel, N., and Gehringer, M. M. (2021). Diurnal Fe(II)/Fe(III) cycling and enhanced O_2 production in a simulated Archean marine oxygen oasis. *Nat. Commun.* 12, 1–11. doi: 10.1038/s41467-021-22258-1

Hoehler, T. M., Bebout, B. M., and Des Marais, D. J. (2001). The role of microbial mats in the production of reduced gases on the early Earth. *Nature* 412, 324–327.

Holland, H. D. (1973). The oceans: a possible source of iron in iron-formations. *Econ. Geol.* 68, 1169–1172.

Homann, M., Sansjofre, P., Van Zuilen, M., Heubeck, C., Gong, J., Killingsworth, B., et al. (2018). Microbial life and biogeochemical cycling on land 3,220 million years ago. *Nat. Geosci.* 11, 665–671. doi: 10.1038/s41561-018-0190-9

Hug, L. A., Baker, B. J., Anantharaman, K., Brown, C. T., Probst, A. J., Castelle, C. J., et al. (2016). A new view of the tree of life. *Nat. Microbiol.* 1:16048. doi: 10.1038/nmicrobiol.2016.48

Imachi, H., Nobu, M. K., Nakahara, N., Morono, Y., Ogawara, M., Takaki, Y., et al. (2020). Isolation of an archaeon at the prokaryote–eukaryote interface. *Nature* 577, 519–525. doi: 10.1038/s41586-019-1916-6

Isson, T. T., and Planavsky, N. J. (2018). Reverse weathering as a long-term stabilizer of marine pH and planetary climate. *Nature* 560, 471–475. doi: 10.1038/s41586-018-0408-4

Ji, X., Verspagen, J. M., Van de Waal, D. B., Rost, B., and Huisman, J. (2020). Phenotypic plasticity of carbon fixation stimulates cyanobacterial blooms at elevated CO_2. *Sci. Adv.* 6:eaax2926. doi: 10.1126/sciadv.aax2926

Jones, C., Nomosatryo, S., Crowe, S. A., Bjerrum, C. J., and Canfield, D. E. (2015). Iron oxides, divalent cations, silica, and the early earth phosphorus crisis. *Geology* 43, 135–138. doi: 10.1130/G36044.1

Jørgensen, B. B., and Boetius, A. (2007). Feast and famine — microbial life in the deep-sea bed. *Nat. Rev. Microbiol.* 5, 770–781. doi: 10.1038/nrmicro1745

Kamennaya, N. A., Zemla, M., Mahoney, L., Chen, L., Holman, E., Holman, H. Y., et al. (2018). High pCO2-induced exopolysaccharide-rich ballasted aggregates of planktonic cyanobacteria could explain Paleoproterozoic carbon burial. *Nat. Commun.* 9, 1–8. doi: 10.1038/s41467-018-04588-9

Kappler, A., Pasquero, C., Konhauser, K. O., and Newman, D. K. (2005). Deposition of banded iron formations by anoxygenic phototrophic Fe(II)-oxidizing bacteria. *Geology* 33, 865–868. doi: 10.1130/G21658.1

Kasting, J. F. (1987). Theoretical constraints on oxygen and carbon dioxide concentrations in the Precambrian atmosphere. *Precambrian Res.* 34, 205–229. doi: 10.1016/0301-9268(87)90001-5

Kasting, J. F. (1993). Earth's early atmosphere. *Science* 259, 920–926. doi: 10.1126/science.11536547

Kelley, C. A., Prufert-Bebout, L. E., and Bebout, B. M. (2006). Changes in carbon cycling ascertained by stable isotopic analyses in a hypersaline microbial mat. *J. Geophys. Res. Biogeosci.* 111:G04012. doi: 10.1029/2006JG000212

Klatt, J. M., Chennu, A., Arbic, B. K., Biddanda, B. A., and Dick, G. J. (2021). Possible link between Earth's rotation rate and oxygenation. *Nature Geoscience* 14, 564–570.

Knoll, A. H., Javaux, E. J., Hewitt, D., and Cohen, P. (2006). Eukaryotic organisms in Proterozoic oceans. *Philos. Trans. R. Soc. B Biol. Sci.* 361, 1023–1038. doi: 10.1098/rstb.2006.1843

Köehler, I., Papineau, D., Konhauser, K. O., and Kappler, A. (2013). Biological carbon precursor to diagenetic siderite spherulites in banded iron formations. *Nat. Commun.* 4:1741. doi: 10.1038/ncomms2770

Konhauser, K. O., Lalonde, S. V., Amskold, L., and Holland, H. D. (2007). Was there really an Archean phosphate crisis? *Science* 315:1234. doi: 10.1126/science.1136328

Konhauser, K., Newman, D. K., and Kappler, A. (2005). The potential significance of microbial Fe(III) reduction during deposition of Precambrian banded iron formations. *Geobiology* 3, 167–177. doi: 10.1111/j.1472-4669.2005.00055.x

Konhauser, K. O., Planavsky, N. J., Hardisty, D. S., Robbins, L. J., Warchola, T. J., Haugaard, R., et al. (2017). Iron formations: a global record of Neoarchaean to Palaeoproterozoic environmental history. *Earth Sci. Rev.* 172, 140–177. doi: 10.1016/j.earscirev.2017.06.012

Kugler, A., and Dong, H. (2019). Phyllosilicates as protective habitats of filamentous cyanobacteria Leptolyngbya against ultraviolet radiation. *PLoS One* 14:e0219616. doi: 10.1371/journal.pone.0219616

Lalonde, S. V., and Konhauser, K. O. (2015). Benthic perspective on Earth's oldest evidence for oxygenic photosynthesis. *Proc. Natl. Acad. Sci.* 112, 995–1000. doi: 10.1073/pnas.1415718112

Lecoeuvre, A., Ménez, B., Cannat, M., Chavagnac, V., and Gérard, E. (2021). Microbial ecology of the newly discovered serpentinite-hosted Old City hydrothermal field (southwest Indian ridge). *ISME J.* 15, 818–832. doi: 10.1038/s41396-020-00816-7

Lenton, T. M., Daines, S. J., and Mills, B. J. W. (2018). COPSE reloaded: an improved model of biogeochemical cycling over Phanerozoic time. *Earth-Sci. Rev.* 178, 1–28. doi: 10.1016/j.earscirev.2017.12.004

Lewis, W. H., Tahon, G., Geesink, P., Sousa, D. Z., and Ettema, T. J. G. (2020). Innovations to culturing the uncultured microbial majority. *Nat. Rev. Microbiol.* 19, 225–240. doi: 10.1038/s41579-020-00458-8

Li, J. L., Konhauser, K. O., Cole, D. R., and Phelps, T. J. (2011). Mineral ecophysiological data provide growing evidence for microbial activity in banded-iron formations. *Geology* 39, 707–710. doi: 10.1130/G32003.1

Lin, W., Kirschvink, J. L., Paterson, G. A., Bazylinski, D. A., and Pan, Y. (2019). On the origin of microbial magnetoreception. *Natl. Sci. Rev.* 7, 472–479. doi: 10.1093/nsr/nwz065

Liu, J., Zhang, W., He, K., Liu, L., Wang, C., Jiang, Y., et al. (2022). Survival of the magnetotactic bacterium *Magnetospirillum gryphiswaldense* exposed to Earth's lower near space. *Sci. Bull.* 67, 1335–1339. doi: 10.1016/j.scib.2022.03.005

Logan, G. A., Hayes, J. M., Hieshima, G. B., and Summons, R. E. Terminal Proterozoic reorganization of biogeochemical cycles. *Nature* 376, 53–56. doi: 10.1038/376053a0

Luckiesh, M., and Knowles, T. (1948). Resistivity of Escherichia coli to ultraviolet energy (lambda 2537) as affected by irradiation of preceding cultures. *J. Bacteriol.* 55, 369–372. doi: 10.1128/jb.55.3.369-372.1948

Ludwig, R., (2004). Carbon cycling and calcification in hypersaline microbial mats (Doctoral dissertation, Universität Bremen).

Lyons, T. W., Reinhard, C. T., and Planavsky, N. J. (2014). The rise of oxygen in Earth's early ocean and atmosphere. *Nature* 506, 307–315. doi: 10.1038/nature13068

Maliva, R. G., Knoll, A. H., and Simonson, B. M. (2005). Secular change in the Precambrian silica cycle: insight from chert petrology. *Geol. Soc. Am. Bull.* 117, 835–845. doi: 10.1130/B25555.1

Margulis, L., Walker, J. C. G., and Rambler, M. (1976). Reassessment of roles of oxygen and ultraviolet light in Precambrian evolution. *Nature* 264, 620–624. doi: 10.1038/264620a0

Martin, W., Baross, J., Kelley, D., and Russell, M. J. (2008). Hydrothermal vents and the origin of life. *Nat. Rev. Microbiol.* 6, 805–814. doi: 10.1038/nrmicro1991

McCain, J. S. P., Allen, A. E., and Bertrand, E. M. (2022). Proteomic traits vary across taxa in a coastal Antarctic phytoplankton bloom. *ISME J.* 16, 569–579. doi: 10.1038/s41396-021-01084-9

Michiels, C. C., Darchambeau, F., Roland, F. A. E., Morana, C., Llirós, M., García-Armisen, T., et al. (2017). Iron-dependent nitrogen cycling in a ferruginous lake and the nutrient status of Proterozoic oceans. *Nat. Geosci.* 10, 217–221. doi: 10.1038/ngeo2886

Mloszewska, A. M., Cole, D. B., Planavsky, N. J., Kappler, A., Whitford, D. S., Owttrim, G. W., et al. (2018). UV radiation limited the expansion of cyanobacteria in early marine photic environments. *Nat. Commun.* 9, 1–8. doi: 10.1038/s41467-018-05520-x

Moore, E. K., Jelen, B. I., Giovannelli, D., Raanan, H., and Falkowski, P. G. Archaean eon. Nat. Geosci. 10, (2017). Metal availability and the expanding network of microbial metabolisms in the Archaean eon. *Nat. Geosci.* 10, 629–636. doi: 10.1038/ngeo3006

Munk, W. H., and MacDonald, G. J. F. (1960). *The Rotation of the Earth: A Geophysical Discussion.* London: Cambridge University Press.

Nobu, M. K., Nakai, R., Tamazawa, S., Mori, H., Toyoda, A., Ijiri, A., et al. (2022). Unique H2-utilizing lithotrophy in serpentinite-hosted systems. *ISME J.* 17, 95–104. doi: 10.1038/s41396-022-01197-9

O'Brian, P. A., and Houghton, J. A. (1982). Photoreactivation and excision repair of UV induced pyrimidine dimers in the unicellular cyanobacterium Gloeocapsa alpicola (Synechocystis PCC 6308). *Photochem. Photobiol.* 35, 359–364. doi: 10.1111/j.1751-1097.1982.tb02574.x

Olsson-Francis, K., and Cockell, C. S. (2010a). Experimental methods for studying microbial survival in extraterrestrial environments. *J. Microbiol. Methods* 80, 1–13. doi: 10.1016/j.mimet.2009.10.004

Olsson-Francis, K., and Cockell, C. S. (2010b). Use of cyanobacteria for in-situ resource use in space applications. *Planet. Space Sci.* 58, 1279–1285. doi: 10.1016/j.pss.2010.05.005

Oren, A. (1997). Mycosporine-like amino acids as osmotic solutes in a community of halophilic cyanobacteria. *Geomicrobiology Journal* 14, 231–240.

Owttrim, G. W., and Coleman, J. R. (1989). Regulation of expression and nucleotide sequence of the Anabaena variabilis recA gene. *J. Bacteriol.* 171, 5713–5719. doi: 10.1128/jb.171.10.5713-5719.1989

Ozaki, K., Tajika, E., Hong, P. K., Nakagawa, Y., and Reinhard, C. T. (2018). Effects of primitive photosynthesis on Earth's early climate system. *Nat. Geosci.* 11, 55–59. doi: 10.1038/s41561-017-0031-2

Ozaki, K., Thompson, K. J., Simister, R. L., Crowe, S. A., and Reinhard, C. T. (2019). Anoxygenic photosynthesis and the delayed oxygenation of Earth's atmosphere. *Nat. Commun.* 10, 1–10. doi: 10.1038/s41467-019-10872-z

Pavlov, A. A., and Kasting, J. F. (2002). Mass-independent fractionation of sulfur isotopes in Archean sediments: strong evidence for an anoxic Archean atmosphere. *Astrobiology* 2, 27–41. doi: 10.1089/153110702753621321

Peters, S. E., Husson, J. M., and Wilcots, J. (2017). The rise and fall of stromatolites in shallow marine environments. *Geology* 45, 487–490. doi: 10.1130/G38931.1

Phoenix, V. R., Bennett, P. C., Engel, A. S., Tyler, S. W., and Ferris, F. G. (2006). Chilean high-altitude hot-spring sinters: a model system for UV screening mechanisms by early Precambrian cyanobacteria. *Geobiology* 4, 15–28. doi: 10.1111/j.1472-4669.2006.00063.x

Phoenix, V. R., Konhauser, K. O., Adams, D. G., and Bottrell, S. H. (2001). Role of biomineralization as an ultraviolet shield: implications for Archean life. *Geology* 29, 823–826. doi: 10.1130/0091-7613(2001)029<0823:ROBAAU>2.0.CO;2

Pierson, B. K., Mitchell, H. K., and Ruff-Roberts, A. L. (1993). Chloroflexus aurantiacus and ultraviolet radiation: implications for archean shallow-water stromatolites. *Orig. Life Evol. Biosph.* 23, 243–260. doi: 10.1007/BF01581902

Planavsky, N. J., Bekker, A., Hofmann, A., Owens, J. D., and Lyons, T. W. (2012). Sulfur record of rising and falling marine oxygen and sulfate levels during the Lomagundi event. *Proc. Natl. Acad. Sci.* 109, 18300–18305. doi: 10.1073/pnas.1120387109

Planavsky, N. J., Crowe, S. A., Fakhraee, M., Beaty, B., Reinhard, C. T., Mills, B. J., et al. (2021). Evolution of the structure and impact of Earth's biosphere. *Nature Rev. Earth Environ.* 2, 123–139. doi: 10.1038/s43017-020-00116-w

Planavsky, N. J., Reinhard, C. T., Isson, T. T., Ozaki, K., and Crockford, P. W. (2020). Large mass-independent oxygen isotope fractionations in mid-proterozoic sediments: evidence for a low-oxygen atmosphere? *Astrobiology* 20, 628–636. doi: 10.1089/ast.2019.2060

Planavsky, N. J., Reinhard, C. T., Wang, X., McGoldrick, P., Thompson, D., Rainbird, R. H., et al. (2014). Low mid-Proterozoic atmospheric oxygen levels and the delayed rise of animals. *Science* 346, 635–638. doi: 10.1126/science.1258410

Posth, N. R., Canfield, D. E., and Kappler, A. (2014). Biogenic Fe(III) minerals: from formation to diagenesis and preservation in the rock record. *Earth Sci. Rev.* 135, 103–121. doi: 10.1016/j.earscirev.2014.03.012

Posth, N. R., Hegler, F., Konhauser, K. O., and Kappler, A. (2008). Alternating Si and Fe deposition caused by temperature fluctuations in Precambrian oceans. *Nat. Geosci.* 1, 703–708. doi: 10.1038/ngeo306

Posth, N. R., Konhauser, K. O., and Kappler, A. (2013). Microbiological processes in banded iron formation deposition. *Sedimentology* 60, 1733–1754. doi: 10.1111/sed.12051

Rettberg, P., Horneck, G., Strauch, W., Facius, R., and Seckmeyer, G. (1998). Simulation of planetary UV radiation climate on the example of the early earth. *Adv. Space Res.* 22, 335–339. doi: 10.1016/S0273-1177(98)00190-2

Reynolds, C. S., Oliver, R. L., and Walsby, A. E. (1987). Cyanobacterial dominance: the role of buoyancy regulation in dynamic lake environments. *N. Z. J. Mar. Freshwater Res.* 21, 379–390. doi: 10.1080/00288330.1987.9516234

Riding, R., Awramik, S. M., Winsborough, B. M., Griffin, K. M., and Dill, R. F. (1991). Bahamian giant stromatolites – microbial composition of surface mats. *Geol. Mag.* 128, 227–234. doi: 10.1017/S001675680002207X

Rodriguez-Caballero, E., Belnap, J., Büdel, B., Crutzen, P. J., Andreae, M. O., Pöschl, U., et al. (2018). Dryland photoautotrophic soil surface communities endangered by global change. *Nat. Geosci.* 11, 185–189. doi: 10.1038/s41561-018-0072-1

Rogers, T. J., Buongiorno, J., Jessen, G. L., Schrenk, M. O., Fordyce, J. A., de Moor, J. M., et al. (2022). Chemolithoautotroph distributions across the subsurface of a convergent margin. *ISME J.* 17, 140–150. doi: 10.1038/s41396-022-01331-7

Royer, D. L., Berner, R. A., Montañez, I. P., Tabor, N. J., and Beerling, D. J. (2004). CO_2 as a primary driver of phanerozoic climate. *GSA Today* 14, 4–10. doi: 10.1130/1052-5173(2004)014<4:CAAPDO>2.0.CO;2

Rye, R., and Holland, H. D. (1998). Paleosols and the evolution of atmospheric oxygen: a critical review. *Am. J. Sci.* 298, 621–672. doi: 10.2475/ajs.298.8.621

Sagan, C. (1973). Ultraviolet selection pressure on the earliest organisms. *J. Theor. Biol.* 39, 195–200. doi: 10.1016/0022-5193(73)90216-6

Sancar, A. (1994). Mechanisms of DNA excision repair. *Science* 266, 1954–1956. doi: 10.1126/science.7801120

Schad, M., Halama, M., Bishop, B., Konhauser, K. O., and Kappler, A. (2019). Temperature fluctuations in the Archean Ocean as trigger for varve-like deposition of iron and silica minerals in banded iron formations. *Geochim. Cosmochim. Acta* 265, 386–412. doi: 10.1016/j.gca.2019.08.031

Schopf, J. W., Kudryavtsev, A. B., Walter, M. R., Van Kranendonk, M. J., Williford, K. H., Kozdon, R., et al. (2015). Sulfur-cycling fossil bacteria from the 1.8-Ga Duck Creek formation provide promising evidence of evolution's null hypothesis. *Proc. Natl. Acad. Sci.* 112, 2087–2092. doi: 10.1073/pnas.1419241112

Sinha, R. P., and Häder, D.-P. (2002). UV-induced DNA damage and repair: a review. *Photochem. Photobiol. Sci.* 1, 225–236. doi: 10.1039/b201230h

Sinha, R. P., and Häder, D.-P. (2008). UV-protectants in cyanobacteria. *Plant Sci.* 174, 278–289. doi: 10.1016/j.plantsci.2007.12.004

Sperling, E. A., Wolock, C. J., Morgan, A. S., Gill, B. C., Kunzmann, M., Halverson, G. P., et al. (2015). Statistical analysis of iron geochemical data suggests limited late Proterozoic oxygenation. *Nature* 523, 451–454. doi: 10.1038/nature14589

Steen, A. D., Crits-Christoph, A., Carini, P., DeAngelis, K. M., Fierer, N., Lloyd, K. G., et al. (2019). High proportions of bacteria and archaea across most biomes remain uncultured. *ISME J.* 13, 3126–3130. doi: 10.1038/s41396-019-0484-y

Sutherland, B. M. (1981). Photoreactiation. *Bioscience* 31, 439–444. doi: 10.2307/1308431

Swanner, E. D., Mloszewska, A. M., Cirpka, O. A., Schoenberg, R., Konhauser, K. O., and Kappler, A. (2015). Modulation of oxygen production in Archaean oceans by episodes of Fe(II) toxicity. *Nat. Geosci.* 8, 126–130. doi: 10.1038/ngeo2327

Szeinbaum, N., Toporek, Y. J., Reinhard, C. T., and Glass, J. B. (2021). Microbial helpers allow cyanobacteria to thrive in ferruginous waters. *Geobiology* 19, 510–520. doi: 10.1111/gbi.12443

Tevini, M. (1993). *UV-B Radiation and Ozone Depletion*. Boca Raton: Lewis.

Thomazo, C., Couradeau, E., and Garcia-Pichel, F. (2018). Possible nitrogen fertilization of the early Earth Ocean by microbial continental ecosystems. *Nat. Commun.* 9, 1–8. doi: 10.1038/s41467-018-04995-y

Thompson, K. J., Kenward, P. A., Bauer, K. W., Warchola, T., Gauger, T., Martinez, R., et al. (2019). Photoferrotrophy, deposition of banded iron formations, and meth- ane production in Archean oceans. *Sci. Adv.* 5:eaav2869. doi: 10.1126/sciadv.aav2869

Trembath-Reichert, E., Morono, Y., Ijiri, A., Hoshino, T., Dawson, K. S., Inagaki, F., et al. (2017). Methyl-compound use and slow growth characterize microbial life in 2-km-deep subseafloor coal and shale beds. *Proc. Natl. Acad. Sci. U. S. A.* 114, E9206–E9215. doi: 10.1073/pnas.1707525114

Viacava, K., Qiao, J., Janowczyk, A., Poudel, S., Jacquemin, N., Meibom, K. L., et al. (2022). Meta-omics-aided isolation of an elusive anaerobic arsenic-methylating soil bacterium. *ISME J.* 16, 1740–1749. doi: 10.1038/s41396-022-01220-z

Walker, J. C. G. *Evolution of the Atmosphere*. Macmillan, New York, (1977).

Ward, L. M., Idei, A., Nakagawa, M., Ueno, Y., Fischer, W. W., and McGlynn, S. E. (2019). Geochemical and metagenomic characterization of Jinata Onsen, a Proterozoic-analog hot spring, reveals novel microbial diversity including iron-tolerant phototrophs and thermophilic lithotrophs. *Microbes Environ.* 34, 278–292. doi: 10.1264/jsme2.ME19017

Wassmann, M., Moeller, R., Reitz, G., and Rettberg, P. (2010). Adaptation of Bacillus subtilis cells to Archean-like UV climate: relevant hints of microbial evolution to remarkably increased radiation resistance. *Astrobiology* 10, 605–615.

Weiss, M. C., Sousa, F. L., Mrnjavac, N., Neukirchen, S., Roettger, M., Nelson-Sathi, S., et al. (2016). The physiology and habitat of the last universal common ancestor. *Nat. Microbiol.* 1, 1–8. doi: 10.1038/NMICROBIOL.2016.116

Williams, G. E. (2000). Geological constraints on the Precambrian history of Earth's rotation and the Moon's orbit. *Rev. Geophys.* 38, 37–59. doi: 10.1029/1999RG900016

Wu, H., Gao, K., Villafañe, V. E., Watanabe, T., and Helbling, E. W. (2005). Effects of solar UV radiation on morphology and photosynthesis of filamentous cyanobacterium Arthrospira platensis. *Appl. Environ. Microbiol.* 71, 5004–5013. doi: 10.1128/AEM.71.9.5004-5013.2005

Xiao, X., and Yu, Z. (2014). Life in extreme environments: approaches to study life-environment co-evolutionary strategies. *Sci. China Earth Sci.* 57, 869–877. doi: 10.1007/s11430-014-4858-8

Zaharescu, D. G., Burghelea, C. I., Dontsova, K., Presler, J. K., Hunt, E. A., Domanik, K. J., et al. (2019). Ecosystem-bedrock interaction changes nutrient compartmentalization during early oxidative weathering. *Sci. Rep.* 9, 1–16. doi: 10.1038/s41598-019-51274-x

Zahnle, K., and Walker, J. C. (1987). A constant daylength during the Precambrian era? *Precambrian Res.* 37, 95–105. doi: 10.1016/0301-9268(87)90073-8

Zhao, M., Reinhard, C. T., and Planavsky, N. (2018). Terrestrial methane fluxes and Proterozoic climate. *Geology* 46, 139–142. doi: 10.1130/G39502.1

Zhu, S., Zhu, M., Knoll, A. H., Yin, Z., Zhao, F., Sun, S., et al. (2016). Decimetre-scale multicellular eukaryotes from the 1.56-billion-year-old Gaoyuzhuang formation in North China. *Nat. Commun.* 7, 1–8. doi: 10.1038/ncomms11500

frontiers | Frontiers in Microbiology

TYPE Original Research
PUBLISHED 27 January 2023
DOI 10.3389/fmicb.2023.869907

OPEN ACCESS

EDITED BY
Andreas Teske,
The University of North Carolina at Chapel Hill, United States

REVIEWED BY
Grégoire Michoud,
Swiss Federal Institute of Technology Lausanne, Switzerland
Danny Ionescu,
Leibniz-Institute of Freshwater Ecology and Inland Fisheries (IGB), Germany

*CORRESPONDENCE
Zeina Bourhane
✉ zeina.bourhane@univ-pau.fr
Robert Duran
✉ robert.duran@univ-pau.fr

SPECIALTY SECTION
This article was submitted to Extreme Microbiology, a section of the journal Frontiers in Microbiology

RECEIVED 05 February 2022
ACCEPTED 03 January 2023
PUBLISHED 27 January 2023

CITATION
Bourhane Z, Cagnon C, Castañeda C, Rodríguez-Ochoa R, Álvaro-Fuentes J, Cravo-Laureau C and Duran R (2023) Vertical organization of microbial communities in Salineta hypersaline wetland, Spain. *Front. Microbiol.* 14:869907. doi: 10.3389/fmicb.2023.869907

Vertical organization of microbial communities in Salineta hypersaline wetland, Spain

Zeina Bourhane[1]*, Christine Cagnon[1], Carmen Castañeda[2], Rafael Rodríguez-Ochoa[3], Jorge Álvaro-Fuentes[2], Cristiana Cravo-Laureau[1] and Robert Duran[1]*

[1]Université de Pau et des Pays de l'Adour, E2S UPPA, CNRS, IPREM, Pau, France, [2]Estación Experimental de Aula Dei, EEAD-CSIC, Zaragoza, Spain, [3]Departamento de Medio Ambiente y Ciencias del Suelo, Universidad de Lleida, Lleida, Spain

Microbial communities inhabiting hypersaline wetlands, well adapted to the environmental fluctuations due to flooding and desiccation events, play a key role in the biogeochemical cycles, ensuring ecosystem service. To better understand the ecosystem functioning, we studied soil microbial communities of Salineta wetland (NE Spain) in dry and wet seasons in three different landscape stations representing situations characteristic of ephemeral saline lakes: S1 soil usually submerged, S2 soil intermittently flooded, and S3 soil with halophytes. Microbial community composition was determined according to different redox layers by 16S rRNA gene barcoding. We observed reversed redox gradient, negative at the surface and positive in depth, which was identified by PERMANOVA as the main factor explaining microbial distribution. The Pseudomonadota, Gemmatimonadota, Bacteroidota, Desulfobacterota, and Halobacteriota phyla were dominant in all stations. Linear discriminant analysis effect size (LEfSe) revealed that the upper soil surface layer was characterized by the predominance of operational taxonomic units (OTUs) affiliated to strictly or facultative anaerobic halophilic bacteria and archaea while the subsurface soil layer was dominated by an OTU affiliated to *Roseibaca*, an aerobic alkali-tolerant bacterium. In addition, the potential functional capabilities, inferred by PICRUSt2 analysis, involved in carbon, nitrogen, and sulfur cycles were similar in all samples, irrespective of the redox stratification, suggesting functional redundancy. Our findings show microbial community changes according to water flooding conditions, which represent useful information for biomonitoring and management of these wetlands whose extreme aridity and salinity conditions are exposed to irreversible changes due to human activities.

KEYWORDS

ephemeral hypersaline lakes, hypersaline ecosystem, functional redundancy, reverse redox gradient, archaeal biomarkers

Introduction

Saline lakes are numerous and geographically widespread in inland ecosystems, particularly in arid and semi-arid areas (Williams, 1996, 2002). Endorheic basins cover approximately one-tenth of the Earth's surface (Casamayor et al., 2013). They are rare in Europe (Casamayor et al., 2013), playing crucial ecosystem services. Particularly, as they are important habitats

for migrating birds, they are included in biodiversity-protected areas under the RAMSAR convention (Ramsar Convention Secretariat, 2010). However, they are threatened by human activities and anthropogenic freshwater inputs (Williams, 2002). Saline lakes are very dynamic environments, with soil and water salinity and temperature fluctuations and thus highly responsive to climate changes (Menéndez-Serra et al., 2021). Among inland saline lakes, athalassohaline lakes, known for the lack of connections to marine environments, are characterized by a high content of sulfate, carbonate, and ionic composition different from that observed in seawater (Demergasso et al., 2008). The ecology of athalassohaline lakes is influenced by a high content of "chaotropic" ions such as Ca^{2+} and Mg^{2+} (Oren, 2015), having major effects on the abundance and growth of microbes (Gasol et al., 2004; Oren, 2013). Studies on microbial communities in several athalassohaline lakes revealed the presence of previously unidentified microorganisms, adapted to salinity fluctuations (Jiang et al., 2006; Demergasso et al., 2008; Menéndez-Serra et al., 2021). As athalassohaline lakes vary in ionic composition according to their location, they exhibit distinct microbial communities more divergent than that observed for thalassohaline environments (Pagaling et al., 2009; McGenity and Oren, 2012), representing genomic islands with limited microbial exchange and own evolution (Pagaling et al., 2009). Nevertheless, athalassohaline ecosystems represent specific habitats for halophilic prokaryotes and eukaryotes, most of them being also polyextremophile able to survive under extreme conditions of salinity, pH, and UV radiation (McGenity and Oren, 2012). The halophilic microorganisms include various aerobes and anaerobes covering diverse functional groups, such as heterotrophs, oxygenic and anoxygenic phototrophs, lithotrophs, methanogens, and methylotrophs, fermenters, sulfate reducers, and sulfide oxidizers (Sorokin et al., 2011; Lanzén et al., 2013).

The Salineta at "Saladas de Bujaraloz-Sástago" (Spain), located in the south of Monegros, one of the most arid areas in Europe, is a lake of an endorheic complex constituted by a large set of inland ephemeral saline lakes subjected to temporary flooding according to seasons (Castañeda and Herrero, 2005; Casamayor et al., 2013; Menéndez-Serra et al., 2021). Similar microbial communities have been described among different saline lakes, constituted by microorganisms with a competitive advantage, characteristic of these dynamic ephemeral lakes (Casamayor et al., 2013; Menéndez-Serra et al., 2019, 2021). The saline lakes are vulnerable to diffuse pollution from agricultural activities surrounding fields and pig farming (Castañeda et al., 2015). The transfer of pollutants is enhanced by the loamy-sandy soil texture and the abundance of gypsum (Castañeda et al., 2015). Chronic accumulation of pollutants is known to contribute to the disruption of microbial community diversity and biogeochemical cycle functions (Bordenave et al., 2004; Duran and Cravo-Laureau, 2016). It is thus of paramount importance to obtain a characterization of the Salineta wetland prior to the intensification of the farming activities that will serve as a baseline for the management of this RAMSAR-protected area.

Among these saline lakes, the Salineta wetland, surrounded by newly irrigated areas, is characterized by three different landscapes corresponding to water flooding conditions: usually submerged soil, intermittently flooded soil, and soil being vegetated with halophytes. The Salineta hydric regime, depending on the rains and the shallow water table dynamics (Castañeda and García-Vera, 2008), contributes to the development of contrasting soil surface microenvironments (Dominguez-Beisiegel et al., 2011), leading to distinct soil redox conditions. We hypothesized that different microbial communities inhabit these three different water-related soil environments corresponding to microbial communities adapted to the different soil and water characteristics of ephemeral saline lakes. To test our hypothesis, we characterized the microbial community composition and inferred the metabolic functional profiles involved in carbon, nitrogen, and sulfur cycles in the wetland soil at different depths according to the soil layering observed in both dry (summer) and wet (winter) periods.

Materials and methods

Site description

The Salineta at "Saladas de Bujaraloz-Sástago" (NE, Spain) is located in Monegros, one of the most arid regions in Europe, with a mean annual precipitation of 350 mm and an annual reference evapotranspiration (ET_0) of 1,225 mm (Castañeda and Herrero, 2005). It is included in the RAMSAR convention list for bird protection and in the Natura, 2000 network. The Monegros endorheic complex contains more than a hundred seasonal inland saline lakes whose salinity is linked to climatic aridity and geologic materials. Salineta, with 23 ha, is one of the northernmost saline lakes of the complex and has the greatest presence of water (Castañeda and García-Vera, 2008; **Figure 1**). The groundwater discharges at the lakebed coming from two long-standing saline aquifers (salinity 294 ± 34 g/l) whose high salinity is due to the chemical and lithological characteristics of the sediments. Wetland soils are very saline and rich in gypsum and carbonates (Menéndez-Serra et al., 2019).

Sampling

Three different soil stations were selected in the Salineta wetland based on the habitat maps (Conesa et al., 2011). S1, S2, and S3 corresponded to usually submerged soil, intermittently flooded soil, and soil covered with halophytes (**Figure 1**). These stations were considered representative of water-related soil conditions in these ephemeral saline lakes. In each sampling station, triplicate cores of soil surface horizons up to 30–40 cm were sampled by an auger (7 cm in diameter). For each site, soil layers were identified according to their color following the Munsell color chart, which relies on different soil chemical and physical characteristics (Kalev and Toor, 2018). Soil samples for molecular and chemical analysis were taken within the three soil layers. Two sampling campaigns, in winter (March 2019, wet period) and summer (September 2019, dry period), were performed. For station S1, three different soil layers were identified by their color (L1, greenish black 0–5 cm; L2, olive gray 5–18 cm; L3, yellowish brown 18–25 cm), while only two layers (L1 and L2) for stations S2 and S3 were distinguished (**Supplementary Figure 1**). Similar vertical layering was collected in both seasons. Thus, 42 samples ([3 stations × layers (3 for S1, 2 for S2 and S3) × 2 seasons] × 3 replicates) were obtained. For each layer, soil samples were collected with a sterile spatula. After homogenization, the soil samples were distributed in 2 ml sterile cryotubes frozen in liquid nitrogen and were conserved at −80°C for microbial analysis. For physical–chemical analyses, samples were collected in 25-ml tubes and stored at −20°C until use.

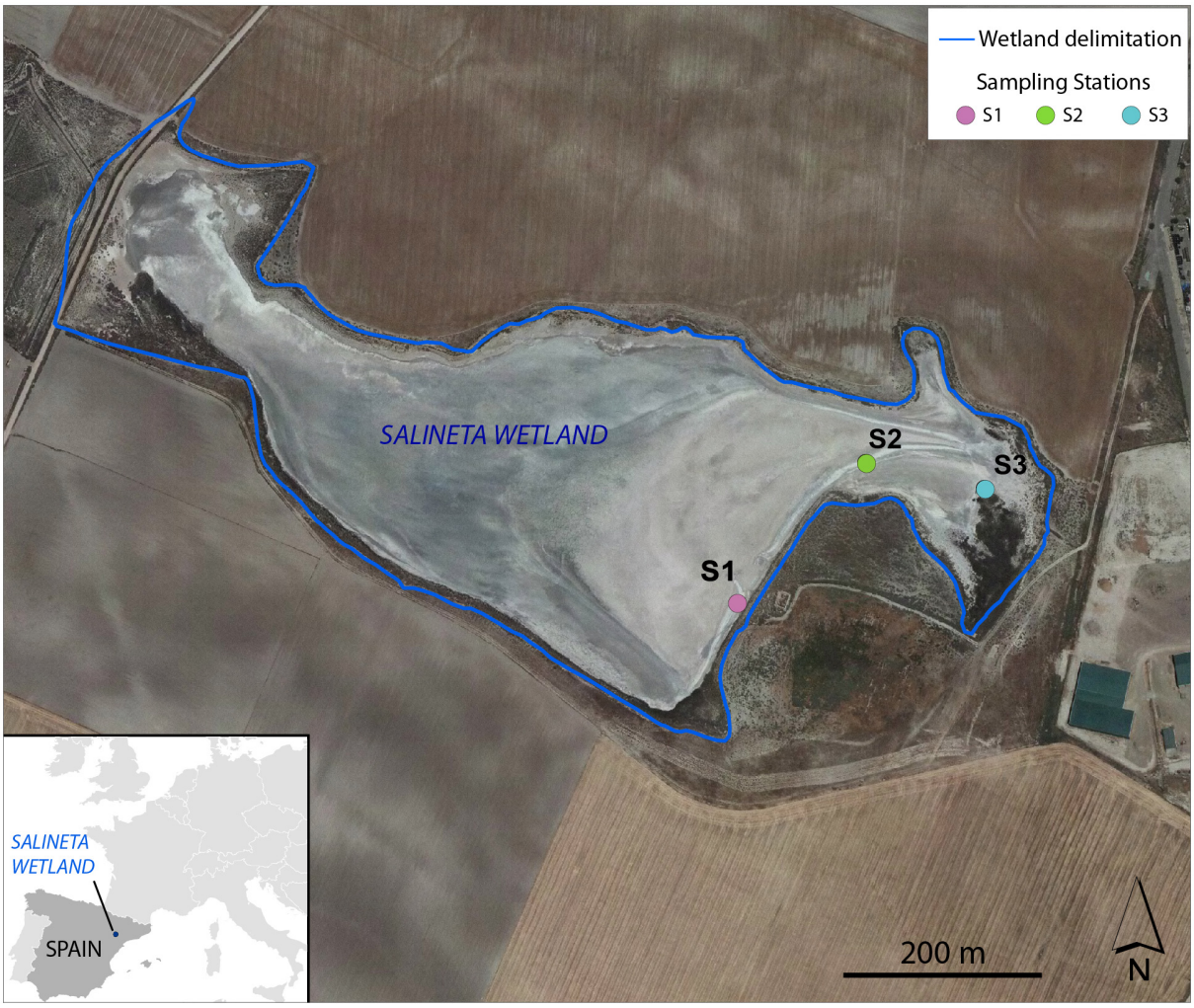

FIGURE 1
Location of the sampling stations (S1, S2, and S3) at Salineta wetland in the orthophotograph of PNOA 2015 (National Geographic Institute of Spain).

Physical–Chemical analysis

Gas emissions (CO_2, N_2O, and CH_4) were measured *in situ* using closed chambers placed on top of the soil and gas chromatography (Agilent 7890B) equipped with a flame ionization detector (FID) coupled to a methanizer for CO_2 determination (Franco-Luesma et al., 2020). For station S3, in order to limit the effect of plants, the chambers were placed in a part of the soil surrounded by halophytes but without plants inside.

Physical–chemical parameters [temperature, pH, salinity, electrical conductivity (EC), redox potential (ORP), and dissolved oxygen] were determined in the field with a multiparameter system (WTW Multi-197i) (Ben Salem et al., 2016). Calcium carbonate equivalent (CCE), gypsum content, organic matter (OM), particle-size distribution, and major ions (ammonium, nitrite, nitrate, fluoride, chloride, bromide, sulfate, bicarbonate, sodium, potassium, calcium, and magnesium) were determined (Castañeda et al., 2017). Briefly, the Bernard calcimeter method (reaction with HCl) was used to determine the CCE, gypsum content was determined by thermogravimetry, and OM by spectrophotometry after chromic acid digestion using a UV/V UNICAM 8625 spectrophotometer. Particle-size distribution was assessed by laser diffraction (Malvern MASTERSIZER 2000). Ion chromatography Metrohm 861 (Metrohm AG, Herisau, Suisse) was used to determine the major ions.

DNA extraction, PCR amplification, and sequencing

Microbial communities were extracted by suspending 250 mg of ground soil (in liquid nitrogen) in 1.2 ml of distilled water. After mixing for 45 s at 6,000 rpm using Precellys Evolution homogenizer (Bertin technology, Montigny-le-Bretonneux, France) and centrifugation for 30 s at 10,000 × *g* the supernatant was recovered. This operation was performed six times. A total of 7.2 ml for each sample was filtered using 0.2-μm MicroFunnel (PALL Corporation, Portsmouth, United Kingdom). DNA was extracted from the cut filters using PowerSoil DNA Kit (MoBio Laboratories Inc., Courtaboeuf, France) following the manufacturer's instructions with few modifications (Giloteaux et al., 2013). The region V4–V5 of 16S rRNA was amplified using prokaryotic universal primers U515-532-GTGYCAGCMGCCGCGGTA and U909-928-CCCCGYCAATTCMTTT (Wang and Qian, 2009), which match

80% of the Bacteria domain and the same for Archaea domain (tested with).[1] The primers include the linkers for barcoding provided by the GenoToul platform. The amplifications were performed in triplicates (Bourhane et al., 2022). Briefly, the amplifications were performed in a total volume of 25 µl, using 12.5 µl of AmpliTaq Gold 360 Master Mix, 0.5 µl of each forward and reverse primers (20 µM), and 5 µl of the DNA extract, as follows: 95°C for 10 min, 30 cycles of 95°C for 30 s, 60°C for 30 s, 72°C for 40 s, and a final extension step at 72°C for 10 min. For each sample, the three PCR products were pooled and sequenced by Illumina-MiSeq (paired-end 2 × 250 bp) at the GenoToul platform (Toulouse, France). The complete protocol is available at https://sites.google.com/site/olivierzembwebsite/16s-sequencing.

Sequence data analysis

Sequence data analysis was performed (Lanzén et al., 2021). Briefly, the sequences were trimmed as follows: reads were overlapped using *vsearch* version 2.7.1 (Rognes et al., 2016), then primers were removed using *cutadapt* version 1.15 (Martin, 2011). The remaining sequences were de-replicated and sorted by abundance using *vsearch*. Then, they were used to cluster the reads into operational taxonomic units (OTUs) with a minimum linkage of one nucleotide using SWARM version 2.2.1 (Mahé et al., 2015). Abundances of unique sequences across samples were retained and used to build an OTU contingency table based on SWARM version 2.2.1 output using SLIM (Dufresne et al., 2019). Singleton OTUs were discarded and then applied reference-based and *de novo* UCHIME chimera filtering as implemented in *vsearch* (Lanzén et al., 2012), with SilvaMod version 138 as the reference database (Lanzén et al., 2021).[2] Then, we applied LULU post-clustering curation with a minimum 97% similarity cutoff point (Frøslev et al., 2017) to correct the remaining sequencing artifacts and merge OTUs with intra-specific or intra-genomic differences. Final SWARM OTUs were aligned to SilvaMod version 138 using *blastn* version 2.6.0 + and taxonomically classified using CREST version 3.1.0 (Lanzén et al., 2021). The data set was deposited in the NCBI Sequence Read Archive (SRA) database under accession number ID PRJNA763109.

Predicted cross-contaminant reads were removed using a procedure analogous to UNCROSS (Edgar, 2016) by setting sample-specific OTU abundances to zero when encountered at an abundance below 2% of the average OTU abundance across samples. In addition, in order to compensate for the possible bias introduced by uneven sequencing depths, OTUs present with a maximum abundance across samples below 0.01% were discarded (Elbrecht et al., 2018).

The functional predictions of microbial communities involved in the main biogeochemical cycles were determined using Phylogenetic Investigation of Communities by Reconstruction of Unobserved States, version 2 (PICRUSt2) from the 16S rRNA gene sequences (Douglas et al., 2020). The recommended maximum NSTI cutoff point of 2 was implemented by default in PICRUSt2 to prevent unconsidered interpretation of overly speculative inferences (Douglas et al., 2020), which excluded 2.2% of OTUs (211 out of 9,557). These removed OTUs represented 1.1% of the relative abundance of the microbial community. The Kyoto Encyclopedia of Genes and Genomes (KEGG) databases were used for functional prediction annotation and metabolic pathways analysis. The weighted nearest sequenced taxon index (NSTI) was calculated to assess the accuracy of PICRUSt analysis (Langille et al., 2013). The KOs associated with nitrogen, sulfur, and carbon metabolisms were identified.

Statistical analysis

Statistical analyses were run in R environments[3] using vegan packages (Oksanen et al., 2019). Alpha diversity indices (including species richness, Shannon—Wiener, and evenness) of microbial community were calculated for each sample based on the rarefied OTU table using the alpha function of the vegan package in R.

Multiple comparison of gas flux was computed by applying the least significant difference (LSD) test within the "agricolae" package using the "LSD.test" function for multiple comparisons after the ANOVA test. Permutational multivariate analysis of variance (Permanova) was performed to estimate the effect of physical–chemical parameters on the microbial communities (999 permutations). Microbial community similarity was performed by non-metric multidimensional scaling (NMDS), based on Bray–Curtis index, correlating communities with physical–chemical parameters. The significant environmental variables were fitted to the NMDS as vectors with the envfit function on the R statistics software.

Linear discriminant analysis effect size (LEfSe) (Segata et al., 2011) was performed to determine significant seasonal and spatiotemporal OTUs biomarkers among the most abundant genera. Briefly, the non-parametric Kruskal–Wallis (KW) sum-rank test was first applied to detect significant differential taxa abundance ($p < 0.05$). Then, the biological consistency was investigated by performing a Wilcoxon pairwise test ($p < 0.05$). The linear discriminant analysis (LDA) threshold was set up to 2 and 1,000 bootstrap interactions. The chordogram profile, performed using the chordDiagram function, showed the distribution of functions in each sample. Ternary plot performed using the PAST software presented the distribution of functions according to the layer depths. Principal component analysis (PCA) showed the distribution of samples and the functional genes correlating microbial community with the environmental factors.

Results

Physical–Chemical characterization

Microbial activities were estimated by the production of CO_2, N_2O, and CH_4 in soil from each station (**Supplementary Table 1**). The main difference was observed for CO_2 fluxes, with station S3 showing higher CO_2 fluxes (ANOVA, $p < 0.01$) in both seasons. The three stations showed similar CH_4 fluxes in summer, but they exhibited different CH_4 fluxes in winter (ANOVA, $p < 0.1$) (**Supplementary Table 1**). Station S3 differs from stations S1 and S2 in physical–chemical parameters (**Supplementary Table 2** and **Supplementary Figure 2**). Such a difference was expected

1 https://www.arb-silva.de/search/testprime

2 https://github.com/lanzen/CREST

3 http://www.rproject.org

since the sampling stations represent a gradient of surface water persistence in the wetland. The soil is usually submerged at S1, intermittently flooded at S2, and covered by halophytes at S3. Furthermore, considering all physical–chemical parameters, significantly different characteristics were also observed according to layers (two-way ANOVA, $p < 0.005$), except at S1 with layer L3 having similar physical–chemical characteristics as layer L2 (**Supplementary Table 2**). The NMDS showed that layer L1 is linked with higher ion concentrations and low (ORP, -155 ± 193 mV), while L2 has higher redox (ORP, 88 ± 118 mV) and soil texture (silt, sand, clay; **Supplementary Figure 2**). The differences between L1 and L2 were further supported by two-way ANOVA (**Supplementary Table 2**). Noteworthy, the layers showed distinct ORP with seasonal variability (**Supplementary Table 2**), probably related to the difference in soil temperature observed between winter (9°C) and summer (28°C). However, despite the observed differences, the general trend was that the negative ORP values of the soil surface (L1) shifted to positive ORP values in depth (L2 first and then L3).

Microbial community composition

To determine the microbial community organization, the microbial composition was characterized by 16S rRNA gene barcoding. A total of 483,501 reads were obtained from 42 samples. The rarefaction curves showed a plateau (**Supplementary Figure 3**), indicating that the sequencing effort was sufficient to assess the prokaryotic diversity, except for the sample S.S1.L2.R3 that has been removed for the analysis because the number of sequences obtained is low. After trimming, the retained 287,781 sequences were distributed within 1,158 OTUs (**Table 1**). The microbial community was composed of 74% of Bacteria (21 main phyla) and 26% of Archaea (5 main phyla) (**Figure 2**). The microbial richness and diversity indices were significantly different between the samples (ANOVA, $p < 0.05$, **Table 1**), showing that the microbial communities were affected by the conditions prevailing in the stations according to layers and seasons. In all stations, Pseudomonadota (15–33%), Gemmatimonadota (6–16%), Bacteroidota (6–13%), and Desulfobacterota (3–9%) phyla dominated the Bacteria, while Halobacteriota (18–31%) phylum dominated the Archaea (**Figure 2**), representing 93% of the Archaea. Although the samples showed similar patterns, it is worth noting that some differences can be observed. Especially, Bacteroidota were more abundant in layer L1 of stations S2 and S3 in winter, while Halobacteriota were more abundant in layer L2 of stations S2 and S3 in summer (**Figure 2**). In addition, the relative abundance of Actinobacteriota and Deinococcota decreased with depth and season. To further characterize the differences, multivariate analyses were conducted.

Spatiotemporal microbial community distribution

The comparison of microbial communities by NMDS separated the layers L1, L2, and L3 in clusters and then according to the stations (S1, S2, and S3) and seasons (summer and winter) (**Figure 3A**), which was consistent with PERMANOVA indicating that the variation between samples was explained mainly by layers ($R^2 = 0.2, p < 0.001$), stations, and seasons (**Figure 3B**). It is likely that the microbial community organization was driven by environmental factors, with L1 being controlled by ion concentrations, OM, and total nitrogen, whereas L2 was mainly influenced by redox (**Figure 3A**).

Linear discriminant analysis effect size revealed OTUs found significantly more abundant according to layers (**Figure 4A**), stations (**Figure 4B**), and seasons (**Figure 4C**), which serve as biomarkers (Mehrshad et al., 2013). Layer L1 was characterized by seven OTU biomarkers, which are usually detected in hypersaline ecosystems, some of them being detected in salt-saturated ecosystems with pH around 8, conditions prevailing at Salineta wetland. These OTU biomarkers include five bacterial OTUs affiliated to the Anaerolineaceae family and the *Salinarimonas*, *Rhodopirellula*, *Desulfonatronobacter*, and *Aliifodinibius* genera; and two archaeal OTUs affiliated to the *Halorubellus* genus and *Halodesulfurarchaeum formicicum* (**Figure 4A**). Three OTUs related to *Coxiella* and *Anaerophaga* genera and the Balneolaceae family were the biomarkers for layer L2.

Regarding station biomarkers, only two OTUs were identified for station S3 that were affiliated with the archaeal *Haloplanus* and *Halonotius* genera (**Figure 4B**). These biomarkers further support the specificity of station S3 that differs from stations S1 and S2 in physical–chemical parameters (**Supplementary Table 2** and **Supplementary Figure 2**), being covered by halophytes. Seasonal biomarkers were also identified (**Figure 4C**), three for winter (*Halanaerobium*, Coxiellaceae genus 1, and *Candidatus Halobonum*) and two for summer (*Halofilum ochraceum* and *Desulfovibrio*), supporting seasonal fluctuation, probably related to the salinity variations according to wet and dry periods.

Functional distribution

To estimate whether the functional capabilities involved in the main biogeochemical cycles (nitrogen, sulfur, and carbon) are affected by taxonomic composition variability, functional profiles were determined by PICRUSt2, with an NSTI score of 0.32 showing the accuracy of the prediction analysis. Although predictive, such an approach is a useful tool to obtain an overview of specific microbial process dynamics (Menéndez-Serra et al., 2019). Focusing on nitrogen, sulfur, and carbon metabolisms, the functional profiles were similar in all samples (**Figure 5A** and **Supplementary Table 3**). Considering the differences observed in the microbial community (**Figure 3A**), this observation indicated that the same metabolic functions are ensured by different microbial communities. Except for nitrification, the metabolic functions were equally distributed according to layers (**Figure 5B**), characterized by different redox (ANOVA, $p < 0.05$) suggesting functional redundancy. However, the PCA based on functional groups (**Figure 5C**) showed a dispersion of the microbial communities, confirming the distribution and differences observed with the phylogenetic analysis (**Figures 3A, B**). The distribution is explained by the presence of different KOs for each functional group (**Figure 5D**), confirming the functional redundancy.

Metabolic function associations

The correlation analysis between the studied functional groups (**Figure 6A**) showed a significant ($p < 0.05$) and positive

TABLE 1 Alpha diversity indices of prokaryotic community from the study sites located at the stations S1, S2, and S3 in Salineta wetland in winter (W) and summer (S) in different layers (L1, L2, and L3).

Indices		Stations						
		S1			S2		S3	
		L1	L2	L3	L1	L2	L1	L2
Reads	W	39126 ± 6540^{a}	40536 ± 11948^{a}	43489 ± 9118^{a}	45297 ± 18095^{a}	31602 ± 5187^{a}	39515 ± 2538^{a}	36334 ± 8543^{a}
	S	34672 ± 3461^{a}	25392 ± 19798^{a}	19286 ± 2748^{a}	29249 ± 5697^{a}	28812 ± 8666^{a}	38386 ± 8977^{a}	31805 ± 10261^{a}
Trimmed sequences	W	211867 ± 687^{a}	26174 ± 6874^{a}	27235 ± 4398^{a}	22464 ± 2365^{a}	20519 ± 3214^{a}	22401 ± 2295^{a}	22319 ± 4863^{a}
	S	21206 ± 3915^{a}	22380 ± 275^{a}	12253 ± 1691^{a}	17889 ± 2204^{a}	17801 ± 5638^{a}	22831 ± 6381^{a}	19911 ± 6611^{a}
Species richness (R)	W	1635 ± 58^{ab}	1004 ± 229^{c}	1106 ± 59^{c}	1919 ± 69^{a}	1337 ± 158^{bc}	1878 ± 71^{a}	1308 ± 323^{bc}
	S	1253 ± 186^{ab}	1032 ± 98^{abc}	579 ± 44^{b}	855 ± 232^{b}	664 ± 135^{b}	1706 ± 283^{a}	848 ± 240^{b}
Simpson *(1-D)*	W	0.98 ± 0.004^{abc}	0.97 ± 0.002^{c}	0.98 ± 0.004^{bc}	0.98 ± 0.002^{a}	0.95 ± 0.057^{abc}	0.99 ± 0.003^{ab}	0.98 ± 0.014^{ab}
	S	0.98 ± 0.004^{a}	0.97 ± 0.002^{a}	0.98 ± 0.0005^{a}	0.99 ± 0.0009^{a}	0.99 ± 0.002^{a}	0.99 ± 0.0008^{a}	0.99 ± 0.001^{a}
Shannon *(H)*	W	5.39 ± 0.11^{bc}	4.77 ± 0.38^{d}	4.96 ± 0.01^{cd}	6 ± 0.09^{a}	5.68 ± 0.19^{ab}	5.91 ± 0.11^{ab}	5.81 ± 0.06^{ab}
	S	5.24 ± 0.34^{ab}	4.98 ± 0.09^{ab}	5.25 ± 0.23^{ab}	5.21 ± 0.29^{ab}	4.63 ± 0.61^{b}	5.71 ± 0.06^{a}	5.14 ± 0.27^{ab}
Pielou Evenness *(E)*	W	0.73 ± 0.011^{bc}	0.7 ± 0.03^{c}	0.7 ± 0.0069^{c}	0.8 ± 0.01^{a}	0.8 ± 0.01^{ab}	0.78 ± 0.01^{ab}	0.81 ± 0.03^{a}
	S	0.73 ± 0.032^{a}	0.72 ± 0.003^{a}	0.82 ± 0.03^{a}	0.77 ± 0.02^{a}	0.71 ± 0.11^{a}	0.77 ± 0.02^{a}	0.77 ± 0.02^{a}

Mean ± SD are presented ($n = 3$; except for S.S1.L2, $n = 2$).
The same small letter indicates no significant difference of means compared by ANOVA, $p < 0.05$.

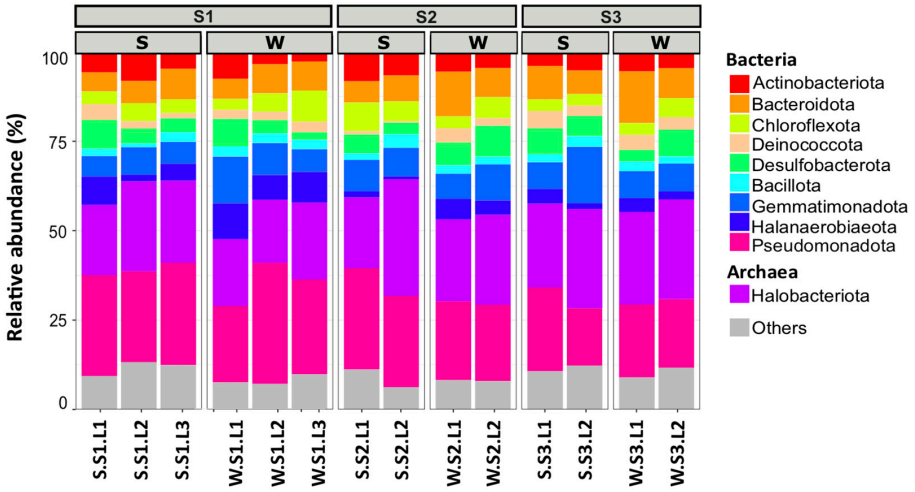

FIGURE 2
Microbial community composition of the 10 most abundant phyla in different layers (L1, L2, L3 or L1, L2) from each station (S1, S2, S3) at summer (S, dry period) and winter (W, wet period). Each bar plots represents the mean of three biological replicates (except for S.S1.L2, $n = 2$). Others represent phyla with relative abundance <5%.

correlation between the functions involved in the sulfur cycle, with the functions related to the nitrogen cycle including denitrification, dissimilatory nitrate reduction to ammonium (DNRA), and complete ammonium oxidation (COMAMMOX), but not significantly correlated with nitrogen fixation and nitrification. Noteworthy, the functions involved in the sulfur cycle were positively correlated with the functions of the carbon cycle (**Figure 6A**). When the methane metabolism functions (methanogenesis and methanotrophy) were abundant, the sulfate reduction functions were also abundant. Particularly, the layers showing the lowest redox at the S1 station exhibited abundant methane metabolism and sulfate reduction functions, especially layer L1 at both seasons (**Figure 6B**). In addition, it is important to note that these functions were more abundant during the wet season (winter), showing the effect of flooding on microbial functions.

Discussion

The ephemeral saline lake of Salineta wetland is driven by the hydric regime (Castañeda and García-Vera, 2008) that results in three different landscapes (Dominguez-Beisiegel et al., 2011) observable according to the water flooding conditions: usually submerged soil (station S1), intermittently flooded soil (station S2), and soil being vegetated with halophytes (station S3). The microbial activities, estimated by gas fluxes (CO_2, N_2O, and CH_4), were different in the three stations, being particularly observable in winter for methane

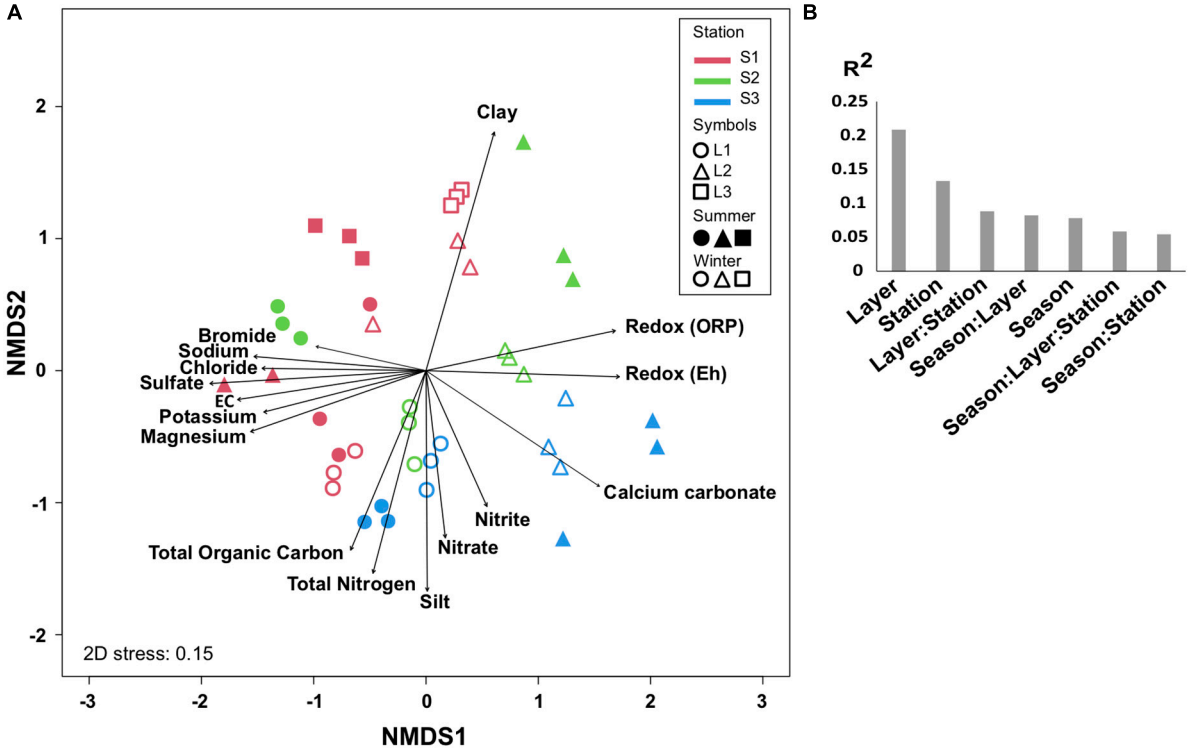

FIGURE 3
Comparison of microbial communities. **(A)** Non-metric multidimensional scale (NMDS) at OTU level in different layers (L1, L2, L3 or L1, L2) from each station (S1, S2, S3) at summer (S, dry period) and winter (W, wet period). The significant environmental variables are represented by vectors. **(B)** PERMANOVA partitioning (R^2 value, $p < 0.001$) according to layers, stations, seasons, and their interactions. Three biological replicates (except for S.S1.L2, $n = 2$) were analyzed per sample.

fluxes. It has been shown that the production of greenhouse gases is affected by flooding and variations in salinity (Ringeval et al., 2010; Kroeger et al., 2017), which relies on the control of microbial activities by the dynamics of redox gradients (Reddy and DeLaune, 2008), suggesting that the flooding conditions affect the microbial activities in Salineta wetland. Consistently, we observed physical–chemical differences between the three landscapes, particularly according to ORP, but the more stricky observation was the stratification of the soil exhibiting significantly different physical–chemical characteristics according to layers. Especially, ORP negative values were observed at the soil surface shifting to positive ORP values with depth, despite the seasonal variations. Such observation constitutes a distinctive feature of the Salineta wetland in comparison to other subaqueous ecosystems where the ORP decreases with depth, such as in marine sediments (Kristensen, 2000). The seasonal presence of different types of salt crusts, the physical and chemical characteristics of soil and water, and the hydric regime of the Salineta wetland (Castañeda and García-Vera, 2008) as well as the OM content (Schultz, 2000) may explain the observed reversed redox gradient in the soil profile, which affects the microbial community assemblages. Future studies will benefit from the fine-scale determination of oxygen and sulfide micro-profiles to better characterize redox gradients in the soil.

The microbial community characterization by 16S rRNA gene meta-barcoding analysis revealed that above 26% of the sequences belonged to Archaea. Although the inherent biases of the sequencing approach for the quantification, it is important to note that Archaea have been found in similar proportion in hypersaline ecosystems, such as the Karak Salt Mine, Pakistan (Cycil et al., 2020), and ocean waters (Karner et al., 2001). Archaea often make the main component of the microbial community in hypersaline systems (Andrei et al., 2012). They have also been found abundant in many extreme ecosystems (Kan et al., 2006; Bruneel et al., 2008) and hydrocarbon-polluted sediments (Stauffert et al., 2014) where they play an important role in biogeochemical cycles influencing the emission of greenhouse gases (Offre et al., 2013). It has been demonstrated that the Archaea proportion reflects the influence of the differences in environmental parameters (Wang et al., 2020). The alpha diversity indices were significantly different between the samples (ANOVA, $p < 0.05$, **Table 1**), indicating that the microbial communities were affected by the conditions prevailing in the stations according to layers and seasons. The dominant Bacteria (Pseudomonadota, Gemmatimonadota, Bacteroidota, and Desulfobacterota) and Archaea (Halobacteriota) phyla observed in Salineta wetland include genera usually found dominant in sediment from hypersaline and saline lakes (Dong et al., 2006; Menéndez-Serra et al., 2019), microbial mats (Kirk Harris et al., 2013; Bolhuis et al., 2014; Mazière et al., 2021), and salt mines (Cycil et al., 2020).

The Pseudomonadota phylum was dominated by *Thiohalorhabdus* (4%), Acidithiobacillaceae group RCP1-48 (4%), and *Wenzhouxiangella* (2%) genera (representing, respectively, 8, 8, and 4% of the phylum) that have been found in hypersaline ecosystems (Sorokin et al., 2008; Caton and Schneegurt, 2012; Zhang et al., 2020). Members of the *Thiohalorhabdus* and *Acidithiobacillaceae* group RCP1-48 are known to play an important role in sulfur and iron compounds oxidation (Sorokin et al., 2008; Arce-Rodríguez et al., 2020), while *Wenzhouxiangella*, described

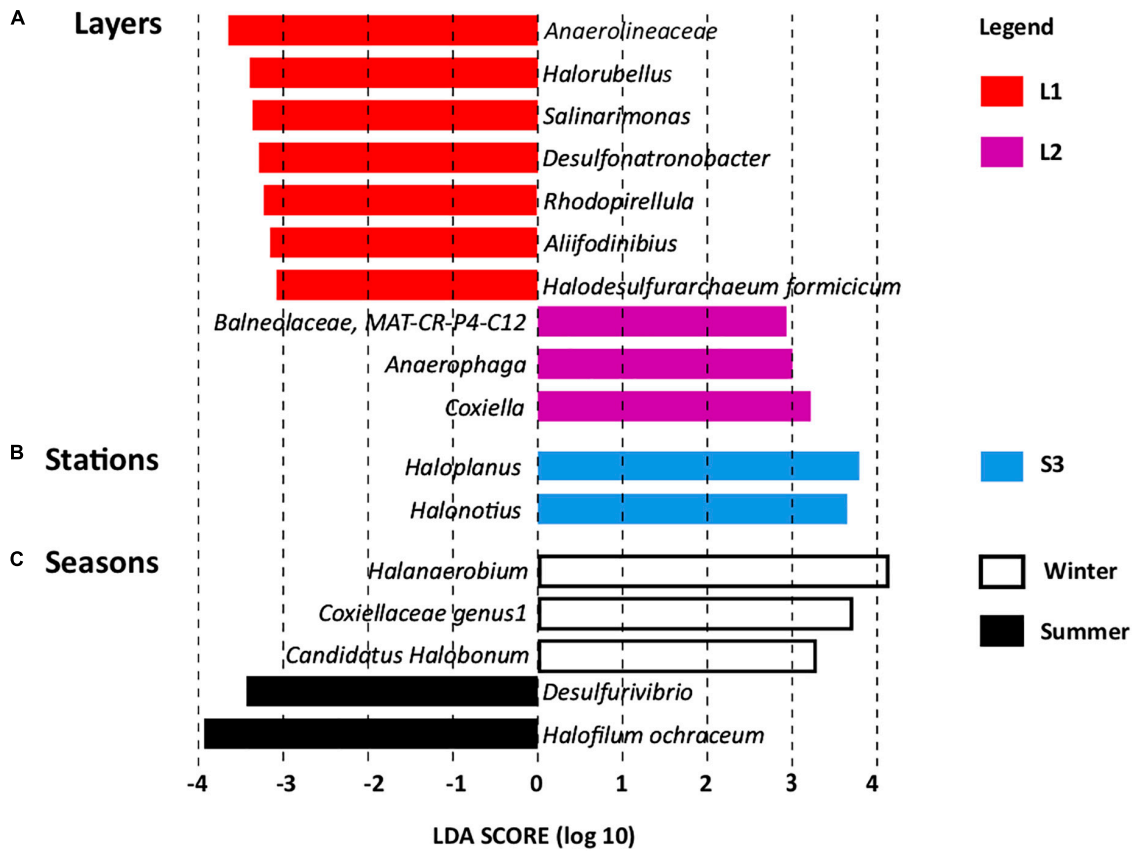

FIGURE 4
Linear discriminant analysis effect size (LEfSe) identifying microbial genera specifically more abundant according to **(A)** layers (L1 and L2), **(B)** stations (S1, S2, and S3), and **(C)** seasons (summer and winter, dry and wet periods, respectively).

as a predator of Gram-positive bacteria cells, exhibit proteolytic activity (Sorokin et al., 2020). The aerobic anoxygenic phototroph *Gemmatimonas* genus dominating the Gemmatimonadota (0.01, 0.1% of the phylum) has been detected in gypsum-rich soil (Yuan et al., 2021). Its ability to grow under micro-oxic conditions (Zeng et al., 2015) provides advantages to survive in intermittently flooded soil (Yuan et al., 2021), such as in the Salineta wetland. In addition, members of the *Gemmatimonas* genus have been found in the rhizosphere of alkali vegetation (Yue et al., 2020; Borsodi et al., 2021) playing a key role in vegetated saline soil, as OM-decomposing and polyphosphate-accumulating bacterium (Mau et al., 2015). The Bacteroidota was dominated by the *Gillisia* genus (1.4%, representing 7.7% of the phylum), in which members have been detected in cold saline (Dorador et al., 2009; Maida et al., 2014) and athalassohaline (Montoya et al., 2013) environments. The pangenome of the *Gillisia* genus reveals the presence of genes involved in the adaptation to cold and high salinity (Maida et al., 2014). The *Geothermobacter* (2.3%) and *Desulfovermiculus* (2.2%) were the dominant genera of the Desulfobacterota, representing, respectively, 19.1 and 18.1% of the phylum. The *Geothermobacter* genus, iron-reducing bacterium (Gomez-Saez et al., 2017), and the *Desulfovermiculus*, sulfate-reducing bacterium (Nigro et al., 2020) are usually found in hypersaline environments where they play a key role in iron and sulfur cycling. The archaeal phylum Halobacteriota was dominated by *Halapricum* (6.1%), *Halorubrum* (3.6%), and *Natronomonas* (2.2%) genera (representing, respectively, 12, 7, and 4.3% of the phylum), isolated in hypersaline ecosystems where they often represent the dominant archaeal taxa (Tu et al., 2022). *Halorubrum* and *Natronomonas* are known as aerobes (Mora-Ruiz et al., 2018), while *Halapricum* is a sulfate-reducing archaeon (Sorokin et al., 2022). Beside these genera from the dominant phyla, it is worth noting the presence of *Halanaerobium* (8.3%, representing 83.4% of the *Halanaerobiaeota*) and *Truepera* (8.5%, representing 99.8% of the *Deinococcota*), chemoorganotrophic strictly anaerobic and aerobic bacteria, respectively (Oren, 2015; Albuquerque et al., 2018), which are detected in hypersaline ecosystems (Boidi et al., 2022; Solchaga et al., 2022). Therefore, such observation indicated that the microbial community inhabiting the Salineta wetland is characteristic of extreme saline environments.

The comparison of microbial communities from the different landscapes revealed that layer (depth) was the main factor explaining the microbial distribution (PERMANOVA: $R^2 = 0.2$, $p < 0.001$). The layers were identified according to soil colors, which rely on chemical and physical characteristics (Kalev and Toor, 2018), particularly the ORP gradient from low (ORP, -155 ± 193 mV) at the surface to higher redox (ORP, 88 ± 118 mV) in the deeper layer. Such microbial distribution according to depth was in accordance with previous reports, showing a relationship between microbial community structure and the variation of physical–chemical parameters with depth in microbial mats (Fourçans et al., 2004) and marine sediments (Böer et al., 2009). Furthermore, the microbial biomarkers revealed by LEfSe were affiliated with five bacterial OTUs (belonging to the Anaerolineaceae family and the *Salinarimonas*, *Rhodopirellula*, *Desulfonatronobacter*, and *Aliifodinibius* genera) and two archaeal

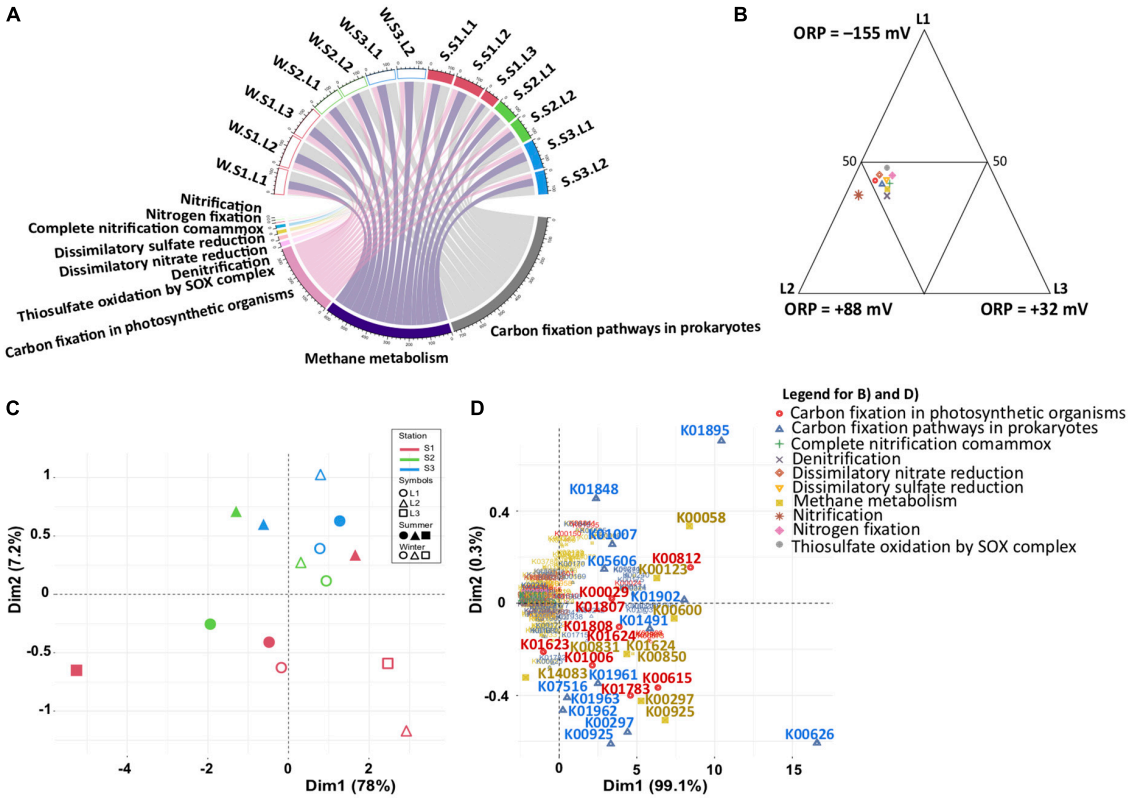

FIGURE 5
Predicted functional analysis for sulfur, nitrogen, and carbon metabolism inferred from 16S rRNA gene data (PICRUSt2). **(A)** Chordogram showing the distribution of functions among samples. **(B)** Ternary plot showing the distribution of functions among layers. **(C,D)** Principal component analysis (PCA) showing the distribution of samples based on the PICRUSt2 predictive functions, and the functional genes, respectively. Winter, W (wet period); Summer, S (dry period); Stations: S1, S2, S3; Layers: L1, L2, L3.

OTUs (*Halorubellus* genus and *H. formicicum*) for the upper layer. Consistent with low ORP observed at the upper layer L1, these OTUs are affiliated with taxa detected in hypersaline ecosystems exhibiting strictly (Anaerolineaceae, *Desulfonatronobacter*, *Aliifodinibius*, *H. formicicum*) or facultative (*Salinarimonas*, *Rhodopirellula*) anaerobic metabolisms (Cai et al., 2011; Cui et al., 2012; d'Avó et al., 2013; Sorokin et al., 2015, 2017; Sugihara et al., 2016). They have also been shown to possess adaptation capacities to sudden environmental changes (Wecker et al., 2009; Cui et al., 2012) that might explain their adaptation to the extreme and fluctuating environmental conditions prevailing at Salineta wetland, especially at the surface soil layer. Interestingly, members of the Anaerolineaceae have been found associated with methanogens (Liang et al., 2015), further supporting that the surface L1 layer was dominated by anaerobic metabolisms.

For the deeper layers, the biomarkers revealed by LEfSe analysis correspond to OTUs affiliated with halophilic bacteria found in hypersaline ecosystems. They include *Coxiella*, *Anaerophaga*, and Balneolaceae for layer L2, exhibiting anaerobic metabolism (Song et al., 2021; Wu et al., 2022). This finding is in agreement with the reversed redox gradient observed in the Salineta wetland. The dominance of *Coxiella*, a genus of endosymbiont bacteria pathogenic for humans and animals (Lory, 2014), is surprising, although the presence of *Coxiella* has been linked to cyanobacterial and algal blooms (Li et al., 2011) in agreement with their lifestyle. Furthermore, members of the *Coxiella* genus have been detected in seawater associated with urban wastewater inputs (Fonti et al., 2021). The farming activities around the Salineta wetland and the presence of migratory birds represent potential sources of *Coxiella* since it has been detected in the feces of livestock (Mcquiston and Childs, 2002) and wild birds (Ebani and Mancianti, 2022).

Linear discriminant analysis effect size also identified *Haloplanus* and *Halonotius* as microbial biomarkers for the halophytes vegetated soil (station S3). *Haloplanus* and *Halonotius* are extremely halophilic archaea, members of which have been isolated from various hypersaline environments (Elevi Bardavid et al., 2007; Burns et al., 2010; Cui et al., 2010). It is likely that the OTUs identified as biomarkers for station S3's own metabolism well adapted to the environmental fluctuation, including variations in salinity, temperature, and UV radiation (Youssef et al., 2012). Finally, LEfSe revealed different biomarkers according to seasons, reflecting probably the variations of not only salinity according to wet and dry periods but also temperature and sun irradiance. The biomarkers taxa have been detected in hypersaline ecosystems: *Candidatus*, *Halobonum*, and *Halanaerobium*, archaeon and sulfidogenic bacterium, respectively (Abdeljabbar et al., 2013; Ugalde et al., 2013) for winter (wet period), and *Desulfurivibrio*, sulfidogenic bacterium (Sorokin et al., 2008) for summer (dry period). The dominance of sulfidogenic bacteria in both seasons is in agreement with the fact that the microbial sulfur cycle is among the most active in alkaline hypersaline lakes (Sorokin et al., 2011). The fact that different taxa ensure similar functions according to seasons suggests functional redundancy.

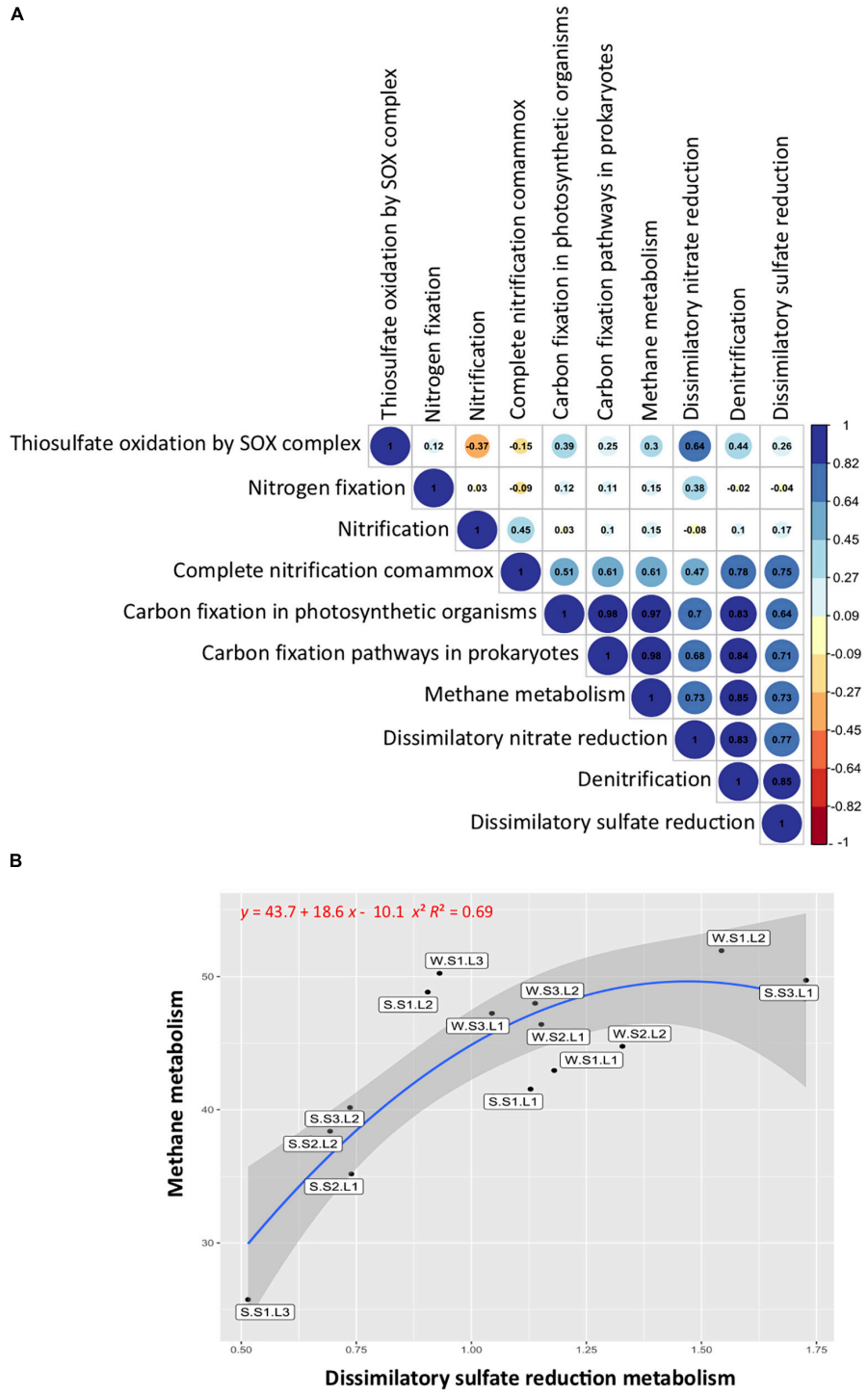

FIGURE 6
Functional group correlations and distributions. **(A)** Pearson's correlations between sulfur, nitrogen, and carbon metabolisms. Blue, positive correlations; red, negative correlations. **(B)** Correlation between methane and dissimilatory sulfate reduction metabolisms. Labels indicate sample names: seasons, summer (S, dry period) and winter (W, wet period); stations (S1, S2, S3); layers (L1, L2, L3).

The PICRUSt2 functional capabilities of microbial communities inferred from 16S rRNA gene meta-barcoding data revealed similar functional patterns, irrespective of the layer, the landscape type, or the season. Consistently, the functional distribution within the microbial community assessed by PCA was explained by the presence of different KOs for each functional group. Such observations suggest functional redundancy; however, further analyses are requested to understand the adaptation strategies for maintaining biogeochemical cycle functioning. Future research will benefit from functional untargeted metagenomic analyses to understand microbial functions in the Salineta hypersaline wetland. Functional redundancy was observed in many ecosystems (Staley et al., 2016; Louca et al., 2018), allowing the microbial community to cope with fluctuating environmental conditions (Stauffert et al., 2014; Terrisse et al., 2017).

Sulfur cycle functions were positively correlated with nitrogen cycle functions (denitrification, DNRA, and COMAMMOX) but not significantly correlated with nitrogen fixation and nitrification. Nitrogen and sulfur cycles are important for ecosystem functioning, and they are coupled in aquatic sediment (Zhu et al., 2018). Our results suggest that the sulfur cycle affects the nitrogen metabolism, some reactions involved in nitrogen species transformation, but not the overall nitrogen cycle functioning. The functions involved in the sulfur cycle were also positively correlated with the functions of the carbon cycle involved in carbon fixation and methane metabolism. Noteworthy, methane metabolism functions (methanogenesis and methanotrophy) were abundant on the surface layer exhibiting the lowest ORP, particularly in the usually submerged soil (station S1). In general, the microorganisms involved in methane metabolisms are described in depth layers with negative redox (Jørgensen, 1982; Kristensen, 2000), competing for carbon sources or establishing syntrophic interactions (Schink and Stams, 2006). Our results suggest that in the reverse redox gradient, methanogens and sulfate reducers are present at the upper layer of the soil, being more abundant during the wet season (winter) showing the effect of flooding on microbial functions. The coexistence of methanogens and sulfate reducers has been described in various ecosystems, such as saline coastal areas (Egger et al., 2016), salt marshes (Parkes et al., 2012), and athalassohaline lakes (Montoya et al., 2011). It has been shown that methanogenesis and sulfate reduction can be coupled even at elevated sulfate concentrations, the competition for a common substrate controlling the activities (Sela-Adler et al., 2017). However, factors favoring sulfate reduction, such as increasing salinity (Huang et al., 2020), resulting in decreasing methane fluxes (McGenity, 2010; Marton et al., 2012). In contrast, the input of freshwater from flooding events reducing salinity favors methane fluxes (McGenity, 2010) and greenhouse gas emissions (Helton et al., 2018). It is likely that climate change with more frequent rainfalls accompanied by heavy flooding events as well as human activities such as intensive agriculture involving important irrigation threatens the equilibrium of ephemeral saline lakes by modifying particularly redox gradient, which, in turn, affects greenhouse gas emissions. Thus, the Salineta wetland represents an adequate model to study the effects of climate change on saline wetlands that would provide information on microbial community modifications and their ecosystem services.

Conclusion

The three sampling stations in the Salineta wetland, within a gradient of water presence (S1 soil usually submerged, S2 soil intermittently flooded, and S3 covered by halophytes), were all characterized by reversed redox gradient in the soil profile (increasing from surface to subsurface soil layer). Thus, the soil layers were the main drivers explaining microbial diversity distribution. Although they exhibited different taxonomic microbial communities, the predictive functional analysis revealed similar functions involved in the main biogeochemical cycles (nitrogen, sulfur, and carbon) in all the soil layers, suggesting functional redundancy. It is likely that the microbial communities inhabiting the Salineta wetland are well adapted to the extreme environmental conditions, characterized by high salinity, high radiance, and seasonal drying. The functioning in this highly dynamic ecosystem is ensured by the redundancy of the biogeochemical cycle functions. Our study provides the first microbial inventory of the Salineta wetland, which is threatened by the direct input of agrochemicals and freshwater from the surrounding irrigated areas. As a consequence, the water change to less saline and polluted may modify the environmental parameters including the redox gradient, which, in turn, affect microbial communities dramatically disturbing the ecosystem. The information from our results is then useful to monitor and manage such an extreme wetland exposed to human activities.

Data availability statement

The datasets presented in this study can be found in online repositories. The names of the repository/repositories and accession number PRJNA763109 can be found in the article/**Supplementary material**.

Author contributions

ZB conducted experimental and performed the bioinformatics and biostatistics analyses. RR-O and JÁ-F conducted the physical–chemical analyses. ZB, CaC, ChC, CC-L, and RD participated in the conceptualization, validation, and writing. All authors contributed to the article and approved the submitted version.

Funding

We acknowledge the European program ERANET-MED through the AQUASALT (NMED-0003-01) project, the French Research Agency (ANR) through the ANR-17-NMED-0003-01, and the Spanish Research Agency (AEI) through the PCI2018-092999 project.

Conflict of interest

The authors declare that the research was conducted in the absence of any commercial or financial relationships that could be construed as a potential conflict of interest.

Publisher's note

Supplementary material

The Supplementary Material for this article can be found online at: https://www.frontiersin.org/articles/10.3389/fmicb.2023.869907/full#supplementary-material

References

Abdeljabbar, H., Cayol, J. L., Ben Hania, W., Boudabous, A., Sadfi, N., and Fardeau, M. L. (2013). *Halanaerobium sehlinense* sp. nov., an extremely halophilic, fermentative, strictly anaerobic bacterium from sediments of the hypersaline lake Sehline Sebkha. *Int. J. Syst. Evol. Microbiol.* 63, 2069–2074. doi: 10.1099/ijs.0.040139-0

Albuquerque, L., Rainey, F. A., and da Costa, M. S. (2018). "Truepera," in *Bergey's manual of systematics of archaea and bacteria*, eds M. E. Trujillo, S. Dedysh, P. DeVos, B. Hedlund, P. Kämpfer, F. A. Rainey, et al. (Hoboken, NJ: John Wiley & Sons). doi: 10.1002/9781118960608.gbm01328

Andrei, A. Ş, Banciu, H. L., and Oren, A. (2012). Living with salt: Metabolic and phylogenetic diversity of archaea inhabiting saline ecosystems. *FEMS Microbiol. Lett.* 330, 1–9. doi: 10.1111/j.1574-6968.2012.02526.x

Arce-Rodríguez, A., Puente-Sánchez, F., Avendaño, R., Libby, E., Mora-Amador, R., Rojas-Jimenez, K., et al. (2020). Microbial community structure along a horizontal oxygen gradient in a Costarican volcanic influenced acid rock drainage system. *Microb. Ecol.* 80, 793–808. doi: 10.1007/s00248-020-01530-9

Ben Salem, F., Ben Said, O., Aissa, P., Mahmoudi, E., Monperrus, M., Grunberger, O., et al. (2016). Pesticides in Ichkeul Lake–Bizerta Lagoon watershed in Tunisia: Use, occurrence, and effects on bacteria and free-living marine nematodes. *Environ. Sci. Pollut. R.* 23, 36–48. doi: 10.1007/S11356-015-4991-8

Böer, S. I., Hedtkamp, S. I. C., van Beusekom, J. E. E., Fuhrman, J. A., Boetius, A., and Ramette, A. (2009). Time–and sediment depth-related variations in bacterial diversity and community structure in subtidal sands. *ISME J.* 3, 780–791. doi: 10.1038/ismej.2009.29

Boidi, F. J., Mlewski, E. C., Fernández, G. C., Flores, M. R., Gérard, E., Farías, M. E., et al. (2022). Community vertical composition of the laguna Negra hypersaline microbial mat, Puna region (Argentinean Andes). *Biology (Basel)* 11:831. doi: 10.3390/biology11060831

Bolhuis, H., Cretoiu, M. S., and Stal, L. J. (2014). Molecular ecology of microbial mats. *FEMS Microbiol. Ecol.* 90, 335–350. doi: 10.1111/1574-6941.12408

Bordenave, S., Fourçans, A., Blanchard, S., Goñi, M. S., and Duran, R. (2004). Structure and functional analyses of bacterial communities changes in microbial mats following petroleum exposure. *Ophelia* 58, 195–203. doi: 10.1080/00785236.2004.10410227

Borsodi, A. K., Mucsi, M., Krett, G., Szabó, A., Felföldi, T., and Szili-Kovács, T. (2021). Variation in sodic soil bacterial communities associated with different alkali vegetation types. *Microorganisms* 9:1673. doi: 10.3390/microorganisms9081673

Bourhane, Z., Lanzén, A., Cagnon, C., Ben Said, O., Mahmoudi, E., Coulon, F., et al. (2022). Microbial diversity alteration reveals biomarkers of contamination in soil-river-lake continuum. *J. Hazard. Mater.* 421:126789. doi: 10.1016/j.jhazmat.2021.126789

Bruneel, O., Pascault, N., Egal, M., Bancon-Montigny, C., Goñi-Urriza, M. S., Elbaz-Poulichet, F., et al. (2008). Archaeal diversity in a Fe-As rich acid mine drainage at Carnoulès (France). *Extremophiles* 12, 563–571. doi: 10.1007/s00792-008-0160-z

Burns, D. G., Janssen, P. H., Itoh, T., Kamekura, M., Echigo, A., and Dyall-Smith, M. L. (2010). *Halonotius pteroides* gen. nov., sp. nov., an extremely halophilic archaeon recovered from a saltern crystallizer in southern Australia. *Int. J. Syst. Evol. Microbiol.* 60, 1196–1199. doi: 10.1099/ijs.0.010017-0

Cai, M., Wang, L., Cai, H., Li, Y., Wang, Y. N., Tang, Y. Q., et al. (2011). *Salinarimonas ramus* sp. nov. and *Tessaracoccus oleiagri* sp. nov., isolated from a crude oil-contaminated saline soil. *Int. J. Syst. Evol. Microbiol.* 61, 1767–1775. doi: 10.1099/ijs.0.025932-0

Casamayor, E. O., Triadó-Margarit, X., and Castañeda, C. (2013). Microbial biodiversity in saline shallow lakes of the Monegros Desert, Spain. *FEMS Microbiol. Ecol.* 85, 503–518. doi: 10.1111/1574-6941.12139

Castañeda, C., and García-Vera, M. Á (2008). Water balance in the playa-lakes of an arid environment, Monegros, NE Spain. *Hydrogeol. J.* 16, 87–102. doi: 10.1007/s10040-007-0230-9

Castañeda, C., and Herrero, J. (2005). The water regime of the Monegros playa-lakes as established from ground and satellite data. *J. Hydrol. (Amst)* 310, 95–110. doi: 10.1016/J.JHYDROL.2004.12.007

Castañeda, C., Javier Gracia, F., Luna, E., and Rodríguez-Ochoa, R. (2015). Edaphic and geomorphic evidences of water level fluctuations in Gallocanta Lake, NE Spain. *Geoderma* 23, 265–279. doi: 10.1016/j.geoderma.2014.11.005

Castañeda, C., Luna, E., and Rabenhorst, M. (2017). Reducing conditions in soil of Gallocanta Lake, northeast Spain. *Eur. J. Soil Sci.* 68, 249–258. doi: 10.1111/ejss.12407

Caton, I. R., and Schneegurt, M. A. (2012). Culture-independent analysis of the soil bacterial assemblage at the Great Salt Plains of Oklahoma. *J. Basic Microbiol.* 52, 16–26. doi: 10.1002/jobm.201100175

Conesa, J. A., Castañeda, C., and Pedrol, J. (2011). *Las saladas de Monegros y su entorno: Habitats y paisaje vegetal*. Zaragoza: Consejo de Protección de la Naturaleza de Aragón.

Cui, H. L., Mou, Y. Z., Yang, X., Zhou, Y. G., Liu, H. C., and Zhou, P. J. (2012). *Halorubellus salinus* gen. nov., sp. nov. and *Halorubellus litoreus* sp. nov., novel halophilic archaea isolated from a marine solar saltern. *Syst. Appl. Microbiol.* 35, 30–34. doi: 10.1016/j.syapm.2011.08.001

Cui, H.-L., Gao, X., Li, X.-Y., Xu, X.-W., Zhou, Y.-G., Liu, H.-C., et al. (2010). *Haloplanus vescus* sp. nov., an extremely halophilic archaeon from a marine solar saltern, and emended description of the genus *Haloplanus*. *Int. J. Syst. Evol. Microbiol.* 60, 1824–1827. doi: 10.1099/ijs.0.018564-0

Cycil, L. M., DasSarma, S., Pecher, W., McDonald, R., AbdulSalam, M., and Hasan, F. (2020). Metagenomic insights into the diversity of halophilic microorganisms indigenous to the Karak salt mine, Pakistan. *Front. Microbiol.* 11:1567. doi: 10.3389/fmicb.2020.01567

d'Avó, A. F., Cunha, S., Mingote, A., Lamosa, P., da Costa, M. S., and Costa, J. (2013). A unique pool of compatible solutes on *Rhodopirellula baltica*, member of the deep-branching phylum Planctomycetes. *PLoS One* 8:e68289. doi: 10.1371/journal.pone.0068289

Demergasso, C., Escudero, L., Casamayor, E. O., Chong, G., Balagué, V., and Pedrós-Alió, C. (2008). Novelty and spatio-temporal heterogeneity in the bacterial diversity of hypersaline Lake Tebenquiche (Salar de Atacama). *Extremophiles* 12, 491–504. doi: 10.1007/s00792-008-0153-y

Dominguez-Beisiegel, M., Herrero, J., and Castañeda, C. (2011). Saline wetlands' fate in inland deserts: An example of 80 years' decline from Monegros, Spain. *Land Degrad. Dev.* 24, 250–265. doi: 10.1002/ldr.1122

Dong, H., Zhang, G., Jiang, H., Yu, B., Chapman, L. R., Lucas, C. R., et al. (2006). Microbial diversity in sediments of saline Qinghai Lake, China: Linking geochemical controls to microbial ecology. *Microb. Ecol.* 51, 65–82. doi: 10.1007/s00248-005-0228-6

Dorador, C., Meneses, D., Urtuvia, V., Demergasso, C., Vila, I., Witzel, K. P., et al. (2009). Diversity of bacteroidetes in high-altitude saline evaporitic basins in northern Chile. *J. Geophys. Res. Biogeosci.* 114:11. doi: 10.1029/2008JG000837

Douglas, G. M., Maffei, V. J., Zaneveld, J., Yurgel, S. N., Brown, J. R., Taylor, C. M., et al. (2020). PICRUSt2: An improved and customizable approach for metagenome inference. *bioRxiv* [Preprint]. doi: 10.1101/672295

Dufresne, Y., Lejzerowicz, F., Perret-Gentil, L. A., Pawlowski, J., and Cordier, T. (2019). SLIM: A flexible web application for the reproducible processing of environmental DNA metabarcoding data. *BMC Bioinform.* 20:88. doi: 10.1186/s12859-019-2663-2

Duran, R., and Cravo-Laureau, C. (2016). Role of environmental factors and microorganisms in determining the fate of polycyclic aromatic hydrocarbons in the marine environment. *FEMS Microbiol. Rev.* 40, 814–830. doi: 10.1093/femsre/fuw031

Ebani, V. V., and Mancianti, F. (2022). Potential role of birds in the epidemiology of *Coxiella burnetii*, *Coxiella*-like agents and *Hepatozoon* spp. *Pathogens* 11:298. doi: 10.3390/pathogens11030298

Edgar, R. C. (2016). UNCROSS: Filtering of high-frequency cross-talk in 16S amplicon reads. *bioRxiv* [Preprint]. doi: 10.1101/088666

Egger, M., Lenstra, W., Jong, D., Meysman, F. J. R., Sapart, C. J., van der Veen, C., et al. (2016). Rapid sediment accumulation results in high methane effluxes from coastal sediments. *PLoS One* 11:e0161609. doi: 10.1371/journal.pone.0161609

Elbrecht, V., Vamos, E. E., Steinke, D., and Leese, F. (2018). Estimating intraspecific genetic diversity from community DNA metabarcoding data. *PeerJ* 2018, 1–13. doi: 10.7717/peerj.4644

Elevi Bardavid, R., Mana, L., and Oren, A. (2007). *Haloplanus natans* gen. nov., sp. nov., an extremely halophilic, gas-vacuolate archaeon isolated from dead sea-red sea water mixtures in experimental outdoor ponds. *Int. J. Syst. Evol. Microbiol.* 57, 780–783. doi: 10.1099/ijs.0.64648-0

Fonti, V., di Cesare, A., Šangulin, J., del Negro, P., and Celussi, M. (2021). Antibiotic resistance genes and potentially pathogenic bacteria in the central Adriatic Sea: Are they connected to urban wastewater inputs? *Water (Switzerland)* 13:3335. doi: 10.3390/w13233335

Fourçans, A., de Oteyza, T. G., Wieland, A., Solé, A., Diestra, E., van Bleijswijk, J., et al. (2004). Characterization of functional bacterial groups in a hypersaline microbial mat community (Salins-de-Giraud, Camargue, France). *FEMS Microbiol. Ecol.* 51, 55–70. doi: 10.1016/j.femsec.2004.07.012

Franco-Luesma, S., Cavero, J., Plaza-Bonilla, D., Cantero-Martínez, C., Arrúe, J. L., and Álvaro-Fuentes, J. (2020). Tillage and irrigation system effects on soil carbon dioxide (CO2) and methane (CH4) emissions in a maize monoculture under Mediterranean conditions. *Soil Tillage Res.* 196:104488. doi: 10.1016/j.still.2019.104488

Frøslev, T. G., Kjøller, R., Bruun, H. H., Ejrnæs, R., Brunbjerg, A. K., Pietroni, C., et al. (2017). Algorithm for post-clustering curation of DNA amplicon data yields reliable biodiversity estimates. *Nat. Commun.* 8:1188. doi: 10.1038/s41467-017-01312-x

Gasol, J. M., Casamayor, E. O., Joint, I., Garde, K., Gustavson, K., Benlloch, S., et al. (2004). Control of heterotrophic prokaryotic abundance and growth rate in hypersaline planktonic environments. *Aqua. Microb. Ecol.* 34, 193–206. doi: 10.3354/ame034193

Giloteaux, L., Duran, R., Casiot, C., Bruneel, O., Elbaz-Poulichet, F., and Goñi-Urriza, M. (2013). Three-year survey of sulfate-reducing bacteria community structure in Carnoulès acid mine drainage (France), highly contaminated by arsenic. *FEMS Microbiol. Ecol.* 83, 724–737. doi: 10.1111/1574-6941.12028

Gomez-Saez, G. V., Ristova, P. P., Sievert, S. M., Elvert, M., Hinrichs, K. U., and Bühring, S. I. (2017). Relative importance of chemoautotrophy for primary production in a light exposed marine shallow hydrothermal system. *Front. Microbiol.* 8:702. doi: 10.3389/fmicb.2017.00702

Helton, A. M., Ardón, M., and Bernhardt, E. S. (2018). Hydrologic context alters greenhouse gas feedbacks of coastal wetland salinization. *Ecosystems* 22, 1108–1125. doi: 10.1007/s10021-018-0325-2

Huang, J., Yang, J., Jiang, H., Wu, G., Liu, W., Wang, B., et al. (2020). Microbial responses to simulated salinization and desalinization in the sediments of the Qinghai–Tibetan lakes. *Front. Microbiol.* 11:1772. doi: 10.3389/fmicb.2020.01772

Jiang, H., Dong, H., Zhang, G., Yu, B., Chapman, L. R., and Fields, M. W. (2006). Microbial diversity in water and sediment of Lake Chaka, an athalassohaline lake in northwestern China. *Appl. Environ. Microbiol.* 72, 3832–3845. doi: 10.1128/AEM.02869-05

Jørgensen, B. B. (1982). Mineralization of organic matter in the sea bed–The role of sulphate reduction. *Nature* 296, 643–645. doi: 10.1038/296643a0

Kalev, S. D., and Toor, G. S. (2018). "The composition of soils and sediments," in *Green chemistry: An inclusive approach*, eds B. Török and T. Dransfield (Amsterdam: Elsevier), 339–357. doi: 10.1016/B978-0-12-809270-5.00014-5

Kan, J., Wang, K., and Chen, F. (2006). Temporal variation and detection limit of an estuarine bacterioplankton community analyzed by denaturing gradient gel electrophoresis (DGGE). *Aquat. Microb. Ecol.* 42, 7–18. doi: 10.3354/ame042007

Karner, M. B., Delong, E. F., and Karl, D. M. (2001). Archaeal dominance in the mesopelagic zone of the Pacific Ocean. *Nature* 409, 507–510.

Kirk Harris, J., Gregory Caporaso, J., Walker, J. J., Spear, J. R., Gold, N. J., Robertson, C. E., et al. (2013). Phylogenetic stratigraphy in the Guerrero Negro hypersaline microbial mat. *ISME J.* 7, 50–60. doi: 10.1038/ismej.2012.79

Kristensen, E. (2000). Organic matter diagenesis at the oxic/anoxic interface in coastal marine sediments, with emphasis on the role of burrowing animals. *Hydrobiologia* 426, 1–24. doi: 10.1023/A:1003980226194

Kroeger, K. D., Crooks, S., Moseman-Valtierra, S., and Tang, J. (2017). Restoring tides to reduce methane emissions in impounded wetlands: A new and potent blue carbon climate change intervention. *Sci. Rep.* 7, 1–12. doi: 10.1038/s41598-017-12138-4

Langille, M. G. I., Zaneveld, J., Caporaso, J. G., McDonald, D., Knights, D., Reyes, J. A., et al. (2013). Predictive functional profiling of microbial communities using 16S rRNA marker gene sequences. *Nat. Biotechnol.* 31, 814–821. doi: 10.1038/nbt.2676

Lanzén, A., Jørgensen, S. L., Huson, D. H., Gorfer, M., Grindhaug, S. H., Jonassen, I., et al. (2012). CREST - classification resources for environmental sequence tags. *PLoS One* 7:e49334. doi: 10.1371/journal.pone.0049334

Lanzén, A., Mendibil, I., Borja, Á, and Alonso-Sáez, L. (2021). A microbial mandala for environmental monitoring: Predicting multiple impacts on estuarine prokaryote communities of the Bay of Biscay. *Mol. Ecol.* 30, 2969–2987. doi: 10.1111/mec.15489

Lanzén, A., Simachew, A., Gessesse, A., Chmolowska, D., Jonassen, I., and Øvreås, L. (2013). Surprising prokaryotic and eukaryotic diversity, community structure and biogeography of Ethiopian Soda Lakes. *PLoS One* 8:e72577. doi: 10.1371/journal.pone.0072577

Li, H., Xing, P., Chen, M., Bian, Y., and Wu, Q. L. (2011). Short-term bacterial community composition dynamics in response to accumulation and breakdown of microcystis blooms. *Water Res.* 45, 1702–1710. doi: 10.1016/j.watres.2010.11.011

Liang, B., Wang, L. Y., Mbadinga, S. M., Liu, J. F., Yang, S. Z., Gu, J. D., et al. (2015). *Anaerolineaceae* and *Methanosaeta* turned to be the dominant microorganisms in alkanes-dependent methanogenic culture after long-term of incubation. *AMB Express* 5:37. doi: 10.1186/s13568-015-0117-4

Lory, S. (2014). "The family Coxiellaceae," in *The prokaryotes*, eds E. Rosenberg, E. F. DeLong, S. Lory, E. Stackebrandt, and F. Thompson (Berlin: Springer). doi: 10.1007/978-3-642-38922-1_371

Louca, S., Polz, M. F., Mazel, F., Albright, M. B. N., Huber, J. A., O'Connor, M. I., et al. (2018). Function and functional redundancy in microbial systems. *Nat. Ecol. Evol.* 2, 936–943. doi: 10.1038/s41559-018-0519-1

Mahé, F., Rognes, T., Quince, C., de Vargas, C., and Dunthorn, M. (2015). Swarmv2: Highly-scalable and high-resolution amplicon clustering. *PeerJ* 3:e1420. doi: 10.7717/peerj.1420

Maida, I., Fondi, M., Papaleo, M. C., Perrin, E., Orlandini, V., Emiliani, G., et al. (2014). Phenotypic and genomic characterization of the Antarctic bacterium *Gillisia* sp. CAL575, a producer of antimicrobial compounds. *Extremophiles* 18, 35–49. doi: 10.1007/s00792-013-0590-0

Martin, M. (2011). Cutadapt removes adapter sequences from high-throughput sequencing reads. *EMBnet J.* 17, 10–12. doi: 10.14806/ej.17.1.200

Marton, J. M., Herbert, E. R., and Craft, C. B. (2012). Effects of salinity on denitrification and greenhouse gas production from laboratory-incubated tidal forest soils. *Wetlands* 32, 347–357. doi: 10.1007/s13157-012-0270-3

Mau, R. L., Liu, C. M., Aziz, M., Schwartz, E., Dijkstra, P., Marks, J. C., et al. (2015). Linking soil bacterial biodiversity and soil carbon stability. *ISME J.* 9, 1477–1480. doi: 10.1038/ismej.2014.205

Mazière, C., Agogué, H., Cravo-Laureau, C., Cagnon, C., Lanneluc, I., Sablé, S., et al. (2021). New insights in bacterial and eukaryotic diversity of microbial mats inhabiting exploited and abandoned salterns at the Ré Island (France). *Microbiol Res.* 252:126854. doi: 10.1016/j.micres.2021.126854

McGenity, T. (2010). "Methanogens and methanogenesis in hypersaline environments," in *Handbook of hydrocarbon and lipid microbiology*, ed. K. N. Timmis (Berlin: Springer). doi: 10.1007/978-3-540-77587-4_53

McGenity, T., and Oren, A. (2012). "Hypersaline environments," in *Life at extremes: Environments, organisms and strategies for survival*, ed. E. Bell (Cambridge, MA: Cabi), 402–437.

Mcquiston, J. H., and Childs, J. E. (2002). Review Q fever in humans and animals in the United States. *Vector Borne Zoonotic Dis.* 2, 179–191.

Mehrshad, M., Amoozegar, M. A., Didari, M., Bagheri, M., Shahzadeh Fazeli, S. A., Schumann, P., et al. (2013). *Bacillus halosaccharovorans* sp. nov., a moderately halophilic bacterium from a hypersaline lake. *Int. J. Syst. Evol. Microbiol.* 63, 2776–2781. doi: 10.1099/ijs.0.046961-0

Menéndez-Serra, M., Triadó-Margarit, X., and Casamayor, E. O. (2021). Ecological and metabolic thresholds in the bacterial, protist, and fungal microbiome of ephemeral saline lakes (Monegros Desert, Spain). *Microb. Ecol.* 82, 885–896. doi: 10.1007/s00248-021-01732-9

Menéndez-Serra, M., Triadó-Margarit, X., Castañeda, C., Herrero, J., and Casamayor, E. O. (2019). Microbial composition, potential functional roles and genetic novelty in gypsum-rich and hypersaline soils of Monegros and Gallocanta (Spain). *Sci. Total Environ.* 650, 343–353. doi: 10.1016/j.scitotenv.2018.09.050

Montoya, L., Lozada-Chávez, I., Amils, R., Rodriguez, N., and Marín, I. (2011). The sulfate-rich and extreme saline sediment of the ephemeral Tirez Lagoon: A biotope for acetoclastic sulfate-reducing bacteria and hydrogenotrophic methanogenic archaea. *Int. J. Microbiol.* 2011:753758. doi: 10.1155/2011/753758

Montoya, L., Vizioli, C., Rodríguez, N., Rastoll, M. J., Amils, R., and Marin, I. (2013). Microbial community composition of Tirez Lagoon (Spain), a highly sulfated athalassohaline environment. *Aquat. Biosyst.* 9:19. doi: 10.1186/2046-9063-9-19

Mora-Ruiz, M., del, R., Cifuentes, A., Font-Verdera, F., Pérez-Fernández, C., Farias, M. E., et al. (2018). Biogeographical patterns of bacterial and archaeal communities from distant hypersaline environments. *Syst. Appl. Microbiol.* 41, 139–150. doi: 10.1016/j.syapm.2017.10.006

Nigro, L. M., Elling, F. J., Hinrichs, K. U., Joye, S. B., and Teske, A. (2020). Microbial ecology and biogeochemistry of hypersaline sediments in Orca Basin. *PLoS One* 15:e0231676. doi: 10.1371/journal.pone.0231676

Offre, P., Spang, A., and Schleper, C. (2013). Archaea in biogeochemical cycles. *Annu. Rev. Microbiol.* 67, 437–457. doi: 10.1146/annurev-micro-092412-155614

Oksanen, A. J., Blanchet, F. G., Friendly, M., Kindt, R., Legendre, P., McGlinn, D., et al. (2019). *Vegan: Community ecology package. R package version 2.2-0.*

Oren, A. (2013). "Life in magnesium–and calcium-rich hypersaline environments: Salt stress by chaotropic ions," in *Polyextremophiles. Cellular origin, life in extreme habitats and astrobiology*, Vol. 27, eds J. Seckbach, A. Oren, and H. Stan-Lotter (Dordrecht: Springer). doi: 10.1007/978-94-007-6488-0_8

Oren, A. (2015). "Life in high-salinity environments," in *Manual of environmental microbiology*, eds M. Yates, C. Nakatsu, R. Miller, and S. Pillai (Washington, DC: ASM Press). doi: 10.1128/9781555818821.ch4.3.2

Pagaling, E., Wang, H., Venables, M., Wallace, A., Grant, W. D., Cowan, D. A., et al. (2009). Microbial biogeography of six salt lakes in Inner Mongolia, China, and a salt lake in Argentina. *Appl. Environ. Microbiol.* 75, 5750–5760. doi: 10.1128/AEM.00040-09

Parkes, R. J., Brock, F., Banning, N., Hornibrook, E. R., Roussel, E. G., Weightman, A. J., et al. (2012). Changes in methanogenic substrate utilization and communities with depth in a salt-marsh, creek sediment in southern England. *Estuar Coast Shelf Sci.* 96, 170–178. doi: 10.1016/j.ecss.2011.10.025

Ramsar Convention Secretariat (2010). *Designating Ramsar sites: Strategic framework and guidelines for the future development of the list of wetlands of international importance. Ramsar handbooks for the wise use of wetlands*. Gland: Ramsar Convention Secretariat.

Reddy, K. R., and DeLaune, R. D. (2008). Biogeochemistry of wetlands: Science and applications. *Biogeochem. Wetlands Sci. Appl.* 73:692. doi: 10.2136/sssaj2008.0013br

Ringeval, B., de Noblet-Ducoudré, N., Ciais, P., Bousquet, P., Prigent, C., Papa, F., et al. (2010). An attempt to quantify the impact of changes in wetland extent on methane emissions on the seasonal and interannual time scales. *Glob. Biogeochem. Cycles* 24, 1–12. doi: 10.1029/2008GB003354

Rognes, T., Flouri, T., Nichols, B., Quince, C., and Mahé, F. (2016). VSEARCH: A versatile open source tool for metagenomics. *PeerJ* 4:e2548. doi: 10.7717/peerj.2584

Schink, B., and Stams, A. J. M. (2006). "Syntrophism among prokaryotes," in *The prokaryotes*, eds M. Dworkin, S. Falkow, E. Rosenberg, K. Schleifer, and E. Stackebrandt (New York, NY: Springer), 309–335. doi: 10.1007/0-387-30742-7_11

Schultz, P. W. (2000). Empathizing with nature: The effects of perspective taking on concern for environmental issues. *J. Soc. Issues* 56, 391–406. doi: 10.1111/0022-4537.00174

Segata, N., Izard, J., Waldron, L., Gevers, D., Miropolsky, L., Garrett, W. S., et al. (2011). Metagenomic biomarker discovery and explanation. *Genome Biol.* 12:R60. doi: 10.1186/gb-2011-12-6-r60

Sela-Adler, M., Ronen, Z., Herut, B., Antler, G., Vigderovich, H., Eckert, W., et al. (2017). Co-existence of methanogenesis and sulfate reduction with common substrates in sulfate-rich estuarine sediments. *Front. Microbiol.* 8:766. doi: 10.3389/fmicb.2017.00766

Solchaga, J. I., Busalmen, J. P., and Nercessian, D. (2022). Unraveling anaerobic metabolisms in a hypersaline sediment. *Front. Microbiol.* 13:811432. doi: 10.3389/fmicb.2022.811432

Song, Q., Chen, X., Zhou, W., and Xie, X. (2021). Application of a spiral symmetric stream anaerobic bioreactor for treating saline heparin sodium pharmaceutical wastewater: Reactor operating characteristics, organics degradation pathway and salt tolerance mechanism. *Water Res.* 205:117671. doi: 10.1016/j.watres.2021.117671

Sorokin, D. Y., Chernyh, N. A., and Poroshina, M. N. (2015). *Desulfonatronobacter acetoxydans* sp. nov.,: A first acetate-oxidizing, extremely salt-tolerant alkaliphilic SRB from a hypersaline soda lake. *Extremophiles* 19, 899–907.

Sorokin, D. Y., Kuenen, J. G., and Muyzer, G. (2011). The microbial sulfur cycle at extremely haloalkaline conditions of soda lakes. *Front. Microbiol.* 2:44. doi: 10.3389/fmicb.2011.00044

Sorokin, D. Y., Merkel, A. Y., Messina, E., Tugui, C., Pabst, M., Golyshin, P. N., et al. (2022). Anaerobic carboxydotrophy in sulfur-respiring haloarchaea from hypersaline lakes. *ISME J.* 16, 1534–1546. doi: 10.1038/s41396-022-01206-x

Sorokin, D. Y., Messina, E., Smedile, F., Roman, P., Damste, J. S., Ciordia, S., et al. (2017). Discovery of anaerobic lithoheterotrophic haloarchaea, ubiquitous in hypersaline habitats. *ISME J.* 11, 1245–1260. doi: 10.1038/ismej.2016.203

Sorokin, D. Y., Mosier, D., Zorz, J. K., Dong, X., and Strous, M. (2020). Wenzhouxiangella strain AB-CW3, a proteolytic bacterium from hypersaline soda lakes that preys on cells of gram-positive bacteria. *Front. Microbiol.* 11:597686. doi: 10.3389/fmicb.2020.597686

Sorokin, D. Y., Tourova, T. P., Mußmann, M., and Muyzer, G. (2008). *Dethiobacter alkaliphilus* gen. nov. sp. nov., and *Desulfurivibrio alkaliphilus* gen. nov. sp. nov.: Two novel representatives of reductive sulfur cycle from soda lakes. *Extremophiles* 12, 431–439. doi: 10.1007/s00792-008-0148-8

Staley, C., Gould, T. J., Wang, P., Phillips, J., Cotner, J. B., and Sadowsky, M. J. (2016). Sediments and soils act as reservoirs for taxonomic and functional bacterial diversity in the upper Mississippi River. *Microb. Ecol.* 71, 814–824. doi: 10.1007/s00248-016-0729-5

Stauffert, M., Duran, R., and Gassie, C. (2014). Response of archaeal communities to oil spill in bioturbated mudflat sediments. *Microb. Ecol.* 67, 108–119.

Sugihara, C., Yanagawa, K., Okumura, T., Takashima, C., Harijoko, A., and Kano, A. (2016). Transition of microbiological and sedimentological features associated with the geochemical gradient in a travertine mound in northern Sumatra, Indonesia. *Sediment. Geol.* 343, 85–98. doi: 10.1016/j.sedgeo.2016.07.012

Terrisse, F., Cravo-Laureau, C., Noël, C., Cagnon, C., Dumbrell, A. J., McGenity, T. J., et al. (2017). Variation of oxygenation conditions on a hydrocarbonoclastic microbial community reveals *Alcanivorax* and *Cycloclasticus* ecotypes. *Front. Microbiol.* 8:1549. doi: 10.3389/fmicb.2017.01549

Tu, D., Ke, J., Luo, Y., Hong, T., Sun, S., Han, J., et al. (2022). Microbial community structure and shift pattern of industry brine after a long-term static storage in closed tank. *Front. Microbiol.* 13:975271. doi: 10.3389/fmicb.2022.975271

Ugalde, J. A., Narasingarao, P., Kuo, S., Podell, S., and Allen, E. E. (2013). Draft genome sequence of "*Candidatus Halobonum tyrrellensis*" strain G22, isolated from the hypersaline waters of Lake Tyrrell, Australia. *Genome Announc.* 1:e01001-13. doi: 10.1128/genomeA.01001-13

Wang, H., Bier, R., Zgleszewski, L., Peipoch, M., Omondi, E., Mukherjee, A., et al. (2020). Distinct distribution of archaea from soil to freshwater to estuary: Implications of archaeal composition and function in different environments. *Front. Microbiol.* 11:576661. doi: 10.3389/fmicb.2020.576661

Wang, Y., and Qian, P.-Y. (2009). Conservative fragments in bacterial 16S RRNA genes and primer design for 16s ribosomal DNA amplicons in metagenomic studies. *PLoS One* 4:7401. doi: 10.1371/journal.pone.0007401

Wecker, P., Klockow, C., Ellrott, A., Quast, C., Langhammer, P., Harder, J., et al. (2009). Transcriptional response of the model planctomycete *Rhodopirellula baltica* SH1Tto changing environmental conditions. *BMC Genomics* 10:410. doi: 10.1186/1471-2164-10-410

Williams, W. D. (1996). The largest, highest and lowest lakes of the world: Saline lakes. *Verh. Int. Verein Limnol.* 26, 61–79. doi: 10.1080/03680770.1995.11900693

Williams, W. D. (2002). Environmental threats to salt lakes and the likely status of inland saline ecosystems in 2025. *Environ. Conserv.* 29, 154–167. doi: 10.1017/S0376892902000103

Wu, S., Wang, J., Wang, J., Du, X., Ran, Q., Chen, Q., et al. (2022). *Halalkalibacterium roseum* gen. nov., sp. nov., a new member of the family Balneolaceae isolated from soil. *Int. J. Syst. Evol. Microbiol.* 72:005339. doi: 10.1099/ijsem.0.005339

Youssef, N. H., Ashlock-Savage, K. N., and Elshahed, M. S. (2012). Phylogenetic diversities and community structure of members of the extremely halophilic archaea (order halobacteriales) in multiple saline sediment habitats. *Appl. Environ. Microbiol.* 78, 1332–1344. doi: 10.1128/AEM.07420-11

Yuan, C., Na, S., Li, F., and Hu, H. (2021). Impact of sulfate and iron oxide on bacterial community dynamics in paddy soil under alternate watering conditions. *J. Hazard. Mater.* 408:124417. doi: 10.1016/j.jhazmat.2020.124417

Yue, Y., Shao, T., Long, X., He, T., Gao, X., Zhou, Z., et al. (2020). Microbiome structure and function in rhizosphere of Jerusalem artichoke grown in saline land. *Sci. Total Environ.* 724:138259. doi: 10.1016/j.scitotenv.2020.138259

Zeng, Y., Selyanin, V., Lukeŝ, M., Dean, J., Kaftan, D., Feng, F., et al. (2015). Characterization of the microaerophilic, bacteriochlorophyll a-containing bacterium *Gemmatimonas phototrophica* sp. Nov., and emended descriptions of the genus *Gemmatimonas* and *Gemmatimonas aurantiaca*. *Int. J. Syst. Evol. Microbiol.* 65, 2410–2419. doi: 10.1099/ijs.0.000272

Zhang, X. Y., Zhang, R., Wang, J. C., Zhang, T., and Du, Z. J. (2020). *Wenzhouxiangella limi* sp. Nov., isolated from a salt lake. *Int. J. Syst. Evol. Microbiol.* 70, 4610–4615. doi: 10.1099/ijsem.0.004320

Zhu, J., He, Y., Zhu, Y., Huang, M., and Zhang, Y. (2018). Biogeochemical sulfur cycling coupling with dissimilatory nitrate reduction processes in freshwater sediments. *Environ. Rev.* 26, 121–132. doi: 10.1139/er-2017-0047

frontiers | Frontiers in Microbiology

TYPE Original Research
PUBLISHED 09 February 2023
DOI 10.3389/fmicb.2023.1097595

OPEN ACCESS

EDITED BY
Andreas Teske,
University of North Carolina at Chapel Hill,
United States

REVIEWED BY
Henry Joseph Oduor Ogola,
Jaramogi Oginga Odinga
University of Science and Technology,
Kenya
Spyridon Ntougias,
Democritus University of Thrace,
Greece

*CORRESPONDENCE
Isao Yumoto
✉ i.yumoto@aist.go.jp

SPECIALTY SECTION
This article was submitted to
Extreme Microbiology,
a section of the journal
Frontiers in Microbiology

RECEIVED 14 November 2022
ACCEPTED 16 January 2023
PUBLISHED 09 February 2023

CITATION
Farjana N, Tu Z, Furukawa H and
Yumoto I (2023) Environmental factors
contributing to the convergence of bacterial
community structure during indigo reduction.
Front. Microbiol. 14:1097595.
doi: 10.3389/fmicb.2023.1097595

Environmental factors contributing to the convergence of bacterial community structure during indigo reduction

Nowshin Farjana[1,2], Zhihao Tu[1,2], Hiromitsu Furukawa[3] and Isao Yumoto[1,2]*

[1]Bioproduction Research Institute, National Institute of Advanced Industrial Science and Technology (AIST), Sapporo, Japan, [2]Laboratory of Environmental Microbiology, Graduate School of Agriculture, Hokkaido University, Sapporo, Japan, [3]Sensing System Research Center, National Institute of Advanced Industrial Science and Technology (AIST), Sapporo, Japan

Indigo is solubilized through the reducing action of the microbiota that occurs during alkaline fermentation of composted leaves of *Polygonum tinctorium* L. (*sukumo*). However, the environmental effects on the microbiota during this treatment, as well as the mechanisms underlying the microbial succession toward stable state remain unknown. In this study, physicochemical analyses and Illumina metagenomic sequencing was used to determine the impact pretreatment conditions on the subsequent initiation of bacterial community transition and their convergence, dyeing capacity and the environmental factors critical for indigo reducing state during aging of *sukumo*. The initial pretreatment conditions analyzed included 60°C tap water (heat treatment: batch 1), 25°C tap water (control; batch 2), 25°C wood ash extract (high pH; batch 3) and hot wood ash extract (heat and high pH; batch 4), coupled with successive addition of wheat bran from days 5 to 194. High pH had larger impact than heat treatment on the microbiota, producing more rapid transitional changes from days 1 to 2. Although the initial bacterial community composition and dyeing intensity differed during days 2–5, the microbiota appropriately converged to facilitate indigo reduction from day 7 in all the batches, with *Alkaliphilus oremalandii*, *Amphibacillus*, *Alkalicella caledoniensis*, *Atopostipes suicloalis* and *Tissierellaceae* core taxa contributing to the improvement of when the dyeing intensity. This convergence is attributed to the continuous maintenance of high pH (day 1 ~) and low redox potential (day 2~), along with the introduction of wheat bran at day 5 (day 5~). PICRUSt2 predictive function profiling revealed the enrichment of phosphotransferease system (PTS) and starch and sucrose metabolism subpathways key toward indigo reduction. Seven NAD(P)-dependent oxidoreductases KEGG orthologs correlating to the dyeing intensity was also identified, with *Alkalihalobacillus macyae*, *Alkalicella caledoniensis*, and *Atopostipes suicloalis* contributing significantly toward the initiation of indigo reduction in batch 3. During the ripening period, the staining intensity was maintained by continuous addition of wheat bran and the successive emergence of indigo-reducing bacteria that also contributed to material circulation in the system. The above results provide insight into the interaction of microbial system and environmental factors in *sukumo* fermentation.

KEYWORDS

indigo reduction ecosystem, alkaline environment, alkaliphilic bacteria, alkaline treatment, convergence of microbiota

Introduction

Indigo fermentation is facilitated by the reducing function of a microbial community based on the natural fermentation. There are two sources of natural indigo dye, namely precipitated indigo (extracted indigo) and composted plants that contain indigo. Precipitated indigo has been used as a source of indigo dye in India, China, Southeast Asia, and Japan (Okinawa Prefecture) (Toyama et al., 1978; Li et al., 2019, 2022; Lopes et al., 2021). Since the microorganisms in the seeds are not associated with the precipitated indigo for fermentation, spontaneous initiation of indigo reduction can be time consuming. Therefore, for earlier initiation of indigo reduction, it is necessary to add a seed culture (e.g., previous fermentation fluid or materials extracted from plants) that contains substrates for microorganisms, chemicals that act as electron mediators or oxygen eliminators, and other materials that create suitable conditions that facilitate indigo reduction (Lopes et al., 2021). Whether indigo reduction depends on the fermentation batch remains uncertain since it is a natural fermentation. The most popular procedure for reducing indigo is *via* sodium dithionite (Etters, 1989), which is not environmentally friendly. Therefore, it is desirable to establish a highly reliable, and environmentally friendly fermentation method based on the fundamentals of microflora formation to induce indigo reduction especially when using extracted indigo.

Procedures involving the composting of plants that contain indigo have been previously performed in Europe (Clark et al., 1993; Padden et al., 2000; Osimani et al., 2012; Hartl et al., 2015; Milanović et al., 2017). The composting process increases indigo concentration compared with the concentrations of the input plant and is more suitable for preservation and transportations. In this case, seed cultures for the indigo-reducing fermentation are derived from composting materials. The seed culture would comprise post-composted plant debris, microbial metabolites, and dead microorganismal cells, which serve as the microbial substrates in the fermented liquor. The composted indigo plant *Polygonum tinctorium* L. (*sukumo*) is a traditional indigo-dyeing material in Japan (Aino et al., 2018; Nakagawa et al., 2021). Composting of indigo plant is performed on an indoor earthen floor and is initiated by adding water to a pile of the dried indigo plant leaves. This process takes approximately 100 days, wherein the appropriate turnover frequency and water addition of the pile are maintained to enable continuous aerobic microbial digestion; this process requires a trained craftsperson. The fermentation temperature (center temperature) of the piled indigo leaves is approximately 70°C. The *sukumo* production process produces indigo (indigotin) from the precursor indican *via* indoxyl.

The period from the fermentation preparation to indigo reduction initiation differs depending on the procedure and quality of raw materials. Transitional changes in the redox state of indigo may be related to changes in the microbiota, which is in turn, associated with the indigo reduction initiation, as previously have suggested using clone library analysis (Aino et al., 2010) and next-generation sequencing (Tu et al., 2019a,b, 2021; Lopes et al., 2021, 2022; Nakagawa et al., 2022). On days 0–1, oxygen metabolizable *Bacillaceae* (e.g., *Sutcliffiella cohnii*) and *Actinobacteria* (e.g., *Nocardiopsis ganjiahuensis*) appear, following which their numbers significantly decrease during days 2–10 as the redox potential (ORP) decreases due to their consumption of oxygen. From days 2 to 5, the more anaerobic conditions become favorable for *Bacillaceae* [e.g., *Amphibacillus indicireducens* (type strain: C40^T; Hirota et al., 2013a), *Amphibacillus iburiensis* (type strain: N314^T; Hirota et al., 2013b) and *Alkalihalobacillus* spp. (formerly *Bacillus* spp.; Nishita et al., 2017)], obligate anaerobes [e.g., *Alkalicella* spp. (formerly *Proteinivoraceae* or *Anaerobranca*) and *Alkaliphilus* spp.], and *Lactobacillales* [e.g., *Alkalibacterium psychrotolerans* (type strain: IDR2-2^T; Yumoto et al., 2004), *Alkalibacterium iburiense* (type strain: M3^T: Nakajima et al., 2005), and *Alkalibacterium indicireducens* (type strain: A11^T: Yumoto et al., 2008)], which begin to appear. Concomitant with these transitional changes in the microbiota, indigo reduction is initiated on days 4–7. The changing velocity of the microbiota is more rapid during the early period of fermentation then the later periods, e.g., later than day 20 (Okamoto et al., 2017; Tu et al., 2021). At a later phase (e.g., later than day 100), wheat bran decomposers [e.g., *Amphibacillus* spp. and *Polygonibacillus* spp. (Hirota et al., 2016, 2020)] and/or obligate anaerobes (e.g., *Proteinivoraceae* and/or *Anerobacillus*) become the dominant members in the fermentation fluids (Okamoto et al., 2017; Tu et al., 2021).

Appropriate selection for the initial microbial community is essential for the earlier initiation of indigo reduction since the microbiota of *sukumo* are different from that of the fermentation fluid (Tu et al., 2019a, 2021). The initial preparation procedure differs based on the craft center. Therefore, a standard procedure for the preparation of indigo fermentation remains lacking. For example, one craftsperson may treat *sukumo* with room temperature wood ash extract, while another may use hot water at the beginning. However, treating *sukumo* with hot wood ash extract (60°C–70°C, pH > 10.5) has been commonly conducted. Although the initial condition for fermentation is important for the early initiation of indigo reduction, the influence of environmental factors on the initial treatment for the transitional changes of microbial community in the fermentation fluid remains unclear.

Indigo fermentation employing *sukumo* is performed by natural fermentation. Therefore, it is difficult to prepare the same fermentation fluid in the microbiota due to subtle differences in pH and temperature producing different microbial communities. However, fermentation fluids with different microbiota proceed to the indigo-reducing state using the appropriate maintenance procedures (e.g., maintaining pH and gently stirring the fluid once a day). In addition, indigo fermentation includes two different phases regardless of their preparations (Tu et al., 2021). Appropriately prepared and maintained indigo fermentation fluid exhibits exquisite robustness that retains the indigo dyeing function for more than 1 year, even with continuous fabric dyeing in an open-air environment. Although the continuous presence of indigo reducing bacteria has been previously reported (Okamoto et al., 2017; Tu et al., 2021), the relationship between the environmental factors, dyeing intensity, and core indigo reducing bacteria base on the aging state remains to be determined.

Therefore, in this study, we determined the selective factors for the microbiota involved in the raw material among 4 different methods. Herein, we show that the microbiota exhibited independent feature based on each pretreatment. In addition, the intensity of the transitional change in the microbiota influenced by the pH maintenance is larger based on pretreatment with high pH and low redox potential, while introduction of wheat bran converges the microbiota to facilitate indigo reduction. Furthermore, we analyzed the relationship between indigo reduction and existing taxa in the fluid and their predicted functions. Analyzing the relationship between the environmental factors and the microbiota's transitions under extreme conditions provides insights into the complex microbial for better management.

Materials and methods

Preparation of indigo fermentation fluid

Four different small-scale batches were prepared to evaluate the effect of the initial treatment of *sukumo* (produced by A.S. Tokushima, Shikoku, Japan) on indigo reduction initiation. *Sukumo* (76 g/batch) was treated with 60°C tap water (heat treatment alone, batch 1), 25°C tap water [neither heat nor high alkaline treatment, batch 2 (control)], 25°C wood ash extract (pH ≥ 11.0; high alkaline treatment alone, batch 3), and 60°C wood ash extract (both heat and high alkaline treatments, batch 4) at half volume (500 ml) for preparation. The next day, another half volume of 25°C wood ash extract (500 ml) was added to each batch (day 1). The wood ash extract was prepared by immersing 380 g wood ash (*Quercus phillyraeoides* A. Gray, Nagomi Co., Gobo, Wakayama, Japan) into 5 l tap water. The solution was boiled for 10 min and then the supernatant was extracted and used for the aiming temperature after the wood ash settled in the water. Triplicate batches were prepared to confirm the difference in the initiation of indigo reduction and changes in the dyeing intensity based on the initial preparation.

Maintenance procedure of indigo fermentation and sampling

The fermentation batches were kept at 26°C in a temperature-regulated room and gently stirred once a day using a laboratory spoon with a top width of 30 mm, to prevent the localization of acid produced by the bacteria in the fermentation fluid. Wheat bran (1 g) was added on days 5, 19, 51, 85, and 194. The pH and redox potential (ORP) of the fermentation fluids were measured with a D-71 pH meter (Horiba, Kyoto, Japan) and a D-75 pH/ORP/CO meter (Horiba), respectively. The pH of the fermentation fluid was maintained between 9.67 and 11.2 using $Ca(OH)_2$ to increase pH. The reducing state was tested by the dying ability of the fermentation fluid after dipping a small piece of cotton cloth into the fluid for 1 min and exposing it to air. After 2–5 min, the cloth was rinsed and dried. Dyeing intensity was measured by scanning the dyed cloth and analyzing the image using Mathematica (version 12.2). The intensity was expressed as $L^*a^*b^*$ value, which is the square root of $L^{*2}+a^{*2}+b^{*2}$ in International Commission on Illumination and its System Colorimetry (CIE) $L^*a^*b^*$ color space where $L^*a^*b^*$ color space, L^* represents lightness, and a^* and b^* represent chromaticity, which indicates hue and saturation, respectively. The extension of a^* and b^* indicates color direction as follows: a^*, red; $-a^*$, green; b^*, yellow; and $-b^*$, the blue. Before sampling, the fluid was stirred using a laboratory spoon to homogenize the fluid, and 700 µL aliquots were collected and stored in 35% (w/v) glycerol at −80°C until use.

Illumina MiSeq sequencing

For DNA extraction, the FastDNA™ Spin kit for soil (MP Biomedicals, Santa Ana, CA, USA) was used according to the manufacturer's instructions. The bacterial 16S rRNA gene sequence of the V3–V4 region (341F–805R) was amplified using the primer pair (5′-3′): V3V4f_MIX (ACACTCTTTCCCTACACGACGACGCTC TTCC-GATCT-NNNNN-CCTACGGG-NGGCWGCAG) and V3V4r_ MIX(GTGACTGGAGTTCAGACGTG-TGCTCTTCCGATCT-NNNNN-GACTACHVGGGTATCTAATCC) purchased from Bioengineering Lab. Co. Ltd. (Sagamihara, Kanagawa, Japan). The primers consisted of an overhang necessary for the 2nd PCR, 0–5 bases of random sequences (described as N; adaptor), and a gene-specific sequence necessary for the amplification of 16S rRNA. The random sequences were used for quality control. The PCR solution (40 µL) consisted of 4 µL of 10× Ex buffer (TaKaRa Bio, Otsu, Shiga, Japan), 3.2 µL dNTPs (TaKaRa Bio), 2 µL each of the forward and reverse primers, 2 ng extracted DNA sample, and 0.4 µL of 5 U/ml Ex Taq polymerase (TaKaRa Bio). The cycling conditions were as follows: 94°C for 2 min; 25–35 cycles of 94°C for 30 s, 55°C for 30 s, and 72°C for 30 s; extension of 72°C for 5 min. The amplification products were purified using the QIAquick PCR Purification Kit (Qiagen, Mississauga, ON, Canada) following the manufacturer's instructions. Product identity and quality were confirmed by agarose gel electrophoresis.

For next generation sequencing (NGS) analysis, the first PCR products were submitted to Bioengineering Lab. Co. Ltd. (Sagamihara, Kanagawa, Japan). The second PCR was performed with index-adapted primers to generate paired-end libraries (2 × 300 bp) for NGS using the MiSeq platform (Illumina, San Diego, CA, United States) and the MiSeq reagent kit v3 (Illumina).

Sequencing data analysis

The 1st sequence primers and N-sequences were removed from the resulting gene sequences using Cutadapt version 1.18, the fastq files obtained from NGS were processed using QIIME2 ver. 2020.2 (Bolyen et al., 2019). Paired end read merge, quality control, and creation amplicon sequence variants (ASVs) were performed using DADA2 (Callahan et al., 2016). Taxonomic classification was conducted using the feature-classifier for the 16S rRNA gene sequence based on the primer pair of 341F–805R created based on the Silva database (Quast et al., 2013; Yilmaz et al., 2014). For updated taxonomic identification, representative sequences were used for a BLAST search in National Center for Biotechnology Information (NCBI[1]) (Miura et al., 2019). Rarefaction curves of observed Operational Taxonomic Units (OTUs) and Shannon index of diversity (Shannon, 1948) were plotted according to the QIIME2 alpha diversity script. Linear discriminant analysis (LDA) effect size (LEfSe) was conducted to identify the biomarkers for each batch by the Galaxy of Huttenhower Lab.[2] Redundancy analysis (RDA) between the microbial community and environmental parameters was performed with R package (vegan ver. 2.6–4, ggrepel ver. 0.9.2, ggplot2 ver. 3.4.0, ggpubr ver. 0.5.0). Networks of the bacterial community based on the relative content change trend was analyzed as previously described (Tu et al., 2021). Predictive functions of the metagenomes were estimated using PICRUSt2 (Douglas et al., 2020). Based on the PICRUSt2 and QIIME2 results, taxa-functional relationships were analyzed using BURRITO (McNally et al., 2018). Correlation coefficient between changes in dyeing intensity of samples and corresponding changes in the intensity of the KEGG ortholog in "pred metagenome unstrat" file produced by the PICRUSt2 results was estimated.

1 https://blast.ncbi.nlm.nih.gov/Blast.cgi

2 https://huttenhower.sph.harvard.edu/galaxy/

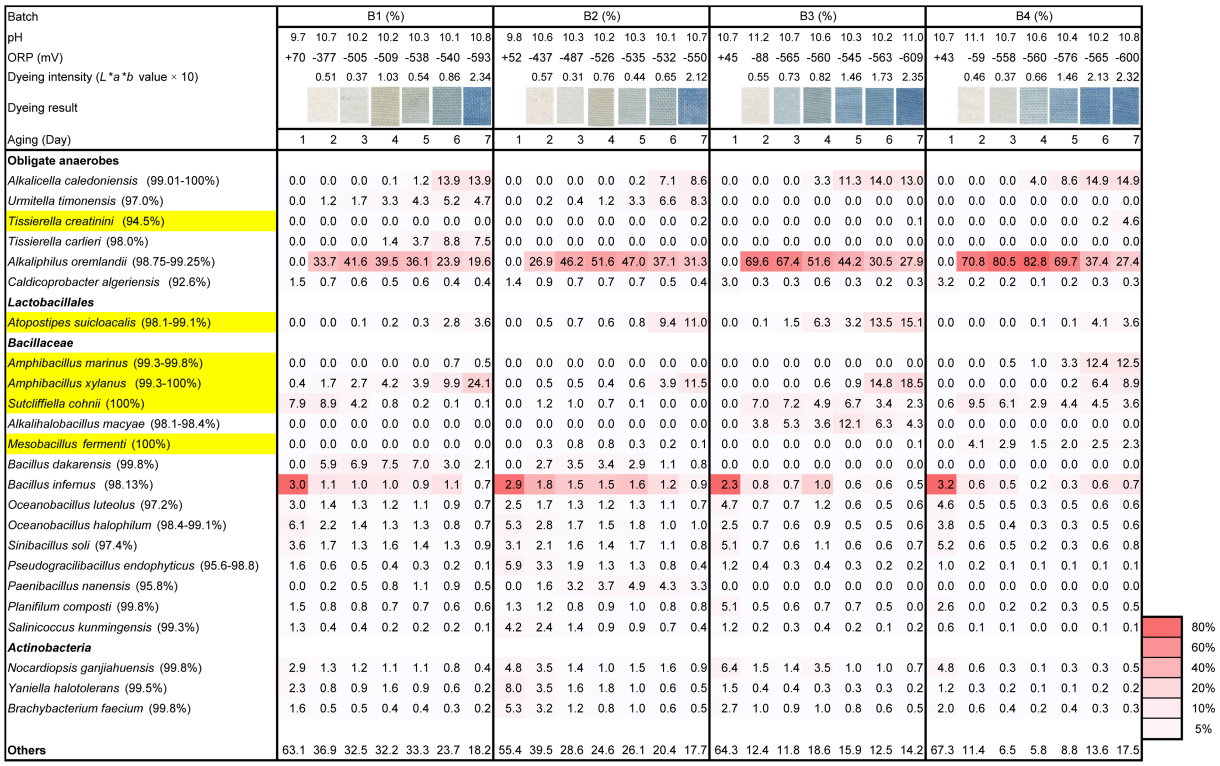

Batch	B1 (%)							B2 (%)							B3 (%)							B4 (%)						
pH	9.7	10.7	10.2	10.2	10.3	10.1	10.8	9.8	10.6	10.3	10.2	10.3	10.1	10.7	10.7	11.2	10.7	10.6	10.3	10.2	11.0	10.7	11.1	10.7	10.6	10.4	10.2	10.8
ORP (mV)	+70	-377	-505	-509	-538	-540	-593	+52	-437	-487	-526	-535	-532	-550	+45	-88	-565	-560	-545	-563	-609	+43	-59	-558	-560	-576	-565	-600
Dyeing intensity (*L*a*b* value × 10)		0.51	0.37	1.03	0.54	0.86	2.34		0.57	0.31	0.76	0.44	0.65	2.12		0.55	0.73	0.82	1.46	1.73	2.35		0.46	0.37	0.66	1.46	2.13	2.32
Dyeing result																												
Aging (Day)	1	2	3	4	5	6	7	1	2	3	4	5	6	7	1	2	3	4	5	6	7	1	2	3	4	5	6	7
Obligate anaerobes																												
Alkalicella caledoniensis (99.01-100%)	0.0	0.0	0.0	0.1	1.2	13.9	13.9	0.0	0.0	0.0	0.0	0.2	7.1	8.6	0.0	0.0	0.0	3.3	11.3	14.0	13.0	0.0	0.0	0.0	4.0	8.6	14.9	14.9
Urmitella timonensis (97.0%)	0.0	1.2	1.7	3.3	4.3	5.2	4.7	0.0	0.2	0.4	1.2	3.3	6.6	8.3	0.0	0.0	0.0	0.0	0.0	0.0	0.0	0.0	0.0	0.0	0.0	0.0	0.0	0.0
Tissierella creatinini (94.5%)	0.0	0.0	0.0	0.0	0.0	0.0	0.0	0.0	0.0	0.0	0.0	0.0	0.0	0.2	0.0	0.0	0.0	0.0	0.0	0.0	0.1	0.0	0.0	0.0	0.0	0.0	0.2	4.6
Tissierella carlieri (98.0%)	0.0	0.0	0.0	1.4	3.7	8.8	7.5	0.0	0.0	0.0	0.0	0.0	0.0	0.0	0.0	0.0	0.0	0.0	0.0	0.0	0.0	0.0	0.0	0.0	0.0	0.0	0.0	0.0
Alkaliphilus oremlandii (98.75-99.25%)	0.0	33.7	41.6	39.5	36.1	23.9	19.6	0.0	26.9	46.2	51.6	47.0	37.1	31.3	0.0	69.6	67.4	51.6	44.2	30.5	27.9	0.0	70.8	80.5	82.8	69.7	37.4	27.4
Caldicoprobacter algeriensis (92.6%)	1.5	0.7	0.6	0.5	0.6	0.4	0.4	1.4	0.9	0.7	0.7	0.7	0.5	0.4	3.0	0.3	0.3	0.6	0.3	0.2	0.3	3.2	0.2	0.2	0.1	0.2	0.3	0.3
Lactobacillales																												
Atopostipes suicloacalis (98.1-99.1%)	0.0	0.0	0.1	0.2	0.3	2.8	3.6	0.0	0.5	0.7	0.6	0.8	9.4	11.0	0.0	0.1	1.5	6.3	3.2	13.5	15.1	0.0	0.0	0.0	0.1	0.1	4.1	3.6
Bacillaceae																												
Amphibacillus marinus (99.3-99.8%)	0.0	0.0	0.0	0.0	0.0	0.7	0.5	0.0	0.0	0.0	0.0	0.0	0.0	0.0	0.0	0.0	0.0	0.0	0.0	0.0	0.0	0.0	0.0	0.5	1.0	3.3	12.4	12.5
Amphibacillus xylanus (99.3-100%)	0.4	1.7	2.7	4.2	3.9	9.9	24.1	0.0	0.5	0.5	0.4	0.6	3.9	11.5	0.0	0.0	0.0	0.6	0.9	14.8	18.5	0.0	0.0	0.0	0.0	0.2	6.4	8.9
Sutcliffiella cohnii (100%)	7.9	8.9	4.2	0.8	0.2	0.1	0.1	0.0	1.2	1.0	0.7	0.1	0.0	0.0	0.0	7.0	7.2	4.9	6.7	3.4	2.3	0.6	9.5	6.1	2.9	4.4	4.5	3.6
Alkalihalobacillus macyae (98.1-98.4%)	0.0	0.0	0.0	0.0	0.0	0.0	0.0	0.0	0.0	0.0	0.0	0.0	0.0	0.0	0.0	3.8	5.3	3.6	12.1	6.3	4.3	0.0	0.0	0.0	0.0	0.0	0.0	0.0
Mesobacillus fermenti (100%)	0.0	0.0	0.0	0.0	0.0	0.0	0.0	0.0	0.3	0.8	0.8	0.3	0.2	0.1	0.0	0.0	0.0	0.0	0.0	0.0	0.1	0.0	4.1	2.9	1.5	2.0	2.5	2.3
Bacillus dakarensis (99.8%)	0.0	5.9	6.9	7.5	7.0	3.0	2.1	0.0	2.7	3.5	3.4	2.9	1.1	0.8	0.0	0.0	0.0	0.0	0.0	0.0	0.0	0.0	0.0	0.0	0.0	0.0	0.0	0.0
Bacillus infernus (98.13%)	3.0	1.1	1.0	1.0	0.9	1.1	0.7	2.9	1.8	1.5	1.5	1.6	1.2	0.9	2.3	0.8	0.7	1.0	0.6	0.6	0.5	3.2	0.6	0.5	0.2	0.3	0.6	0.7
Oceanobacillus luteolus (97.2%)	3.0	1.4	1.3	1.2	1.1	0.9	0.7	2.5	1.7	1.3	1.2	1.3	1.1	0.7	4.7	0.7	0.7	1.2	0.6	0.5	0.6	4.6	0.5	0.5	0.3	0.5	0.6	0.6
Oceanobacillus halophilum (98.4-99.1%)	6.1	2.2	1.4	1.3	1.3	0.8	0.7	5.3	2.8	1.7	1.5	1.8	1.0	1.0	2.5	0.7	0.6	0.9	0.5	0.5	0.6	3.8	0.5	0.4	0.3	0.3	0.5	0.6
Sinibacillus soli (97.4%)	3.6	1.7	1.3	1.6	1.4	1.3	0.9	3.1	2.1	1.6	1.4	1.7	1.1	0.8	5.1	0.7	0.6	1.1	0.6	0.6	0.7	5.2	0.6	0.5	0.2	0.3	0.6	0.8
Pseudogracilibacillus endophyticus (95.6-98.8)	1.6	0.6	0.5	0.4	0.3	0.2	0.1	5.9	3.3	1.9	1.3	1.3	0.8	0.4	1.2	0.4	0.3	0.4	0.3	0.2	0.2	1.0	0.2	0.1	0.1	0.1	0.1	0.1
Paenibacillus nanensis (95.8%)	0.0	0.2	0.5	0.8	1.1	0.9	0.5	0.0	1.6	3.2	3.7	4.9	4.3	3.3	0.0	0.0	0.0	0.0	0.0	0.0	0.0	0.0	0.0	0.0	0.0	0.0	0.0	0.0
Planifilum composti (99.8%)	1.5	0.8	0.8	0.7	0.7	0.6	0.6	1.3	1.2	0.8	0.9	1.0	0.8	0.8	5.1	0.5	0.6	0.7	0.7	0.5	0.0	2.6	0.0	0.2	0.2	0.3	0.5	0.5
Salinicoccus kunmingensis (99.3%)	1.3	0.4	0.4	0.2	0.2	0.2	0.1	4.2	2.4	1.4	0.9	0.9	0.7	0.4	1.2	0.2	0.3	0.4	0.2	0.1	0.2	0.6	0.1	0.1	0.0	0.0	0.1	0.1
Actinobacteria																												
Nocardiopsis ganjiahuensis (99.8%)	2.9	1.3	1.2	1.1	1.1	0.8	0.4	4.8	3.5	1.4	1.0	1.5	1.6	0.9	6.4	1.5	1.4	3.5	1.0	1.0	0.7	4.8	0.6	0.3	0.1	0.3	0.3	0.5
Yaniella halotolerans (99.5%)	2.3	0.8	0.9	1.6	0.9	0.6	0.2	8.0	3.5	1.6	1.8	1.0	0.6	0.5	1.5	0.4	0.4	0.3	0.3	0.3	0.2	1.2	0.3	0.2	0.1	0.1	0.2	0.2
Brachybacterium faecium (99.8%)	1.6	0.5	0.5	0.4	0.4	0.3	0.2	5.3	3.2	1.2	0.8	1.0	0.6	0.5	2.7	1.0	0.9	1.0	0.8	0.6	0.5	2.0	0.6	0.4	0.2	0.4	0.3	0.3
Others	63.1	36.9	32.5	32.2	33.3	23.7	18.2	55.4	39.5	28.6	24.6	26.1	20.4	17.7	64.3	12.4	11.8	18.6	15.9	12.5	14.2	67.3	11.4	6.5	5.8	8.8	13.6	17.5

FIGURE 1
Changes in the relative abundance (%) of bacterial communities (≥ 4.1% in any sample) based on 16S rRNA analysis, dyeing intensity (dyeing result and *L*a*b** value), ORP, and pH during days 1–7 following different initial treatments of *sukumo*. B1: batch 1 (*sukumo* treated with 60°C tap water); B2: batch 2 (*sukumo* treated with 25°C tap water [control]); B3: batch 3 (*sukumo* treated with 25°C wood ash extract); B4: batch 4 (control; *sukumo* treated with 60°C wood ash extract). Yellow marked taxa indicate the confirmed indigo-reducing taxa (including unpublished results). The percentages in the brackets indicate the similarities with the top hit taxa as revealed *via* a BLAST (blastn) search in NCBI.

Results

Changes in the microbial community during the early fermentation phase

From the 28 samples, 1,442,013 raw sequences were obtained, with an average of 51,500 sequences per sample (days 1–7) following fermentation preparation. After adapter trimming, and filtering for quality checking and chimeric exclusion, 687,015 sequences (average: 24,536 per sample) were obtained.

Triplicate experiments confirmed the reproducibility of initiation of indigo reduction based on the treatment of *sukumo*. Microbiota analysis was performed with one sample set. Although wood ash treatment produced only approximately one unit difference in pH (batches 3 and 4; pH 10.7) compared with tap water treatment (batches 1 and 2; pH 9.7–9.8), contents of "others" were much higher in batches 1 and 2 than those in batches 3 and 4 after day 2. "Others" represents the sum of taxa present in less than 4.1% of all the samples (miscellaneous taxa), indicating that initial exposure of the microbial community in *sukumo* at approximately one unit higher than pH 9.7–9.8 strongly converged the microflora. However, the differences in the content of "others" were not observed between batches 1 and 2 on day 2, suggesting that heat treatment of 60°C of tap water was not very effective in converging the microflora. The lowest percentage of "others" (5.8%) and the highest percentage of the relative abundance of obligate anaerobic *Alkaliphilus oremlandii* (similarity: 98.8%–99.3%; abundance: 82.8%) in batch 4 at day 4 were observed (Figure 1). Moreover, the highest percentage of "others" (41.4%) and the lowest percentage of the relative abundance of *A. oremlandii* in batch 2 on day 2 were observed. The higher abundance (>50%) of *A. oremlandii* in batch 4 continued longer than in the other batches. These results suggest a strong relationship between the selection intensity of existing microorganisms in *sukumo* and relative abundance of obligate anaerobes in the initial treatment and the successive environmental changes.

The effect of the initial high pH treatment that was maintained was more pronounced in batches 2 and 4 than 1 and 2. However, the abundance of the alkaliphilic obligate anaerobic bacterium *A. oremlandii* was increased until days 3 and 4 in batches 3 and 4, respectively. In addition, the ratio of "others" decreased until day 4 in batch 4. Considering the ratio of "others," which constitute miscellaneous low ratio constituent microorganisms, the converging effect for the microbial community was further enhanced in batches 1 and 2 by the addition of wheat bran on day 5.

Considering the rapid decrease in ORP, the remaining microorganisms in batches 1 and 2 after the preparation consumed oxygen more rapidly than those in batches 3 and 4 (Figure 1, Supplementary Figure S1A). Meanwhile, a pH of 11.2 in batch 3 and 11.1 in batch 4 deterred the metabolism of oxygen metabolizable microorganisms (Supplementary Figure S1B). However, the selected microorganisms of the initial treatments in batches 3 and 4 produced acid, which reduced the pH and allowed them to consume oxygen.

The earliest initiation of indigo reduction was observed in batch 3. The appearance of *Alkalihalobacillus macyae* (similarities: 98.1%–98.4%;

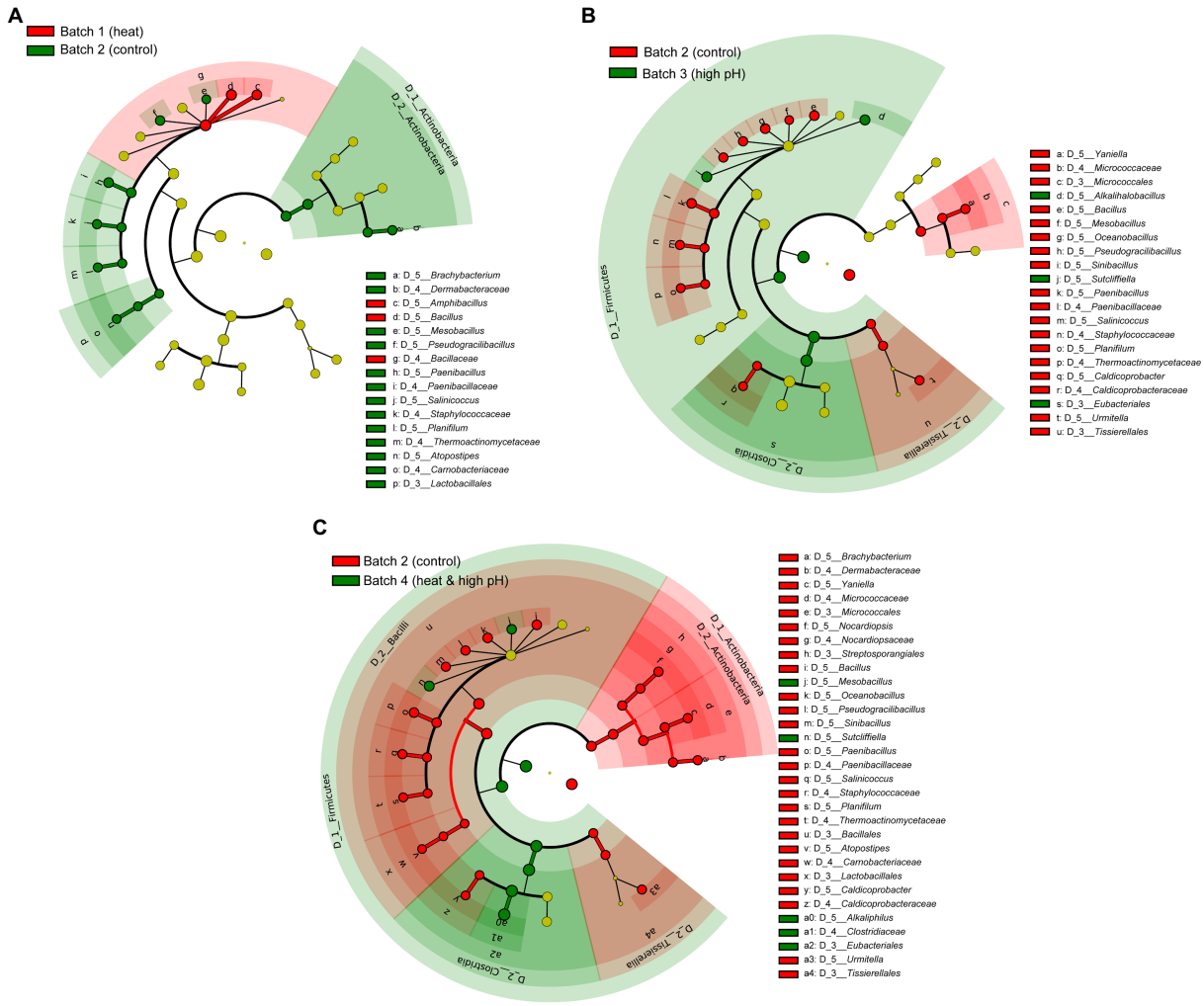

FIGURE 2
Bacterial markers of differently treated *sukumo* during days 2–5 following different initial treatments. **(A)** comparison between B1: batch 1 (*sukumo* treated with 60°C tap water) and B2: batch 2 (*sukumo* treated with 25°C tap water [control]). **(B)** comparison between B2 and B3: batch 3 (*sukumo* treated with 25°C wood ash extract) **(C)** comparison between B2 and B4: batch 4 (sukumo treated with 60°C wood ash extract). The LDA effect size (LEfSe) analysis was performed to identify the markers for each group (significant when LAD score > 3.6).

content ratio: 5.3%) on day 3 in batch 3 was considered a contributing factor to the earlier indigo reduction. Initiation of indigo reduction was observed following the appearance of *Alkalicella caledoniensis* (formerly *Proteinivoraceae*; 99.0%–100%; Tu et al., 2019b) in batches 1, 2, and 4. Indigo reduction was initiated on day 6 in batches 1 and 2. The appearance of *Tissierella* spp., *Amphibacillus* spp., and *Atopostipes* spp. may also contribute to the initiation of the indigo reduction. Although characterizations of these taxa were our unpublished results, these bacteria are indigo-reducing bacteria. This conversion effect by continuous high pH and low ORP was reflected in the ratio of "others" on day 7.

Comparison of microbiota based on the heat or/and high pH treatment during days 2–5

Differences in the microbiota due to treatment method of *sukumo* was most noticeable from day 2, when the effect of treatment began, prior to the effect of adding wheat bran, which appeared after day 6. Biomarker detection in each treatment batch was performed during days 2–5 (Figure 2). Heat treated (60°C) batch 1 compared with non-treated batch 2 showed that *Actinobacteria* (*Brachybacterium*), *Bacillaceae* (*Mesobacillus*, *Pseudogracillibacillus*, *Paenibacillus*, *Salinicoccus*, and *Planifilum*), and *Lactobacillales* (*Atopostipes*) were inhibited by treatment, while *Amphibacillus* (*Bacillaceae*) was enhanced (Figure 2A). High pH (pH ≥ 11.0) treated batch 3 compared with batch 2 showed that *Actinobacteria* (*Yaniella*), *Bacillaceae* (*Bacillus*, *Mesobacillus*, *Oceanobacillus*, *Pseudogracillibacillus*, *Sinibacillus*, *Paenibacillus*, *Salinicoccus*, *Planifilum* and *Thermoactinomyce*), and *Caldicoprobacteraceae* (*Caldicoprobacter*) were inhibited by the alkaline treatment, while *Bacillaceae* (*Alkalihalobacillus* and *Sutcliffiella*) and *Eubacteriales* were enhanced (Figure 2B). Heat and high pH treated batch 4 compared with batch 2 showed wider range of inhibited taxa compared with alkaline treatment (Figure 2C). Indeed, *Actinobacteria* (*Brachybacterium* and *Nocardiopsis*), *Bacillaceae* (*Paenibacillus*) and *Lactobacillales* (*Atopostipes*) were further inhibited compared with alkaline treatment alone; meanwhile, *Mesobacillus*, *Sutcliffiella*, and

10.3389/fmicb.2023.1097595

Batch	B2 (%)						B3 (%)						B4 (%)					
pH	10.5	11.0	10.5	10.5	11.4	9.6	10.7	10.9	10.6	10.5	10.7	9.7	10.5	10.9	10.5	10.6	10.8	10.1
ORP (mV)	-583	-608	-594	-607	-657	-562	-610	-624	-601	-614	-644	-580	-583	-620	-600	-611	-640	-582
Dyeing intensity (*L*a*b* value × 10)	2.36	2.41	1.73	2.11	2.10	2.12	2.47	2.46	1.82	1.99	2.25	2.02	2.62	2.38	1.41	1.99	2.06	2.26
Dyeing result																		
Aging (Day)	10	16	29	49	75	209	10	16	29	49	75	209	10	16	29	49	75	209
Obligate anaerobes																		
Alkalicella caledoniensis (99.01-100%)	17.8	13.3	13.3	12.4	11.5	1.4	14.7	16.2	16.3	17.7	19.2	3.9	20.6	16.5	15.5	10.8	13.3	5.0
Urmitella timonensis (97.0%)	4.4	2.0	0.8	0.6	0.2	0.2	0.0	0.0	0.0	0.0	0.0	0.1	0.0	0.0	0.0	0.0	0.0	0.0
Tissierella creatinini (94.5%)	3.7	7.4	9.0	6.9	9.4	4.5	1.4	10.6	3.2	4.0	4.9	5.0	9.3	2.5	10.4	12.2	9.9	5.1
Alkaliphilus oremlandii (98.8-99.3%)	27.4	17.3	12.4	8.9	8.2	2.1	23.7	6.8	14.3	11.4	14.5	1.9	14.1	18.7	3.1	1.9	1.1	0.4
Rhabdanaerobium thermarum (92.6%)	0.0	1.0	2.8	5.8	3.1	0.8	0.0	1.0	9.1	4.5	3.7	0.8	0.0	0.1	10.0	9.3	3.1	0.8
Clostridium septicum (89.0%)	0.0	0.1	3.5	3.4	1.4	3.7	0.0	3.7	2.0	2.6	2.0	1.1	3.2	0.2	4.4	3.9	4.1	3.5
Erysipelotrichaceae																		
Erysipelothrix inopinata (93.2%)	0.0	0.0	0.0	0.0	0.0	2.1	0.0	0.0	0.0	0.0	0.0	3.3	0.0	0.0	0.0	0.0	0.0	7.1
Lactobacillales																		
Enterococcus gallinarum (99.8-100%)	0.5	1.0	9.9	16.9	6.6	0.1	0.0	0.0	5.6	13.5	11.5	0.0	0.0	1.0	3.3	6.9	8.3	0.1
Atopostipes suicloacalis (98.1-99.1%)	8.6	12.1	8.2	4.0	4.0	0.4	11.1	3.7	6.5	6.5	3.8	1.0	4.1	9.6	4.7	8.7	6.7	1.3
Alkalibacterium pelagium (100%)	0.0	0.0	0.0	0.0	0.2	9.4	0.0	0.0	0.0	0.0	0.1	2.6	0.0	0.0	0.0	0.0	0.3	5.2
Alkalibacterium iburiense (99.1-100%)	0.0	0.1	2.5	4.2	5.3	3.7	0.0	0.0	0.0	0.0	0.4	2.3	0.0	0.0	0.0	0.5	4.0	3.0
Bacillaceae																		
Amphibacillus marinus (99.3-99.8%)	0.0	0.0	0.0	0.0	0.0	0.0	0.0	5.1	0.3	0.3	0.1	0.0	6.0	0.0	2.5	1.1	0.5	0.0
Amphibacillus indicireducens (99.8-100%)	0.0	0.0	0.0	0.0	4.0	16.2	0.0	1.6	0.0	0.0	1.9	5.0	0.9	0.0	0.8	2.6	2.3	8.9
Amphibacillus xylanus (99.3-100%)	11.3	6.7	3.1	9.9	1.1	6.6	28.3	19.6	21.2	15.6	5.0	1.7	14.2	27.4	15.4	11.1	8.6	2.8
Pseudogracilibacillus endophyticus (95.6-98.8%)	0.3	0.3	0.3	0.1	0.1	0.0	0.2	0.2	0.2	0.1	0.2	3.4	0.1	0.3	0.2	0.1	0.1	7.1
Pseudogracilibacillus marinus (95.3%)	0.0	0.0	0.0	0.4	0.1	0.0	0.0	0.0	0.0	3.0	3.2	0.2	0.0	0.0	0.0	2.0	6.3	0.6
Pseudogracilibacillus auburnensis (98.8%)	0.0	0.0	0.0	0.0	0.0	0.0	0.0	0.0	0.0	0.0	0.0	2.3	0.0	0.0	0.0	0.0	0.0	4.3
Actinobacteria																		
Yaniella halotolerans (99.5%)	0.5	2.1	4.4	1.7	0.8	0.1	0.2	0.4	0.6	1.8	1.7	0.2	0.2	0.2	2.1	2.4	1.8	0.3
Corynebacterium efficiens (99.5%)	0.0	0.0	0.0	0.0	0.1	1.4	0.0	0.0	0.0	0.0	0.0	6.6	0.0	0.0	0.0	0.0	0.0	3.8
Proteobacteria																		
Halopseudomonas pertucinogena (97.7%)	0.0	0.0	0.0	0.0	0.0	9.0	0.0	0.0	0.0	0.0	0.0	3.7	0.0	0.0	0.0	0.0	0.0	2.2
Alcaligenes aquatilis (99.5%)	0.0	0.0	0.0	0.0	0.0	13.8	0.0	0.0	0.0	0.0	0.0	32.7	0.0	0.0	0.0	0.0	0.0	18.0
Pusillimonas ginsengisoli (97.4%)	0.0	0.0	0.0	0.0	0.0	2.4	0.0	0.0	0.0	0.0	0.0	5.6	0.0	0.0	0.0	0.0	0.0	5.9
Others	25.6	36.6	29.8	24.8	44.0	22.2	20.3	31.0	20.6	18.9	27.7	16.6	27.2	23.4	27.5	26.5	29.6	14.6

30%
20%
10%
5%

FIGURE 3
Changes in the relative abundance (%) of bacterial communities (≥ 4.1% in any sample) based on 16S rRNA analysis, dyeing intensity (dyeing result and *L*a*b** value), ORP, and pH during days 10–209 following different initial treatments of *sukumo*. B2: batch 2 (*sukumo* treated with 25°C tap water [control]); B3: batch 3 (*sukumo* treated with 25°C wood ash extract); B4: batch 4 (*sukumo* treated with 60°C wood ash extract). Yellow marked taxa indicate the confirmed indigo-reducing taxa (including unpublished results). The percentages in the brackets indicate the similarities with the top hit taxa as revealed *via* a BLAST (blastn) search in NCBI.

Eubacteriales (*Alkaliphilus*) were enhanced by the treatment. Therefore, high pH treatment had larger impact than heat treatment on microbiota, while heat combined with high pH treatment showed the biggest impact on microbiota among the three treatments.

Changes in the microbial community in the stable and aged states of fermentation

Since batches 1 and 2 showed similar changes in their microbiota on 7, we focused on batches 2, 3 and 4 from days 10–209 for subsequent microbiota analysis. A total of 873,986 raw sequences were obtained from a total of 18 samples (average: 48,555/sample), one from each day (days 10–209) after fermentation preparation. After adapter trimming, filtering for quality checking, and chimeric exclusion, 353,688 sequences (average: 19,649/sample) were obtained.

The batches exhibited clear dyeing on day 7 and further strong dyeing on day 10. This may be attributed to the effect of the maintained high pH from day 2, low ORP, and the introduction of wheat bran on day 5 across all batches. Consequently, all three batches exhibited relatively strong dyeing intensity and the constituents in the microbiota were relatively similar after day 10, indicating that all the batches reached a stable state for indigo reduction in fermentation, regardless of the initial treatment.

Although no strong selection was observed in batch 2 on day 0 compared with the other batches, the microbiota converged appropriately on day 7 due to the continuously high pH starting on day 2 with the addition of $Ca(OH)_2$, low ORP and wheat bran. Furthermore, the establishment of desirable microbiota was observed on day 10, and relatively similar microbiota among the batches was observed on day 75 in this batch (Figure 3). The microbiota in batch 2 were mainly comprised of *A. caledoniensis* (similarity: 99.0%–100%; abundance ratio: 11.5%–17.8% on days 10–75), *A. oremlandii* (similarity: 98.8%–99.3%; abundance ratio: 8.2%–27.4% on days 10–75), *Enterococcus gallinarum* (similarity: 99.8%–100%; abundance ratio: 6.6%–16.9% on days 29–75), *Atopostipes suicloacalis* (similarity: 98.1%–99.1%; abundance ratio: 4.0%–12.1% on days 10–49) and *Amphibacillus xylanus* (similarity: 99.3%–100%; abundance ratio: 3.1–11.3 on days 10–49). The microbiota

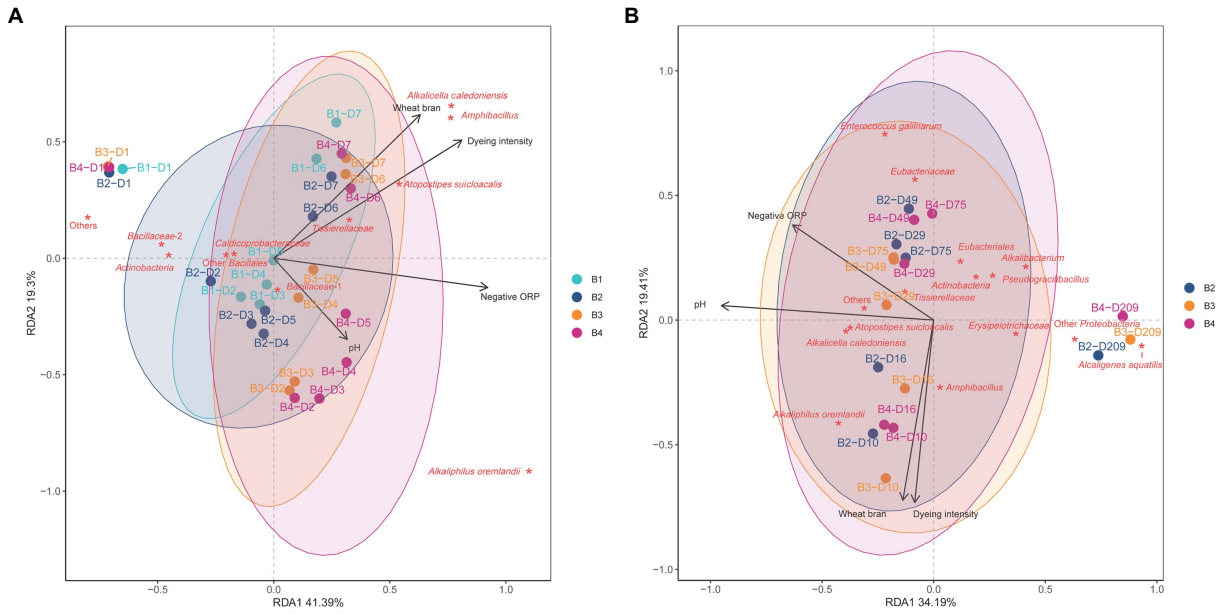

FIGURE 4
Redundancy analysis (RDA) of indigo fermentations during days 1–7 **(A)** and days 10–209 **(B)** following different initial treatments of *sukumo*. B1: batch 1 (*sukumo* treated with 60°C tap water); B2: batch 2 (*sukumo* treated with 25°C tap water [control]); B3: batch 3 (*sukumo* treated with 25°C wood ash extract); B4: batch 4 (*sukumo* treated with 60°C wood ash extract). The labels for samples indicate the batch number and the number of days of fermentation (B, batch; D, day). Red asterisks represent the core microbiota. Black arrows indicate different environmental factor. Wheat bran was considered an environmental factor given that it would be consumed within 1month. Percentages on the axes represent the eigenvalues of principal components. **(A)** *Bacillaceae*-1 contains *Sutcliffiella cohnii*, *Alkalihalobacillus macyae*, *Mesobacillus fermenti*, and *Bacillus dakarensis*; *Bacillaceae*-2 contain *Oceanobacillus*, *Sinibacillus*, and *Pseudogracilibacillus*; Other *Bacillales* contains *Paenibacillus* and *Salinicoccus kunmingensis*. **(B)** *Eubacteriaceae*: *Rhabdanaerobium thermarum* (92.6%); *Eubacteriales*: *Clostridium septicum* (89.0%).

of batch 2 was different with regards to the lower abundance ratio of *A. xylanus*, the earlier appearance of *Alkalibacterium iburiense* and the higher ratio of "others."

The microbiota of batch 3 was relatively similar to that of batch 4. However, the present ratio in *Tissierella creatini* (similarity: 94.5%) to *A. oremalandii* (similarity: 98.8%–99.3%) differed in the taxa comprising obligate anaerobes. Moreover, the ratio in the fluctuations of *A. xylanus* (similarity: 99.3%–100%) was also different.

On day 209, all three batches contained *Proteobacteria* in their microbiota, which comprised more than 20% in the microbiota ratio suggesting that although *sukumo* introduced Gram-positive bacteria into the fermentation system. However, Gram-negative bacteria exhibited superior adaptation ability compared with Gram-positive bacteria in the liquid environments. In addition, the ratio in *Alkalibacterium* spp. was increased, while other taxa existed categorized in *Lactobacillales* [e.g., *Atopostipes suicloacalis* and *Enterococcus gallinarum* (99.8%–100%)] were decreased. In the obligate anaerobes category, the ratio of preferred taxa on day 75 (e.g., *Alkakucella caledoniensis* and *Alkaliphilus oremlandii*) was decreased and facultative anaerobic *Erysipelotrichaceae* (93.2% similarity with *Erysipelothrix inopinate*) and *Corynebacterium efficiens* (similarity: 99.5%) appeared.

Changes in alpha diversities

Changes in alpha diversity at a sampling depth of 8,825 reads from the rarefaction curves based on the observed OTUs and Shannon index of the four batches are shown in Supplementary Figure S2. High alkaline treated batches 3 and 4 showed significant decreases in both the observed OTUs and Shannon index from days 1 to 2. Moreover, the decrease in these values by heat (60°C) treated batch 1 was not as intense as a high alkaline treatment (batches 3 and 4). Although the high pH treatment (batch 3) and both high pH and heat treatment (batch 4) were performed at the preparation of fermentation (day 0), the decrease in the diversity of microbial constituents continued until days 2 and 4, respectively. After the decrease in diversity, recovery was observed on days 3 and 5 in batches 3 and 4, respectively.

Although the Shannon index of batches 1 and 2 did not changed the diversity from days 3–7, the observed OTUs gradually decreased. Furthermore, the introduction of wheat brane caused a further decrease in the observed OTUs. Surprisingly, all the alpha-diversity of the four batches, except for observed OTUs in batch 1, converged to almost the same values. These results are comparable with the similar dyeing intensity among the four batches and the ratio changes of the "others."

Identification of environmental factors influencing the convergence of microbiota to indigo reducing state

The relationship between the changes in microbial communities among the three batches (batches 2–4) and the influence of environmental parameters were estimated using RDA (Figures 4A,B). The high impact of hot wood ash extract in batch 4 on microbiota was reflected in the distance between day 1 and after day 2 (Figure 4A). Meanwhile, the higher impact of the high pH in batch 3 compared with the heat treatment in batch 1 was reflected by the distances between days 1 and 2. Changes in microbiota of batch 1 was very similar that of the non-heat-treated batch 2. High pH treatment (batches 3 and 4) produced more rapid transitional changes from days 1 to 2. The microbiota treated with high pH was changed and

influenced by low ORP from day 2. However, susceptibility to low ORP decreased in batches 1 and 2 compared with 3 and 4. The changing velocity of each microbiota was lower during days 2–5 compared with until day 2. However, the velocity became increased by the wheat bran introduced at day 5. Although the microbiota of each batch was differed, the wheat bran strongly shifted the microbiota towered indigo reducing state from day 5. The contribution to indigo reducing state remains unknown, however the appearance of *Alkaliphilus oremlandii* is strongly linked to the high pH and low ORP. Furthermore, *Tissierellaceae*, *Atopostipes suicloacalis*, *Amphibacillus* and *Alkalicella caledoniensis* are core members at days 6–7 (Figure 4A). Batch 3 started indigo reduction on day 3, which was attributed to the contribution of *Bacillaceae*-1. Although the transitional change from days 1 to 5 of each batch differed, all day 7 positions were similar. This is comparable with the changes in the Shannon index of alpha diversity in the 4 batches converged to nearly the same values on day 7.

Relationship between changes in microbiota after day 10, environmental parameters, and related microorganisms

All batches exhibited similar changing tendencies from day 10 compared with the changes in days 1–7 (Figure 4B). The changing direction was the same with similar positioning of microbiota. Figure 4B shows that the change rate of microbiota was low based on the slow decomposing substrate, wheat bran, while the continuous introduction of the substrate is strongly associated with the maintenance of the dyeing intensity during the aging of each microbiota. However, the dyeing intensity gradually decreased with aging during fermentation. During the convergence of each microbiota toward an aging state, successive changes in several functional-redundant-indigo-reducing different taxa appeared and sustained indigo reduction for a long duration. Around day 29, *Alkaliphilus oremlandii*, *Amphbacillus Atopstipes suicloacalis*, and *Alcalicela caledoniensis* were the core bacteria that sustained this ecosystem. However, after day 29, in addition to *Atopstipes suicloacalis*, and *Alcalicela caledoniensis*, *Tissierellaceae* and *Alkalibacterium* were the core members in the microbiota. Meanwhile, after day 75, *Eubacteriaceae*, *Eubacteriales*, and *Enterococcus gallinarum* were added as the core members in the ecosystem, and at day 209, Gram-negative bacteria became the core members of the microbiota. The isolated positioning of the microbiota in this series of change to day 209 was in the opposite to the high pH, possibly due to local changes in pH of the fermentation fluid.

Microbial interaction network

We analyzed the interaction of existing bacteria on days 1–7 (Figure 5A) and 10–209 (Figure 5B) and found insignificance differences in the detail between the batches, with similar tendencies. Therefore, the results from batch 4 are presented as the representative. Firstly, a relatively strong network was constructed based on the survived oxygen-metabolizing taxa such the 3 taxa of *Actinobacteria* and *Sinibacillus*, and 2 taxa of *Oceanobacillus*, *Salinicoccus kunmingensis*, *Bacillus infernus*, *Planifilum composti* and *Caldicoprobacteraceae*. This initial network was destroyed by the high pH and the low ORP. Subsequently, *Msobacillus fermenti*, *Sutcliffiella cohnii* and *Alkaliphilus oremlandii* appeared. Toward an enhanced indigo reducing state at day 7, network consisted of 2 taxa of *Amphibacillus*, *Tissierellaceae*, *Atopstipes suicloacalis*, and *Alcalicela caledoniensis* was constructed. After day 10, the similar network, constructed until day 7, was succeeded; however, the inter positive relationship had weakened. The gravity of the network gradually moved to the latter stage as shown in Figure 5B. Networks containing Gram-negative bacteria established after day 75 were relatively strong.

Functional abundance for the initiation of indigo reduction

The predictive function of the metagenomes was estimated to clarify the prerequisite functional abundances for the initiation of indigo reduction. Since the initiation of indigo reduction was observed only in batch 3 on day 3, the functional abundance ratio between batch 3 and the other batches was estimated. The ratio in the functional subpathways containing a ratio > 1.05 in batch 3(B3)/batches 1(B1), B3/batch 2 (B2), or B3/batch 4 (B4) on day 3 are listed in Supplementary Figure S3. Among the presented subpathways, "phosphotransferase system (PTS)" and "starch and sucrose metabolisms" followed by "Prokaryotic defense system" and "nicotinate and nicotinamide metabolism" were identified. In addition, although their ratios are not very high, the subpathways related to the reconstitution of cellular functions and metabolism related to electron carriers and motility were also found.

Although the dyeing intensities during the initiation days were not always strong, batches 2–4 exhibited strong dyeing intensities compared with day 10. To understand the prerequisite functional subpathways that initiate dyeing, the functional abundance ratios of day 10 (beginning of intense dyeing)/day 2 (before initiation of dyeing) was estimated. In addition, ratio of day 16 (stable phase in intense dyeing)/day 2 in batches 2–4 were estimated (Supplementary Figure S4). To understand the important functions for enhancing dyeing intensity, the functional abundance ratios of day 10/day at the initiation of dyeing and day 16/ day at the initiation of dyeing in batches 2–4 were estimated (Supplementary Figure S4). The listed categories and super pathways were similar to the list in Supplementary Figure S3, except for the subpathways in super pathways of cell motility and metabolism (category of unclassified). Subpathways in the category of "unclassified" are important based on the subpathway in either batch 2 or 4. Increased items from Supplementary Figure S3 were reflected in the diversity change in the microorganisms related to indigo reduction. Although the listed subpathways were increased, it was considered that the "phosphotransferase system (PTS)" and "starch and sucrose metabolisms" remain important for the initiation of dyeing and enhancement of the dyeing intensity. In addition, although their ratios were lower in the two subpathways, "Prokaryotic defense system" and "nicotinate and nicotinamide metabolism" were relatively high.

The functional abundance of the subpathways, which were picked up in Supplementary Figure S4 and the contribution of the subpathways by major constituted taxa were estimated (Supplementary Figure S5) on day 3. The initial fermentation stage in batch 3 could be explained by the functional abundances of the subpathways of "phosphotransferase system (PTS)" and "starch and sucrose metabolisms." The specific abundancies in batch 3 were attributed to the genus *Alkalihalobacterium*, which specifically existed in this batch. This genus exhibited a higher contribution than other taxa considering the existing abundance ratio. The contribution for the listed subpathways by the genus *Alkaliphilus* was relatively low considering the existing ratio. However, this genus contributed to "amino acid metabolisms" rather than that of the carbohydrates.

The time from the preparation (day 0) to the initiation of indigo dyeing was different depending on the initial preparation. However, a moderate

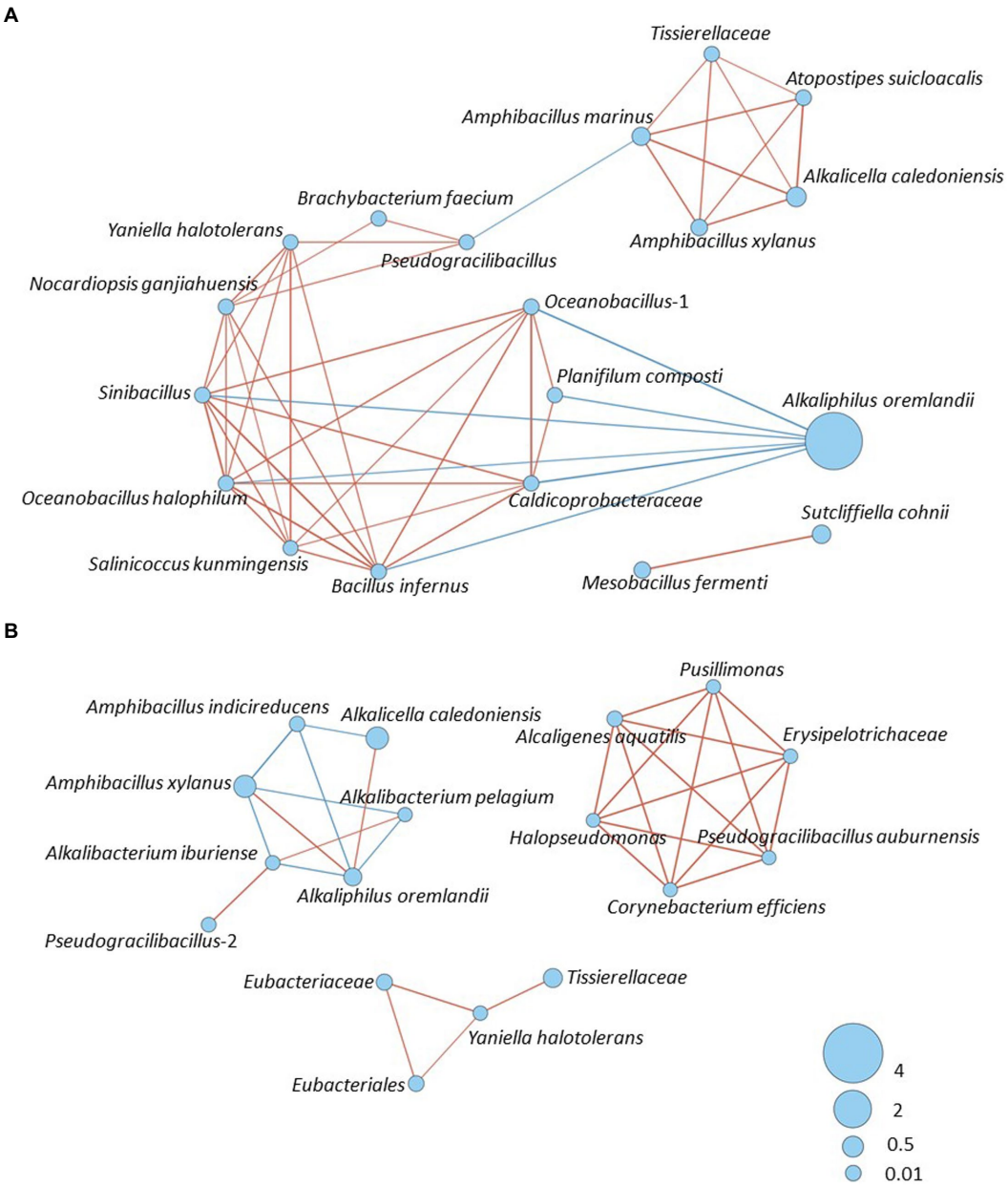

FIGURE 5
Bacterial community networks of the bacterial community based on the relative content change trend analyzed with Speaman's rank correlation coefficient [rs>0.6, p<0.05]; **(A)** Batch 4, days 1–7. **(B)** Batch 4, days 10–209. The red and blue lines represent positive and negative correlation, respectively. The thickness of the lines corresponds to the strength of the relationship (0.6<rs≤1), while circle size shows accumulated taxon abundances during each fermentation period.

and similar intensity of dyeing was observed on day 7 in all batches (Figure 1). All four batches exhibited high functional abundance ratios in the three subpathways of "phosphotransferase system (PTS)" and "starch and sucrose metabolisms" (Figure 6). These findings consistent with the dyeing results. Taxa that occupied major constituents were increased as the abundance ratio of *Alkaliphilus* was decreased in all the batches. The functional abundance of subpathways by genera *Amphibacullus* and/or *Atopstipes* contributed to fulfilling the abundance of the important subpathways involved in indigo dyeing. The contributions of subpathways important for dyeing in obligate anaerobes (e.g., *Alkaliphilus* and *Umitella*) were relatively low considering the present ratio. However, the contribution by genus *Tissierella* in batch was high considering the existing ratio. These obligate anaerobes most likely did not significantly contribute to the metabolisms of carbohydrates in this ecosystem.

Functional abundance in the stable and aged states of the fermentation

From days 7 to 10, the dyeing intensity increased; however, no significant change was found in the ratio of the functional abundance ratio, which was important for indigo reduction (Figure 6 and Supplementary Figure S6). The increase in staining intensity was likely due to the qualitatively improved metabolic function of the microbiota

Category/SuperPathway	SubPathway	B1-D7 (%)					B2-D7 (%)						B3-D7 (%)						B4-D7 (%)					
		Function abundance	*Alkalicella* (13.9%)*	*Urmiella* (4.7%)	*Tissierella* (7.5%)	*Alkaliphilus* (19.6%)	*Amphibacillus* (24.1%)	Function abundance	*Alkalicella* (8.6%)	*Urmiella* (8.3%)	*Alkaliphilus* (31.3%)	*Atopostipes* (11%)	*Amphibacillus* (11.5%)	Function abundance	*Alkalicella* (13.0%)	*Alkaliphilus* (29.7%)	*Atopostipes* (15.1%)	*Amphibacillus* (20.8%)	*Alkalihabacillus* (4.3%)	Function abundance	*Alkalicella* (14.9%)	*Tissierella* (4.6%)	*Alkaliphilus* (27.4%)	*Atopostipes* (3.6%)	*Amphibacillus* (8.9%)	*Sutcliffiella*/*Mesobacillus* (5.9%)
Cellular Processes																									
Cell motility:	Bacterial chemotaxis	0.82	11.0	0.1	17.3	4.4	38.5	0.77	8.1	1.0	8.1	12.8	25.3	0.79	11.9	6.9	15.5	35.9	10.9	0.76	12.5	0.1	7.2	16.2	37.7	6.2
	Bacterial motility proteins	2.34	12.4	0.1	18.7	4.0	35.9	2.15	9.3	0.1	7.5	11.3	24.1	2.20	13.8	6.4	13.9	34.5	10.7	2.22	13.7	0.1	6.4	13.7	34.2	6.4
	Flagellar assembly	0.93	12.7	0.1	17.6	3.6	35.1	0.88	9.2	0.0	6.6	16.6	22.8	0.93	13.4	5.5	19.8	31.7	9.9	0.89	13.9	0.1	5.7	20.5	32.9	6.3
Transport and catabolism:	**Prokaryotic Defense System**	**0.96**	12.1	0.2	21.4	3.5	33.9	**0.95**	8.4	0.4	6.2	18.1	21.2	**0.96**	12.8	5.4	22.5	30.9	7.0	**0.84**	14.6	0.2	6.1	25.6	35.1	7.3
Environmental Information Processing																										
Membrane transport:	**Phosphotransferase system (PTS)**	**0.33**	0.0	0.0	2.2	0.4	56.0	**0.39**	0.0	0.0	0.6	44.5	28.7	**0.52**	0.0	0.4	41.8	31.4	14.0	**0.34**	0.0	0.0	0.6	63.7	47.9	5.4
Genetic Information Processing																										
Replication and repair:	DNA replication proteins	0.81	10.2	0.1	16.8	3.4	35.4	0.81	7.0	0.3	5.9	16.4	21.8	0.83	10.7	4.8	20.9	31.0	9.4	0.80	10.8	0.1	5.2	20.8	32.3	7.0
Translation:	Aminoacyl-tRNA biosynthesis	0.75	12.8	0.1	18.1	3.7	31.9	0.75	8.9	0.3	6.4	16.9	19.8	0.76	13.3	5.5	20.9	28.6	8.9	0.73	13.9	0.1	5.7	21.8	29.8	6.4
	Ribosome	4.46	12.9	0.1	17.0	3.5	33.6	4.43	9.0	0.3	6.2	17.8	20.8	4.61	13.1	5.2	21.4	29.2	9.3	4.33	13.9	0.1	5.5	22.8	31.1	6.1
	Ribosome biogenesis	3.38	12.0	0.1	16.2	3.4	34.8	3.35	8.4	0.3	5.9	16.5	21.6	3.45	12.3	5.0	20.1	30.7	9.5	3.32	12.8	0.1	5.2	20.9	31.9	6.6
	Transfer RNA biogenesis	2.98	12.5	0.1	17.5	3.6	31.9	2.92	8.6	0.3	6.7	16.0	20.0	2.97	13.2	5.6	19.7	28.8	9.1	2.90	13.5	0.1	5.9	20.2	29.5	6.7
	Translation factors	0.98	12.9	0.1	17.9	3.8	32.3	0.98	8.9	0.3	6.7	17.1	20.0	0.99	13.4	5.7	21.1	28.8	9.0	0.94	14.2	0.1	6.0	22.3	30.4	6.0
Metabolism																										
Amino acid metabolism:	Lysine biosynthesis	0.72	10.0	0.2	22.7	4.2	31.7	0.70	7.1	0.4	7.4	14.5	20.0	0.67	11.3	6.8	19.1	30.7	9.0	0.70	10.9	0.2	6.6	18.3	29.5	5.7
	Phenylalanine, tyrosine and tryptophan biosynthesis	1.20	13.6	0.1	10.3	3.4	40.3	1.15	9.8	0.2	6.1	13.0	25.8	1.27	13.5	4.9	14.8	34.3	10.1	1.23	13.9	0.1	5.0	15.2	35.3	6.3
Carbohydrate metabolism:	Amino sugar and nucleotide sugar metabolism	1.04	8.9	0.1	9.2	2.6	43.2	1.09	5.9	0.1	4.4	18.8	25.7	1.16	8.4	3.6	22.0	35.2	9.1	1.00	9.8	0.1	4.2	25.6	40.9	7.2
	Glycolysis / Gluconeogenesis	0.54	8.6	0.1	10.5	3.1	39.0	0.58	5.6	0.2	5.0	24.0	22.6	0.65	7.6	3.9	27.0	29.7	10.3	0.53	9.3	0.1	4.8	33.1	36.4	7.5
	Starch and sucrose metabolism	**1.19**	5.1	0.1	6.9	2.1	49.1	**1.32**	3.2	0.1	3.2	33.3	27.4	**1.65**	3.9	2.2	33.3	31.9	13.4	**1.21**	5.3	0.0	3.1	45.5	43.7	6.8
Metabolism of cofactors and vitamins:	Nicotinate and nicotinamide metabolism	0.78	11.9	0.1	14.0	3.4	40.3	0.72	8.9	0.2	6.3	12.0	26.7	0.79	12.3	5.0	13.7	35.4	11.6	0.79	12.3	0.1	5.0	13.7	35.6	6.5
Unclassified																										
Genetic information processing:	Replication, recombination and repair proteins	1.15	11.7	0.1	18.7	3.7	32.8	1.13	8.2	0.3	6.5	14.3	20.5	1.15	12.2	5.6	17.6	29.5	12.0	1.11	12.7	0.1	5.8	18.4	30.7	6.5
Metabolism:	Amino acid metabolism	0.57	6.6	0.3	36.9	12.1	14.8	0.59	4.3	0.6	19.9	12.4	8.7	0.45	8.7	22.9	20.4	16.7	5.2	0.49	7.9	0.3	21.0	18.7	15.3	7.0
	Carbohydrate metabolism	0.50	4.8	0.1	9.9	1.1	44.3	0.49	3.4	0.2	2.0	9.1	28.3	0.52	4.9	1.7	10.8	39.1	13.8	0.46	5.5	0.1	1.9	12.1	43.9	11.0
	Energy metabolism	1.48	12.5	0.2	22.1	6.2	28.3	1.48	8.7	0.4	10.7	13.9	17.4	1.37	14.2	10.0	18.8	27.5	7.5	1.34	14.6	0.2	10.3	19.3	28.2	5.6
	Others	0.73	3.9	0.0	6.0	1.6	46.2	0.75	2.6	0.1	2.6	19.7	27.6	0.84	3.6	2.1	22.1	36.1	9.4	0.79	3.8	0.0	2.2	23.5	38.5	10.2

60.0%
40.0%
20.0%
10.0%
5.0%
1.0%

FIGURE 6
Functional abundance ratio (%) of the total subpathways and the contributing ratio (%) of the major constituent taxa in the subpathways related to the initiation and enhancement of indigo reduction at D7 samples in B1–4. *: The number in the parentheses is the existence ratio (%) in the microbiota. The metagenomic prediction produced using PICRUSt2 and BURRITO is shown. The important subpathways and functional abundance ratios are indicated in bold letters. B, batch; D, day.

Category/SuperPathway	SubPathway	B2-D49 (%)									B3-D49 (%)								B4 (control)-D49 (%)							
		Function abundance	*Alcalicella* (12.4%)*	*Tissierella* (6.9%)	*Alkaliphilus* (8.9%)	*Rhabdaneorobium* (5.8%)	*Enterococcus* (16.8%)	*Atopostipes* (4.0%)	*Alkalibacterium* (4.2%)	*Amphibacillus* (9.9%)	Function abundance	*Alcalicella* (17.7%)	*Trisierella* (4.0%)	*Alkaliphilus* (11.4%)	*Rhabdaneorobium* (4.5%)	*Enterococcus* (13.5%)	*Atopostipes* (6.5%)	*Amphibacillus* (16.0%)	Function abundance	*Alcalicella* (10.8%)	*Tissierella* (12.2%)	*Rhabdaneorobium* (8.3%)	*Enterococcus* (6.9%)	*Atopostipes* (8.7%)	*Amphibacillus* (14.8%)	
Cellular Processes																										
Cell motility:	Bacterial chemotaxis	0.63	12.8	12.7	2.3	8.8	6.2	4.2	4.4	18.8	0.68	16.2	6.8	2.8	6.5	4.9	6.6	29.4	0.73	7.8	17.0	11.1	2.0	8.6	22.7	
	Bacterial motility proteins	1.86	13.9	13.0	2.1	9.2	7.0	3.5	3.8	17.0	1.98	17.8	7.0	2.4	6.8	5.5	5.6	26.8	2.13	8.6	17.5	11.6	2.2	7.3	20.8	
	Flagellar assembly	0.78	13.6	11.0	1.8	8.9	9.5	5.1	5.3	15.7	0.82	17.5	6.0	2.1	6.7	7.6	8.1	25.1	0.87	8.6	15.2	11.5	3.1	10.8	19.8	
Transport and catabolism:	Prokaryotic Defense System	0.90	11.7	14.0	1.6	7.9	12.9	5.2	5.3	13.8	0.90	15.8	8.0	2.0	6.2	10.6	8.8	23.0	0.98	7.5	19.8	10.4	4.6	11.3	17.4	
Environmental Information Processing																										
Membrane transport:	**Phosphotransferase system (PTS)**	**0.66**	0.0	0.6	0.1	0.5	64.4	7.1	6.5	10.3	**0.63**	0.0	0.3	0.1	0.4	56.0	12.6	18.3	**0.46**	0.0	1.3	1.0	34.8	24.1	20.8	
Genetic Information Processing																										
Replication and repair:	DNA replication proteins	0.81	9.1	9.8	1.4	5.9	21.2	4.4	4.5	13.3	0.81	12.3	5.6	1.8	4.7	17.3	7.4	22.2	0.82	6.3	15.0	8.5	8.0	10.3	18.4	
Translation:	Aminoacyl-tRNA biosynthesis	0.79	10.9	9.0	1.4	7.5	19.9	4.4	4.5	11.4	0.78	15.1	5.2	1.8	6.0	16.6	7.4	19.5	0.79	7.7	13.9	10.9	7.6	10.3	16.1	
	Ribosome	4.70	11.0	8.5	1.4	7.3	20.1	4.6	4.8	12.0	4.67	15.0	4.9	1.8	5.8	16.6	7.7	20.3	4.70	7.7	13.0	10.5	7.7	10.8	16.9	
	Ribosome biogenesis	3.47	10.5	8.4	1.3	7.2	20.7	4.3	4.8	12.7	3.47	14.2	4.8	1.7	5.7	17.0	7.3	21.4	3.47	7.3	12.9	10.4	7.9	10.2	18.0	
	Transfer RNA biogenesis	2.97	11.2	9.1	1.6	7.5	18.1	4.3	4.7	12.0	2.96	15.3	5.2	2.0	5.9	14.9	7.2	20.3	3.02	7.8	13.7	10.6	6.8	9.9	16.7	
	Translation factors	1.02	11.1	9.0	1.5	7.7	19.5	4.5	4.7	11.7	1.01	15.3	5.2	1.9	6.1	16.2	7.6	19.8	1.02	7.8	13.8	11.1	7.4	10.5	16.4	
Metabolism																										
Amino acid metabolism:	Lysine biosynthesis	0.70	9.4	13.1	1.8	6.5	17.4	4.0	4.2	12.3	0.68	12.9	7.7	2.3	5.3	14.7	6.8	21.2	0.72	6.2	19.5	9.1	6.4	9.0	16.9	
	Phenylalanine, tyrosine and tryptophan biosynthesis	1.18	12.3	5.7	1.4	7.3	15.5	3.4	4.1	15.4	1.23	16.2	3.1	1.7	5.5	12.3	5.6	24.8	1.20	8.7	8.6	10.3	5.8	8.0	21.4	
Carbohydrate metabolism:	Amino sugar and nucleotide sugar metabolism	1.18	7.2	4.4	1.0	4.7	29.8	4.7	5.4	14.4	1.17	9.6	2.6	1.2	3.7	24.7	7.9	24.3	1.08	5.3	7.5	7.4	12.4	12.1	21.9	
	Glycolysis / Gluconeogenesis	0.66	6.4	4.6	1.1	4.2	32.0	5.8	6.0	12.2	0.64	8.8	2.7	1.3	3.4	26.8	9.8	20.8	0.59	5.0	7.8	6.7	13.4	15.1	18.8	
	Starch and sucrose metabolism	**1.49**	3.7	2.9	0.7	2.4	40.0	8.0	8.3	14.8	**1.49**	5.0	1.7	0.9	1.8	32.9	13.5	24.9	**1.30**	2.8	5.1	3.8	17.3	21.7	23.6	
Metabolism of cofactors and vitamins:	Nicotinate and nicotinamide metabolism	0.72	11.5	7.8	1.5	7.4	14.3	3.2	3.3	16.2	0.75	15.1	4.3	1.8	5.6	11.3	5.3	26.4	0.76	7.7	11.5	10.1	5.2	7.3	21.9	
Unclassified																										
Genetic information processing:	Replication, recombination and repair proteins	1.24	9.7	9.5	1.4	6.1	26.1	3.6	3.7	11.5	1.22	13.4	5.5	1.8	4.9	21.7	6.1	19.6	1.19	7.2	15.2	9.2	10.5	8.8	16.9	
Metabolism:	Amino acid metabolism	0.47	7.0	24.2	6.0	4.1	12.3	4.3	4.5	6.7	0.43	10.5	15.0	8.2	3.6	11.1	7.8	12.3	0.51	4.7	34.4	5.5	4.3	9.3	8.7	
	Carbohydrate metabolism	0.51	4.0	6.0	0.5	2.8	26.8	2.4	3.3	16.6	0.51	5.8	3.4	0.6	2.1	22.1	4.0	27.6	0.48	3.5	9.7	4.1	10.7	5.9	23.9	
	Energy metabolism	1.44	11.8	13.6	2.6	8.6	18.9	3.9	4.1	10.9	1.42	16.0	8.0	3.3	6.9	15.9	6.7	18.7	1.46	7.8	20.8	12.3	7.1	9.1	15.0	
	Others	0.84	3.1	2.7	0.6	1.6	32.1	4.8	6.0	15.0	0.83	4.2	1.6	0.7	1.3	26.8	8.1	25.6	0.75	2.3	4.7	2.6	13.5	12.6	23.6	

60.0%
40.0%
20.0%
10.0%
5.0%
1.0%

FIGURE 7
Functional abundance ratio (%) of the total subpathways and the contributing ratio (%) of the major constituent taxa in the subpathways related to the initiation and enhancement of indigo reduction at D49 samples in B2–4B. *: The number in the parentheses is the existence ratio (%) in the microbiota. The metagenomic prediction produced using PICRUSt2 and BURRITO is shown. There important subpathways and the functional abundance ratios are indicated in bold letters. B, batch; D, day.

rather than a quantitative increase in abundance. The decrease in the ratio of *Alkaliphilus* and increase in the ratio of *Amphibacillus* and/or *Alcalicella* and *Tissierella* were improved during days 7–10. The former exhibited a relatively low contribution for the important subpathways for indigo reduction, while the latter exhibited relatively high contribution for the important subpathways for indigo reduction (Supplementary Figure S6). In this way, important functions for the reduction of indigo and material circulation in the system shifted to the main constituent taxa on day 10.

After day 10, the functional abundance ratio of the subpathways of "phosphotransferase system (PTS)" and "starch and sucrose metabolisms" remained relatively high. The established effective metabolic pathway was maintained after day 10. The contribution of the subpathways by major taxa was also estimated in the microbiota at day 49 (Figure 7). The highly contributed taxa for the important subpathways were different based on the batch. *Alcalicella*, *Tissierella*, *Enterococcus*, and *Ampibacillus* were the major contributors to the important subpathways in batch 2. Meanwhile, *Alcalicella*, *Enterococcus*, and *Amphibacillus* were the major contributors to the indigo reduction in batch 3.

KEGG ortholog related to the dyeing intensity and initiation of indigo reduction

Table 1 lists the KEGG orthology correlated with staining intensity, which shows the correlation coefficients of ≥ 0.69 selected up from

TABLE 1 KEGG orthologies predicted by PICRUSt2 correlated with changes in dyeing intensity (correlation coefficient≥0.69).

KEGG orthology	Correlation coefficient	Symbol	Description	Function
K08977	0.79	cruF	bisanhydrobacterioruberin hydratase [EC:4.2.1.161]	Metabolism of terpenoids and polyketides; Carotenoid biosynthesis
K02538	0.79	manR	mannose operon transcriptional activator	Protein families: genetic information processing; Transcription factors
K16788	0.76	niaX	niacin transporter	Protein families: signaling and cellular processes; Transporters
K03973	0.76	pspC	phage shock protein C	Protein families: signaling and cellular processes;**Prokaryotic defense system**
K01224	0.76	E3.2.1.89	arabinogalactan endo-1,4-beta-galactosidase [EC:3.2.1.89]	Unclassified: metabolism; Enzymes with EC numbers
K00325	0.76	pntB	H^+-translocating NAD(P) transhydrogenase subunit beta [EC:1.6.1.2 7.1.1.1]	Metabolism of cofactors and vitamins;**Nicotinate and nicotinamide metabolism**
K02791	0.75	malX	maltose/glucose **PTS system** EIICB component [EC:2.7.1.199 2.7.1.208]	Amino sugar and nucleotide sugar metabolism; Metabolic pathways
K11646	0.75	K11646	3-dehydroquinate synthase II [EC:1.4.1.24]	Amino acid metabolism; Phenylalanine, tyrosine and tryptophan biosynthesis
K14660	0.75	nodE	nodulation protein E [EC:2.3.1.-]	Unclassified: metabolism; Enzymes with EC numbers
K00324	0.73	pntA	H^+-translocating NAD(P) transhydrogenase subunit alpha [EC:1.6.1.2 7.1.1.1]	Metabolism of cofactors and vitamins;**Nicotinate and nicotinamide metabolism**
K03339	0.73	iolJ	6-phospho-5-dehydro-2-deoxy-D-gluconate aldolase [EC:4.1.2.29]	**Carbohydrate metabolism**; Inositol phosphate metabolism
K09163	0.72	K09163	uncharacterized protein	Poorly characterized; Function unknown
K00197	0.72	cdhE, acsC	acetyl-CoA decarbonylase/synthase, CODH/ACS complex subunit gamma [EC:2.1.1.245]	Metabolic pathways; Microbial metabolism in diverse environments
K15023	0.72	acsE	5-methyltetrahydrofolate corrinoid/iron sulfur protein methyltransferase [EC:2.1.1.258]	Metabolic pathways; Microbial metabolism in diverse environments
K11261	0.72	fwdE, fmdE	formylmethanofuran dehydrogenase subunit E [EC:1.2.7.12]	Metabolic pathways; Microbial metabolism in diverse environments
K03389	0.72	hdrB2	heterodisulfide reductase subunit B2 [EC:1.8.7.3 1.8.98.4 1.8.98.5 1.8.98.6]	Metabolic pathways; Microbial metabolism in diverse environments
K00198	0.71	cooS, acsA	anaerobic carbon-monoxide dehydrogenase catalytic subunit [EC:1.2.7.4]	Metabolic pathways; Microbial metabolism in diverse environments
K15051	0.71	endA	DNA-entry nuclease	Unclassified: signaling and cellular processes; Unclassified viral proteins
K02173	0.71	yggC	(RefSeq) P-loop NTPase domain-containing protein YggC K02173 putative kinase	Unclassified: metabolism; Cofactor metabolism
K02750	0.71	glvC, malP, aglA	alpha-glucoside**PTS system** EIICB component [EC:2.7.1.208 2.7.1.-]	**Carbohydrate metabolism;Starch and sucrose metabolism**
K13677	0.71	dgs, bgsA	1,2-diacylglycerol-3-alpha-glucose alpha-1,2-glucosyltransferase [EC:2.4.1.208]	Lipid metabolism; Glycerolipid metabolism
K00105	0.71	E1.1.3.21	alpha-glycerophosphate oxidase [EC:1.1.3.21]	Lipid metabolism; Glycerolipid metabolism
K02530	0.71	lacR	DeoR family transcriptional regulator, lactose phosphotransferase system repressor	Protein families: genetic information processing; Transcription factors
K08325	0.71	yqhD	NADP-dependent alcohol dehydrogenase [EC:1.1.1.2]	**Carbohydrate metabolism**; Propanoate metabolism
K10530	0.71	lctO	L-lactate oxidase [EC:1.1.3.2]	Unclassified: metabolism; Enzymes with EC numbers
K18217	0.71	steB, tetB46	ATP-binding cassette, subfamily B, tetracycline resistant protein	Membrane transport; ABC transporters
K09952	0.71	csn1, cas9	CRISPR-associated endonuclease Csn1 [EC:3.1.-.-]	Protein families: signaling and cellular processes;**Prokaryotic defense system**

(Continued)

TABLE 1 (Continued)

KEGG orthology	Correlation coefficient	Symbol	Description	Function
K03390	0.71	hdrC2	heterodisulfide reductase subunit C2 [EC:1.8.7.3 1.8.98.4 1.8.98.5 1.8.98.6]	Energy metabolism; Methane metabolism
K02291	0.71	crtB	15-cis-phytoene synthase [EC:2.5.1.32]	Metabolism of terpenoids and polyketides; Carotenoid biosynthesis
K01215	0.71	dexB	glucan 1,6-alpha-glucosidase [EC:3.2.1.70]	Unclassified: metabolism; Enzymes with EC numbers
K06896	0.71	mapP	maltose 6′-phosphate phosphatase [EC:3.1.3.90]	**Carbohydrate metabolism**;**Starch and sucrose metabolism**
K02779	0.71	ptsG	glucose**PTS system** EIICB or EIICBA component [EC:2.7.1.199]	**Carbohydrate metabolism**; Glycolysis / Gluconeogenesis
K01071	0.71	MCH	medium-chain acyl-[acyl-carrier-protein] hydrolase [EC:3.1.2.21]	Lipid metabolis; Fatty acid biosynthesis
K09758	0.71	asdA	aspartate 4-decarboxylase [EC:4.1.1.12]	Amino acid metabolism; Alanine, aspartate and glutamate metabolism
K02781	0.71	srlB	glucitol/sorbitol**PTS system** EIIA component [EC:2.7.1.198]	**Carbohydrate metabolism**; Fructose and mannose metabolism
K07078	0.71	FRM2, YCLX08C	(RefSeq) type II nitroreductase	Poorly characterized; Function unknown
K03388	0.71	hdrA2	heterodisulfide reductase subunit A2 [EC:1.8.7.3 1.8.98.4 1.8.98.5 1.8.98.6]	Energy metabolism; Methane metabolism
K18981	0.70	udh	uronate dehydrogenase [EC:1.1.1.203]	**Carbohydrate metabolism**; Ascorbate and aldarate metabolism
K15780	0.70	tilS-hprT	bifunctional protein TilS/HprT [EC:6.3.4.19 2.4.2.8]	Nucleotide metabolism; Purine metabolism
K03778	0.70	ldhA	D-lactate dehydrogenase [EC:1.1.1.28]	**Carbohydrate metabolism**; Pyruvate metabolism
K02769	0.69	fruAb	fructose**PTS system** EIIB component [EC:2.7.1.202]	**Carbohydrate metabolism**; Fructose and mannose metabolism
K01669	0.69	phr, PHR1	deoxyribodipyrimidine photo-lyase [EC:4.1.99.3]	Protein families: genetic information processing; DNA repair and recombination proteins
K02793	0.69	manXa	mannose**PTS system** EIIA component [EC:2.7.1.191]	**Carbohydrate metabolism**; Fructose and mannose metabolism

Bold letters in Description and Function exhibit referred with the results of BRRITO. Items exhibit bold letter in KEGG orthology are candidate enzymes directly related with extracellular electron transportation. K00198 and K11261: related to obligate anaerobes; K03778, K08325 and K18981: related to lactic acid bacteria; K00324 and K00325; related to facultative anaerobes.

KEGG orthology items of 5,458 described in "pred metagenome unstrat" file created with PICRUSt2. Although the functional category differed from the results of the BURRITO analysis, the functions described the "phosphotransferase system (PTS)," "starch and sucrose metabolisms," "Prokaryotic defense system," and "nicotinate and nicotinamide metabolism" were found in the list. Among the KEGG orthology items, seven NAD(P)-dependent oxidoreductases were selected and the related taxa in each orthology and ratio "CountContributedByOTU" at the initiation of indigo reduction in batches 3 [from days 2 to 3 (D3/D2)] and 4 was [from days 3 to 4 (D4/D3)] were estimated using the "pred metagenome contrib.legacy" produced by PICRUSt2 analysis (Table 2). Enhancement of H^+-translocating NAD(P) transhydrogenase subunit beta [EC:1.6.1.2 7.1.1.1] (K00324, K00325) of *Alkalihalobacillus macyae* and NADP-dependent alcohol dehydrogenase [EC:1.1.1.2], uronate dehydrogenase [EC:1.1.1.203], and D-lactate dehydrogenase [EC:1.1.1.28] of *Atopostipes suicloacalis* caused the initiation of indigo reduction in batch 3 (Table 2). Meanwhile, enhancement of formylmethanofuran dehydrogenase subunit E [EC:1.2.7.12] and anaerobic carbon-monoxide dehydrogenase catalytic subunit [EC:1.2.7.4] of *Alkalicella caledoniensis* might have contributed to the initiation of indigo reduction in batch 4 (Table 2). In batches 1 and 2, changes toward the indigo reduction are attributed to the increase in the ratio of *Atopostipes suicloacalis* and *Alkalicella caledoniensis* (Figure 1).

Discussion

An initial treatment of *sukumo* with hot wood ash extract (60°C–80°C, pH > 10.5) has been conventionally used in indigo fermentation for reducing indigo. However, the environmental effects on the microbiota during this treatment, as well as the mechanisms underlying the microbial succession toward stable state remain unknown. Subsequently, wheat bran is added to the fermentation fluid as a substrate for the microorganisms, but the timing of this treatment varies depending on the craftsperson. We tested the effect of pH and heat treatment on *sukumo* and found that a high pH has larger impact on the microbiota in *sukumo* than a high temperature when selecting for microorganisms that contribute to indigo reduction. In addition, the microbiota in the *sukumo* treated with high pH exhibited more rapid change than those of non-alkaline treated batches. In the initial state of the fermentation (days 2–5), the different microbial communities with different dyeing intensities appropriately converged to facilitate indigo

TABLE 2 The KEGG orthologies belonging to the NAD(P)-dependent oxidoreductase that exhibited.

KEGG orthology	Taxon identified from DNA sequencing of OTU	Ratio in D3/D2 in CountContributedByOTU
K08325, K03778, K18981		
	Atopostipes suicloacalis (99.1%)	11.0
	Atopostipes suicloacalis (99.1%)	9.1
K00324, K00325		
	Alkalihalobacillus macyae (98.1%)	1.4
		Ratio in D4/D3 in CountContributedByOTU
K00198, K11261		
	Alkalicella caledoniensis (99.3%)	88.1

Highly correlated with the initiation of indigo reduction in batch 3 in day 3/day 2 (D3/D2) and batch 4 in day 4/day 3(D4/D3) in Table 1.

reduction on day 7 by the effect of wheat bran added at day 5. This convergence is occurred based on the maintenance of a high pH (day 1~) and low redox potential (day 2~) and the introduction of wheat bran at day 5. Indigo reducing functions of the microbiota were initiated or enhanced concomitant with major substrate changes from readily utilizable substrates derived from *sukumo* and dead microbial cells resulting from transitional changes of microbiota to hardly utilizable substrates (wheat bran or cellulose and xylan in *sukumo*) (Lopes et al., 2021). Wheat bran was not added in the early fermentation phase in most of our previous experimental batches, and the microbiota did not reach to the maturation phase within day 30 and a decrease in staining intensity was observed around day 56 (Tu et al., 2021). The present study showed that the addition of wheat bran in the early fermentation stage led to a stable state of indigo reduction (day 10) in all the fermentation batches tested. Introducing the carbohydrate as a source of energy for microbiota also increased dyeing intensity. Finally, the microbiota maintained their indigo reducing function in the closed ecosystem as the wheat bran was the sole external nutrient and changed the slowly circling substances involved in the high pH conditions. This stable stage is similar to the maturation in the general fermentation process. During the maturation period of indigo reduction fermentation, circulating substances in the ecosystem and indigo reduction function are synchronized.

Considering the relationship between the predicted functional abundance based on the microbial community and the differences in the dyeing results attributed to differences in the preparation procedures, fulfillment of the "phosphotransferease system (PTS)" and "starch and sucrose metabolism" subpathways helped to increase the dyeing intensity and the initiation of indigo reduction. In addition to the two main subpathways, other enhanced subpathways related to the indigo reduction included: carbohydrate metabolisms, accession for the substrates, reconstitution of cellular functions, defense for bacteriophage and antibiotics, and metabolism related to electron carriers. These functions indicate that indigo reduction occurs when the bacteria with indigo-reducing abilities that overcome the intense competition with other microorganisms for substrates and niches in the environment, undergone a drastic change in ORP and major substrates change under high alkaline conditions (pH 9.8–11.2). The importance of "PTS" was indicated in the later phase (maturation phase) in which the indigo fermentation consisted of two phases (Tu et al., 2021). Lopes et al. (2021) also reported the importance of "PTS" in fermentation, which accelerated indigo reduction by the addition of Indian indigo leaf powder during early fermentation. The importance of "starch and sucrose metabolism" in indigo reduction has been reported in comparative studies between of rapid and slow time-to-indigo reduction *sukumo* (Lopes et al., 2022). Using various preparation samples in this study, we clarified the significance of the two subpathways, "PTS" and "starch and sucrose metabolism," by assessing the relationship between dyeing intensity and functional abundance during early fermentation. In addition, the earlier introduction of wheat bran brought about an earlier realization of high-intensity dyeing compared with the previous trials.

Two possible indigo reducing systems have been considered so far. The indigo particle reduction is induced by azoreductase (AzoA), which oxidizes NADH (Suzuki et al., 2018); however, this AzoA was found in *Alkalihalobacillus wakoensis* (similarity: 98.9%), which is not an essential member of the microbiota in *sukumo* fermentation. Therefore, there is a possibility that this reaction has negligible effect on indigo reduction during fermentation. Conversely, the acetate$^-$/acetaldehyde couple is a strong electron donor than the NAD$^+$/NADH couple (ORP = −0.601 V at pH10), with an ORP of −1.044 V at pH10. The acetate$^-$/acetaldehyde coupled reaction can be catalyzed by (NAD-dependent) acetaldehyde dehydrogenases (Nakagawa et al., 2021). Acetaldehyde can be supplied from ethanol *via* the catalytic reaction facilitated by alcohol dehydrogenase. Another possible indigo reducing system is flavin-based extracellular electron transfer system found in *Listeria monocytogenes* (Light et al., 2018). The extracellular electron transfer is achieved *via* a series of intracellular electron transfers. NADH dehydrogenase (Ndh2) transfers electrons from NADH to the demethylmenaquinone (DMK) pool, which separates ordinary menaquinone (MK). Electrons are transferred from DMK to flavin adenine dinucleotide (FAD) on two FMNylased domain of PplA (outer membrane anchored electron transfer protein) or free flavin shuttles. Final electron acceptors, such as iron, accept electrons from FAD group on PplA or free flavin shuttles. This FAD-based extracellular electron transfer system expects widely distributed in Gram-positive bacteria. Seven NAD(P)-dependent oxidoreductases predicted using the PICRUSt2 analysis correlated with dyeing intensity were identified as the candidates for the initiation of indigo reductions in the KEGG orthologs level analysis. The intensity of these enzymes correlated with the initiation of indigo reduction in batches 3 and 4. These oxidoreductases, which are associated with the energy metabolism and the metabolisms of microbial metabolic products such as ethanol and lactic acid, were considered as candidate enzymes for reducing indigo particles.

Concerning the importance of favorable substrates, it has been reported that a period of accelerated convergence exists concurrent with

a bloom of *Bifidobacterium* associated with the metabolism of oligosaccharides in breast milk (de Muink and Trosvik, 2018). The succession of microbiota and metabolic functional change in the microbial ecosystem influenced by environments and the substrates have been reported (Zhou et al., 2019; Kong et al., 2020). In addition to the pathways related to substrate metabolisms, the "prokaryotic defense system" was also identified as a pathway related to indigo reduction. The "prokaryotic defense system" is essential for defense against external DNA attachment by bacteriophages and exposure to antibiotics produced by the other bacterial in a highly competitive environment (Tajkarimi and Wexler, 2017; Alessandri et al., 2021). The abundance of bacteriophages in the gut microbiome has been reported (Carasso et al., 2020). These findings suggest that bacteriophages affect various microbial ecosystems. These findings and our analyses of the functional abundance ratios suggest that intense bacteria–bacteriophage or antibiotic relationships exist in the indigo fermentation system. The resulting microbiota that realizes indigo reducing state can survive a competition with other microorganisms for their nutrients and niches under the succession of the environmental changes.

Indigo fermentation is roughly divided into two phases (Tu et al., 2021). During the first phase, the microbiota changes relatively rapidly, while in the second phase, the changes stabilize. The first phase could be altered by the succession of decay and regeneration of the microbiota depending on their adaptabilities (e.g., high pH and low ORP) and the availabilities of substrates derived from *sukumo*. Our results of the functional prevalence for indigo reduction suggest that the substrate utilization and adaptation to the environment under the succession of the microbial community are important to access the indigo reduction state. The stable indigo reduced state is realized by the convergence of microbiota *via* a succession of decay and replacement of the microbial community from the initial community (first phase) and transformation into the second phase community in the presence of the limited substrates (mainly wheat bran) under alkaline environments. Besides the pretreatment of *sukumo*, continuous maintenance of high pH, low ORP, and introduction of wheat bran on day 5 during the maintenance of the fermentation fluid converged microbiota toward indigo reduction on day 7. This finding can be explained by RDA, the decrease in the ratio of "others," which expresses miscellaneous low ratio constituent microorganisms, and the fluctuation in the alpha diversity change. This state may be the turning point from phase 1 (microbial community constructed after pretreatment of *sukumo*) toward phase 2 (relatively slow changing of the microbiota) (Tu et al., 2021). Previous studies have introduced wheat bran after day 22, which slowed the transition from phase 1 to phase 2 (Tu et al., 2019a,b, 2021). After day 22 of fermentation, the nutrition derived from *sukumo* was exhausted and the *sukumo* shifted to the phase of using nutrition from wheat bran. In other words, after fermentation begins and anaerobic microorganisms become dominant around day 3, the reduction of indigo starts around day 5, and after day 20, an ecosystem based on wheat bran is formed. This time, by introducing wheat bran during a highly flexible state of microbiota at the beginning of fermentation, the above stages were compressed, and even with different microbiota from different *sukumo* treatment, the effect of wheat bran started at day 6. A relatively strong indigo reduction occurs on day 6. This desirable state for indigo reduction was maintained until day 209. The long-term maintained state in the microbiota brought high-intensity of dyeing and a stable microbial community.

Indigo fermentation fluids exhibit exquisite resilience and maintain their indigo reducing ability for more than 1 year, even the fluids maintain under open air where there are many chances for contamination occur through immersed textiles (Okamoto et al., 2017; Aino et al., 2018). The first reason for the resilient ecosystem is the primary substrate in the fermentation which is wheat bran in this case. Wheat bran contains hard-to-utilizable substrates for microorganisms, such as starch, xylan, and cellulose. These hard-to-utilizable substrates produce slow changes and maintain a stable microbial community. If some bacteria contaminate the fermentation fluid, it is difficult for them to propagate using the hard-to-utilizable substrates under high pH and low ORP conditions. The second reason for the resilient ecosystem might be related to the microbiota formation process, which is converged by the succession of bacterial cells death and the regeneration of other taxa in the microbial community in the first phase. We suspect that the converged microbiota are maintained by the circulation of dead bacterial cells and the resulting generation of cell components that are utilizable microorganisms, which will lead the converged microbiota to adapt to the anaerobic alkaline environment. Some of the important functions of resistance to transitional changes in microbiota are shared in the converged microbial community. In addition, the microbial community exists in an anaerobic alkaline environment in the presence of limited substrates that exclude ordinary microorganisms. Therefore, the microbial community can converge easier than ordinary microbial community. The third reason for the stability of this ecosystem is that the stable ecosystem is based on the sharing of indispensable functions for indigo reduction among the major constituent microorganisms and obligate and facultative anaerobic acid producing bacteria. It is thought that the facultative anaerobic acid producing bacteria (e.g., *Amphibacillus* and *Alkalibacterium*) highly contribute to indigo reduction. In addition, these taxa are necessary to maintain this ecosystem. The predicted functional abundance suggests that obligate anaerobes utilize dead cells, which are produced by the pretreatment of *sukumo* and the initial transitional changes in microbiota owing to the high pH and the drastic decrease in ORP. This is in accordance with previous reports that described these obligate anaerobes-related taxa observed in this system such as *Alcalicella* (formerly *Anaerobrancaceae* or *Proteinivoraceae*) and *Tissierella* exhibited the ability for sludge degradations or bacterial cell lysis (Maspolim et al., 2015; Boltyanskaya and Kevbrin, 2016; Huang et al., 2018; Lavrentyeva et al., 2019; Wang et al., 2019). Dead cells are produced from the bacterial cells that died in the microbiota during the long-term fermentation period. Lactic acid bacteria utilize carbohydrates originating from wheat bran. Thus, a circulated system was constructed among the microbiota involved. The fourth reason is the functional redundancy among the constituted taxa. Several functions are necessary to maintain the circulation of this ecosystem, which exhibits simultaneously produces extracellular electrons *via* carbohydrate metabolisms. In this study, we identified functional redundancy between the same categories of the microorganisms such as obligate anaerobes and lactic acid bacteria. Resilient microbial systems have been found in other microbial communities due to their functional redundancy (Weimer, 2015; Luan et al., 2020; Zhao et al., 2021). The sharing of important functions for indigo reduction and the maintenance of this fermentation system were illustrated *via* the predicted functional abundance in major members of the microbiota. Furthermore, these important functions are shared in the predominant taxa.

Anaerobic fermentation systems with high pH can be observed in other ecosystems. Anaerobic alkaline conditions limit the survival of microorganisms; therefore, only limited members of alkaliphiles that

can adapt anaerobic environment can be present. However, the core microorganisms change based on the substrates in the conditions. Proteins are major substrates; indeed, proteins such as those in fermented fish, *Tissierella* stains are core microorganisms (Osimani et al., 2019). Meanwhile, in plant derived materials treated with salt, such as green table-olive fermentation, *Alkalibacterium*, *Halolactibacillus*, and *Marinilactibacullus* are major members in the microbiota (Lucena-Padrós and Ruiz-Barba, 2016). A cementitious geological disposal facility for radioactive wastes provides a niche for microorganisms that can survive in hyperalkaline conditions. In the environment, formation of flocs composed of a complex mixture of extracellular polymers has been reported. *Alishewanella* and *Dietzia* were dominated in the flock (Charles et al., 2017). Some of the taxa mentioned above have also been found in indigo fermentation liquids. Compared with neutralophilic environments, possible members in the alkaline environments are limited. The members of ecosystems in alkaline environments may therefore be predictable according to their physicochemical conditions and nutrient availability for microorganisms. In *sukumo* fermentation, most microorganisms are derived from *sukumo*, which is itself derived from plant. However, it is produced solid fermentation on the in-house earthen floor. Gram-positive microorganisms are predominant in earthen floor, which may explain the predominance of Gram-positive bacteria in the indigo fermentation fluid. Gram-negative bacteria possess higher adaptability in aqueous alkaline environments than Gram-positive bacteria (Takebayashi et al., 2007). Therefore, there is a predominance of Gram-negative bacteria in the aged fermentation for indigo reduction (Lopes et al., 2021; Tu et al., 2021).

Conclusion

Sukumo the composted leaves of *Polygonum tinctorium* L., provides autochthonous microorganisms and indigo dye to indigo reducing fermentation. The treatment procedure of *sukumo* is influenced by the artisanal practice. Although the aim of this treatment is to activate and select of microorganisms, the relationship between the involved environmental factors and microbiota remains unclear. *Sukumo* was treated in 4 different conditions and transitional change of the microbiota was analyzed. During days 2–5, before the effects of wheat bran were observed, treatment with high pH had higher impact than high temperature, while each pretreatment batch exhibited its own microbiota. Transitional changes in microbiota in alkaline treated *sukumo* were more rapid than those in non-alkaline-treated batches at the beginning of fermentation. High pH and low ORP altered the microbiota until day 5. Although the microbial community differed based on the treatment until day 5, each microbiota converged toward indigo reducing state at day 7 by the effect of the added wheat brane at day 5. *Amphibacillus*, *Alkalicella*, *Atopostipes*, and *Tissierellaceae* were core members at day 7. The relationship between the predicted functional abundance in the microbiota and the differences in the dyeing results between batches suggests that transportation and metabolisms of carbohydrates are important for initiation and acceleration of indigo reduction. Seven NAD(P)-dependent oxidoreductases with high correlation with indigo reduction intensity were identified as candidate enzymes for the extracellular electron transportation. The continuous addition of slowly decomposing wheat bran and the functional redundancy and successive changes of different indigo reducing taxa, which sustained the circulations of the ecosystem based on the fermentation aging, attributed to the sustainability of indigo reducing state. In this study, we demonstrated that alkaline treatment of *sukumo* and the addition of wheat bran are important for the secure realization of indigo reduction and maintenance at later stages of fermentation. In the future, adjustments for accurate alkaline pH and temperature for pretreatment of *sukumo* along with effective timing and more appropriate amount of wheat bran for early realization and maintenance of indigo reduction and to optimize conditions, better operation and performance of indigo fermentation can be accomplished.

Data availability statement

The datasets presented in this study can be found in online repositories. The names of the repository/repositories and accession number(s) can be found at: https://www.ddbj.nig.ac.jp/, DRA014811.

Author contributions

NF and IY: conceived and designed the experiments. NF, ZT, and HF: performed the experiments. IY, ZT, and HF: analyzed the data. IY: wrote the manuscript. All authors contributed to the article and approved the submitted version.

Funding

This work was supported by the Institute for Fermentation (IFO), Osaka (G-2020-3-035; I.Y.).

Acknowledgments

We would like to thank Editage (www.editage.com) for English language editing.

Conflict of interest

The authors declare that the research was conducted in the absence of any commercial or financial relationships that could be construed as a potential conflict of interest.

Publisher's note

Supplementary material

The Supplementary material for this article can be found online at: https://www.frontiersin.org/articles/10.3389/fmicb.2023.1097595/full#supplementary-material

References

Aino, K., Hirota, K., Okamoto, T., Tu, Z., Matsuyama, H., and Yumoto, I. (2018). Microbial communities associated with indigo fermentation that thrive in anaerobic alkaline environments. *Front. Microbiol.* 9:2196. doi: 10.3389/fmicb.2018.02196

Aino, K., Narihiro, T., Minamida, K., Kamagata, Y., Yoshimune, K., and Yumoto, I. (2010). Bacterial community characterization and dynamics of indigo fermentation. *FEMS Microbiol. Ecol.* 74, 174–183. doi: 10.1111/j.1574-6941.2010.00946.x

Alessandri, G., van Sinderen, D., and Ventura, M. (2021). The genus *Bifidobacterium*: from genomics to functionality of an important component of the mammalian gut microbiota. *Comput. Struct. Biotechnol. J.* 19, 1472–1487. doi: 10.1016/j.csbj.2021.03.006

Boltyanskaya, Y. V., and Kevbrin, V. V. (2016). Trophic interactions of proteolytic bacteria *Proteinivorax tanatarense* in an alkaliphilic microbial community. *Microbiology (Moscow, Engl Transl)* 85, 481–487. doi: 10.1134/S0026261716040032

Bolyen, E., Rideout, J. R., Dillon, M. R., Bokulich, N. A., Abnet, C. C., Al-Ghalith, G. A., et al. (2019). Reproducible, interactive, scalable and extensible microbiome data science using QIIME 2. *Nat. Biotechnol.* 37, 852–857. doi: 10.1038/s41587-019-0209-9

Callahan, B. J., McMurdie, P. J., Rosen, M. J., Han, A. W., Johnson, A. J. A., and Holmes, S. P. (2016). DADA2: high resolution sample inference from Illumina amplicon data. *Nat. Methods* 13, 581–583. doi: 10.1038/nmeth.3869

Carasso, S., Hajo, H., and Geva-Zatorsky, N. (2020). Phage-bacteria associations: analyze. Match. Develop therapies. *Cell Host Microbe* 28, 353–355. doi: 10.1016/j.chom.2020.08.009

Charles, C., Rout, S., Patel, K., Akbar, S., Laws, A., Jackson, B., et al. (2017). Floc formation reduces the pH stress experienced by microorganisms living in alkaline environments. *Appl. Environ. Microbiol.* 83, e02985–e02916. doi: 10.1128/AEM.02985-16

Clark, R. J. H., Cooksey, C. J., Daniels, M. A. M., and Withnall, R. (1993). Indigo, woad, and Tyrian purple: important vat dyes from antiquity to the present. *Endeavour* 17, 191–199. doi: 10.1016/0160-9327(93)90062-8

de Muink, E. J., and Trosvik, P. (2018). Individuality and convergence of the infant gut microbiota during the first year of life. *Nat. Commun.* 9:2233. doi: 10.1038/s41467-018-04641-7

Douglas, G.-M., Maffei, V.-J., Zaneveld, J., Yurgel, S.-N., Brown, J.-R., Taylor, C.-M., et al. (2020). PICRUSt2 for prediction of metagenome function. *Nat. Biotechnol.* 38, 685–688. doi: 10.1038/s41587-020-0548-6

Etters, J. N. (1989). Efficient use of sodium hydrosulfite in commercial vat dyeing processes. *Am. Dyest Rep.* 78, 18–26.

Hartl, A., Proaño Gaibor, A. N., van Bommel, M. R., and Hofmann-de Keijzer, R. (2015). Searching for blue: experiments with woad fermentation vats and an explanation of the colours through dye analysis. *J. Archaeol. Sci. Rep.* 2, 9–39. doi: 10.1016/j.jasrep.2014.12.001

Hirota, K., Aino, K., Nodasaka, Y., Morita, N., and Yumoto, I. (2013a). *Amphibacillus indicireducens* sp. nov., an alkaliphile that reduces an indigo dye. *Int. J. Syst. Evol. Microbiol.* 63, 464–469. doi: 10.1099/ijs.0.037622-0

Hirota, K., Aino, K., and Yumoto, I. (2013b). *Amphibacillus iburiensis* sp. nov., an alkaliphile that reduces an indigo dye. *Int. J. Syst. Evol. Microbiol.* 63, 4303–4308. doi: 10.1099/ijs.0.048009-0

Hirota, K., Okamoto, T., Matsuyama, H., and Yumoto, I. (2016). *Polygonibacillus indicireducens* gen. Nov., sp. nov., an indigo-reducing and obligate alkaliphile isolated from indigo fermentation liquor for dyeing. *Int. J. Syst. Evol. Microbiol.* 66, 4650–4656. doi: 10.1099/ijsem.0.001405

Hirota, K., Okamoto, T., Matsuyama, H., and Yumoto, I. (2020). "Polygonibacillus" in *Bergey's Manual of Systematics of Archaea and Bacteria*. eds. S. B. Kim and M. Goodfellow (Chichester, UK: JohnWiley & Sons, Ltd), 1–7.

Huang, X., Dong, W., Wang, H., and Feng, Y. (2018). Role of acid/alkali-treatment in primary sludge anaerobic fermentation: insights into microbial community structure, functional shifts and metabolic output by high-throughput sequencing. *Bioresour. Technol.* 249, 943–952. doi: 10.1016/j.biortech.2017.10.104

Kong, W., Sun, B., Zhang, J., Zhang, Y., Gu, L., Bao, L., et al. (2020). Metagenomic analysis revealed the succession of microbiota and metabolic function in corncob composting for preparation of cultivation medium for *Pleurotus ostreatus*. *Bioresour. Technol.* 306:123156. doi: 10.1016/j.biortech.2020.123156

Lavrentyeva, E. V., Erdyneeva, E. B., Dunaevskii, Y. E., Boltyanskaya, Y. V., and Kevbrin, V. V. (2019). Peptidase activity of *Proteinivorax* bacteria and their possible ecological role in the microbial communities of Tanatar Soda Lakes (Altai Krai, Russia). *Microbiology (Moscow, Engl Transl)* 88, 773–776. doi: 10.1134/S0026261719060079

Li, S., Cunningham, A. B., Fan, R., and Wang, Y. (2019). Identity blues: the ethnobotany of the indigo dyeing by Landian Yao (Iu mien) in Yunnan, Southwest China. *J. Ethnobiol. Ethnomed.* 15, 1–14. doi: 10.1186/s13002-019-0289-0

Li, S., Shi, Y., Huang, H., Tong, Y., Wu, S., and Wang, Y. (2022). Fermentation blues: analyzing the microbiota of traditional inigo vat dyeing in Hunan, China. *Microbiol. Spectr.* 10:e0166322. doi: 10.1128/spectrum.01663-22

Light, S. H., Su, L., Rivera-Lugo, R., Cornejo, J. A., Louie, A., Iavarone, A. T., et al. (2018). A flavin-based extracellular electron transfer mechanism in diverse gram-positive bacteria. *Nature* 562, 140–144. doi: 10.1038/s41586-018-0498-z

Lopes, H. F. S., Tu, Z., Sumi, H., and Yumoto, I. (2021). Analysis of bacterial flora of bacterial flora of indigo fermentation fluid utilizing composted indigo leaves (*Sukumo*) and indigo extraction from plants (Ryukyu-ai and Indian indigo). *J. Biosci. Bioeng.* 132, 279–286. doi: 10.1016/j.jbiosc.2021.05.004

Lopes, H. F. S., Tu, Z., Sumi, H., and Yumoto, I. (2022). *Indigofera tinctria* L. leaf powder promotes initiation of indigo reduction by inducing of rapid transition of the microbial community. *Front. Microbiol.* 13:957809. doi: 10.3389/fmicb.2022.957809

Luan, X., Zhang, H., Tian, Z., Yang, M., Wen, X., and Zhang, Y. (2020). Microbial community functional structure in an aerobic biofilm reactor: impact of streptomycin and recovery. *Chemosphere* 255:127032. doi: 10.1016/j.chemosphere.2020.127032

Lucena-Padrós, H., and Ruiz-Barba, J. L. (2016). Diversity and enumeration of halophilic and alkaliphilic bacteria in Spanish-style green table-olive fermentations. *Food Microbiol.* 53, 53–62. doi: 10.1016/j.fm.2015.09.006

Maspolim, Y., Zhou, Y., Guo, C., Xiao, K., and Ng, W. J. (2015). The effect of pH on solubilization of organic matter and microbial community structures in sludge fermentation. *Bioresour. Technol.* 190, 289–298. doi: 10.1016/j.biortech.2015.04.087

McNally, C. P., Eng, A., Noecker, C., Gagne-Maynard, W. C., and Borenstein, E. (2018). BURRITO: an interactive multi-omic tool for visualizing taxa-function relationships in microbiome data. *Front. Microbiol.* 9:365. doi: 10.3389/fmicb.2018.00365

Milanović, V., Osimani, A., Taccari, M., Garofalo, C., Butta, A., Clementi, F., et al. (2017). Insight into the bacterial diversity of fermentation woad dye vats as revealed by PCR-DGGE and pyrosequencing. *J. Ind. Microbiol. Biotechnol.* 44, 997–1004. doi: 10.1007/s10295-017-1921-4

Miura, A., Kurumisawa, T., Kano, R., Ito, T., Suzuki, K., and Kamata, H. (2019). Next-generation sequencing analysis of bacterial flora in bovine prototheca mastitic milk and feces. *J. Vet. Med. Sci.* 81, 1547–1551. doi: 10.1292/jvms.18-0649

Nakagawa, K., Takeuchi, M., Kikuchi, M., Kiyofuji, S., Kugo, M., Sakamoto, T., et al. (2021). Mechanistic insights into indigo reduction in indigo fermentation: a voltametric study. *Electrochemistry* 89, 25–30. doi: 10.5796/electrochemistry.20-00123

Nakagawa, K., Takeuchi, M., Tada, M., Matsunaga, M., Kugo, M., Kiyofuji, S., et al. (2022). Isolation and characterization of indigo-reducing bacteria of microbiota from indigo fermentation. *Biosci. Biotechnol. Biochem.* 86, 273–281. doi: 10.1093/bbb/zbab209

Nakajima, K., Hirota, K., Nodasaka, Y., and Yumoto, I. (2005). *Alkalibacterium iburiense* sp. nov., an obligate alkaliphile that reduces an indigo dye. *Int. J. Syst. Evol. Microbiol.* 55, 1525–1530. doi: 10.1099/ijs.0.63487-0

Nishita, M., Hirota, K., Matsuyama, H., and Yumoto, I. (2017). Development of media to accelerate the isolation of indigo-reducing bacteria, which are difficult to isolate using conventional media. *World J. Microbiol. Biotechnol.* 33:133. doi: 10.1007/s11274-017-2300-z

Okamoto, T., Aino, K., Narihiro, T., Matsuyama, H., and Yumoto, I. (2017). Analysis of microbiota involved in the aged natural fermentation of indigo. *World J. Microbiol. Biotechnol.* 33, 1–10. doi: 10.1007/s11274-017-2238-1

Osimani, A., Aquilanti, L., Baldini, G., Silvestri, G., Butta, A., and Clementi, F. (2012). Implementation of a biotechnological process for vat dyeing with woad. *J. Ind. Microbiol. Biotechnol.* 39, 1309–1319. doi: 10.1007/s10295-012-1139-4

Osimani, A., Ferrocino, I., Agnolucci, M., Cocolin, L., Giovannetti, M., Cristani, C., et al. (2019). Unveiling *hákarl*: a study of the microbiota of the traditional Icelandic fermented fish. *Food Microbiol.* 82, 560–572. doi: 10.1016/j.fm.2019.03.027

Padden, A. N., John, P., Collins, M. D., Hutson, R., and Hall, A. R. (2000). Indigo-reducing *clostridium isatidis* isolated from a variety of sources, including a 10th-century Viking dye vat. *J. Archaeol. Sci.* 27, 953–956. doi: 10.1006/jasc.1999.0524

Quast, C., Pruesse, E., Yilmaz, P., Gerken, J., Schweer, T., Yarza, P., et al. (2013). The SILVA ribosomal RNA gene database project: improved data processing and web-based tools. *Nucleic Acids Res.* 41, D590–D596. doi: 10.1093/nar/gks1219

Shannon, C. E. (1948). A mathematical theory of communication. *Bell Syst. Tech. J.* 27, 379–423. doi: 10.1002/j.1538-7305.1948.tb01338.x

Suzuki, H., Abe, T., Doi, K., and Ohshima, T. (2018). Azoreductase from alkaliphilc *bacillus* sp. AO1 catalyzes indigo reduction. *Appl. Microbiol. Biotechnol.* 102, 9171–9181. doi: 10.1007/s00253-018-9284-y

Tajkarimi, M., and Wexler, H. M. (2017). CRISPR-Cas system in *Bacteroides fragilis*, an important pathobiont in human gut microbiome. *Front. Microbiol.* 8:2234. doi: 10.3389/fmicb.2017.02234

Takebayashi, S., Narihiro, T., Fujii, Y., and Hiraishi, A. (2007). Water availability is a critical determinant of a population shift from Proteobacteria to Actinobacteria during start-up operation of mesophilic fed-batch composting. *Microb. Environ.* 22, 279–289. doi: 10.1264/jsme2.22.279

Toyama, S., Kawaguchi, Y., and Yonaha, K. (1978). Studies on the vat fermentation with Ryukyu: (3) on the indigo-reducing bacteria. *Sci. Bill. Coll. Agric. Univ. Ryukyu* 25, 225–233.

Tu, Z., de Fátima Silva Lopes, H., Hirota, K., and Yumoto, I. (2019a). Analysis of the microbiota involved in the early changes associated with indigo reduction in the natural fermentation of indigo. *World J. Microbiol. Biotechnol.* 35:123. doi: 10.1007/s11274-019-2699-5

Tu, Z., de Fátima Silva Lopes, H., Igarashi, K., and Yumoto, I. (2019b). Characterization of the microbiota in long- and short-term natural indigo fermentation. *J. Ind. Microbiol. Biotechnol.* 46, 1657–1667. doi: 10.1007/s10295-019-02223-0

Tu, Z., de Fátima Silva Lopes, H., Narihiro, T., and Yumoto, I. (2021). The mechanism underlying of long-term stable indigo reduction state in indigo fermentation using *Sukumo* (composted Polygonum tinctorium leaves). *Front. Microbiol.* 12:698674. doi: 10.3389/fmicb.2021.698674

Wang, X., Li, Y., Zhang, Y., Pan, Y. R., Li, L., Liu, J., et al. (2019). Stepwise pH control to promote synergy of chemical and biological processes for augmenting short-chain fatty acid production from anaerobic sludge fermentation. *Water Res.* 155, 193–203. doi: 10.1016/j.watres.2019.02.032

Weimer, P. J. (2015). Redundancy, resilience, and host specificity of the ruminal microbiota: implications for engineering improved ruminal fermentations. *Front. Microbiol.* 6:296. doi: 10.3389/fmicb.2015.00296

Yilmaz, P., Parfrey, L. W., Yarza, P., Gerken, J., Pruesse, E., Quast, C., et al. (2014). The SILVA and "all-species living tree project (LTP)" taxonomic frameworks. *Nucleic Acids Res.* 42, D643–D648. doi: 10.1093/nar/gkt1209

Yumoto, I., Hirota, K., Nodasaka, Y., Tokiwa, Y., and Nakajima, K. (2008). *Alkalibacterium indicireducens* sp. nov., an obligate alkaliphile that reduces indigo dye. *Int. J. Syst. Evol. Microbiol.* 58, 901–905. doi: 10.1099/ijs.0.64995-0

Yumoto, I., Hirota, K., Nodasaka, Y., Yokota, Y., Hoshino, T., and Nakajima, K. (2004). *Alkalibacterium psychrotolerans* sp. nov., a psychrotolerant obligate alkaliphile that reduces an indigo dye. *Int. J. Syst. Evol. Microbiol.* 54, 2379–2383. doi: 10.1099/ijs.0.63130-0

Zhao, X., Yang, Y., Feng, K., Wang, X., Liu, B., Xie, G., et al. (2021). Self-regulating microbiome networks ensure functional resilience of biofilms in sand biofilters during manganese load fluctuations. *Water Res.* 188:116473. doi: 10.1016/j.watres.2020.116473

Zhou, G., Xu, X., Qiu, X., and Zhang, J. (2019). Biochar influences the succession of microbial communities and the metabolic functions during rice straw composting with pig manure. *Bioresour. Technol.* 272, 10–18. doi: 10.1016/j.biortech.2018.09.135

frontiers | Frontiers in Microbiology

TYPE Original Research
PUBLISHED 23 February 2023
DOI 10.3389/fmicb.2023.1136514

OPEN ACCESS

EDITED BY
Andreas Teske,
University of North Carolina at Chapel Hill,
United States

REVIEWED BY
William T. Doerrler,
Louisiana State University,
United States
Etana Padan,
Hebrew College,
United States

*CORRESPONDENCE
Masahiro Ito
masahiro.ito@toyo.jp

†These authors have contributed equally to this work

SPECIALTY SECTION
This article was submitted to Extreme Microbiology, a section of the journal Frontiers in Microbiology

RECEIVED 03 January 2023
ACCEPTED 20 January 2023
PUBLISHED 23 February 2023

CITATION
Ishida Y, Koretsune T, Ishiuchi E, Teshima M and Ito M (2023) A magnesium transporter is involved in the cesium ion resistance of the high-concentration cesium ion-resistant bacterium *Microbacterium* sp. TS-1. *Front. Microbiol.* 14:1136514. doi: 10.3389/fmicb.2023.1136514

A magnesium transporter is involved in the cesium ion resistance of the high-concentration cesium ion-resistant bacterium *Microbacterium* sp. TS-1

Yoshiki Ishida[1†], Takahiro Koretsune[1†], Eri Ishiuchi[2], Miyu Teshima[2] and Masahiro Ito[1,2,3,4*]

[1]Graduate School of Life Sciences, Toyo University, Oura-gun, Gunma, Japan, [2]Faculty of Life Sciences, Toyo University, Oura-gun, Gunma, Japan, [3]Bio-Nano Electronics Research Center, Toyo University, Kawagoe, Saitama, Japan, [4]Bio-Resilience Research Project (BRRP), Toyo University, Oura-gun, Gunma, Japan

Cesium ion (Cs^+) resistance has been reported in bacteria but is poorly understood as reports on Cs^+-resistant bacteria have been limited. We previously reported a novel Cs^+/H^+ antiporter CshA implicated in Cs^+-resistance in *Microbacterium* sp. TS-1. The present study used the same screening method to isolate novel Cs^+-sensitive mutants and their revertants from TS-1. A comparative mutation site analysis using whole-genome sequencing revealed that *MTS1_03028* encodes the Mg^{2+} transporter MgtE and is a candidate Cs^+ resistance-related gene. We performed a bioinformatic analysis of *MTS1_03028* and complementation experiments on Cs^+ resistance in the TS-1 MTS1_03028 mutants Mut5 and Mut7 as well as *Escherichia coli* expressing *MTS1_03028* in the presence of Mg^{2+}. We established the role of MgtE in Cs^+ resistance through a functional analysis of TS-1. Enhancing Mg^{2+} transport by expression of MTS_03028 conferred increased Cs^+ resistance. When this strain was exposed to Cs^+ concentrations exceeding 200 mM, CshA consistently lowered the intracellular Cs^+ concentration. To our knowledge, the present study is the first to clarify the mechanism of Cs^+ resistance in certain bacteria. The study findings offer important insights into the mechanism of bacterial resistance to excess Cs^+ in the environment, suggesting the potential for bioremediation in high Cs-contaminated areas.

KEYWORDS

cesium-resistant microorganism, magnesium transporter, *Microbacterium*, alkaliphile bacteria, alkaliphiles, jumping spider, Cs^+/H^+ antiporter

1. Introduction

Cesium (Cs) has received global attention because large amounts of its radioactive isotopes (^{134}Cs and ^{137}Cs) were released into the environment after the 1986 Chernobyl and 2011 Fukushima nuclear power plant accidents (Buesseler et al., 2012; Hirose, 2016; Vasylenko et al., 2021; Nakamura et al., 2022; Wu et al., 2022). Since the latter half of the 2010s, there has been an increase in the amount of research on radioactive Cs^+ contamination of the soil (Sakai et al., 2021; Singh et al., 2022), decontamination and bioremediation efforts (Liu et al., 2014; Singh et al., 2022), and the quest to identify Cs^+-resistant microorganisms (Dekker et al., 2014; Kato et al., 2016; Swer et al., 2016; Zhang et al., 2021). By utilizing the cesium resistance mechanism of Cs^+-resistant microorganisms, it can be used by imparting high-concentration cesium-tolerant functions to radioresistant bacteria

with low Cs^+-resistant performance; it is thought that this will lead to the creation of highly functional radioresistant bacteria that efficiently recover radioactive cesium from radioactive cesium-contaminated environments. Therefore, such highly functional microorganisms can be used for bioremediation in contaminated environments.

As the chemical properties of Cs^+ resemble those of potassium (K^+), erroneous cellular Cs^+ influx through the K^+ uptake system may occur in microorganisms and animal and plant cells and inhibit their growth (Hampton et al., 2004; Kato et al., 2016). Prior studies on Cs^+ cytotoxicity in *Escherichia coli* reported that Cs^+ erroneously entered the cells *via* the K^+ uptake system and intracellularly accumulated as the bacterium lacks a Cs^+ efflux mechanism. Hence, the intracellular Cs^+ content increased over time (Bossemeyer et al., 1989). Moreover, K^+ homeostasis and cellular turgor are maintained by the transport of K^+ out of the cell *via* the K^+ excretion system. It has been reported that *E. coli* growth declines with low intracellular K^+ concentration.

Microbacterium sp. TS-1 was isolated from Jumping Spider ground extract in 2012, and its genomic information was reported in 2013 (Fujinami et al., 2013). This bacterium is a facultative alkaliphilic bacterium with a growth pH range of 6.0 to 10.0 and an optimum pH of 8.0 to 9.0. In addition, it can withstand up to 1.2 M CsCl, making it a high-concentration Cs^+-resistant bacterium (Koretsune et al., 2022). Previously, the upper growth limit of CsCl concentration for Cs^+-resistant bacteria was 700 mM for *Bacillus* sp. strain C700 (Zhang et al., 2021). Therefore, strain TS-1 was expected to have a unique Cs^+ resistance mechanism.

Although there are multiple reports of isolation of Cs^+-resistant bacteria, the mechanism of their Cs^+ resistance remains unknown (Dekker et al., 2014; Kato et al., 2016; Swer et al., 2016; Ito and Hasunuma, 2022a,b; Yukawa et al., 2022). We reported that a Cs^+/H^+ antiporter called CshA is involved in Cs^+ resistance in *Microbacterium* sp. TS-1 (Koretsune et al., 2022). In addition to this, another Cs^+ resistance mechanism was expected.

Herein, we aimed to isolate novel Cs^+-sensitive mutant strains through continuous screening and identify candidate Cs^+ resistance-related genes *via* spontaneous mutagenesis and next-generation sequencing. The discoveries made herein could elucidate the mechanisms by which bacteria adapt to cesium ion exposure.

2. Materials and methods

2.1. Bacterial strains and plasmids

The bacterial strains and plasmids used in the present study are listed in Table 1. The primers used in this investigation are available upon request to the corresponding author. Whole-genome sequencing (WGS) was previously performed on the alkaliphilic *Microbacterium* sp. TS-1 strain (Fujinami et al., 2013).

2.2. Growth media and conditions

Escherichia coli was grown at 37°C in Luria-Bertani (LB) medium (BD Difco™, Franklin Lakes, NJ, United States). Alkaliphilic *Microbacterium* sp. TS-1 was grown at 30°C in neutral complex medium (NC medium) and Tris medium (Imazawa et al., 2016). The latter consisted of 3.63 g L^{-1} Tris base, 1.47 g L^{-1} citric acid monohydrate, 0.5 g L^{-1} yeast extract, 9 g L^{-1} glucose, and 1% (w/v) trace elements (Cohen-Bazire et al., 1957). The solvent was deionized water. The pH was adjusted to 8 and 9 with 1 M *N*-methyl-*D*-glucamine. The pH was adjusted to 7 with 5 N H_2SO_4. Tris medium was used for the monovalent cation resistance test as cation influx can be underestimated. The NC medium consisted of 15.5 g L^{-1} K_2HPO_4, 4.5 g L^{-1} KH_2PO_4, 0.05 g L^{-1} $MgSO_4 \bullet 7H_2O$, 0.34 g L^{-1} citric acid, 5 g L^{-1} peptone, 2 g L^{-1} yeast extract, 5 g L^{-1} glucose, and 11.7 g L^{-1} NaCl. The solvent was deionized water. The final pH was adjusted to the desired value as required with KOH or H_2SO_4 (Fujinami et al., 2011). The *E. coli* KNabc transformants were grown in LBK medium (10 g L^{-1} tryptone, 5 g L^{-1} yeast extract, and 6 g L^{-1} KCl; pH 7.5). For growth selection, the medium was supplemented

TABLE 1 Bacterial strains and plasmids used in the present study.

Strain	Genotype	References
Microbacterium sp. TS-1	Wild type	Fujinami et al. (2013)
Mut3	Cs^+-sensitive mutant from TS-1, *MTS1_00475* (*cshA*)	Koretsune et al. (2022)
Mut4	Cs^+-sensitive mutant from TS-1, *MTS1_00475* (*cshA*)	Koretsune et al. (2022)
Mut5	Cs^+-sensitive mutant from TS-1	This study
Mut5R	Cs^+-resistant revertant from Mut5	This study
Mut7	Cs^+-sensitive mutant from TS-1	This study
Mut7R	Cs^+-resistant revertant from Mut7	This study
Escherichia coli		
KNabc	*ΔnhaA*, *ΔnhaB*, *ΔchaA*, Kan^+, Ery^+, Cam^+, *supE*, *hsd*, *Δ5thi*, *Δ* (*lac-proAB*)/F′, [*traD36*, *proAB*$^+$, *lacLq*, *lacZ*, ΔM15]	Nozaki et al. (1998)
Mach1	F^-, [φ80*lacZ*ΔM15], Δ*lac*X74, *hsd*R, (r_K^-, m_K^+), Δ*rec*A1398, *end*A1, *ton*A	Thermo Fisher Scientific, Waltham, MA, United States
Plasmid		
pBAD24	Cloning expression vector, P_{BAD} promoter, Ap^R	Guzman et al. (1995)
pBAD-00475	pBAD24 carrying *MTS1-00475* (*E. coli* codon-optimized sequence)	Koretsune et al. (2022)
pGEM7zf (+)	Cloning vector; Ap^R	Promega, Madison, WI, United States
pGEM-03028	pGEM7zf (+) carrying *MTS1_ 03028* (*E. coli* codon-optimized sequence)	This study

with kanamycin (25 μg mL^{-1}) or ampicillin (100 μg mL^{-1}). The cells were grown with shaking at 200 rpm and 30°C, and their growth was monitored by measuring OD_{600} in a spectrophotometer UV-1800 (Shimadzu Corporation, Kyoto Japan).

2.3. Isolation of novel Cs^+-sensitive mutants *via* chemical mutation and replica plating

Cs^+-sensitive strains and their Cs^+-resistant revertants were generated *via* chemical mutagenesis with ethyl methane sulfonate (EMA), as previously reported (Koretsune et al., 2022). The Cs^+-sensitive mutants obtained here were designated Mut5 and Mut7. Single colony isolation was performed for the isolated Mut5 and Mut7 on NC agar medium (pH 8). The colonies were inoculated into 2 ml NC medium (pH 8.0) and reciprocally shake-cultured at 200 rpm at 30°C for 18 h. The culture (100 μl) was independently plated on NC agar medium (pH 8) containing 200 mM or 400 mM CsCl to obtain spontaneous mutants whose cesium resistance was restored. Their Cs^+-resistant revertants obtained here were designated Mut5R and Mut7R.

2.4. Cs^+ resistance test of Cs^+-sensitive mutants and Cs^+-resistant revertants

Each TS-1 mutant was isolated from a single colony on NC agar (pH 8.0). Each colony was inoculated into a 14-mL culture tube containing 2 ml neutral composite medium (pH 8.0). The tubes were shaken at 200 rpm and 30°C for 18 h. The culture broth was used as the preculture medium. Two milliliters test medium and 10 μl preculture were placed in each 14-mL culture tube. The tubes were shaken at 200 rpm and 30°C for 16 h. OD_{600} was measured and Cs^+ resistance was assessed for each strain. Three independent experiments were performed.

2.5. Investigation of effects of Mg^{2+} on Cs^+ resistance in Mut5 and Mut7

Tris medium (pH 8.0) was supplemented with 100–1,200 mM Cs^+ and it was determined whether Mg^{2+} addition to semisynthetic medium improved Cs^+ resistance in Mut5 and Mut7. Single colonies were isolated from the TS-1, Mut5, and Mut7 strains on NC agar (pH 8.0). Each TS-1 mutant colony was then inoculated into a culture tube containing 2 ml NC medium and shaken at 200 rpm and 30°C for 18 h. The culture broth was used as the preculture medium. Two milliliters Tris medium was supplemented with various concentrations of Tris medium plus 100–1,200 mM CsCl with or without 2 μl of 1 M $MgCl_2$. Then, 10 μl preculture (0.5% (v/v)) was inoculated into the duplicated medium and shaken at 200 ppm and 30°C for 18 h. Then, OD_{600} was measured using a spectrophotometer. Three independent experiments were performed.

2.6. TS-1 mutant chromosomal DNA preparation

Single Mut5, Mut5R, Mut7, and Mut7R colonies were each inoculated into 2 ml NC medium (pH 8.0) and shaken at 200 rpm and 30°C for 18 h. Five hundred microliters preculture was inoculated into a 24φ test tube containing 4.5 ml NC medium (pH 8.0) and shaken at 200 rpm and 30°C for 4 h. The entire culture medium was then centrifuged at 9,100 × *g* and 4°C for 5 min and the supernatant was removed. Chromosomal DNA was extracted using a DNeasy Blood and Tissue kit (QIAGEN, Tokyo, Japan) according to the manufacturer's instructions.

2.7. Comparative analysis of WGS data

The chromosomal DNA was subjected to WGS with HiSeq X 2 × 150 bp (Illumina, San Diego, CA, United States) by Eurofins Genomics K.K. (Tokyo, Japan). The genome sequences of the mutant strain were then subjected to single-nucleotide polymorphism (SNP) analysis and the mutation sites were extracted. Variant calls were analyzed using samtools v. 1.6,[1] and bases differing from the reference were extracted from the mapping results. Variants were filtered using vcfutils.pl. in bcftools v. 1.6[2] and selected if they met the default settings for the called variants. Genes with different mutation sites were selected as candidates for Cs^+ resistance. The selected Cs^+ resistance-related candidate gene was identified from the annotation results for the TS-1 genome sequence. It was then determined whether the mutation caused nonsynonymous amino acid substitution. Mutations were detected in the genes overlapping Cs^+-sensitive mutant strains. Those with reverse mutations common to both revertant strains were selected as candidate Cs^+ resistance-related genes. The nucleotide sequence data are available in the DDBJ Sequenced Read Archive[3] under accession Nos. DRR328007 (Mut5), DRR328008 (Mut5R), DRR328009 (Mut7), and DRR328010 (Mut7R).

2.8. Artificial gene synthesis

MTS1_03028 was optimized for *E. coli* codons with GENEius,[4] and each identified gene was artificially synthesized by Eurofins Genomics. The gene sequence was registered in the DNA Data Bank of Japan (DDBJ).[5] The accession number for *MTS1_03028* is LC655172.

2.9. Alignment of the Mg^{2+} transporter-related genes with protein homologs in several bacterial species

The amino acid sequences of the Cs^+ resistance-related candidate genes and their homologs were obtained using the BLASTP algorithm at NCBI[6]. The amino acid residues selected in the alignment were analyzed using ClustalW[7] (Larkin et al., 2007). ETE3[8] was used to construct a phylogenetic tree for MTS1_03028 and its homologs using the neighbor-joining (NJ) method (Huerta-Cepas et al., 2016). Each

1 https://sourceforge.net/projects/samtools/files/samtools/0.1.6/
2 https://github.com/samtools/bcftools/releases/download/1.16/bcftools-1.16.tar.bz2
3 https://ddbj.nig.ac.jp/
4 http://www.geneius.de/GENEius/
5 https://www.ddbj.nig.ac.jp/index-e.html
6 https://blast.ncbi.nlm.nih.gov/Blast.cgi?PAGE=Proteins
7 https://www.genome.jp/tools-bin/clustalw
8 https://www.genome.jp/tools-bin/ete

protein structure was inferred from the amino acid sequence of the Cs^+ resistance-related genes using TMHMM 2.0.[9]

2.10. Construction of plasmids to express *MTS1_03028* optimized for *Escherichia coli* codons

Both 5′ ends of the phosphorylated synthetic *MTS1_03028* fragments optimized for *E. coli* codons were ligated with *Sma*I and pGEM7zf (+) and digested with T4 DNA ligase. The product was then transformed into Mach1-competent *E. coli*. A hundred microliters were spread onto LB agar containing 100 μg/ml ampicillin and statically incubated at 37°C overnight. The plasmids were then isolated and designated pGEM-03028.

2.11. Cs^+ growth test and intracellular Mg^{2+} concentrations for *Escherichia coli* Mach1 transformants subjected to various CsCl concentrations

Single Mach1/pGEM7zf (+) and Mach1/pGEM-03028 colonies were inoculated into 2 ml LB medium (pH 7.5) containing 100 μg/ml ampicillin and shaken at 200 rpm and 37°C for 16 h. Two milliliters LB medium and 50 mM, 100 mM, or 150 mM CsCl plus 100 μg/ml ampicillin were combined with 10 μl preculture. The cultures were shaken at 200 rpm and 37°C for 16 h. OD_{600} was measured in a spectrophotometer and the Cs^+ resistance of each strain was evaluated. Three independent experiments were performed.

The cultures were then centrifuged at 9,100 × *g* and 4°C for 5 min. The supernatants were removed, and the cell pellets were resuspended in 2 ml of 300 mM sucrose and centrifuged at 9,100 × *g* and 4°C for 5 min. The supernatants were removed, and the cell pellets were suspended in 2 ml of 300 mM sucrose. The cell count was adjusted based on the measured OD_{600}. Three microliters of 6 N HCl was added to the suspensions, and they were centrifuged at 9,100 × *g* and 4°C for 5 min. Then, 250 μl Mg assay solution was decanted into a 1.5-mL tube and subjected to the quantitative determination of Mg using a Metallo Assay Magnesium Measurement LS kit (Metallogenics Co. Ltd., Chiba, Japan; Osman et al., 1983) following the manufacturer's instructions. Then, 3 μl supernatant was added. The reaction was allowed to proceed at 20–25°C for 5 min and OD_{600} was measured. The latter values were used to calculate the intracellular Mg^{2+} concentrations according to the formula and instructions provided by the kit manufacturer.

3. Results

3.1. Cs^+-sensitive mutant isolation *via* chemical mutagenesis and replica plating

Mutagenesis was chemically induced by subjecting the TS-1 to 3% (v/v) EMS for 2 h. The cells were cultured until the early stationary phase, spread on NC medium plates, and incubated at 37°C for 2 day. Approximately 41,500 colonies were subjected to replica plating. Two candidate mutants designated Mut5 and Mut7 were sensitive to 200 mM Cs^+ (Supplementary Figure S1). They were subsequently isolated.

3.2. Isolation of Cs^+-resistant revertants and CsCl growth tests

The reversion mutation rates for Mut5 and Mut7 were 5.8×10^{-9} and 1.9×10^{-8}, respectively.

CsCl growth tests were performed using the mutant strains (Figure 1). All Cs^+-sensitive mutants presented with slower growth than the wild type. The revertants recovered the same level of Cs^+ resistance as the wild type (Table 2).

3.3. Comparative WGS analysis using next-generation sequencing

WGS analyzes indicated that the Cs^+-sensitive Mut5 and Mut7 harbored 177 and 166 mutations, respectively. They shared a common mutated gene encoding a magnesium transporter designated *MTS1_03028*. Comparison of the genome sequences of Mut5 and the revertant Mut5R confirmed that the latter had the reversion mutation Mut5: T396I → Mut5R: I396T on *MTS1_030285*. In contrast, comparison of the genome sequences of Mut7 and the revertant Mut7R confirmed that the latter had a reversion mutation Mut7: E310K → Mut7R: K310E on *MTS1_030285*. The *MTS1_030285* nucleotides were sequenced for both revertants.

3.4. Bioinformatics analysis of MTS1_03028

Multiple sequence alignment of MTS1_03028 and its protein homologs revealed that it is the Mg^{2+} transporter MgtE (Smith and Maguire, 1998), which is widely distributed among *Microbacterium* spp. (Figure 2). MTS1_03028 showed 99% homology with the MgtE of *Microbacterium paludicola*. Its homologs were detected in *Brevibacterium casei*, *Leucobacter weissii*, and *Actinotalea caeni*, and their amino acid identities were 70, 70, and 69%, respectively. According to protein structure prediction using TMHMM-2.0[10], MTS1_03028 is a five-transmembrane protein. A schematic diagram of the secondary structure prediction is shown in Figure 3.

3.5. Effects of Mg^{2+} on Cs^+ resistance in the Cs^+-sensitive TS-1 mutants

Tris medium (pH 8.0) was supplemented with 100–1,200 mM Cs^+ plus 1 mM Mg^{2+}. A Cs^+ resistance growth test in the conditions supplemented with 1 mM $MgCl_2$ indicated that Mut5 and Mut7 recovered Cs^+ resistance to the same level as that of the TS-1 wild type (Figure 4). Therefore, it is suggested that Mg^{2+} plays an important role in the Cs^+ resistance of TS-1. Mut5 and Mut7 might have been

9 https://services.healthtech.dtu.dk/service.php?TMHMM-2.0

10 https://services.healthtech.dtu.dk/service.php?TMHMM-2.0

10.3389/fmicb.2023.1136514

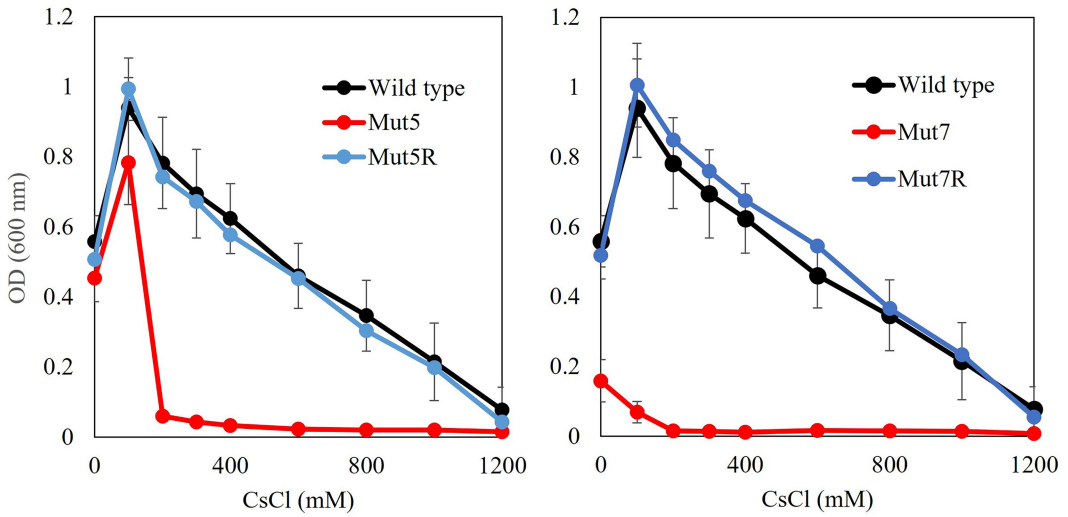

FIGURE 1
Cs^+ resistance growth tests on Cs^+-sensitive mutants and Cs^+-resistant revertants. Single colonies of each mutant were inoculated into 2 ml NC medium (pH 8.0) and shaken at 200 rpm and 30°C for 18 h. Ten microliters preculture was inoculated into 2 ml Tris medium (pH 8.0) containing 100–1,200 mM CsCl and shaken at 200 rpm and 30°C for 18 h. OD_{600} was measured using spectrophotometry. Error bars show SD for three independent experiments.

TABLE 2 Rates of mutation reversion of each Cs^+-sensitive mutant strain and proteins encoded by genes with revertant mutations.

Mutant	Frequency of Cs^+-resistant revertant strains	Amino acid mutation site (Cs^+ sensitive mutant→revertant mutant)	Accession no.
Mut5R	5.8×10^{-9}	MTS1_00841 phenylalanyl-tRNA synthetase beta subunit (A730V → V730A) (true reversion)	BASQ01000001.1889132–891,651 (minus strand)
		MTS1_02354 putative DNA segregation ATPase (P142S → S142P) (true reversion)	BASQ01000001.12498595–2,499,221
		MTS1_03028 magnesium transporter (T396I → I396T) (true reversion)	BASQ01000002.124174–25,532 (minus strand)
Mut7R	1.9×10^{-8}	MTS1_03028 magnesium transporter (E310K → K310E) (true reversion)	BASQ01000002.124174–25,532 (minus strand)

Table summarizes the proteins encoded by the genes confirmed to be mutated in the Cs^+-sensitive mutants and reverted in the Cs^+-resistant revertants. For genes with mutations and nonsynonymous amino acid substitutions, the mutations are shown in parentheses in the following order: wild type, Cs^+-sensitive mutant, and Cs^+-resistant revertant.

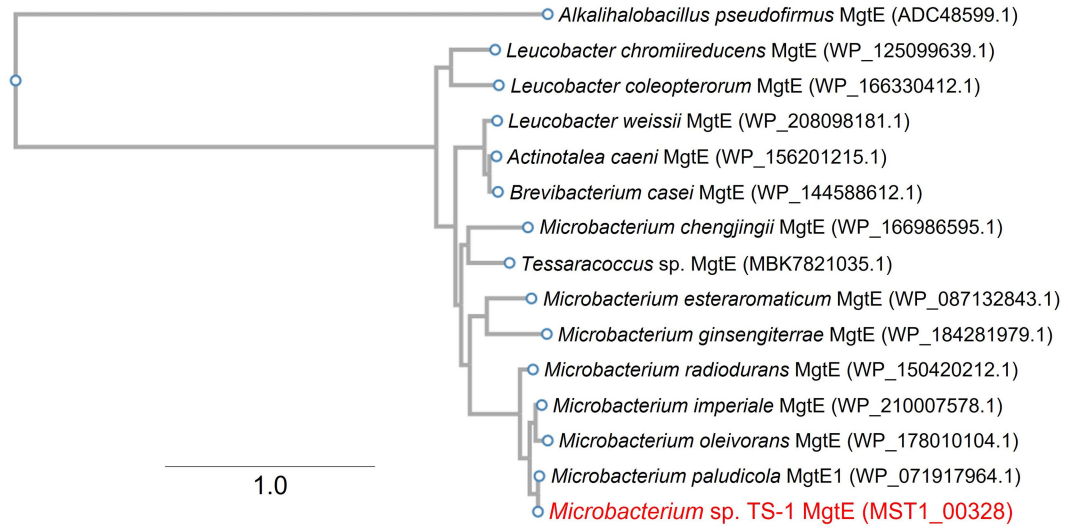

FIGURE 2
Phylogenetic clustering of MTS1_00328. A phylogenetic tree was constructed based on multiple sequence alignment with MTS1_00328 homolog. Details of this procedure are described in Materials and Methods. MTS1_00328 from *Microbacterium* sp. TS-1 is shown in red. MgtE from gram-positive alkaliphile *Alkalihalobacillus pseudofirmus* was used as an outgroup. The number between branches indicates the bootstrap value. GenBank accession Nos. are provided in parentheses.

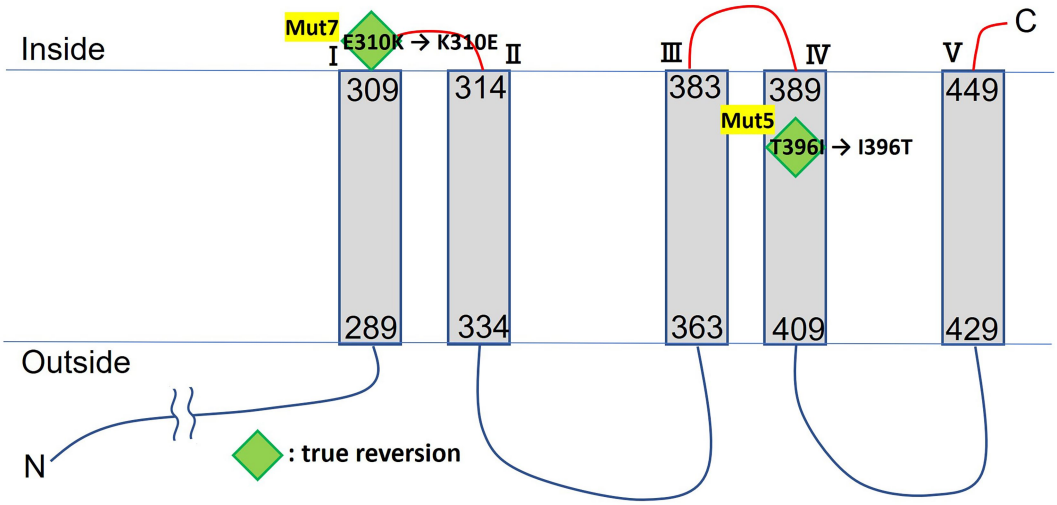

FIGURE 3
TMHMM transmembrane model of MTS1_00328. Mutation sites of Cs^+-sensitive mutants are indicated by diamonds. Green diamonds indicate true reversion in Cs^+-resistant revertant.

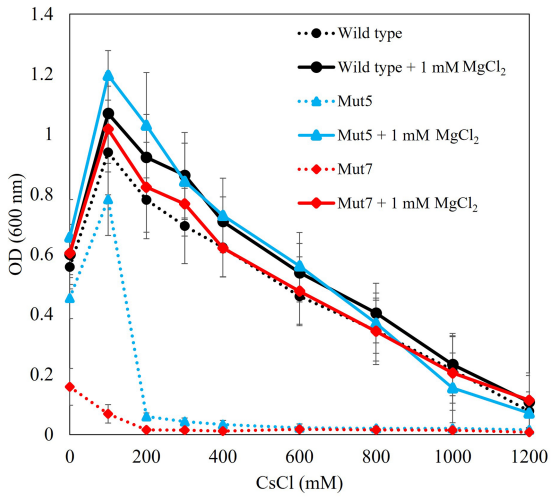

FIGURE 4
Cs^+ resistance growth test on each strain with and without Mg^{2+} addition. Each strain was cultured in Tris medium for 18 h. Dotted line denotes results in the absence of $MgCl_2$. Solid line denotes results when 1 mM $MgCl_2$ was added. Vertical axis indicates turbidity (OD_{600}). Horizontal axis indicates CsCl concentration in the medium. Error bars indicate SD for three independent experiments.

Cs^+-sensitive as they could not take in sufficient Mg^{2+} because of the mutation in each MgtE.

3.6. Cs^+ resistance growth and intracellular Mg^{2+} concentration of *Escherichia coli* Mach1/pGEM-03028

The Cs^+ resistance growth test was conducted, and intracellular Mg^{2+} concentration was measured to determine whether MgtE expression in pGEM7zf (+) improved Mg^{2+} uptake and Cs^+ resistance. OD_{600} was measured after 16 h of culturing in media containing various CsCl concentrations (Figure 5A). The intracellular Mg^{2+} concentrations are shown in Figure 5B. The minimum inhibitory concentration (MIC) of CsCl was 200 mM for *E. coli* Mach1 harboring the negative control pGEM7zf (+). The *E. coli* Mach1 harboring the MgtE-encoding plasmid pGEM-03028 exhibited resistance to 200 mM CsCl and its MIC was increased to 300 mM. Hence, its Cs^+ resistance was augmented. The intracellular Mg^{2+} concentration was ~20 mM in the CsCl-free medium both in the presence and absence of MgtE expression. In the latter case, however, the intracellular Mg^{2+} concentration increased by ~50% at elevated CsCl concentrations, whereas in the former case, it increased to ~100%. Thus, *E. coli* Mach1 absorbs Mg^{2+} in the presence of Cs^+. Furthermore, MgtE expression improved both Mg^{2+} uptake and Cs^+ resistance.

3.7. Cs^+ resistance in *Escherichia coli* KNabc/pBAD-00475 in the presence of Mg^{2+}

A Cs^+ resistance growth test was conducted to confirm whether MTS1_00475 expression improved Cs^+ resistance in *E. coli* KNabc. MTS1_00475 is a *cshA* gene product that encodes a low-affinity Cs^+/H^+ antiporter. In previous studies, KNabc/pBAD-00475 displayed the same degree of Cs^+ resistance as that of the negative control KNabc/pBAD24 (vector) (Koretsune et al., 2022). In previous study, the reason why MTS_00475 (CshA) could not improve the Cs^+ resistance of *E. coli* KNabc is that *E. coli* cannot grow in the presence of 200 mM CsCl, and the apparent K_m value of CshA for Cs^+ is 250 mM (pH 8), which is a low affinity. Therefore, it was thought that *E. coli* could not grow at Cs^+ concentrations at which CshA functions (Koretsune et al., 2022).

The addition of Mg^{2+} to the medium improved Cs^+ resistance in *E. coli* (Figure 5A). Therefore, we conducted a Cs^+ resistance growth test to evaluate whether the combination of *E. coli* KNabc/pBAD-00475 plus Mg^{2+} addition enhanced Cs^+ resistance. In the presence of Mg^{2+}, *E. coli* KNabc/pBAD-00475 growth was observed at 300 mM CsCl (Figure 6). These observations suggest that the MTS1_00475 product encoding the Cs^+/H^+ antiporter CshA effluxed Cs^+ at this condition and improved its Cs^+ resistance.

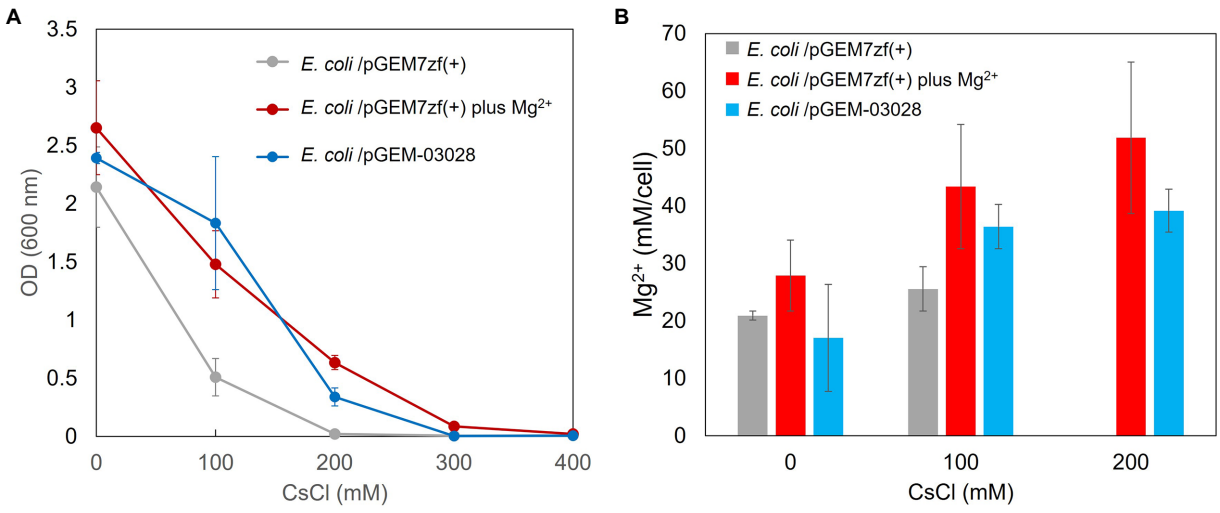

FIGURE 5
Cs^+ resistance growth test **(A)** and intracellular Mg^{2+} concentrations **(B)** of *Escherichia coli* Mach1 harboring pGEM-03028 and *E. coli* Mach1 harboring pGEM7zf (+) in presence of Mg^{2+}. **(A)** Turbidity (OD_{600}) of *E. coli* Mach1/pGEM-03028 in LB medium and Mach1/pGEM7zf (+) in LB medium plus 50 mM $MgCl_2$ at each CsCl concentration and after 16 h of culturing. Error bars indicate SD for three independent experiments. *E. coli* Mach1/pGEM7zf (+) was used as the negative control. **(B)** Intracellular Mg^{2+} content at each CsCl concentration for *E. coli*/pGEM-03028 cultured in LB medium (pH 7.5) for 16 h. Vertical axis indicates intracellular Mg^{2+} concentration. Horizontal axis indicates CsCl concentration in the medium. Error bars indicate SD for three independent experiments. An empty vector pGEM7zf (+) was used as the negative control.

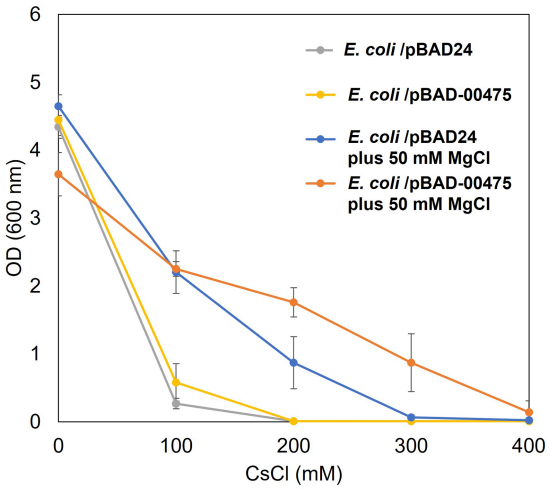

FIGURE 6
Cs^+ resistance growth test on *Escherichia coli* KNabc harboring pBAD-00475 in the presence of Mg^{2+}. Turbidity (OD_{600}) of *E. coli* KNabc/pBAD-00475 in LBK medium and *E. coli* KNabc/pBAD-00475 in LBK medium plus 50 mM $MgCl_2$ at each CsCl concentration and after 16 h of culturing. Error bars indicate SD for three independent experiments. *E. coli* KNabc/pBAD24 was used as the negative control.

4. Discussion

4.1. Identification of a novel Cs^+ resistance-related gene in Cs^+-sensitive mutants

We attempted to obtain a Cs^+-sensitive mutant from the TS-1 strain. We used EMS to induce Cs^+ resistance through chemical mutagenesis. We obtained Mut5 and Mut7 which had reduced Cs^+ resistance and no *CshA* mutation. We determined that the reversion frequencies in Mut5 and Mut7 were 5.8×10^{-9} and 1.9×10^{-8}, respectively. Unstable and stable mutations had reversion frequencies of $\geq 1.0 \times 10^{-6}$ and $\leq 1.0 \times 10^{-8}$, respectively. Here, we successfully obtained a Cs^+-resistant revertant. Analyzes of Cs^+ resistance in the Cs^+-sensitive mutant and its revertants disclosed that the phenotype varied with the tested strain.

Mut5 grew at the same rate as that of the wild type in the absence of Cs^+. The growth of both strains was inhibited by 200 mM Cs^+. Hence, the Cs^+ resistance-related gene was mutated in Mut5 and differed from those in Mut3 and Mut4 (Koretsune et al., 2022). A whole-genome analysis revealed no mutation in the MTS1-00475 region of Mut5 or Mut7. A comparison of Mut5 and Mut5R disclosed a back mutation in the *mgtE* region. Mut5R grew at the same rate as that of the wild type whether or not Cs^+ was present in the medium. As Cs^+ resistance was fully rescued in Mut5R, *mgtE* is a vital Cs^+ resistance-related gene.

Mut7 exhibited slower growth than the wild type in the absence of Cs^+, and its growth was inhibited by 100 mM Cs^+. Furthermore, its revertant Mut7R grew at the same rate as that of the wild type regardless of Cs^+ addition. In the absence of Cs^+, Mut7R rescued both growth and Cs^+ resistance. A comparison of the mutation sites in Mut7 and Mut7R revealed that the back mutation occurred in the *mgtE* region similar to that in Mut5. Therefore, *mgtE* is critical for growth and Cs^+ resistance.

4.2. Importance of Mg^{2+} in TS-1 Cs^+ resistance

It was proposed that Mut5 and Mut7 were sensitive to Cs^+ because of mutations in their MgtE Mg^{2+} uptake system (MTS1_03028). Mg^{2+} addition to the medium increased the intracellular Mg^{2+} concentration and restored Cs^+ resistance to the wild-type level. Hence, Mut5 and Mut7 were sensitive to Cs^+ as they could not incorporate sufficient Mg^{2+}. For this reason, adequate Mg^{2+} uptake is required for Cs^+ resistance in TS-1.

The Group 2 metal magnesium is an essential trace element in many living organisms. Magnesium maintains ribosome structure, stabilizes cell membranes and Mg^{2+}-dependent enzymatic reactions involved in ribosome synthesis, and has numerous functions in animals, fungi, microorganisms, plants, and other life forms (Akanuma et al., 2014).

Depletion of Mg^{2+} in *E. coli* growth medium induces ribosome disassembly, and binding of ribosomal subunits to form 70S ribosomes is forced at Mg^{2+} concentrations above 15 mM. When the Mg^{2+} concentration is lowered below 1 mM, the 70S ribosomes dissociate and eventually unfold. A single *E. coli* ribosome contains at least 170 Mg^{2+}. The presence of divalent and monovalent cations stabilizes the tertiary structure of 23S rRNA by mediating interactions between its structural domains (Akanuma et al., 2014). Based on the above, ribosomes are speculated to be one of the candidates affected by intracellular Cs^+ elevation. Therefore, in the future, we would like to verify the stability of the ribosome structure in the presence of Cs^+ in the TS-1 and the Cs^+-sensitive mutant strains using methods such as sucrose density-gradient centrifugation.

The present study demonstrated that 50 mM $MgCl_2$ addition improved Cs^+ resistance in *E. coli*. On the other hand, TS-1 recovered Cs^+ resistance when one mM $MgCl_2$ was added to the Cs^+-sensitive mutants. Wild-type strain TS-1 is already highly resistant to Cs^+ due to MgtE and Cs^+/H^+ antiporter (CshA). However, the importance of Mg^{2+} in TS-1 was discovered by the MgtE mutant obtained in this study. *E. coli*, which does not have a Cs^+ efflux mechanism such as a Cs^+/H^+ antiporter, is presumed to acquire Cs^+ resistance by requiring higher concentrations of Mg^{2+}. It is speculated that it might have a similar effect in other microbial taxa. The next challenge is to verify whether Mg^{2+} constitutively enhances Cs^+-resistance in different microorganisms.

To the best of our knowledge, no prior studies have shown that Mg^{2+} plays an essential role in microbial Cs^+ resistance. However, the present work was the first to reveal this association in TS-1.

4.3. Cs^+ resistance mechanism in TS-1

In our recent study, we reported using intracellular Cs^+ (CsCl) concentrations of 0 mM to 400 mM in *E. coli* and strain TS-1 (Koretsune et al., 2022). When CsCl was added to the culture medium of *E. coli*, intracellular Cs^+ concentrations accumulated at levels similar to or higher than extracellular concentrations. Conversely, strain TS-1 suppressed intracellular Cs^+ concentrations below 150 mM even when exposed to 400 mM CsCl. Comprehensively judging this result and those of the present study, there are two central Cs^+ resistance mechanisms in strain TS-1. First, strain TS-1 acquired resistance to ≤200 mM Cs^+ by absorbing Mg^{2+} *via* MgtE. Second, when strain TS-1 was exposed to >200 mM Cs^+, Cs^+ was excreted *via* the low affinity Cs^+/H^+ antiporter CshA. High-concentration Cs^+-resistant bacterium strain TS-1 utilizes Mg^{2+} accumulation by Mg^{2+} transporter and Cs^+ efflux by Cs^+/H^+ antiporter to maintain Cs^+ resistance against low to high Cs^+ concentrations in the external environment. Several studies have endeavored to isolate Cs^+-resistant bacteria. To our knowledge, however, this study is the first to elucidate a physiological Cs^+ resistance mechanism.

5. Conclusion

In the present work, we isolated two Cs^+-sensitive mutants from the *Microbacterium* sp. strain designated TS-1, identified revertant strains, compared their mutation sites, and identified novel Cs^+ resistance-related gene candidates. The strains Mut5 and Mut7 were obtained in the process of isolating Cs^+-sensitive strains lacking any mutation in *MTS1_00475*. It was confirmed that Mut5 and Mut7 harbored mutations in *MTS1_03028*. When a single mutation was induced in *MTS1_00475* or *MTS1_03028*, Cs^+ resistance was significantly reduced. Thus, both of these genes play critical roles in Cs^+ resistance. Future research should aim to develop a strategy for utilizing TS-1 and other bacteria with the aforementioned Cs^+ resistance mechanism in the bioremediation of Cs^+-contaminated soil adjacent to nuclear power plants, radioactive ore tailings, and others.

Data availability statement

The datasets presented in this study can be found in online repositories. The names of the repository/repositories and accession number(s) can be found at: NCBI - https://www.ncbi.nlm.nih.gov/sra/DRR328007; https://www.ncbi.nlm.nih.gov/sra/?term=DRR328008; https://www.ncbi.nlm.nih.gov/sra/?term=DRR328009; https://www.ncbi.nlm.nih.gov/sra/?term=DRR328010.

Author contributions

MI designed the research and wrote the manuscript. YI, TK, EI, MT, and MI conducted the research. TK, YI, and MI analyzed the data. All authors contributed to the article and approved the submitted version.

Funding

This work was supported by a grant for the Toyo University Top Priority Research Promotion Program and the Toyo University intellectual property practical application promotion program.

Acknowledgments

We would like to thank Editage (www.editage.com) for English language editing.

Conflict of interest

The authors declare that the research was conducted in the absence of any commercial or financial relationships that could be construed as a potential conflict of interest.

Publisher's note

Supplementary material

The Supplementary material for this article can be found online at: https://www.frontiersin.org/articles/10.3389/fmicb.2023.1136514/full#supplementary-material

References

Akanuma, G., Kobayashi, A., Suzuki, S., Kawamura, F., Shiwa, Y., Watanabe, S., et al. (2014). Defect in the formation of 70S ribosomes caused by lack of ribosomal protein L34 can be suppressed by magnesium. *J. Bacteriol.* 196, 3820–3830. doi: 10.1128/JB.01896-14

Bossemeyer, D., Schlösser, A., and Bakker, E. P. (1989). Specific cesium transport via the *Escherichia coli* Kup (TrkD) K^+ uptake system. *J. Bacteriol.* 171, 2219–2221. doi: 10.1128/jb.171.4.2219-2221.1989

Buesseler, K. O., Jayne, S. R., Fisher, N. S., Rypina, I., Baumann, H., Baumann, Z., et al. (2012). Fukushima-derived radionuclides in the ocean and biota off Japan. *Proc. Natl. Acad. Sci. U. S. A.* 109, 5984–5988. doi: 10.1073/pnas.1120794109

Cohen-Bazire, G., Sistrom, W. R., and Stanier, R. Y. (1957). Kinetic studies of pigment synthesis by non-sulfur purple bacteria. *J. Cell. Comp. Physiol.* 49, 25–68. doi: 10.1002/jcp.1030490104

Dekker, L., Osborne, T. H., and Santini, J. M. (2014). Isolation and identification of cobalt-and caesium-resistant bacteria from a nuclear fuel storage pond. *FEMS Microbiol. Lett.* 359, 81–84. doi: 10.1111/1574-6968.12562

Fujinami, S., Sato, T., and Ito, M. (2011). The relationship between a coiled morphology and Mbl in alkaliphilic *Bacillus halodurans* C-125 at neutral pH values. *Extremophiles* 15, 587–596. doi: 10.1007/s00792-011-0389-9

Fujinami, S., Takeda, K., Onodera, T., Satoh, K., Sano, M., Narumi, I., et al. (2013). Draft genome sequence of sodium-independent alkaliphilic *Microbacterium* sp. strain TS-1. *Genome Announc.* 1:e01043. doi: 10.1128/genomeA.01043-13

Guzman, L. M., Belin, D., Carson, M. J., and Beckwith, J. (1995). Tight regulation, modulation, and high-level expression by vectors containing the arabinose PBAD promoter. *J. Bacteriol.* 177, 4121–4130. doi: 10.1128/jb.177.14.4121-4130.1995

Hampton, C. R., Bowen, H. C., Broadley, M. R., Hammond, J. P., Mead, A., Payne, K. A., et al. (2004). Cesium toxicity in Arabidopsis. *Plant Physiol.* 136, 3824–3837. doi: 10.1104/pp.104.046672

Hirose, K. (2016). Fukushima Daiichi nuclear plant accident: atmospheric and oceanic impacts over the five years. *J. Environ. Radioact.* 157, 113–130. doi: 10.1016/j.jenvrad.2016.01.011

Huerta-Cepas, J., Serra, F., and Bork, P. (2016). ETE 3: reconstruction, analysis, and visualization of phylogenomic data. *Mol. Biol. Evol.* 33, 1635–1638. doi: 10.1093/molbev/msw046

Imazawa, R., Takahashi, Y., Aoki, W., Sano, M., and Ito, M. (2016). A novel type bacterial flagellar motor that can use divalent cations as a coupling ion. *Sci. Rep.* 6:19773. doi: 10.1038/srep19773

Ito, M., and Hasunuma, S. (2022a). Complete genome sequence of *Bacillus* sp. strain NC3, isolated from *Trichonephila* spider ground extract. *Microbiol. Resour. Announc.* 11, e01110–e01121. doi: 10.1128/mra.01110-21

Ito, M., and Hasunuma, S. (2022b). Complete genome sequence of *Bacillus* sp. strain TM2, isolated from ground *Tetragnatha* spider extract. *Microbiol. Resour. Announc.* 11:e0013022. doi: 10.1128/mra.00130-22

Kato, S., Goya, E., Tanaka, M., Kitagawa, W., Kikuchi, Y., Asano, K., et al. (2016). Enrichment and isolation of *Flavobacterium* strains with tolerance to high concentrations of cesium ion. *Sci. Rep.* 6:20041. doi: 10.1038/srep20041

Koretsune, T., Ishida, Y., Kaneda, Y., Ishiuchi, E., Teshima, M., Marubashi, N., et al. (2022). Novel cesium resistance mechanism of alkaliphilic bacterium isolated from jumping spider ground extract. *Front. Microbiol.* 13:841821. doi: 10.3389/fmicb.2022.841821

Larkin, M. A., Blackshields, G., Brown, N. P., Chenna, R., Mcgettigan, P. A., Mcwilliam, H., et al. (2007). Clustal W and Clustal X version 2.0. *Bioinformatics* 23, 2947–2948. doi: 10.1093/bioinformatics/btm404

Liu, X., Chen, G. R., Lee, D. J., Kawamoto, T., Tanaka, H., Chen, M. L., et al. (2014). Adsorption removal of cesium from drinking waters: a mini review on use of biosorbents and other adsorbents. *Bioresour. Technol.* 160, 142–149. doi: 10.1016/j.biortech.2014.01.012

Nakamura, K., Chiba, S., Kiuchi, T., Nabeshi, H., Tsutsumi, T., Akiyama, H., et al. (2022). Comprehensive analysis of a decade of cumulative radiocesium testing data for foodstuffs throughout Japan after the 2011 Fukushima Daiichi nuclear power plant accident. *PLoS One* 17:e0274070. doi: 10.1371/journal.pone.0274070

Nozaki, K., Kuroda, T., Mizushima, T., and Tsuchiya, T. (1998). A new Na^+/H^+ antiporter, NhaD, of *Vibrio parahaemolyticus*. *Biochim. Biophys. Acta* 1369, 213–220. doi: 10.1016/S0005-2736(97)00223-X

Osman, M. A., Patel, R. B., Schuna, A., Sundstrom, W. R., and Welling, P. G. (1983). Reduction in oral penicillamine absorption by food, antacid, and ferrous sulfate. *Clin. Pharmacol. Ther.* 33, 465–470. doi: 10.1038/clpt.1983.63

Sakai, M., Tsuji, H., Ishii, Y., Ozaki, H., Takechi, S., Jo, J., et al. (2021). Untangling radiocesium dynamics of forest-stream ecosystems: a review of Fukushima studies in the decade after the accident. *Environ. Pollut.* 288:117744. doi: 10.1016/j.envpol.2021.117744

Singh, B. S. M., Dhal, N. K., Kumar, M., Mohapatra, D., Seshadri, H., Rout, N. C., et al. (2022). Phytoremediation of (137) Cs: factors and consequences in the environment. *Radiat. Environ. Biophys.* 61, 341–359. doi: 10.1007/s00411-022-00985-3

Smith, R. L., and Maguire, M. E. (1998). Microbial magnesium transport: unusual transporters searching for identity. *Mol. Microbiol.* 28, 217–226. doi: 10.1046/j.1365-2958.1998.00810.x

Swer, P. B., Joshi, S. R., and Acharya, C. (2016). Cesium and strontium tolerant *Arthrobacter* sp. strain KMSZP6 isolated from a pristine uranium ore deposit. *AMB Express* 6:69. doi: 10.1186/s13568-016-0247-3

Vasylenko, V. V., Kuriata, M. S., Morozov, V. V., Lytvynets, L. O., Kramarenko, M. S., Bilonyk, A. B., et al. (2021). Comprehensive radiation and hygienic monitoring in population of the Rivne oblast radiologically contaminated territories. *Probl. Radiac. Med. Radiobiol.* 26, 124–140. doi: 10.33145/2304-8336-2021-26-124-140

Wu, J., Zheng, X., Chen, J., Yang, G., Zheng, J., and Aono, T. (2022). Distributions and impacts of plutonium in the environment originating from the Fukushima Daiichi nuclear power plant accident: an overview of a decade of studies. *J. Environ. Radioact.* 248:106884. doi: 10.1016/j.jenvrad.2022.106884

Yukawa, T., Bamba, T., Matsuda, M., Yoshida, T., Inokuma, K., Kim, J., et al. (2022). Enhanced production of 3,4-dihydroxybutyrate from xylose by engineered yeast via xylonate re-assimilation under alkaline condition. *Biotechnol. Bioeng.* 120, 511–523. doi: 10.1002/bit.28278

Zhang, F., Guo, Y., Ji, J., Li, G., Zhang, H., and Yu, T. (2021). Complete genome sequence of a high cesium ion-tolerating bacterium *Bacillus* sp. Cs-700 isolated from the South China Sea sediment. Mar. *Genomics* 56:100810. doi: 10.1016/j.margen.2020.100810

frontiers | Frontiers in Microbiology

TYPE Original Research
PUBLISHED 29 March 2023
DOI 10.3389/fmicb.2023.1147162

OPEN ACCESS

EDITED BY
Andreas Teske,
University of North Carolina, Chapel Hill, United States

REVIEWED BY
Anirban Chakraborty,
Idaho State University, United States
Kevin R. Sowers,
University of Maryland, Baltimore, United States

*CORRESPONDENCE
Mahmoud Shavandi
✉ shavandim@ripi.ir
Mohammad Ali Amoozegar
✉ amoozegar@ut.ac.ir

SPECIALTY SECTION
This article was submitted to Extreme Microbiology, a section of the journal Frontiers in Microbiology

RECEIVED 18 January 2023
ACCEPTED 13 March 2023
PUBLISHED 29 March 2023

CITATION
Yavari-Bafghi M, Rezaei Somee M, Amoozegar MA, Dastgheib SMM and Shavandi M (2023) Genome-resolved analyses of oligotrophic groundwater microbial communities along phenol pollution in a continuous-flow biodegradation model system.
Front. Microbiol. 14:1147162.
doi: 10.3389/fmicb.2023.1147162

Genome-resolved analyses of oligotrophic groundwater microbial communities along phenol pollution in a continuous-flow biodegradation model system

Maryam Yavari-Bafghi[1], Maryam Rezaei Somee[2], Mohammad Ali Amoozegar[1]*, Seyed Mohammad Mehdi Dastgheib[3] and Mahmoud Shavandi[3]*

[1]Extremophiles Laboratory, Department of Microbiology, School of Biology, College of Science, University of Tehran, Tehran, Iran, [2]Centre for Ecology and Evolution in Microbial Model Systems (EEMiS), Linnaeus University, Kalmar, Sweden, [3]Microbiology and Biotechnology Group, Environment and Biotechnology Research Division, Research Institute of Petroleum Industry, Tehran, Iran

Groundwater pollution is one of the major environmental concerns. The entrance of pollutants into the oligotrophic groundwater ecosystems alters native microbial community structure and metabolism. This study investigated the application of innovative Small Bioreactor Chambers and CaO_2 nanoparticles for phenol removal within continuous-flow sand-packed columns for 6 months. Scanning electron microscopy and confocal laser scanning microscopy analysis were conducted to indicate the impact of attached biofilm on sand surfaces in bioremediation columns. Then, the influence of each method on the microbial biodiversity of the column's groundwater was investigated by next-generation sequencing of the 16S rRNA gene. The results indicated that the simultaneous application of biostimulation and bioaugmentation completely eliminated phenol during the first 42 days. However, 80.2% of phenol remained in the natural bioremediation column at the end of the experiment. Microbial diversity was decreased by CaO_2 injection while order-level groups known for phenol degradation such as *Rhodobacterales* and *Xanthomonadales* dominated in biostimulation columns. Genome-resolved comparative analyses of oligotrophic groundwater prokaryotic communities revealed that *Burkholderiales*, *Micrococcales*, and *Cytophagales* were the dominant members of the pristine groundwater. Six-month exposure of groundwater to phenol shifted the microbial population towards increasing the heterotrophic members of *Desulfobacterales*, *Pseudomonadales*, and *Xanthomonadales* with the degradation potential of phenol and other hydrocarbons.

KEYWORDS

oligotrophic groundwater, biodiversity, metagenome, phenol, bioremediation

1. Introduction

In recent decades, increasing demand for petroleum hydrocarbon, leakage from storage tanks and pipelines, and unsafe waste transportation have become severe global environmental issues. The pollutants are easily transported by the natural water flow and contaminate the downstream groundwater (Koshlaf et al., 2016; Wang et al., 2016; Lu et al., 2017). Phenols are the major organic compounds present in the effluents of various industries (e.g., petroleum), which contaminate groundwater by infiltration through the soil of the polluted area (Mohammadi et al., 2015; Sun et al., 2015). They are considered the main pollutants having high solubility in water (84.2 g L^{-1}) and hence carcinogenic impacts on humans, animals, and plants (Villegas et al., 2016).

Groundwater, as a most critical water resource, is widely used in washing and irrigation processes for about 40% of the world's agricultural products and also influences the rates and types of biogeochemical cycles in water networks (Lall et al., 2020). Although all domains of life are present and active in groundwater, archaea and bacteria showed a clear dominance over eukarya (Lopez-Fernandez et al., 2018). Prokaryotes, with estimated total abundances of 10^2–10^6 cells, have a vital role in the biogeochemical cycles (Clark et al., 2018). The entrance of hydrocarbon pollutants into the oligotrophic groundwater ecosystems will increase microbial metabolism, change their community structure, and affect their role in cycling elements (Flynn et al., 2008). Therefore, pollutant removal from groundwater has great importance.

Among the numerous physical, chemical, and biological groundwater treatment approaches, bioremediation has been widely used as a safe, economical, and eco-friendly method in recent years (Dong et al., 2019; Cecconet et al., 2020). However, it is a time-consuming process due to the limited amount of dissolved oxygen (DO) and low microbial count of the groundwater (Lu et al., 2017). To overcome this problem, biostimulation [by injection of oxygen-releasing compounds (ORCs)] and bioaugmentation (using exogenous microbial consortia inoculation) were applied in several studies (Pickup et al., 2001; Mikkonen et al., 2018).

Oxygen-releasing compounds, like calcium peroxide (CaO_2), decompose to oxygen and hydroxyl radicals after exposure to water and accelerate the contaminant degradation (Mosmeri et al., 2018, 2019). According to previous studies, the generated O_2 stimulates the intrinsic groundwater microorganisms, and OH' radicals destroy the aromatic structure of pollutants (Yeh et al., 2010; Gholami et al., 2019). CaO_2 nanoparticles have been applied for groundwater treatment in a lot of research (Cassidy and Irvine, 1999; Xue et al., 2018; Mosmeri et al., 2019). For instance, in Qian et al. (2016) study, 2,4-dichlorophenol was removed by nanoscale CaO_2 from groundwater. On the other side, the application of bioaugmentation to treat groundwater samples polluted with phenol, arsenic, and total petroleum-hydrocarbons (TPH) has recently received increasing interest (Dey et al., 2016; Hedbavna et al., 2016; Poi et al., 2018; Zhuang and Fang, 2020). However, achieving and maintaining a sufficient microbial mass over time is the main challenge for implementing bioaugmentation. In our previous study, Small Bioreactor Chambers (SBCs) were developed that enabled high concentrations of external specific microbial consortiums to stay active (alive) and grow normally inside the 3D chambers in a suspended state for phenol removal of groundwater. The innovative design of SBCs allowed diffusion of phenol, DO, and nutrients into the encapsulated culture, however, confined the inner bacteria due to the presence of cellulose acetate membranes with pores of up to 0.22 μm in diameter. In addition, the SBCs contained a lyophilized specific consortium which was in a dry state and not active. The penetration of water through the membrane activated the freeze-dried culture and as long as the nutrients and DO were present in the water, the consortium was active and stable (Yavari-Bafghi et al., 2022). Due to the specific SBCs structure, indigenous or consortium bacteria, cannot pass through the 0.22 microfiltration (MF) membrane and as a result, SBCs are more environmentally friendly than polymer beads (González, 2001; Duan et al., 2016).

Despite the vast number of publications on the ecological characteristics of groundwater, the microbial community dynamics and the metabolic context in response to pollutant exposure during the bioremediation process, especially in Iran, have been less noticed.

Current work aims to (i) investigate the performance and impact of simultaneous use of CaO_2 nanoparticles and SBCs on the intrinsic microorganisms of oligotrophic groundwater within phenol bioremediation during continuous-flow experiments (pilot level), (ii) survey the microbial community dynamics of the groundwater along the phenol pollution, and (iii) study the microbial potential metabolic capabilities in hydrocarbon degradation and biogeochemical cycles. To achieve these objectives, we conducted a 6-month biostimulation and bioaugmentation investigation through the sand-packed columns with a continuous flow of phenol-polluted groundwater. The genome-resolved comparative analyses of the pristine and phenol-contaminated groundwater were performed afterward.

2. Materials and methods

2.1. Chemical

Phenol (99.99%), calcium chloride (99.99%), sodium hydroxide (99.99%), sodium azide, and glutaraldehyde (25% in H_2O, grade I) were prepared from Sigma-Aldrich, R_2A agar, and H_2O_2 (30%) were purchased from Merck. All other chemicals were of analytical grade and obtained from commercial sources. The sand and groundwater used in this study were prepared as described in our previous work (Yavari-Bafghi et al., 2022).

2.2. Calcium peroxide nanoparticles synthesis

Calcium peroxide nanoparticles were synthesized based on calcium chloride ($CaCl_2$) and hydrogen peroxide reaction conforming to the procedure described by Khodaveisi et al. (2011).

Abbreviations: SBCs, Small Bioreactor Chambers; CaO_2, calcium peroxide; NGS, next-generation sequencing; DO, dissolved oxygen; ORCs, oxygen-releasing compounds; PRB, permeable reactive barrier; SEM, scanning electron microscopy; CLSM, confocal laser scanning microscopy.

2.3. Column experiments

According to the results of batch experiments in our previous work (Yavari-Bafghi et al., 2022), column experiments were conducted to investigate the CaO_2 nanoparticles and SBCs performance in phenol removal from oligotrophic groundwater through the permeable reactive barrier (PRB). Four continuous up-flow Plexiglas reactors (100 cm length and 9 cm inner diameter) were packed with underground originated acid-washed and autoclaved sands with particle size in the 2–4 mm range. The phenol (100 mg/L) contaminated groundwater was passed through the columns with a 20 cm/day flow rate. To simulate the underground conditions, all the experiments were carried out in a cold room with a temperature of 15 ± 0.5°C.

As illustrated in **Figure 1**, column I was considered the abiotic column in which the filter-sterilized phenol-contaminated groundwater containing 1 g/L sodium azide was used as the inlet flow to study the chemical phenol removal efficiency by calcium peroxide nanoparticles. Column II was used to simulate the natural bioremediation process as the blank column. Columns III (CaO_2 injected) and (IV) (CaO_2 injected + SBCs placed) were applied to investigate the efficiency of biostimulation and bioaugmentation processes, respectively in the phenol removal of groundwater.

Before the experiments, groundwater from the feed tank (pH 7.4 ± 0.01 and DO of 4 mg/L) flowed through the packed columns for 4 weeks to perform the adaptation phase. Initially, 15 g of CaO_2 nanoparticles were injected into columns I, III, and IV. Then, to maintain the desired conditions in the columns, 15 and 5 g of CaO_2 were re-injected after 8 and 16 weeks, respectively. SBCs were placed in column IV simultaneously with the first CaO_2 injection. DO, pH, phenol concentration, and microbial count were measured within 6 months.

2.3.1. Sampling and chemical analysis

The DO and pH of the water samples of each column effluent were measured using HQ40d multimeter (HACH). Phenol concentration in groundwater was analyzed by high-performance liquid chromatography (HPLC) (SPD-M10 A, Shimadzu, Japan). The HPLC analysis conditions were as previously presented by Yavari-Bafghi et al. (2022). Moreover, the total culturable microbial count of the effluent samples was measured by the standard plate count (SPC) method on R2A agar, and the colonies were counted by a standard colony counter (SC6 Plus, Stuart). At the end of the experiments, the physicochemical parameters of the effluent of each column were analyzed through standard methods (**Supplementary Table 1**) and compared with groundwater parameters reported in the authors' previous study (Yavari-Bafghi et al., 2022).

Additionally, scanning electron microscopy (SEM) (VEGA\\TESCAN-XMU) and confocal laser scanning microscopy (CLSM) (Leica TCS SPE) were applied according to Gholami et al. (2018) and Inoué (2006), respectively, to study the microbial attachment and biofilm formation on the sand surfaces.

2.3.2. DNA extraction and microbial diversity analysis

To study the effects of CaO_2 and SBCs application on the structure and diversity of the oligotrophic groundwater microbial community by 16S rRNA gene amplicon sequencing, total microbial DNA was extracted from column's sand surfaces using DNeasy® PowerSoil® (QIAGEN) according to the manufacturer's protocol. In addition, the genomic DNA of the SBC's consortium was extracted through the NucleoSpin® Microbial DNA isolation kit (Macherey-Nagel) according to the manufacturer's protocol to investigate the consortium dynamics during the experiment in comparison to our previous study (Yavari-Bafghi et al., 2022). The quality and concentration of the extracted DNA were analyzed by NanoDrop UV–Vis spectrophotometer (ND-1000, USA). Additionally, to ensure the structural integrity of the extracted DNA, 5 μl DNA was loaded on 1.0% agarose gel and visualized under UV in a gel documentation system. The V3–V4 region of the 16S rRNA gene was analyzed using 341F and 806R universal primers and sequenced on the Illumina MiSeq platform (Novogene company, Hong Kong).

Paired-end reads were merged to tags based on overlaps using FLASH (V1.2.7) (Magoc and Salzberg, 2011). To obtain high-quality clean tags, quality filtering on the raw tags was performed according to the Qiime (V1.7.0) (Caporaso et al., 2010). Operational taxonomic units (OTUs) were generated using Uparse software (V7.0.1090) with a 97% similarity threshold for the tags (Edgar, 2013). SSUrRNA database (SILVA138.1) was applied for species annotation of each representative sequence at each taxonomic rank, using Mothur software. The phylogenetic relationship of all sequences was obtained by MUSCLE (V3.8.31) which can compare multiple sequences rapidly (Edgar, 2004; Quast et al., 2013). Histograms of the relative abundance (%) of taxa in different samples were plotted in RStudio (V3.1.1).

2.4. Comparative metagenomic analyses of groundwater prokaryotic communities

2.4.1. Sampling site description, sample collection, and DNA extraction

Comparative metagenomic analyses were performed during 6 months of continuous phenol pollution (100 mg/L) to investigate the dynamics of oligotrophic groundwater microbial communities due to phenol contamination. Sampling from the deep groundwater well located in the research institute of the petroleum industry, Tehran, Iran (35°44′18.7″ N 51°15′34.0″ E) was done in May 2020 using a water pump. This water sample was considered a control point without any pollution (GW). The sands used in the second column in the PRB studies were collected after 6 months of experiments. As mentioned before, the phenol (100 mg/L) contaminated groundwater was passed through the column for 6 months and the sands, which were autoclaved before applying into the column, were considered a suitable substrate for the formation of microbial biofilms during the experiment (second point, R2).

For the first sampling point, 80 L of water sample were collected and pre-filtered through 20 μm (Albet DP5891150, Germany), and 5 μm pore-size (Albet DP5895150, Germany) filters (15 cm in diameter). Microbial biomass was finally concentrated on 0.22 μm pore-size cellulose acetate filters (Sartorius 11107-142-N, Germany) using a peristaltic pump. Sand samples were collected from the sampling port of the column using sterile laboratory

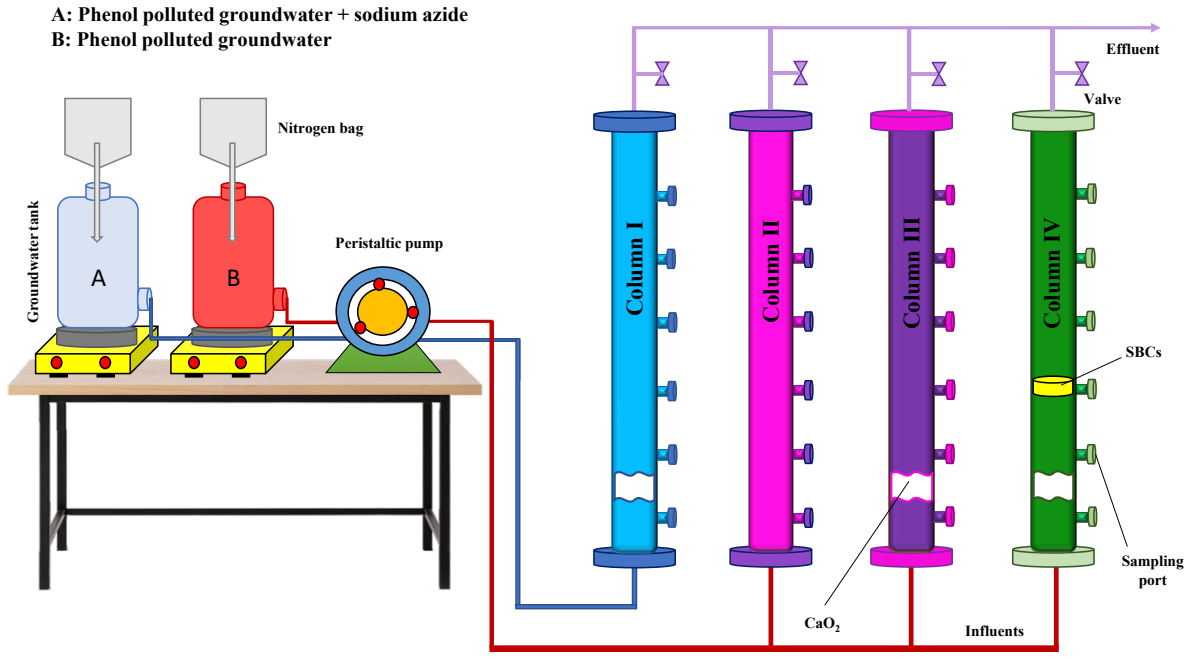

FIGURE 1
Schematic representation of column experiments. Column I: phenol removal in the abiotic condition by CaO_2 nanoparticles (chemical), column II: natural bioremediation of phenol (blank), column III: phenol remediation by CaO_2 nanoparticles and native groundwater microbial population (biostimulation), and column IV: phenol remediation by CaO_2 nanoparticles and SBCs (biostimulation and bioaugmentation).

pincers. Water filters and sand samples were stored at −80°C until DNA extraction.

A standard phenol-chloroform protocol (Martín-Cuadrado et al., 2007) was used for extracting community DNA from the water sample. DNeasy PowerMax Soil DNA Extraction Kit (QIAGEN 12988-10, Germany) was applied for DNA extraction of the sand samples, according to the manufacturer's instructions. Extracted DNA samples were sequenced using Illumina Novaseq 6000 platform (PE150) (Novogene, Hong Kong).

2.4.2. Ribosomal RNA classification

A subset of 5 million reads was separated from each dataset, and the reads affiliated with ribosomal RNA genes were detected using SSU-ALIGN (Nawrocki, 2009). Then, the putative prokaryotic 16S rRNA gene sequences were blasted against the SILVA reference database (release 138.1 SSUParc) using BLAST, and their taxonomic affiliation was assigned based on their closest hit if the read was ≥90 bp at the similarity threshold of ≥90.

2.4.3. Sequence assembly, binning, and annotation

Paired-end reads of the sequenced datasets were interleaved and quality trimmed using reformat.sh and bbduck.sh scripts of the BBMap toolkit, respectively (Bushnell, 2014). All trimmed sequences of each dataset were assembled separately using MEGAHIT (k-mer list 49, 69, 89, 109, 129, and 149) (Li et al., 2015). MetaBat2 software binned contigs ≥1 kb into metagenome-assembled genomes (MAGs) based on their different mapping depth and tetranucleotide frequency (Kang et al., 2019). The quality and completeness of the reconstructed MAGs were evaluated with CheckM (Parks et al., 2015). The taxonomy of MAGs with ≥40% completeness and ≤5% contamination was assigned using GTDB-tk (release 202) (Chaumeil et al., 2020). Putative genes were predicted with Prodigal (Hyatt et al., 2010) and preliminarily annotated using Prokka in the metagenomics mood (Seemann, 2014). Finally, the eggNOG-mapper was used to annotate further each MAG's predicted protein sequences (Huerta-Cepas et al., 2019).

3. Results and discussion

3.1. Column experiments

3.1.1. Phenol removal experiments

Four continuous-flow columns were set up to investigate the phenol removal rate from oligotrophic groundwater by CaO_2 nanoparticles and SBCs. The experimental columns were as follows: (I) abiotic control column (CaO_2 + sodium azide), (II) natural remediation column (without CaO_2 and SBCs), (III) biostimulation column (CaO_2), and (IV) simultaneous biostimulation and bioaugmentation column (CaO_2 + SBCs).

As presented in **Figure 2**, the DO in the chemical column I effluent increased notably after the first injection and peaked on the 21st day, reaching 14.14 mg/L. Production of $Ca(OH)_2$ from calcium peroxide decomposition increased the pH in the injection zone (**Figure 2B**), resulting in the higher stability of solid peroxide (Gholami et al., 2018). According to Northup and Cassidy (2008), CaO_2 in an alkaline environment tends to produce O_2 rather than OH'. Therefore, most CaO_2 nanoparticles in column I were converted to oxygen, which completely remained in the abiotic column.

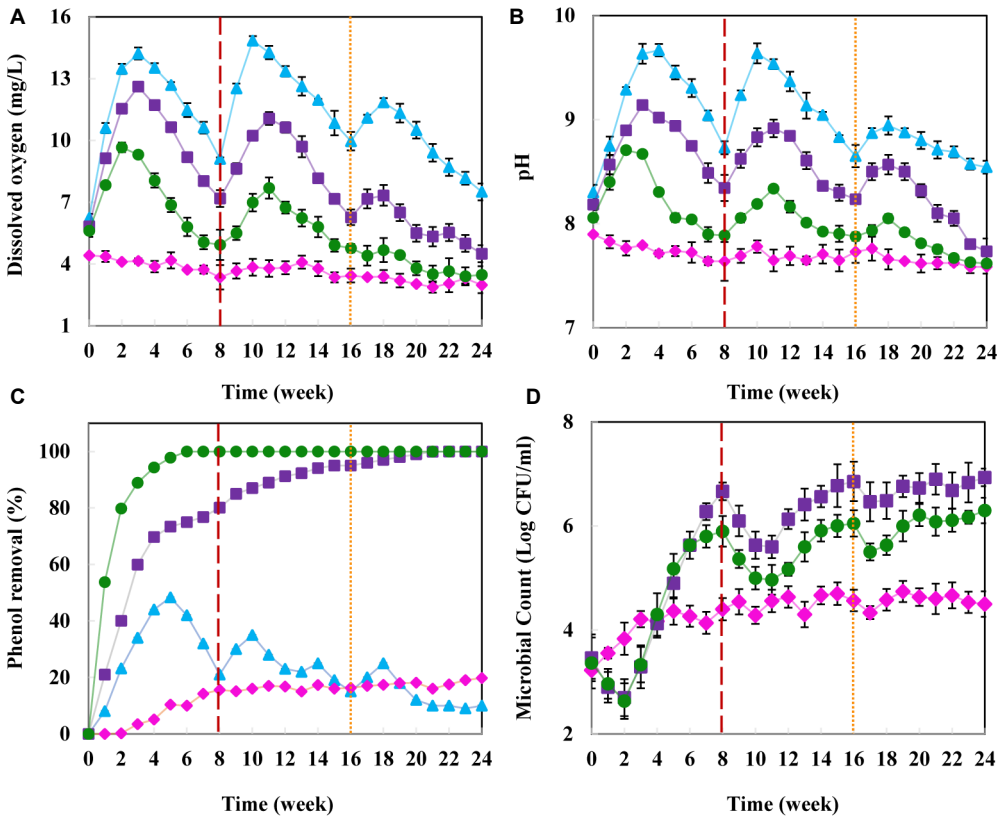

FIGURE 2
Remediation of phenol from groundwater in the column experiments. **(A)** Dissolved oxygen concentration (mg/L), **(B)** pH, **(C)** phenol removal (%), and **(D)** intrinsic microbial count (log CFU/mL). Abiotic column (▲), natural remediation column II (♦), biostimulation column III (■), and simultaneous biostimulation and bioaugmentation column IV (●). The red and orange dashed lines, respectively indicate 15 and 5 g CaO_2 nanoparticles re-injection to provide the proper contaminant removal condition.

By injection of nanoparticles into columns III and IV, the DO increased in comparison to the blank column II (**Figure 2A**). Within 21 days, it reached 12.62 and 9.31 mg/L in columns III and IV, respectively. However, due to the high microbial count (intrinsic and SBCs' communities) (**Figure 2D**) and oxygen consumption in column IV, DO dropped sharply (**Figure 2A**). To overcome this problem, the oxidative agents were re-injected into the groundwater after 8 and 16 weeks of the experiment.

After the first nanoparticle injection, the pH of column I effluent significantly increased and reached to 9.17 within 4 weeks (**Figure 2B**). In the three other columns, the pH slowly decreased, consistent with previous studies (Gholami et al., 2018; Mosmeri et al., 2019). According to Padhi and Gokhale (2017), it seems possible that these results are due to the production of acidic metabolites from the degradation of contaminants by microorganisms.

Only 19.8% of the phenol was naturally removed from groundwater in column II within 6 months (**Figure 2C**). Meanwhile, the addition of CaO_2 and SBCs to column IV resulted in the complete phenol remediation after 42 days. The contaminant removal efficiency in column III containing CaO_2 increased to 90% after 12 weeks and reached 100% in the 22nd week. In the abiotic column I, 48.3% of the phenol was removed within 5 weeks; however, a remarkable reduction in the contaminant removal efficiency was observed afterward.

Further CaO_2 injection into column I at weeks 8 and 16 could not improve the phenol removal by more than 48.3%. The majority of H_2O_2 generated from CaO_2 was converted to oxygen in the abiotic column I, and $OH^{\bullet}$ content in water was not enough to degrade 100 mg/L of phenol (**Figure 2C**). These results were consistent with previous studies (Northup and Cassidy, 2008; Mosmeri et al., 2017; Gholami et al., 2018). Moreover, in accordance to prior surveys, our results indicated that by increasing the groundwater DO, microbial growth and activity gradually increased (Mosmeri et al., 2017; Gholami et al., 2019; Yavari-Bafghi et al., 2022).

In the natural bioremediation column I, the culturable microbial count was increased logarithmically to more than 3.2×10^4 CFU/ml, then significantly limited due to the lack of enough available oxygen for microorganisms. After injecting CaO_2 nanoparticles into the biotic columns III and IV, the microbial count dropped initially due to the negative impacts of OH radicals generated from nanoparticles on the intrinsic microorganisms. Then, the count increased by adapting the microbial population to the oxidative condition (**Figure 2D**).

In summary, the results showed that the phenol remediation of oligotrophic groundwater was entirely successful in the presence of CaO_2 and SBCs. Furthermore, the simultaneous application of biostimulation and bioaugmentation methods significantly increased the contaminant removal efficiency. Our results agree

with Liu N. et al. (2018), which used a PRB containing CaO_2 to remediate nitrobenzene-contaminated groundwater and observed the highest removal rate in the presence of calcium peroxide and nitrobenzene-degrading bacteria after 20 days. Additionally, a comparison of the phenol removal in the natural remediation column II and the abiotic column I indicates the crucial role of microorganisms in the remediation process. The innovative SBCs concept of macro-encapsulation allowed the possibility of selective contaminant removal in the water using the encapsulation of a specific bacterial culture. This study proved the beneficial effects of native bacterial biostimulation and bioaugmentation with external bacteria in oligotrophic environments through continuous-flow reactors. Besides, this bioremediation procedure is considered in-situ cost-effective, environmentally friendly, and performs at high efficiencies compared to conventional *ex situ* pump and treat technologies.

3.1.2. Microscopic analysis of microbial biofilm on the sand surface

Apart from the planktonic groundwater microorganisms, the attached microbial population (biofilm) on the sand surfaces also plays a key role in contaminant remediation. Therefore, bacterial adhesion to the sand surface and biofilm thickness was respectively examined by SEM and CLSM.

As represented in **Figure 3** and **Supplementary Figure 1**, no recognizable microorganism was observed on the sand surface in the abiotic column I (**Figure 3A** and **Supplementary Figure 1A**). It proved that no microbial degradation was involved in phenol removal from the column I effluent, and remediation was conducted by hydroxyl radicals ($OH^{\bullet}$). The groundwater microorganisms were attached to the sand surfaces and formed a thin biofilm layer (**Figure 3B** and **Supplementary Figure 1B**). However, by stimulating the microbial activity, the attached microbial communities with a thick biofilm layer can be seen on the sand surfaces (**Figures 3C, D** and **Supplementary Figures 1C, D**). It has resulted from the direct effect of oxygen-releasing nanoparticles on microbial growth. Present findings seem to be consistent with the results of Mosmeri et al. (2019) and Gholami et al. (2018), which investigated the impact of CaO_2 on groundwater microbial communities. It can also be indicated from **Figure 3C** that the attached microbial communities, due to more desirable oxygen conditions in column III, formed a thicker biofilm compared to others.

3.1.3. Water characteristics after treatment in each column

The concentration of NO_3^-, NO_2^-, $CaCO_3$, Cl^-, Fe (total), PO_4^-, color, and turbidity of the effluents from each column were examined at the end of the experiment and were compared with oligotrophic groundwater parameters (**Supplementary Table 2**). Among mentioned factors, PO_4^-, Fe (total), Cl^-, and color showed no significant changes. However, there was a substantial decrease in the NO_3^- and NO_2^- concentrations of the biotic columns II, III, and IV effluent (**Supplementary Table 2**). These results indicate that groundwater microorganisms consume nitrate as a nitrogen source during phenol biodegradation. In line with the study of Ye et al. (2017), nitrate in groundwater can also be removed by the denitrification process.

$CaCO_3$ concentration was increased from 184 mg/L in the groundwater to 253 mg/L by flowing through the abiotic column I, which contained sodium azide. However, in columns II, III, and IV effluents, the concentration of $CaCO_3$ trend was decreased. According to previous reports, the coincidence of the denitrification and high pH leads to the precipitation of bicarbonates in groundwater (Dupraz et al., 2004; Hamdan et al., 2017). Meanwhile, microbial growth in columns III, IV, and II, raised the water turbidity from 1.8 to 2.5, 2.2, and 1.9, respectively. In contrast, abiotic column I effluent, which lacked microbial growth, was the most transparent sample.

3.1.4. Microbial community analysis

Microbial community compositions of columns at the order level are visualized in **Supplementary Figure 2**. Although *Rhodobacterales* with more than 70% relative abundance were dominated in samples from columns III and IV, they were present in lower than one percent in another column. In accordance with the current results, Jehmlich et al. (2010) demonstrated that the order *Rhodobacterales* abundance increased along the chronic hydrocarbon pollution in groundwater. Therefore, the presence of this order in columns III and IV indicates its ability to remove phenol under aerobic conditions. The order *Burkholderiales* showed a high abundance (45.01%) in column II, while it had a percentage of around three in other columns. The reduction in the prevalence of order *Burkholderiales* in biostimulation columns III and IV was probably due to the toxic effects of hydroxyl radical generation, which was previously mentioned in section "3.1.1. Phenol removal experiments."

The order *Xanthomonadales* had relatively similar frequency in all three columns. Despite the presence of *Syntrophobacterales* in the natural bioremediation column II, its frequency reached zero in the third and fourth columns. Orders *Desulfobacterales*, *Bacteriovoracales*, *Pseudomonadales,* and *Bdellovibrionales,* which were identified in column II, were not detected in columns III and IV. Representatives of *Syntrophobacterales*, *Desulfobacterales,* and *Bacteriovoracales* generally have anaerobic respiration or fermentation metabolism (Koval et al., 2015; Dyksma et al., 2018; Liu P. et al., 2018); thus, their abundance was higher in the oxygen-deficient column II than in the biostimulation columns (**Supplementary Figure 2**).

According to **Supplementary Figure 2**, column II (natural bioremediation) exhibited the highest species richness among the samples collected at the end of the experiment. It seems that the application of ORCs had a remarkable impact on the microbial diversity of two other columns (III and IV). The same results were obtained in the bioremediation of benzene-contaminated groundwater by ORC (Mosmeri et al., 2019). Although the composition of the microbial community was changed in the presence of CaO_2 nanoparticles, it significantly increased the remediation efficiency.

Considering the environmental concerns about using the bioaugmentation method, the microbial community dynamics of the ph100 consortium were investigated at the end of the experiment. This microbial community was compared with the initial consortium's composition which was indicated in our previous study (Yavari-Bafghi et al., 2022). According to the results, the microbial composition of the ph100 consortium was constant during the continuous-flow experiment. Representatives

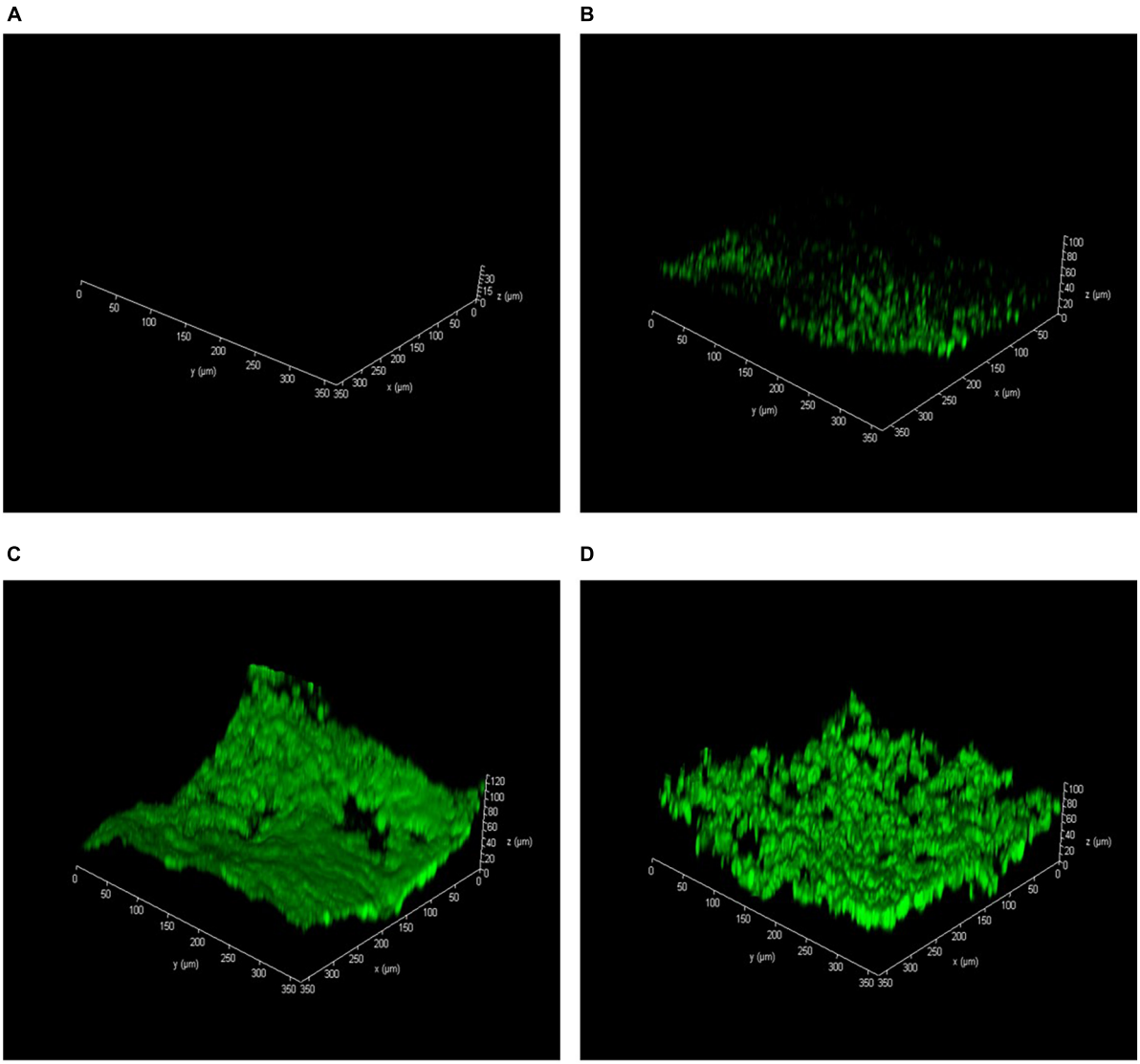

FIGURE 3
Acridine orange-stained confocal laser scanning microscopy (CLSM) images of biofilm thickness on the sand surface after 6 months. **(A)** Abiotic column I, **(B)** natural bioremediation column II, **(C)** biostimulation column III, and **(D)** biostimulation and bioaugmentation column IV.

of *Burkholderiales* from *Gammaproteobacteria* were the dominant order with almost the same relative abundance in both samples (**Supplementary Figure 3**). Based on the stability of the consortium's composition, it can be concluded that the SBCs have no microbial leakage, and only the contaminated water penetrates through the SBCs microfiltration structure membrane. As a result, the SBCs can solve a significant part of the environmental concern of the bioaugmentation method.

3.2. Comparative metagenomic analyses

3.2.1. Prokaryotic community composition, along the phenol pollution of groundwater

Comparative metagenomic analyses demonstrated that continuous exposure to phenol pollution in oligotrophic groundwater samples causes a shift in the microbial community composition. Hydrogen and CO_2 are frequently found in deep groundwater ecosystems since they are formed in the Earth's crust or mantle. Chemolithotrophs in these environments obtain their metabolic energy and carbon from the oxidation of reduced inorganic compounds and fixation of CO_2, respectively (Purkamo, 2017). As demonstrated in **Figure 4**, the microbial community of pristine groundwater (GW sample) was dominated by *Burkholderiales* (*Burkholderiaceae*), *Micrococcales*, *Cytophagales,* and *Sphingomonadales*. In a previous study, it has been proved that the family *Burkholderiaceae* belongs to the order *Burkholderiales* including obligate and facultative chemolithotroph members (Pérez-Pantoja et al., 2012).

The entrance of phenol as a carbon source into the oligotrophic groundwater altered the microbial community towards a higher relative abundance of *Desulfobacterales*, *Burkholderiales* (*Rhodocyclaceae*), *Pseudomonadales*, and *Xanthomonadales* in the R2 sample.

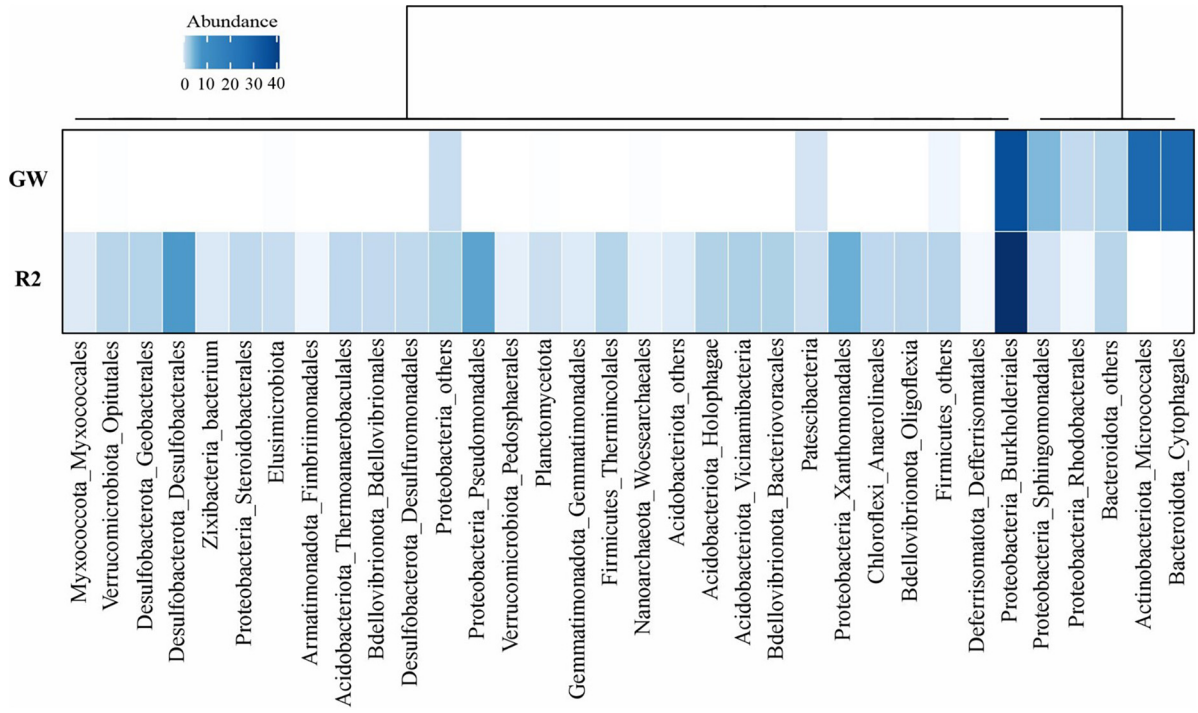

FIGURE 4
Prokaryotic community composition of the groundwater samples according to the abundance of 16S rDNA gene reads in unassembled metagenomes. Rows are the name of samples (GW: unpolluted and R2: phenol polluted groundwater). Column names are microbial taxa at the phylum and order level. For some taxa with lower frequency, the sum of orders is displayed as others or in their corresponding higher taxonomic level. There are a total number of 34 taxa for both samples. Dendrograms represent the clustering of columns based on Pearson correlation. The figure was plotted using "circlize" and "ComplexHeatmap" packages in R.

The order *Burkholderiales* of the phylum *Proteobacteria* was the most abundant member of the community in both R2 and GW samples. Its relative abundance increased from 35.57% (*Burkholderiaceae*) in GW to 45.01% (*Rhodocyclaceae*) in R2. According to Silva et al. (2013), the most effective bacteria that harbor the metabolic pathways for phenol degradation are represented by genera from the order *Burkholderiales*.

Furthermore, sulfate-reducing bacteria (SRB) in the R2 sample comprised up to 11% of the community (*Desulfobacterales*, *Geobacterales*, *Desulfuromonadales,* and *Myxococcales*). The nitrate- and sulfate-reducing bacteria were presented in almost all samples of marine oil-polluted sediments and are considered the most crucial hydrocarbon (HC) degrading communities in aquatic ecosystems with low levels of DO (Paissé et al., 2008; Stagars et al., 2017; Rezaei Somee et al., 2021). Additionally, the orders *Pseudomonadales* and *Xanthomonadales* were prevalent in the diesel-contaminated soils and have caused the efficient removal of pollutants (Koshlaf et al., 2016). It indicated that the bioremediation process successfully raised the population of the phenol-degrading species.

Among microbial members of groundwater samples, the representatives of *Woesearchaeales* from the phylum *Nanoarchaeota* were the only archaea observed in both metagenomic samples with 1% frequency.

In accordance with the previous study that reported the negative response of *Cytophagales* to oil pollution in marine ecosystems (Rezaei Somee et al., 2021), **Figure 4** represents that phenol pollution also significantly reduced the relative abundance of orders *Micrococcales* and *Cytophagales*. However, the relative abundance of *Firmicutes*, *Chloroflexi*, *Acidobacteriota,* and *Verrucomicrobiota* consistently increased from GW to R2 in response to phenol pollution. The entrance of high concentrations of HC pollutant (phenol) into the oligotrophic groundwater environment introduces new sources of carbon and more taxonomic groups were able to consume these carbon sources. As a result, the frequency of microbial groups increased and the amount of DO showed a significant reduction. In the absence of oxygen, alternative final electron acceptors such as nitrate and sulfate increased and consequently, a higher relative abundance of nitrate- and sulfate-reducing bacteria besides phenol-degrading members became dominant in the microbial community of the R2 sample. Furthermore, the alpha diversity of samples has been calculated based on the Shannon–Wiener index in R using the "vegan" package. As could be seen in **Supplementary Figure 4**, the R2 sample has a higher alpha index (2.3) than the pristine groundwater sample (1.4), indicating increased microbial diversity after phenol entrance.

3.2.2. Genome-resolved metabolic analysis of the groundwater prokaryotic community along the phenol pollution

A total of 47 metagenome-assembled genomes (MAGs) with completeness ≥40% and contamination ≤5% were recovered from two sequenced metagenomes, among which 46 belonged to domain bacteria and one to domain Archaea. Reconstructed bacterial MAGs were mainly affiliated with

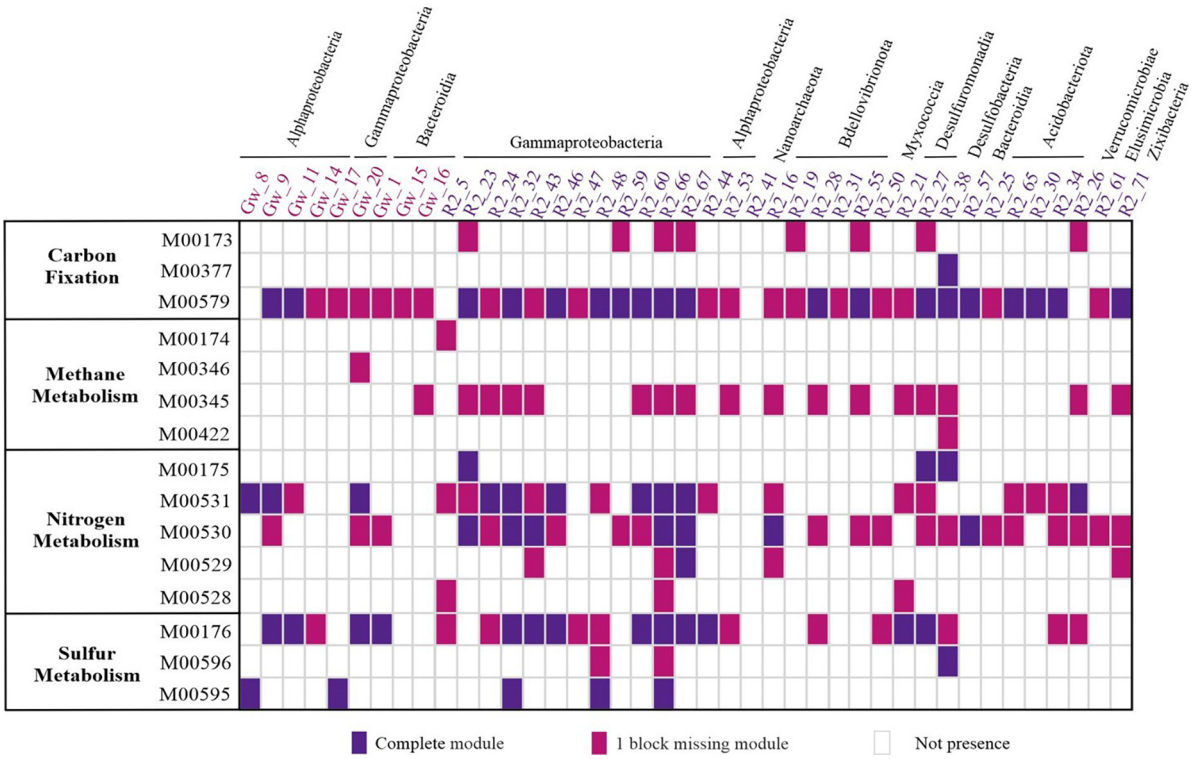

FIGURE 5
Energy metabolism pathways modules present in recovered MAGs from the groundwater metagenomes. The columns represent the taxonomy recovered of MAGs. The color of each MAG indicates the MAG origin. The row shows the cluster of metabolic pathways. Reductive citrate cycle (Arnon–Buchanan cycle) (M00173), reductive acetyl-CoA pathway (Wood–Ljungdahl pathway) (M00377), and phosphate acetyltransferase-acetate kinase pathway (M00579). Methane oxidation, methanotroph (M00174), formaldehyde assimilation, serine pathway (M00346), formaldehyde assimilation, ribulose monophosphate pathway (M00345), and Acetyl-CoA pathway (M00422). Nitrogen fixation (M00175), assimilatory nitrate reduction (M00531), dissimilatory nitrate reduction (M00530), nitrification (M00528), and denitrification (M00529). Assimilatory sulfate reduction (M00176), dissimilatory sulfate reduction (M00596), and thiosulfate oxidation by SOX complex (M00595). For the presence of a module that has all the enzymes of a pathway the value 2 and for the module that lacks one of the enzymes of a pathway the value 1 is considered.

Proteobacteria (46.8%), *Bdellovibrionota* (10.63%), *Bacteroidota* (8.51%), and *Desulfobacterota* (6.38%), along with some representatives of other phyla.

Metabolic pathways in each MAG have been recovered based on the KEGG orthologous (KO) list of corresponding MAG via the KEGG Mapper Reconstruct website tool[1] (**Supplementary Table 3**). The distribution of energy-related modules (e.g., carbon, nitrogen, and sulfur) present in at least one MAG is represented in **Figure 5**.

The KEGG orthologous accession numbers (KOs) of a collection of reported enzymes involved in the degradation of different aromatic and aliphatic hydrocarbons (HCs) under aerobic and anaerobic conditions were collected and surveyed in the annotated MAGs (Abbasian et al., 2015, 2016; Rabus et al., 2016). **Figure 6** represents the distribution of KEGG orthologues detected at least in one MAG (n = 93 genes). Mono/dioxygenases triggering the degradation of alkane, cyclododecane, biphenyl, phenol, toluene, xylene, and naphthalene/phenanthrene were detected in 43 recovered MAGs of the groundwater samples. Furthermore, the key enzymes responsible for initiating the degradation of alkane, ethylbenzene, phenol, and toluene exclusively under anaerobic conditions were detected in four reconstructed MAGs.

The metabolic context of pristine groundwater (GW sample) reconstructed MAGs suggested a primarily heterotrophic and autotrophic lifestyle. In oligotrophic groundwater, chemolithotrophs are responsible for organic matter production through CO_2 fixation (Purkamo, 2017). Representatives of *Alphaproteobacteria* (GW_9 and GW_11) in the GW sample were autotrophs capable of fixing carbon dioxide and producing acetate by using the phosphate acetyltransferase-acetate kinase pathway (**Figure 5**). Acetate is a key intermediate for heterotrophic bacteria in anaerobic conditions and is also considered as a carbon source for SRBs (Dyksma et al., 2018). Furthermore, sulfur-oxidizing chemolithoautotrophic bacteria such as NBD.18 (GW_17) and *Alphaproteobacteria* member (GW_8) are probably among the primary producers in GW sample by converting thiosulfate to sulfate through sulfate oxidation with SOX complex.

According to **Figure 6**, the distribution of HC-degrading enzymes is less frequent in reconstructed MAGs of the GW sample. However, sulfur-oxidizing MAGs, including GW_17, GW_20 (*Burkholderiales*), as well as GW_15 and GW_16 (*Algoriphagus*), potentially have enzymes involved in the degradation of phenol, toluene, xylene, ethylbenzene, alkanes, and naphthalene under both aerobic and anaerobic conditions. They were among

1 https://www.genome.jp/kegg/mapper/reconstruct.html

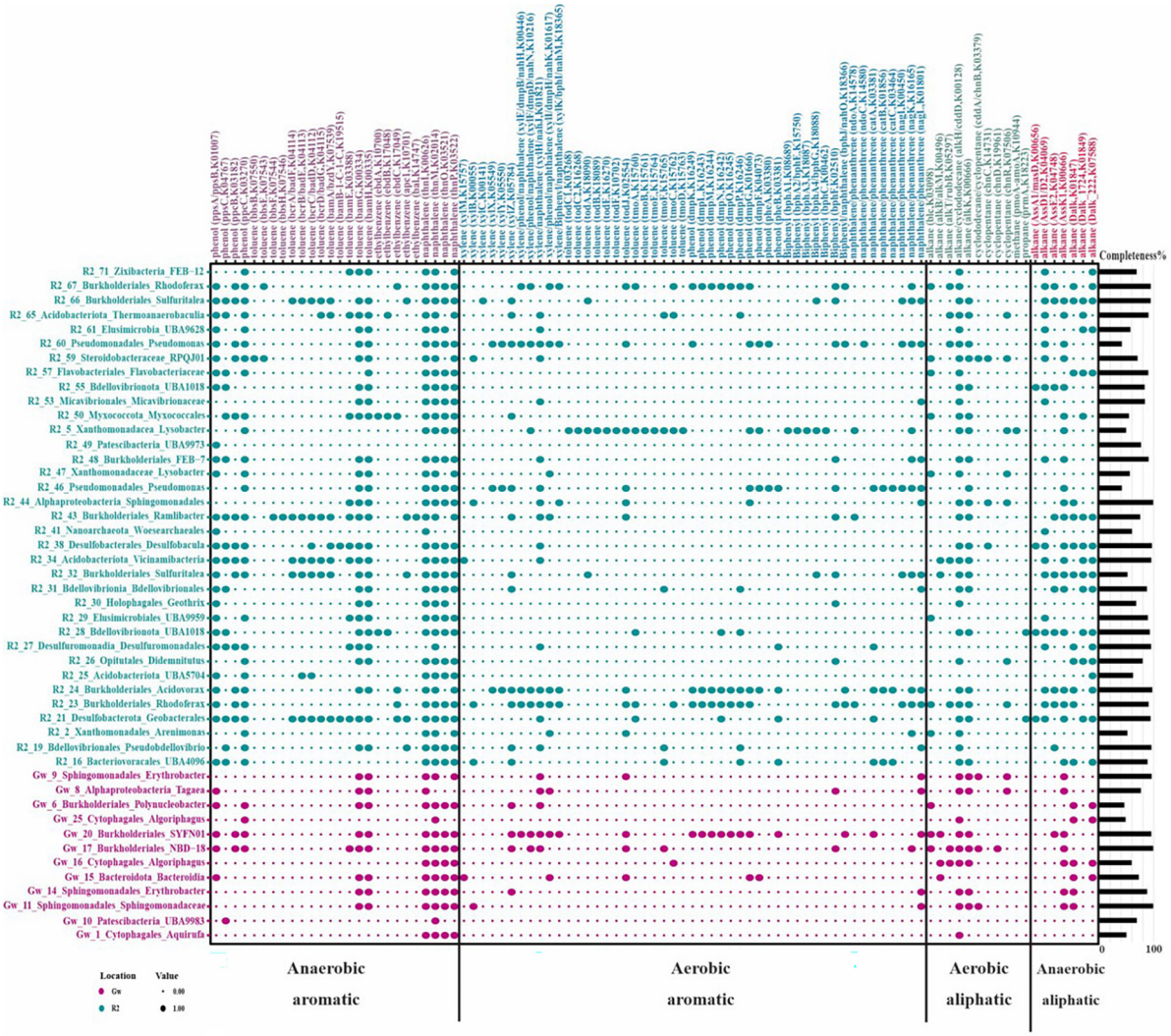

FIGURE 6
Hydrocarbon-degrading enzymes present in recovered MAGs from the groundwater metagenomes. Row names represent the taxonomy of recovered MAGs and their completeness is provided as a bar plot on the right side. The color indicates the MAG origin. Columns indicate the type of hydrocarbon and in the parenthesis is the name of the enzyme hydrolyzing this compound, followed by its corresponding KEGG orthologous accession number. The size of the dots indicates the presence or absence of each enzyme in each recovered MAG. The figure was plotted using the "reshape2" and "ggplot2" packages in RStudio.

microorganisms with alkB/M genes and were initiating the degradation of HCs under aerobic conditions in waters (Rezaei Somee et al., 2021).

In the R2 sample, despite recovering chemolithotrophic MAGs that potentially were capable of carbon fixation (**Figure 5**), MAGs with HC degradation ability were more prevalent due to the high concentrations of phenol as a carbon source (**Figure 6**).

R2_23 and R2_24 MAGs, affiliated to *Rhodoferax* and *Acidovorax*, respectively, had the genomic potential to degrade a diverse range of HCs, including phenol, alkane, biphenyl, toluene, ethylbenzene, and xylene under both aerobic and anaerobic conditions (**Figure 6**). Members of *Acidovorax* have been reported to potentially degrade various organic compounds like chlorobenzene (Monferrán et al., 2005), phenanthrene (Singleton et al., 2009), trichloroethylene (Futamata et al., 2005) and polyhydroxyalkanoates (Masood, 2017). Therefore, the genus *Acidovorax* can be one of the main genera that play a crucial role in the bioremediation of a wide range of oil derivatives in polluted ecosystems.

According to previous studies, the entrance of a carbon source into groundwater causes the activation of denitrification and increases nitrate reduction (Lee et al., 2021). *Sulfuritalea* (R2_32/66), *Rhodoferax* (R2_23), *Ramlibacter* (R2_43), and *Zixibacteria* (R2_71) had denitrification potential in the R2 sample. *Sulfuritalea* members have been identified in HC-polluted environments and reported to have conserved genes of the anaerobic benzoyl-CoA pathway, such as bamA, to initiate the degradation process under anaerobic conditions (Sperfeld et al., 2018). In the present study, the existence of aromatic and aliphatic compounds degradation genes under anaerobic conditions in the *Sulfuritalea* genome was confirmed and the presence of genes related to pollutant degradation in aerobic conditions was also reported. It seems that SRB members of *Burkholderiales* and *Desulfobacteraceae,* such as *Sulfuritalea* and FEB-7, have substrate

specificity in degrading hydrocarbon compounds. According to a recent study, they often degrade HCs in samples that have aliphatic compounds (Shin et al., 2019).

Representatives of *Zixibacteria* (R2_71) had genes for the degradation of phenol, toluene, ethylbenzene, alkanes, and naphthalene under anaerobic conditions. The phylum *Zixibacteria* has no cultured representative, and its genome was first introduced in 2013 by metagenomics studies of sediment samples of a reservoir near the Colorado River (USA) (Castelle et al., 2013).

Phenol, naphthalene, and phenanthrene degradation genes have also been reported for representatives of *Lysobacter* (Maeda et al., 2009; Brescia et al., 2020). According to **Figure 6**, the *Lysobacter* (R2_5) genome also had toluene degradation genes under aerobic conditions. However, there is no report on this ability in previous studies.

Woesearchaeales from *Nanoarchaeota* that have been reported in metagenomics analyses of groundwater samples (Mehrshad et al., 2021) were recovered from both GW and R2 samples and contained several enzymes contributing to phenol (ppsA/ppsB), naphthalene (thnl), and alkane (AssD1/D2) degradation under aerobic conditions.

A nitrate-reducing member of *Flavobacteriaceae* (R2_57) was recovered from the R2 sample and contained aromatic compounds' degrading enzymes under anaerobic conditions. They mostly have enzymes that participate in the degradation of PAHs under anaerobic conditions (Rezaei Somee et al., 2021) and are potent aquatic indigenous degraders that bloom in response to HC pollution (Momper et al., 2017).

4. Conclusion

The present study investigated the application of SBCs and CaO2 nanoparticles in phenol-contaminated groundwater remediation through the continuous flow of sand-packed plexiglass columns. In addition, the influence of each treatment approach on the diversity and richness of the oligotrophic groundwater microbial communities was evaluated using next-generation sequencing (NGS) technology. The results indicated that applying SBCs into the simulated groundwater substrate remarkably affected the phenol removal rate. During the first 42 days of experiment, simultaneous use of CaO_2 nanoparticles and SBCs showed great potential in the complete phenol removal efficiency. Meanwhile, the natural bioremediation process was able to remove only 19.8% of the contaminant of the column's effluent within 6 months.

The attached microbial communities on the sand surfaces were observed by SEM and CLSM, where their crucial role in the remediation process was specified. Furthermore, studying the biodiversity of the attached biofilm in each remediation process by NGS demonstrated that the addition of CaO_2 nanoparticles into the groundwater stimulates the contaminant biodegrading microorganisms without any adverse effect on the groundwater. Consequently, the biostimulation and bioaugmentation process is suggested for phenol-contaminated groundwater bioremediation.

Moreover, our understanding of microbial dynamics in response to phenol pollution in oligotrophic groundwater enrolled as a valuable model for advancing knowledge of managing organic and hydrocarbon spill accidents, especially in Iran. In this work, the extensive analysis of groundwater metagenome along phenol pollution illustrated the 6-month exposure to 100 mg/L phenol altered the microbial community, and microbes with the capability of pollutant degradation became the dominant population in the pollution zone. Higher-resolution analysis of the microbial community of this ecosystem in future studies can reveal critical ecological adaptations to different pollutants.

Data availability statement

The data presented in the study are deposited in the DDBJ/EMBL/GenBank repository, accession number PRJNA741716. All data have been released and are available at https://www.ncbi.nlm.nih.gov/bioproject/?term=PRJNA741716.

Author contributions

MS: conceptualization, supervision, review and editing, and funding acquisition. SD and MA: conceptualization, project administration, and review and editing. MY-B: methodology, investigation, software, validation, visualization, and writing—original draft. MR: software, validation, formal analysis, and review and editing. All authors contributed to the article and approved the submitted version.

Funding

This study was supported by a grant from the Research Institute of Petroleum Industry (RIPI), Tehran, Iran (grant number: 35670221).

Conflict of interest

The authors declare that the research was conducted in the absence of any commercial or financial relationships that could be construed as a potential conflict of interest.

Publisher's note

Supplementary material

The Supplementary Material for this article can be found online at: https://www.frontiersin.org/articles/10.3389/fmicb.2023.1147162/full#supplementary-material

References

Abbasian, F., Lockington, R., Mallavarapu, M., and Naidu, R. (2015). A comprehensive review of aliphatic hydrocarbon biodegradation by bacteria. *Appl. Biochem. Biotechnol.* 176, 670–699.

Abbasian, F., Lockington, R., Megharaj, M., and Naidu, R. (2016). A review on the genetics of aliphatic and aromatic hydrocarbon degradation. *Appl. Biochem. Biotechnol.* 178, 224–250.

Brescia, F., Pertot, I., and Puopolo, G. (2020). "Lysobacter," in *Beneficial Microbes in Agro-Ecology*, eds N. Amaresan, M. Senthil Kumar, and K. Annapurna (Amsterdam: Elsevier).

Bushnell, B. (2014). *BBMap: a Fast, Accurate, Splice-Aware Aligner*. Berkeley, CA: Lawrence Berkeley National Laboratory.

Caporaso, J., Stombaugh, J., Costello, E. K., Lozupone, C. A., McDonald, D., Pirrung, M., et al. (2010). QIIME allows analysis of high-throughput community sequencing data. *Nat. Methods* 7, 335–336.

Cassidy, D. P., and Irvine, R. L. (1999). Use of calcium peroxide to provide oxygen for contaminant biodegradation in a saturated soil. *J. Hazard. Mater.* 69, 25–39. doi: 10.1016/s0304-3894(99)00051-5

Castelle, C. J., Hug, L. A., Wrighton, K. C., Thomas, B. C., Williams, K. H., Wu, D., et al. (2013). Extraordinary phylogenetic diversity and metabolic versatility in aquifer sediment. *Nat. Commun.* 4:2120. doi: 10.1038/ncomms3120

Cecconet, D., Sabba, F., Devecseri, M., Callegari, A., and Capodaglio, A. G. (2020). In situ groundwater remediation with bioelectrochemical systems: a critical review and future perspectives. *Environ. Int.* 137:105550. doi: 10.1016/j.envint.2020.105550

Chaumeil, P. A., Mussig, A. J., Hugenholtz, P., and Parks, D. H. (2020). GTDB-Tk: a toolkit to classify genomes with the genome taxonomy database. *Bioinformatics* 36, 1925–1927.

Clark, D. R., Ferguson, R. M. W., Harris, D. N., Matthews Nicholass, K. J., Prentice, H. J., Randall, K. C., et al. (2018). Streams of data from drops of water: 21st century molecular microbial ecology. *WIREs Water* 5:e1280.

Dey, U., Chatterjee, S., and Mondal, N. K. (2016). Isolation and characterization of arsenic-resistant bacteria and possible application in bioremediation. *Biotechnol. Rep.* 10, 1–7.

Dong, H., Li, L., Lu, Y., Cheng, Y., Wang, Y., Ning, Q., et al. (2019). Integration of nanoscale zero-valent iron and functional anaerobic bacteria for groundwater remediation: a review. *Environ. Int.* 124, 265–277. doi: 10.1016/j.envint.2019.01.030

Duan, L., Wang, H., Sun, Y., and Xie, X. (2016). Biodegradation of phenol from wastewater by microorganism immobilized in bentonite and carboxymethyl cellulose gel. *Chem. Eng. Commun.* 203, 948–956.

Dupraz, C., Visscher, P. T., Baumgartner, L. K., and Reid, R. P. (2004). Microbe-mineral interactions: early carbonate precipitation in a hypersaline lake (Eleuthera Island. Bahamas). *Sedimentology* 51, 745–765.

Dyksma, S., Lenk, S., Sawicka, J. E., and Mußmann, M. (2018). Uncultured gammaproteobacteria and desulfobacteraceae account for major acetate assimilation in a coastal marine sediment. *Front. Microbiol.* 9:3124. doi:10.3389/fmicb.2018.03124

Edgar, R. C. (2004). MUSCLE: multiple sequence alignment with high accuracy and high throughput. *Nucleic Acids Res.* 32, 1792–1797.

Edgar, R. C. (2013). UPARSE: highly accurate OTU sequences from microbial amplicon reads. *Nat. Methods* 10, 996–998. doi: 10.1038/nmeth.2604

Flynn, T. M., Sanford, R. A., and Bethke, C. M. (2008). Attached and suspended microbial communities in a pristine confined aquifer. *Water Resour. Res.* 44:W07425.

Futamata, H., Nagano, Y., Watanabe, K., and Hiraishi, A. (2005). Unique kinetic properties of phenol-degrading variovorax strains responsible for efficient trichloroethylene degradation in a chemostat enrichment culture. *Appl. Environ. Microbiol.* 71, 904–911. doi: 10.1128/AEM.71.2.904-911.2005

Gholami, F., Shavandi, M., Dastgheib, S. M. M., and Amoozegar, M. A. (2018). Naphthalene remediation from groundwater by calcium peroxide (CaO2) nanoparticles in permeable reactive barrier (PRB). *Chemosphere* 212, 105–113.

Gholami, F., Shavandi, M., Dastgheib, S. M. M., and Amoozegar, M. A. (2019). The impact of calcium peroxide on groundwater bacterial diversity during naphthalene removal by permeable reactive barrier (PRB). *Environ. Sci. Pollut. Res.* 26, 35218–35226. doi: 10.1007/s11356-019-06398-y

González, G. (2001). Biodegradation of phenolic industrial wastewater in a fluidized bed bioreactor with immobilized cells of *Pseudomonas putida*. *Bioresour. Technol.* 80, 137–142. doi: 10.1016/s0960-8524(01)00076-1

Hamdan, N., Kavazanjian, E., Rittmann, B. E., and Karatas, I. (2017). Carbonate mineral precipitation for soil improvement through microbial denitrification. *Geomicrobiol. J.* 34, 139–146.

Hedbavna, P., Rolfe, S. A., Huang, W. E., and Thornton, S. F. (2016). Biodegradation of phenolic compounds and their metabolites in contaminated groundwater using microbial fuel cells. *Bioresour. Technol.* 200, 426–434. doi: 10.1016/j.biortech.2015.09.092

Huerta-Cepas, J., Szklarczyk, D., Heller, D., Hernández-Plaza, A., Forslund, S. K., Cook, H., et al. (2019). eggNOG 5.0: a hierarchical, functionally and phylogenetically annotated orthology resource based on 5090 organisms and 2502 viruses. *Nucleic Acids Res.* 47, D309–D314. doi: 10.1093/nar/gky1085

Hyatt, D., Chen, G.-L., LoCascio, P. F., Land, M. L., Larimer, F. W., and Hauser, L. J. (2010). Prodigal: prokaryotic gene recognition and translation initiation site identification. *BMC Bioinformatics* 11:119. doi: 10.1186/1471-2105-11-119

Inoué, S. (2006). "Foundations of confocal scanned imaging in light microscopy," in *Handbook Of Biological Confocal Microscopy*, ed. J. Pawley (Boston, MA: Springer).

Jehmlich, N., Kleinsteuber, S., Vogt, C., Benndorf, D., Harms, H., Schmidt, F., et al. (2010). Phylogenetic and proteomic analysis of an anaerobic toluene-degrading community. *J. Appl. Microbiol.* 109, 1937–1945.

Kang, D. D., Li, F., Kirton, E., Thomas, A., Egan, R., An, H., et al. (2019). MetaBAT 2: an adaptive binning algorithm for robust and efficient genome reconstruction from metagenome assemblies. *PeerJ* 7:e7359. doi: 10.7717/peerj.7359

Khodaveisi, J., Banejad, H., Afkhami, A., Olyaie, E., Lashgari, S., and Dashti, R. (2011). Synthesis of calcium peroxide nanoparticles as an innovative reagent for in situ chemical oxidation. *J. Hazard. Mater.* 192, 1437–1440. doi: 10.1016/j.jhazmat.2011.06.060

Koshlaf, E., Shahsavari, E., Aburto-Medina, A., Taha, M., Haleyur, N., Makadia, T. H., et al. (2016). Bioremediation potential of diesel-contaminated Libyan soil. *Ecotoxicol. Environ. Saf.* 133, 297–305. doi: 10.1016/j.ecoenv.2016.07.027

Koval, S. F., Williams, H. N., and Stine, O. C. (2015). Reclassification of Bacteriovorax marinus as Halobacteriovorax marinus gen. nov., comb. nov. and Bacteriovorax litoralis as Halobacteriovorax litoralis comb. nov.; description of Halobacteriovoraceae fam. nov. in the class Deltaproteobacteria. *Int. J. Syst. Evol. Microbiol.* 65, 593–597. doi: 10.1099/ijs.0.070201-0

Lall, U., Josset, L., and Russo, T. (2020). A snapshot of the world's groundwater challenges. *Annu. Rev. Environ. Resour.* 45, 171–194.

Lee, D., Ahn, Y., Pandi, K., Park, J., Yun, S.-T., Jang, M., et al. (2021). Evaluation of natural attenuation-potential and biogeochemical analysis in nitrate contaminated bedrock aquifers by carbon source injection. *Sci. Total Environ.* 780:146459. doi: 10.1016/j.scitotenv.2021.146459

Li, D., Liu, C. M., Luo, R., Sadakane, K., and Lam, T. W. (2015). MEGAHIT: an ultra-fast single-node solution for large and complex metagenomics assembly via succinct de Bruijn graph. *Bioinformatics* 31, 1674–1676. doi: 10.1093/bioinformatics/btv033

Liu, N., Zhang, Y., An, Y., and Wang, L. (2018). Preparation of integrative cubes as a novel biological permeable reactive barrier medium for the enhancement of in situ aerobic bioremediation of nitrobenzene-contaminated groundwater. *Environ. Earth Sci.* 77, 707.

Liu, P., Pommerenke, B., and Conrad, R. (2018). Identification of syntrophobacteraceae as major acetate-degrading sulfate reducing bacteria in Italian paddy soil. *Environ. Microbiol.* 20, 337–354. doi: 10.1111/1462-2920.14001

Lopez-Fernandez, M., Simone, D., Wu, X., Soler, L., Nilsson, E., Holmfeldt, K., et al. (2018). Metatranscriptomes reveal that all three domains of life are active but are dominated by bacteria in the fennoscandian crystalline granitic continental deep biosphere. *MBio* 9:e1792-18. doi: 10.1128/mBio.01792-18

Lu, S., Zhang, X., and Xue, Y. (2017). Application of calcium peroxide in water and soil treatment: a review. *J. Hazard. Mater.* 337, 163–177. doi: 10.1016/j.jhazmat.2017.04.064

Maeda, R., Nagashima, H., Zulkharnain, A., Bin, Iwata, K., and Omori, T. (2009). Isolation and characterization of a car gene cluster from the naphthalene, phenanthrene, and carbazole-degrading marine isolate Lysobacter sp. strain OC7. *Curr. Microbiol.* 59, 154–159. doi: 10.1007/s00284-009-9414-y

Magoc, T., and Salzberg, S. L. (2011). FLASH: fast length adjustment of short reads to improve genome assemblies. *Bioinformatics* 27, 2957–2963. doi: 10.1093/bioinformatics/btr507

Martín-Cuadrado, A.-B., López-García, P., Alba, J.-C., Moreira, D., Monticelli, L., Strittmatter, A., et al. (2007). Metagenomics of the deep mediterranean, a warm bathypelagic habitat. *PLoS One* 2:e914. doi: 10.1371/journal.pone.0000914

Masood, F. (2017). "Polyhydroxyalkanoates in the food packaging industry," in *Nanotechnology Applications in Food*, 153–177. Available online at: https://doi.org/10.1016/B978-0-12-811942-6.00008-X

Mehrshad, M., Lopez-Fernandez, M., Sundh, J., Bell, E., Simone, D., Buck, M., et al. (2021). Energy efficiency and biological interactions define the core microbiome of deep oligotrophic groundwater. *Nat. Commun.* 12:4253. doi: 10.1038/s41467-021-24549-z

Mikkonen, A., Yläranta, K., Tiirola, M., Dutra, L. A. L., Salmi, P., Romantschuk, M., et al. (2018). Successful aerobic bioremediation of groundwater contaminated with higher chlorinated phenols by indigenous degrader bacteria. *Water Res.* 138, 118–128. doi: 10.1016/j.watres.2018.03.033

Mohammadi, S., Kargari, A., Sanaeepur, H., Abbassian, K., Najafi, A., and Mofarrah, E. (2015). Phenol removal from industrial wastewaters: a short review. *Desalin. Water Treat.* 53, 2215–2234.

Momper, L., Jungbluth, S. P., Lee, M. D., and Amend, J. P. (2017). Energy and carbon metabolisms in a deep terrestrial subsurface fluid microbial community. *ISME J.* 11, 2319–2333. doi: 10.1038/ismej.2017.94

Monferrán, M. V., Echenique, J. R., and Wunderlin, D. A. (2005). Degradation of chlorobenzenes by a strain of Acidovorax avenae isolated from a polluted aquifer. *Chemosphere* 61, 98–106. doi:10.1016/j.chemosphere.2005.03.003

Mosmeri, H., Alaie, E., Shavandi, M., Dastgheib, S. M. M., and Tasharrofi, S. (2017). Bioremediation of benzene from groundwater by calcium peroxide (CaO2) nanoparticles encapsulated in sodium alginate. *J. Taiwan Inst. Chem. Eng.* 78, 299–306.

Mosmeri, H., Gholami, F., Shavandi, M., Dastgheib, S. M. M., and Alaie, E. (2019). Bioremediation of benzene-contaminated groundwater by calcium peroxide (CaO2) nanoparticles: continuous-flow and biodiversity studies. *J. Hazard. Mater.* 371, 183–190. doi: 10.1016/j.jhazmat.2019.02.071

Mosmeri, H., Tasharrofi, S., Alaie, E., and Sadegh Hassani, S. (2018). "Controlled-release oxygen nanocomposite for bioremediation of benzene contaminated groundwater," in *New Polymer Nanocomposites for Environmental Remediation*, 601–622. Available online at: https://doi.org/10.1016/B978-0-12-811033-1.00023-8

Nawrocki, E. (2009). *Structural RNA Homology Search and Alignment Using Covariance Models*. St. Louis, MO: Washington University in St. Louis.

Northup, A., and Cassidy, D. (2008). Calcium peroxide (CaO2) for use in modified fenton chemistry. *J. Hazard. Mater.* 152, 1164–1170.

Padhi, S. K., and Gokhale, S. (2017). Benzene biodegradation by indigenous mixed microbial culture: kinetic modeling and process optimization. *Int. Biodeterior. Biodegradation* 119, 511–519.

Paissé, S., Coulon, F., Goñi-Urriza, M., Peperzak, L., McGenity, T. J., and Duran, R. (2008). Structure of bacterial communities along a hydrocarbon contamination gradient in a coastal sediment. *FEMS Microbiol. Ecol.* 66, 295–305. doi: 10.1111/j.1574-6941.2008.00589.x

Parks, D. H., Imelfort, M., Skennerton, C. T., Hugenholtz, P., and Tyson, G. W. (2015). CheckM: assessing the quality of microbial genomes recovered from isolates, single cells, and metagenomes. *Genome Res.* 25, 1043–1055. doi: 10.1101/gr.186072.114

Pérez-Pantoja, D., Donoso, R., Agulló, L., Córdova, M., Seeger, M., Pieper, D. H., et al. (2012). Genomic analysis of the potential for aromatic compounds biodegradation in Burkholderiales. *Environ. Microbiol.* 14, 1091–1117.

Pickup, R., Rhodes, G., Alamillo, M., Mallinson, H. E., Thornton, S., and Lerner, D. (2001). Microbiological analysis of multi-level borehole samples from a contaminated groundwater system. *J. Contam. Hydrol.* 53, 269–284. doi: 10.1016/s0169-7722(01)00169-3

Poi, G., Shahsavari, E., Aburto-Medina, A., Mok, P. C., and Ball, A. S. (2018). Large scale treatment of total petroleum-hydrocarbon contaminated groundwater using bioaugmentation. *J. Environ. Manage.* 214, 157–163. doi: 10.1016/j.jenvman.2018.02.079

Purkamo, L. (2017). Thriving microbial life in ancient groundwater deep inside earth's crust. *Front. Young Minds* 5:65. doi: 10.3389/FRYM.2017.00065/PDF

Qian, Y., Zhang, J., Zhang, Y., Chen, J., and Zhou, X. (2016). Degradation of 2,4-dichlorophenol by nanoscale calcium peroxide: implication for groundwater remediation. *Sep. Purif. Technol.* 166, 222–229.

Quast, C., Pruesse, E., Yilmaz, P., Gerken, J., Schweer, T., Yarza, P., et al. (2013). The SILVA ribosomal RNA gene database project: improved data processing and web-based tools. *Nucleic Acids Res.* 41, D590–D596. doi: 10.1093/nar/gks1219

Rabus, R., Boll, M., Heider, J., Meckenstock, R. U., Buckel, W., Einsle, O., et al. (2016). Anaerobic microbial degradation of hydrocarbons: from enzymatic reactions to the environment. *J. Mol. Microbiol. Biotechnol.* 26, 5–28. doi: 10.1159/000443997

Rezaei Somee, M., Dastgheib, S. M. M., Shavandi, M., Ghanbari Maman, L., Kavousi, K., Amoozegar, M. A., et al. (2021). Distinct microbial community along the chronic oil pollution continuum of the Persian Gulf converge with oil spill accidents. *Sci. Rep.* 11:11316. doi: 10.1038/s41598-021-90735-0

Seemann, T. (2014). Prokka: rapid prokaryotic genome annotation. *Bioinformatics* 30, 2068–2069.

Shin, B., Kim, M., Zengler, K., Chin, K.-J., Overholt, W. A., Gieg, L. M., et al. (2019). Anaerobic degradation of hexadecane and phenanthrene coupled to sulfate reduction by enriched consortia from northern Gulf of Mexico seafloor sediment. *Sci. Rep.* 9:1239. doi: 10.1038/s41598-018-36567-x

Silva, C. C., Hayden, H., Sawbridge, T., Mele, P., De Paula, S. O., Silva, L. C. F., et al. (2013). Identification of genes and pathways related to phenol degradation in metagenomic libraries from petroleum refinery wastewater. *PLoS One* 8:e61811. doi: 10.1371/journal.pone.0061811

Singleton, D. R., Guzmaìn Ramirez, L., and Aitken, M. D. (2009). Characterization of a polycyclic aromatic hydrocarbon degradation gene cluster in a phenanthrene-degrading acidovorax strain. *Appl. Environ. Microbiol.* 75, 2613–2620. doi: 10.1128/AEM.01955-08

Sperfeld, M., Diekert, G., and Studenik, S. (2018). Anaerobic aromatic compound degradation in Sulfuritalea hydrogenivorans sk43H. *FEMS Microbiol. Ecol.* 95:fiy199. doi: 10.1093/femsec/fiy199

Stagars, M. H., Mishra, S., Treude, T., Amann, R., and Knittel, K. (2017). Microbial community response to simulated petroleum seepage in Caspian sea sediments. *Front. Microbiol.* 8:764.

Sun, X., Wang, C., Li, Y., Wang, W., and Wei, J. (2015). Treatment of phenolic wastewater by combined UF and NF/RO processes. *Desalination* 355, 68–74.

Villegas, L. G. C., Mashhadi, N., Chen, M., Mukherjee, D., Taylor, K. E., and Biswas, N. (2016). A short review of techniques for phenol removal from wastewater. *Curr. Pollut. Reports* 2, 157–167.

Wang, H., Zhao, Y., Li, T., Chen, Z., Wang, Y., and Qin, C. (2016). Properties of calcium peroxide for release of hydrogen peroxide and oxygen: a kinetics study. *Chem. Eng. J.* 303, 450–457.

Xue, Y., Lu, S., Fu, X., Sharma, V. K., Mendoza-Sanchez, I., Qiu, Z., et al. (2018). Simultaneous removal of benzene, toluene, ethylbenzene and xylene (BTEX) by CaO2 based fenton system: enhanced degradation by chelating agents. *Chem. Eng. J.* 331, 255–264.

Yavari-Bafghi, M., Shavandi, M., Dastgheib, S. M. M., and Amoozegar, M. A. (2022). Simultaneous application of CaO2 nanoparticles and microbial consortium in Small bioreactor chambers (SBCs) for phenol removal from groundwater. *Process Saf. Environ. Prot.* 160, 465–477.

Ye, L., Yu, G., Zhou, S., Zuo, S., and Fang, C. (2017). Denitrification of nitrate-contaminated groundwater in columns packed with PHBV and ceramsites for application as a permeable reactive barrier. *Water Supply* 17, 1241–1248.

Yeh, C.-H., Lin, C.-W., and Wu, C.-H. (2010). A permeable reactive barrier for the bioremediation of BTEX-contaminated groundwater: microbial community distribution and removal efficiencies. *J. Hazard. Mater.* 178, 74–80. doi: 10.1016/j.jhazmat.2010.01.045

Zhuang, H., and Fang, F. (2020). Bioaugmentation with phenol-degrading bacteria (PDB) as a strategy for improving start-up and stability of sequencing biofilm batch reactor (SBBR) for coal gasification wastewater (CGW) treatment. *Polish J. Environ. Stud.* 29, 3955–3964.

frontiers | Frontiers in Microbiology

TYPE Original Research
PUBLISHED 12 May 2023
DOI 10.3389/fmicb.2023.1192029

OPEN ACCESS

EDITED BY
Anirban Chakraborty,
Idaho State University, United States

REVIEWED BY
Xiyang Dong,
Third Institute of Oceanography of the Ministry of Natural Resources, China
Sabrina Beckmann,
Oklahoma State University, United States

*CORRESPONDENCE
Mark A. Lever
✉ mark.lever@austin.utexas.edu

RECEIVED 22 March 2023
ACCEPTED 24 April 2023
PUBLISHED 12 May 2023

CITATION
Lever MA, Alperin MJ, Hinrichs K-U and Teske A (2023) Zonation of the active methane-cycling community in deep subsurface sediments of the Peru Trench.
Front. Microbiol. 14:1192029.
doi: 10.3389/fmicb.2023.1192029

Zonation of the active methane-cycling community in deep subsurface sediments of the Peru trench

Mark A. Lever[1,2]*, Marc J. Alperin[2], Kai-Uwe Hinrichs[3] and Andreas Teske[2]

[1]Department of Marine Science, Marine Science Institute, University of Texas at Austin, Port Aransas, TX, United States, [2]Earth, Marine and Environmental Sciences, University of North Carolina at Chapel Hill, Chapel Hill, NC, United States, [3]Organic Geochemistry Group, MARUM-Center for Marine Environmental Sciences and Department of Geosciences, University of Bremen, Bremen, Germany

The production and anaerobic oxidation of methane (AOM) by microorganisms is widespread in organic-rich deep subseafloor sediments. Yet, the organisms that carry out these processes remain largely unknown. Here we identify members of the methane-cycling microbial community in deep subsurface, hydrate-containing sediments of the Peru Trench by targeting functional genes of the alpha subunit of methyl coenzyme M reductase (*mcrA*). The *mcrA* profile reveals a distinct community zonation that partially matches the zonation of methane oxidizing and –producing activity inferred from sulfate and methane concentrations and carbon-isotopic compositions of methane and dissolved inorganic carbon (DIC). *Mcr*A appears absent from sulfate-rich sediments that are devoid of methane, but *mcr*A sequences belonging to putatively methane-oxidizing ANME-1a-b occur from the zone of methane oxidation to several meters into the methanogenesis zone. A sister group of ANME-1a-b, referred to as ANME-1d, and members of putatively aceticlastic *Methanothrix* (formerly *Methanosaeta*) occur throughout the remaining methanogenesis zone. Analyses of 16S rRNA and *mcr*A-mRNA indicate that the methane-cycling community is alive throughout (rRNA to 230 mbsf) and active in at least parts of the sediment column (mRNA at 44 mbsf). Carbon-isotopic depletions of methane relative to DIC (–80 to –86‰) suggest mostly methane production by CO_2 reduction and thus seem at odds with the widespread detection of ANME-1 and *Methanothrix*. We explain this apparent contradiction based on recent insights into the metabolisms of both ANME-1 and *Methanothricaceae*, which indicate the potential for methanogenetic growth by CO_2 reduction in both groups.

KEYWORDS

deep biosphere, methanogenesis, anaerobic oxidation of methane, subseafloor sediment, ocean drilling, methane hydrate, carbon isotopes, *mcrA*

Introduction

The detection of active microbial populations to 80 mbsf in Peru Margin sediments during Ocean Drilling Program (ODP) Leg 112 in 1988, was the first demonstration of an deep subseafloor biosphere (Cragg et al., 1990). Since then, numerous studies and multiple lines of evidence from a range of locations have shown a vast microbial biomass in deep subseafloor sediments (for syntheses, see D'Hondt et al., 2004; Kallmeyer et al., 2012; Parkes et al., 2014)

with metabolically active cells to at least 1,500 mbsf (Roussel et al., 2008; Inagaki et al., 2015; Heuer et al., 2020), and the existence of a subsurface microbiome that is distinct from that found in marine surface sediments (e.g., Deng et al., 2020; Hoshino et al., 2020).

Several sites sampled during ODP Leg 112 were revisited in 2002 during ODP Leg 201, now 22 years ago, during the first ocean drilling expedition to focus on subseafloor life (D'Hondt et al., 2003). Porewater concentration gradients of microbially consumed electron acceptors such as nitrate or sulfate indicated active microbial populations to depths of >400 mbsf in the sediment column (D'Hondt et al., 2004). Molecular biological studies, e.g., polymerase-chain-reaction (PCR) assays of 16S rRNA genes (Parkes et al., 2005; Inagaki et al., 2006; Webster et al., 2006) and 16S rRNA gene transcripts (Biddle et al., 2006; Sørensen and Teske, 2006), fluorescence-*in-situ*-hybridization (FISH; Mauclaire et al., 2005, Schippers et al., 2005), and metagenomic signatures of whole-genome amplified DNA (Biddle et al., 2008) provided insights into the community structure and metabolic potential of microbial populations. Yet, specific links between microbial activity based on geochemical gradients and microbial identity based on genetic and genomic assays could not be established. For instance, sulfate and methane profiles suggested that sulfate reduction, anaerobic oxidation of methane (AOM), and methanogenesis were all important microbially-driven *in situ* processes (D'Hondt et al., 2004). However, sulfate-reducing, methanogenic, or methane-oxidizing microorganisms were surprisingly rare or absent from clone libraries of transcribed, PCR-amplified 16S rRNA (Biddle et al., 2006; Sørensen and Teske, 2006) and PCR-amplified 16S rRNA genes (Parkes et al., 2005; Inagaki et al., 2006).

Functional genes that encode for enzymes that are unique to certain metabolisms can be targeted to identify microorganisms that are involved in these metabolisms. Functional genes that have been investigated in targeted studies at ODP Leg 201 sites include the gene for dissimilatory sulfite reductase (*dsrAB*), a key enzyme of dissimilatory sulfate reduction (Wagner et al., 2005), the gene for reductive dehalogenase (*rdh*A) of reductive dehalorespiration (Futagami et al., 2009), the gene for formyl tetrahydrofolate synthetase (*fhs*A), a crucial enzyme of acetogenewsis (Lever et al., 2010), and the gene for the α subunit of methyl coenzyme M reductase (*mcrA*), an enzyme that catalyzes the terminal step of biological methanogenesis and is also present in anaerobic methane oxidizers (Friedrich, 2005; Knittel and Boetius, 2009; Wang et al., 2021). Patchy PCR detections of *dsr*AB *and mcr*A in only a few samples (Parkes et al., 2005; Inagaki et al., 2006; Webster et al., 2006) remain at odds with porewater concentration profiles of sulfate and methane, which indicate microbial sulfate reduction, AOM, and methanogenesis (D'Hondt et al., 2004). Similar observations were made based on quantitative PCR and metagenome sequencing in methane-rich deep subseafloor sediments of Hydrate Ridge in the Northeastern Pacific (Colwell et al., 2008), the Black Sea and off Namibia (Schippers et al., 2012), the Baltic Sea (Marshall et al., 2018), and Adélie Basin off Antarctica (Carr et al., 2018). It was thus proposed that methanogens account for low percentages (<1%) of microbial cells in subseafloor sediments, or are not detected by PCR assays due to primer mismatches or use of unrecognized genetic pathways (Lever, 2013).

Here we take a closer look at the *in situ* community of methanogens and anaerobic methanotrophs in the sediment column of ODP Site 1230 in the Peru Trench via PCR assays of *mcrA*. We investigate the relationship between community zonation and geochemical profiles [sulfate, methane, formate, acetate, hydrogen, δ^{13}C-methane and -dissolved inorganic carbon (DIC)], and identify active members of the methane-cycling community via reverse transcription-PCR (RT-PCR) of 16S rRNA and *mcrA*-mRNA. Redesigned general *mcrA* primers (Lever and Teske, 2015) and new group-specific *mcrA* and 16S rRNA gene primers allow us to detect methane-cycling functional genes in the AOM and methanogenesis zones inferred from porewater chemical gradients. While updated primers improve the detection of methane-cycling archaea, they reinforce the notion that methane-cycling archaea only account for a small proportion of microbial subsurface communities even in sediments with clear geochemical evidence for methanogenesis and AOM.

Materials and methods

Field site and sampling

The Peru Trench is part of the larger Atacama Trench that is located between the continental South American Plate and the accretionary wedge of the oceanic Nazca Plate (Suess, 1981). ODP Site 1230 is located on the lower slope of the Peru Trench at 5,086 m water depth (Figure 1). Sediments were drilled to ~270 mbsf during ODP Leg 201 in 2002 (D'Hondt et al., 2003). Three boreholes (A, B, and C) were within ~20 m of one another (D'Hondt et al., 2003). Sediment temperatures are low, increasing linearly from 2°C at the seafloor to 12°C at 270 mbsf. The upper 200 m of sediment consist of clay-rich, diatomaceous mud that was largely relocated from the continental shelf throughout the Holocene and Pleistocene. At approximately 216 mbsf, the sediment column changes to Miocene diatom ooze in a stratigraphic hiatus of 4.5 million years (Shipboard Scientific Party, 1988; Meister et al., 2005). Throughout the sediment column, organic carbon contents mostly range from 2 to 4% dry sediment weight (Meister et al., 2005). DIC concentrations to 160 mM and sulfate depletion in the upper ~10 mbsf indicate active microbial remineralization of organic matter, largely by sulfate reduction (D'Hondt et al., 2003). After sulfate is depleted, methane concentrations increase rapidly and reach *in situ* saturation by 28 mbsf (Spivack et al., 2005). Geophysical and chemical data suggest that hydrates are first present at ~70 mbsf and occur intermittently to 278 mbsf (D'Hondt et al., 2003).

For molecular biological analyses, 5-cm whole-round intervals of cores were frozen at −80°C. Only sediment from the nearly contamination-free core interiors was used (House et al., 2003; Lever et al., 2006). For carbon isotope analyses, 5-mL subsamples were frozen in pre-combusted glass vials.

Porewater geochemical concentrations

We used published depth profiles of DIC, sulfate, methane, dihydrogen (H_2), formate and acetate concentrations

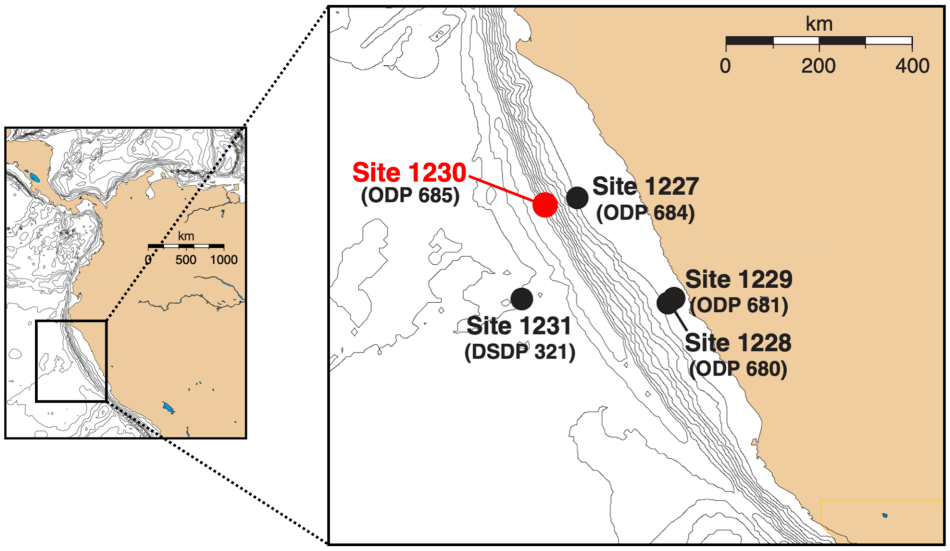

FIGURE 1
Map of Peru Margin sites sampled during ODP Leg 201 and ODP Leg 112 (in parentheses) [adapted from D'Hondt et al., 2003]. Samples used in this study were collected at ODP Site 1230 in the Peru Trench, which was in the same location as the previously studied ODP Site 685.

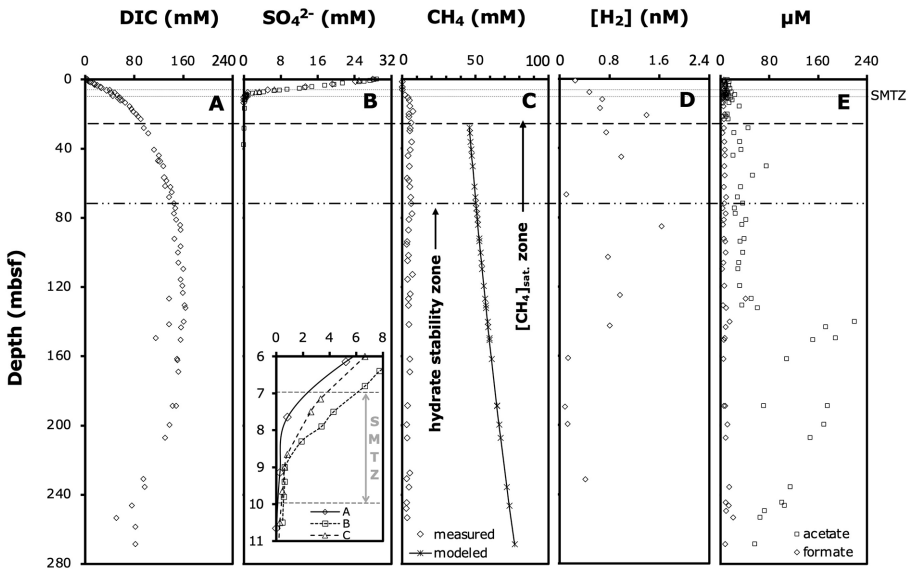

FIGURE 2
Relevant porewater geochemical profiles: **(A)** DIC concentrations, **(B)** sulfate concentrations (note: the insert shows an enlarged view of the SMTZ and concentrations in individual boreholes), **(C)** measured methane concentrations, modeled methane saturation concentrations, and distribution of hydrate stability zone (D'Hondt et al., 2003) and methane saturation zone (Spivack et al., 2005), **(D)** dihydrogen (H_2) concentrations, and **(E)** formate and acetate concentrations. Modeled methane concentrations from this study, all other data from D'Hondt et al. (2003). Horizontal lines indicate the approximate depth interval of the SMTZ, and the depths below which we estimate methane concentrations to be saturated and methane hydrates to be present. All data are from Borehole A, except where noted.

(Figures 2A–E; D'Hondt et al., 2003). Due to outgassing during core retrieval, measured methane concentrations below ~12 mbsf were underestimates of *in situ* concentrations. We calculated methane concentrations below the saturation depth at *in situ* temperature, pressure, and salinity, assuming a uniform pore size of 1.0 µm based on the equilibrium model for methane hydrate-seawater-porous media (Sun and Duan, 2007). Modeled methane concentrations generally agree with measured *in situ* methane concentrations based on pressure coring (4 depths analyzed at ODP Site 1230; Spivack et al., 2005).

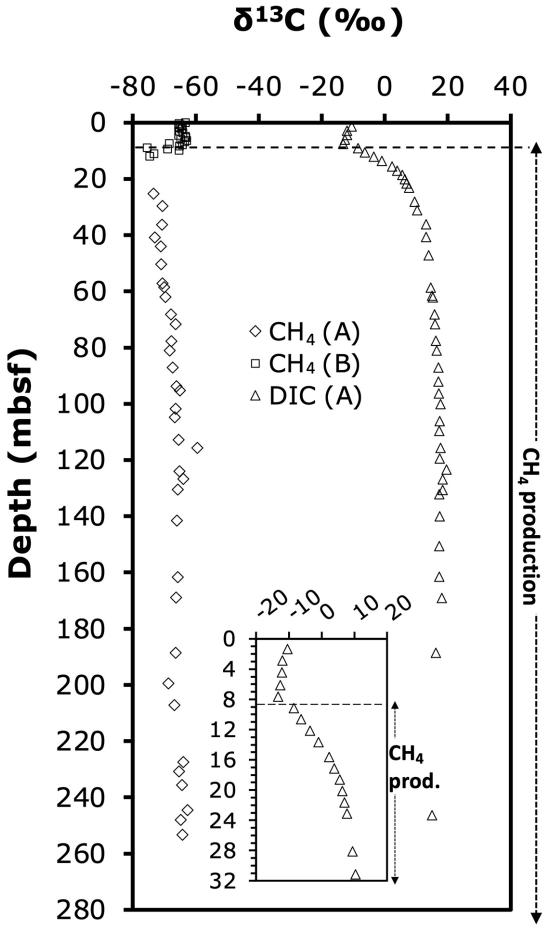

FIGURE 3
Depth profile of δ^{13}C-CH_4 and δ^{13}C-DIC. Letters in parentheses indicate borehole in which samples were analyzed. Depth profile of difference between δ^{13}C-CH_4 and δ^{13}C-DIC. The dashed line marks the abrupt shift in δ^{13}C-DIC from decreasing to increasing values.

δ^{13}C-C_1 and DIC

δ^{13}C-C_1 (~99% ^{13}C-CH_4) and -DIC (Figure 3) were measured as described previously (Biddle et al., 2006). All values are shown in Supplementary Table S1.

Nucleic acid extraction

RNA was extracted as in Biddle et al. (2006), except that the extraction buffer was supplemented with 120 mM sodium phosphate. DNA was extracted using the same protocol as for RNA, except that the pH of the extraction buffer and phenol were raised to 8.0, the bead beating time reduced to 15 s, and the bead beating speed reduced to 4.0 (Qbiogene, Carlsbad, CA). Moreover, the DNase incubation was omitted, and DNA purified with the PowerClean DNA Clean-Up Kit (MOBIO laboratories, Carlsbad, CA) instead of the RNeasy Mini Kit (Qiagen, Valencia, CA).

PCR primers

Two previously published general *mcrA* primer pairs yielded no amplification (ME1/ME2, Hales et al., 1996), or amplification at only one depth interval (mcrI, Springer et al., 1995; see Inagaki et al., 2006). The mcrIRD primer pair, a modified version of the mcrI primer pair with a reduced number of nucleotide degeneracies and consequently improved detection sensitivity, was used in conjunction with the ANME-1-specific ANME-1-mcrI primer pair [both published in Lever and Teske (2015)]. Special primers for ANME-1 detection were necessary due to the high number of nucleotide mismatches between the mcrI primer pair primer and the genetically divergent *mcrA* sequences of ANME-1. To confirm that detected *mcr*A detected belonged to active and living members of the methane-cycling community, we performed RT-PCR of *mcrA*-mRNA and 16S rRNA in several depth horizons using new group-specific primers for maximum amplification efficiency and hence detection sensitivity (mRNA: ODP1230, ANME-1; 16S rRNA: Msaeta 268F/927R, ANME-1 42F/898R; ANME-1-SG 35F/1038R). All primer sequences used in this study are shown in Table 1. All nucleotide sequences are publicly accessible at GenBank.

PCR protocols

PCR assays of *mcr*A were performed using the Takara SpeedSTAR HS DNA polymerase kit (TaKaRa Bio USA, Madison, WI) using (1) 1 × 2 min denaturation (98°C), (2) 40 × (a) 10s denaturation (98°C), (b) 30s annealing (Table 1 for temperatures), (c) 1 min extension (72°C), and (3) 1 × 5 min extension (72°C). Negative controls and reaction blanks were included.

RT-PCR assays were carried out using TaKaRa RNA PCR Kits (AMV) Version 3.0 (TaKaRa Bio USA, Madison, WI) and (1) 1 × 15 min reverse transcription, (2) 5 min denaturation (98°C), (3) 40 × (a) 30s denaturation (98°C), (b) 30s annealing (Table 1 for temperatures), (c) 1 min extension (72°C), and (4) 1 × 5 min extension (72°C). Negative controls and reaction blanks were included. Absence of DNA was confirmed by DNA-PCR with the same treatments but omitting the reverse transcription step.

Cloning and sequencing

PCR products were purified in a 2.5% low-melting point agarose gel using 1 × Tris acetate - EDTA buffer (TAE). Gel slices containing PCR fragments of the correct length were excised and purified using a S.N.A.P. Mini Kit (Invitrogen, Carlsbad, USA). Purified PCR fragments were cloned using the Topo TA Kit (Invitrogen, Carlsbad, USA) and transformed into TOP10 electrocompetent cells following the manufacturer's instructions. Plasmid extraction and purification was done using the GeneJET Plasmid Miniprep Kit (ThermoFisher Scientific) and cycle sequencing was performed on an ABI 3730 Sequencer with M13 universal primers (SP010-SP030) at the Josephine Bay Paul Center at MBL (Woods Hole, MA). Sequences were BLAST analyzed using

TABLE 1 Overview of PCR primer pairs used in this study.

Gene	Primer pair	Nucleotide sequences (5′-3′)	Reference	Target organisms	$T_{annealing}$ (°C)
mcrA	mcrI	F: TAY GAY CAR ATH TGG YT; R: ACR TTC ATN GCR TAR TT	Springer et al. (1995)	General *mcr*A	51
mcrA	ME1/ME2	F: GCM ATG CAR ATH GGW ATG TC; R: TCA TKG CRT AGT TDG GRT AGT	Hales et al. (1996)	General *mcr*A	58
mcrA	*mcrIRD*	F: TWY GAC CAR ATM TGG YT; R: ACR TTC ATB GCR TAR TT	Lever and Teske (2015)	General *mcr*A	55
mcrA	*ANME-1-mcrI*	F: GAC CAG TTG TGG TTC GGA AC; R: ATC TCG AAT GGC ATT CCC TC	Lever and Teske (2015)	ANME-1 *mcr*A	63
mcrA	ODP1230-mcrI	F: GCT ACA TGT CCG GTG G; R: CGG ATA GTT GGG TCC TCT	This study	ODP 1230 *M.thrix*	59
16S	M.saeta 268F/927R	F: CCT ACT AGC CTA CGA CGG GT; R: CCC GCC AAT TCC TTT AAG TTT	This study	All *Methanothrix*	63
16S	ANME-1 42F/898R	F: GAG TTC GAT TAA GCC ATG TTA GT; R: CGA CCG TAC TCC CCA GAT	This study	ANME-1a-b	61
16S	ANME-1-SG 35F/1038R	F: GCT ATC AGC GTC CGA CTA AGC; R: TAA TCC GGC AGG GTC TTC A	This study	ANME-1d	65
16S	ARC 8F/915R	F: TCC GGT TGA TCC TGC C; R: GTG CTC CCC CGC CAA TTC CT	Stahl and Amann (1991)	All Archaea	55

PCR assays involving the universal ARC 8F/915R primer pair were solely used to confirm the recovery of PCR-amplifiable nucleic acids from Archaea in all samples based on gel electrophoresis images of PCR products.

the nucleotide collection in GenBank.[1] Phylogenetic trees were created and bootstrap analyses (1,000 replicates) performed in ARB[2] using manually optimized SILVA 16S rRNA gene alignments, and a custom-built, publicly accessible *mcr*A database (name: mcrA4All)[3] with >2,400 high-quality, aligned *mcr*A amplicon and genome sequences.

Thermodynamic calculations

Gibbs energy yields (ΔG_r) of methanogenesis reactions from $H_2 + CO_2$ ($2\ HCO_3^- + 4\ H_2 + H^+ \rightarrow CH_4 + 3\ H_2O$) and acetate ($CH_3COO^- + H_2O \rightarrow CH_4 + HCO_3^-$), and the methanogenic conversion of formate to methane [$4\ HCOO^- + H_2O + H^+ \rightarrow CH_4 + 3\ HCO_3^-$; note: this reaction presumably involves the initial oxidation of formate to H_2 and HCO_3^-, which is not known to conserve energy except in certain hyperthermophiles (Schink et al., 2017)] were calculated based on the equation:

$$\Delta G_r = \Delta G_r^0 + RT \ln Q_r$$

where ΔG_r^0 is the Gibbs energy (kJ mol^{-1} of reaction) at standard concentrations (1 M for reactants and products, pH 7.0), corrected for *in situ* temperature T (K) and pressure *p* (bar) based on standard enthalpies and molar volumes as outlined in Stumm and Morgan (1996), R is the universal gas constant (0.008314 kJ mol^{-1} K^{-1}), and Q_r the quotient of product and reactant activities. Calculations were done for measured pH and concentrations of DIC (HCO_3^-), H_2, and acetate. Measured methane concentrations were used for the upper 12 mbsf, while modeled concentrations were used below. Activities of all chemical species were calculated by multiplying concentrations by their activity coefficients. These were $\gamma_{HCO32-} = 0.532$ (Millero and Schreiber, 1983), and $\gamma_{CH4} = 1.24$ (Millero, 2000). The activity coefficients of H_2, acetate, and formate were approximated with those of CH_4 (H_2) and HCO_3^- (acetate, formate). Standard Gibbs energies (ΔG_f°), standard enthalpies (ΔH_f°), and standard molal volumes (ΔV_f°) of formation are shown in Supplementary Table S2.

Results

Porewater gradients of chemical species determined on ODP Leg 201 provided the initial framework for our study and indicated ODP Site 1230 as a deep-sea site with unusually organic-rich sediments and highly active anaerobic microbial communities. Organic matter remineralization by microbes to at least 140 mbsf was indicated by DIC concentrations that increased steeply in the upper 25 mbsf and continued to increase gradually to 140 mbsf (Figure 2A). Sulfate reducing microbial communities depleted sulfate at ~9 mbsf in borehole A and up to 1 m deeper in boreholes B and C (Figure 2B). Porewater methane concentrations in borehole A were at background values (0.06 mM) at 6.10 mbsf, but had increased to 1.86 mM at 9.1 mbsf (Figure 2C). We thus estimate that the sulfate–methane transition zone (SMTZ), where most AOM takes place, was located within the depth interval from 7 to 9 mbsf in borehole A and up to 1 m deeper in boreholes B and C (Figure 2B, insert; for enlarged view of sulfate and methane profiles across the SMTZ in borehole A, see

1 www.ncbi.nlm.nih.gov/blast

2 http://www.arb-home.de/

3 https://drive.google.com/drive/u/0/folders/1G8GeJuYsIX4MLv5-LaUQHD9f9F9rfIAu

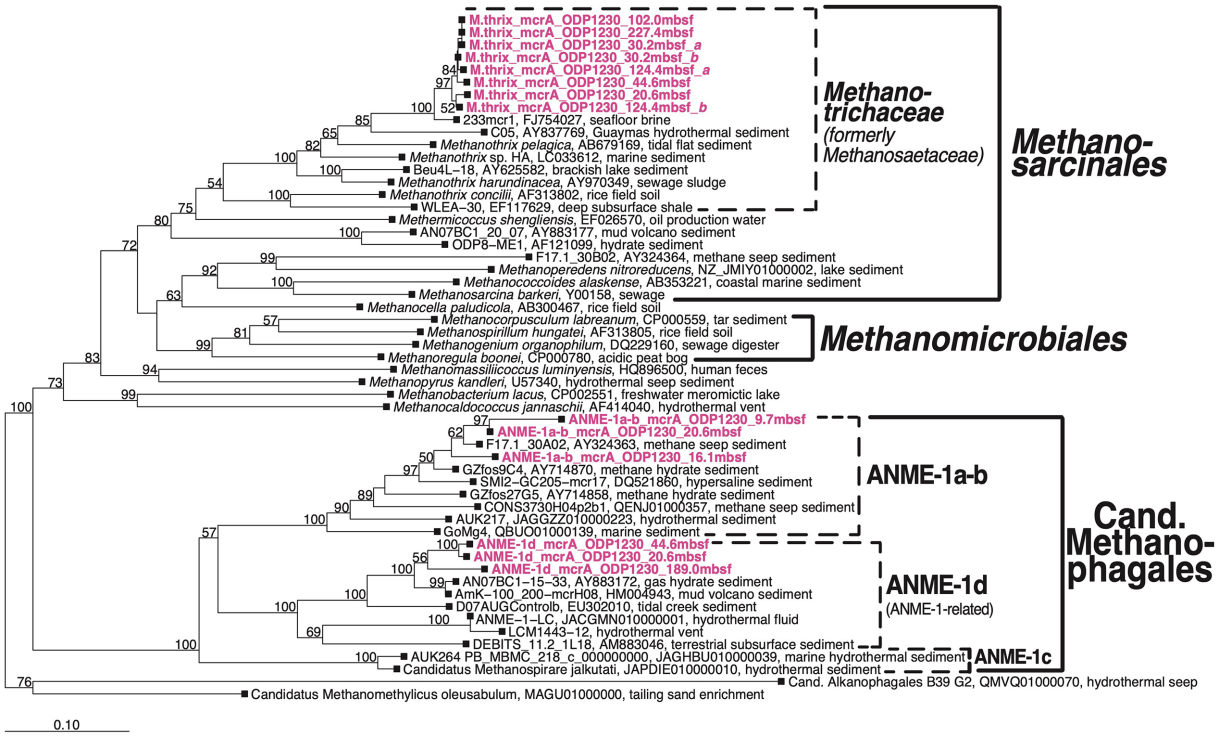

FIGURE 4
Bootstrap phylogenetic tree based on *mcrA* nucleotide sequences. Created using Jukes-Cantor correction in ARB neighbor-joining (Ludwig et al., 2004). Cand., Candidatus.

Supplementary Figure S1). Below the SMTZ, methane concentrations increased steeply, reaching saturation by ~28 mbsf, and hydrates appeared by ~50 mbsf. Hydrogen (H_2) concentrations fluctuated greatly, but generally increased throughout the sulfate reduction zone, stabilized in the methanogenesis zone to ~140 mbsf, and decreased below (Figure 2D). Formate concentrations showed no clear depth-related trend and fluctuated between 3–15 μM throughout the entire cored interval (Figure 2E). By contrast, acetate concentrations increased from 3–11 μM in the sulfate reduction zone and SMTZ (upper 10 mbsf) to concentrations of ~20–60 μM in the methanogenesis zone between 30 to 140 mbsf (Figure 2E; see Supplementary Figure S2 for enlarged view of upper 20 mbsf). Below 140 mbsf, acetate concentrations rose sharply to 220 μM and remained >50 μM to the deepest cores sampled.

Carbon isotope geochemistry

^{13}C-isotopic signatures of porewater methane and DIC provide insights into the zones of biological methane production and oxidation (Figure 3). Throughout the sediment column, methane was ^{13}C-depleted relative to DIC. δ^{13}C-DIC-values (only determined in borehole A) decreased slightly from −10.4‰ in the upper meter to −13.3‰ by 7.65 mbsf, then increased sharply in the uppermost methanogenic layer to +6‰ at 20 mbsf. The steepest increase in δ^{13}C-DIC occurred within the interval from 7.65 mbsf (δ^{13}C-DIC: −13.2‰) to 9.15 mbsf (δ^{13}C-DIC: −8.4‰), and suggests onset of methanogenesis by CO_2 reduction in this interval. Below 20 mbsf, δ^{13}C-DIC-values continued to gradually increase to reach a maximum of +20‰ at 123 mbsf, below which values slightly fell off to +15‰ at 246 mbsf (Figure 3). The ^{13}C-isotopic compositions of methane, determined in the methanogenesis zones of boreholes A (>25 mbsf) and B (0–12 mbsf), were in a range typical of biological methanogenesis (Whiticar et al., 1986; Whiticar, 1999). δ^{13}C-CH_4 was ~ −65‰ in the upper 6 mbsf, and then decreased to −75‰ at 12 mbsf. This increase in δ^{13}C-CH_4 upward through the SMTZ is consistent with isotopic discrimination of AOM against ^{13}C-CH_4. Below, values gradually increased from to ~ −65‰ at 246 mbsf (Figure 3). The difference in δ^{13}C-CH_4 relative to δ^{13}C-DIC was ~ −53‰ in the upper 6 mbsf, decreased across the SMTZ reaching −71‰ in the upper methanogenesis zone at 12 mbsf, and stabilized at −80‰ to −85‰ below 25 mbsf (Figure 3).

*mcr*A sequence diversity

We detected *mcrA* sequences of three phylogenetic groups (Figure 4): (1) putatively anaerobic methanotrophic ANME-1a-b Archaea, (2) a sister group of ANME-1, which we here refer to as ANME-1d, and (3) sequences of *Methanotrichales* that cluster with a genus-level group that includes the known aceticlastic methanogens *Methanothrix harundinacea* and *Methanothrix pelagica*.

The three groups were vertically zonated (Figure 5). ANME-1a-b *mcrA* sequences were found in horizons near the upper (7.8 mbsf) and lower limit (9.7 mbsf) of the STMZ in Borehole B and four horizons in the upper methanogenesis zone (10.25–20.6 mbsf; Table 2). Sequences of ANME-1d were detected with ANME-1a-b sequences at one depth in the upper methanogenesis zone (20.6 mbsf) and in

10.3389/fmicb.2023.1192029

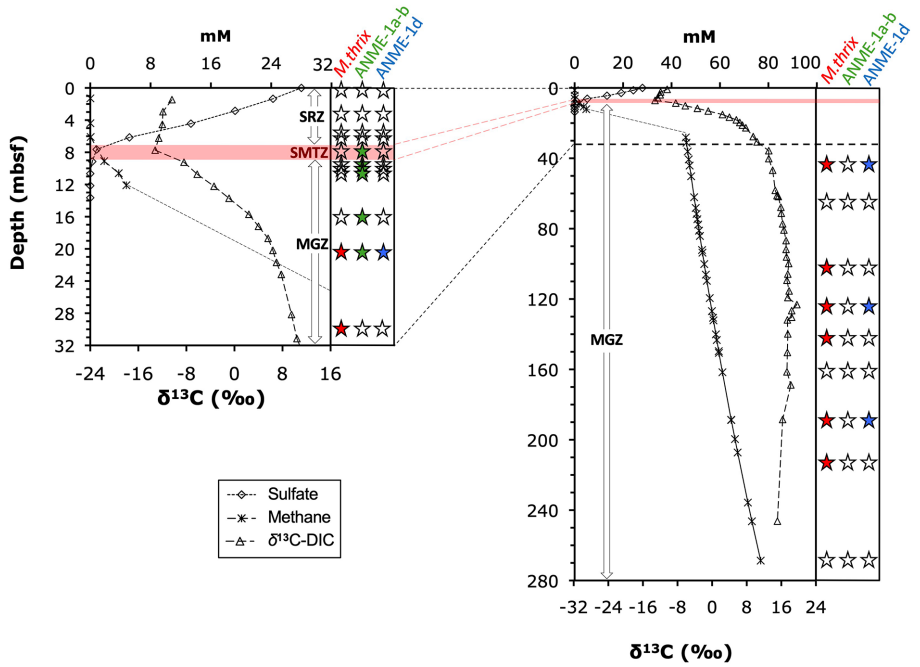

FIGURE 5
Distribution of *mcr*A groups along depth and geochemical gradients of sulfate, methane, and δ^{13}C-DIC. Panel on right side of each graph indicates detection/absence of detection of (1) ANME-1a-b, (2) ANME-1d, and (3) *Methanothrix* sequences. Solid black symbols indicate detection, empty symbols indicate lack of detection (example: ✦✧✧ indicates presence of ANME-1, and absence of ANME-1d and *Methanothrix*). Horizontal red bar indicates the depth interval of the SMTZ, where most AOM takes place, for Borehole A (7 to 9 mbsf). This interval extended ~1m deeper (~10 mbsf) in Borehole B. The uppermost detections of ANME1-a-b *mcr*A were at 7.8 and 9.7 mbsf in Borehole B and thus near the upper and lower limits of the SMTZ in this borehole.

TABLE 2 Overview of boreholes, core samples, sediment depths, and biogeochemical zones from which DNA and RNA were extracted, and the results of PCR amplifications with different primers with number of clones sequenced in parentheses.

Bore-hole	Core, section, interval (cm)	Depth (mbsf)	Biogeo-chemical zone	DNA			mRNA	16S rRNA
				*mcr*IRD	ODP1230_ *M.thrix*-*mcr*A	ANME-1-*mcr*I-DNA	ANME-1-*mcr*I-mRNA	*M.thrix*-16S-rRNA-268F/927R
A	1H-1, 25–30	0.3	SRZ	bd	-	bd	-	-
A	1H-3, 25–30	3.3	SRZ	bd	-	bd	-	-
B	2H-2, 120–125	5.70	SRZ	bd	-	bd	bd	-
B	2H-3, 30–40	6.30	SRZ	bd	-	bd	bd	-
B	2H-4, 30–40	7.80	SMTZ	bd	-	ANME-1a-b	bd*	-
B	2H-5, 70–80	9.70	SMTZ (MGZ?)	bd	-	ANME-1a-b	bd*	-
B	2H-5, 120–125	10.20	MGZ	bd	-	ANME-1a-b	bd*	-
C	2H-5, 25–30	10.8	MGZ	bd	-	ANME-1a-b	bd*	-
A	3H-2, 25–30	16.1	MGZ	bd	-	ANME-1a-b (45)	-	-
A	3H-5, 25–30	20.6	MGZ	M.thrix (17)	-	ANME-1a-b (1), ANME-1d (40)	-	-
A	4H-5, 35–40	30.2	MGZ	M.thrix (28)	-	bd	-	-
A	6H-2, 25–30	44.6	MGZ	M.thrix (9)	-	ANME-1d (40)	ANME-1d (3)	M.thrix (7)
A	9H-5, 23–28	65.7	MGZ	bd	bd	bd	-	-
A	13H-3, 20–25	102.0	MGZ	M.thrix (30)	-	bd	-	-
A	15H-6, 25–30	124.4	MGZ	bd	M.thrix (19)	ANME-1d (47)	bd	M.thrix (12)
A	18H-3, 35–40	142.2	MGZ	bd	M.thrix (20)	bd	-	-
A	21H-3, 25–30	160.5	MGZ	bd	-	bd	-	-
A	24H-2, 24–29	189.0	MGZ	M.thrix (25)	-	ANME-1d (44)	-	-
A	30X-1, 108–115	227.4	MGZ	M.thrix (30)	-	bd	bd	bd
A	38X-1, 130–135	268.5	MGZ	bd	bd	-	-	-

SRZ, sulfate reduction zone; SMTZ, sulfate–methane transition zone; MGZ, methanogenesis zone; bd, below PCR detection; –, not tested; M.thrix, Methanothrix [we did not detect mcrA-mRNA using the general mcrIRD primer pair].

three horizons below (to 189.0 mbsf). *Methanothrix mcr*A showed a distribution similar to ANME-1d, but was detected in more sediment horizons and to greater depth (to 227 mbsf; Table 2).

We detected *mcr*A-mRNA of ANME-1-d in one of the 9 samples examined using the ANME-1-*mcr*A primer pair (core 6H-2, 44 mbsf; Table 2). In 11 replicate RT-PCRs of RNA extracts, controls (PCR negative, extraction blank, DNA controls) always tested negative, whereas 8/11 RNA extracts tested positive. By comparison, four other samples (from 7.8, 9.7, 10.2, 10.8 mbsf) yielded RT-PCR detection with the same primers, but DNA controls were positive (albeit weaker than cDNA bands), indicating that traces of DNA had resisted the DNAse treatment. We cloned cDNA of *mcr*A-mRNA from core 6H-2 and confirmed the presence of *mcr*A of ANME-1d.

In addition to *mcr*A-mRNA, we examined 16S rRNA sequences. RT-PCRs with new *Methanothrix*-specific 16S rRNA gene primers (Table 1) yielded *Methanothrix*-like sequences in two additional depth horizons (Table 2; Supplementary Figure S3). This primer pair also generated 16S rRNA sequences of a sister group of *Methanosarcinales*, previously detected in methane seep and mud volcano environments, with unknown metabolism at two depths (15H-6, 30H-1; Supplementary Figure S3). Interestingly, despite detecting mRNA with ANME-1-*mcr*A primers, we were unable to detect 16S rRNA of ANME-1a-b or ANME-1d with newly designed group-specific 16S rRNA gene primers (Table 1).

Discussion

We present a depth profile of *mcrA* that relates distribution patterns of deep subseafloor methanogens and anaerobic methanotrophs to the geochemical context. While the genetic and gene transcript analyses in our study are present-day snapshots of methane-cycling activity, the measured geochemical data in part capture much longer time scales, such as the accumulation of methane over millions of years. Nonetheless, we observe a clear relationship between the community profile of methane-cycling archaea and porewater geochemical gradients. We, moreover, resolve the paradox of earlier studies in which methane-rich sediments at ODP Site 1230 appeared largely devoid of methanogens in the methanogenesis zone (Inagaki et al., 2006), and completely devoid of anaerobic methanotrophs in the SMTZ (Biddle et al., 2006).

Geochemical and functional gene profiles indicate a distinct depth stratification of the active methane cycling community (Table 2; Figure 5). No nucleic acid evidence of present-day methane-cycling was detected in the upper part of the sulfate reduction zone (0 to ~7 mbsf) despite methane concentrations in the micromolar range. Throughout the SMTZ (~7 to 9 mbsf in borehole A, up to 1 m deeper in boreholes B and C), sulfate concentrations diminished in typical concave-down profiles, and methane concentrations increased. These gradients coincide with the detection of *mcr*A of ANME-1a-b (Figure 5), members of which are known to be anaerobic methanotrophs (Knittel and Boetius, 2009). Therefore, our sulfate and methane concentration profiles and *mcrA* composition in the SMTZ are consistent with AOM. In the underlying methanogenesis zone (~9 to 269+ mbsf), methane concentrations and δ^{13}C-DIC increase drastically in the upper tens of meters and stay high throughout, while sulfate remains depleted (Figures 2, 3). Interestingly, ANME-1a-b Archaea were detected in the upper meters of the methanogenesis zone (from 9.7 to 16.1 mbsf), in line with past indications that ANME-1a-b might be capable of methanogenesis in addition to methanotrophy (House et al., 2009; Lloyd et al., 2011; Beulig et al., 2019). Moreover, ANME-1a-b were vertically separated from ANME-1d and *Methanothrix mcr*A sequences, which were only found in deeper, methanogenic sediment layers. The three groups only overlapped in core 3H-5 (20.6 mbsf), which marked the deepest sample in which ANME-1a-b and shallowest sample in which ANME-1d and *Methanothrix* were detected.

Implications of the ^{13}C-isotopic data

The changes in δ^{13}C-DIC and –methane provide insights into the sources of DIC and pathways of methane production at ODP Site 1230. The δ^{13}C-DIC isotopic values in the upper ~9 mbsf (−10.4 to −13.2‰) are consistent with organic matter mineralization becoming the main DIC source with increasing sediment depth. Most of this organic matter is likely to be phytoplankton-derived organic matter (δ^{13}C-total organic carbon: ~22–23‰; Biddle et al., 2006) that was initially deposited under the upwelling regime of the Peru Margin, and subsequently reworked and laterally transported downslope to the Peru Trench. Toward the sediment surface, the δ^{13}C-DIC increases, most likely due to an increasing contribution of ^{13}C-enriched DIC from deep sea bottom water, which typically bears a ^{13}C-composition of ~0 to +1.2‰ (Lynch-Stieglitz et al., 1995).

Notably, despite the strong geochemical evidence for AOM in the SMTZ, which might be expected to produce highly ^{13}C-depleted DIC from the oxidation of methane, we do not observe a strong downward swing in δ^{13}C-DIC within the SMTZ. This phenomenon has been observed previously in SMTZs and has been explained with concomitant AOM and methane production (Beulig et al., 2019), microbially mediated isotope exchange between methane and DIC (Yoshinaga et al., 2014), and reversibility of intracellular methane-cycling reactions at low sulfate concentrations (Wegener et al., 2021). In our case, the *mcr*A data argue against the first scenario, if ANME-1a-b are assumed to only perform methanotrophy. Yet, if – as proposed previously - ANME-1a-b are facultative methanogens, which matches the detection of this group throughout the upper ~12 m of the methanogenesis zone, then the first scenario is also plausible. Notably, porewater dissolved barium concentrations increase sharply throughout the AOM and upper methanogenesis zone (e.g., from 2.7 µM at 6.15 mbsf to 290 µM at 23.15 mbsf at ODP Site 1230A; D'Hondt et al., 2003), consistent with (slow) release of sulfate through chemical dissolution of barite ($BaSO_4$). This sulfate could fuel low rates of AOM, and thus also support concomitant AOM and methane production throughout the upper methanogenesis zone. AOM coupled to iron or manganese reduction could also support low rates of AOM, as was recently proposed for subsurface sediments of the South China Sea, where ANME-1 were detected meters below the SMTZ (Zhang et al., 2023). Yet, the low porewater concentrations of Fe^{2+} (0.6 to 3.9 µM) and Mn^{2+}(0 to 0.3 µM) in the upper methanogenic sediment layer where we detected ANME-1a-b at ODP Site 1230 (D'Hondt et al., 2003) do not support an important role of AOM coupled to metal reduction.

Below 9 mbsf, the δ^{13}C-DIC increased, consistent with a strong isotopic imprint of methanogenesis by CO_2 reduction. Strong isotopic discrimination against ^{13}C-CO_2 is the norm in methanogenesis from H_2/CO_2 (Whiticar, 1999; Penning et al., 2005) and can result in

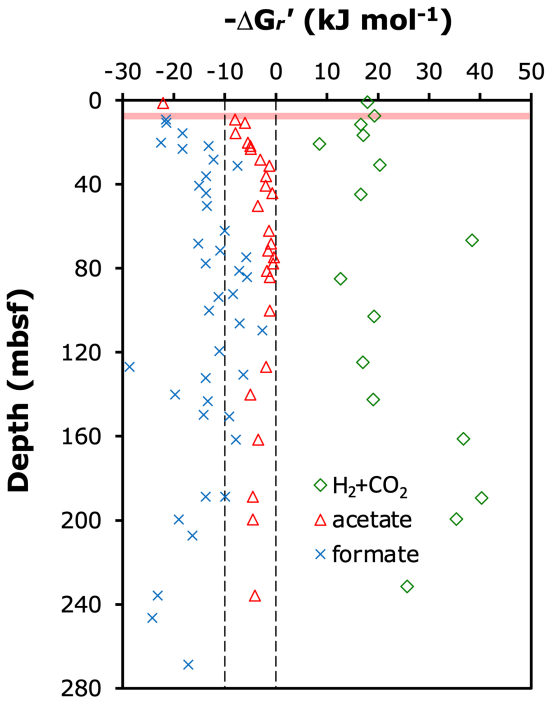

FIGURE 6
Calculated *in situ* Gibbs energy yields ($\Delta Gr'$) of methanogenesis reactions from $H_2 + CO_2$ ($HCO_3^- + 4\ H_2 + H^+ \rightarrow CH_4 + 3\ H_2O$) and acetate ($CH_3COO^- + H_2O \rightarrow CH_4 + HCO_3^-$), and the methanogenic conversion of formate to methane ($4\ HCOO^- + H_2O + H^+ \rightarrow CH_4 + 3\ HCO_3^-$; note: this reaction includes the initial oxidation of formate to H_2 and HCO_3^-, which may not be coupled to energy conservation). Calculations were done for *in situ* conditions as described in the Materials & Methods.

significant ^{13}C-enrichment of the residual DIC pool (Alperin and Hoehler, 2009; House et al., 2009). Based on measured porewater geochemical data, methanogenesis from H_2/CO_2 is, however, not thermodynamically favorable (Figure 6), with *in situ* Gibbs energies in the positive (i.e., endergonic) range ($\Delta G_r' > 0\ kJ\ mol^{-1}$) throughout the sediment column of ODP Site 1230. Since methanogenesis from formate follows the same biochemical route as hydrogenotrophic methanogenesis after the initial oxidation of formate to CO_2 and H_2 by formate dehydrogenase (Sparling and Daniels, 1986), a similar isotopic fractionation can be expected. Indeed, the complete conversion reaction of formate to methane is thermodynamically favorable, and based on that alone formate a potential methanogenic substrate at ODP Site 1230 (Figure 6). Yet, assuming that energy is not conserved during the initial formate oxidation step, but only in the second step involving methanogenic CO2 reduction with H_2 (Schink et al., 2017), then formate conversion to methane appears less plausible. This is because intracellular H_2 concentrations can be expected to be close to equilibrium with H_2 concentrations in the surrounding sediment due to H_2 leakage out of methanogenic cells (Finke et al., 2007). As stated above, however, measured H_2 concentrations in the surrounding sediment are too low to energetically support hydrogenotrophic methanogenesis. A more recently documented form of methanogenic CO_2 reduction involves interspecies electron transfer (IET). This form of methanogenesis, which was first discovered in *Methanothrix harundinaceae* (Rotaru et al., 2014), involves cellular structures, e.g., cytochromes, that attach to conductive mineral surfaces or syntrophic partner organisms (Gao and Lu, 2021). The isotopic fractionations of these reactions are not known but most likely also cause $\delta^{13}C$-enrichment of residual DIC. In principle, the conversion of formate to methane could also operate via a direct electron transfer mechanism, e.g., from syntrophic bacteria to methanogens. This mechanism could bypass H_2 as a catabolic intermediate and even render formate catabolism a potential source of methane. Thus, based on the available geochemical data, the dominance of methanogenic CO_2 reduction at Site 1230, which was inferred from the $\delta^{13}C$-DIC profile below 9 mbsf, is most plausibly explained with electron transfer from syntrophic partner organisms or mineral surfaces to methanogens.

By contrast, chemoautotrophy, acetogenesis or other methanogenic pathways are unlikely drivers of the observed $\delta^{13}C$-DIC increase in the methanogenesis zone. Although (certain) ANME-1a-b are chemoautotrophs (Kellermann et al., 2012), past studies indicate that AOM of isotopically highly depleted methane (~ −75 per mil) to CO_2 occurs at much (≥40-fold) higher rates than C-assimilation by chemoautotrophy (e.g., Nauhaus et al., 2007; Wegener et al., 2008). Consequently, AOM would be expected to overprint any C-isotopic enrichment of DIC by chemoautotrophy. Acetogenesis from H_2/CO_2, which also strongly discriminates against ^{13}C (Gelwicks et al., 1989), is unlikely based on $\delta^{13}C$-acetate values of −12 to −18‰ at ODP Site 1230 that indicate fermentation as the main acetate source (Heuer et al., 2006). The other widespread methanogenesis pathways from acetate (aceticlastic methanogenesis) and methylated substrates (e.g., methanol, dimethyl sulfide and methyl amines; methylotrophic methanogenesis), produce rather than consume CO_2 (Whitman et al., 2014). In aceticlastic methanogenesis, this CO_2 has the same ^{13}C-depleted isotopic composition as the methane produced (Gelwicks et al., 1994) and would thus lower (rather than increase) the $\delta^{13}C$-DIC. Despite high concentrations of acetate, our calculations, moreover, indicate that aceticlastic methanogenesis is close to thermodynamic equilibrium throughout most of the methanogenesis zone (Figure 6), with Gibbs energies not reaching the theoretical minimum required for biological energy conservation by proton translocation ($\Delta G_r' \cong 10\ kJ\ mol^{-1}$; Hoehler et al., 2001; Lever et al., 2015). ^{13}C-depletion of DIC is also expected for methylotrophic methanogenesis, even though this pathway produces methane with similar isotopic fractionations as CO_2 reduction (Conrad, 2005). The reason for ^{13}C-depletion of DIC is that the main isotopic fractionation of methylotrophic methanogenesis is produced by the first enzymes in the reaction chain (methyl transferase I and/or II; Krzycki et al., 1987) and hence upstream of where C fractions enter separate enzymatic pathways to produce CO_2 and methane (Thauer, 1998). Notably, another form of methylotrophic methanogenesis, which involves methylated substrates and hydrogen, e.g., methanol + H_2 does not produce CO_2 (Dridi et al., 2012; Whitman et al., 2014). A fourth methanogenic pathway that involves the conversion of methoxy-groups from lignin monomers to methane with CO_2 as a co-substrate (Mayumi et al., 2016) is in theory also possible. Yet, this pathway is unlikely to be important given the primarily phytoplanktonic origin of organic matter at ODP Site 1230 (Shipboard Scientific Party, 1988; D'Hondt et al., 2003) and recent evidence suggesting minimal long-term degradation of lignin in anoxic sediment (Han et al., 2022).

The increase in $\delta^{13}C$-DIC with depth is steepest from the lower SMTZ to ~20 mbsf (Figures 3, 5), consistent with rates of methanogenic CO_2 reduction being highest in this interval. The

subsequent decrease in the slope of δ^{13}C-DIC with depth can be explained with an increase in the DIC pool size and decline in the rates of CO_2 reduction. In addition, it is possible that the relative contributions of other methanogenic pathways, e.g., aceticlastic methanogenesis, increase below this depth. Nonetheless, the ^{13}C-isotopic depletions of −80 to −86‰ of δ^{13}C-methane relative to δ^{13}C-DIC that were consistently measured below 18 mbsf (Figure 3) indicate that CO_2 reduction accounts for most of the methane that has accumulated throughout the methanogenesis zone of ODP Site 1230.

Community zonation

When examined in the geochemical context, the distribution of *mcrA* genes within the methanogenesis zone of ODP Site 1230 may be surprising. Isotopic compositions of DIC and methane suggest predominance of methanogenesis by CO_2 reduction, whereas detected *mcr*A sequences belong to phylotypes of putatively anaerobic methane-oxidizing ANME-1a-b, its catabolically uncharacterized sister group ANME-1d, and *Methanothrix*, a genus that was traditionally believed to consist uniformly of obligately aceticlastic methanogens.

The presence of ANME-1a-b in the SMTZ and in underlying sediment that is net methanogenic can be explained with different scenarios. The first one is that ANME-1a-b are indeed facultatively methanogenic, as proposed previously based on strong heterogeneity in δ^{13}C of ANME-1-biomass in seep sediments (House et al., 2009), detection of ANME-1a-b *mcr*A transcripts in methanogenic sediment (Lloyd et al., 2011), and combined methanogenesis rate measurements and *mcr*A analyses across anaerobic methane-oxidizing and methanogenic sediment (Beulig et al., 2019). This environmental evidence has been supported by recent genomic detections of hydrogenase genes, that are potentially involved in hydrogenotrophic methanogenesis, across multiple ANME-1a-b and ANME-1c taxa (Laso-Pérez et al., 2023). Alternatively, AOM by ANME-1a-b may continue as a cryptic process in the presence of methanogenesis throughout the uppermost part of the methanogenesis zone. Our thermodynamic calculations indicate that a reversal of methanogenic CO_2 reduction with H_2 is thermodynamically favorable throughout bulk sediments of ODP Site 1230 (Figure 6), though the electron acceptor is unclear. As discussed earlier, the increase in dissolved barium indicates barite ($BaSO_4$) dissolution in this part of the sediment column as a potential source of sulfate, whereas the very low Fe^{2+} and Mn^{2+} concentrations argue against a significant role of AOM coupled to metal reduction. Under this scenario, the organisms that were responsible for the production of the measured methane are unknown. While neither possibility can be ruled out, the available evidence from this and past studies supports ANME-1a-b contributing to the production of methane by CO_2 reduction in the upper methanogenesis zone of ODP 1230.

The metabolism of ANME-1d, which replaces ANME-1a-b in deeper sediment layers of the methanogenesis zone, is even less understood than that of ANME-1a-b. This group, which was previously also referred to as "ANME-1-related group" and represents a poorly studied, sister family, or even sister order, of ANME-1a-b (Lever and Teske, 2015), has been found across a range of anoxic environments. These include hydrothermal vents in ultramafic settings (Kelley et al., 2005), deeply buried terrestrial coalbeds (Fry et al., 2009), marine gas hydrate sediments (Kormas et al., 2005), and tidal creek sediments (Edmonds et al., 2008). Given the sole detection of ANME-1d DNA and mRNA deep in the methanogenesis zone, a methanogenic lifestyle seems likely. This group could reduce CO_2 to methane using electrons from IET and thus contribute to the observed strong δ^{13}C-depletion of methane relative to DIC.

The predominant detection of *Methanothrix-mcr*A sequences below 20 mbsf, despite δ^{13}C-DIC compositions that indicate mainly methanogenesis by CO_2 reduction, and Gibbs energies of aceticlastic methanogenesis near thermodynamic equilibrium, is perplexing, given that members of *Methanothrix* are traditionally considered to be obligate aceticlasts. One explanation is that these sequences belong to inactive or dead cells. Yet, this explanation does not match the detection of rRNA of *Methanothrix* (Table 2), and is at odds with research suggesting that the vast majority of DNA from dead microorganisms is degraded over time scales of centuries in subsurface sediments (Torti et al., 2018). Instead, the *Methanothrix mcr*A and 16S rRNA sequences may not belong to (obligate) aceticlasts. While genomic data of *Methanothrix thermophila* indicate potential for hydrogenotrophic metabolism in this group (Smith and Ingram-Smith, 2007), methanogenesis involving H_2 has never been shown for *Methanothricaceae*. Yet, more recent experiments with pure cultures have demonstrated that members of *Methanothrix* - including *Methanothrix harundinacea*, which *mcr*A sequences from ODP Site 1230 cluster with (Figure 5) - are capable of methanogenic growth by CO_2 reduction using electrons received directly or through mineral intermediates from syntrophic partner organisms (Rotaru et al., 2014; Yang et al., 2019; Gao and Lu, 2021). Experiments involving rice paddy soils and lake sediments have provided additional evidence for CO_2 reduction by *Methanothrix* in the environment (Holmes et al., 2017; Rotaru et al., 2019). Consequently, the observed δ^{13}C-DIC and δ^{13}C-methane compositions and dominance of *mcr*A sequences of *Methanothrix* may not be a contradiction, but instead match revised knowledge on the metabolic capabilities of *Methanothrix*.

Conclusion

We provide the first complete community profile of active methane-cycling archaea in deep subseafloor sediments, and show based on DNA and RNA sequence data that anaerobic methane-cycling archaea are present throughout the SMTZ and methanogenesis zone of ODP Site 1230 in the Peru Trench. Of essential importance for the detection of *mcr*A, *mcr*A-mRNA, and 16S rRNA of methane-cycling archaea was the use of redesigned general *mcrA* primers and development of new group-specific *mcrA* and 16S rRNA gene primers. While these primers improved the detection sensitivity of methane-cycling archaea, they confirm the notion that methane-cycling archaea only account for a small fraction of deep subsurface microbial communities, even in AOM and methanogenesis zones (Lever, 2013).

Even though DNA- and RNA-based detections of methane-cycling archaea generally match the distributions of AOM and methanogenesis based on geochemical data, the detected phylogenetic groups appear at odds with the inferred dominant methane-cycling pathways. ANME-1, which are historically considered to be anaerobic methanotrophs, were detected to sediment depths that were > 10 m (ANME-1a-b) and > 100 m (ANME-1d) below the SMTZ. Based on published sedimentation rates for Site 1230 (0.25 mm yr.$^{-1}$; Shipboard Scientific Party, 1988), these distances suggest the continued existence of ANME-1a-b and ANME-1d populations in methanogenic sediments for >40,000 and > 400,000 years after their burial below the SMTZ, respectively. Given the measured

methane concentration and DIC-isotopic data, and that no other methane-cycling archaea were detected, a switch to methanogenesis by CO_2 reduction offers the most parsimonious explanation for the occurrence of ANME-1a-b far below the SMTZ. Similarly, methanogenesis by CO_2 reduction may sustain populations of ANME-1d in deeper layers, and also explain why members of *Methanothrix* – that were historically assumed to be aceticlastic - are pervasive throughout sediments that appear to be dominated by methanogenic CO_2 reduction. Herein, the pathway of CO_2 reduction remains unclear, but could bypass H_2 as an electron source through direct electron transfer.

Data availability statement

The original contributions presented in the study are publicly available. This data can be found here: All isotopic data (d13C-CH4, d13C-DIC) are included in Supplementary Table 1. All geochemical concentration data, including pH, are publicly available in D'Hondt et al. (2003). All nucleotide sequences can be retrieved from GenBank (mcrA: OQ603043-OQ603056; 16S rRNA: OQ658172-OQ658186).

Author contributions

ML, MA, and AT designed the research. AT and K-UH obtained the samples. ML and K-UH produced the data. ML analyzed the data with input from MA and AT and wrote the manuscript with input from all co-authors. All authors contributed to the article and approved the submitted version.

Funding

Sequencing was supported by the NASA Astrobiology Institute "From Early Biospheric Metabolisms to the Evolution of complex systems" and performed at the Josephine Bay Paul Center for Comparative Molecular Biology and Evolution at the Marine Biological Laboratory, Woods Hole, MA. ML was supported by a Schlanger Ocean Drilling Fellowship, and a University of North Carolina Dissertation Completion Fellowship.

Acknowledgments

The authors thank the Ocean Drilling Program (ODP) and in particular the ODP Leg 201 Shipboard Scientific Party for sampling support, Ketil Sørensen and Christopher S. Martens for helpful discussions, and Barbara J. MacGregor for intellectual input to earlier manuscript versions.

Conflict of interest

The authors declare that the research was conducted in the absence of any commercial or financial relationships that could be construed as a potential conflict of interest.

Publisher's note

Supplementary material

The Supplementary material for this article can be found online at: https://www.frontiersin.org/articles/10.3389/fmicb.2023.1192029/full#supplementary-material

References

Alperin, M. J., and Hoehler, T. M. (2009). Anaerobic methane oxidation by Archaea/sulfate-reducing bacteria aggregates: 2 Isotopic constraints. *Am. J. Sci.* 309, 958–984. doi: 10.2475/10.2009.02

Beulig, F., Røy, H., McGlynn, S. E., and Jørgensen, B. B. (2019). Cryptic CH_4 cycling in the sulfate-methane transition of marine sediments apparently mediated by ANME-1 archaea. *ISME J.* 13, 250–262. doi: 10.1038/s41396-018-0273-z

Biddle, J. F., Fitz-Gibbon, S., Schuster, S. C., Brenchley, J. E., and House, C. H. (2008). Metagenomic signatures of the Peru margin subseafloor biosphere show a genetically distinct environment. *Proc. Natl. Acad. U. S. A.* 105, 10583–10588. doi: 10.1073/pnas.0709942105

Biddle, J. F., Lipp, J. S., Lever, M. A., Lloyd, K., Sørensen, K., Anderson, R., et al. (2006). Heterotrophic Archaea dominate sedimentary subsurface ecosystems off Peru. *Proc. Natl. Acad. U. S. A.* 103, 3846–3851. doi: 10.1073/pnas.0600035103

Carr, S. A., Schubotz, F., Dunbar, R. B., Mills, C. T., Dias, R., Summons, R. E., et al. (2018). Acetoclastic *Methanosaeta* are dominant methanogens in organic-rich Antarctic marine sediments. *ISME J.* 12, 330–342. doi: 10.1038/ismej.2017.150

Colwell, F. S., Boyd, S., Delwiche, M. E., Reed, D. W., Phelps, T. J., and Newby, D. T. (2008). Estimates of biogenic methane production rates in deep marine sediments at hydrate ridge, Cascadia margin. *Appl. Environ. Microbiol.* 74, 3444–3452. doi: 10.1128/AEM.02114-07

Conrad, R. (2005). Quantification of methanogenic pathways using stable carbon isotopic signatures: a review and a proposal. *Org. Geochem.* 36, 739–752. doi: 10.1016/j.orggeochem.2004.09.006

Cragg, B. A., Parkes, R. J., Fry, J. C., Herbert, R. A., Wimpenny, J. W. T., and Getliff, J. M. (1990). "Bacterial biomass and activity profiles within deep sediment layers" in *Proc. ODP, Scientific Res.* eds. E. Suess and R. von Huene, vol. *112* (College Station, TX: Ocean Drilling Program)

D'Hondt, S. L., Jørgensen, B. B., and Miller, D. J.. (2003). *1. Leg 201 summary. Proc. ODP, Init. Repts*. College Station, TX: Ocean Drilling Program. 201.

D'Hondt, S., Jørgensen, B. B., Miller, D. J., Batzke, A., Blake, R., Cragg, B. A., et al. (2004). Distributions of microbial activities in deep subseafloor sediments. *Science* 306, 2216–2221. doi: 10.1126/science.1101155

Deng, L., Bölsterli, D., Kristensen, E., Meile, C., Su, C.-C., Bernasconi, S. M., et al. (2020). Macrofaunal control of microbial community structure in continental margin sediments. *Proc. Natl. Acad. Sci. U. S. A.* 117, 15911–15922. doi: 10.1073/pnas.1917494117

Dridi, B., Fardeau, M.-L., Ollivier, B., Raoult, D., and Drancourt, M. (2012). *Methanomassiliicoccus luminyensis* gen. Nov., sp. nov., a methanogenic archaeon isolated from human faeces. *Int. J. Syst. Evol. Microbiol.* 62, 1902–1907. doi: 10.1099/ijs.0.033712-0

Edmonds, J. W., Weston, N. B., Joye, S. B., and Moran, M. A. (2008). Variation in prokaryotic community composition as a function of resource availability in tidal creek sediments. *Appl. Environ. Microbiol.* 74, 1836–1844. doi: 10.1128/AEM.00854-07

Finke, N., Hoehler, T. M., and Jørgensen, B. B. (2007). Hydrogen 'leakage' during methanogenesis from methanol and methylamine: implications for anaerobic carbon

degradation pathways in aquatic sediments. *Environ. Microbiol.* 9, 1060–1071. doi: 10.1111/j.1462-2920.2007.01248.x

Friedrich, M. W. (2005). Methyl-coenzyme M reductase genes: unique functional markers of methanogenic and anaerobic methane-oxidizing Archaea. *Meth. Enzymol.* 397, 428–442. doi: 10.1016/S0076-6879(05)97026-2

Fry, J. C., Horsfield, B., Sykes, R., Cragg, B. A., Heywood, C., Kim, G. T., et al. (2009). Prokaryotic populations and activities in an interbedded coal deposit, including a previously deeply buried section (1.6–2.3 km) above ~150 ma basement rock. *Geomicrobiol J.* 26, 163–178. doi: 10.1080/01490450902724832

Futagami, T., Morono, Y., Terada, T., Kaksonen, A. H., and Inagaki, F. (2009). Dehalogenation activities and distribution of reductive dehalogenase homologous genes in marine subsurface sediments. *Appl. Environ. Microbiol.* 75, 6905–6909. doi: 10.1128/AEM.01124-09

Gao, K., and Lu, Y. (2021). Putative extracellular electron transfer in methanogenic archaea. *Front. Microbiol.* 12:611739. doi: 10.3389/fmicb.2021.611739

Gelwicks, J. T., Risatti, J. B., and Hayes, J. M. (1989). Carbon isotope effects associated with autotrophic acetogenesis. *Org. Geochem.* 14, 441–446. doi: 10.1016/0146-6380(89)90009-0

Gelwicks, J. T., Risatti, J. B., and Hayes, J. M. (1994). Carbon isotope effects associated with aceticlastic methanogenesis. *Appl. Environ. Microbiol.* 60, 467–472. doi: 10.1128/aem.60.2.467-472.1994

Hales, B. A., Edwards, C., Ritchie, D. A., Hall, G., Pickup, R. W., and Saunders, J. R. (1996). Isolation and identification of methanogen-specific DNA from blanket bog peat by PCR amplification and sequence analysis. *Appl. Environ. Microbiol.* 62, 668–675. doi: 10.1128/aem.62.2.668-675.1996

Han, X., Tolu, J., Deng, L., Fiskal, A., Schubert, C. J., Winkel, L. H. E., et al. (2022). Physical shielding promotes long-term preservation of biomolecules in lake sediments. *PNAS Nexus* 1, 1–15. doi: 10.1093/pnasnexus/pgac076

Heuer, V. B., Elvert, M., Tille, S., Krummen, M., Prieto Mollar, X., Hmelo, L. R., et al. (2006). Online δ13C analysis of volatile fatty acids in sediment/porewater systems by liquid chromatography-isotope ratio mass spectrometry. *Limnol. Oceanogr. Meth.* 4, 346–357. doi: 10.4319/lom.2006.4.346

Heuer, V. B., Inagaki, F., Morono, Y., Kubo, Y., Spivack, A. J., Viehweger, B., et al. (2020). Temperature limits to deep subseafloor life in the Nankai trough subduction zone. *Science* 370, 1230–1234. doi: 10.1126/science.abd7934

Hoehler, T. M., Alperin, M. J., Albert, D. B., and Martens, C. S. (2001). Apparent minimum free energy requirements for methanogenic archaea and sulfate-reducing bacteria in an anoxic marine sediment. *FEMS Microbiol. Ecol.* 38, 33–41. doi: 10.1111/j.1574-6941.2001.tb00879.x

Holmes, D. E., Shrestha, P. M., Walker, D. J. F., Dang, Y., Nevin, K. P., Woodard, T. L., et al. (2017). Metatranscriptomic evidence for direct interspecies electron transfer between *Geobacter* and *Methanothrix* species in methanogenic rice paddy soils. *Appl. Environ. Microbiol.* 83, e00223–e00217. doi: 10.1128/AEM.00223-17

Hoshino, T., Doi, H., Uramoto, G.-I., Wörmer, L., Adhikari, R. R., Xiao, N., et al. (2020). Global diversity of microbial communities in marine sediment. *Proc. Natl. Acad. Sci. U. S. A.* 117, 27587–27597. doi: 10.1073/pnas.1919139117

House, C. H., Cragg, B. A., and Teske, A.the Leg 201 Scientific Party (2003). "Drilling contamination tests during ODP leg 201 using chemical and particulate tracers" in *ODP Leg 201*, eds. D'Hondt, S. L. Jørgensen, B. B. Miller, D. J. et. al. *Proc. ODP, Init. Repts.*, 201 [Online]. Available at: http://www-odp.tamu.edu/publications/201_IR/chap_02/chap_02.htm

House, C. H., Orphan, V. J., Turk, K. A., Thomas, B., Pernthaler, A., Vrentas, J. M., et al. (2009). Extensive carbon isotopic heterogeneity among methane seep microbiota. *Environ. Microbiol.* 11, 2207–2215. doi: 10.1111/j.1462-2920.2009.01934.x

Inagaki, F., Hinrichs, K.-U., Kubo, Y., Bowles, M. W., Heuer, V. B., Hong, W. L., et al. (2015). Exploring deep microbial life in coal-bearing sediment down to ~2.5 km below the ocean floor. *Science* 349, 420–424. doi: 10.1126/science.aaa6882

Inagaki, F., Nunoura, T., Nakagawa, S., Teske, A., Lever, M., Lauer, A., et al. (2006). Biogeographical distribution and diversity of microbes in methane-bearing deep marine sediments on the Pacific Ocean margin. *Proc. Natl. Acad. U. S. A.* 103, 2815–2820. doi: 10.1073/pnas.0511033103

Kallmeyer, J., Pockalny, R., Adhikari, R. R., Smith, D. C., and D'Hondt, S. (2012). Global distribution of microbial abundance and biomass in subseafloor sediment. *Proc. Natl. Acad. Sci. U. S. A.* 109, 16213–16216. doi: 10.1073/pnas.1203849109

Kellermann, M. Y., Wegener, G., Elvert, M., Yoshinaga, M. Y., Lin, Y.-S., Holler, T., et al. (2012). Autotrophy as a predominant mode of carbon fixation in anaerobic methane-oxidizing microbial communities. *Proc. Natl. Acad. Sci. U. S. A.* 109, 19321–19326. doi: 10.1073/pnas.1208795109

Kelley, D. S., Karson, J. A., Früh-Green, G. L., Yoerger, D. R., Shank, T. M., Butterfield, D. A., et al. (2005). A serpentinite-hosted ecosystem: the lost City hydrothermal field. *Science* 307, 1428–1434. doi: 10.1126/science.1102556

Knittel, K., and Boetius, A. (2009). Anaerobic oxidation of methane: progress with an unknown process. *Annu. Rev. Microbiol.* 63, 311–334. doi: 10.1146/annurev.micro.61.080706.093130

Kormas, K. A., Meziti, A., Dählmann, A., de Lange, G. J., and Lykousis, V. (2005). Characterization of methanogenic and prokaryotic assemblages based on mcrA and 16S rRNA gene diversity in sediments of the Kazan mud volcano (Mediterranean Sea). *Geobiology* 6, 450–460. doi: 10.1111/j.1472-4669.2008.00172.x

Krzycki, J. A., Kenealy, W. R., DeNiro, M. J., and Zeikus, J. G. (1987). Stable carbon isotope fractionation by *Methanosarcina barkeri* during methanogenesis from acetate, methanol, or carbon dioxide-hydrogen. *Appl. Environ. Microbiol.* 53, 2597–2599. doi: 10.1128/aem.53.10.2597-2599.1987

Laso-Pérez, R., Wu, F., Crémière, A., Speth, D. R., Magyar, J. S., Zhao, K., et al. (2023). Evolutionary diversification of methanotrophic ANME-1 archaea and their expansive virome. *Nature Microbiol.* 8, 231–245. doi: 10.1038/s41564-022-01297-4

Lever, M. A. (2013). Functional gene surveys from ocean drilling expeditions – a review and perspective. *FEMS Microbiol. Ecol.* 84, 1–23. doi: 10.1111/1574-6941.12051

Lever, M. A., Alperin, M. A., Engelen, B., Inagaki, F., Nakagawa, S., Steinsbu, B., et al. (2006). Trends in basalt and sediment core contamination during IODP expedition 301. *Geomicrobiol J.* 23, 517–530. doi: 10.1080/01490450600897245

Lever, M. A., Heuer, V. B., Morono, Y., Masui, N., Schmidt, F., Alperin, M. J., et al. (2010). Acetogenesis in deep subseafloor sediments of the Juan de Fuca ridge flank: a synthesis of geochemical, thermodynamic, and gene-based evidence. *Geomicrobiol J.* 27, 183–211. doi: 10.1080/01490450903456681

Lever, M. A., Rogers, K., Lloyd, K. G., Overmann, J. O., Schink, B., Thauer, R. K., et al. (2015). Microbial life under extreme energy limitation: a synthesis of laboratory- and field-based investigations. *FEMS Microbiol. Rev.* 39, 688–728. doi: 10.1093/femsre/fuv020

Lever, M. A., and Teske, A. P. (2015). Diversity of methane-cycling archaea in hydrothermal sediment investigated by general and group-specific PCR primers. *Appl. Environ. Microbiol.* 81, 1426–1441. doi: 10.1128/AEM.03588-14

Lloyd, K. G., Alperin, M. J., and Teske, A. (2011). Environmental evidence for net methane production and oxidation in putative anaerobic Methanotrophic (ANME) archaea. *Environ. Microbiol.* 13, 2548–2564. doi: 10.1111/j.1462-2920.2011.02526.x

Ludwig, W., Strunk, O., Westram, R., Richter, L., Meier, H., Yadhukumar, , et al. (2004). ARB: a software environment for sequence data. *Nucleic Acids Res.* 32, 1363–1371. doi: 10.1093/nar/gkh293

Lynch-Stieglitz, J., Stocker, T. F., Broecker, W. S., and Fairbanks, R. G. (1995). The influence of air-sea exchange on the isotopic composition of oceanic carbon: observations and modeling. *Global Biogeochem. Cycles* 9, 653–665. doi: 10.1029/95GB02574

Marshall, I. P. G., Karst, S. M., Nielsen, P. H., and Jørgensen, B. B. (2018). Metagenomes from deep Baltic Sea sediments reveal how past and present environmental conditions determine microbial community composition. *Mar. Genomics* 37, 58–68. doi: 10.1016/j.margen.2017.08.004

Mauclaire, L., Zepp, K., Meister, P., and McKenzie, J. (2005). Direct in situ detection of cells in deep-sea sediment cores from the Peru margin (ODP leg 201, site 1229). *Geobiology* 2, 217–223. doi: 10.1111/j.1472-4677.2004.00035.x

Mayumi, D., Mochimaru, H., Tamaki, H., Yamamoto, K., Yoshioka, H., Suzuki, Y., et al. (2016). Methane production from coal by a single methanogen. *Science* 354, 222–225. doi: 10.1126/science.aaf8821

Meister, P., Prokopenko, M., Skilbeck, C. G., Watson, M., and McKenzie, J. A. (2005). "Data report: compilation of total organic and inorganic carbon data from Peru margin and eastern equatorial Pacific drill sites (ODP legs 112, 138, and 201)" in, eds. Jørgensen, B. B. D'Hondt, S. L. and Miller, D. J. *Proc. ODP, Sci. Results*, 201, 1–20 [Online]. Available at: http://www-odp.tamu.edu/ publications/201_SR/VOLUME/ CHAPTERS/105.PDF

Millero, F. J. (2000). The activity coefficients of non-electrolytes in seawater. *Marine Chem.* 70, 5–22. doi: 10.1016/S0304-4203(00)00011-6

Millero, F. J., and Schreiber, D. R. (1983). Use of the ion pairing model to estimate activity coefficients of the ionic components of natural waters. *Am. J. Sci.* 282, 1508–1540. doi: 10.2475/ajs.282.9.1508

Nauhaus, K., Albrecht, M., Elvert, M., Boetius, A., and Widdel, F. (2007). *In vitro* cell growth of marine archaeal-bacterial consortia during anaerobic oxidation of methane with sulfate. *Environ. Microbiol.* 9, 187–196. doi: 10.1111/j.1462-2920.2006.01127.x

Parkes, R. J., Cragg, B. A., Bale, S. J., Getliff, J. M., Goodman, K., Rochelle, P. A., et al. (2005). Deep sub-seafloor prokaryotes stimulated at interfaces over geological time. *Nature* 436, 390–394. doi: 10.1038/nature03796

Parkes, R. J., Cragg, B., Roussel, E., Webster, G., Weightman, A., and Sass, H. (2014). A review of prokaryotic populations and processes in sub-seafloor sediments, including biosphere: geosphere interactions. *Mar. Geol.* 352, 409–425. doi: 10.1016/j.margeo.2014.02.009

Penning, H., Claus, P., Casper, P., and Ralf Conrad, R. (2005). Carbon isotope fractionation during acetoclastic methanogenesis by *Methanosaeta concilii* in culture and a lake sediment. *Appl. Environ. Microbiol.* 72, 5648–5652. doi: 10.1128/AEM.00727-06

Rotaru, A.-E., Posth, N. R., Löscher, C. R., Miracle, M. R., Vicente, E., Cox, R. P., et al. (2019). Interspecies interactions mediated by conductive minerals in the sediments of the iron-rich meromictic Lake La Cruz, Spain. *Limnetica* 38, 21–40. doi: 10.23818/limn.38.10

Rotaru, A.-E., Shrestha, P. M., Liu, F., Shrestha, M., Shrestha, D., Embree, M., et al. (2014). A new model for electron flow during anaerobic digestion: direct interspecies

electron transfer to *Methanosaeta* for the reduction of carbon dioxide to methane. *Energy Environ. Sci.* 7, 408–415. doi: 10.1039/C3EE42189A

Roussel, E. G., Bonavita, M. A. C., Querellou, J., Cragg, B. A., and Webster, G. (2008). Extending the sub-sea-floor biosphere. *Science* 320:1046. doi: 10.1126/science.1154545

Schink, B., Montag, D., Keller, A., and Müller, N. (2017). Hydrogen or formate: alternative key players in methanogenic degradation. *Environ. Microbiol. Repts.* 9, 189–202. doi: 10.1111/1758-2229.12524

Schippers, A., Kock, D., Höft, C., Köweker, G., and Siegert, M. (2012). Quantification of microbial communities in subsurface marine sediments of the Black Sea and off Namibia. *Front. Microbiol.* 3:16. doi: 10.3389/fmicb.2012.00016

Schippers, A., Neretin, L., Kallmeyer, J., Ferdelman, T., Cragg, B. A., Parkes, J. R., et al. (2005). Prokaryotic cells of the deep sub-seafloor biosphere identified as living bacteria. *Nature* 433, 861–864. doi: 10.1038/nature03302

Shipboard Scientific Party (1988). "Introduction, objectives, and principal results, leg 112, Peru continental margin" in E. Suess, R. von Huene, et al. *Proc. ODP, Init. Repts.*, 112. (College Station, TX: Ocean Drilling Program), 5–23. doi: 10.2973/odp.proc.ir.112.102.1988

Smith, K. S., and Ingram-Smith, C. (2007). *Methanosaeta*, the forgotten methanogen? *Trends Microbiol.* 15, 150–155. doi: 10.1016/j.tim.2007.02.002

Sørensen, K. B., and Teske, A. (2006). Stratified communities of active Archaea in deep marine subsurface sediments. *Appl. Environ. Microbiol.* 72, 4596–4603. doi: 10.1128/AEM.00562-06

Sparling, R., and Daniels, L. (1986). Source of carbon and hydrogen in methane produced from formate by *Methanococcus thermolithotrophicus*. *J. Bacteriol.* 168, 1402–1407. doi: 10.1128/jb.168.3.1402-1407.1986

Spivack, A. J., McNeil, C., Holm, N. G., and Hinrichs, K.-U. (2005). "Determination of in situ methane based on analysis of void gas" in *ODP Leg 201*, eds. B. B. Jørgensen, S. L. D'Hondt, and D. J. Miller, *Proc. ODP, Sci. Results*, 201 [Online]. Available at: http://www-odp.tamu.edu/publications/201_SR/119/119.htm

Springer, E., Sachs, M. S., Woese, C. R., and Boone, D. R. (1995). Partial gene sequences for the a subunit of methyl-coenzyme M reductase (mcrI) as a phylogenetic tool for the family *Methanosarcinaceae*. *Int. J. Syst. Bacteriol.* 45, 554–559. doi: 10.1099/00207713-45-3-554

Stahl, D. A., and Amann, R. (1991). "Development and application of nucleic acid probes" in *Nucleic acid techniques in bacterial systematics*. eds. E. Stackebrandt and M. Goodfellow, vol. *8* (London: John Wiley & Sons), 207–248.

Stumm, W., and Morgan, J. J. (1996). Aquatic chemistry, chemical equilibria and rates in natural waters, 3rd ed. New York: John Wiley & Sons, Inc.

Suess, E. (1981). Phosphate regeneration from sediment of the Peru continental margin by dissolution of fish debris. *Geochim. Cosmochim. Acta* 45, 577–588. doi: 10.1016/0016-7037(81)90191-5

Sun, R., and Duan, Z. (2007). An accurate model to predict the thermodynamic stability of methane hydrate and methane solubility in marine environments. *Chem. Geol.* 244, 248–262. doi: 10.1016/j.chemgeo.2007.06.021

Thauer, R. K. (1998). Biochemistry of methanogenesis: a tribute to Marjory Stephenson. *Microbiology* 144, 2377–2406. doi: 10.1099/00221287-144-9-2377

Torti, A., Jørgensen, B. B., and Lever, M. A. (2018). Preservation of microbial DNA in marine sediments: insights from extracellular DNA pools. *Environ. Microbiol.* 20, 4526–4542. doi: 10.1111/1462-2920.14401

Wagner, M., Loy, A., Klein, M., Lee, N., Ramsing, N. B., Stahl, D. A., et al. (2005). Functional marker genes for identification of sulfate-reducing prokaryotes. *Meth. Enzymol.* 397, 469–489. doi: 10.1016/S0076-6879(05)97029-8

Wang, Y., Wegener, G., Ruff, S. E., and Wang, F. (2021). Methyl/alkyl-coenzyme M reductase-based anaerobic alkane oxidation in archaea. *Environ. Microbiol.* 23, 530–541. doi: 10.1111/1462-2920.15057

Webster, G., Parkes, R. J., Cragg, B. A., Newberry, C. J., Weightman, A. J., and Fry, J. C. (2006). Prokaryotic community composition and biogeochemical processes in deep subseafloor sediments from the Peru margin. *FEMS Microbiol. Ecol.* 58, 65–85. doi: 10.1111/j.1574-6941.2006.00147.x

Wegener, G., Gropp, J., Taubner, H., Halevy, I., and Elvert, M. (2021). Sulfate-dependent reversibility of intracellular reactions explains the opposing effects in the anaerobic oxidation of methane. *Sci. Adv.* 7:eabe4939. doi: 10.1126/sciadv.abe4939

Wegener, G., Niemann, H., Elvert, M., Hinrichs, K.-U., and Boetius, A. (2008). Assimilation of methane and inorganic carbon by microbial communities mediating the anaerobic oxidation of methane. *Environ. Microbiol.* 10, 2287–2298. doi: 10.1111/j.1462-2920.2008.01653.x

Whiticar, M. J. (1999). Carbon and hydrogen isotope systematics of bacterial formation and oxidation of methane. *Chem. Geol.* 161, 291–314. doi: 10.1016/S0009-2541(99)00092-3

Whiticar, M. J., Faber, E., and Schoell, M. (1986). Biogenic methane formation in marine and freshwater environments: CO_2 reduction vs. acetate fermentation – isotope evidence. *Geochim. Cosmochim. Acta* 50, 693–709. doi: 10.1016/0016-7037(86)90346-7

Whitman, W. B., Bowen, T. L., and Boone, D. R. (2014). "The methanogenic Bacteria" in *The prokaryotes*. eds. E. Rosenberg, E. F. DeLong, S. Lory, E. Stackebrandt and F. Thompson, vol. 3, (Heidelberg:Springer, Berlin) 124–163. doi: 10.1007/978-3-642-38954-2_407

Yang, P., Amy Tan, G.-Y., Aslam, M., Kim, J., and Lee, P.-H. (2019). Metatranscriptomic evidence for classical and RuBisCO-mediated CO_2 reduction to methane facilitated by direct interspecies electron transfer in a methanogenic system. *Sci. Rep.* 9:4116. doi: 10.1038/s41598-019-40830-0

Yoshinaga, M. Y., Holler, T., Goldhammer, T., Wegener, G., Pohlman, J. W., Brunner, B., et al. (2014). Carbon isotope equilibration during sulphate-limited anaerobic oxidation of methane. *Nat. Geosci.* 7, 190–194. doi: 10.1038/ngeo2069

Zhang, C., Fang, Y.-X., Yin, X., Lai, H., Kuang, Z., Zhang, T., et al. (2023). The majority of microorganisms in gas hydrate-bearing subseafloor sediments ferment macromolecules. *Microbiome* 11:37. doi: 10.1186/s40168-023-01482-5

frontiers | Frontiers in Microbiology

TYPE Mini Review
PUBLISHED 16 May 2023
DOI 10.3389/fmicb.2023.1186847

OPEN ACCESS

EDITED BY
Andreas Teske,
University of North Carolina at Chapel Hill, United States

REVIEWED BY
Ian P. G. Marshall,
Aarhus University, Denmark

*CORRESPONDENCE
Pierre Amato
✉ pierre.amato@uca.fr

†PRESENT ADDRESSES
Raphaëlle Péguilhan,
IPREM – Institut des Sciences Analytiques et de Physico-Chimie pour l'Environnement et les Matériaux, Pau, France
Florent Rossi,
Département de Biochimie, de Microbiologie et de Bio-informatique, Faculté des Sciences et de Génie, Université Laval, Quebec City, QC, Canada
Jonathan Vyskocil,
CSTB – Scientific and Technical Center for Construction, Division for Biological Agents and Air Contaminants, Champs-sur-Marne, France

RECEIVED 15 March 2023
ACCEPTED 24 April 2023
PUBLISHED 16 May 2023

CITATION
Amato P, Mathonat F, Nuñez Lopez L, Péguilhan R, Bourhane Z, Rossi F, Vyskocil J, Joly M and Ervens B (2023) The aeromicrobiome: the selective and dynamic outer-layer of the Earth's microbiome. *Front. Microbiol.* 14:1186847. doi: 10.3389/fmicb.2023.1186847

The aeromicrobiome: the selective and dynamic outer-layer of the Earth's microbiome

Pierre Amato*, Frederic Mathonat, Leslie Nuñez Lopez, Raphaëlle Péguilhan†, Zeina Bourhane, Florent Rossi†, Jonathan Vyskocil†, Muriel Joly and Barbara Ervens

Université Clermont Auvergne, CNRS, Institut de Chimie de Clermont-Ferrand (ICCF), Clermont-Ferrand, France

The atmosphere is an integral component of the Earth's microbiome. Abundance, viability, and diversity of microorganisms circulating in the air are determined by various factors including environmental physical variables and intrinsic and biological properties of microbes, all ranging over large scales. The aeromicrobiome is thus poorly understood and difficult to predict due to the high heterogeneity of the airborne microorganisms and their properties, spatially and temporally. The atmosphere acts as a highly selective dispersion means on large scales for microbial cells, exposing them to a multitude of physical and chemical atmospheric processes. We provide here a brief critical review of the current knowledge and propose future research directions aiming at improving our comprehension of the atmosphere as a biome.

KEYWORDS

atmosphere, bioaerosol, aeromicrobiome, bacteria, fungi, cloud

1. Introduction

Airborne microbial cell concentrations range from <10 to ~10^7 cells m^{-3} depending on altitude, location, time of day, and season (Bowers et al., 2011; Tignat-Perrier et al., 2020). The global atmosphere contains ~10^{20} bacteria cells (Whitman et al., 1998), which is approximately 10 orders of magnitude less than in soil and in the oceans, respectively (Šantl-Temkiv et al., 2022). At first sight, such biomass thus seems insignificant, but it is renewed with high turnover (typical particle residence time of a few days) and selectivity (high mortality rates), while providing efficient dispersion at large scale.

Since pioneering visionary scientists investigated the microbes transported in the air [the most prominent of which include (Pasteur, 1862; Molisch, 1922; Meier and Lindbergh, 1935; Moulton, 1942; Lacey, 1986)], aeromicrobiology has emerged as a full-fledged field of environmental microbiology. Over time, it benefited from general technological and knowledge advances in microbiology, and from interactions between disciplines including microbiology, ecology, meteorology, atmospheric physics, and chemistry.

The aeromicrobiome demonstrates some level of organization at different scales of space and time, through physical and biological processes as depicted in Figure 1. This contributes to the many aspects of the Earth system, *via* the regulation of ecosystems and populations, hydrological and biochemical cycles, atmospheric composition, climate, biogeography, and microbial evolution. However, despite apparent proximity, the atmospheric biotic system is one of the least studied on the planet and its implications remain still poorly characterized. The

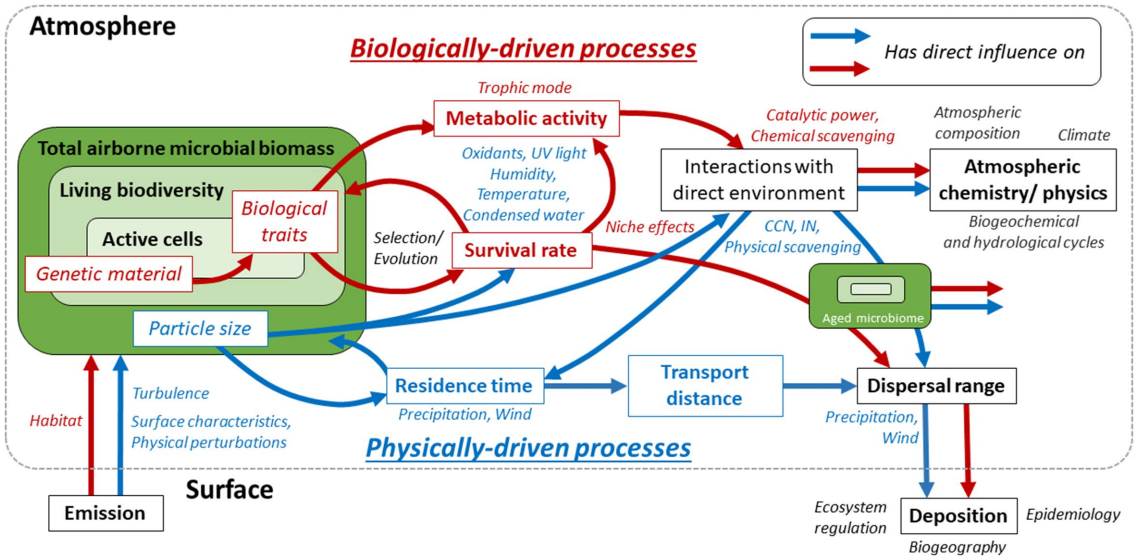

FIGURE 1
The aeromicrobiome and its identified biological and physical drivers, in red and blue, respectively (arrows and text). Its main intrinsic characteristics are italicized and framed, and major biological and physical factors of regulation are in blue and red italics. Wider hypothesized or proven outcomes, through the processes framed in black, are mentioned in black italics. For example: (i) the survival rate of emitted microorganisms determines the composition of the living aeromicrobiome; it depends on both microorganism's biological traits, which rely on genetic material, and particle size, and is under pressure from atmospheric conditions (oxidants, UV light, etc.); (ii) microbial cells interact with their atmospheric environment as aerosol particles, with impacts on their residence time (e.g., precipitation), and through metabolic activity, depending on survival and biological traits, which influences chemical processes. More largely, atmospheric composition, hydrogeochemical and hydrological cycles and climate are affected. Aged aeromicrobiome is depicted on the right; it includes a fraction of the emitted cells, and selected viable and active fractions. Once deposited, genetic material and living organisms interact with surface ecosystems, including hosts in the case of pathogens, and contribute to biogeographical and pathogeographical patterns.

selective pressures exerted by atmospheric conditions toward microorganisms depend on physical and biological parameters, and is heterogeneous among the great biodiversity potentially exposed. Some microorganisms remain viable longer than others and, thus, have larger dispersal ranges, while maintaining different degrees of metabolic activity and interaction with their environment. Independently from viability, genetic material is also dispersed and can contribute to large-scale horizontal gene transfer. Microbial cells and biological material also undergo and can affect atmospheric processes, such as cloud formation, precipitation, and chemical reactivity. In this mini-review, we summarize some of the latest developments and key findings related to the atmospheric microbiome, and emphasize major directions for future research.

2. Structuration of the aeromicrobiome

2.1. Interactions with Earth surfaces

It is largely accepted that anywhere on the planet, the airborne microbial abundance and diversity result exclusively from exchanges with the surface, i.e., emission and deposition processes. At first approximation, emissions and deposition are globally balanced (Burrows et al., 2009b; Fröhlich-Nowoisky et al., 2016), which implies that all aerosolized microorganisms are finally deposited back, without significant production or loss of microbial biomass in the atmosphere, resulting in atmospheric transport as a neutral process. The simplified assumption could be discussed, but it forms the basis of our current view on microbial aerial dispersion. Thus, studying the aeromicrobiome starts by characterizing inputs and losses from and to surfaces.

Aerosolization, i.e., the detachment from surfaces, depends in complex ways on factors such as surface roughness, humidity, and electrical charges, which act against drag forces. Once detached from the surface, particles are lifted by turbulent fluxes (Carotenuto et al., 2017), and their residence time largely depends on particle size and hygroscopicity; these are described in aerosol dispersion models of different resolutions and scales (local to global). However, emission fluxes and dispersion of microorganisms are currently poorly constrained in atmospheric models.

Globally, ~10^{24} bacteria cells are emitted each year from surfaces to the atmosphere (Burrows et al., 2009a), i.e., on average ~60 cells/m^2/s. The aeromicrobiome is highly variable over short spatial and temporal scales (Fierer et al., 2008; Bowers et al., 2011). It has a large species-time relationship compared to, for example, soil or marine environments (Shade et al., 2013), which is directly related to the high turnover (replacement) of taxa (Baselga, 2010; Péguilhan et al., 2021) and the large proportions of rare species (Shade et al., 2014). Its composition and dynamics reflect underlying ecosystem patterns, their spatial extension, and seasonal variations (Bowers et al., 2011; Tignat-Perrier et al., 2020; Archer et al., 2023). The aerial parts of plants notably host a large number of diverse microorganisms that can be readily aerosolized (Vorholt, 2012; Schlechter et al., 2019). Therefore, vegetation acts as a major source of airborne microorganisms with emissions fluxes of up to ~500 viable bacteria

cells/m^2/s measured (Lindemann et al., 1982; Lindemann and Upper, 1985). However, on average, these fluxes rarely exceed ~10 cells/m^2/s (Carotenuto et al., 2017) and are hence extremely difficult to quantify with accuracy.

Technical and analytical limitations certainly contribute to the current inability to account for microbial emission fluxes. In their current development, these can be experimentally assessed through the Bowen ratio method, approximating that microorganisms' fluxes above surfaces follow that of sensible heat (Lighthart and Shaffer, 1994). This method involves micrometeorological measurements at high frequency to characterize turbulent fluxes, efficient and accurate sampling devices positioned at 2 heights above ground, e.g., typically ~1 m and 2 m a.g.l. to assess the gradient of microbial abundance (Carotenuto et al., 2017), and the characterization of the surface area "seen" by the samplers and probes, referred to as "footprint" (Schmid, 2002).

In the absence of actual data, emission fluxes are thus to be inferred *a posteriori* based on airborne concentrations measured near the ground, and assuming that removal processes can be appropriately represented. This way, bacteria emission fluxes from major ecosystems were constrained on a global scale by a multivariate approach (Burrows et al., 2009a,b). The underlying assumptions implied underestimated (or ignored) emissions from poorly characterized surfaces, such as oceans, and no temporal variations. The uplift of microorganisms from surfaces is nevertheless highly variable in space and time, in relation for instance with solar irradiance imposing diurnal and seasonal cycles on turbulent fluxes (Lighthart, 1999; Gusareva et al., 2019). Mechanical disturbance of surfaces by wind, rainfall, animals and human activities, and wildland fire can cause efficient aerosolization of microorganisms (Evans et al., 2006; Huffman et al., 2013; Joung et al., 2017; Kobziar et al., 2022). High productivity ecosystems, such as vegetated areas tend to act as long-term net sources (Burrows et al., 2009a), alike the organic-rich microlayer at the ocean–atmosphere interface (sea-surface microlayer) (Aller et al., 2005; Cunliffe and Murrell, 2009; Malfatti et al., 2019; Alsante et al., 2021).

Not all microorganisms have equal chances to enter the aeromicrobiome: those located at the surface-air-interface are inherently more prone to aerosolization than those embedded in complex matrices or deep layers. Therefore, it is conceivable for instance that aerobic organisms are more prone to aerosolization than anaerobes. Some microorganisms have structures designed for aerial dispersion, such as spores in certain fungi, for which emissions can be active processes predictable from meteorological variables (Burns et al., 2022). For other microorganisms, differential aerosolization may occur depending on taxa and their physiological characteristics, some of which can lead to increased buoyancy and flotation (pigmentation linked with cell' surface hydrophobicity, allometry, …), as shown from aquatic environments using controlled bubble-bursting (Burger and Bennett, 1985; Gauthier-Levesque et al., 2016; Michaud et al., 2018). Microbial biofilms covering Earth surfaces are designed to break up under specific conditions and release free cells, including genetic variants, to colonize distant environments or hosts (McDougald et al., 2012). Aerial dispersion could be integral parts of their life cycle.

Airborne microbial cells finally exit the aeromicrobiome by dry or wet deposition processes, including scavenging by precipitation (Slinn, 1982; Triadó-Margarit et al., 2019; Moore et al., 2020; Péguilhan et al., 2021). Deposition fluxes are much more accessible than those of emission, as deposits can be easily collected and analyzed and directly expressed as per surface area and time. For bacteria, wet deposition is associated with highest fluxes, reaching up to ~10^7–10^8 cells/m^2/h (Reche et al., 2018; Woo and Yamamoto, 2020; Péguilhan et al., 2021). The microbial mixture permanently deposited from air on surfaces brings invaders and competitors to surface environments (Hervas and Casamayor, 2009; Morris and Sands, 2017; Noirmain et al., 2022). The continuous flow of foreign genetic material from atmospheric deposition is hypothesized to contribute to ecosystems stability and microbial evolution (Jalasvuori, 2020).

2.2. Microscale distribution

Microorganisms are distributed among aerosol particles in the atmosphere. Size determines the velocity at which particles are removed from the atmosphere by dry deposition, and so their transport range. Settling rates are on the order of ~7 to 750 µm s^{-1} for typical sizes of microbial aerosol particles (0.5 and 5 µm of aerodynamic diameter, respectively, i.e., the equivalent diameter of a perfect sphere of unit density) (Scheuch, 2020); these vary with temperature and pressure. Single bacteria cells with aerodynamic diameter of ~1 µm are estimated to remain airborne for 3–4 days (Burrows et al., 2009a), about twice as short as the residence time of water molecules (van der Ent and Tuinenburg, 2017). This still allows long distance travel over transcontinental scales, as attested for instance by tracers such as Saharan desert dust carrying specific bioaerosols deposited with snow in the Alps, or reaching North America (Creamean et al., 2013; Smith et al., 2013; Barberán et al., 2015; Weil et al., 2017). Such large-scale spread of microorganisms connects distant ecosystems and affects global biogeographical patterns (Morris et al., 2010; Barberán et al., 2014; Leyronas et al., 2018).

The range of sizes of microorganism-carrying particles leads to their zonal separation, horizontally with the distance from emission sources (Gat et al., 2021) and vertically along the altitude (Prass et al., 2021). Very few data exist about the size distribution of microbe-containing particles, that associated with living organisms in particular, or the number of cells and taxa carried together on individual aerosol particles, i.e., the biological mixing state of microbial aerosols, which may affect gene transfer while airborne.

3. Aerial fate of microorganisms

3.1. Survival of microorganisms during aerial transport

The proportion of living cells, their level of metabolic activity, and the functions expressed are key parameters in the characterization of the aeromicrobiome. A fraction of the emitted microorganisms could already be dead at the time of aerosolization. Moreover, microbial survival is greatly impaired during atmospheric transport due direct exposure to extremely harsh and variable conditions including water availability, temperature, oxidants, and UV radiation (Smith et al., 2011; Joly et al., 2015; Šantl-Temkiv et al., 2022). Most living microbial cells occur as agglomerates larger than 2 µm (Lighthart and Shaffer, 1995b; Lighthart, 1997; Monier and Lindow, 2003). While cell clusters

and cells agglomerated to other material have higher survival capacity than single cells, they have a shorter atmospheric residence time; both aspects (particle size and sheltering effect) contribute to the dispersal range of microorganisms. The few available studies assessing the size distribution of microbial particles do not discriminate between viable and total organisms.

Experiments on *Pseudomonas syringae* aerosolized in a cloud chamber determined a half-life time of ~4 h (Amato et al., 2015), indicating that statistically only ~1 individual out of one million survives atmospheric transport from emission to deposition. This is much higher than the mortality rates of bacteria in aquatic ecosystems, on the order of ~10^{-3} h^{-1}, mostly driven by predators (Menon et al., 2003). During their atmospheric transport, cells undergo highly selective processes, and the living fraction of microbial aerosols may sharply decrease with time airborne, i.e., increasing horizontal and vertical distance from the emission source. As differential survival capacity exists among the enormous microbial diversity transiting through the atmosphere, aeromicrobiome's richness and structure may be altered during atmospheric aging.

The proportion of viable organisms is not frequently reported; quantitative data can be difficult to obtain reliably from atmospheric samples due to the necessity to preserve cell integrity and the complex microbial assemblages. Viability is not accounted for by DNA-based techniques, which most current studies rely on. Data derived from cultures represent a conservative underestimate of viability; they typically indicate ~1% viable bacteria, and ~ 50% viable fungal cells (Vaïtilingom et al., 2012). Differential staining (e.g., live/dead staining), a more reliable method, indicated proportions of viable bacteria varying from 2.8 to 6.6% in air sampled from a high mountain site, with higher proportions during the night (Šantl-Temkiv et al., 2017).

Microbial survival rates in relation with environmental variables such as humidity, temperature, particle size distribution, sun radiation, or chemical composition were explored in numerous studies (Ehrlich et al., 1970; Lighthart et al., 1971; Lighthart and Frisch, 1976; Lighthart, 1989; Lighthart and Shaffer, 1997; Tong and Lighthart, 1998; Amato et al., 2015). The survival of bacteria upon water evaporation depends on environmental parameters such as temperature and salinity, and is favored at higher evaporation rates (Marthi et al., 1990; Alsved et al., 2018). In addition, physiological characteristics of taxa are linked with their capacity to maintain viability, including forming resistance spores, pigments, efficient oxidative stress responses and repair systems (Tong and Lighthart, 1998; Ochsner et al., 2000; Fredrickson et al., 2008; Joly et al., 2015). In *E. coli*, series of genes differentially expressed after aerosolization were found to contribute to higher survival, including proteins involved in stress response and DNA protection (Ng et al., 2018). In addition, multiple resistance genes, such as efflux pumps involved in the resistance to quinolones, could provide selective advantage to microorganisms in stressful environments like the atmosphere, even in the absence of such compound, and enhance their capacity to aerial dispersion (Rossi et al., 2022; Smith and King, 2022). *Sphingomonas*, one of the most frequent bacteria taxa in continental atmosphere, often carries multiple resistance genes (Vaz-Moreira et al., 2011).

Overall, some biological traits favoring microbial survival in the atmosphere have been identified. Their selective advantage may vary with atmospheric conditions, i.e., water availability, light radiation, temperature, presence of toxic chemical, etc, and this needs to be better characterized.

3.2. Metabolic activity, biological functioning, and potential niche effects in clouds

Biomarkers such as ATP and ribosomal RNA in air and cloud samples indicate the presence of metabolically active bacteria, such as Alpha-Proteobacteria (Rhodospirillales, Sphingomonadales, and Rhizobiales) and Gamma-Proteobacteria (Pseudomonadales) (Klein et al., 2016; Amato et al., 2017; Wirgot et al., 2017; Šantl-Temkiv et al., 2018). This was corroborated by experiments under controlled conditions, in which airborne Alpha-Proteobacteria (*Sphingomonas aerolata*) responded to the presence of volatile compounds by elevating ribosome content (Krumins et al., 2014). Such responses suggest some extent of acclimation to environmental conditions.

The metabolic functioning of airborne microorganisms is expected to vary widely in space and time and with environmental conditions, with potential niche effects in particular in clouds where condensed water could promote biological processes. Only a single study so far demonstrated a general microbial functioning in natural clouds oriented toward the response to stress factors (temperature, oxidants, etc.); metatranscriptomics data indicated series of defense mechanisms associated with central metabolic functions known to participate to stress management (Amato et al., 2019). Microbial multiplication in fog and cloud was suggested based on observations (Fuzzi et al., 1997; Sattler et al., 2001). Further modeling work suggested that significant microbial proliferation is not likely given the short life time of clouds (Ervens and Amato, 2020), but the whole aeromicrobiome functioning could be affected, which still needs to be evaluated.

In situ observations of microbial activity in clouds is not possible yet. Enzymatic assays (Vaïtilingom et al., 2010; Qi et al., 2015) as well as chemical fingerprinting of the impacts of microbial activity (Bianco et al., 2019), including isotope-based assays (Sattler et al., 2001), require laboratory incubation. More direct approaches, such as transcriptomics combined with powerful sampling solutions are, thus, preferred. Controlled experiments in simulation chambers might provide further insight into quantitative aspects of microbial activity and its modulations by environmental factors.

Microorganisms are considered specialists or generalists depending on the range of conditions (temperature, salinity, substrates, *etc.*) compatible with their development. Their assembly can be described by niche-driven or neutral (i.e., random) processes, respectively (Liao et al., 2016). Generalists are metabolically more flexible than specialists, resulting in selective advantage in frequently disturbed ecosystems (Chen et al., 2021); these might thus be favored in the atmosphere. The relative abundance of Proteobacteria and Actinobacteria, which include higher proportions of generalists than other phyla, increases with altitude in soils (Luo et al., 2019); these are also frequent in viable airborne assemblages (Vaïtilingom et al., 2012).

The capacity to utilize various sources of nutrients and energy thus seems advantageous for survival and maintenance in the atmosphere. This may contribute to the high abundance of *Pseudomonas* species that are known for their versatility and opportunism (Rojo, 2010). While chemoheterotrophic and photoautotrophic modes are regularly investigated (Amato et al., 2007; Vaïtilingom et al., 2010; Tesson et al., 2016; Dillon et al., 2020),

photoheterotrophy, by which cells can harvest additional biochemical energy from light through bacteriochlorophylls and rhodopsins is barely studied. This function may however provide strong selective advantage during atmospheric transport, as suggested by the occurrence of *Sphingomonas*, whose certain species contain anoxygenic phototrophy pigments (Kopejtka et al., 2020). Comparative analyses between the aeromicrobiome and other ecosystems can help deciphering biological functions that provide selective advantage or intimate relation with atmospheric transport, by identifying anomalies in their occurrence.

3.3. Impact of microorganisms on the atmosphere

While the previous sections addressed the role of atmospheric conditions for the microbial viability and activity, microbiological processes might, in turn, also affect the atmospheric composition. The role of biological ice nuclei, their distribution in the atmosphere, and their impact on clouds and precipitation have been investigated over the last decade (Hoose and Möhler, 2012; Joly et al., 2014; Pouzet et al., 2017; Patade et al., 2021; Hartmann et al., 2022). Certain plant pathogen bacteria can initiate ice nucleation at higher temperatures than other atmospheric particles. Ice-nucleation active strains of *Pseudomonas syringae* were found at a particularly high frequency in snowfall compared to other environments, and they were identified in feedback processes called "bioprecipitation," linking vegetation, epiphytic microorganisms, and precipitation (Morris et al., 2008; Bigg et al., 2015). However, to date, the conclusions are not totally clear on the role of ice nucleating bacteria for precipitation (DeMott et al., 2010; Hoose et al., 2010; Burrows et al., 2013; Sahyoun et al., 2017). In addition, chemical, physical, and biological aging processes can modify the ice nucleation ability of biological particles during atmospheric residence time, which makes it difficult to represent them in atmospheric models (Attard et al., 2012; Worthy et al., 2021; Zhang et al., 2021).

Microorganisms have also been suggested to influence the chemical composition of the atmosphere. The biodegradation rates of common cloud-water constituents (e.g., small carboxylic acids) by bacteria were determined in laboratory bulk studies (Vaïtilingom et al., 2013; Bianco et al., 2019; Jaber et al., 2021). Such approaches omitted the fact that cloud droplets are distinct, small environments (~10^{-12} liters), physically spread and exposed to gas uptake, and that biological processes only occur in the small fraction of cloud droplets containing bacteria (statistically <1 out of ~1,000 droplets). Atmospheric model studies found that biodegradation in cloud water may represent a significant sink for water-soluble organic carbon (8 to 11 Tg $yr.^{-1}$), comparable to chemical losses in cloud droplets (Ervens and Amato, 2020; Khaled et al., 2021). The multiple potential impacts of biological activity on the complex atmospheric chemical reactivity should thus be better evaluated and specified.

4. Concluding remarks—synthesis of research needs

The atmosphere is a biotic environment. While the need seems obvious to characterize the transport and residence of pathogens for Human, animal, and plant health-related issues, the present review highlights much broader implications of the aeromicrobiome for the planetary health. It is coupled by numerous transport and exchange processes to the Earth surface, the extent of which needs to be better characterized to predict not only the evolution of the aeromicrobiome but also its implications upon deposition.

Future research directions for better characterization of the aeromicrobiome' organization and its impacts include:

- Characterizing emissions from surfaces: data of airborne microbial concentrations and emission fluxes from surfaces should be collected in particular over vast and poorly characterized areas such as oceans (Burrows et al., 2009b; Hasenecz et al., 2020; Alsante et al., 2021) and forests (Huffman et al., 2012; Crawford et al., 2014), and over sources with potentially important socio-economic impacts, such as agricultural fields and crops (Lindemann et al., 1982; Lighthart and Shaffer, 1995a; Morris et al., 2000; Brunet et al., 2013; Carotenuto et al., 2017). The mass and diversity of microorganisms susceptible to aerosolization has to be constrained for each defined surface category, as well as temporal variations linked with microclimatic and meteorological parameters (turbulence, precipitation, and wind) (Evans et al., 2006), and disturbances such as animal and human activities and wildfires (Kobziar et al., 2022).
- Assessing the dependence of microbial survival, metabolic functioning and activity on atmospheric conditions and biological traits. This includes potential niche effects such as clouds, nutritive conditions, the dependence on particle size, and altitude above ground, along with biological drivers related with trophic modes and biological traits. Size-resolved data of microbial concentration, biodiversity, viability, and functioning should be acquired at defined altitudes from ground, i.e., using towers (Prass et al., 2021), unmanned vehicles (Powers et al., 2018), tethered balloons, or aircraft (DeLeon-Rodriguez et al., 2013), preferably to mountain sites that can be affected by local emissions. Experiments in atmospheric simulation chambers or microcosms can help testing hypotheses. Current basic models of microbial survival rates in aerosol, in relation with environmental variables, should be improved to account for differences between taxa and functions, for implementation in dispersion models (Ehrlich et al., 1970; Lighthart et al., 1971; Lighthart and Frisch, 1976; Lighthart, 1989; Lighthart and Shaffer, 1997; Tong and Lighthart, 1998; Amato et al., 2015).
- Specifying the importance of biological particles for atmospheric processes, and their dependence on atmospheric conditions, e.g., presence of liquid water, temperature, and oxidant levels, which may affect the utilization of nutritive resources as well as cell properties (aging, i.e., destructuration, oxidation of the surface, release of intracellular compounds, *etc.*) (Ballesteros et al., 2001; Bianco et al., 2019). Due to the lack of data, atmospheric model studies are currently limited to the investigation of the biodegradation of a few organic compounds in clouds (Jaber et al., 2020, 2021; Khaled et al., 2021). However, there are indications that similar processes might also occur in the aqueous phase of deliquescent aerosol particles outside clouds. Finally, the aeromicrobiome clearly

harbors living organisms interacting with their environment, but the possibility of interactions between airborne microbes (predation, symbiosis, exchange of genetic material, communication, etc.) needs to be elucidated as well.

Such studies will require interdisciplinary efforts by multiple science communities including atmospheric chemistry and physics, meteorology, ecology, microbiology, and also concerted efforts in the development of new measurement and analysis techniques and concepts.

Whether or not the aeromicrobiome can be considered an ecosystem, a mosaic of adjacent ecosystems, or simply a major ecotone extending the boundaries of surface ecosystems and pressuring their microbiomes remains an open question. This environment is still poorly characterized while it may be affected by the rapidly changing conditions on various scales on the planet, with eventual feedbacks stabilizing or aggravating global change trends.

Author contributions

PA wrote the manuscript with the help and input from all co-authors. All authors contributed to the article and approved the submitted version.

Funding

This research has been supported by the French National Research Agency (ANR) through the projects MOBIDIC (grant no. ANR-17-MPGA-0013) and METACLOUD (grant no. ANR-19-CE01-0004-02). The authors also acknowledge funding from the Fédération des Recherches en Environnement of Clermont-Ferrand, Clermont Auvergne University, and CNRS.

Conflict of interest

The authors declare that the research was conducted in the absence of any commercial or financial relationships that could be construed as a potential conflict of interest.

Publisher's note

All claims expressed in this article are solely those of the authors and do not necessarily represent those of their affiliated organizations, or those of the publisher, the editors and the reviewers. Any product that may be evaluated in this article, or claim that may be made by its manufacturer, is not guaranteed or endorsed by the publisher.

References

Aller, J. Y., Kuznetsova, M. R., Jahns, C. J., and Kemp, P. F. (2005). The sea surface microlayer as a source of viral and bacterial enrichment in marine aerosols. *J. Aerosol Sci.* 36, 801–812. doi: 10.1016/j.jaerosci.2004.10.012

Alsante, A. N., Thornton, D. C. O., and Brooks, S. D. (2021). Ocean aerobiology. *Front. Microbiol.* 12:764178. doi: 10.3389/fmicb.2021.764178

Alsved, M., Holm, S., Christiansen, S., Smidt, M., Ling, M., Boesen, T., et al. (2018). Effect of aerosolization and drying on the viability of *Pseudomonas syringae* cells. *Front. Microbiol.* 9:3086. doi: 10.3389/fmicb.2018.03086

Amato, P., Besaury, L., Joly, M., Penaud, B., Deguillaume, L., and Delort, A.-M. (2019). Metatranscriptomic exploration of microbial functioning in clouds. *Sci. Rep.* 9:4383. doi: 10.1038/s41598-019-41032-4

Amato, P., Demeer, F., Melaouhi, A., Fontanella, S., Martin-Biesse, A. S., Sancelme, M., et al. (2007). A fate for organic acids, formaldehyde and methanol in cloud water: their biotransformation by micro-organisms. *Atmos. Chem. Phys.* 7, 4159–4169. doi: 10.5194/acp-7-4159-2007

Amato, P., Joly, M., Besaury, L., Oudart, A., Taib, N., Moné, A. I., et al. (2017). Active microorganisms thrive among extremely diverse communities in cloud water. *PLoS One* 12:e0182869. doi: 10.1371/journal.pone.0182869

Amato, P., Joly, M., Schaupp, C., Attard, E., Möhler, O., Morris, C. E., et al. (2015). Survival and ice nucleation activity of bacteria as aerosols in a cloud simulation chamber. *Atmos. Chem. Phys.* 15, 6455–6465. doi: 10.5194/acp-15-6455-2015

Archer, S. D. J., Lee, K. C., Caruso, T., Alcami, A., Araya, J. G., Cary, S. C., et al. (2023). Contribution of soil bacteria to the atmosphere across biomes. *Sci. Total Environ.* 871:162137. doi: 10.1016/j.scitotenv.2023.162137

Attard, E., Yang, H., Delort, A. M., Amato, P., Poschl, U., Glaux, C., et al. (2012). Effects of atmospheric conditions on ice nucleation activity of Pseudomonas. *Atmos. Chem. Phys.* 12, 10667–10677. doi: 10.5194/acp-12-10667-2012

Ballesteros, M., Fredriksson, Å., Henriksson, J., and Nyström, T. (2001). Bacterial senescence: protein oxidation in non-proliferating cells is dictated by the accuracy of the ribosomes. *EMBO J.* 20, 5280–5289. doi: 10.1093/emboj/20.18.5280

Barberán, A., Henley, J., Fierer, N., and Casamayor, E. O. (2014). Structure, inter-annual recurrence, and global-scale connectivity of airborne microbial communities. *Sci. Total Environ.* 487, 187–195. doi: 10.1016/j.scitotenv.2014.04.030

Barberán, A., Ladau, J., Leff, J. W., Pollard, K. S., Menninger, H. L., Dunn, R. R., et al. (2015). Continental-scale distributions of dust-associated bacteria and fungi. *Proc. Natl. Acad. Sci.* 112, 5756–5761. doi: 10.1073/pnas.1420815112

Baselga, A. (2010). Partitioning the turnover and nestedness components of beta diversity. *Glob. Ecol. Biogeogr.* 19, 134–143. doi: 10.1111/j.1466-8238.2009.00490.x

Bianco, A., Deguillaume, L., Chaumerliac, N., Vaïtilingom, M., Wang, M., Delort, A.-M., et al. (2019). Effect of endogenous microbiota on the molecular composition of cloud water: a study by Fourier-transform ion cyclotron resonance mass spectrometry (FT-ICR MS). *Sci. Rep.* 9:7663. doi: 10.1038/s41598-019-44149-8

Bigg, E. K., Soubeyrand, S., and Morris, C. E. (2015). Persistent after-effects of heavy rain on concentrations of ice nuclei and rainfall suggest a biological cause. *Atmos. Chem. Phys.* 15, 2313–2326. doi: 10.5194/acp-15-2313-2015

Bowers, R. M., McLetchie, S., Knight, R., and Fierer, N. (2011). Spatial variability in airborne bacterial communities across land-use types and their relationship to the bacterial communities of potential source environments. *ISME J.* 5, 601–612. doi: 10.1038/ismej.2010.167

Brunet, Y., Bonnefond, J.-M., Garrigou, D., Delmas, F., Leyronas, C., and Morris, C. E. (2013). A relaxed-eddy accumulation system for measuring microbial emission fluxes from the vegetation, AAAR annual conference, American Association for Aerosol Research, Sep 2013, Portland, Oregon, United States. Available at: https://hal.inrae.fr/view/index/identifiant/hal-02807518

Burger, S., and Bennett, B. (1985). Droplet enrichment factors of pigmented and nonpigmented *Serratia marcescens*: possible selective function for prodigiosin. *Appl. Environ. Microbiol.* 50, 487–490. doi: 10.1128/aem.50.2.487-490.1985

Burns, P., Timmermann, V., and Yearsley, J. M. (2022). Meteorological factors associated with the timing and abundance of *Hymenoscyphus fraxineus* spore release. *Int. J. Biometeorol.* 66, 493–506. doi: 10.1007/s00484-021-02211-z

Burrows, S. M., Butler, T., Jöckel, P., Tost, H., Kerkweg, A., Pöschl, U., et al. (2009a). Bacteria in the global atmosphere – part 2: modeling of emissions and transport between different ecosystems. *Atmos. Chem. Phys.* 9, 9281–9297. doi: 10.5194/acp-9-9281-2009

Burrows, S. M., Elbert, W., Lawrence, M. G., and Pöschl, U. (2009b). Bacteria in the global atmosphere – part 1: review and synthesis of literature data for different ecosystems. *Atmos. Chem. Phys.* 9, 9263–9280. doi: 10.5194/acp-9-9263-2009

Burrows, S. M., Hoose, C., Pöschl, U., and Lawrence, M. G. (2013). Ice nuclei in marine air: biogenic particles or dust? *Atmos. Chem. Phys.* 13, 245–267. doi: 10.5194/acp-13-245-2013

Carotenuto, F., Georgiadis, T., Gioli, B., Leyronas, C., Morris, C. E., Nardino, M., et al. (2017). Measurements and modeling of surface–atmosphere exchange of microorganisms in Mediterranean grassland. *Atmos. Chem. Phys.* 17, 14919–14936. doi: 10.5194/acp-17-14919-2017

Chen, Y.-J., Leung, P. M., Wood, J. L., Bay, S. K., Hugenholtz, P., Kessler, A. J., et al. (2021). Metabolic flexibility allows bacterial habitat generalists to become dominant in a frequently disturbed ecosystem. *ISME J.* 15, 2986–3004. doi: 10.1038/s41396-021-00988-w

Crawford, I., Robinson, N. H., Flynn, M. J., Foot, V. E., Gallagher, M. W., Huffman, J. A., et al. (2014). Characterisation of bioaerosol emissions from a Colorado pine forest: results from the BEACHON-RoMBAS experiment. *Atmos. Chem. Phys.* 14, 8559–8578. doi: 10.5194/acp-14-8559-2014

Creamean, J. M., Suski, K. J., Rosenfeld, D., Cazorla, A., DeMott, P. J., Sullivan, R. C., et al. (2013). Dust and biological aerosols from the Sahara and Asia influence precipitation in the Western U.S. *Science* 339, 1572–1578. doi: 10.1126/science.1227279

Cunliffe, M., and Murrell, J. C. (2009). The sea-surface microlayer is a gelatinous biofilm. *ISME J.* 3, 1001–1003. doi: 10.1038/ismej.2009.69

DeLeon-Rodriguez, N., Lathem, T. L., Rodriguez-R, L. M., Barazesh, J. M., Anderson, B. E., Beyersdorf, A. J., et al. (2013). Microbiome of the upper troposphere: species composition and prevalence, effects of tropical storms, and atmospheric implications. *Proc. Natl. Acad. Sci.* 110, 2575–2580. doi: 10.1073/pnas.1212089110

DeMott, P. J., Prenni, A. J., Liu, X., Kreidenweis, S. M., Petters, M. D., Twohy, C. H., et al. (2010). Predicting global atmospheric ice nuclei distributions and their impacts on climate. *Proc. Natl. Acad. Sci. U. S. A.* 107, 11217–11222. doi: 10.1073/pnas.0910818107

Dillon, K. P., Correa, F., Judon, C., Sancelme, M., Fennell, D. E., Delort, A.-M., et al. (2020). Cyanobacteria and algae in clouds and rain in the area of puy de Dôme. *Central France. Appl. Environ. Microbiol.* 87:e01850–20. doi: 10.1128/AEM.01850-20

Ehrlich, R., Miller, S., and Walker, R. L. (1970). Relationship between atmospheric temperature and survival of airborne Bacteria. *Appl. Microbiol.* 19, 245–249. doi: 10.1128/am.19.2.245-249.1970

Ervens, B., and Amato, P. (2020). The global impact of bacterial processes on carbon mass. *Atmos. Chem. Phys.* 20, 1777–1794. doi: 10.5194/acp-20-1777-2020

Evans, C. A., Coombes, P. J., and Dunstan, R. H. (2006). Wind, rain and bacteria: the effect of weather on the microbial composition of roof-harvested rainwater. *Water Res.* 40, 37–44. doi: 10.1016/j.watres.2005.10.034

Fierer, N., Liu, Z., Rodríguez-Hernández, M., Knight, R., Henn, M., and Hernandez, M. T. (2008). Short-term temporal variability in airborne bacterial and fungal populations. *Appl. Environ. Microbiol.* 74, 200–207. doi: 10.1128/AEM.01467-07

Fredrickson, J. K., Li, S. W., Gaidamakova, E. K., Matrosova, V. Y., Zhai, M., Sulloway, H. M., et al. (2008). Protein oxidation: key to bacterial desiccation resistance? *ISME J.* 2, 393–403. doi: 10.1038/ismej.2007.116

Fröhlich-Nowoisky, J., Kampf, C. J., Weber, B., Huffman, J. A., Pöhlker, C., Andreae, M. O., et al. (2016). Bioaerosols in the earth system: climate, health, and ecosystem interactions. *Atmos. Res.* 182, 346–376. doi: 10.1016/j.atmosres.2016.07.018

Fuzzi, S., Mandrioli, P., and Perfetto, A. (1997). Fog droplets—an atmospheric source of secondary biological aerosol particles. *Atmos. Environ.* 31, 287–290. doi: 10.1016/1352-2310(96)00160-4

Gat, D., Reicher, N., Schechter, S., Alayof, M., Tarn, M. D., Wyld, B. V., et al. (2021). Size-resolved community structure of bacteria and fungi transported by dust in the Middle East. *Front. Microbiol.* 12:744117. doi: 10.3389/fmicb.2021.744117

Gauthier-Levesque, L., Bonifait, L., Turgeon, N., Veillette, M., Perrott, P., Grenier, D., et al. (2016). Impact of serotype and sequence type on the preferential aerosolization of *Streptococcus suis*. *BMC. Res. Notes* 9:273. doi: 10.1186/s13104-016-2073-8

Gusareva, E. S., Acerbi, E., Lau, K. J. X., Luhung, I., Premkrishnan, B. N. V., Kolundžija, S., et al. (2019). Microbial communities in the tropical air ecosystem follow a precise diel cycle. *Proc. Natl. Acad. Sci.* 116, 23299–23308. doi: 10.1073/pnas.1908493116

Hartmann, S., Ling, M., Dreyer, L. S. A., Zipori, A., Finster, K., Grawe, S., et al. (2022). Structure and protein-protein interactions of ice nucleation proteins drive their activity. *Front. Microbiol.* 13:872306. doi: 10.3389/fmicb.2022.872306

Hasenecz, E. S., Jayarathne, T., Pendergraft, M. A., Santander, M. V., Mayer, K. J., Sauer, J., et al. (2020). Marine Bacteria affect saccharide enrichment in sea spray aerosol during a phytoplankton bloom. *ACS Earth Space Chem.* 4, 1638–1649. doi: 10.1021/acsearthspacechem.0c00167

Hervas, A., and Casamayor, E. O. (2009). High similarity between bacterioneuston and airborne bacterial community compositions in a high mountain lake area. *FEMS Microbiol. Ecol.* 67, 219–228. doi: 10.1111/j.1574-6941.2008.00617.x

Hoose, C., Kristjánsson, J. E., and Burrows, S. M. (2010). How important is biological ice nucleation in clouds on a global scale? *Environ. Res. Lett.* 5:024009. doi: 10.1088/1748-9326/5/2/024009

Hoose, C., and Möhler, O. (2012). Heterogeneous ice nucleation on atmospheric aerosols: a review of results from laboratory experiments. *Atmos. Chem. Phys.* 12, 9817–9854. doi: 10.5194/acp-12-9817-2012

Huffman, J. A., Prenni, A. J., DeMott, P. J., Pöhlker, C., Mason, R. H., Robinson, N. H., et al. (2013). High concentrations of biological aerosol particles and ice nuclei during and after rain. *Atmos. Chem. Phys.* 13, 6151–6164. doi: 10.5194/acp-13-6151-2013

Huffman, J. A., Sinha, B., Garland, R. M., Snee-Pollmann, A., Gunthe, S. S., Artaxo, P., et al. (2012). Size distributions and temporal variations of biological aerosol particles in the Amazon rainforest characterized by microscopy and real-time UV-APS fluorescence techniques during AMAZE-08. *Atmos. Chem. Phys.* 12, 11997–12019. doi: 10.5194/acp-12-11997-2012

Jaber, S., Joly, M., Brissy, M., Leremboure, M., Khaled, A., Ervens, B., et al. (2021). Biotic and abiotic transformation of amino acids in cloud water: experimental studies and atmospheric implications. *Biogeosciences* 18, 1067–1080. doi: 10.5194/bg-18-1067-2021

Jaber, S., Lallement, A., Sancelme, M., Leremboure, M., Mailhot, G., Ervens, B., et al. (2020). Biodegradation of phenol and catechol in cloud water: comparison to chemical oxidation in the atmospheric multiphase system. *Atmos. Chem. Phys.* 20, 4987–4997. doi: 10.5194/acp-20-4987-2020

Jalasvuori, M. (2020). Silent rain: does the atmosphere-mediated connectivity between microbiomes influence bacterial evolutionary rates? *FEMS Microbiol. Ecol.* 96:fiaa096. doi: 10.1093/femsec/fiaa096

Joly, M., Amato, P., Deguillaume, L., Monier, M., Hoose, C., and Delort, A.-M. (2014). Quantification of ice nuclei active at near 0°C temperatures in low-altitude clouds at the Puy de Dôme atmospheric station. *Atmos. Chem. Phys.* 14, 8185–8195. doi: 10.5194/acp-14-8185-2014

Joly, M., Amato, P., Sancelme, M., Vinatier, V., Abrantes, M., Deguillaume, L., et al. (2015). Survival of microbial isolates from clouds toward simulated atmospheric stress factors. *Atmos. Envion.* 117, 92–98. doi: 10.1016/j.atmosenv.2015.07.009

Joung, Y. S., Ge, Z., and Buie, C. R. (2017). Bioaerosol generation by raindrops on soil. *Nat. Commun.* 8:14668. doi: 10.1038/ncomms14668

Khaled, A., Zhang, M., Amato, P., Delort, A.-M., and Ervens, B. (2021). Biodegradation by bacteria in clouds: an underestimated sink for some organics in the atmospheric multiphase system. *Atmos. Chem. Phys.* 21, 3123–3141. doi: 10.5194/acp-21-3123-2021

Klein, A. M., Bohannan, B. J. M., Jaffe, D. A., Levin, D. A., and Green, J. L. (2016). Molecular evidence for metabolically active Bacteria in the atmosphere. *Front. Microbiol.* 7:772. doi: 10.3389/fmicb.2016.00772

Kobziar, L. N., Vuono, D., Moore, R., Christner, B. C., Dean, T., Betancourt, D., et al. (2022). Wildland fire smoke alters the composition, diversity, and potential atmospheric function of microbial life in the aerobiome. *ISME Commun.* 2, 1–9. doi: 10.1038/s43705-022-00089-5

Kopejtka, K., Tomasch, J., Zeng, Y., Selyanin, V., Dachev, M., Piwosz, K., et al. (2020). Simultaneous presence of bacteriochlorophyll and xanthorhodopsin genes in a freshwater bacterium. *mSystems* 5, e01044–e01020. doi: 10.1128/mSystems.01044-20

Krumins, V., Mainelis, G., Kerkhof, L. J., and Fennell, D. E. (2014). Substrate-dependent rRNA production in an airborne bacterium. *Environ. Sci. Technol. Lett.* 1, 376–381. doi: 10.1021/ez500245y

Lacey, J. (1986). Philip Herries Gregory (1907–1986). *Grana* 25, 159–160. doi: 10.1080/00173138609427716

Leyronas, C., Morris, C. E., Choufany, M., and Soubeyrand, S. (2018). Assessing the aerial interconnectivity of distant reservoirs of *Sclerotinia sclerotiorum*. *Front. Microbiol.* 9:2257. doi: 10.3389/fmicb.2018.02257

Liao, J., Cao, X., Zhao, L., Wang, J., Gao, Z., Wang, M. C., et al. (2016). The importance of neutral and niche processes for bacterial community assembly differs between habitat generalists and specialists. *FEMS Microbiol. Ecol.* 92:fiw174. doi: 10.1093/femsec/fiw174

Lighthart, B. (1989). A statistical model of laboratory death rate measurements for airborne bacteria. *Aerobiologia* 5, 138–144. doi: 10.1007/BF02486511

Lighthart, B. (1997). The ecology of bacteria in the alfresco atmosphere. *FEMS Microbiol. Ecol. Ecol.* 23, 263–274. doi: 10.1111/j.1574-6941.1997.tb00408.x

Lighthart, B. (1999). An hypothesis describing the general temporal and spatial distribution of alfresco bacteria in the earth's atmospheric surface layer. *Atmos. Environ.* 33, 611–615. doi: 10.1016/S1352-2310(98)00215-5

Lighthart, B., and Frisch, A. S. (1976). Estimation of viable airborne microbes downwind from a point source. *Appl. Environ. Microbiol.* 31, 700–704. doi: 10.1128/aem.31.5.700-704.1976

Lighthart, B., Hiatt, V. E., and Rossano, A. T. Jr. (1971). The survival of airborne *Serratia marcescens* in urban concentrations of sulfur dioxide. *J. Air Pollut. Control Assoc.* 21, 639–642. doi: 10.1080/00022470.1971.10469580

Lighthart, B., and Shaffer, B. T. (1994). Bacterial flux from chaparral into the atmosphere in mid-summer at a high desert location. *Atmos. Environ.* 28, 1267–1274. doi: 10.1016/1352-2310(94)90273-9

Lighthart, B., and Shaffer, B. T. (1995a). Airborne Bacteria in the atmospheric surface layer: temporal distribution above a grass seed field. *Appl. Environ. Microbiol.* 61, 1492–1496. doi: 10.1128/aem.61.4.1492-1496.1995

Lighthart, B., and Shaffer, B. T. (1995b). Viable bacterial aerosol particle size distributions in the midsummer atmosphere at an isolated location in the high desert chaparral. *Aerobiologia* 11, 19–25. doi: 10.1007/BF02136140

Lighthart, B., and Shaffer, B. T. (1997). Increased airborne bacterial survival as a function of particle content and size. *Aerosol Sci. Technol.* 27, 439–446. doi: 10.1080/02786829708965483

Lindemann, J., Constantinidou, H. A., Barchet, W. R., and Upper, C. D. (1982). Plants as sources of airborne bacteria, including ice nucleation-active bacteria. *Appl. Environ. Microbiol.* 44, 1059–1063. doi: 10.1128/aem.44.5.1059-1063.1982

Lindemann, J., and Upper, C. D. (1985). Aerial dispersal of epiphytic bacteria over bean plants. *Appl. Environ. Microbiol.* 50, 1229–1232. doi: 10.1128/aem.50.5.1229-1232.1985

Luo, Z., Liu, J., Zhao, P., Jia, T., Li, C., and Chai, B. (2019). Biogeographic patterns and assembly mechanisms of bacterial communities differ between habitat generalists and

specialists across elevational gradients. *Front. Microbiol.* 10:169. doi: 10.3389/fmicb.2019.00169

Malfatti, F., Lee, C., Tinta, T., Pendergraft, M. A., Celussi, M., Zhou, Y., et al. (2019). Detection of active microbial enzymes in nascent sea spray aerosol: implications for atmospheric chemistry and climate. *Environ. Sci. Technol. Lett.* 6, 171–177. doi: 10.1021/acs.estlett.8b00699

Marthi, B., Fieland, V. P., Walter, M., and Seidler, R. J. (1990). Survival of bacteria during aerosolization. *Appl. Environ. Microbiol.* 56, 3463–3467. doi: 10.1128/aem.56.11.3463-3467.1990

McDougald, D., Rice, S. A., Barraud, N., Steinberg, P. D., and Kjelleberg, S. (2012). Should we stay or should we go: mechanisms and ecological consequences for biofilm dispersal. *Nat. Rev. Microbiol.* 10, 39–50. doi: 10.1038/nrmicro2695

Meier, F. C., and Lindbergh, C. A. (1935). Collecting micro-organisms from the atmosphere. *Sci. Mon.* 40, 5–20.

Menon, P., Billen, G., and Servais, P. (2003). Mortality rates of autochthonous and fecal bacteria in natural aquatic ecosystems. *Water Res.* 37, 4151–4158. doi: 10.1016/S0043-1354(03)00349-X

Michaud, J. M., Thompson, L. R., Kaul, D., Espinoza, J. L., Richter, R. A., Xu, Z. Z., et al. (2018). Taxon-specific aerosolization of bacteria and viruses in an experimental ocean-atmosphere mesocosm. *Nat. Commun.* 9:2017. doi: 10.1038/s41467-018-04409-z

Molisch, H. (1922). *Populäre biologische Vorträge. 2. durchgesehene und erw. Aufl.* Jena: G. Fischer

Monier, J.-M., and Lindow, S. E. (2003). Differential survival of solitary and aggregated bacterial cells promotes aggregate formation on leaf surfaces. *Proc. Natl. Acad. Sci.* 100, 15977–15982. doi: 10.1073/pnas.2436560100

Moore, R. A., Hanlon, R., Powers, C., Schmale, D. G., and Christner, B. C. (2020). Scavenging of sub-Micron to Micron-sized microbial aerosols during simulated rainfall. *Atmos.* 11:80. doi: 10.3390/atmos11010080

Morris, C. E., Glaux, C., Latour, X., Gardan, L., Samson, R., and Pitrat, M. (2000). The relationship of host range, physiology, and genotype to virulence on cantaloupe in *Pseudomonas syringae* from cantaloupe blight epidemics in France. *Phytopathology* 90, 636–646. doi: 10.1094/PHYTO.2000.90.6.636

Morris, C. E., and Sands, D. C. (2017). "Impacts of microbial aerosols on natural and agro-ecosystems: immigration, invasions and their consequences" in *Microbiology of aerosols* (Hoboken, NJ: Delort, A.M. and Amato, P)

Morris, C. E., Sands, D. C., Vanneste, J. L., Montarry, J., Oakley, B., Guilbaud, C., et al. (2010). Inferring the evolutionary history of the plant pathogen *Pseudomonas syringae* from its biogeography in headwaters of Rivers in North America, Europe, and New Zealand. *mBio* 1, e00107–e00110. doi: 10.1128/mBio.00107-10

Morris, C. E., Sands, D. C., Vinatzer, B. A., Glaux, C., Guilbaud, C., Buffière, A., et al. (2008). The life history of the plant pathogen *Pseudomonas syringae* is linked to the water cycle. *ISME J.* 2, 321–334. doi: 10.1038/ismej.2007.113

Moulton, R.F. (1942). *Aerobiology. The science press printing company*. Lancaster, PA: American Association for the Advancement of Science

Ng, T. W., Ip, M., Chao, C. Y. H., Tang, J. W., Lai, K. P., Fu, S. C., et al. (2018). Differential gene expression in *Escherichia coli* during aerosolization from liquid suspension. *Appl. Microbiol. Biotechnol.* 102, 6257–6267. doi: 10.1007/s00253-018-9083-5

Noirmain, F., Baray, J.-L., Tridon, F., Cacault, P., Billard, H., Voyard, G., et al. (2022). Interdisciplinary strategy to assess the impact of meteorological variables on the biochemical composition of the rain and the dynamics of a small eutrophic lake under rain forcing. *Biogeosciences* 19, 5729–5749. doi: 10.5194/bg-19-5729-2022

Ochsner, U. A., Vasil, M. L., Alsabbagh, E., Parvatiyar, K., and Hassett, D. J. (2000). Role of the *Pseudomonas aeruginosa* oxyR-recG operon in oxidative stress defense and DNA repair: OxyR-dependent regulation of katB-ankB, ahpB, and ahpC-ahpF. *J. Bacteriol.* 182, 4533–4544. doi: 10.1128/JB.182.16.4533-4544.2000

Pasteur, L. (1862). *Mémoire sur les corpuscules organisés qui existent dans l'atmosphère: examen de la doctrine des générations spontanées*. Annales de Chimie et de Physique. Mallet-Bachelier.

Patade, S., Phillips, V. T. J., Amato, P., Bingemer, H. G., Burrows, S. M., DeMott, P. J., et al. (2021). Empirical formulation for multiple groups of primary biological ice nucleating particles from field observations over Amazonia. *J. Atmos. Sci.* 78, 2195–2220. doi: 10.1175/JAS-D-20-0096.1

Péguilhan, R., Besaury, L., Rossi, F., Enault, F., Baray, J.-L., Deguillaume, L., et al. (2021). Rainfalls sprinkle cloud bacterial diversity while scavenging biomass. *FEMS Microbiol. Ecol.* 97:fiab144. doi: 10.1093/femsec/fiab144

Pouzet, G., Peghaire, E., Aguès, M., Baray, J.-L., Conen, F., and Amato, P. (2017). Atmospheric processing and variability of biological ice nucleating particles in precipitation at Opme. *France. Atmosphere* 8:229. doi: 10.3390/atmos8110229

Powers, C. W., Hanlon, R., Grothe, H., Prussin, A. J. I., Marr, L. C., and Schmale, D. G. I. (2018). Coordinated sampling of microorganisms over freshwater and saltwater environments using an unmanned surface vehicle (USV) and a small unmanned aircraft system (sUAS). *Front. Microbiol.* 9:1668. doi: 10.3389/fmicb.2018.01668

Prass, M., Andreae, M. O., de Araùjo, A. C., Artaxo, P., Ditas, F., Elbert, W., et al. (2021). Bioaerosols in the Amazon rain forest: temporal variations and vertical profiles of Eukarya, Bacteria, and Archaea. *Biogeosciences* 18, 4873–4887. doi: 10.5194/bg-18-4873-2021

Qi, J., Zhong, X., Shao, Q., Gao, D., Wu, L., Huang, L., et al. (2015). Microbial activity levels in atmospheric bioaerosols in Qingdao. *Aerobiologia* 31, 353–365. doi: 10.1007/s10453-015-9369-3

Reche, I., D'Orta, G., Mladenov, N., Winget, D. M., and Suttle, C. A. (2018). Deposition rates of viruses and bacteria above the atmospheric boundary layer. *ISME J.* 12, 1154–1162. doi: 10.1038/s41396-017-0042-4

Rojo, F. (2010). Carbon catabolite repression in Pseudomonas: optimizing metabolic versatility and interactions with the environment. *FEMS Microbiol. Rev.* 34, 658–684. doi: 10.1111/j.1574-6976.2010.00218.x

Rossi, F., Péguilhan, R., Turgeon, N., Veillette, M., Baray, J.-L., Deguillaume, L., et al. (2022). Quantification of antibiotic resistance genes (ARGs) in clouds at a mountain site (puy de Dôme, Central France). *Sci. Total Environ.* 865:161264. doi: 10.1016/j.scitotenv.2022.161264

Sahyoun, M., Korsholm, U. S., Sørensen, J. H., Šantl-Temkiv, T., Finster, K., Gosewinkel, U., et al. (2017). Impact of bacterial ice nucleating particles on weather predicted by a numerical weather prediction model. *Atmos. Environ.* 170, 33–44. doi: 10.1016/j.atmosenv.2017.09.029

Šantl-Temkiv, T., Amato, P., Casamayor, E. O., Lee, P. K. H., and Pointing, S. B. (2022). Microbial ecology of the atmosphere. *FEMS Microbiol. Rev.* 46:fuac009. doi: 10.1093/femsre/fuac009

Šantl-Temkiv, T., Amato, P., Gosewinkel, U., Thyrhaug, R., Charton, A., Chicot, B., et al. (2017). High-flow-rate Impinger for the study of concentration, viability, metabolic activity, and ice-nucleation activity of airborne Bacteria. *Environ. Sci. Technol.* 51, 11224–11234. doi: 10.1021/acs.est.7b01480

Šantl-Temkiv, T., Gosewinkel, U., Starnawski, P., Lever, M., and Finster, K. (2018). Aeolian dispersal of bacteria in Southwest Greenland: their sources, abundance, diversity and physiological states. *FEMS Microbiol. Ecol.* 94:fiy031. doi: 10.1093/femsec/fiy031

Sattler, B., Puxbaum, H., and Psenner, R. (2001). Bacterial growth in supercooled cloud droplets. *Geophys. Res. Lett.* 28, 239–242. doi: 10.1029/2000GL011684

Scheuch, G. (2020). Breathing is enough: for the spread of influenza virus and SARS-CoV-2 by breathing only. *J. Aerosol Med. Pulm. Drug Deliv.* 33, 230–234. doi: 10.1089/jamp.2020.1616

Schlechter, R. O., Miebach, M., and Remus-Emsermann, M. N. P. (2019). Driving factors of epiphytic bacterial communities: a review. *J. Adv. Res.* 19, 57–65. doi: 10.1016/j.jare.2019.03.003

Schmid, H. P. (2002). Footprint modeling for vegetation atmosphere exchange studies: a review and perspective. *Agric. For. Meteorol.* 113, 159–183. doi: 10.1016/S0168-1923(02)00107-7

Shade, A., Gregory Caporaso, J., Handelsman, J., Knight, R., and Fierer, N. (2013). A meta-analysis of changes in bacterial and archaeal communities with time. *ISME J.* 7, 1493–1506. doi: 10.1038/ismej.2013.54

Shade, A., Jones, S. E., Caporaso, J. G., Handelsman, J., Knight, R., Fierer, N., et al. (2014). Conditionally rare taxa disproportionately contribute to temporal changes in microbial diversity. *MBio* 5, e01371–e01314. doi: 10.1128/mBio.01371-14

Slinn, W. G. N. (1982). Predictions for particle deposition to vegetative canopies. *Atmos. Environ.* 16, 1785–1794. doi: 10.1016/0004-6981(82)90271-2

Smith, D. J., Griffin, D. W., McPeters, R. D., Ward, P. D., and Schuerger, A. C. (2011). Microbial survival in the stratosphere and implications for global dispersal. *Aerobiologia* 27, 319–332. doi: 10.1007/s10453-011-9203-5

Smith, B. L., and King, M. D. (2022). Aerosolization triggers immediate antibiotic resistance in bacteria. *J. Aerosol Sci.* 164:106017. doi: 10.1016/j.jaerosci.2022.106017

Smith, D. J., Timonen, H. J., Jaffe, D. A., Griffin, D. W., Birmele, M. N., Perry, K. D., et al. (2013). Intercontinental dispersal of bacteria and archaea by transpacific winds. *Appl. Environ. Microbiol.* 79, 1134–1139. doi: 10.1128/AEM.03029-12

Tesson, S. V. M., Skjøth, C. A., Šantl-Temkiv, T., and Löndahl, J. (2016). Airborne microalgae: insights, opportunities, and challenges. *Appl. Environ. Microbiol.* 82, 1978–1991. doi: 10.1128/AEM.03333-15

Tignat-Perrier, R., Dommergue, A., Thollot, A., Magand, O., Amato, P., Joly, M., et al. (2020). Seasonal shift in airborne microbial communities. *Sci. Total Environ.* 716:137129. doi: 10.1016/j.scitotenv.2020.137129

Tong, Y., and Lighthart, B. (1998). Effect of simulated solar radiation on mixed outdoor atmospheric bacterial populations. *FEMS Microbiol. Ecol.* 26, 311–316. doi: 10.1111/j.1574-6941.1998.tb00515.x

Triadó-Margarit, X., Caliz, J., Reche, I., and Casamayor, E. O. (2019). High similarity in bacterial bioaerosol compositions between the free troposphere and atmospheric depositions collected at high-elevation mountains. *Atmos. Environ.* 203, 79–86. doi: 10.1016/j.atmosenv.2019.01.038

Vaïtilingom, M., Amato, P., Sancelme, M., Laj, P., Leriche, M., and Delort, A.-M. (2010). Contribution of microbial activity to carbon chemistry in clouds. *Appl. Environ. Microbiol.* 76, 23–29. doi: 10.1128/AEM.01127-09

Vaïtilingom, M., Attard, E., Gaiani, N., Sancelme, M., Deguillaume, L., Flossmann, A. I., et al. (2012). Long-term features of cloud microbiology at the puy de Dôme (France). *Atmos. Environ.* 56, 88–100. doi: 10.1016/j.atmosenv.2012.03.072

Vaïtilingom, M., Deguillaume, L., Vinatier, V., Sancelme, M., Amato, P., Chaumerliac, N., et al. (2013). Potential impact of microbial activity on the oxidant capacity and organic carbon budget in clouds. *Proc. Natl. Acad. Sci.* 110, 559–564. doi: 10.1073/pnas.1205743110

van der Ent, R. J., and Tuinenburg, O. A. (2017). The residence time of water in the atmosphere revisited. *Hydrol. Earth Syst. Sci.* 21, 779–790. doi: 10.5194/hess-21-779-2017

Vaz-Moreira, I., Nunes, O. C., and Manaia, C. M. (2011). Diversity and antibiotic resistance patterns of Sphingomonadaceae isolates from drinking water. *Appl. Environ. Microbiol.* 77, 5697–5706. doi: 10.1128/AEM.00579-11

Vorholt, J. A. (2012). Microbial life in the phyllosphere. *Nat. Rev. Microbiol.* 10, 828–840. doi: 10.1038/nrmicro2910

Weil, T., Filippo, C. D., Albanese, D., Donati, C., Pindo, M., Pavarini, L., et al. (2017). Legal immigrants: invasion of alien microbial communities during winter occurring desert dust storms. *Microbiome* 5:32. doi: 10.1186/s40168-017-0249-7

Whitman, W. B., Coleman, D. C., and Wiebe, W. J. (1998). Prokaryotes: the unseen majority. *Proc. Natl. Acad. Sci.* 95, 6578–6583. doi: 10.1073/pnas.95.12.6578

Wirgot, N., Vinatier, V., Deguillaume, L., Sancelme, M., and Delort, A.-M. (2017). H2O2 modulates the energetic metabolism of the cloud microbiome. *Atmos. Chem. Phys.* 17, 14841–14851. doi: 10.5194/acp-17-14841-2017

Woo, C., and Yamamoto, N. (2020). Falling bacterial communities from the atmosphere. *Environ. Microbiol.* 15:22. doi: 10.1186/s40793-020-00369-4

Worthy, S. E., Kumar, A., Xi, Y., Yun, J., Chen, J., Xu, C., et al. (2021). The effect of (NH4)2SO4 on the freezing properties of non-mineral dust ice-nucleating substances of atmospheric relevance. *Atmos. Chem. Phys.* 21, 14631–14648. doi: 10.5194/acp-21-14631-2021

Zhang, M., Khaled, A., Amato, P., Delort, A.-M., and Ervens, B. (2021). Sensitivities to biological aerosol particle properties and ageing processes: potential implications for aerosol–cloud interactions and optical properties. *Atmos. Chem. Phys.* 21, 3699–3724. doi: 10.5194/acp-21-3699-2021

frontiers | Frontiers in Microbiology

TYPE Original Research
PUBLISHED 25 May 2023
DOI 10.3389/fmicb.2023.1145781

OPEN ACCESS

EDITED BY
Andreas Teske,
University of North Carolina, Chapel Hill, United States

REVIEWED BY
James F. Holden,
University of Massachusetts Amherst, United States
Aude Picard,
University of Nevada, Las Vegas, United States

*CORRESPONDENCE
Chloé Truong
✉ chloe.truong1@mnhn.fr

RECEIVED 16 January 2023
ACCEPTED 02 May 2023
PUBLISHED 25 May 2023

CITATION
Truong C, Bernard S, Le Pape P, Morin G, Baya C, Merrot P, Gorlas A and Guyot F (2023) Production of carbon-containing pyrite spherules induced by hyperthermophilic Thermococcales: a biosignature? *Front. Microbiol.* 14:1145781. doi: 10.3389/fmicb.2023.1145781

Production of carbon-containing pyrite spherules induced by hyperthermophilic Thermococcales: a biosignature?

Chloé Truong[1]*, Sylvain Bernard[1], Pierre Le Pape[1], Guillaume Morin[1], Camille Baya[1], Pauline Merrot[1], Aurore Gorlas[2] and François Guyot[1,3]

[1]Institut de Minéralogie, de Physique des Matériaux et de Cosmochimie (IMPMC), MNHN, CNRS, IRD, Sorbonne Université, Paris, France, [2]CEA, CNRS, Institute for Integrative Biology of the Cell, Université Paris-Saclay, Gif-sur-Yvette, France, [3]Institut Universitaire de France (IUF), Paris, France

Thermococcales, a major order of hyperthermophilic archaea inhabiting iron- and sulfur-rich anaerobic parts of hydrothermal deep-sea vents, are known to induce the formation of iron phosphates, greigite (Fe_3S_4) and abundant quantities of pyrite (FeS_2), including pyrite spherules. In the present study, we report the characterization of the sulfide and phosphate minerals produced in the presence of Thermococcales using X-ray diffraction, synchrotron-based X ray absorption spectroscopy and scanning and transmission electron microscopies. Mixed valence Fe(II)-Fe(III) phosphates are interpreted as resulting from the activity of Thermococcales controlling phosphorus–iron–sulfur dynamics. The pyrite spherules (absent in abiotic control) consist of an assemblage of ultra-small nanocrystals of a few ten nanometers in size, showing coherently diffracting domain sizes of few nanometers. The production of these spherules occurs via a sulfur redox swing from S^0 to S^{-2} and then to S^{-1}, involving a comproportionation of (-II) and (0) oxidation states of sulfur, as supported by S-XANES data. Importantly, these pyrite spherules sequester biogenic organic compounds in small but detectable quantities, possibly making them good biosignatures to be searched for in extreme environments.

KEYWORDS

archaea, biosignatures, hydrothermal vents, pyrite, greigite

1. Introduction

The activity of microorganisms may promote mineral dissolution and/or precipitation in hydrothermal mineral environments (e.g., Holden and Adams, 2003; Templeton et al., 2009; Houghton and Seyfried, 2010). Hydrothermal systems, in particular sulfur-rich hydrothermal vents, allow exchange of heat and chemical species between seawater and ocean rocks (Edmond et al., 1979; Stein and Stein, 1994; Elderfield and Schultz, 1996; Wheat et al., 2000). The mixture of the hot – up to 400°C – reduced fluid discharging from the vents with the cold – about 2°C – oxygenated sea water, results in the formation of chimneys accommodating very steep temperature and geochemical gradients (Tivey, 1995; Von Damm, 1995; Charlou et al., 2002; Schmidt et al., 2007; Flores et al., 2011). Iron sulfide

minerals, such as pyrite (FeS_2) and chalcopyrite ($CuFeS_2$), are predominant in the inner and hotter parts (>250°C) of active chimneys (Feely et al., 1994; Ludford et al., 1996). The cooler middle layers (80–150°C) of the chimneys are mainly composed of calcium and magnesium sulfate minerals, such as anhydrite ($CaSO_4$), but contain iron sulfides such as pyrite and marcasite (FeS_2) as well (e.g., Langmuir et al., 1997; Schrenk et al., 2003; Rouxel et al., 2004). It has been proposed that those middle layers harbor a population of hyperthermophilic archaea (Schrenk et al., 2003; Lin et al., 2016), probably mainly composed of sulfur-reducers Thermococcales (Takai et al., 2001; Prieur et al., 2004; Kormas et al., 2006).

Thermococcales could be an important contributor to the precipitation of minerals in the middle and external cooler layers dominated by anhydrite. Gorlas et al. (2018, 2022) reported that Thermococcales induce the formation of greigite (Fe_3S_4) nanocrystals and of great amounts of pyrite (FeS_2) when they are cultivated in an iron and sulfur-rich synthetic medium simulating mineralizing hydrothermal fluids. These studies also showed that the production of pyrite only occurs in the cases where Thermococcales produce sulfur-rich vesicles (S(0)-vesicles), i.e., if they grow in a medium containing sulfur at zero valent state [S(0)] (Gorlas et al., 2015, 2018, 2022). In fact, fermentation-assisted by elemental sulfur reduction made by Thermococcales involves an NAD(P)H elemental sulfur oxidoreductase (NSR) enzyme (Liu et al., 2005; Kobori et al., 2010; Bridger et al., 2011; Herwald et al., 2013) and can lead to the rapid accumulation of elemental sulfur in the cytoplasm, as was reported for *Pyrococcus furiosus* exposed to high concentrations of elemental sulfur (>6.4 g/L) (Schut et al., 2007). The production of sulfur-rich vesicles could thus be seen as a detoxifying process, involving the sequestration of excess sulfur at oxidation state of (0) or close to (0) within the cell and its transport outside of the cell (Gorlas et al., 2015). This mechanism likely occurs in natural environments, since hydrothermal fluids are generally rich in polysulfides (Luther et al., 2001; Waite et al., 2008; Gartman et al., 2011) or colloidal reactive zero-valent sulfur.

In contact with an Fe (II)-rich fluid, these sulfur-rich vesicles could act as a precursor for pyrite formation, most likely after their release by the cells. In contrast, the production of greigite derives from the sulfurization of amorphous Fe (III) phosphates close to the surface of the cells (Gorlas et al., 2018, 2022). Although the excess of sulfide species (H_2S and HS^-) in the system should quickly convert greigite into pyrite (Posfai et al., 1998; Hunger and Benning, 2007), greigite was observed over a period ranging from a few days to several weeks in previous cultures (Gorlas et al., 2018, 2022). Because the stability of greigite depends on the balance between the abundance of reactive iron and the sulfide or polysulfide activities (Kao et al., 2004), its presence over rather long periods suggests that Thermococcales influence the reactivity of at least one, if not both, of these species. More data on the sequence of production and relative abundance of these mineral phases (pyrite, greigite, iron phosphates) in the presence of Thermococcales are needed to better understand the possible role of high temperature microorganisms in the mineralogy of hydrothermal systems. Special attention needs to be given to the habitus of these phases as identifying mineral phases with characteristics specific to the presence of Thermococcales (e.g., shape, size, crystallinity, content in organics), which could be used to track their presence in sulfur-rich hydrothermal vents.

To better understand how archaeal cells influenced the mineral environment and *vice versa*, this study focuses on the mineral characterization of the iron sulfides and iron phosphates produced in the presence/absence of *Thermococcus kodakarensis* in a medium containing zero-valent sulfur S(0). We determined the sequence of production and the habitus of the mineral phases produced in the cultures using X-ray diffraction (XRD), X-ray absorption (XAS) and electron microscopies (SEM and TEM). In addition to proposing a unified explanation of cell growth in strongly mineralized media, we documented the production of pyrite spherules. The specific shape and microstructure of these spherules possibly make them biosignature which presence in natural hydrothermal settings could be used to track the current or past activity of hyperthermophilic archaea.

2. Materials and methods

2.1. Mineralization process in anoxic conditions

Thermococcus kodakarensis KOD1 (JCM 12380) cultures were prepared under strictly anaerobic conditions under N_2 atmosphere in an anoxic Jacomex^{TM} glove box (<1 ppm O_2), as described in Gorlas et al. (2018). Cultures were performed in glass serum vials set with rubber stoppers and aluminium caps. Cells were grown during 12 h at 85°C in 10 mL of a modified Ravot medium (containing, per liter of distilled water : 1 g NH_4Cl, 0.2 g $MgCl2.6H_2O$, 0.1 g $CaCl_2.2H_2O$, 0.1 g KCl, 0.83 g $CH_3COONa.2H_2O$, 20 g NaCl, 1 g yeast extract, 1 g tryptone, 3 g PIPES, 0.001 g resazurin and Na_2S to reduce the medium at 0.05% (w/v) (final concentration) in presence of S(0) (1 g/L) in order to reach 10^8 cells/mL^{-1}. Then an anoxic solution of ferrous sulfate ($FeSO_4$) was added to the cultures (leading to a final concentration of 5 mM) to induce iron mineral precipitation. The mineralized cultures were incubated for different durations determined in previous studies (Gorlas et al., 2018, 2022), namely 5 h for the presence of amorphous iron phosphates, 96 h corresponding to the formation of iron sulfides, 192 h for the demineralization process correlated to the presence of iron phosphates and 35 days to document a very long mineralization period.

Two control experiments were conducted at 85°C for 96 h (i.e., the duration required to observe the production of iron sulfides in the presence of cells): (1) a cell-free abiotic control consisting of the modified Ravot medium with S(0) 1 g/L, Na_2S at 0.05% (w/v) (final concentration) and the $FeSO_4$ solution at 5 mm (final concentration), and (2) a biotic control, consisting of *T. kodakarensis* cells grown in the modified Ravot medium with S(0) (1 g/L), Na_2S at 0.05% (w/t) (final concentration), but without $FeSO_4$ supplementation.

2.2. X-ray absorption near edge structure at the S K-edge

The sulfur speciation in the bulk samples was determined by X-ray absorption near edge structure (XANES) spectroscopy analysis at the S K-edge. Samples were prepared using

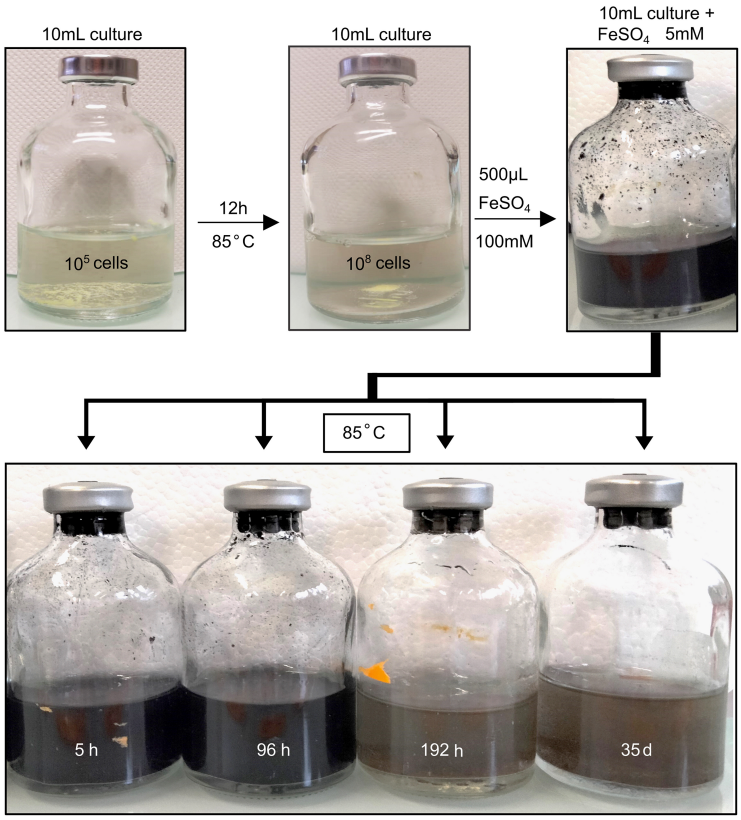

FIGURE 1
Schematic representation of the experimental protocol. *T. kodakarensis* cells were cultivated during 12 h in Ravot medium at 85°C which corresponds to the early stationary phase. Then, upon addition of aqueous $FeSO_4$ solution (5 mM), mineralization occurred as observed visually. Mineralization experiments were conducted for 5 h, 96 h, 192 h, and 35 days. The mineral phases composing the solid residues were then studied by using a combination of XRD, SEM, XANES, TEM, and STXM. Two control experiments were conducted at 85°C for 96 h (i.e., the duration required to observe the production of iron sulfides in the presence of cells): (1) a cell-free abiotic control consisting of the modified Ravot medium with S(0) (1 g/L), Na_2S at 0.05% (w/v) (final concentration), and the $FeSO_4$ solution at 5 mM (final concentration) and (2) a biotic control, consisting of *T. kodakarensis* cells grown in the modified Ravot medium with S(0) (1 g/L), Na_2S at 0.05% (w/v) (final concentration), but without $FeSO_4$ supplementation.

centrifugation (15 mL of each sample were centrifugated at 5000 g for 10 min).

X-ray absorption near edge structure (XANES) was performed in fluorescence mode at the 4–3 beamline at the Stanford Synchrotron Radiation Light Source (SSRL, California, CA, USA) with a Hitachi^{TM} HTA 4-element solid-state Si drift detector for the samples produced in our experiments or a PIPS detector for some of the concentrated reference samples. The incident energy was set up with a Si(111) monochromator and calibrated by measuring a thiosulfate reference (absorption edge at 2472 eV) between each sample holder during the experiment. Samples were shipped to SSRL within anoxic containers, and a few mg of pure solid powders were spread over sulfur-free tape, mounted into sample holders in a COY^{TM} glove box onsite, and analyzed at room temperature under He flow. Between 1 to 4 scans were collected for each sample. Data were calibrated and averaged using the SIXPACK software (Webb, 2005). Then, averaged spectra were normalized using the ATHENA software (Ravel and Newville, 2005).

For data analysis, a Linear Combination Fitting (LCF) procedure was conducted on the S K-edge XANES data with model compounds. LCF analysis of the XANES spectra at the S K-edge was performed using a custom-built program (Morin et al., 2003) based on the Levenberg-Marquardt minimization algorithm. Fit quality was estimated by a R-factor and a reduced chi-square, and the uncertainty on each fitting parameter was estimated to 99.7% confidence (3 sigma) [see Baya et al. (2021) for details]. The set of model compounds included biogenic nanocrystalline mackinawite (FeS), elemental sulfur [S(0)], synthetic nanocrystalline pyrite (FeS_2), and synthetic nanocrystalline greigite (Fe_3S_4). For nano-mackinawite, elemental sulfur, and pyrite, the spectra of model compounds are given in Baya et al. (2021). Briefly, nano-mackinawite refers to a biogenic mackinawite synthesized by incubating *Desulfovibrio capillatus* with Fe(III)-citrate in Ikogou et al. (2017). A powder sample of α-sulfur S(0) was taken from the IMPMC chemical stocks, and pyrite was pure pyrite synthesized according to the protocol reported in Baya et al. (2021). The additional sample of nanocrystalline greigite (Fe_3S_4) was synthesized at ambient temperature in a glove box by mixing an appropriate volume of ferric chloride ($FeCl_3$) and ferrous chloride ($FeCl_2$) solutions with a sodium sulfide (Na_2S) solution while gently stirring, and was then kept under magnetic stirring during 3 months until being dried under vacuum in the IMPMC glove box. This last sample contains traces of FeS.

2.3. Powder X-ray diffraction and Rietveld refinement

Sample preparation was carried out under N_2 atmosphere in an anoxic Jacomex^{TM} glove box (<1 ppm O_2). Samples were prepared using centrifugation (5 mL of each sample were centrifugated at 5000 g for 10 min). The supernatant was discarded and the solid phase was vacuum-dried in an anoxic glove-box (no rinsing). Powder samples were placed on a zero-background Si wafer and inserted in a custom-built anoxic sample chamber equipped with a Kapton® window. The sealed chamber was then removed from the glove-box and XRD patterns were collected using an XPert Pro Panalytical diffractometer. Data were collected using Co Kα radiation in continuous scan mode with an equivalent 0.03°2 θ step counting 2.5 h per sample over the 5–100°2 θ. Scans were then shortened to the 10–100°2 θ because of the bump signal from the Kapton® window at 7.2°2 θ. Rietveld analysis was performed with the xnd_1.3 code (Berar and Baldinozzi, 1998) using pseudo-Voigt line-shape profiles. Starting crystallographic parameters including space group, unit-cell parameters, atomic positions and isotropic Debye-Waller factors were taken from Rettig and Trotter (1987) for α elemental sulfur S(0), from Lennie et al. (1995) for mackinawite FeS, from Stanjek and Schneider (2000) for greigite Fe_3S_4 and from Bayliss (1977) for pyrite FeS_2. The structure of β-Fe_2PO_4O from Ijjaali et al. (1990) was used for the barbosalite-like compound within the $Fe_4(PO_4)_2O_2$ – $Fe_4(PO_4)_3(OH)_3$ solid solution. Unit-cell and line-shape parameters were varied for major phases only. Iron occupation was refined for the barbosalite-like compounds in order to properly account for relative intensities. Scale factors were refined for all phases and were used to calculate relative weight fraction of the mineral phases in the samples using the classical procedure by Bish and Post (1993), assuming a sum of weight fractions equal to one.

2.4. Scanning electron microscopy coupled with energy dispersive X-ray spectroscopy

Sample preparation was carried out under N_2 atmosphere in an anoxic Jacomex^{TM} glove box (<1 ppm O_2). 1 mL of each sample was filtered through a 0.2 μm polycarbonate filter in order to conserve the solid part of the samples (no rinsing). Filters were then deposited on a carbon tape and carbon-coated. SEM-EDXS data were collected at IMPMC, with a GEMINI ZEISSTM Ultra55 Field Emission Gun Scanning Electron Microscope equipped with a Bruker silicon drift detector for EDXS. Both images and EDXS data were collected using an acceleration voltage of 10 kV at a working distance of 7.5 mm.

2.5. Sample preparation by focused ion beam

Focused ion beam (FIB) foils (20 μm × 5 μm × 100 nm) were extracted from pyrite spherules using a FEI Strata DB 235 (IEMN, Lille, France). Milling at low gallium ion currents allowed minimizing common artifacts including local gallium implantation, mixing of components, redeposition of the sputtered material on the sample surface and significant changes in the speciation of carbon-based polymers (Bernard et al., 2009; Schiffbauer and Xiao, 2009).

2.6. Scanning transmission X-ray microscopy

Scanning transmission X-ray microscopy (STXM) analyses were performed on FIB foils to document the carbon speciation of the organics present within the pyrite spherules using the HERMES STXM beamline at the synchrotron SOLEIL (Saint-Aubin, France - Belkhou et al., 2015; Swaraj et al., 2017). Energy calibration was done using the well-resolved 3 p Rydberg peak of gaseous CO2 at 294.96 eV for the C K-edge. XANES hypercube data (stacks) were collected with a spatial resolution of 100 nm at energy increments of 0.1 eV over the carbon (270–340 eV) absorption range with a dwell time of less than 1 ms per pixel to prevent irradiation damage (Wang et al., 2009). Stack alignments and extraction of XANES spectra were done using the Hyperspy python-based package (De la Peña et al., 2018). Normalization of data was done using the QUANTORXS freeware (Le Guillou et al., 2018).

2.7. Transmission electron microscopy (TEM)

Samples were examined using a JEOL JEM-2100F at IMPMC, equipped with a field emission gun (FEG) operating at 200 kV. Mineral characterization was completed by selected-area electron diffraction (SAED) and high-resolution transmission electron microscopy (HRTEM).

3. Results

3.1. Optical appearance

Upon addition of ferrous sulfate ($FeSO_4$) in the medium, abundant black precipitates were immediately generated both in abiotic controls (S(0)+Na_2S+$FeSO_4$) and in experiments conducted in the presence of cells (**Figure 1**). In presence of *T. kodakarensis*, the deep dark aspect of the precipitates faded after 192 h of mineralization (**Figure 1**), consistently with the observations reported in Gorlas et al. (2022). The abiotic controls retained their initial appearance over the entire duration of the experiments, no fading of the deep dark aspect of the precipitates occurred (**Supplementary Figure 1**).

3.2. Sulfur speciation

X-ray absorption near edge structure (XANES) at the S K-edge of mineralized cultures of *T. kodakarensis* indicate a peculiar

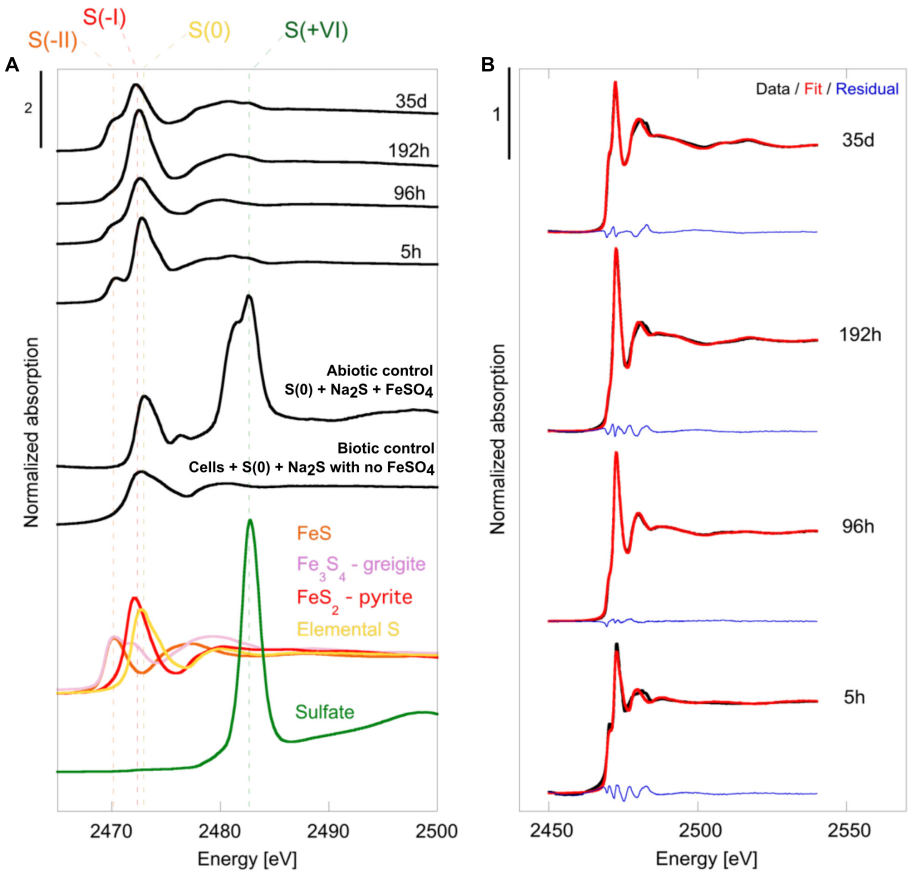

FIGURE 2
(A) Normalized S K-edge XANES spectra of selected reference compounds [FeS (S^{-II}) in orange, Fe_3S_4 greigite in pink, FeS_2 pyrite (S^{-I}) in red, elemental sulfur S(0) in yellow and sulfate in green (S^{+VI})] of the cell-free abiotic control [S(0)+Na_2S+$FeSO_4$], of the biotic control [cells+S(0)+Na_2S with no $FeSO_4$] and of the solid residues of mineralization experiments conducted with *T. kodakarensis* in a sulfur and Fe^{2+} rich medium at 85°C for 5 h, 96 h, 192 h and 35 days. **(B)** Plot presenting linear combination fits performed on normalized S K-edge spectra of the 5 h, 96 h, 192 h and 35 days mineralization experiments conducted with *T. kodakarensis* (data in black, fit in red and residual in blue). Parameters relative to the LCF analysis, such as relative proportions of standard reference compounds and indicators of fit quality, are listed in **Table 2**.

TABLE 1 Results of the LCF analysis applied to normalized S K-edge XANES spectra using chosen reference compounds (see the section "2. Materials and methods").

Sample	FeS %	S(0) %	Fe_3S_4 %	FeS_2 %	Sum	χ^2_R (0.10^{-4})	R-factor (0.10^{-5})
5 h	38 (4)	63 (4)	–	–	101	40.9	80.8
96 h	–	60 (3)	25 (1)	14 (3)	99	3.8	7.7
192 h	–	42 (8)	19 (3)	40 (8)	101	19.1	36.5
35 days	–	–	53 (2)	46 (2)	99	16.3	33.3

Uncertainties on the reported values are given considering a 99% confidence interval. Fit quality is estimated by a reduced chi-square and a R-factor (see the section "2. Materials and methods").

dynamic of sulfur redox evolution (**Figure 2** and **Table 1**). The solid residues of the 5 h long mineralization experiments are dominated by the elemental sulfur [S(0)] introduced in the medium (63% (± 4) of the S atoms), nano-mackinawite (FeS) being also detected (38% (±4) of the S atoms). The proportion of sulfur as elemental sulfur corresponds to 60% (±3) of the S atoms in the solid residues of the 96 h long mineralization experiments. Nano-mackinawite is not present, while greigite (Fe_3S_4) and pyrite (FeS_2) represent 25% (±1) and 14 (±3) of the S atoms, respectively. In the solid residues of the 192 h long mineralization experiments, the proportion of elemental sulfur only corresponds to 43% (±8) of the S atoms, while the proportion of sulfur as greigite corresponds to 19% (±3) of the S atoms and that of sulfur as pyrite to 40% (±8) of the S atoms. The solid residues of the 35 days long mineralization experiments do not contain any elemental sulfur, and sulfur is distributed between greigite (53% (±2) of the S atoms) and pyrite (46% (±2) of the S atoms). The solid residues of the abiotic control (S(0)+Na_2S+$FeSO_4$) and of the biotic control (cells+S(0)+Na_2S with no $FeSO_4$) (**Figure 2**) do not contain nano-mackinawite, greigite nor pyrite according to XANES data at the S K-edge. Although they are detected in the solid residues of the abiotic control (**Figure 2**), sulfates are not detected in the solid residues of mineralized cultures nor in the biotic control due to a common ion effect or a lack of iron in these experiments. The non-indexed

peaks at 2472 and 2481 eV (close to the sulfate peak) in the abiotic control could be attributed to thiosulfate (Fleet et al., 2005).

3.3. X-ray diffraction identification of the crystalline phases formed in the presence of Thermococcales

X-ray diffraction patterns of the solid residues collected during the time-course mineralization experiments are displayed in Figure 3. After 5 h of mineralization, α-sulfur [S(0)] and halite (NaCl) are the major crystalline phases, halite having been likely crystallized upon drying (no rinsing). An additional broadened mackinawite (FeS) pattern is also detected and was included in the Rietveld analysis for this sample. After 96 h of mineralization, α-sulfur is still the dominant crystalline phase but pyrite (FeS_2) and greigite (Fe_3S_4) are also observed in significant amounts, whereas halite is minor. After 192 h of mineralization, an iron (II)-(III) phosphate referred to as "barbosalite-like" is observed in large amount, in addition to pyrite and greigite. Based on Rietveld analysis it can be assigned to a member of the $Fe^{3+}_{(4-x)}Fe^{2+}_{3x}(PO_4)_3(OH)_{(3-3x)}O_{3x}$ solution (Schmid-Beurmann, 2000) with an x value of 0.28 as determined from iron occupancy-factor refinement, i.e., $Fe^{3+}_{2.53}Fe^{2+}_{0.42}(PO_4)_2O_{0.42}(OH)_{1.58}$ when compared to barbosalite $(Fe^{3+})_2Fe^{2+}(PO_4)_2(OH)_2$ (Redhammer et al., 2000). After 35 days of mineralization, greigite, pyrite and some halite were the sole crystalline phases (Figure 3). Neither elemental sulfur nor crystalline iron (II)-(III) phosphate were detected. Note that large crystals may have not been sampled during preparation. Neither greigite, nor pyrite, nor barbosalite-like iron phosphate were detected in the solid residues of the abiotic control ($S(0)+Na_2S+FeSO_4$) and in the biotic control (cells+$S(0)+Na_2S$ with no $FeSO_4$) (Figure 3 and Supplementary Figure 2).

Rietveld refinement (Table 2) allowed us to determine weight fractions of the crystalline phases composing the residues of the mineralization experiments and of the abiotic control ($S(0)+Na_2S+FeSO_4$). Mackinawite was detected in the form of "nano-mackinawite" after 5 h of mineralization with mean coherent domain size (MCD) <3 nm (Table 3) and unit-cell parameters close to those of mackinawite (Lennie et al., 1995). In this sample, elemental sulfur and nano-mackinawite accounted for 22(±6) wt% and 31(±9) wt% of the crystalline phases, respectively. After 96 h of mineralization, greigite and pyrite were present in similar proportions, 23(±1) wt% and 21(±4) wt%, respectively, and nano-mackinawite could not be quantified because of a too low amount. After 192 h of mineralization, greigite accounted for only 4(±1) wt% of the crystalline phases, whereas the barbosalite-like iron (II)-(III) phosphate was present at 50(±3) wt% and pyrite at 29(±3) wt%. After 35 days of mineralization, the proportion of greigite represented 34(±6) wt% of the crystalline fraction, while pyrite represented 52(±11) wt%. In the abiotic control ($S(0)+Na_2S+FeSO_4$), elemental sulfur accounted for 84(±16) wt% and the amount of nano-mackinawite was qualitatively estimated at ≤16 wt% (Table 2). After 96 h of mineralization, Rietveld refinement (Table 3) indicated isotropic mean coherent domain (MCD) size of 61(±11) nm greigite, and slightly anisotropic MCD for pyrite, with (111)-plane pseudo-platelets of 14(±4) nm width and 10(±4) nm thickness. MCD of both greigite and pyrite did not significantly evolve through time.

3.4. Electron and X-ray microscopies on the minerals produced in the presence of Thermococcales

3.4.1. Nano-mackinawite (FeS)

In the solid residues of the 5 h long mineralization experiments, an iron-sulfur-phosphorus amorphous or poorly crystalline material was observed, containing sometimes NaCl crystals, as well as carbon, nitrogen and potassium (Figures 4A, B). At longer times, this amorphous material disappears for the benefit of crystalline phases. Those observations are consistent with XANES and XRD results. A similar iron-sulfur-phosphorus amorphous material is also detected in the abiotic control [$S(0)+Na_2S+FeSO_4$], but neither nitrogen nor potassium were detected (Supplementary Figure 3).

3.4.2. Greigite nano-crystals (Fe_3S_4)

Tiny greigite crystals are present in the solid residues of the 96 h long mineralization experiments (Figure 4C). These greigite crystals of about 40–60 nm are no longer present in the solid residues of the 192 h long mineralization experiments (Figure 4E), but crystals of greigite are present in the solid residues of the 35 days long mineralization experiments (Figure 4F). The nature of the nano-crystals as greigite was confirmed by Selected Area Electron Diffraction Pattern (SAED) and High Resolution TEM (HRTEM) images collected on the solid residues of the 96 h long mineralization experiments (Figures 5A–D).

3.4.3. Pyrite (FeS_2)

Submicrometric (from 200 nm to 1 μm) pyrite spherules are present in the solid residues of the 96 h, 192 h and 35 days long mineralization experiments (Figure 4). Their size, shape and smooth surface texture are very similar in all residues. Low magnification observations show homogeneous aggregates of pyrite spherules with relatively low disparities over the whole mineralization experiments (Supplementary Figure 3).

Focused ion beam (FIB) foils extracted from aggregates of pyrite spherules found in the solid residues of the 96 h long mineralization experiments reveal that each spherule is made of pure pyrite (Figure 5A). The SAED patterns reveal very tiny crystalline domains with some common orientations between adjacent domains (Figure 5E). These observations are consistent with Rietveld refinement of XRD data according to which pyrites are made of small anisotropic coherent domains of 15 nm by 10 nm (Table 3). Moreover, STXM characterization of pyrite sections reveal the presence of organic compounds trapped within the spherules and in the matrix surrounding the spherules (Figure 5F). Absorption features at 285.0, 286.4, 287.4, 288.0, and 288.6 eV can be attributed to aromatic groups, unsaturated C-S bonds, aliphatic groups, amide groups and carboxylic groups, respectively, (Le Guillou et al., 2018). The organic material that can be found in the matrix exhibits the same absorption features as the one

10.3389/fmicb.2023.1145781

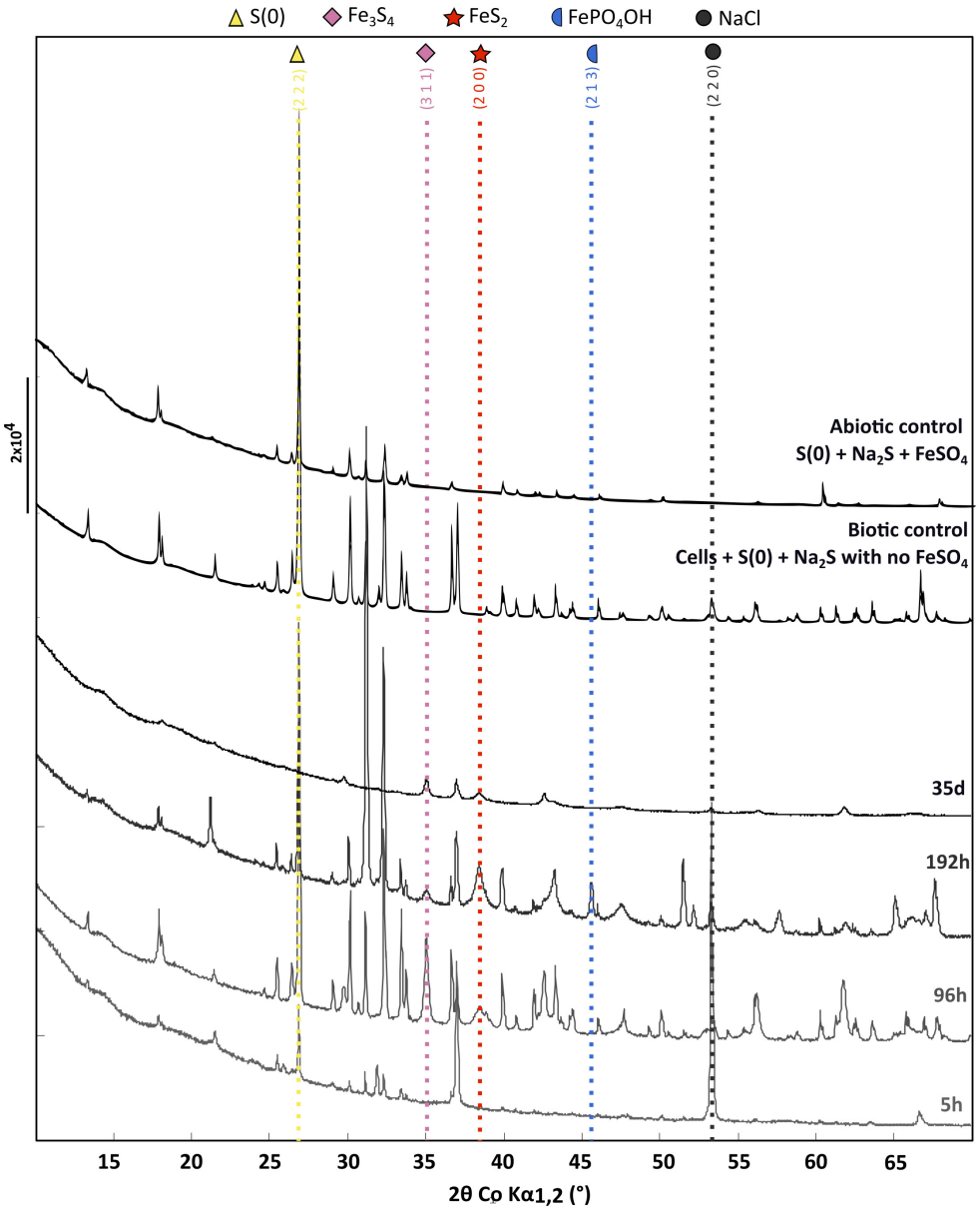

FIGURE 3
X-ray diffraction of the cell-free abiotic control [S(0)+Na_2S+$FeSO_4$], of the biotic control [cells+S(0)+Na_2S with no $FeSO_4$] and of the solid residues of mineralization experiments conducted with *T. kodakarensis* in a sulfur and Fe^{2+} rich medium at 85°C for 5 h, 96 h, 192 h and 35 days. For each phase, peaks corresponding to a line of significant intensity are labeled with concerned (h k l) of elemental sulfur (COD ID: 00-008-0247; yellow triangle), NaCl (halite COD ID: 00-005-0628; gray round), Greigite (COD ID: 00-016-0713; pink diamond), Pyrite (00-006-0710; red star) and Barbosalite-like (iron phosphate oxide hydroxide COD ID: 01-070-5888; blue moon).

TABLE 2 Relative weight fraction of the mineral phases determined by Rietveld analysis applied to samples XRD patterns using pseudo-Voigt line-shape profiles (see the section "2. Materials and methods").

Sample	FeS %	S(0) %	Fe_3S_4 %	FeS_2 %	NaCl	$FePO_4(OH)$	Sum
5 h	31 (9)	22 (6)	–	–	47 (11)	–	100
96 h	–	52 (1)	23 (1)	21 (4)	4 (1)	–	100
192 h	–	12 (1)	4 (1)	29 (3)	5 (5)	50 (3)	100
35 days	–	–	34 (6)	52 (11)	12 (3)	–	100
Abiotic control S(0)+Na_2S+$FeSO_4$	16	84 (16)	–	–	–	–	100

TABLE 3 Mean coherent domain size of the mineral phases based on Rietveld analysis applied to samples XRD patterns.

Sample	FeS	Fe_3S_4	FeS_2		$FePO_4(OH)$
			L_0[2]	L_2[2]	
5 h	<3	–	–	–	–
96 h	–	61 (10.7)	14.1 (3.5)	10.5 (3.5)	–
192 h	–	41.6 (0.1)	15.7 (1.9)	9.3 (1.6)	>1000
35 days	–	46.5 (11.4)	12.5 (3)	5.7 (1.8)	–

Mineral particle size was calculated by using the Scherrer equation.

trapped into the pyrite spherules (Figure 5F). The carbon amount is rather low (~0.15 optical density units) but still detectable. As a comparison, the spectrum of the organic-rich platinum only shows a feature at 285.0 eV, attributed to aromatic groups (Le Guillou et al., 2018).

3.4.4. Barbosalite-like ($Fe^{3+}_{2.53}Fe^{2+}_{0.42}(PO_4)_2O_{0.42}(OH)_{1.58}$)

Barbosalite-like crystals are only observed in the solid residues of the 192 h long mineralization experiments. They exhibit heterogeneous shapes and sizes (Figures 4E, F). Some are several micrometers wide and display a spherical or broken spherical shape, while some submicrometric ones display a spherule shape and are in direct contact with pyrite.

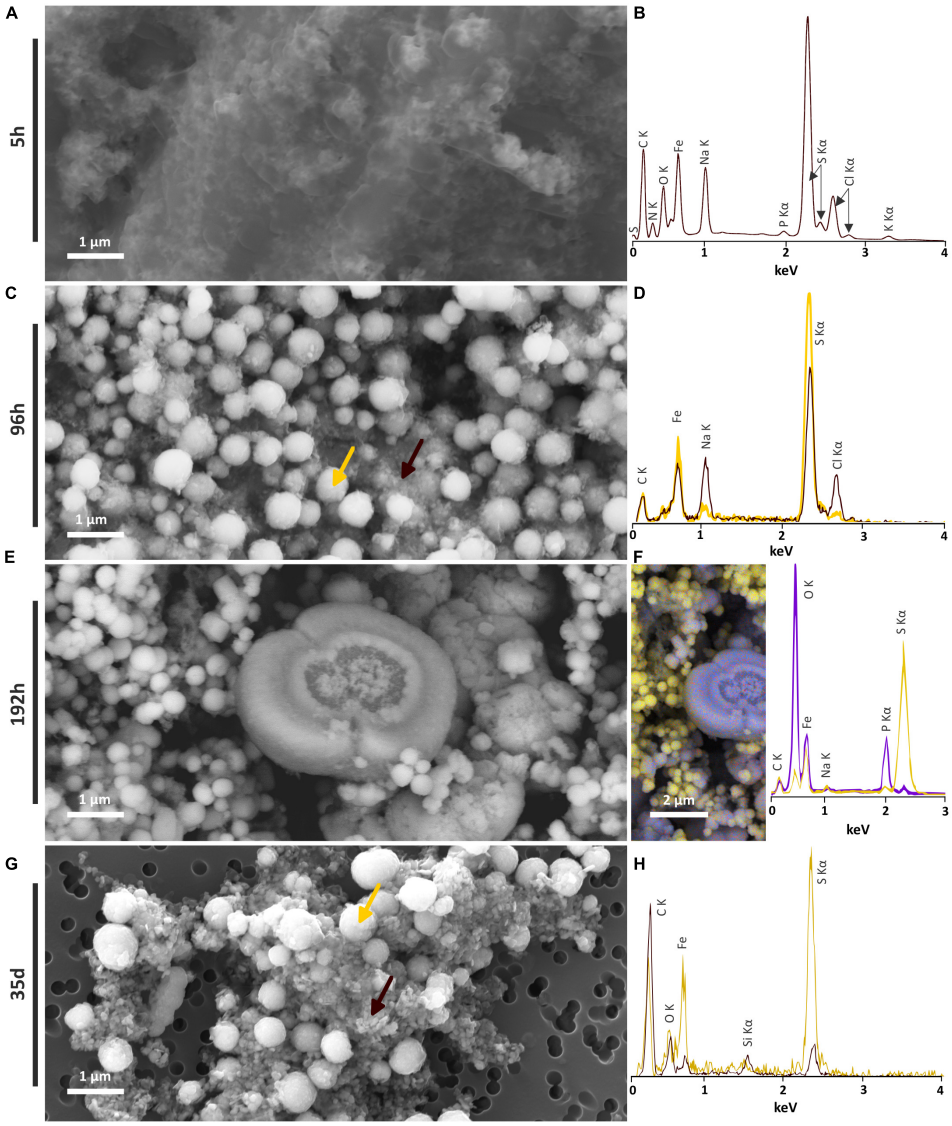

FIGURE 4
SEM investigations of the solid residues of mineralization experiments conducted with *T. kodakarensis* in a sulfur and Fe^{2+} rich medium at 85°C for 5 h, 96 h, 192 h and 35 days. **(A)** Iron sulfide matrix after 5 h of mineralization and **(B)** associated EDXS spectrum. **(C)** Iron sulfide spherules (indicated by a yellow arrow) and nanocrystals in the matrix (indicated by a brown arrow) after 96 h of mineralization and **(D)** associated EDXS spectra in yellow and brown, respectively. **(E)** Iron sulfide spherules and iron phosphate after 192 h of mineralization and **(F)** associated EDXS hypermap and spectra of iron phosphates (blue) and iron sulfides (yellow). **(G)** Iron sulfide spherules and crystallized iron sulfide matrix after 35 days of mineralization and **(H)** associated EDXS spectra in yellow and brown, respectively.

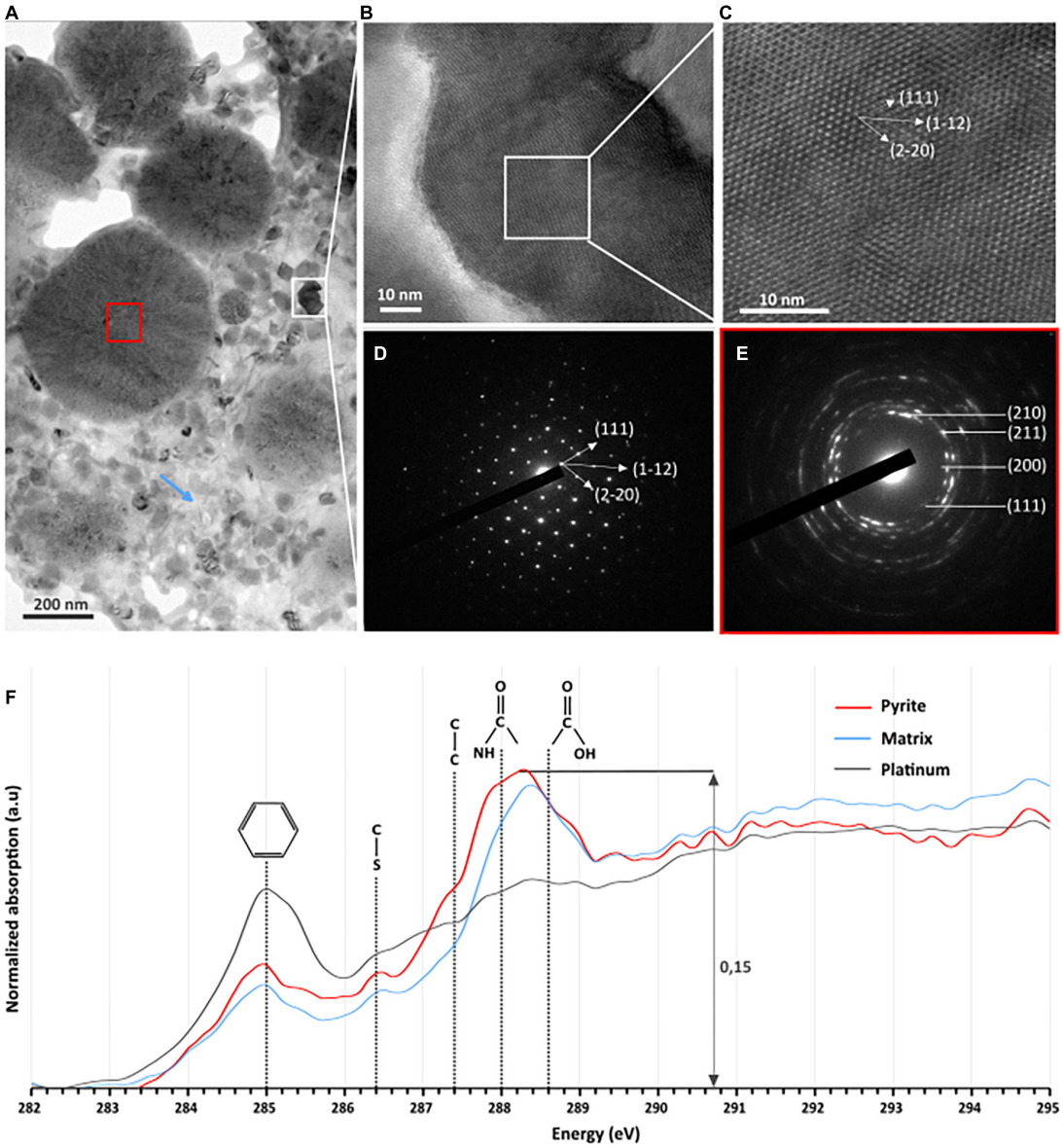

FIGURE 5
TEM, HRTEM, and STXM characterization of FIB sections of pyrite spherules observed in the solid residues of mineralization experiments conducted with *T. kodakarensis* in a sulfur and Fe^{2+} rich medium at 85°C for 96 h. **(A)** TEM image of sections of pyrite spherules. **(B)** TEM image and **(C)** HRTEM of greigite [zone axis ($1\bar{1}0$)] and **(D)** associated electron diffraction pattern. **(E)** Electron diffraction pattern of polycrystalline pyrite (red square in panel **A**) showing a preferential orientation. **(F)** C-XANES spectra of the organic material trapped into the pyrite spherules (red spectrum) and into the matrix surrounding the spherules (blue spectrum). The spectrum of the organic-rich platinum is also shown (in gray) for comparison. Absorption features at 285.0, 286.4, 287.4, 288.0, and 288.6 eV are attributed to aromatic groups, unsaturated C-S bonds, aliphatic groups, amide groups, and carboxylic groups, respectively.

4. Discussion

4.1. Evolution of the system over time: phosphorus–iron–sulfur dynamics

The formation of a black precipitate immediately after the addition in the medium of iron as Fe^{2+} (Figure 1) is caused by the precipitation of amorphous or poorly crystalline nanophases such as FeS nano-mackinawite [unambiguously detected by Rietveld refinement (Table 2) and XANES (Figure 2 and Table 1)] and iron phosphates (Figure 4B; Gorlas et al., 2018, 2022), the two phases forming a three-dimensional matrix observed by electron microscopy. A similar amorphous matrix is observed in the abiotic control [S(0) + Na_2S + $FeSO_4$] at 96 h (Supplementary Figure 3), identified as FeS nano-mackinawite by Rietveld refinement (Table 2). Note that the nano-mackinawite contribution, estimated at ≤16% ± while elemental sulfur accounted for 84 (± 16) wt %, likely is overestimated by Rietveld refinement (Table 2) since we were not able to detect it in XANES S K-edge analysis (Figure 2 and Table 1). Thermococcales promote a redox evolution of both sulfur and iron: S(0) is reduced by cellular metabolism producing sulfide (S^{-2}) which is then progressively oxidized into S^{-1} as pyrite

while Fe^{2+}, although not directly involved in cellular metabolism, is partially oxidized into Fe^{3+} in greigite and in barbosalite-like phosphate (**Figures 2**, **6** and **Tables 1**, **2**). In parallel with the continuous reduction of sulfur (0), the system thus evolves from almost pure nano-mackinawite (FeS) at 5 h (**Figures 4A, B**, **6**) to greigite (Fe_3S_4) nanocrystals and pyrite (FeS_2) submicrometric spherules starting 96 h (**Figures 4C, D**, **6**).

While the precipitation of pyrite increases with increasing duration of mineralization (**Figures 6A–C**), the initial production of greigite, a sulfide containing 2 Fe(III) for 1 Fe(II), seems to be intimately related to that of Fe (II/III) phosphates in the present system: the proportion of greigite first decreases while barbosalite-like phosphates precipitate, before it increases once barbosalite-like are no longer present (**Figures 6A, D**). A number of studies have reported the microbial production of greigite either intracellularly (by magnetotactic bacteria for instance) or extracellularly (e.g., Mann et al., 1990; Bertel et al., 2012; Gorlas et al., 2018, 2022; Picard et al., 2018, 2019). Some authors proposed that the production of greigite requires a precursor already containing some Fe (III) (Etique et al., 2018; Picard et al., 2018; Berg et al., 2020; Duverger et al., 2020; Gorlas et al., 2022). This Fe(III) may come from Fe(III)-phosphates (e.g., Duverger et al., 2020) or from the oxidation of the Fe(II) of mackinawite (e.g., Lennie et al., 1997). Here, the FeS nano-mackinawite three-dimensional matrix contains some amorphous or poorly crystallized iron phosphates (**Figure 4B**), likely Fe(III)-phosphates as previously reported by Gorlas et al. (2022). Still, the initial production of Fe(III)-phases remains enigmatic since the experiments are conducted in strict anoxia. The oxidation of iron could have involved the S(0) contained in the cells, organic acids, or water (H^+), which reductions could have been catalyzed by the cell surfaces. Kish et al. (2016) have reported that *Sulfolobus acidocaldarius* S-layer of both active and ghost cells and membrane vesicles are effective nucleation sites for amorphous or crystalline Fe-phosphate phases in a phosphate-rich and sulfate-rich medium. This possibility is also consistent with the observations of iron phosphates on Thermococcales cell surfaces or extracellular materials (Gorlas et al., 2022).

Between 96 and 192 h, the proportions of well crystallized pyrite and large iron phosphates, namely barbosalite-like [resembling barbosalite (Schmid-Beurmann, 2000) or lipscombite (Ech-Chahed et al., 1988)], increase over that of greigite (**Figures 6A, D**). The crystallized phosphates could be formed by interaction between poorly crystallized phosphates and greigite. Moreover, when sulfur is present in the medium, it has been shown that the cells accumulate S(0) vesicles leading to the formation of pyrite when in contact with Fe^{2+} (Gorlas et al., 2022), which explains the abundance of this phase. The predominance of such large grain size phases over nanophases of iron phosphate, nano-mackinawite and greigite likely explains the clarification of the medium (**Figure 1** and **Supplementary Figure 1**). In similar 192 h long mineralization experiments, Gorlas et al. (2022) detected significant amounts of intracellular ATP and visualized living cells and cell divisions suggesting that some cells had resisted the toxic initial high nanoparticle-rich medium and benefited from clear enough medium to resume growth and cell division. It is then likely that these cells largely depleted the stock of sulfur (0) in the medium and shift to an H_2 generating fermentative metabolism, below a certain threshold of zero valent sulfur in the system (**Figure 6**; Kanai et al., 2013; Schut et al., 2013). This may result in some pyrite dissolution producing H_2S and greigite according to:

$$3FeS_2 + 2H_2 \rightarrow Fe_3S_4 + 2H_2S \quad (1)$$

and possibly iron (II)-(III) phosphates, which allow the cell population to recover additional phosphorus. Such phosphorus-iron-sulfur dynamics would constitute an ecological strategy in natural environments (Xiong et al., 2019; Wilfert et al., 2020). Such mobilization of the phosphorus reservoir by the cells leaves an excess of Fe(III) which can then be used for greigite precipitation. This model is consistent with the second phase of greigite precipitation (**Figure 6**) and the absence of well crystallized phosphates in the solid residues of 35 days long mineralization experiments (**Figure 6**).

4.2. Carbon-containing pyrite spherules: a biosignature?

In contrast to amorphous ferrous sulfide (FeS), greigite (Fe_3S_4) or mackinawite (FeS), which biological production has been extensively reported (Posfai et al., 1998; Picard et al., 2016, 2018; Stanley and Southam, 2018; Park and Faivre, 2022), pyrite is generally produced abiotically in natural settings (e.g., Yuan et al., 2020). Still, biogenic production of pyrite can be achieved by some microorganisms, including sulfate-reducing microorganisms (SRM) (Thiel et al., 2019; Berg et al., 2020; Duverger et al., 2020) or methanogenic archaea (Thiel et al., 2019). Pyrite may form from greigite and ferrous sulfide (Rickard, 1997; Hunger and Benning, 2007; Rickard and Luther, 2007) or from elemental sulfur and ferrous sulfide (Wilkin and Barnes, 1996; Benning et al., 2000). Here, an early ferrous sulfide phase is unambiguously detected by XANES (**Figure 2** and **Table 1**), Rietveld refinement (**Table 2**) and SEM (**Figures 4A, B**), confirming previous results (Gorlas et al., 2018, 2022). This ferrous sulfide phase has likely been produced via interactions between S(-II) and Fe(II). The presence of both sulfides and hydrogen sulfide (HS^-) results from the reduction of S(0) by *T. kodakarensis*, occurring partially before the addition of iron in the system (Morikawa et al., 1994). Note that it is likely that some sulfide ions come from the Na_2S, explaining the production of black precipitates identified as ferrous sulfides by Rietveld refinement (**Table 2**) in the abiotic control (S(0) + Na_2S + $FeSO_4$) after addition of $FeSO_4$.

As stated above, with increasing duration of mineralization, phases containing iron and/or sulfur more oxidized than mackinawite (FeS) are produced, namely greigite (Fe_3S_4), pyrite (FeS_2) and barbosalite-like ($Fe_{1.47}PO_4(OH)_{0.79}$) (**Figures 2**, **3**, **4**, **6**). The sulfur of pyrite is at a formal oxidation state S(-I), i.e., it is more oxidized than that in mackinawite, which is formally S(-II), while both phases contain Fe(II). An oxidation process is thus necessary to form pyrite from mackinawite, i.e., electron acceptors must be present in the system. It is known that Thermococcales produce many extracellular vesicles (Soler et al., 2008; Gorlas et al., 2015; Liu et al., 2021), and particularly S(0)-vesicles which have been suggested to be involved in the detoxification of polysulfides (Gorlas et al., 2015). Here, the production of S(0)-vesicles may have enhanced the production of pyrite. Accordingly, Gorlas et al. (2015, 2018, 2022) have shown that no pyrite forms in culture devoid of

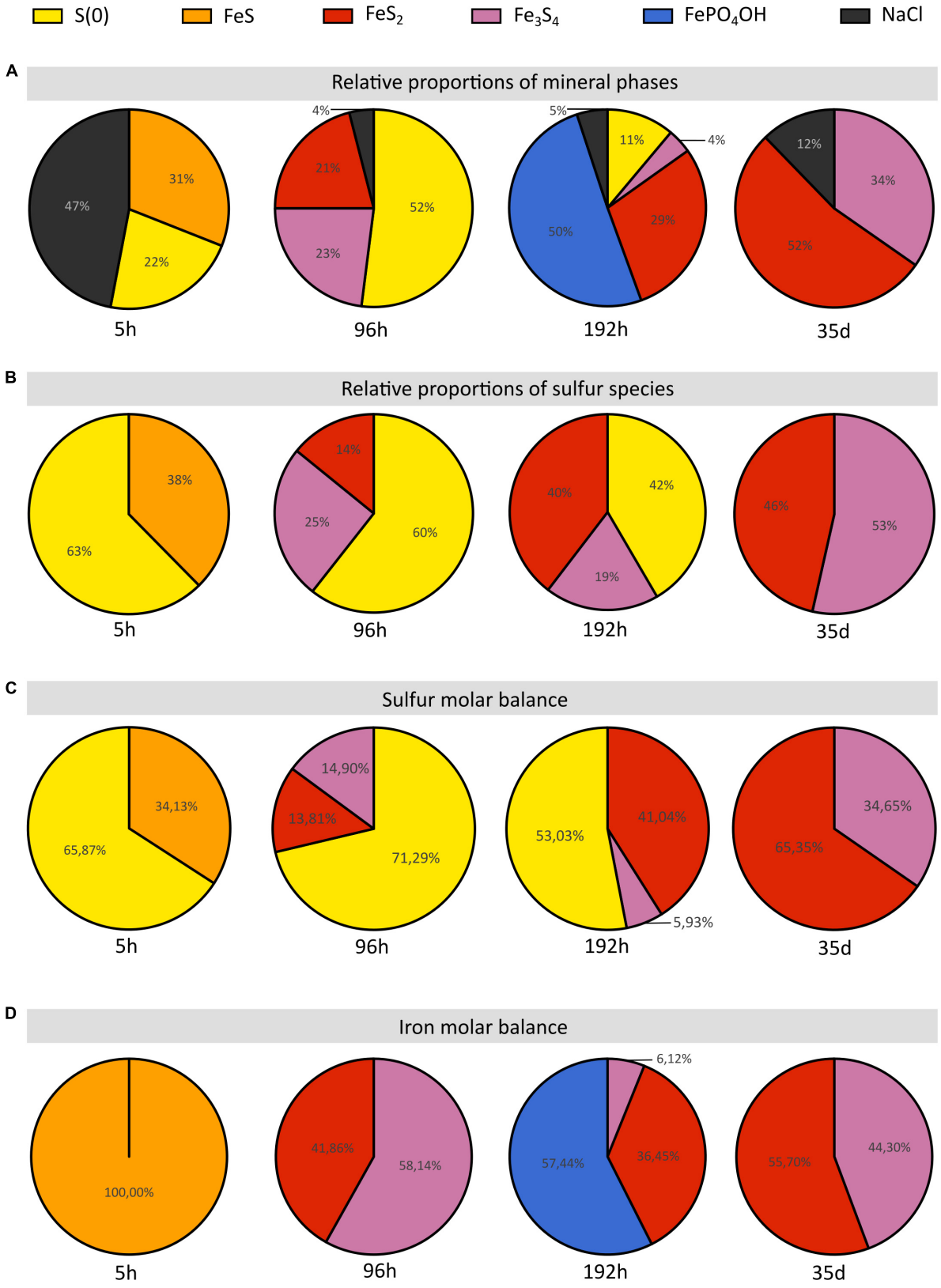

FIGURE 6
Proportions of sulfur and iron species and of the iron species of the solid residues of mineralization experiments conducted with *T. kodakarensis* in a sulfur and Fe^{2+} rich medium at 85°C for 5 h, 96 h, 192 h and 35 days. **(A)** Relative proportions of mineral phases according to Rietveld refinements. **(B)** Relative proportions of sulfur species according to S K-edge XANES data. **(C)** Sulfur and **(D)** iron molar balances based on Rietveld analyses (cf **Table 2**).

S(0)-vesicles. Thus, the main process of pyrite formation in this system likely involves S(0)-vesicles, S(0) acting in such a scheme as an acceptor of sulfide electrons, according to:

$$FeS + S \rightarrow FeS_2 \quad (2)$$

The present study suggests that the presence of metabolically active *T. kodakarensis* influences the sulfur reactivity by producing S(0)-vesicles, which leads to a redox comproportionation of S(0) from elemental sulfur and S(-II) from FeS, to S(-I) in pyrite. Of note, using zero valent sulfur as an oxidant does not exclude greigite as a pyrite intermediate (Hunger and Benning, 2007).

The pyrite produced in the presence of Thermococcales present a peculiar spherical shape. The spherules with a diameter of 200 nm to 1 μm exhibit a very smooth surface texture (**Figures 4C, E, G**) and consist in an accumulation of many ultra-small domains sharing common preferential orientations in the spherules (**Figure 5E**). The ultra-small domains are anisotropic and about 15 nm by 10 nm (**Table 3**), which explains the very smooth aspect of the spherules. Moreover, the presence of complex organic matter is detected within these pyrite spherules, although in low quantity. These compounds exhibit several functional groups, including aromatic groups, unsaturated C-S bonds, aliphatic groups, amide groups and carboxylic groups (**Figure 5F**), i.e., typical of the functional groups measured in mineralization studies involving prokaryotes (Benzerara et al., 2006; Miot et al., 2009; Li et al., 2013, 2014; Picard et al., 2021).

Pyrite mineralization by Thermococcales has been proposed to constitute a survival strategy at the population level (Gorlas et al., 2022). Still, the production of the pyrite spherules described here may be bio-induced rather than bio-controlled. Frankel and Bazylinski (2003), described biological induced mineralization (BIM) as the unintended and uncontrolled result of metabolic products reacting with ions or compounds present in the environment, making BIM products rather difficult to distinguish from abiotic minerals (Beveridge, 1989; Konhauser, 1998; Banfield and Zhang, 2001; Bäuerlein, 2003). In contrast, biologically controlled mineralization (BCM) minerals leads to the production of structurally well-ordered, narrow size distributed minerals exhibiting specific morphologies (Frankel and Bazylinski, 2003; Liu et al., 2012). Given the homogeneity in texture, shape and size of the pyrite spherules discussed here, it seems that they rather correspond to BCM than to BIM. But BCM minerals are usually formed within intracellular organic matrices or vesicles, and their nucleation and growth are genetically controlled by the organism itself (Bazylinski and Frankel, 2000a,b), which is not the case here since pyrite most likely precipitates after the release of the S(0)-vesicles outside the cells. However, it could be argued that the BCM concept is relevant to the S(0)-vesicles themselves. Further studies, especially of the transcriptome, are necessary to determine if Thermococcales genetics are able to control the characteristics of pyrite spherules.

5. Conclusion

When cultivated in a ferrous and sulfur-rich medium, Thermococcales influence the reactivity of both species through iron sulfur and iron phosphate precipitation. After an initial precipitation of iron sulfide and phosphate nanophases that are toxic to most cells, the medium clears by evolving to the formation of larger structures of hundreds of nanometres pyrite spherules and well-crystallized iron II-III phosphates that are compatible with proper cell development. Moreover, this study shows that pyrite precipitation results from a redox comproportionation of S(0) (from elemental sulfur) and S(-II) (from FeS) to S(-I) (in pyrite), induced by the presence of Thermococcales and their production of S(0)-vesicles. Pyrites thus formed present specific textural features such as a peculiar spherule shape, ultra-small and anisotropic domains and a content in organic compounds that make them good candidates as biosignatures. However, before using them as tracers of the activity of Thermococcales in natural hydrothermal settings such as hydrothermal chimneys, additional experiments should be conducted to determine whether or not similar spherules containing similar organic compounds can be produced abiotically, and whether or not these specificities (shape, crystallinity and content in organics) may withstand hydrothermal and diagenetic conditions over long durations.

Data availability statement

The original contributions presented in this study are included in the article/**Supplementary material**, further inquiries can be directed to the corresponding author.

Author contributions

CT, AG, SB, and FG contributed to the conception and design of the study. CT and AG conducted the Thermococcales cultures, the mineralization process in anoxic conditions, and the powder X-ray diffraction. CT and FG conducted the electron microscopy analyses. PL, GM, CB, and PM conducted the XANES S K-edge measurements. GM realized the Rietveld refinement. CT and SB conducted the STXM analyses. CT wrote the first draft of the manuscript. CT, SB, FG, GM, and PL wrote the sections of the manuscript. All authors contributed to the manuscript revision, read, and approved the submitted version.

Funding

CT was supported by the Muséum National d'Histoire Naturelle (MNHN), Sorbonne Université (SU) and the Ministère de l'Enseignement Supérieur et de la Recherche. AG was supported by the Agence Nationale de la Recherche, project HYPERBIOMIN (ANR-20-CE02-0001-01). FG was supported by Institut Universitaire de France. The SEM facility at IMPMC was supported by the Region Île-de-France grant SESAME Number I-07-593/R, INSU-CNRS, INP-CNRS, and UPMC-Paris 6, and the Agence Nationale de la Recherche (ANR-07-BLAN-0124-01). The HERMES beamline (SOLEIL) was supported by the CNRS, the CEA, the Region Île-de-France, the Departmental Council of Essonne, and the Region Centre.

Acknowledgments

We acknowledge the support of the IMPMC microscopy platform, IMPMC X-ray diffraction platform, SSRL experimental station 4-3, and SOLEIL HERMES beamline. We thank Elisabeth Malassis (IMPMC) for her administrative support, Imène Estève (IMPMC) for her help in SEM-EDXS, Jean-Michel Guigner (IMPMC) for his help in TEM, Ludovic Delbes (IMPMC) for his help in XRD, David Troadec (IEMN) for the preparation of the FIB sections, Corentin Le Guillou (UMET) for his help with STXM, Pierre Lefebvre (ETH) for his help with XANES at SSRL, and Stefan Stanescu for his expert support of HERMES beamline at SOLEIL.

Conflict of interest

The authors declare that the research was conducted in the absence of any commercial or financial relationships that could be construed as a potential conflict of interest.

Publisher's note

All claims expressed in this article are solely those of the authors and do not necessarily represent those of their affiliated organizations, or those of the publisher, the editors and the reviewers. Any product that may be evaluated in this article, or claim that may be made by its manufacturer, is not guaranteed or endorsed by the publisher.

Supplementary material

The Supplementary Material for this article can be found online at: https://www.frontiersin.org/articles/10.3389/fmicb.2023.1145781/full#supplementary-material

SUPPLEMENTARY FIGURE 1
(A) Mineralization experiments conducted with *T. kodakarensis* in a sulfur and Fe^{2+} rich medium at 85°C for 192 h. **(B)** Abiotic control [S(0) + Na_2S + $FeSO_4$] after 192 h of mineralization at 85°C.

SUPPLEMENTARY FIGURE 2
X-ray diffractograms of the solid residues of mineralization experiments conducted with *T. kodakarensis* in a sulfur and Fe^{2+} rich medium at 85°C for 5 h **(A)**, 96 h **(B)**, 192 h **(C)** and 35 days **(D)** and of abiotic control [S(0) + Na_2S + $FeSO_4$] **(E)** and of biotic control (cells + S(0) + Na_2S with no $FeSO_4$) **(F)**. Each identified peaks are labeled with Elemental sulfur (COD ID: 00-008-0247; yellow triangle), NaCl (halite COD ID: 00-005-0628; gray round), Greigite (COD ID: 00-016-0713; pink diamond), Pyrite (00-006-0710; red star) and Barbosalite-like (iron phosphate oxide hydroxide COD ID: 01-070-5888; blue moon).

SUPPLEMENTARY FIGURE 3
Low magnification SEM images of the solid residues of mineralization experiments conducted with *T. kodakarensis* in a sulfur and Fe^{2+} rich medium at 85°C for 5 h **(A)**, 96 h **(B)**, 192 h **(C)**, 35 days **(D)**, and of abiotic control [S(0) + Na_2S + $FeSO_4$] after 96 h of mineralization **(E)**.

References

Banfield, J., and Zhang, H. (2001). Nanoparticles in the environment. *Rev. Mineral Geochem.* 44, 1–58.

Bäuerlein, E. (2003). Biomineralization of unicellular organisms: An unusual membrane biochemistry for the production of inorganic nano- and microstructures. *Angew. Chem. Int. Ed.* 42, 614–641. doi: 10.1002/anie.200390176

Baya, C., Le Pape, P., Baptiste, B., Brest, J., Landrot, G., Elkaim, E., et al. (2021). Influence of trace level As or Ni on pyrite formation kinetics at low temperature. *Geochim. Cosmochim. Acta* 300, 333–353. doi: 10.1016/j.gca.2021.01.042

Bayliss, P. (1977). Crystal structure refinement of a weakly anisotropic pyrite. *Am. Mineral.* 62, 1168–1172.

Bazylinski, D., and Frankel, R. (2000a). "Magnetic iron oxide and iron sulfide minerals within organisms," in *Biomineralization: From biology to biotechnology and medical application*, ed. E. Bäuerlein (Weinheim: Wiley-VCH), 25–46.

Bazylinski, D., and Frankel, R. (2000b). "Biologically controlled mineralization of magnetic iron minerals by magnetotactic bacteria," in *Environmental microbe-mineral interactions*, ed. D. Lovley (Washington, DC: ASM Press), 109–144. doi: 10.1128/9781555818098.ch5

Belkhou, R., Stanescu, S., Swaraj, S., Besson, A., Ledoux, M., Hajlaoui, M., et al. (2015). HERMES: A soft X-ray beamline dedicated to X-ray microscopy. *J. Synchrotron Radiat.* 22, 968–979. doi: 10.1107/S1600577515007778

Benning, L., Wilkin, R., and Barnes, H. (2000). Reaction pathways in the Fe–S system below 100°C. *Chem. Geol.* 167, 25–51.

Benzerara, K., Menguy, N., López-García, P., and Brown, G. Jr. (2006). Nanoscale detection of organic signatures in carbonate microbialites. *PNAS* 103, 9440–9445. doi: 10.1073/pnas.0603255103

Berar, J.-F., and Baldinozzi, G. (1998). XND code: From X-ray laboratory data to incommensurately modulated phases. Rietveld modeling of complex materials. *CPD Newsletter* 20, 3–5.

Berg, J., Duverger, A., Cordier, L., Laberty-Robert, C., Guyot, F., and Miot, J. (2020). Rapid pyritization in the presence of a sulfur/sulfate-reducing bacterial consortium. *Sci. Rep.* 10:8264. doi: 10.1038/s41598-020-64990-6

Bernard, S., Benzerara, K., Beyssac, O., Brown, G. E., Grauvogel Stamm, L., and Duringer, P. (2009). Ultrastructural and chemical study of modern and fossil sporoderms by scanning transmission X-ray microscopy (STXM). *Rev. Palaeobot. Palynol.* 156, 248–261.

Bertel, D., Peck, J., Quick, T. J., and Senko, J. M. (2012). Iron transformations induced by an acid-tolerant *Desulfosporosinus* species. *Appl. Environ. Microbiol.* 78, 81–88. doi: 10.1128/AEM.06337-11

Beveridge, T. J. (1989). Role of cellular design in bacterial metal accumulation and mineralization. *Annu. Rev. Microbiol.* 43, 147–171.

Bish, D., and Post, J. E. (1993). Quantitative mineralogical analysis using the rietveld full-pattern fitting method. *Am. Mineral.* 789, 932–940. doi: 10.1016/j.dib.2021.107746

Bridger, S., Clarkson, S., Stirrett, K., DeBarry, M., Lipscomb, G., Schut, G., et al. (2011). Deletion strains reveal metabolic roles for key elemental sulfur-responsive proteins in *Pyrococcus furiosus*. *J. Bacteriol.* 193, 6498–6504. doi: 10.1128/JB.05445-11

Charlou, J., Donval, J., Fouquet, Y., Jean-Baptiste, P., and Holm, N. (2002). Geochemistry of high H2 and CH4 vent fluids issuing from ultramafic rocks at the Rainbow hydrothermal field (36 degrees 14'N. MAR). *Chem. Geol.* 191, 345–359. doi: 10.1016/S0009-2541(02)00134-1

De la Peña, F., Ostasevicius, T., Fauske, V. T., Burdet, P., Prestat, E., Jokubauskas, P., et al. (2018). *HyperSpy v1. 4.*

Duverger, A., Berg, J. S., Busigny, V., Guyot, F., Bernard, S., and Miot, J. (2020). Mechanisms of pyrite formation promoted by sulfate-reducing bacteria in pure culture. *Front. Earth Sci.* 8:588310. doi: 10.3389/feart.2020.588310

Ech-Chahed, B., Jeannot, F., Malaman, B., and Gleitzer, C. (1988). Préparation et étude d'une variété basse température de l'oxyphosphate de fer de valence mixte β-Fe2(PO4)O et de $NiCr(PO_4)O$: Un cas d'échange électronique rapide. *J. Solid State Chem.* 74, 47–59. doi: 10.1016/0022-4596(88)90330-1

Edmond, J., Measures, C., McDuff Chan, L., Collier, R., and Grant, B. (1979). Ridge crest hydrothermal activity and the balances of the major and minor element in the ocean : The Galapagos data. *Earth Planet. Sci. Lett.* 46, 1–18. doi: 10.1016/0012-821X(79)90061-X

Elderfield, H., and Schultz, A. (1996). Mid-ocean ridge hydrothermal fluxes and the chemical composition of the ocean. *Annu. Rev. Earth Planet. Sci.* 24, 191–224. doi: 10.1146/annurev.earth.24.1.191

Etique, M., Romaine, A., Bihannic, I., Gley, R., Carteret, C., Abdelmoula, M., et al. (2018). Abiotically or microbially mediated transformations of magnetite by sulphide species: The unforeseen role of nitrate-reducing bacteria. *Corros. Sci.* 142, 31–44. doi: 10.1016/j.corsci.2018.06.032

Feely, R., Massoth, G., Trefry, J., Baker, E., Paulson, A., and Lebon, G. (1994). Composition and sedimentation of hydrothermal plume particles from north Cleft segment, Juan de Fuca Ridge. *J. Geophys. Res.* 99, 4985–5006. doi: 10.1029/93JB02509

Fleet, M., Xiaoyang, L., Harmer, S., and Nesbitt, W. (2005). Chemical state of sulfur in natural and synthetic lazurite by S K-edge XANES and X-ray photoelectron spectroscopy. *Canad. Mineral.* 43, 1589–1603.

Flores, G., Campbell, J., Kirshtein, J., Meneghin, J., Seewald, J., Tivey, M., et al. (2011). Microbial community structure of hydrothermal deposits from geochemically different vent fields along the Mid-Atlantic Ridge. *Environ. Microbiol.* 13, 2158–2171. doi: 10.1111/j.1462-2920.2011.02463.x

Frankel, R., and Bazylinski, D. (2003). Biologically induced mineralization by bacteria. *Rev. Mineral. Geochem.* 54, 95–114.

Gartman, A., Yücel, M., Madison, A., Chu, D., Ma, S., Janzen, C., et al. (2011). Sulfide oxidation across diffuse flow zones of hydrothermal vents. *Aquat. Geochem.* 17, 583–601. doi: 10.1007/s10498-011-9136-1

Gorlas, A., Jacquemot, P., Guigner, J. M., Gill, S., Forterre, P., and Guyot, F. (2018). Greigite nanocrystals produced by hyperthermophilic archaea of *Thermococcales* order. *PLoS One* 13:e0201549. doi: 10.1371/journal.pone.0201549

Gorlas, A., Marguet, E., Gill, S., Geslin, C., Guigner, J.-M., Guyot, F., et al. (2015). Sulfur vesicles from *Thermococcales*: A possible role in sulfur detoxifying mechanisms. *Biochimie* 118, 356–364. doi: 10.1016/j.biochi.2015.07.026

Gorlas, A., Mariotte, T., Morey, L., Truong, C., Bernard, S., Guigner, J.-M., et al. (2022). Precipitation of greigite and pyrite induced by *Thermococcales*: An advantage to live in Fe- and S-rich environments? *Environ. Microbiol.* 24, 626–642. doi: 10.1111/1462-2920.15915

Herwald, S., Liu, A., Zhu, B., Sea, K., Lopez, K., Sazinsky, M., et al. (2013). Structure and substrate specificity of the pyrococcal coenzyme A disulphide reductases/polysulfide reductases (CoADR/Psr): Implications for S(0)-based respiration and a sulfur-dependent antioxidant system in *Pyrococcus*. *Biochemistry* 52, 2764–2773. doi: 10.1021/bi3014399

Holden, J., and Adams, M. (2003). Microbe-metal interactions in marine hydrothermal environments. *Curr. Opin. Chem. Biol.* 7, 160–165. doi: 10.1016/s1367-5931(03)00026-7

Houghton, J., and Seyfried, Jr (2010). An experimental and theoretical approach to determining linkages between geochemical variability and microbial diversity in sea floor hydrothermal chimneys. *Geobiology* 8, 457–470. doi: 10.1111/j.1472-4669.2010.00255.x

Hunger, S., and Benning, L. G. (2007). Greigite: A true intermediate on the polysulfide pathway to pyrite. *Geochem. Trans.* 8:1. doi: 10.1186/1467-4866-8-1

Ijjaali, M., Malaman, B., Gleitzer, C., Warner, J., Hriljac, J., and Cheetham, A. (1990). Stability, structure refinement, and magnetic properties of β-Fe2PO4O. *J. Solid State Chem.* 86, 195–205. doi: 10.1016/0022-4596(90)90135-K

Ikogou, M., Ona-Nguema, G., Juillot, F., Le Pape, P., Menguy, N., Richeux, N., et al. (2017). Long-term sequestration of nickel in mackinawite formed by *Desulfovibrio capillatus* upon Fe(III)-citrate reduction in the presence of thiosulfate. *Appl. Geochem.* 80, 143–154. doi: 10.1016/j.apgeochem.2017.02.019

Kanai, T., Imanaka, T., and Atomi, H. (2013). Hydrogen production by the hyperthermophilic archeon *Thermococcus* kodakaraensis. *J. Japan Pet. Ins.* 56, 267–279. doi: 10.1016/j.jbiotec.2004.11.002

Kao, S., Horng, C., Roberts, A., and Liu, K. (2004). Carbon-sulfur-iron relationships in sedimentary rocks from Southwestern Taiwan: Influence of geochemical environment on greigite and pyrrhotite formation. *Chem. Geol.* 203, 153–168. doi: 10.1016/j.chemgeo.2003.09.007

Kish, A., Miot, J., Lombard, C., Guigner, J., Bernard, S., Zirah, S., et al. (2016). Preservation of archaeal surface layer structure during mineralization. *Sci. Rep.* 6:26152. doi: 10.1038/srep26152

Kobori, H., Ogino, M., Orita, I., Nakamura, S., Imanaka, T., and Fukui, T. (2010). Characterization of NADH oxidase/NADPH polysulfide oxidoreductase and its unexpected participation in oxygen sensitivity in an anaerobic hyperthermophilic archaeon. *J. Bacteriol.* 192, 5192–5202. doi: 10.1128/JB.00235-10

Konhauser, K. O. (1998). Diversity of bacterial iron mineralization. *Earth Sci. Rev.* 43, 91–121.

Kormas, L., Tivey, M., Von Damm, K., and Teske, A. (2006). Bacterial and archaeal phylotypes associated with distinct mineralogical layers of a white smoker spire from a deep-sea hydrothermal vent site (9°N, East Pacific Rise). *Environ. Microbiol.* 8, 909–920. doi: 10.1111/j.1462-2920.2005.00978.x

Langmuir, C., Humphris, S., Fornari, D., VanDover, C., VonDamm, K., Tivey, M., et al. (1997). Hydrothermal vents near a mantle hot spot: The Lucky Strike vent field at 37 degrees N on the Mid-Atlantic Ridge. *Earth Planet Sci. Lett.* 148, 69–91.

Le Guillou, C., Bernard, S., De la Peña, F., and Le Brech, Y. (2018). XANES-based quantification of carbon functional group concentrations. *Anal. Chem.* 90, 8379–8386. doi: 10.1021/acs.analchem.8b00689

Lennie, A. R., Redfern, S. A. T., Champness, P. E., Stoddart, C. P., Schofield, P. F. and Vaughan, D. J. (1997). Transformation of mackinawite to greigite; an in situ X-ray powder diffraction and transmission electron microscope study. *Am. Mineral.* 82, 302–309.

Lennie, A. R., Redfern, S. A. T., Schofield, P. F., and Vaughan, D. J. (1995). Synthesis and rietveld crystal structure refinement of mackinawite, tetragonal FeS. *Mineral. Mag.* 59, 677–683. doi: 10.1180/minmag.1995.059.397.10

Li, J. H., Benzerara, K., Bernard, S., and Beyssac, O. (2013). The link between biomineralization and fossilization of bacteria: Insights from field and experimental studies. *Chem. Geol.* 359, 49–69. doi: 10.1016/j.chemgeo.2013.09.013

Li, J. H., Bernard, S., Benzerara, K., Beyssac, O., Allard, T., Cosmidis, J., et al. (2014). Impact of biomineralization on the preservation of microorganisms during fossilization: An experimental perspective. *Earth Planet. Sci. Lett.* 400, 113–122. doi: 10.1016/j.epsl.2014.05.031

Lin, T., Ver Eecke, H., Breves, E., Dyar, M., Jamieson, J., Hannington, M., et al. (2016). Linkages between mineralogy, fluid chemistry, and microbial communities within hydrothermal chimneys from the Endeavour segment, Juan de Fuca ridge. *Geochem. Geophys. Geosyst.* 17, 300–323. doi: 10.1002/2015GC006091

Liu, G., Natarajan, S., and Kim, S. (2005). Photochemical production of oligothiophene and polythiophene micropatterns from 2,5-diiodothiophene on Au in UHV. *Surf. Sci.* 592, 305–309.

Liu, J., Soler, N., Gorlas, A., Krupovic, V., Krupovic, M., and Forterre, P. (2021). Extracellular membrane vesicles and nanotubes in *archaea*. *Microlife* 2:uqab007.

Liu, Y., Beer, L., and Whitman, W. (2012). Sulfur metabolism in *archaea* reveals novel processes. *Environ. Microbiol.* 14, 2632–2644. doi: 10.1111/j.1462-2920.2012.02783.x

Ludford, E., Palmer, M., German, C., and Klinkhammer, G. (1996). The geochemistry of Atlantic hydrothermal particles. *Geophys. Res. Lett.* 23, 3503–3506.

Luther, G., Glazer, B., Hohmann, L., Popp, J., Taillefert, M., Rozan, T., et al. (2001). Sulfur speciation monitored in situ with solid state gold amalgam voltammetric micro-electrodes: Polysulfides as a special case in sediments, microbial mats and hydrothermal vent waters. *J. Environ. Monit.* 3, 61–66. doi: 10.1039/b006499h

Mann, S., Sparks, N. H. C., Frankel, R., Bazylinski, D., and Jannasch, H. W. (1990). Biomineralization of ferromagnetic greigite (Fe3S4) and iron pyrite (FeS2) in a magnetotactic bacterium. *Nature* 343, 258–261.

Miot, J., Benzerara, K., Obst, M., Kappler, A., Hegler, F., Schädler, S., et al. (2009). Extracellular iron biomineralization by photoautotrophic iron-oxidizing bacteria. *Appl. Environ. Microbiol.* 75, 5586–5591. doi: 10.1128/AEM.00490-09

Morikawa, M., Izawa, Y., Rashid, N., Hoaki, T., and Imanakai, T. (1994). Purification and characterization of a thermostable thiol protease from a newly isolated hyperthermophilic *Pyrococcus* sp. *Appl. Environ. Microbiol.* 60, 4559–4566. doi: 10.1128/aem.60.12.4559-4566.1994

Morin, G., Juillot, F., Casiot, C., Bruneel, O., Personné, J.-C., Elbaz- Poulichet, F., et al. (2003). Bacterial formation of tooeleite and mixed arsenic(III) or arsenic(V)-iron(III) gels in the Carnoulès acid mine drainage, France. A XANES, XRD, and SEM study. *Environ. Sci. Technol.* 37, 1705–1712. doi: 10.1021/es025688p

Park, Y., and Faivre, D. (2022). Diversity of microbial metal sulfide biomineralization. *Chempluschem* 87:20.

Picard, A., Gartman, A., and Girguis, P. (2016). What do we really know about the role of microorganisms in iron sulfide mineral formation? *Front. Earth Sci.* 4:68. doi: 10.3389/feart.2016.00068

Picard, A., Gartman, A., and Girguis, P. (2021). Interactions between iron sulfide minerals and organic carbon: Implications for biosignature preservation and detection. *Astrobiology* 21, 587–604. doi: 10.1089/ast.2020.2276

Picard, A., Gartman, A., Clarke, D. R., and Girguis, P. R. (2018). Sulfate-reducing bacteria influence the nucleation and growth of mackinawite and greigite. *Geoch. Cosmochim. Acta* 220, 363–384.

Picard, A., Gartman, A., Cosmidis, J., Obst, M., Vidoudez, C., Clarke, D. R., et al. (2019). Authigenic metastable iron sulfide minerals preserve microbial organic carbon in anoxic environments. *Chem. Geol.* 530, 1–13. doi: 10.1016/j.chemgeo.2019.119343

Posfai, M., Buseck, P., Bazylinski, D., and Frankel, R. (1998). Iron sulfides from magnetotactic bacteria; structure, composition, and phase transitions. *Am. Min.* 83, 1469–1481. doi: 10.2138/am-1998-11-1235

Prieur, D., Erauso, G., Geslin, C., Lucas, S., Gaillard, M., Bidault, A., et al. (2004). Genetic elements of *Thermococcales*. *Biochem. Soc. Trans.* 32, 184–187. doi: 10.1042/bst0320184

Ravel, B., and Newville, M. (2005). ATHENA, ARTEMIS, HEPHAESTUS: Data analysis for X-ray absorption spectroscopy using IFEFFIT. *J. Synchrotron. Rad.* 12, 537–541. doi: 10.1107/S0909049505012719

Redhammer, G. J., Tippelt, G., Roth, G., Lottermoser, W., and Amthauer, G. (2000). Structure and mossbauer spectroscopy of barbosalite $Fe^{2+}Fe3^{+2}$ $(PO_4)_2(OH)_2$ between 80 K and 300 K. *Phys. Chem. Min.* 27, 419–429. doi: 10.1007/s0026999 00078

Rettig, S. J., and Trotter, J. (1987). Refinement of the structure of orthorhombic sulfur, α -S8. *Acta Cryst.* 43, 2260–2262. doi: 10.1107/S0108270187088152

Rickard, D. (1997). Kinetics of pyrite formation by the H_2S oxidation of iron (II) monosulfide in aqueous solutions between 25 and 125°C: The mechanism. *Geochim. Cosmochim. Acta* 61, 135–147. doi: 10.1016/S0016-7037(96)00322-5

Rickard, D., and Luther, G. W. (2007). Chemistry of iron sulfides. *Chem. Rev.* 107, 514–562.

Rouxel, O., Fouquet, Y., and Ludden, J. N. (2004). Subsurface processes at the Lucky Strike hydrothermal field, mid-atlantic ridge: Evidence from sulfur, selenium, and iron isotopes. *Geochim. Cosmochim. Acta* 68, 2295–2311.

Schiffbauer, J., and Xiao, S. (2009). Novel application of focused ion beam electron microscopy (FIB-EM) in preparation and analysis of microfossil ultrastructures: A new view of complexity in early Eukaryotic organisms. *PALAIOS* 24, 616–626.

Schmid-Beurmann, P. (2000). Synthesis and phase characterization of a solid solution series between β-$Fe_2(PO_4)O$ and $Fe_4(PO_4)_3(OH)_3$. *J. Solid State Chem.* 153, 237–247.

Schmidt, K., Koschinsky, A., Garbe-Schonberg, D., de Carvalho, L. M., and Seifert, R. (2007). Geochemistry of hydrothermal fluids from the ultramafic-hosted Logatchev hydrothermal field, 15 degrees N on the Mid-Atlantic Ridge: Temporal and spatial investigation. *Chem. Geol.* 242, 1–21.

Schrenk, M., Kelley, D., Delaney, J., and Baross, J. (2003). Incidence and diversity of microorganisms within the walls of an active deep-sea sulfide chimney. *Appl. Environ. Microbiol.* 69, 3580–3592. doi: 10.1128/AEM.69.6.3580-3592.2003

Schut, G., Boyd, E., Peters, J., and Adams, M. (2013). The modular respiratory complexes involved in hydrogen and sulfur metabolism by heterotrophic *hyperthermophilic archaea* and their evolutionary implications. *FEMS Microbiol. Rev.* 37, 182–203. doi: 10.1111/j.1574-6976.2012.00346.x

Schut, G., Bridger, S., and Adams, M. (2007). Insights into the metabolism of elemental sulfur by the hyperthermophilic archaeon *Pyrococcus furiosus*: Characterization of a coenzyme A-dependent NAD(P)H sulfur oxidoreductase. *J. Bacteriol.* 189, 4431–4441. doi: 10.1128/JB.00031-07

Soler, N., Krupovic, M., Marguet, E., and Forterre, P. (2008). Membrane vesicles in natural environments: A major challenge in viral ecology. *ISME J.* 9, 793–796. doi: 10.1038/ismej.2014.184

Stanjek, H., and Schneider, J. (2000). Anisotropic peak broadening analysis of a biogenic soil greigite (Fe_3S_4) with Rietveld analysis and single peak fitting. *Am. Mineral.* 85, 839–846.

Stanley, W., and Southam, G. (2018). The effect of grampositive (*Desulfosporosinus orientis*) and gram-negative (*Desulfovibrio desulfuricans*) sulfate-reducing bacteria on iron sulfide mineral precipitation. *Can. J. Microbiol.* 64, 629–637. doi: 10.1139/cjm-2017-0545

Stein, C., and Stein, S. (1994). Constraints on hydrothermal Heat-Flux through the oceanic lithosphere from global heat-flow. *J. Geophys. Res.* 99, 3081–3095.

Swaraj, S., Stanescu, S., Rioult, M., Besson, A., and Hitchcock, A. P. (2017). Performance of the HERMES beamline at the carbon K-edge. *J. Phys.* 849:012046.

Takai, K., Komatsu, T., Inagaki, F., and Horikoshi, K. (2001). Distribution of *archaea* in a black smoker chimney structure. *Appl. Environ. Microbiol.* 67, 3618–3629. doi: 10.1128/AEM.67.8.3618-3629.2001

Templeton, A., Knowles, E., Eldridge, D., Arey, B., Dohnalkova, A., Webb, S., et al. (2009). A seafloor microbial biome hosted within incipient ferromanganese crusts. *Nat. Geosci.* 2, 872–876. doi: 10.1038/ngeo696

Thiel, J., Byrne, J., Kappler, A., Schink, B., and Pester, M. (2019). Pyrite formation from FeS and H_2S is mediated through microbial redox activity. *Proc. Natl. Acad. Sci. U.S.A.* 116, 6897–6902. doi: 10.1073/pnas.1814412116

Tivey, M. (1995). The influence of hydrothermal fluid composition and advection rates on black smoker chimney mineralogy: Insights from modelling transport and reaction. *Geochim. Cosmochim. Acta* 59, 1933–1949. doi: 10.1016/0016-7037(95) 00118-2

Von Damm, K. L. (1995). "Controls on the chemistry and temporal variability of seafloor hydrothermal fluids," in *Seafloor hydrothermal systems: Physical, chemical, biological, and geological interactions*, eds S. Humphris, R. Zierenberg, L. Mullineaux, and R. Thomson (Washington, DC: American Geophysical Union), 222–247. doi: 10.1029/GM091p0222

Waite, T., Moore, T., Childress, J., Hsu-Kim, H., Mullaugh, K., Nuzzio, D., et al. (2008). Variation in sulfur speciation with shellfish presence at a Lau Basin diffuse flow vent site. *J. Shellfish Res.* 27, 163–168. doi: 10.2983/0730-8000(2008)27[163:VISSWS] 2.0.CO;2

Wang, J., Morin, C., Li, L., Hitchcock, A. P., Scholl, A., and Doran, A. (2009). Radiation damage in soft X-ray microscopy. *J. Electron Spectros. Relat. Phenomena* 170, 25–36.

Webb, S. M. (2005). SIXpack: A graphical user interface for XAS analysis using IFEFFIT. *Phys. Scr.* 115:1011. doi: 10.1238/Physica.Topical.115a01011

Wheat, C., Jannasch, W., Plant, J., Moyer, C., Sansone, F., and McMurtry, G. (2000). Continuous sampling of hydrothermal fluids from Loihi Sea mount after the 1996 event. *J. Geophys. Res. Earth* 105, 19353–19367. doi: 10.1029/2000JB90 0088

Wilfert, P., Meerdink, J., Degaga, B., Temmink, H., Korving, L., Witkamp, G. J., et al. (2020). Sulfide induced phosphate release from iron phosphates and its potential for phosphate recovery. *Water Res.* 171:115389.

Wilkin, R., and Barnes, H. (1996). Pyrite formation by reactions of iron monosulfides with dissolved inorganic and organic sulfur species. *Geochim. Cosmochim. Acta* 60, 4167–4179. doi: 10.1016/S0016-7037(97)81 466-4

Xiong, Y., Guilbaud, R., Peacock, C. L., Cox, R. P., Canfield, D. E., Krom, M. D., et al. (2019). Phosphorus cycling in Lake Cadagno, Switzerland: A low sulfate euxinic ocean analogue. *Geochim. Cosmochim. Acta* 251, 116–135.

Yuan, Y., Wang, L., and Gao, L. (2020). Nano-sized iron sulfide: Structure, synthesis, properties, and biomedical applications. *Front. Chem.* 8:818. doi: 10.3389/fchem.2020. 00818

frontiers | Frontiers in Microbiology

TYPE Review
PUBLISHED 02 June 2023
DOI 10.3389/fmicb.2023.1167718

OPEN ACCESS

EDITED BY
Andreas Teske,
University of North Carolina at Chapel Hill, United States

REVIEWED BY
Anirban Chakraborty,
Idaho State University, United States
Melanie R. Mormile,
Missouri University of Science and Technology, United States

*CORRESPONDENCE
Alexandre Soares Rosado
✉ alexandre.rosado@kaust.edu.sa

RECEIVED 16 February 2023
ACCEPTED 09 May 2023
PUBLISHED 02 June 2023

CITATION
Schultz J, Modolon F, Peixoto RS and Rosado AS (2023) Shedding light on the composition of extreme microbial dark matter: alternative approaches for culturing extremophiles.
Front. Microbiol. 14:1167718.
doi: 10.3389/fmicb.2023.1167718

Shedding light on the composition of extreme microbial dark matter: alternative approaches for culturing extremophiles

Júnia Schultz[1,2], Flúvio Modolon[1,3], Raquel Silva Peixoto[1,2] and Alexandre Soares Rosado[1,2]*

[1]Red Sea Research Center, King Abdullah University of Science and Technology, Thuwal, Saudi Arabia, [2]Computational Bioscience Research Center, King Abdullah University of Science and Technology, Thuwal, Saudi Arabia, [3]Laboratory of Molecular Microbial Ecology, Institute of Microbiology, Federal University of Rio de Janeiro, Rio de Janeiro, Brazil

More than 20,000 species of prokaryotes (less than 1% of the estimated number of Earth's microbial species) have been described thus far. However, the vast majority of microbes that inhabit extreme environments remain uncultured and this group is termed "microbial dark matter." Little is known regarding the ecological functions and biotechnological potential of these underexplored extremophiles, thus representing a vast untapped and uncharacterized biological resource. Advances in microbial cultivation approaches are key for a detailed and comprehensive characterization of the roles of these microbes in shaping the environment and, ultimately, for their biotechnological exploitation, such as for extremophile-derived bioproducts (extremozymes, secondary metabolites, CRISPR Cas systems, and pigments, among others), astrobiology, and space exploration. Additional efforts to enhance culturable diversity are required due to the challenges imposed by extreme culturing and plating conditions. In this review, we summarize methods and technologies used to recover the microbial diversity of extreme environments, while discussing the advantages and disadvantages associated with each of these approaches. Additionally, this review describes alternative culturing strategies to retrieve novel taxa with their unknown genes, metabolisms, and ecological roles, with the ultimate goal of increasing the yields of more efficient bio-based products. This review thus summarizes the strategies used to unveil the hidden diversity of the microbiome of extreme environments and discusses the directions for future studies of microbial dark matter and its potential applications in biotechnology and astrobiology.

KEYWORDS

extremophiles, extreme environments, microbial cultivation, applied microbiology, culturomics

1. Introduction

Although extreme environments are complex and inhospitable, they often harbor a high microbial diversity (Shu and Huang, 2022). Extensive efforts have been made to fully characterize and describe novel extremophilic microbes and their metabolic functions in these harsh conditions using culture-dependent techniques (Vester et al., 2015; Topçuoglu and Holden, 2019; Sood et al., 2021; Schultz et al., 2022b). However, although there has been enormous progress in the isolation and culture of extremophiles, most of these microorganisms cannot be cultivated and fail to grow in conventional laboratory settings. Recent studies have estimated

that 80% of microbial taxa remain uncultured (Lloyd et al., 2018) and 85% of the phylogenetic diversity of prokaryotes consists of yet-to-be-cultured taxa (Nayfach et al., 2021). Although there is no consensus regarding the percentage of the culturable fraction of prokaryotes and eukaryotes, most taxa, including extremophiles, clearly lack cultivated representatives. In turn, these yet-to-be-cultured taxa are termed "microbial dark matter" (Marcy et al., 2007; Rinke et al., 2013).

In view of the metabolic adaptations required for extremophiles to thrive in the severe conditions of extreme environments, studies on these organisms can expand our knowledge of the origin of life (on our planet and beyond), evolution, ecology, physiology, and biotechnology. However, the first step toward unlocking the full potential of extremophiles is to overcome the challenge of culturing them. In order to obtain pure cultures and fully understand the inadequately exploited cultured extremophiles, developing innovative culturing methods is crucial (Vartoukian et al., 2010; Bull and Goodfellow, 2019). Several old and recently developed techniques and strategies have been applied to isolate previously uncultured microbes from extreme habitats, such as prolonging incubation times (Davis et al., 2005; de Jesus et al., 2015; Pulschen et al., 2017), using different concentrations of oxygen and other gases (Lopez et al., 2019; Volpiano et al., 2021), using low-nutrient culture media (Do Carmo et al., 2011; Peixoto et al., 2011; Grzesiak et al., 2015; Pulschen et al., 2017), adding antibiotics to inhibit fast-growing microorganisms and prevent contamination with unwanted microbial groups (Bender et al., 2020), changing the gelling agent, e.g., gellan gum (Das et al., 2015), or using a cellulose plate (Tsudome et al., 2009) instead of agar, *in situ* diffusion devices (Nichols et al., 2010; Palma Esposito et al., 2018), and cell-targeting methods (Huber et al., 2000; Antunes et al., 2008a). However, although these alternative strategies may yield new microbes, most of the microbes presumed to occur in extreme environments remain uncultured.

This review summarizes methods and technologies used to recover the microbial diversity of extreme environments (often involving multiple extreme conditions; Figure 1) and discusses the advantages and disadvantages of each of these approaches (see Table 1). Additionally, we describe alternative culturing strategies to retrieve novel taxa and reveal previously unknown genes, metabolic processes, ecological roles, and more efficient bio-based products. Therefore, this study provides a comprehensive synthesis of the strategies used to unveil the hidden microbial diversity in extreme environments, while also suggesting further directions and improvements to make new discoveries and shed light on the microbial dark matter thriving in extreme environments.

2. Strategies to access extreme microbiomes

Culture-dependent and -independent methods are widely used to gain insights into the ecology, physiology, microbial interactions and dynamics, and functional roles of the culturable fraction of microbiome members. These techniques mainly use standardized methods, with nutrient-rich culture media and standard pH, salinity, oxygen, and temperature parameters. Alternative approaches have been used in an attempt to cultivate hard-to-culture microbes by varying the cultivation settings (Pulschen et al., 2017; Lagier et al., 2018), *in situ* cultivation, using diffusion-based devices (Steinert et al., 2014; Berdy et al., 2017), and a combination of the aforementioned technologies.

Cultivation-independent techniques enable the study of the overall function and activity of microbial communities in the environment and have allowed for the identification of novel bacterial groups and the assessment of the biotechnological potential of microbial communities by identifying useful pathways and genes (Sysoev et al., 2021). The number of known taxa can also be further expanded by omitting culture steps. Zamkovaya et al. (2021) recently demonstrated that the members of the microbial "dark matter" from different environments (including extremes) play key roles in ecological networking within their respective communities.

Recently, Shu and Huang (2022) made a substantial effort to summarize the current state of the characterization of prokaryotes inhabiting the major extreme environments on Earth. Data from culture-independent methods provided insights regarding the microbial composition and diversity of complex environments. For instance, hot springs (water and sediment) are dominated by the phyla Aquificae, Proteobacteria, and Crenarchaeota, whereas Proteobacteria is the dominant phylum in the deep sea and the archaeal phylum Crenarchaeota is the most abundant in hypersaline habitats. Prokaryotes in the cryosphere (glaciers and permafrost) are diverse, particularly the phyla Proteobacteria, Chloroflexi, and Actinobacteria. Diversity surveys using marker genes and genome-resolved metagenomics have unveiled a vast range of previously unknown microorganisms in extreme environments, thus substantially expanding the phylogenetic breadth and genome representation of the tree of life (Hug et al., 2016; Shu and Huang, 2022). However, the understanding of their physiology and ecology is hampered by the lack of pure cultures (Hedlund et al., 2015). The lack of cultured representatives of many of the known microbial taxa reinforces the need for more efficient tools to culture these organisms, especially given that many play key functional roles in communities (e.g., biogeochemical cycles) in extreme environments and are important to explain the origin and evolutionary processes of microorganisms (Merino et al., 2019; Martínez-Espinosa, 2020). Here, we describe the factors that strongly influence the culturability of extremophiles in laboratory conditions, highlighting the main techniques and strategies used to culture these microbes.

2.1. Sample processing

Sample processing interferes with the culturability of the microbial community from any environment. This problem can be even more challenging for samples from extreme environments. The first step to successfully culture extremophiles, as with any other microbe (Bellali et al., 2019; Schultz et al., 2022a), is to effectively detach the microbial cells from the sample substrate. Using three different resuspension buffers (Ringer's solution, PBS, and sterile cave water, pH 8.2) for rocks from cave samples, Bender et al. (2020) identified the largest number of colonies and diverse phenotypes in water. This suggests that suspension solutions buffered to physiological conditions (i.e., pH, sodium, and potassium) should be effective in increasing microbial culturability (Padan et al., 2005). For extremophiles, resuspending samples in sterilized water obtained from a given environment or suspensions using a buffer that is geochemically similar to the environment could be the best option, as osmotic stress and low salinity may induce a viable but non-culturable state in bacteria (Gin and Goh, 2013; Li et al., 2014; Dong et al., 2020). Sprinkling portions of the sample onto Petri dishes containing culture

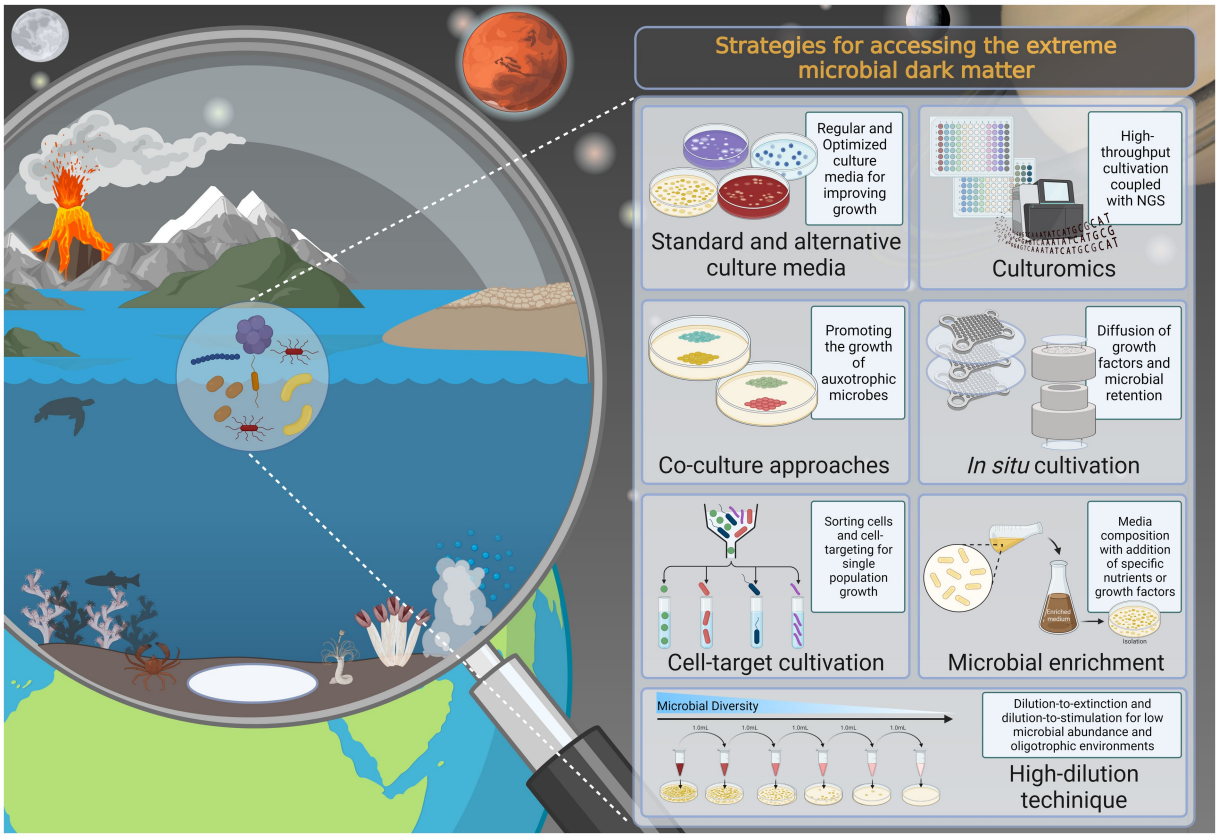

FIGURE 1
Overview of the current knowledge of standard and alternative culture-dependent approaches that can be applied for culturing microbiomes from extreme environments and unveiling the members of the extreme microbial dark matter, in addition to enabling the culture of uncultivated extremophiles. The figure was created by the authors using Biorender.com.

media (e.g., R2A and MA media) could be an alternative to resuspension and could eventually increase the recovery of different and more-pigmented microbial morphotypes compared to classical serial dilution, as reported by Paulino-Lima et al. (2016), who cultured bacteria from sand samples collected from the Atacama Desert.

Extreme environments are usually remote, difficult to access, and far from the laboratory. Processing time and primary incubation after sampling also directly impact culturability. Bender et al. (2020) evaluated the significance of crushing and plating the samples immediately after sampling versus 6 h later. When sample processing was delayed, the number of colonies and their diversity were sharply reduced (Bender et al., 2020). Similarly, Bellali et al. (2019) described the negative impact of delaying the processing and first cultivation of gut microbiota, as the viability and diversity of microbes were significantly reduced when sample processing was delayed for increasingly long periods.

2.2. Moving forward: advances in microbial cultivation

In the early 1980s, Staley and Konopka described the discrepancy between the total number of microbial cells in an environmental sample and the culturable population of that sample as the "great plate count anomaly." Only a small fraction of the true microbial diversity and cell abundance in any environment can be retrieved by culturing (Nichols et al., 2008), whereas the remaining microbes are recalcitrant to cultivation (Joint et al., 2010). Classical methods include using nutrient-rich or nutrient-poor culture media coupled with standard incubation times, pH, salinity, oxygen, and temperature (Pulschen et al., 2017; Schultz et al., 2022a). However, these methods appear to work best for fast-growing organisms, which represent only a small fraction of natural microbial communities (Pham and Kim, 2012; Sysoev et al., 2021).

Cultivation-based tools are still paramount to achieve a comprehensive understanding of the biology, ecology, and bioactivity of extremophiles, and are essential for future bioprospecting and other applications (Joint et al., 2010). The value of culturing the extremosphere microbiome is undeniable. For example, cultivation has enabled the discovery of several widely used enzymes (Chien et al., 1976; Mesbah, 2022) and has provided valuable insights into the origin and evolution of life on Earth (Merino et al., 2019; Thombre et al., 2020), in addition to providing a means to evaluate the prospect of extraterrestrial life, planetary protection, and space exploration (Cavicchioli, 2002; Carré et al., 2022; Blachowicz et al., 2022). For this reason, there is a growing interest in culturing and recovering a larger proportion of extremophilic microorganisms from a sample, and this can be achieved by improving cultivation methods. The use of alternative approaches such as different cultivation settings (Song et al., 2009), the formulation of new culture media (Tyson et al., 2005; Ñancucheo et al., 2016), complex microfluid and laser manipulation systems (Imachi et al., 2011), filters and membrane systems to simulate

TABLE 1 Summary of the main strategies to improve the culturability and isolation of extremophilic microorganisms from extreme environments.

Strategy	Approach	Microbial target	Previous uses	Advantages	Disadvantages	References
Culture media and incubation settings for microbial growth	Standard and alternative culture media, modifications of composition and incubation conditions	Generalist and specialized microorganisms	Environmental and clinical microbes. Commonly used for cultivation of microbes from extreme environments	-Easy formulation and manipulation -Established methods and commercial options -Low cost -The equipment is not necessarily complex	Cultivation bias of isolating more members of Proteobacteria, Firmicutes, Bacteroidetes and Actinobacteria	Landreau et al. (2016); Kurm et al. (2019); Pulschen et al. (2018); Yasir et al. (2019); Bender et al. (2020); Gómez-Acata et al. (2021); Molina-Menor et al. (2021)
	Enriched culture	Generalist and specialized microorganisms	Environmental and clinical microbes. Commonly used for Archaea	-Enrichment of wanted groups by manipulating the conditions (e.g., adding inhibitors or growth factors) -Separation of specific species from a mixed community	-Long incubation period -In some cases, lack of pure cultures	Bae et al. (2005); Könneke et al. (2005); Klein et al. (2022)
	Co-culture	Autotrophic and syntrophic microbes	Environmental and clinical microbes	-Microbial interactions -Growth of microbes that depend on specific (sometimes unknown) compounds generated by other microorganisms -Low cost	-May require optimization for some requirements -Lack of pure cultures	Plugge and Stams (2002); Stewart et al. (2012); Sánchez-Andrea et al. (2018); Pillot et al. (2020)
	Culturomics	Generalist and selective microorganisms	Environmental microbes and human gut microbiota	-High-throughput isolation -Multiple and simultaneous microbial growth under different conditions	-Labor-intensive. Large numbers of samples and data to process -Significant cost	Lagier et al. (2012); Khelaifia et al. (2018); Yasir et al. (2019); Sood et al. (2021)
Diffusion-based devices and *in-situ* cultivation	Cultivation chambers	Generalist microbes	Microorganisms from soil, marine environments, activated sludge	-*In situ* cultivation -Small, low-cost device	Competition between cells may occur in the chamber, leading to selectivity	Kaeberlein et al. (2002); Bollmann and Lewis (2007)
	Isolation chips	Generalist microbes	Environmental microbes	-High-throughput cultivation -*In-situ* cultivation -Easy observation of colonies under a microscope	Difficulty of loading cells into the chip wells	Nichols et al. (2010); Berdy et al. (2017)
	Multiwell microbial culture chip	Generalist microbes	Environmental microbes	-High cultivation efficiency - High-throughput screening for phenotypes and microbial products -Rapid changes in environment and analysis under a variety of culture conditions	Difficult to pick and recover microcolonies from the wells	Ingham et al. (2007)

(Continued)

TABLE 1 (Continued)

Strategy	Approach	Microbial target	Previous uses	Advantages	Disadvantages	References
	Hollow-fiber membrane-based chamber	Generalist and specialized microorganisms	Environmental microbes	-Simple handling -Rapid molecular exchange	-Oversize device -Culture of microbes from surface water layer	Aoi et al. (2009); Fu et al. (2017)
	Paper-based analytical device	Generalist microbes	Environmental, human and clinical microbes	-Multifunctional, used for biological and chemical purposes -Low cost -Efficient for clinical diagnostics	Selective growth of well-known cultured microbes	Kim and Yeo (2016); Noiphung and Laiwattanapaisal (2019); Levy et al. (2020)
Targeted cell-sorting and cultivation	Reverse genomics	Targeted microbial groups	Human oral microbiome	Isolation and cultivation of targeted microbes	-Significant cost -Use of different robust equipment -Required technical abilities	Cross et al. (2019); Ibrahim et al. (2022)
	FACS	Targeted microbial groups	Environmental and clinical microbes	Isolation and cultivation of targeted microbes	-Not compatible for anaerobe growth -In some cases, it is not possible to culture	Alvarez-Barrientos et al. (2000); Zengler et al. (2002); Espina et al. (2022)
	Live-FISH	Targeted microbial groups	Marine microbes	-Isolation and cultivation of targeted microbes -No sophisticated probe design is required	-Advances skills in fluorescence due to variations in fluorescent signals can decrease the detectability of some microorganisms	Batani et al. (2019)
	Micromanipulators and laser manipulation system	Generalist and selective microorganisms	Marine microbes, human cells, microorganisms from deep-sea brine pools and hydrothermal systems	-Selection of cells of interest from a mixed microbial community -Pure colonies obtained by sorting cells with microscope	-Required technical abilities -Laser manipulation	Huber et al. (1995); Huber et al. (2000); Antunes et al. (2008a,b)

the natural environment (Ferrari et al., 2008; Benaud et al., 2022), co-culture approaches (Nichols et al., 2008; Shaw et al., 2020), and *in situ* cultivation using diffusion-based devices (Kaeberlein et al., 2002; Nichols et al., 2010; Pope et al., 2022) could overcome challenges in mimicking the natural environment and isolating hard-to-culture microbes (Figure 1; Table 1).

2.2.1. All-you-can-eat: standard and alternative culture media and growth conditions

To effectively cultivate a given microorganism, its physiological and metabolic needs must first be addressed (Leadbetter, 2003). These factors are especially important in feeding extremophiles. An all-you-can-eat buffet of amino acids and sugars, such as those found in standard media formulations, is not necessarily the best approach. The most basic approach used to culture microbes from different sources (e.g., extreme environments) is the use of conventional nutrient-rich culture media (e.g., tryptic soy broth, lysogen broth, marine broth, nutrient broth, etc.). New materials may revolutionize microbiology by improving access to organisms that were previously recalcitrant to culture. The design of alternative media may increase the number of different microorganisms, including modification of culture medium composition, the addition of specific chemicals and promoters, depleting carbon sources, and altering the gelling agent. However, this requires in-depth insights into the nature and characteristics of the samples to better understand the factors that determine bacterial growth (Pham and Kim, 2012).

Hamaki et al. (2005) developed an innovative soil-extract agar medium in an effort to mimic the characteristics of the soil environment and cultivate soil microbes. This newly developed synthetic medium enabled the growth of novel bacteria (Actinomycetes) due to the presence of soil constituents that are required for the growth of some groups of microorganisms. Gómez-Acata et al. (2021) used a soil-extract agar medium to recover 37 haloalkaliphilic strains from volcanic samples. Most of the samples collected in extreme environments have a low level of organic carbon. Excessive amounts of carbon in conventional culture media can interfere with microbial growth, and therefore reducing the organic-carbon input might be an effective strategy for bacterial culture, particularly for oligotrophic taxa (Kurm et al., 2019; Bender et al., 2020). The same is true for nutrient concentrations (Reasoner and Geldreich, 1985). Extreme environments tend to be nutrient-poor, and the large amounts of nutrients in rich culture media can induce a high-nutrient shock and impair the growth of microorganisms that inhabit stressful

low-nutrient environments. This problem led to the development of the low-nutrient R2A culture medium, which is extensively used in cultivating extremophiles (Reasoner and Geldreich, 1985; Bendia et al., 2018; Kusuma et al., 2022). Using low-nutrient media (usually diluting standard culture media), Pulschen et al. (2017) and Molina-Menor et al. (2021) were able to retrieve microorganisms belonging to rare or recently described genera and to cultivate previously uncultured Antarctic and European desert bacteria, respectively.

The gelling agent is also an important but often overlooked factor that can strongly influence microbial culturability, and is a key driver of the structure of different cultured communities (Mac Rygaard et al., 2017). Agar is the most commonly used gelling agent. However, there are other compounds with similar gelling properties, including xanthan gum, carrageenan, isubgol, and gellan gum. These polymers can be used to culture organisms that grow poorly or not at all on agar and may increase their growth rates (Das et al., 2015). Agar is derived from a group of red marine algae (genera *Gelidium* and *Gracilaria*) and has been used in microbiology since 1882 (Hitchens and Leikind, 1939). Gellan gum is an extracellular polysaccharide secreted by the bacterium *Sphingomonas elodea*. This compound is commercially manufactured by a fermentation process and possesses unique colloidal and gelling properties, a good ability to form coatings, and high clarity (Das et al., 2015). Due to its high thermal stability, gellan gum has been used to culture (hyper)thermophiles (Shungu et al., 1983; Landreau et al., 2016). Several studies have reported that gellan gum improves the culturability of certain microorganisms. For instance, Sari et al. (2020) cultivated rare thermophilic Actinobacteria; Landreau et al. (2016) cultured several anaerobic (hyper)thermophilic marine microbes; and Ferrari et al. (2008) isolated and studied previously unculturable bacteria from soil using an alternative gelling gum. Regarding acidophiles, Johnson (1995) found that agarose or gellan gum must be used instead of agar, as agar is prone to hydrolysis in low pH conditions. Moreover, the gelling agent must be sterilized separately and later combined with the acidic medium components. Johnson (1995) also found that culturing of heterotrophic acidophiles is improved when they are grown in a double-layer overlay solid medium. The use of polycarbonate filters floating on an acidic liquid medium containing ferrous sulfate enables the growth of acidophiles on a solid medium (de Bruyn et al., 1990). These examples demonstrate the importance of selecting the optimal gelling agent for a particular purpose, especially when culturing extremophiles. In another example, Tsudome et al. (2009) described the advantages of a matrix made of nanofibrous cellulose instead of agar, which is more stable, even at temperatures exceeding 100°C.

In an attempt to grow unculturable microbes, microbiologists also often change the growth conditions, such as the incubation period, inoculum size, temperature, pH, and atmosphere (CO_2/O_2 level). By applying a combination of simple techniques such as low temperatures (12°C) and a long incubation period (up to 15 weeks), Pulschen et al. (2017) increased the culturable diversity and recovered previously uncultured microorganisms, thus revealing a rare bacterial diversity in a soil sample from Antarctica. Additionally, the plates were incubated in the dark and in polyethylene bags to prevent drying. Similarly, prolonged incubation (3 months) was crucial for the growth of rarely isolated phyla of soil microbes (Davis et al., 2005; Steven et al., 2007). Burns et al. (2004) obtained an increased diversity of Haloarchaea with incubation times as long as 12 weeks. Extended incubation times (more than 8 months) yielded the highest diversity of cultured bacteria and unknown species from a cold and alkaline environment (Vester et al., 2013).

Different culture-based strategies can be applied for slow-growing bacteria, especially due to the bias toward the cultivation of fast-growing bacteria. For instance, recovery of slower-growing species can be improved by adding low concentrations of antibiotics (e.g., chloramphenicol, amphotericin B, and nalidixic acid), which will slow down or completely inhibit the growth of opportunistic fast-growing species with flexible metabolisms (Alain and Querellou, 2009). Weissman et al. (2021) compared the growth rates of cultivated and uncultivated organisms to illustrate how culture collections are strongly biased toward organisms capable of rapid growth. The authors found that organisms naturally group into two growth classes and observed a bias in growth predictions for extremely slow-growing organisms. In an effort to recover slow-growing bacteria from hot springs, Yasir et al. (2019) used low-nutrient media supplemented with water from each respective hot spring. The authors also added amphotericin B to the medium to prevent fungal contamination and supplemented it with ascorbic acid to support the growth of anaerobic bacteria in an aerobic environment. With these adaptations, 536 strains affiliated with 139 distinct species were isolated after 15 days of incubation. From cave samples, Bender et al. (2020) evaluated the effect of antibiotics on culturability, preparing media with and without 10 μg/mL chloramphenicol and nalidixic acid, and observed inhibition of the growth of rapidly growing species and a statistically significant increase in colony counts. For the cultivation of extreme halophiles, Robinson et al. (2005) obtained higher diversity when the solid medium was supplemented with penicillin.

A novel strategy termed "selective medium-design algorithm restricted by two constraints" (SMART) was developed by Kawanishi et al. (2011). This method for the culture of a target microorganism from a complex environment is based on two selective agents: (i) a carbon source, enabling proliferation of the target microorganism, and (ii) antimicrobials, suppressing unwanted microorganisms in the medium. The authors were able to successfully grow only the intended microbes and effectively suppress the growth of unwanted microorganisms. Likewise, the SMART approach allowed for the isolation of the fish pathogen *Edwardsiella tarda*, which was inoculated into a culture medium containing a mixture of other fish pathogens (Yamamoto et al., 2017). However, additional tests using the SMART approach in microbial cultures from extreme environments are needed to confirm the potential of this alternative method to culture extremophiles.

2.2.2. Enrichment as a strategy to increase culture diversity

In microbial cultivation, enriched media are commonly used to facilitate the growth of certain microbes with specific metabolic requirements that are not supplied (and/or could be inhibited) by conventional culture methods. One example is the cultivation of archaeons, which commonly requires extreme conditions, and the enrichment step must use specific molecules to mimic environmental conditions. These requirements include physical and chemical conditions besides growth factors, such as energy and nutrient sources (Sun et al., 2020). For instance, archaeons from the phyla Thaumarchaeota and Crenarchaeota have been successfully grown by using ammonia as an electron donor (Könneke et al., 2005), as they oxidize ammonia to nitrite as a primary energy source.

Enrichment is another strategy that has also allowed for the culture of Asgardarchaeal members. Imachi et al. (2020) have succeeded in culturing an Asgard archaeon, *Candidatus* Prometheoarchaeum syntrophicum strain MK-D1, from deep marine sediment. This strain was characterized as a syntrophy between either a methanogenic archaeon, a sulfate-reducing deltaproteobacterium, or both. Moreover, the authors reported that the archaeon grows very slowly, taking over a decade for enrichment. The cultivation of *Ca. P. syntrophicum* was crucial to rest criticisms regarding their existence since their first discovery from binning metagenome-assembled genomes (MAGs; López-García and Moreira, 2020). Later, Rodrigues-Oliveira et al. (2023) reported a highly enriched culture of *Candidatus* Lokiarchaeum ossiferum, another member of the Asgard phylum. This species grew anaerobically at 20°C in the presence of organic carbon sources and exhibited a significantly larger genome compared with the single previously cultivated Asgard strain (Imachi et al., 2020). Additionally, enrichment is a great strategy to culture methane- and alkane-oxidizing microbial consortia. To achieve this, a sample of the target environment (e.g., soil, sediment, or water) is collected and then placed in a suitable growth medium that contains methane or alkane as the sole source of carbon and energy, after which the media is adjusted to the required temperature. Over time, the microbial community will adapt to the new conditions, and the methane- and alkane-oxidizing consortia will enrich and become more abundant (Holler et al., 2011; Dowell et al., 2016). For example, Holler et al. (2011) were able to enrich a consortium of anaerobic methane-oxidizing archaea of the ANME-1 lineage consortia and the deltaproteobacterial HotSeep-1 cluster, which were thriving under thermophilic enrichment conditions.

Unknown growth factors could be supplemented using raw extracts from the original source (Schultz et al., 2022a). Some microbes use cell components of other microbes as growth factors and microbial extracts could enhance the cultivation of these extremophiles (Bae et al., 2005). However, depending on the nature of the sample, the extruded components can be toxic to some microbes after extraction or sterilization. Overgrowth of other (unwanted) microbes such as generalist bacteria or fungi may also inhibit the growth of archaea. Extremophile microorganisms generally exhibit slow growth rates and cannot be easily differentiated based on colony morphology. Additionally, these microorganisms are often inhibited by competition or by specific components of a culture medium (Sun et al., 2020; Klein et al., 2022). To inhibit the overgrowth of such unwanted microbes, antibiotics could be added to the culture medium (see topic 2.2.1). Once the enrichment steps are successfully carried out, isolation could be performed in some cases.

2.2.3. High-dilution techniques

High-dilution strategies are commonly used for culturing microorganisms from very low abundance samples, including soil, seawater, or other environmental samples. The basic principle of high-dilution culturing is to serially dilute the given sample until individual cells or colonies can be isolated from separate cultures (Button et al., 1993; Connon and Giovannoni, 2002). This technique is useful for studying microbial diversity and physiology in environments with low microbial abundance.

In seawater, for instance, oligotrophic and ultra-oligotrophic prokaryotes are typically found in very low abundance, making them difficult to study. However, high-dilution approaches have been used to successfully cultivate these organisms (Rappé et al., 2002; Cho and Giovannoni, 2004; Henson et al., 2016). The "dilution-to-extinction" method involves serially diluting mixed culture samples to the point where individual cells are isolated (Button et al., 1993). This technique has been used to cultivate a wide range of oligotrophic bacteria and archaea from seawater and later utilized to cultivate groundwater (Connon and Giovannoni, 2002) and lake water (Salcher et al., 2015) bacterioplankton. Using this approach, previously uncultured marine oligotrophic bacterioplankton, including the predominant SAR11 clade (*Candidatus* Pelagibacter; Rappé et al., 2002; Song et al., 2009), the SAR 116 clade (*Candidatus* Puniceispirillum; Henson et al., 2016), the OM43 clade (Giovannoni et al., 2008), the OM60 clade (Cho et al., 2007), the SUP05 clade (Spietz et al., 2019), and the oligotrophic marine Gammaproteobacteria group (Cho and Giovannoni, 2004), have been successfully cultivated in a laboratory setting and their physiologies and genomes have been successfully investigated. Additionally, the "dilution-to-extinction" technique has been used for the isolation of ammonia-oxidizing bacteria (e.g., *Nitrosospira* spp. and *Nitrosomonas* spp.) from soil samples (Aakra et al., 1999), as well as for the isolation of thermophilic piezophiles (Kato, 2011).

The "dilution-to-stimulation" method is another strategy that involves adding a small amount of nutrients to seawater samples before diluting them (Ho et al., 2012). This approach has been used to successfully cultivate ultra-oligotrophic bacteria, which require extremely low levels of nutrients to grow, as well as to isolate a functional consortium for the production of hydrogen from cellulosic feedstocks (Ho et al., 2012). Another example was the experiment developed by Díaz-García et al. (2021), in which the authors presented a strategy to assemble a minimal and effective lignocellulolytic bacterial consortium where the first step was the "dilution-to-stimulation" approach. From the "dilution-to-stimulation" phase, several bacterial types were significantly enriched, including members of the Paenibacillaceae, Sphingobacteriaceae, Enterobacteriaceae, and Pseudomonadaceae families. Both of these high-dilution approaches require careful attention to sterile technique and appropriate culturing conditions, as well as time and persistence. Nevertheless, they have proven to be valuable tools for exploring the diversity and physiology of oligotrophic microorganisms and functional microbial consortia from environmental samples.

2.2.4. Syntrophy

Another limitation in extremophile cultivation is the syntrophic metabolism of some microbes. In other words, microbes may lack some metabolic apparatus and supplement it by feeding on metabolites produced by other microbes. In the natural environment, most microorganisms grow in a consortium with other microbes of the same or different taxa. In general, syntrophy allows a consortium of microorganisms to gain energy by coupling processes that can, for bioenergetic reasons, be accomplished only through microbial interlinkage (Moissl-Eichinger et al., 2018). Cooperative interaction among microbes is an important survival strategy (Mee et al., 2014). Mimicking complex networks that naturally occur in extreme environments can also provide insights into the limitations of the traditional cultivation of individual microorganisms (Marmann et al., 2014), in which microbes can cooperate through the exchange of metabolites and signaling molecules within a shared pool of micronutrients (Pande and Kost, 2017). Thus, coculturing enables

obligate symbionts to grow with their microbial partners and may activate genes that are not expressed in laboratory settings and in pure cultures, thus improving culturing success (Bertrand et al., 2014). For example, the coculture approach successfully enabled the culture of *Candidatus* Prometheoarchaeum syntrophicum strain MK-D1, a member of the Asgardarchaeota (proposed superphylum) cultured from deep marine sediments (for more information, see section 2.2.2).

Extremophiles are uniquely difficult to investigate due to their complex syntrophy. Nevertheless, the results derived from these studies are often fascinating. For example, by using the coculture strategy, Sánchez-Andrea et al. (2018) successfully enhanced sulfidogenesis by adding the sulfur reducer *Desulfurella amilsii* to a culture of the acidophilic fermentative bacterium *Lucifera butyrica*. Similarly, Pillot et al. (2020) reported the generation of electricity through the syntrophy between exoelectrogenic and fermentative hyperthermophilic microbes from hydrothermal vents. These experiments demonstrated the direct production of electric current from acetate, pyruvate, and H_2 and indirect production from yeast extract and peptone through the production of H_2 and acetate from fermentation. Methanogenesis is a well-studied process performed by syntrophic microbes (Sieber et al., 2010; Phan et al., 2021; Tilahun et al., 2021). Syntrophic acetate oxidation is catalyzed by syntrophic acetate-oxidizing bacteria, whereas H_2-consuming methanogenesis is catalyzed by hydrogenotrophic methanogens. The two microbes obligately require each other, since the bacterium requires hydrogen scavengers (i.e., partner methanogens) and the archaeon requires hydrogen suppliers (i.e., syntrophic acetate-oxidizing bacteria). Although this mutual syntrophy theoretically yields energy, the amount is quite small ($\Delta G0' = 31.0$ kJ/mol). Moreover, the syntrophic acetate-oxidizer and partner methanogens must share this small amount of energy. This energy disadvantage may cause these syntrophs to grow slowly and adopt a rigid mutualism, which may explain why the isolation of syntrophic acetate-oxidizing co-cultures was long considered extremely difficult or even impossible (Hattori, 2008).

2.2.5. *In situ* diffusion-based devices in extreme environments

Platforms for *in situ* cultivation that were successfully developed in the last decade have improved the cultivation of certain microbial groups that were previously difficult or impossible to culture. These improvements were made based on observations of the natural environment, which provides all of the initiation factors required for microbial growth (Jung et al., 2021). These platforms could be implemented as devices customized for different environments and specific purposes. Some examples of applications include the cultivation of microbes from wet soil (Ling et al., 2015; Berdy et al., 2017; Chaudhary et al., 2019), marine systems (Aoi et al., 2009; Alkayyali et al., 2021), and different hosts such as sponges (Steinert et al., 2014; Jung et al., 2021) and corals (Schultz et al., 2022b).

Chaudhary and Kim (2019) developed a diffusion bioreactor that consisted of a container wrapped with a polycarbonate membrane (0.4 μm) filled with culture media, which was then placed in the soil. Similar to other *in situ* diffusion-based devices, the polycarbonate membrane allowed for the exchange of essential compounds with the environment (nutrients and oxygen, for example), thus enabling the culture of soil microbes such as members of the Proteobacteria, Firmicutes, Actinobacteria, and Bacteroidetes phyla (Chaudhary et al., 2019). Multiwell microbial culture chips are another alternative tool for microbial culturing, which were first used in freshwater by Ingham et al. (2007). The authors successfully conducted a high-throughput screening and their proposed approach enabled the rapid growth of novel bacterial species with potential for biotechnology (Ingham et al., 2007). Likewise, Palma Esposito et al. (2018) designed a miniaturized culture chip (microscreen plate), which was then applied to culture microorganisms from Antarctic sediments. Using this approach, the authors were able to isolate *Aequorivita* sp., a rare species with antimicrobial and anthelmintic activities. Based on the same concept of *in situ* incubation, Zengler et al. (2005) added single cells into microcapsules and exposed them to a continuous flow of culture medium under *in vitro* conditions, which enabled the retrieval of nearly 10,000 microcolonies of environmental microbes. Similarly, Alkayyali et al. (2021) created Microbe Domestication Pod (MD Pod), a microfluidics platform with chambers and sealed membranes, aiming to load agarose microbeads containing marine bacteria and incubate them *in situ* in marine sediments. Another noteworthy example includes an *in situ* hollow-fiber membrane platform integrated with injectors to maintain the flow of substrates, which was particularly used for continuous fermentation (Aoi et al., 2009). The authors improved the culturability of the cells by up to 12% in comparison to microbial cells inoculated in Petri dishes (Aoi et al., 2009). Lastly, the development of transwell plates by Svenning et al. (2003) allowed for the recovery of methane-oxidizing bacteria by enabling the diffusion of nutrients from the environment to the plate.

Halophilic bacteria and ammonia-oxidizing archaea from coral mucus, for example, have been cultivated using these approaches (Schultz et al., 2022a). Cai et al. (2022) conducted an *in situ* investigation of cold seeps using simple dialysis tubes loaded with a previously cultivated strain of *Erythrobacter flavus*. The authors were able to describe the thiosulfate oxidation pathway for this strain under natural conditions. This study shows how diffusion-based approaches could be used to study microbial metabolism, in addition to improving cultivation methods. This research paves the way for *in situ* screening for exoplanetary biosignatures, where microbes could be grown under natural conditions similar to those occurring on other planets, after which their metabolic traits can be tracked as potential biosignatures. Gevi et al. (2022) used a similar approach to mimic Martian conditions *in vitro* and grow the black fungus *Cryomyces antarcticus*. Metabolomic profiles of the cultures increased the range of possible biosignatures of life on Mars. Variations of *in situ* cultivation techniques include devices designed without membranes, where microbial cells are trapped in micro-wells and fully exposed to the environment (Ingham et al., 2007), as well as membranes with different pore sizes that allow only certain desired microbial cells to pass (Gavrish et al., 2008).

Although these devices vary in application, shape, composition, and size, some of their basic principles are quite similar. Specifically, these instruments often consist of chambers or microchambers where the desired microbial cells are loaded, with membranes separating the inside of the chamber from the external environment. The microbial cells are usually retrieved from an environment of interest and once they are loaded and trapped in the devices, the platforms are set up at the original sampling site. The growth factors naturally occurring in the environment can pass freely through the membranes, allowing the cells to grow (Berdy et al., 2017). This principle could be easily adapted to extreme environments. The optimal device design will depend on the goal. For example, platforms without membranes could be used to

cultivate thermophilic, psychrophilic, and piezophilic microbes, since the membrane integrity could be affected by high temperatures, formation of micro-ice crystals, and high hydrostatic pressures, respectively. Even changes in pore sizes caused by dilation could yield uncertain results. All the diffusion-based alternatives discussed herein might be adapted and applied for the recovery of extremophiles from a given environment.

2.2.6. Culturomics

Culturomics is a novel approach that combines next-generation sequencing with high-throughput cultivation by simultaneously using a wide range of culture media with the goal of identifying different compositions that best promote the growth of different microbes in a given sample (Greub, 2012; Lagier et al., 2012). This strategy uses the above-mentioned improvements in cultivation (low-nutrient media, carbon source, variation in incubation, pH, signaling and antibiotic compounds, and co-culture) as well as high-throughput methods [matrix-assisted laser desorption ionization–time of flight mass spectrometry (MALDI-TOF MS) and amplicon sequencing] to retrieve large numbers of microbial colonies (Greub, 2012). Culturomics emerged with the objective of recovering rare and/or new microbial lineages and has led to the cultivation of microbes from different extreme environments that were previously thought to be uninhabitable by microorganisms (Sysoev et al., 2021). Additionally, genomic information from microorganisms and metagenomic data from extreme environments have led to the discovery of habitat-specific genes (Kumar et al., 2017) and provide a basis for the design of specific and unique culture medium conditions based on the metabolic repertoire of target microorganisms to obtain pure cultures (Nielsen et al., 2014). In the near future, metagenome-assisted culturomics will be increasingly valuable for deciphering the community composition of microbial dark matter.

Culturomics has been successfully used to explore human gut microbiota, extending knowledge of human microbial diversity and providing descriptions of new microbial taxa (Lagier et al., 2016; Diakite et al., 2020), but also of extreme environments. For example, by changing the salt concentrations of the growth media, Khelaifia et al. (2018) first described a new halophilic archaeon species, *Haloferax massiliense*, from the human gut. Other new extremophile species with different metabolisms have been successfully retrieved using similar approaches, including thermophiles (Yasir et al., 2019), microbes resistant to reactive oxygen species (Kapinusova et al., 2022), and hyperhalophilies (Durán-Viseras et al., 2021). Using culturomics, Zeng et al. (2021) cultivated and isolated *Gemmatimonas groenlandica* (a representative bacterial species from the phylum Gemmatimonadetes) for the second time. This phylum consists of photoheterotrophic bacteria; however, its members remain largely uncharacterized because their cultivation is uniquely challenging. Sood et al. (2021) recently proposed the use of this approach with some modifications in order to improve the cultivation of extremophiles. The authors suggested applying metagenomics in natural environments as the first step prior to cultivation. Binning metagenome-assembled genomes (MAGs) and single amplified genomes (SAGs) retrieved from a given source could provide insights into the nutritional requirements of the microbes living there. Carbon and nitrogen cycling, as well as the genes related to degradation pathways and adaptations to specific niches, are good traits to search for. Once the screening is complete, culture media could be formulated to meet previously determined requirements (Sood et al., 2021).

2.2.7. Reverse genomics isolation

Reverse genomics isolation is a relatively new approach that enables the culture of hard-to-culture or yet-to-be-cultured microbes, which focuses on using genomic data to guide the cultivation of previously uncultured microorganisms (Cross et al., 2019). This strategy has the potential to support the growth of extremophiles by first applying metagenomics and single-cell genomics (already-available genomes) to obtain genomic data of the microbial community in their natural environment (e.g., nutritional requirements, growth factors, and coculture). Afterward, this knowledge is used to design specific culture conditions that simulate the natural habitat of the microbes, thus enhancing the chances of successfully culturing the target microbe or group of microorganisms (Cross et al., 2019).

Reverse genomics isolation has been successfully implemented to enable the culture of several previously uncultivated microbes, including members of the candidate phyla radiation (CPR) and the Planctomycetes, Verrucomicrobia, and Chlamydia (PVC) superphylum, both of which are considered unknown and enigmatic clusters of microorganisms. Cross et al. (2019) were the first to cultivate and isolate three lineages of previously uncultured Saccharibacteria from a complex community and one human oral SR1 specimen from the human oral cavity. The authors used genome-engineered antibodies as immunofluorescence probes for Saccharibacteria (TM7) as a means to maintain cell viability. Once the cells were sorted, they were cultured using different solid and liquid culture media based on their genomic information. Ibrahim et al. (2022) also used reverse genomics for creating a universal epitope to isolate different members of the Saccharibacteria lineage from the human oral cavity and successfully obtained specific epitopes from species of this superphylum *in silico*.

Overall, these findings highlight the potential of reverse genomics as a promising approach to culture previously uncultivated microbes including but not limited to CPR and PVC members. Additionally, this approach could enable the culture of other uncultured microbes, as well as rare, low abundance, and slow-growing microorganisms to greatly expand our understanding of microbial diversity and functions.

2.2.8. Cell-targeted cultivation

Up to this point, we have mainly discussed expanding the range of extremophile culturability, aiming to recover a wider diversity of microbial isolates than with conventional methods, as well as to discover new taxa. Other approaches such as enrichment can be used when seeking to cultivate certain groups of microorganisms based on metabolic characteristics and/or nutritional requirements. Microorganism screening, however, can focus on taxa of particular taxonomic groups or with specific functional traits depending on the purpose of the study. Cell-targeted cultivation strategies (Cross et al., 2019; Lee et al., 2021) can be roughly divided into two steps: a first trial of cell sorting using different methods, aiming to segregate the target cell and deplete the unwanted ones; followed by integrated cultivation efforts using suitable media. Both steps are challenging because the first requires keeping the cells viable and the second depends on a well-designed cultivation strategy. Moreover, the success of the first step does not guarantee effective culturability.

Alternatively, more feasible methods to retrieve viable environmental microbes include FACS (fluorescence-activated cell sorting; Espina et al., 2022), Live-FISH (fluorescence *in situ* hybridization; Batani et al., 2019), micromanipulators, and laser manipulation systems (optical tweezers and laser microdissection). Additional technical details are provided by Zhang and Liu (2008), Keloth et al. (2018), and Lee et al. (2019). Briefly, optical tweezers and laser microdissection are used in sorting, culturing, and isolating single bacterial cells from a mixed culture by using a microscope to locate, trap, collect, and transfer a single cell to fresh culture media (Huber et al., 1995; Frumkin et al., 2008). Optical tweezers proved a rapid and efficient tool for successfully isolating hyperthermophiles (Huber et al., 1995, 2000) and an extremely halophilic archaeon (Antunes et al., 2008a,b) from a mixed microbial community. Despite being labor-intensive and requiring particular growth conditions, isolation techniques enable the culture and characterization of a variety of undiscovered strains (Alain and Querellou, 2009).

3. Bioprospecting the metabolic potential of cultured extremophiles

Environmental parameters such as temperature, pH, salinity, anoxia, pressure, UV and ionizing radiation, and water and nutrient availability can limit microbial life and affect the structure and diversity of microbial communities (Paulino-Lima et al., 2013; Shock and Boyd, 2015; Merino et al., 2019). Many natural terrestrial and aquatic environments (e.g., deserts, polar regions, geothermal environments, supersaturated salt pools, acidic or soda lakes, and the deep sea) were originally thought to be too harsh to harbor life (Carré et al., 2022). However, more recent studies have demonstrated the occurrence of a wide diversity of organisms in these extreme habitats (Jurelevicius et al., 2012; Cury et al., 2015; Lopez et al., 2019; Shu and Huang, 2022). Microorganisms able to tolerate, survive, or require extreme conditions to grow optimally are known as extremophiles (Brock and Freeze, 1969; MacElroy, 1974; Rothschild and Mancinelli, 2001), whereas those that grow optimally under multiple extreme stress conditions are known as polyextremophiles (Capece et al., 2013). To thrive in such extreme conditions, extremophiles must develop a range of adaptations that provide a unique perspective on the fundamental characteristics of biological processes, as well as the broad metabolic diversity and physiological capabilities of these microorganisms (Canganella and Wiegel, 2014; Salwan and Sharma, 2020). Although knowledge of extremophile biology has progressed considerably in recent decades, (poly)extremophiles remain largely unexplored mainly due to the difficulty of culturing these microorganisms in a laboratory setting. Here, we highlight the importance of cultured extremophilic microorganisms and briefly discuss their potential for biotechnology and space-related sciences.

3.1. Biotechnological applications of extremophilic microbes

Extremophiles may generate bioproducts with important biotechnological applications (Bull and Goodfellow, 2019) for use in many areas of biotechnology, including agriculture, medicine, and the petroleum and pharmaceutical industries (Reis-Mansur et al., 2019; Schultz and Rosado, 2019, 2020; Zhu et al., 2020; Schultz et al., 2022b). One noteworthy example is the global enzyme market, which was valued at US$6.4 billion in 2021 (BCC, 2022). However, the commercial enzyme market has struggled to meet the increasing requirements of the industrial sectors (i.e., textile manufacturing, pulp and paper, biofuel), mainly because most enzymes currently available in the market are only active within a very narrow range of conditions because they originate from mesophilic organisms. Therefore, they quickly lose activity under the extreme conditions found in industrial processes (temperature, pH, pressure, solvent concentrations, and ion concentration). Enzymes from polyextremophiles hold the promise of fulfilling industrial needs (Kara and Liese, 2019; Sysoev et al., 2021) and may produce robust enzymes with higher activity and stability under the extreme conditions that characterize industrial processes (Rampelotto, 2016; Mesbah, 2022). From samples obtained in Antarctica, Monsalves et al. (2020) isolated a psychrotolerant and UV-C resistant bacterium that produces catalase, an enzyme commonly used in the textile industry, that was thermoactive and thermostable under high temperatures (optimal activity at 50°C at pH 7.0). Sheikhi et al. (2012) screened microorganisms from geothermal sites for thermoalkaliphilic laccase, an important enzyme used in the biofuel industry. Using a sample from a polar volcano, Márquez and Blamey (2019) isolated thermophilic microorganisms capable of producing thermophilic amine-transaminase, an enzyme with important pharmacological applications.

Extremophiles are also promising sources of biosurfactants, a versatile type of chemical that is widely used in the oil, pharmaceutical, and food industries, which generates billions of dollars per year (Cameotra et al., 2010; Schultz and Rosado, 2020; da Silva et al., 2022; Schultz et al., 2022b). Currently, most commercially available surfactants are derived from petroleum products (Jemil et al., 2016). However, replacing chemically synthesized compounds with compounds of biological origin may have advantages (Banat et al., 2014; Perfumo et al., 2018), such as low toxicity, high biodegradability, production from renewable materials, and capability to remain active and stable under extreme temperatures, pH, and salinity (Vijayakumar and Saravanan, 2015; Jemil et al., 2016; Schultz et al., 2022b). For example, Schultz et al. (2022b) screened for oil-degrading and biosurfactant-producing thermophiles by investigating the thermophilic microbial community of Antarctic geothermal sites for applications in the bioremediation of oil-contaminated sites and microbial-enhanced oil recovery processes. The authors reported that the majority of the isolated microbes were able to grow in a culture medium supplemented with crude oil as the only carbon source and exhibited excellent performance in terms of biosurfactant production and emulsification stability at 100°C. Additionally, extremophiles require a large suite of specialized metabolites to overcome their hostile environments and thus represent a potentially valuable reservoir of novel bioactive molecules. However, the secondary metabolites derived from microbiomes thriving in extreme habitats have remained largely unexplored, and thus represent new frontiers in drug discovery (Sayed et al., 2020). Therefore, microbes from extreme environments are a uniquely promising source of novel potent anticancer molecules, as reported by Sagar et al. (2013a,b) and Esau et al. (2019), who screened samples from Red Sea brine pools, in addition to other diseases such as Alzheimer's disease, Parkinson's disease, hypercholesterolemia, and epilepsy. Biomolecules from extremophiles are also valuable for other medical applications such

as the production of halocins, diketopiperazines, DNA polymerase, and lipases (Kumar et al., 2017), as well as carotenoids, which are important for the production of antibiotics and cosmetics related to UV protection and antioxidant agents (Inoue et al., 2017). Additionally, these compounds have important implications for agriculture, as microbial bioactive compounds can be used to achieve high crop yields, mitigate pathogens (Rachid et al., 2015; Rao et al., 2022), and promote soil health (Yadav, 2021).

3.2. Extremophiles on Earth and beyond: implications in astrobiology

In addition to the biotechnological applications of extremophilic microbes or their products, extreme microbes may provide significant insights for astrobiology research due to their capacity to survive in conditions analogous to or simulated extraterrestrial habitats or conditions (Lage et al., 2012). Considering that temperature, radiation, gravity, and salinity are the primary parameters that determine life in outer space, the study of survival strategies in extreme conditions helps to define questions regarding planetary habitability and to identify possible targets for the search for extraterrestrial life (Rothschild and Mancinelli, 2001; Bonch-Osmolovskaya, 2010).

Most ecosystems inhabited by extremophiles on Earth resemble planetary bodies in outer space (Schmid et al., 2020). Microorganisms isolated from these extreme habitats considered analogous to extraterrestrial environments are highly adapted and are good candidates for astrobiological studies [e.g., astrobiological models, adaptation mechanisms, strategies underlying survival in extreme conditions, and potential (novel) biosignatures that can be used in habitable zones beyond Earth; Lopez et al., 2019; Jebbar et al., 2020], yielding potential clues as to whether (and how) life may exist and persist on other planetary bodies (Lopez et al., 2019; Coleine and Delgado-Baquerizo, 2022), and even provide tools to guide future colonization, if this is desired (Lopez et al., 2019). So far, prokaryotes are the most-studied models for astrobiology (Seyler et al., 2020; Abbott and Pearce, 2021), including members of the (i) halophilic archaea (class Haloarchaea), which are typically used for Mars studies, due to their ability to withstand salinity and perchlorates, anaerobic conditions, high levels of UV and ionizing radiation, subzero temperatures, desiccation, and toxic ions (Stan-Lotter and Fendrihan, 2015; DasSarma and DasSarma, 2017); (ii) *Deinococcus radiodurans*, a bacterium that is widely known for its high resistance to radiation (up to 10,000 Gy; Daly, 2011) and its importance in the context of planetary protection and panspermia (Kawaguchi et al., 2013); and (iii) representatives of the genus *Bacillus*, which have repeatedly demonstrated their ability to survive in many extreme conditions encountered in outer space. These members include (i) *Bacillus subtilis*, which is known to survive in conditions similar to those on Mars (extreme dryness, high radiation levels, and high concentrations of perchlorate salts) (Nicholson et al., 2000), and (ii) *Bacillus pumilus*, a model organism that is currently used to assess the habitability of Europa (icy moon of Jupiter) based on its capability to survive in extreme temperatures, low nutrient availability, dryness, and UV-C radiation (Stepanov et al., 2016). Photosynthetic extremophilic organisms and fungi are also reported as good models. Members of the order Chroococcidiopsidales (e.g., *Chroococcidiopsis*) have proved to be interesting candidates for Mars and icy moons, tolerating many years of desiccation, high doses of ionizing radiation, microgravity, high concentrations of perchlorates, and low temperatures (Cosciotti et al., 2019; Billi et al., 2021; Napoli et al., 2022). Additionally, strains of *Cladosporium sphaerospermum* and *Cremonium murorum,* both isolated from a reactor at the Chernobyl Nuclear Plant, are able to extract energy from ionizing radiation, making them viable models of life in space, with its constant cosmic radiation (Blachowicz et al., 2019).

Experiments in the stratosphere and in laboratory-based simulations can facilitate future *in situ* planetary explorations. For instance, fungi, yeasts, bacteria, and cyanobacteria isolated from terrestrial and space-related environments like the International Space Station (ISS) have survived in the stratosphere under multiple Mars-like conditions, such as cold, dry, oligotrophic environments, intense UV radiation, and low pressure (Blachowicz et al., 2019; Cortesão et al., 2019). Additionally, several missions have used balloons to transport biological samples to the high-elevation environment of the stratosphere (Smith et al., 2014; DasSarma et al., 2020). Pulschen et al. (2018) investigated cold-adapted UV-resistant yeasts (black-pigmented *Exophiala* sp. and non-pigment-producing *Naganishia friedmannii*) isolated from a volcano in the Atacama Desert, and both microorganisms showed higher survival rates than *Bacillus subtilis* spores, thus confirming the remarkable resilience of yeast and making them good candidate models for further research. In a recent study, fungal spores (*Aspergillus niger*) and bacterial cells (*Salinisphaera shabanensis, Staphylococcus capitis,* and *Buttiauxella* sp.) were launched on a NASA scientific balloon flight into the stratosphere (Cortesão et al., 2019), and the authors concluded that the halophilic bacterium *S. shabanensis* and spores of the pigmented fungus *A. niger* were the most resistant microbes, with a 2- and 4-log reduction. However, additional efforts are needed to further develop ground-based systems such as laboratory-based simulation chambers to mimic the conditions in outer space, (exo)planets, and moons to determine the capacity of terrestrial microorganisms to survive in extraterrestrial conditions, including microgravity, UV radiation, gas composition, temperature, pressure, and humidity. Among the culturable microorganisms, extremophiles have been extensively placed in simulated conditions, such as the ability of the thermophiles *Sulfolobus solfataricus, Haloterrigena hispanica, Thermotoga neapolitana,* and *Geobacillus thermantarcticus* to survive under Mars-like conditions (Mastascusa et al., 2014). All strains, particularly *S. solfataricus*, proved highly resistant, continuing to grow after exposure to temperature variation, with a slight effect on growth from UV radiation.

4. Final remarks

Extremophile research has consistently remained at the cutting edge of microbiology, opening unexplored territory in our understanding of life and its limits. After more than five decades of research focused on exploiting extreme environments to unveil extremophile taxonomy, functions, and applicability in society, microbes capable of thriving in multiple harsh conditions have garnered increasing attention among the scientific community, particularly in the biotechnology sector and, more recently, in astrobiology and space-related studies. The more we learn about extremophiles, the more intriguing they become, opening broad

questions regarding their evolution, adaptations, and diversity. So far, most attempts to characterize and describe the extremosphere have involved conventional culture methods. However, extremophiles commonly fail to grow under standard laboratory conditions and remain uncharacterized. New cultivation approaches are thus essential to enable the recovery of the still-uncultured fraction of the microbial dark matter, thus improving culturability rates and enabling new discoveries.

Recent years have seen extensive advances in high-throughput cultivation, techniques to mimic the natural environment, and the development of a variety of devices to cultivate yet-to-be-cultured microbes. Culturomics coupled with focused genome-guided cultivation efforts and *in situ* cultivation by using materials modified according to each extreme environment are promising strategies for the characterization of extreme microbiomes. These innovative strategies complement the current cultivation-independent approaches, such as metagenomics and metatranscriptomics, to further understand the physiology of extremophiles. Thus, culturomics is an important approach that has enabled scientists to extend our knowledge about extremophiles, including the description of new species and the discovery of new metabolic pathways with high biotechnological potential. However, the application of this strategy for extremophile research is still in its infancy. In this review, we summarized the current strategies used to culture the environmental microbial diversity, including the extremosphere. We hope that the topics discussed herein will aid microbiologists in untangling the composition and functions of extremophilic microbiomes, describing novel taxa, and screening microorganisms for new biotechnological applications.

Author contributions

JS, FM, RP, and ASR: investigation and writing—original draft, conceptualization, review, and editing. ASR: funding acquisition and supervision. All authors contributed to the article and approved the submitted version.

Funding

This study was supported by a KAUST Baseline Grant (BAS/1/1096-01-01) to ASR. FM received support from the National Council for Scientific and Technological Development (CNPq).

Conflict of interest

The authors declare that the research was conducted in the absence of any commercial or financial relationships that could be construed as a potential conflict of interest.

Publisher's note

References

Aakra, A., Utåker, J. B., Nes, I. F., and Bakken, L. R. (1999). An evaluated improvement of the extinction dilution method for isolation of ammonia-oxidizing bacteria. *J. Microbiol. Methods* 39, 23–31. doi: 10.1016/S0167-7012(99)00094-9

Abbott, C., and Pearce, D. A. (2021). "Antarctic Bacteria as Astrobiological Models" in *Extremophiles as Astrobiological Models*. eds. J. Seckbach and H. Stan-Lotter (In: Scrivener Publishing LLC.) doi: 10.1002/9781119593096.ch6

Alain, K., and Querellou, J. (2009). Cultivating the uncultured: limits, advances and future challenges. *Extremophiles* 13, 583–594. doi: 10.1007/s00792-009-0261-3

Alkayyali, T., Pope, E., Wheatley, S. K., Cartmell, C., Haltli, B., Kerr, R. G., et al. (2021). Development of a microbe domestication pod (MD pod) for in situ cultivation of micro-encapsulated marine bacteria. *Biotechnol. Bioeng.* 118, 1166–1176. doi: 10.1002/bit.27633

Alvarez-Barrientos, A., Arroyo, J., Cantón, R., Nombela, C., and Sánchez-Pérez, M. (2000). Applications of flow cytometry to clinical microbiology. *Clin. Microbiol. Rev.* 13, 167–195. doi: 10.1128/CMR.13.2.167

Antunes, A., Rainey, F. A., Wanner, G., Taborda, M., Pätzold, J., Nobre, M. F., et al. (2008b). A new lineage of halophilic, wall-less, contractile bacteria from a brine-filled deep of the Red Sea. *J. Bacteriol.* 190, 3580–3587. doi: 10.1128/JB.01860-07

Antunes, A., Taborda, M., Huber, R., Moissl, C., Nobre, M. F., and da Costa, M. S. (2008a). *Halorhabdus tiamatea* sp. nov., a non-pigmented, extremely halophilic archaeon from a deep-sea, hypersaline anoxic basin of the Red Sea, and emended description of the genus Halorhabdus. *Int. J. Syst. Evol. Microbiol.* 58, 215–220. doi: 10.1099/ijs.0.65316-0

Aoi, Y., Kinoshita, T., Hata, T., Ohta, H., Obokata, H., and Tsuneda, S. (2009). Hollow-fiber membrane chamber as a device for in situ environmental cultivation. *Appl. Environ. Microbiol.* 75, 3826–3833. doi: 10.1128/AEM.02542-08

Bae, J. W., Rhee, S. K., Park, J. R., Kim, B. C., and Park, Y. H. (2005). Isolation of uncultivated anaerobic thermophiles from compost by supplementing cell extract of *Geobacillus toebii* in enrichment culture medium. *Extremophiles* 9, 477–485. doi: 10.1007/s00792-005-0467-y

Banat, I. M., Satpute, S. K., Cameotra, S. S., Patil, R., and Nyayanit, N. V. (2014). Cost effective technologies and renewable substrates for biosurfactants' production. *Front. Microbiol.* 5:697. doi: 10.3389/fmicb.2014.00697

Batani, G., Bayer, K., Böge, J., Hentschel, U., and Thomas, T. (2019). Fluorescence in situ hybridization (FISH) and cell sorting of living bacteria. *Sci. Rep.* 9:18618. doi: 10.1038/s41598-019-55049-2

BCC (2022). Global Markets for Enzymes in industrial application. Available at: https://www.bccresearch.com/market-research/biotechnology/global-markets-for-enzymes-in-industrial-applications.html (Accessed January 14, 2023).

Bellali, S., Lagier, J. C., Raoult, D., and Bou Khalil, J. (2019). Among live and dead Bacteria, the optimization of sample collection and processing remains essential in recovering gut microbiota components. *Front. Microbiol.* 10:1606. doi: 10.3389/fmicb.2019.01606

Benaud, N., Chelliah, D. S., Wong, S. Y., and Ferrari, B. C. (2022). Soil substrate culturing approaches recover diverse members of Actinomycetota from desert soils of Herring Island. *Extremophiles* 26:24. doi: 10.1007/s00792-022-01271-2

Bender, K., Glover, K., Archey, A., and Barton, H. (2020). The impact of sample processing and media chemistry on the culturable diversity of bacteria isolated from a cave. *Int. J. Speleol.* 49, 209–220. doi: 10.5038/1827-806X.49.3.2337

Bendia, A. G., Araujo, G. G., Pulschen, A. A., Contro, B., Duarte, R. T. D., Rodrigues, F., et al. (2018). Surviving in hot and cold: psychrophiles and thermophiles from Deception Island volcano. *Extremophiles* 22:917. doi: 10.1007/s00792-018-1048-1

Berdy, B., Spoering, A. L., Ling, L. L., and Epstein, S. S. (2017). In situ cultivation of previously uncultivable microorganisms using the Ichip. *Nat. Protoc.* 12, 2232–2242. doi: 10.1038/nprot.2017.074

Bertrand, S., Bohni, N., Schnee, S., Schumpp, O., Gindro, K., and Wolfender, J. L. (2014). Metabolite induction via microorganism co-culture: a potential way to enhance chemical diversity for drug discovery. *Biotechnol. Adv.* 32, 1180–1204. doi: 10.1016/j.biotechadv.2014.03.001

Billi, D., Gallego Fernandez, B., Fagliarone, C., Chiavarini, S., and Rothschild, L. J. (2021). Exploiting a perchlorate-tolerant desert cyanobacterium to support bacterial growth for in situ resource utilization on Mars. *Int. J. Astrobiol.* 20, 29–35. doi: 10.1017/S1473550420000300

Blachowicz, A., Chiang, A. J., Elsaesser, A., Kalkum, M., Ehrenfreund, P., Stajich, J. E., et al. (2019). Proteomic and Metabolomic characteristics of Extremophilic Fungi under simulated Mars conditions. *Front. Microbiol.* 10:1013. doi: 10.3389/fmicb.2019.01013

Blachowicz, A., Mhatre, S., Singh, N. K., Wood, J. M., Parker, C. W., Ly, C., et al. (2022). The isolation and characterization of rare Mycobiome associated with spacecraft assembly cleanrooms. *Front. Microbiol.* 26:777133. doi: 10.3389/fmicb.2022.777133

Bollmann, A,. Lewis, K., and Epstein, S.S. (2007). Incubation of environmental samples in a diffusion chamber increases the diversity of recovered isolates. *Appl. Environ. Microbiol.* 73:6386–6390. doi: 10.1128/AEM.01309-07

Bonch-Osmolovskaya, E. A. (2010). High-temperature deep-subsurface microbial communities as a possible equivalent of ancient ecosystems. *Paleontol. J.* 44, 851–859. doi: 10.1134/S0031030110070130

Brock, T. D., and Freeze, H. (1969). *Thermus aquaticus* gen. n. and sp. n., a nonsporulating extreme thermophile. *J. Bacteriol.* 98, 289–297. doi: 10.1128/jb.98.1.289-297.1969

Bull, A. T., and Goodfellow, M. (2019). Dark, rare and inspirational microbial matter in the extremobiosphere: 16 000 m of bioprospecting campaigns. *Microbiology* 165, 1252–1264. doi: 10.1099/mic.0.000822

Burns, D. G., Camakaris, H. M., Janssen, P. H., and Dyall-Smith, M. L. (2004). Combined use of cultivation-dependent and cultivation-independent methods indicates that members of most haloarchaeal groups in an Australian crystallizer pond are cultivable. *Appl. Environ. Microbiol.* 70, 5258–5265. doi: 10.1128/AEM.70.9.5258-5265.2004

Button, D. K., Schut, F., Quang, P., Martin, R., and Robertson, B. R. (1993). Viability and isolation of marine bacteria by dilution culture: theory, procedures, and initial results. *Appl. Environ. Microbiol.* 59, 881–891. doi: 10.1128/aem.59.3.881-891.1993

Cai, R., He, W., Liu, R., Zhang, J., Zhang, X., and Sun, C. (2022). Deep-Sea in situ insights into the formation of zero-valent sulfur driven by a bacterial thiosulfate oxidation pathway. *MBio* 13:e0014322. doi: 10.1128/mbio.00143-22

Cameotra, S. S., Makkar, R. S., Kaur, J., and Mehta, S. K. (2010). Synthesis of biosurfactants and their advantages to microorganisms and mankind. *Adv. Exp. Med. Biol.* 672, 261–280. doi: 10.1007/978-1-4419-5979-9_20

Canganella, F., and Wiegel, J. (2014). Anaerobic thermophiles. *Lifestyles* 4, 77–104. doi: 10.3390/life4010077

Capece, M. C., Clark, E., Saleh, J. K., Halford, D., Heinl, N., Hoskins, S., et al. (2013). "Polyextremophiles and the constraints for terrestrial habitability" in *Polyextremophiles: Life Under Multiple Forms of Stress*. eds. J. Seckbach, A. Oren and H. Stan-Latter (Dordrecht, the Netherlands: Springer), 3–60.

Carré, L., Zaccai, G., Delfosse, X., Girard, E., and Franzetti, B. (2022). Relevance of earth-bound extremophiles in the search for extraterrestrial life. *Astrobiology* 22, 322–367. doi: 10.1089/ast.2021.0033

Cavicchioli, R. (2002). Extremophiles and the search for extraterrestrial life. *Astrobiology* 2, 281–292. doi: 10.1089/153110702762027862

Chaudhary, D. K., Khulan, A., and Kim, J. (2019). Development of a novel cultivation technique for uncultured soil bacteria. *Sci. Rep.* 9:6666. doi: 10.1038/s41598-019-43182-x

Chaudhary, D. K., and Kim, J. (2019). Experimental setup for a diffusion bioreactor to isolate Unculturable soil Bacteria. *Bioanalysis* 9:e3388. doi: 10.21769/BioProtoc.3388

Chien, A., Edgar, D. B., and Trela, J. M. (1976). Deoxyribonucleic acid polymerase from the extreme thermophile *Thermus aquaticus*. *J. Bacteriol.* 127, 1550–1557. doi: 10.1128/jb.127.3.1550-1557.1976

Cho, J. C., and Giovannoni, S. J. (2004). Cultivation and growth characteristics of a diverse group of oligotrophic marine Gammaproteobacteria. *Appl. Environ. Microbiol.* 70, 432–440. doi: 10.1128/AEM.70.1.432-440.2004

Cho, J. C., Stapels, M. D., Morris, R. M., Vergin, K. L., Schwalbach, M. S., Givan, S. A., et al. (2007). Polyphyletic photosynthetic reaction Centre genes in oligotrophic marine Gammaproteobacteria. *Environ. Microbiol.* 9, 1456–1463. doi: 10.1111/j.1462-2920.2007.01264.x

Coleine, C., and Delgado-Baquerizo, M. (2022). Unearthing terrestrial extreme microbiomes for searching terrestrial-like life in the solar system. *Trends Microbiol.* 30, 1101–1115. doi: 10.1016/j.tim.2022.04.002

Connon, S. A., and Giovannoni, S. J. (2002). High-throughput methods for culturing microorganisms in very-low-nutrient media yield diverse new many isolates. *Appl. Environ. Microbiol.* 68, 3878–3885. doi: 10.1128/AEM.68.8.3878-3885.2002

Cortesão, M., Fuchs, F. M., Commichau, F. M., Eichenberger, P., Schuerger, A. C., Nicholson, W. L., et al. (2019). *Bacillus subtilis* spore resistance to simulated mars surface conditions. *Front. Microbiol.* 10:333. doi: 10.3389/FMICB.2019.00333

Cosciotti, B., Balbi, A., Ceccarelli, A., Fagliarone, C., Mattei, E., Lauro, S. E., et al. (2019). Survivability of Anhydrobiotic Cyanobacteria in salty ice: implications for the habitability of icy worlds. *Life* 9:86. doi: 10.3390/life9040086

Cross, K. L., Campbell, J. H., Balachandran, M., Campbell, A. G., Cooper, C. J., Griffen, A., et al. (2019). Targeted isolation and cultivation of uncultivated bacteria by reverse genomics. *Nat. Biotechnol.* 37, 1314–1321. doi: 10.1038/s41587-019-0260-6

Cury, J., Jurelevicius, D., Villela, H., Jesus, H., Peixoto, R., Schaefer, C., et al. (2015). Microbial diversity and hydrocarbon depletion in low and high diesel-polluted soil samples from Keller peninsula. *Antarctic Sci.* 27, 263–273. doi: 10.1017/S0954102014000728

da Silva, M. B. F., da Mota, F. F., Jurelevicius, D., de Carvalho Azevedo, V. A., da Costa, M. M., Góes-Neto, A., et al. (2022). Genomic analyses of a novel bioemulsifier-producing Psychrobacillus strain isolated from soil of King George Island, Antarctica. *Polar Biol.* 45, 691–701. doi: 10.1007/s00300-022-03028-1

Daly, M. J. (2011). *Deinococcus radiodurans*: revising the molecular basis for radiation effects on cells. *Extremophiles Handbook* 1117–1133. doi: 10.1007/978-4-431-53898-1_53

Das, N., Tripathi, N., Basu, S., Bose, C., Maitra, S., and Khurana, S. (2015). Progress in the development of gelling agents for improved culturability of microorganisms. *Front. Microbiol.* 6:698. doi: 10.3389/fmicb.2015.00698

DasSarma, P., Antunes, A., Simões, M. F., and DasSarma, S. (2020). Earth's stratosphere and microbial life. *Curr. Issues Mol. Biol.* 38, 197–244. doi: 10.21775/cimb.038.197

DasSarma, S., and DasSarma, P. (2017). "Halophiles" in *Encyclopedia of Life Sciences* (Chichester: John Wiley & Sons, Ltd)

Davis, K. E., Joseph, S. J., and Janssen, P. H. (2005). Effects of growth medium, inoculum size, and incubation time on culturability and isolation of soil bacteria. *Appl. Environ. Microbiol.* 71, 826–834. doi: 10.1128/AEM.71.2.826-834.2005

de Jesus, H. E., Peixoto, R. S., Cury, J. C., van Elsas, J. D., and Rosado, A. S. (2015). Evaluation of soil bioremediation techniques in an aged diesel spill at the Antarctic peninsula. *Appl. Microbiol. Biotechnol.* 99, 10815–10827. doi: 10.1007/s00253-015-6919-0

de Bruyn, J. C., Boogerd, F. C., Bos, P., and Kuenen, J. G. (1990). Floating filters, a novel technique for isolation and enumeration of fastidious, acidophilic, iron-oxidizing, autotrophic bacteria. *Appl Environ Microbiol.* 56, 2891–2894. doi: 10.1128/aem.56.9.2891-2894.1990

Diakite, A., Dubourg, G., Dione, N., Afouda, P., Bellali, S., Ngom, I. I., et al. (2020). Optimization and standardization of the culturomics technique for human microbiome exploration. *Sci. Rep.* 10:9674. doi: 10.1038/s41598-020-66738-8

Díaz-García, L., Huang, S., Spröer, C., Sierra-Ramírez, R., Bunk, B., Overmann, J., et al. (2021). Dilution-to-stimulation/extinction method: a combination enrichment strategy to develop a minimal and versatile Lignocellulolytic bacterial consortium. *Appl. Environ. Microbiol.* 87:e02427. doi: 10.1128/AEM.02427-20

Do Carmo, F. L., Dos Santos, H. F., Martins, E. F., et al. (2011). Bacterial structure and characterization of plant growth promoting and oil degrading bacteria from the rhizospheres of mangrove plants. *J. Microbiol.* 49, 535–543. doi: 10.1007/s12275-011-0528-0

Dong, K., Pan, H., Yang, D., Rao, L., Zhao, L., Wang, Y., et al. (2020). Induction, detection, formation, and resuscitation of viable but non-culturable state microorganisms. *Compr. Rev. Food Sci. Food Saf.* 19, 149–183. doi: 10.1111/1541-4337.12513

Dowell, F., Cardman, Z., Dasarathy, S., Kellermann, M. Y., Lipp, J. S., Ruff, S. E., et al. (2016). Microbial communities in methane- and Short chain alkane-rich hydrothermal sediments of Guaymas Basin. *Front. Microbiol.* 29:17. doi: 10.3389/fmicb.2016.00017

Durán-Viseras, A., Andrei, A. Ş., Vera-Gargallo, B., Ghai, R., Sánchez-Porro, C., and Ventosa, A. (2021). Culturomics-based genomics sheds light on the ecology of the new haloarchaeal genus *Halosegnis*. *Environmental Microbiology* 23, 3418–3434. doi: 10.1111/1462-2920.15082

Esau, L., Zhang, G., Sagar, S., Stingl, U., Bajic, V. B., and Kaur, M. (2019). Mining the deep Red-Sea brine pool microbial community for anticancer therapeutics. *BMC Complement. Altern. Med.* 19:142. doi: 10.1186/s12906-019-2554-0

Espina, G., Muñoz-Ibacache, S. A., Cáceres-Moreno, P., Amenabar, M. J., and Blamey, J. M. (2022). From the discovery of Extremozymes to an enzymatic product: roadmap based on their applications. *Front. Bioeng. Biotechnol.* 12:752281. doi: 10.3389/fbioe.2021.752281

Ferrari, B. C., Winsley, T., Gillings, M., and Binnerup, S. (2008). Cultivating previously uncultured soil Bacteria using a soil substrate membrane system. *Nat. Protoc.* 3, 1261–1269. doi: 10.1038/nprot.2008.102

Frumkin, D., Wasserstrom, A., Itzkovitz, S., Harmelin, A., Rechavi, G., Shapiro, E., et al. (2008). Amplification of multiple genomic loci from single cells isolated by laser micro-dissection of tissues. *BMC Biotechnol.* 8:17. doi: 10.1186/1472-6750-8-17

Fu, L., Ding, J., Lu, Y. Z., Ding, Z. W., Bai, Y. N., and Zeng, R. J. (2017). Hollow fiber membrane bioreactor affects microbial community and morphology of the DAMO and Anammox co-culture system. *Bioresour. Technol.* 232, 247–253. doi: 10.1016/j.biortech.2017.02.048

Gavrish, E., Bollmann, A., Epstein, S., and Lewis, K. (2008). A trap for in situ cultivation of filamentous actinobacteria. *J. Microbiol. Methods* 72, 257–262. doi: 10.1016/j.mimet.2007.12.009

Gevi, F., Leo, P., Cassaro, A., Pacelli, C., de Vera, J. P., Rabbow, E., et al. (2022). Metabolomic profile of the fungus Cryomyces antarcticus under simulated Martian and space conditions as support for life-detection missions on Mars. *Front. Microbiol.* 12:749396. doi: 10.3389/fmicb.2022.749396

Gin, K. Y., and Goh, S. G. (2013). Modeling the effect of light and salinity on viable but non-culturable (VBNC) Enterococcus. *Water Res.* 15, 3315–3328. doi: 10.1016/j.watres.2013.03.021

Giovannoni, S. J., Hayakawa, D. H., Tripp, H. J., Stingl, U., Givan, S. A., Cho, J. C., et al. (2008). The small genome of an abundant coastal ocean methylotroph. *Environ. Microbiol.* 10, 1771–1782. doi: 10.1111/j.1462-2920.2008.01598.x

Gómez-Acata, E. S., Ayala-Gámez, L. M., García-Covarrubias, R., Torres-Núñez, M. Y., Vargas-López, L., Hernández-Camargo, S., et al. (2021). Bioprospecting of haloalkaliphilic microorganisms isolated from a dried-out maar in the volcano "Hoya Rincón de Parangueo". *Nova scientia* 13:00006. doi: 10.21640/ns.v13i26.2553

Greub, G. (2012). Culturomics: a new approach to study the human microbiome. *Clin. Microbiol. Infect.* 18, 1157–1159. doi: 10.1111/1469-0691.12032

Grzesiak, J., Górniak, D., Świątecki, A., Aleksandrzak-Piekarczyk, T., Szatraj, K., and Zdanowski, M. K. (2015). Microbial community development on the surface of Hans and Werenskiold glaciers (Svalbard, Arctic): a comparison. *Extremophiles* 19, 885–897. doi: 10.1007/s00792-015-0764-z

Hamaki, T., Suzuki, M., Fudou, R., Jojima, Y., Kajiura, T., Tabuchi, A., et al. (2005). Isolation of novel Bacteria and Actinomycetes using soil-extract agar medium. *J. Biosci. Bioeng.* 99, 485–492. doi: 10.1263/jbb.99.485

Hattori, S. (2008). Syntrophic acetate-oxidizing microbes in methanogenic environments. *Microbes Environ.* 23, 118–127. doi: 10.1264/jsme2.23.118

Hedlund, B. P., Dodsworth, J. A., and Staley, J. T. (2015). The changing landscape of microbial biodiversity exploration and its implications for systematics. *Syst. Appl. Microbiol.* 38, 231–236. doi: 10.1016/j.syapm.2015.03.003

Henson, M. W., Pitre, D. M., Weckhorst, J. L., Lanclos, V. C., Webber, A. T., and Thrash, J. C. (2016). Artificial seawater media facilitate cultivating members of the microbial majority from the Gulf of Mexico. *mSphere* 1, e00028–e00016. doi: 10.1128/mSphere.00028-16

Hitchens, A. P., and Leikind, M. C. (1939). The introduction of agar agar into bacteriology. *J. Bacteriol.* 37, 485–493. doi: 10.1128/jb.37.5.485-493.1939

Ho, K.L., Lee, D.J., and Su, A., and Chang, JS. (2012). Biohydrogen from cellulosic feedstock: dilution-to-stimulation approach. *Int. J. Hydrog. Energy* 37:15582–15587, doi: 10.1016/j.ijhydene.2012.01.093

Holler, T., Widdel, F., K\nittel, K., Amann, R., Kellermann, M. Y., Hinrichs, K. U., et al. (2011). G. Thermophilic anaerobic oxidation of methane by marine microbial consortia. *ISME J.* 5, 1946–1956. doi: 10.1038/ismej.2011.77

Huber, R., Burggraf, S., Mayer, T., Barns, S. M., Rossnagel, P., and Stetter, K. O. (1995). Isolation of a hyperthermophilic archaeum predicted by in situ RNA analysis. *Nature* 376, 57–58. doi: 10.1038/376057a0

Huber, H., Burggraf, S., Mayer, T., Wyschkony, I., Rachel, R., and Stetter, K. O. (2000). Ignicoccus gen. Nov., a novel genus of hyperthermophilic, chemolithoautotrophic Archaea, represented by two new species, *Ignicoccus islandicus* sp. nov. and *Ignicoccus pacificus* sp. nov. *Int. J. Syst. Evol. Microbiol.* 50, 2093–2100.

Hug, L., Baker, B., Anantharaman, K., Brown, C. T., Probst, A. J., Castelle, C. J., et al. (2016). A new view of the tree of life. *Nat. Microbiol.* 1:16048. doi: 10.1038/nmicrobiol.2016.48

Ibrahim, A., Maatouk, M., Raoult, D., and Bittar, F. (2022). Reverse genomics: Design of Universal Epitope Sets to isolate all Saccharibacteria members from the human Oral cavity. *Microorganisms* 10:602. doi: 10.3390/microorganisms10030602

Imachi, H., Aoi, K., Tasumi, E., Yamanaka, Y., Saito, Y., Yamaguchi, T., et al. (2011). Cultivation of methanogenic community from subseafloor sediments using a continuous-flow bioreactor. *ISME J.* 5, 1913–1925. doi: 10.1038/ismej.2011.64

Imachi, H., Nobu, M. K., Nakahara, N., Morono, Y., Ogawara, M., Takaki, Y., et al. (2020). Isolation of an archaeon at the prokaryote–eukaryote interface. *Nature* 577, 519–525. doi: 10.1038/s41586-019-1916-6

Ingham, C. J., Sprenkels, A., Bomer, J., Molenaar, D., van den Berg, A., van Hylckama Vlieg, J. E., et al. (2007). The micro-petri dish, a million-well growth chip for the culture and high-throughput screening of microorganisms. *Proc. Natl. Acad. Sci.* 104, 18217–18222. doi: 10.1073/pnas.0701693104

Inoue, Y., Masamitsu, S., Ryota, N., Yoshiki, K., Kei, T., Kazuhiro, T., et al. (2017). Astaxanthin analogs, adonixanthin and lycopene, activate Nrf2 to prevent light-induced photoreceptor degeneration. *J. Pharmacol. Sci.* 134, 147–157. doi: 10.1016/j.jphs.2017.05.011

Jebbar, M., Hickman-Lewis, K., Cavalazzi, B., Taubner, R. S., Rittmann, S. K.-M. R., Antunes, A., et al. (2020). Microbial diversity and biosignatures: an icy moons perspective. *Space Sci. Rev.* 216:10. doi: 10.1007/s11214-019-0620-z

Jemil, N., Ben Ayed, H., Hmidet, N., and Nasri, M. (2016). Characterization and properties of biosurfactants produced by a newly isolated strain *Bacillus methylotrophicus* DCS1 and their applications in enhancing solubility of hydrocarbon. *World J. Microbiol. Biotechnol.* 32:175. doi: 10.1007/s11274-016-2132-2

Johnson, D. B. (1995). Selective solid media for isolating and enumerating acidophilic bacteria. *J. Microbiol. Methods* 23, 205–218. doi: 10.1016/0167-7012(95)00015-D

Joint, I., Mühling, M., and Querellou, J. (2010). Culturing marine bacteria—an essential prerequisite for biodiscovery. *Microb. Biotechnol.* 3, 564–575. doi: 10.1111/j.1751-7915.2010.00188.x

Jung, D., Liu, B., He, X., Owen, J. S., Liu, L., Yuan, Y., et al. (2021). Accessing previously uncultured marine microbial resources by a combination of alternative cultivation methods. *Microb. Biotechnol.* 14, 1148–1158. doi: 10.1111/1751-7915.13782

Jurelevicius, D., Cotta, S. R., Peixoto, R., Rosado, A. S., and Seldin, L. (2012). Distribution of alkane-degrading bacterial communities in soils from King George Island, maritime Antarctic. *Eur. J. Soil Biol.* 51, 37–44. doi: 10.1016/j.ejsobi.2012.03.006

Kaeberlein, T., Lewis, K., and Epstein, S. S. (2002). Isolating "uncultivable" microorganisms in pure culture in a simulated natural environment. *Science* 296, 1127–1129. doi: 10.1126/science.1070633

Kapinusova, G., Jani, K., Smrhova, T., Pajer, P., Jarosova, I., Suman, J., et al. (2022). Culturomics of Bacteria from radon-saturated water of the World's oldest radium mine. *Microbiology spectrum* 10, e01995–e01922. doi: 10.1128/spectrum.01995-22

Kara, S., and Liese, A. (2019). "Process considerations for the application of enzymes" in *Industrial Enzyme Applications*. eds. A. Vogel and O. May (Hoboken, NJ: Wiley Online Library), 71–94.

Kato, C. (2011). "Methods—isolation and cultivation procedures of piezophiles" in *Extremophiles Handbook*. eds. K. Horikoshi, G. Antranikian, A. Bull, F. Robb and K. Stetter (Tokyo: Springer-Verlag)

Kawaguchi, Y., Yang, Y., Kawashiri, N., Shiraishi, K., Takasu, M., Narumi, I., et al. (2013). The possible interplanetary transfer of microbes: assessing the viability of Deinococcus spp. under the ISS environmental conditions for performing exposure experiments of microbes in the Tanpopo mission. *Orig. Life Evol. Biosph.* 43, 411–428. doi: 10.1007/s11084-013-9346-1

Kawanishi, T., Shiraishi, T., Okano, Y., Sugawara, K., Hashimoto, M., Maejima, K., et al. (2011). New detection Systems of Bacteria Using Highly Selective Media Designed by SMART: selective medium-design algorithm restricted by two constraints. *PLoS One* 6:e16512. doi: 10.1371/journal.pone.0016512

Keloth, A., Anderson, O., Risbridger, D., and Paterson, L. (2018). Single cell isolation using optical tweezers. *Micromachines* 9:434. doi: 10.3390/mi9090434

Khelaifia, S., Caputo, A., Andrieu, C., Cadoret, F., Armstrong, N., Michelle, C., et al. (2018). Genome sequence and description of Haloferax massiliense sp. nov., a new halophilic archaeon isolated from the human gut. *Extremophiles* 22, 485–498. doi: 10.1007/s00792-018-1011-1

Kim, J. Y., and Yeo, M. K. (2016). A fabricated microfluidic paper-based analytical device (μPAD) for in situ rapid colorimetric detection of microorganisms in environmental water samples. *Mol. Cell. Toxicol.* 12, 101–109. doi: 10.1007/s13273-016-0013-2

Klein, T., Poghosyan, L., Barclay, J. E., Murrell, J. C., Hutchings, M. I., and Lehtovirta-Morley, L. E. (2022). Cultivation of ammonia-oxidising archaea on solid medium. *FEMS Microbiol. Lett.* 369:fnac029. doi: 10.1093/femsle/fnac029

Könneke, M., Bernhard, A. E., de La Torre, J. R., Walker, C. B., Waterbury, J. B., and Stahl, D. A. (2005). Isolation of an autotrophic ammonia-oxidizing marine archaeon. *Nature* 437, 543–546. doi: 10.1038/nature03911

Kumar, R., Verma, H., Haider, S., Bajaj, A., Sood, U., Ponnusamy, K., et al. (2017). Comparative genomic analysis reveals habitat-specific genes and regulatory hubs within the genus Novosphingobium. *mSystems* 2, e00017–e00020. doi: 10.1128/mSystems.00020-17

Kurm, V., van der Putten, W. H., and Hol, W. H. G. (2019). Cultivation-success of rare soil bacteria is not influenced by incubation time and growth medium. *PLoS One* 14:e0210073. doi: 10.1371/journal.pone.0210073

Kusuma, A. B., Putra, K. E., Vanggy, L. R., Loh, J., Nouioui, I., Goodfellow, M., et al. (2022). Actinospica acidithermotolerans sp. nov., a novel actinomycete isolated from sediment from an Indonesian hot spring. *Arch. Microbiol.* 204:518. doi: 10.1007/s00203-022-03058-7

Lage, C., Dalmaso, G., Teixeira, L., Bendia, A., Paulino-Lima, I., Galante, D., et al. (2012). Mini-review: probing the limits of extremophilic life in extraterrestrial environment-simulated experiments. *Int. J. Astrobiol.* 11, 251–256. doi: 10.1017/S1473550412000316

Lagier, J. C., Armougom, F., Million, M., Hugon, P., Pagnier, I., Robert, C., et al. (2012). Microbial culturomics: paradigm shift in the human gut microbiome study. *Clin. Microbiol. Infect.* 8, 1185–1193.

Lagier, J.-C., Dubourg, G., Million, M., Cadoret, F., Bilen, M., Fenollar, F., et al. (2018). Culturing the human microbiota and Culturomics. *Nat. Rev. Microbiol.* 16, 540–550. doi: 10.1038/s41579-018-0041-0

Lagier, J.-C., Khelaifia, S., Alou, M. T., Ndongo, S., Dione, N., Hugon, P., et al. (2016). Culture of previously uncultured members of the human gut microbiota by culturomics. *Nat. Microbiol.* 1:16203. doi: 10.1038/nmicrobiol.2016.203

Landreau, M., Duthoit, F., Claeys-Bruno, M., Vandenabeele-Trambouze, O., Aubry, T., Godfroy, A., et al. (2016). Entrapment of anaerobic thermophilic and Hyperthermophilic marine Micro-organisms in a Gellan/xanthan matrix. *J. Appl. Microbiol.* 120, 1531–1541. doi: 10.1111/jam.13118

Leadbetter, J. R. (2003). Cultivation of recalcitrant microbes: cells are alive, well and revealing their secrets in the 21st century laboratory. *Curr. Opin. Microbiol.* 6, 274–281. doi: 10.1016/S1369-5274(03)00041-9

Lee, K. S., Palatinszky, M., Pereira, F. C., Nguyen, J., Fernandez, V. I., Mueller, A. J., et al. (2019). An automated raman-based platform for the sorting of live cells by functional properties. *Nat. Microbiol.* 4, 1035–1048. doi: 10.1038/s41564-019-0394-9

Lee, K. S., Pereira, F. C., Palatinszky, M., Behrendt, L., Alcolombri, U., Berry, D., et al. (2021). Optofluidic Raman-activated cell sorting for targeted genome retrieval or cultivation of microbial cells with specific functions. *Nat. Protoc.* 16, 634–676. doi: 10.1038/s41596-020-00427-8

Levy, A. F., Labrador, A., Knecht, L., and Van Dyken, J. D. (2020). An inexpensive, high-throughput μPAD assay of microbial growth rate and motility on solid surfaces

using Saccharomyces cerevisiae and Escherichia coli as model organisms. *PLoS One* 15:e0225020. doi: 10.1371/journal.pone.0225020

Li, L., Mendis, N., Trigui, H., Oliver, J. D., and Faucher, S. P. (2014). The importance of the viable but non-culturable state in human bacterial pathogens. *Front Microbiol.* 2:258. doi: 10.3389/fmicb.2014.00258

Ling, L. L., Schneider, T., Peoples, A. J., Spoering, A. L., Engels, I., Conlon, B. P., et al. (2015). A new antibiotic kills pathogens without detectable resistance. *Nature* 517, 455–459. doi: 10.1038/nature14098

Lloyd, K. G., Steen, A. D., Ladau, J., Yin, J., and Crosby, L. (2018). Phylogenetically novel uncultured microbial cells dominate earth microbiomes. *mSystems* 3, e00055–e00018. doi: 10.1128/mSystems.00055-18

Lopez, J. V., Peixoto, R. S., and Rosado, A. S. (2019). Inevitable future: space colonization beyond earth with microbes first. *FEMS Microbiol. Ecol.* 95:127. doi: 10.1093/femsec/fiz127

López-García, P., and Moreira, D. (2020). Cultured Asgard Archaea shed light on Eukaryogenesis. *Cells* 181, 232–235. doi: 10.1016/j.cell.2020.03.058

Mac Rygaard, A., Thøgersen, M. S., Nielsen, K. F., Gram, L., and Bentzon-Tilia, M. (2017). 92017. Effects of gelling agent and extracellular signaling molecules on the Culturability of marine Bacteria. *Appl. Environ. Microbiol.* 83, e00243–e00317. doi: 10.1128/AEM.00243-17

MacElroy, R. (1974). Some comments on the evolution of extremophiles. *Biosystems* 6, 74–75. doi: 10.1016/0303-2647(74)90026-4

Marcy, Y., Ouverney, C., Bik, E. M., Lösekann, T., Ivanova, N., Martin, H. G., et al. (2007). Dissecting biological "dark matter" with single-cell genetic analysis of rare and uncultivated TM7 microbes from the human mouth. *Proc. Natl. Acad. Sci. U. S. A.* 104, 11889–11894. doi: 10.1073/pnas.0704662104

Marmann, A., Aly, A. H., Lin, W., Wang, B., and Proksch, P. (2014). Co-cultivation—a powerful emerging tool for enhancing the chemical diversity of microorganisms. *Mar. Drugs* 12, 1043–1065. doi: 10.3390/md12021043

Márquez, S. L., and Blamey, J. M. (2019). Isolation and partial characterization of a new moderate thermophilic Albidovulum sp. SLM16 with transaminase activity from Deception Island, Antarctica. *Biol. Res.* 52:5. doi: 10.1186/s40659-018-0210-7

Martínez-Espinosa, R. M. (2020). Microorganisms and their metabolic capabilities in the context of the biogeochemical nitrogen cycle at extreme environments. *Int. J. Mol. Sci.* 21:4228. doi: 10.3390/ijms21124228

Mastascusa, V., Romano, I., Di Donato, P., Poli, A., Della Corte, V., Rotundi, A., et al. (2014). Extremophiles survival to simulated space conditions: an astrobiology model study. *Orig. Life Evol. Biosph.* 44, 231–237. doi: 10.1007/s11084-014-9397-y

Mee, M. T., Collins, J. J., Church, G. M., and Wang, H. H. (2014). Syntrophic exchange in synthetic microbial communities. *Proc. Natl. Acad. Sci. U. S. A.* 111, E2149–E2156. doi: 10.1073/pnas.1405641111

Merino, N., Aronson, H. S., Bojanova, D. P., Feyhl-Buska, J., Wong, M. L., Zhang, S., et al. (2019). Living at the extremes: extremophiles and the limits of life in a planetary context. *Front. Microbiol.* 10:780. doi: 10.3389/fmicb.2019.00780

Mesbah, N. M. (2022). Industrial biotechnology based on enzymes from extreme environments. *Front. Bioeng. Biotechnol.* 5:870083. doi: 10.3389/fbioe.2022.870083

Moissl-Eichinger, C., Pausan, M., Taffner, J., Berg, G., Bang, C., and Schmitz, R. A. (2018). Archaea are interactive components of complex microbiomes. *Trends Microbiol.* 26, 70–85. doi: 10.1016/j.tim.2017.07.004

Molina-Menor, E., Gimeno-Valero, H., Pascual, J., Peretó, J., and Porcar, M. (2021). High Culturable bacterial diversity from a European Desert: the Tabernas Desert. *Front. Microbiol.* 11:583120. doi: 10.3389/fmicb.2020.583120

Monsalves, M. T., Ollivet-Besson, G. P., Amenabar, M. J., and Blamey, J. M. (2020). Isolation of a Psychrotolerant and UV-C-resistant bacterium from Elephant Island, Antarctica with a highly Thermoactive and thermostable catalase. *Microorganisms.* 8:95. doi: 10.3390/microorganisms8010095

Ñancucheo, I., Oliveira, R., Dall'Agnol, H., Johnson, D. B., Grail, B., Holanda, R., et al. (2016). Draft Genome Sequence of a Novel Acidophilic Iron-Oxidizing Firmicutes Species, "Acidibacillus ferrooxidans" (SLC66T). *Genome Announc.* 19, e00383–e00316. doi: 10.1128/genomeA.00383-16

Napoli, A., Micheletti, D., Pindo, M., Larger, S., Cestaro, A., de Vera, J. P., et al. (2022). Absence of increased genomic variants in the cyanobacterium Chroococcidiopsis exposed to Mars-like conditions outside the space station. *Sci. Rep.* 12:8437. doi: 10.1038/s41598-022-12631-5

Nayfach, S., Roux, S., Seshadri, R., Udwary, D., Varghese, N., Schulz, F., et al. (2021). A genomic catalog of Earth's microbiomes. *Nat. Biotechnol.* 39, 499–509. doi: 10.1038/s41587-020-0718-6

Nichols, D., Cahoon, N., Trakhtenberg, E. M., Pham, L., Mehta, A., Belanger, A., et al. (2010). Use of Ichip for high-throughput in situ cultivation of "uncultivable" microbial species. *Appl. Environ. Microbiol.* 76, 2445–2450. doi: 10.1128/AEM.01754-09

Nichols, D., Lewis, K., Orjala, J., Mo, S., Ortenberg, R., O'Connor, P., et al. (2008). Short peptide induces an "uncultivable" microorganism to grow in vitro. *Appl. Environ. Microbiol.* 74, 4889–4897. doi: 10.1128/AEM.00393-08

Nicholson, W. L., Munakata, N., Horneck, G., Melosh, H. J., and Setlow, P. (2000). Resistance of Bacillus endospores to extreme terrestrial and extraterrestrial environments. *Microbiol. Mol. Biol. Rev.* 64, 548–572. doi: 10.1128/MMBR.64.3.548-572.2000

Nielsen, H., Almeida, M., Juncker, A., Rasmussen, S., Li, J., Sunagawa, S., et al. (2014). Identification and assembly of genomes and genetic elements in complex metagenomic samples without using reference genomes. *Nat. Biotechnol.* 32, 822–828. doi: 10.1038/nbt.2939

Noiphung, J., and Laiwattanapaisal, W. (2019). Multifunctional paper-based analytical device for in situ cultivation and screening of *Escherichia Coli* infections. *Sci. Rep.* 9:1555. doi: 10.1038/s41598-018-38159-1

Padan, E., Bibi, E., Ito, M., and Krulwich, T. A. (2005). Alkaline pH homeostasis in bacteria: new insights. *Biochim. Biophys. Acta BBA-Biomembr.* 1717, 67–88. doi: 10.1016/j.bbamem.2005.09.010

Palma Esposito, F., Ingham, C. J., Hurtado-Ortiz, R., Bizet, C., Tasdemir, D., and de Pascale, D. (2018). Isolation by miniaturized culture Chip of an Antarctic bacterium Aequorivita sp. with antimicrobial and anthelmintic activity. *Biotechnol. Rep.* 20:e00281. doi: 10.1016/j.btre.2018.e00281

Pande, S., and Kost, C. (2017). Bacterial Unculturability and the formation of intercellular metabolic networks. *Trends Microbiol.* 25, 349–361. doi: 10.1016/j.tim.2017.02.015

Paulino-Lima, I. G., Azua-Bustos, A., Vicuña, R., González-Silva, C., Salas, L., Teixeira, L., et al. (2013). Isolation of UVC-tolerant Bacteria from the Hyperarid Atacama Desert, Chile. *Microb. Ecol.* 65, 325–335. doi: 10.1007/s00248-012-0121-z

Paulino-Lima, I. G., Fujishima, K., Navarrete, J. U., Galante, D., Rodrigues, F., Azua-Bustos, A., et al. (2016). Extremely high UV-C radiation resistant microorganisms from desert environments with different manganese concentrations. *J. Photochem. Photobiol. B* 163, 327–336. doi: 10.1016/j.jphotobiol.2016.08.017

Peixoto, R., Chaer, G. M., Carmo, F. L., Araújo, F. V., Paes, J. E., Volpon, A., et al. (2011). Bacterial communities reflect the spatial variation in pollutant levels in Brazilian mangrove sediment. *Antonie Van Leeuwenhoek* 99, 341–354. doi: 10.1007/s10482-010-9499-0

Perfumo, A., Banat, I. M., and Marchant, R. (2018). Going green and cold: biosurfactants from low-temperature environments to biotechnology applications. *Trends Biotechnol.* 36, 277–289. doi: 10.1016/j.tibtech.2017.10.016

Pham, V. H. T., and Kim, J. (2012). Cultivation of Unculturable soil Bacteria. *Trends Biotechnol.* 30, 475–484. doi: 10.1016/j.tibtech.2012.05.007

Phan, H. V., Kurisu, F., Kiba, K., and Furumai, H. (2021). Optimized cultivation and syntrophic relationship of anaerobic benzene-degrading enrichment cultures under methanogenic conditions. *Microbes Environ.* 36:ME21028. doi: 10.1264/jsme2.ME21028

Pillot, G., Davidson, S., Auria, R., Combet-Blanc, Y., Godfroy, A., and Liebgott, P. P. (2020). Production of current by syntrophy between exoelectrogenic and fermentative hyperthermophilic microorganisms in heterotrophic biofilm from a deep-sea hydrothermal chimney. *Microb. Ecol.* 79, 38–49. doi: 10.1007/s00248-019-01381-z

Plugge, C. M., and Stams, A. J. (2002). Enrichment of thermophilic syntrophic anaerobic glutamate-degrading consortia using a dialysis membrane reactor. *Microb Ecol.* 43, 378–387. doi: 10.1007/s00248-001-0047-3

Pope, E., Cartmell, C., Haltli, B., Ahmadi, A., and Kerr, R. G. (2022). Microencapsulation and in situ incubation methodology for the cultivation of marine bacteria. *Front. Microbiol.* 22:958660. doi: 10.3389/fmicb.2022.958660

Pulschen, A. A., Araujo, G. G., Carvalho, A. C. S. R., Cerini, M. F., Fonseca, L. D. M., Galante, D., et al. (2018). Survival of Extremophilic yeasts in the stratospheric environment during balloon flights and in laboratory simulations. *Appl. Environ. Microbiol.* 84, e01942–e01918. doi: 10.3389/fmicb.2017.01346

Pulschen, A. A., Bendia, A. G., Fricker, A. D., Pellizari, V. H., Galante, D., and Rodrigues, F. (2017). Isolation of uncultured Bacteria from Antarctica using long incubation periods and low nutritional media. *Front. Microbiol.* 14:1346. doi: 10.3389/fmicb.2017.01346

Rachid, C. T. C. C., Balieiro, F. C., Fonseca, E. S., Peixoto, R. S., Chaer, G. M., Tiedje, J. M., et al. (2015). Intercropped Silviculture systems, a key to achieving soil fungal Community Management in Eucalyptus Plantations. *PLoS One* 10:e0118515. doi: 10.1371/journal.pone.0118515

Rampelotto, P.H. (2016). *Biotechnology of Extremophiles: Advances and Challenges (Grand Challenges in Biology and Biotechnology)*. New York, NY: Springer, 720

Rao, A. S., Nair, Y., More, V. S., Anantharaju, K. S., and More, S. S. (2022). "Chapter 11—extremophiles for sustainable agriculture" in *New and Future Developments in Microbial Biotechnology and Bioengineering*. eds. H. B. Singh and A. Vaishnav (Amsterdam, Netherlands: Elsevier), 243–264.

Rappé, M. S., Connon, S. A., Vergin, K. L., and Giovannoni, S. J. (2002). Cultivation of the ubiquitous SAR11 marine bacterioplankton clade. *Nature* 418, 630–633. doi: 10.1038/nature00917

Reasoner, D. J., and Geldreich, E. E. (1985). A new medium for the enumeration and subculture of bacteria from potable water. *Appl. Environ. Microbiol.* 49, 1–7. doi: 10.1128/aem.49.1.1-7.1985

Reis-Mansur, M. C. P., Cardoso-Rurr, J. S., Silva, J. V. M. A., de Souza, G. R., da Silva Cardoso, V., Mansoldo, F. R. P., et al. (2019). Carotenoids from UV-resistant Antarctic Microbacterium sp. LEMMJ01. *Sci. Rep.* 9:9554. doi: 10.1038/s41598-019-45840-6

Rinke, C., Schwientek, P., Sczyrba, A., Ivanova, N. N., Anderson, I. J., Cheng, J. F., et al. (2013). Insights into the phylogeny and coding potential of microbial dark matter. *Nature* 499, 431–437. doi: 10.1038/nature12352

Robinson, J. L., Pyzyna, B., Atrasz, R. G., Henderson, C. A., Morrill, K. L., Burd, A. M., et al. (2005). Growth kinetics of extremely halophilic archaea (family halobacteriaceae) as revealed by arrhenius plots. *J. Bacteriol.* 187, 923–929. doi: 10.1128/JB.187.3.923-929.2005

Rodrigues-Oliveira, T., Wollweber, F., Ponce-Toledo, R. I., Chen, W., Ponce-Toledo, R. I., Savvides, S. N., et al. (2023). Actin cytoskeleton and complex cell architecture in an Asgard archaeon. *Nature* 613, 332–339. doi: 10.1038/s41586-022-05550-y

Rothschild, L. J., and Mancinelli, R. L. (2001). Life in extreme environments. *Nature* 409, 1092–1101. doi: 10.1038/35059215

Sagar, S., Esau, L., Hikmawan, T., Antunes, A., Holtermann, K., Stingl, U., et al. (2013b). Cytotoxic and apoptotic evaluations of marine bacteria isolated from brine-seawater interface of the Red Sea. *BMC Complement. Altern. Med.* 13:29. doi: 10.1186/1472-6882-13-29

Sagar, S., Esau, L., Holtermann, K., Hikmawan, T., Zhang, G., Stingl, U., et al. (2013a). Induction of apoptosis in cancer cell lines by the Red Sea brine pool bacterial extracts. *BMC Complement. Altern. Med.* 13:344. doi: 10.1186/1472-6882-13-344

Salcher, M. M., Neuenschwander, S. M., Posch, T., and Pernthaler, J. (2015). The ecology of pelagic freshwater methylotrophs assessed by a high-resolution monitoring and isolation campaign. *ISME J.* 9, 2442–2453. doi: 10.1038/ismej.2015.55

Salwan, R., and Sharma, V. (2020). Molecular and biotechnological aspects of secondary metabolites in Actinobacteria. *Microbiol. Res.* 231:126374. doi: 10.1016/j.micres.2019.126374

Sánchez-Andrea, I., Florentino, A. P., Semerel, J., Strepis, N., Sousa, D. Z., and Stams, A. J. M. (2018). Co-culture of a novel fermentative bacterium, Lucifera butyrica gen. Nov. sp. nov., with the sulfur reducer Desulfurella amilsii for enhanced Sulfidogenesis. *Front. Microbiol.* 13:3108. doi: 10.3389/fmicb.2018.03108

Sari, D. C. A. F., Ningsih, F., Yokota, A., Yabe, S., Sjamsuridzal, W., and Oetari, A. (2020). Aerial mycelium formation in rare thermophilic Actinobacteria on media solidified with agar and Gellan gum. *IOP Conf. Ser. Earth Environ. Sci.* 483:012017. doi: 10.1088/1755-1315/483/1/012017

Sayed, A. M., Hassan, M. H. A., Alhadrami, H. A., Hassan, H. M., Goodfellow, M., and Rateb, M. E. (2020). Extreme environments: microbiology leading to specialized metabolites. *J. Appl. Microbiol.* 128, 630–657. doi: 10.1111/jam.14386

Schmid, A. K., Allers, T., and DiRuggiero, J. (2020). SnapShot: microbial extremophiles. *Cells* 180, 818–818.e1. doi: 10.1016/j.cell.2020.01.018

Schultz, J., Argentino, I. C. V., Kallies, R., Nunes da Rocha, U., and Rosado, A. S. (2022b). Polyphasic analysis reveals potential petroleum hydrocarbon degradation and biosurfactant production by rare biosphere thermophilic Bacteria from Deception Island, an active Antarctic volcano. *Front. Microbiol.* 4:885557. doi: 10.3389/fmicb.2022.885557

Schultz, J., Modolon, F., Rosado, A. S., Voolstra, C. R., Sweet, M., and Peixoto, R. S. (2022a). Methods and strategies to uncover coral-associated microbial dark matter. *mSystems* 7:e0036722. doi: 10.1128/msystems.00367-22

Schultz, J., and Rosado, A. S. (2019). "Use of microbes from extreme environments for biotechnological applications" in *Advanced Techniques for Studying Microorganisms in Extreme Environments*. ed. E. Yergeau (Boston, MA: De Gruyter), 33–56.

Schultz, J., and Rosado, A. S. (2020). Extreme environments: a source of biosurfactant for biotechnological applications. *Extremop. J.* 1, 1–18. doi: 10.1007/s00792-019-01151-2

Seyler, L., Kujawinski, E. B., Azua-Bustos, A., Lee, M. D., Marlow, J., Perl, S. M., et al. (2020). Metabolomics as an emerging tool in the search for astrobiologically relevant biomarkers. *Astrobiology* 20, 1251–1261. doi: 10.1089/ast.2019.2135

Shaw, C., Brooke, C., Hawley, E., Connolly, M. P., Garcia, J. A., Harmon-Smith, M., et al. (2020). Phototrophic co-cultures from extreme environments: community structure and potential value for fundamental and applied research. *Front. Microbiol.* 6:572131. doi: 10.3389/fmicb.2020.572131

Sheikhi, F., Roayaei Ardakani, M., Enayatizamir, N., and Rodriguez-Couto, S. (2012). The determination of assay for laccase of *Bacillus Subtilis* WPI with two classes of chemical compounds as substrates. *Indian J. Microbiol.* 52, 701–707. doi: 10.1007/s12088-012-0298-3

Shock, E. L., and Boyd, E. S. (2015). Principles of Geobiochemistry. *Elements* 11, 395–401. doi: 10.2113/gselements.11.6.395

Shu, W. S., and Huang, L. N. (2022). Microbial diversity in extreme environments. *Nat. Rev. Microbiol.* 20, 219–235. doi: 10.1038/s41579-021-00648-y

Shungu, D., Valiant, M., Tutlane, V., Weinberg, E., Weissberger, B., Koupal, L., et al. (1983). Gelrite as an agar substitute in bacteriological media. *Appl. Environ. Microbiol.* 46, 840–845. doi: 10.1128/aem.46.4.840-845.1983

Sieber, J. R., Sims, D. R., Han, C., Kim, E., Lykidis, A., Lapidus, A. L., et al. (2010). The genome of *Syntrophomonas wolfei*: new insights into syntrophic metabolism and biohydrogen production. *Environ. Microbiol.* 12, 2289–2301. doi: 10.1111/j.1462-2920.2010.02237.x

Smith, D. J., Thakrar, P. J., Bharrat, A. E., Dokos, A. G., Kinney, T. L., James, L. M., et al. (2014). Aballoon-based payload for exposing microorganisms in the stratosphere (E-MIST). *Gravitat. Space Res.* 2, 70–80. doi: 10.2478/gsr-2014-0019

Song, J., Oh, H.-M., and Cho, J.-C. (2009). Improved culturability of SAR11 strains in dilution-to-extinction culturing from the East Sea, West Pacific Ocean. *FEMS Microbiol. Lett.* 295, 141–147. doi: 10.1111/j.1574-6968.2009.01623.x

Sood, U., Kumar, R., and Hira, P. (2021). Expanding culturomics from gut to extreme environmental settings. *Msystems* 6, e00848–e00921. doi: 10.1128/mSystems.00848-21

Spietz, R. L., Lundeen, R. A., Zhao, X. W., Nicastro, D., Ingalls, A. E., and Morris, R. M. (2019). Heterotrophic carbon metabolism and energy acquisition in Candidatus Thioglobus singularis strain PS1, a member of the SUP05 clade of marine Gammaproteobacteria. *Environ. Microbiol.* 21, 2391–2240. doi: 10.1111/1462-2920.14623

Stan-Lotter, H., and Fendrihan, S. (2015). Halophilic Archaea: life with desiccation, radiation and oligotrophy over geological times. *Lifestyles* 5:1487. doi: 10.3390/life5031487

Steinert, G., Whitfield, S., Taylor, M. W., Thoms, C., and Schupp, P. J. (2014). Application of diffusion growth chambers for the cultivation of marine sponge-associated bacteria. *Mar. Biotechnol.* 16, 594–603. doi: 10.1007/s10126-014-9575-y

Stepanov, V. G., Tirumalai, M. R., Montazari, S., Checinska, A., Venkateswaran, K., and Fox, G. E. (2016). *Bacillus pumilus* SAFR-032 genome revisited: sequence update and re-annotation. *PLoS One* 11:e0157331. doi: 10.1371/journal.pone.0157331

Stewart, E. J. (2012). Growing unculturable bacteria. *J Bacteriol.* 194, 4151–4160. doi: 10.1128/JB.00345-12

Steven, B., Briggs, G., McKay, C. P., Pollard, W. H., Greer, C. W., and Whyte, L. G. (2007). Characterization of the microbial diversity in a permafrost sample from the Canadian high Arctic using culture-dependent and culture-independent methods. *FEMS Microbiol. Ecol.* 59, 513–523. doi: 10.1111/j.1574-6941.2006.00247.x

Sun, Y., Liu, Y., Pan, J., Wang, F., and Li, M. (2020). Perspectives on cultivation strategies of Archaea. *Microb. Ecol.* 79, 770–784. doi: 10.1007/s00248-019-01422-7

Svenning, M. M., Wartiainen, I., Hestnes, A. G., and Binnerup, S. J. (2003). Isolation of methane oxidising bacteria from soil by use of a soil substrate membrane system. *FEMS Microbiol. Ecol.* 44, 347–354. doi: 10.1016/S0168-6496(03)00073-4

Sysoev, M., Grötzinger, S. W., Renn, D., Eppinger, J., Rueping, M., and Karan, R. (2021). Bioprospecting of novel Extremozymes from prokaryotes-the advent of culture-independent methods. *Front. Microbiol.* 10:630013. doi: 10.3389/fmicb.2021.630013

Thombre, R. S., Gomez, F., Parkhe, R., Kaur, K., Vaishampayan, P., Shivakarthik, E., et al. (2020). Effect of impact shock on extremophilic Halomonas gomseoemensis EP-3 isolated from hypersaline sulphated Lake Laguna de Peña Hueca, Spain, planetary and space science. *ISSN* 192:105041. doi: 10.1016/j.pss.2020.105041

Tilahun, L., Asrat, A., Wessel, G. M., and Simachew, A. (2021). Prediction of genes that function in Methanogenesis and CO_2 pathways in extremophiles. *Microorganisms* 9:2211. doi: 10.3390/microorganisms9112211

Topçuoglu, B. D., and Holden, J. F. (2019). "Extremophiles: hot environments" in *Encyclopedia of Microbiology*. ed. T. M. Schmidt. *2th* ed (Cambridge, MA: Academic Press), 263–269.

Tsudome, M., Deguchi, S., Tsujii, K., Ito, S., and Horikoshi, K. (2009). Versatile solidified nanofibrous cellulose-containing media for growth of extremophiles. *Appl. Environ. Microbiol.* 75, 4616–4619. doi: 10.1128/AEM.00519-09

Tyson, G. W., Lo, I., Baker, B. J., Allen, E. E., Hugenholtz, P., and Banfield, J. F. (2005). Genome-directed isolation of the key nitrogen fixer Leptospirillum ferrodiazotrophum sp. nov. from an acidophilic microbial community. *Appl. Environ. Microbiol.* 71, 6319–6324. doi: 10.1128/AEM.71.10.6319-6324.2005

Vartoukian, S. R., Palmer, R. M., and Wade, W. G. (2010). Strategies for culture of 'unculturable' bacteria. *FEMS Microbiol. Lett.* 309, 1–7. doi: 10.1111/j.1574-6968.2010.02000.x

Vester, J. K., Glaring, M. A., and Stougaard, P. (2013). Improving diversity in cultures of bacteria from an extreme environment. *Can. J. Microbiol.* 59, 581–586. doi: 10.1139/cjm-2013-0087

Vester, J. K., Glaring, M. A., and Stougaard, P. (2015). Improved cultivation and metagenomics as new tools for bioprospecting in cold environments. *Extremophiles* 19, 17–29. doi: 10.1007/s00792-014-0704-3

Vijayakumar, S., and Saravanan, V. (2015). Biosurfactants-types, sources and applications. *Res. J. Microbiol.* 10, 181–192. doi: 10.3923/jm.2015.181.192

Volpiano, C. G., Sant'Anna, F. H., da Mota, F. F., Sangal, V., Sutcliffe, I., Munusamy, M., et al. (2021). Proposal of Carbonactinosporaceae fam. Nov. within the class Actinomycetia. Reclassification of *Streptomyces thermoautotrophicus* as Carbonactinospora thermoautotrophica gen. Nov., comb. nov. *Syst. Appl. Microbiol.* 44:126223. doi: 10.1016/j.syapm.2021.126223

Weissman, J. L., Hou, S., and Fuhrman, J. A. (2021). Estimating maximal microbial growth rates from cultures, metagenomes, and single cells via codon usage patterns. *Proc. Natl. Acad. Sci. U.S.A.* 118:e2016810118. doi: 10.1073/pnas.2016810118

Yadav, A. N. (2021). Microbial biotechnology for bioprospecting of microbial bioactive compounds and secondary metabolites. *J. Appl. Biol. Biotechnol.* 9, 1–6. doi: 10.7324/JABB.2021.92ed

Yasir, M., Qureshi, A. K., Khan, I., Bibi, F., Rehan, M., Khan, S. B., et al. (2019). Culturomics-based taxonomic diversity of bacterial communities in the hot springs

of Saudi Arabia. Omics: a journal of. *Integr. Biol.* 23, 17–27. doi: 10.1089/omi.2018.0176

Yamamoto, A., Kitano, H., and Araki, K. (2017). Selective medium design for the Japanese eel pathogen Edwardsiella tarda by SMART: selective medium-design algorithm restricted by two constraints. *Gyobyo Kenkyu = Fish Pathology* 52: 1, 42–45. doi: 10.3147/jsfp.52.42

Zamkovaya, T., Foster, J. S., de Crécy-Lagard, V., and Conesa, A. A. (2021). Network approach to elucidate and prioritize microbial dark matter in microbial communities. *ISME J.* 15, 228–244. doi: 10.1038/s41396-020-00777-x

Zeng, Y., Wu, N., Madsen, A. M., Chen, X., Gardiner, A. T., and Koblížek, M. (2021). Gemmatimonas groenlandica sp. nov. is an aerobic anoxygenic phototroph in the phylum Gemmatimonadetes. *Front. Microbiol.* 11:606612. doi: 10.3389/fmicb.2020.606612

Zengler, K., Toledo, G., Rappé, M., Elkins, J., Mathur, E. J., Short, J. M., et al. (2002). Cultivating the uncultured. *Proc. Natl. Acad. Sci. U. S. A.* 99, 15681–15686. doi: 10.1073/pnas.252630999

Zengler, K., Walcher, M., Clark, G., Haller, I., Toledo, G., Holland, T., et al. (2005). High-throughput cultivation of microorganisms using microcapsules. *Methods Enzymol.* 397, 124–130.

Zhang, H., and Liu, K.-K. (2008). Optical tweezers for single cells. *J. R. Soc. Interface* 5, 671–690. doi: 10.1098/rsif.2008.0052

Zhu, D., Adebisi, W. A., Ahmad, F., Sethupathy, S., Danso, B., and Sun, J. (2020). Recent development of Extremophilic Bacteria and their application in biorefinery. *Front. Bioeng. Biotechnol.* 8:483. doi: 10.3389/fbioe.2020.00483

frontiers | Frontiers in Microbiology

TYPE Original Research
PUBLISHED 11 October 2023
DOI 10.3389/fmicb.2023.1173613

OPEN ACCESS

EDITED BY
Virginia P. Edgcomb,
Woods Hole Oceanographic Institution,
United States

REVIEWED BY
Alexandre Soares Rosado,
King Abdullah University of Science and Technology, Saudi Arabia
Jason B. Sylvan,
Texas A&M University, United States

*CORRESPONDENCE
Mirjam Perner
✉ mperner@geomar.de
Nicole Adam-Beyer
✉ nadam@geomar.de

RECEIVED 24 February 2023
ACCEPTED 26 September 2023
PUBLISHED 11 October 2023

CITATION
Adam-Beyer N, Laufer-Meiser K, Fuchs S, Schippers A, Indenbirken D, Garbe-Schönberg D, Petersen S and Perner M (2023) Microbial ecosystem assessment and hydrogen oxidation potential of newly discovered vent systems from the Central and South-East Indian Ridge. *Front. Microbiol.* 14:1173613. doi: 10.3389/fmicb.2023.1173613

Microbial ecosystem assessment and hydrogen oxidation potential of newly discovered vent systems from the Central and South-East Indian Ridge

Nicole Adam-Beyer[1]*, Katja Laufer-Meiser[1], Sebastian Fuchs[2], Axel Schippers[2], Daniela Indenbirken[3], Dieter Garbe-Schönberg[4], Sven Petersen[5] and Mirjam Perner[1]*

[1]Marine Geosystems, GEOMAR Helmholtz Centre for Ocean Research Kiel, Kiel, Germany, [2]Federal Institute for Geosciences and Natural Resources (BGR), Hannover, Germany, [3]Leibniz Institute of Virology, Hamburg, Germany, [4]Institute of Geosciences, Christian-Albrechts-Universität zu Kiel, Kiel, Germany, [5]GEOMAR Helmholtz Centre for Ocean Research Kiel, Kiel, Germany

In order to expand the knowledge of microbial ecosystems from deep-sea hydrothermal vent systems located on the Central and South-East Indian Ridge, we sampled hydrothermal fluids, massive sulfides, ambient water and sediments of six distinct vent fields. Most of these vent sites were only recently discovered in the course of the German exploration program for massive sulfide deposits and no previous studies of the respective microbial communities exist. Apart from typically vent-associated chemosynthetic members of the orders *Campylobacterales*, *Mariprofundales*, and *Thiomicrospirales*, high numbers of uncultured and unspecified Bacteria were identified via 16S rRNA gene analyses in hydrothermal fluid and massive sulfide samples. The sampled sediments however, were characterized by an overall lack of chemosynthetic Bacteria and the presence of high proportions of low abundant bacterial groups. The archaeal communities were generally less diverse and mostly dominated by members of *Nitrosopumilales* and *Woesearchaeales*, partly exhibiting high proportions of unassigned Archaea. Correlations with environmental parameters were primarily observed for sediment communities and for microbial species (associated with the nitrogen cycle) in samples from a recently identified vent field, which was geochemically distinct from all other sampled sites. Enrichment cultures of diffuse fluids demonstrated a great potential for hydrogen oxidation coupled to the reduction of various electron-acceptors with high abundances of *Hydrogenovibrio* and *Sulfurimonas* species. Overall, given the large number of currently uncultured and unspecified microorganisms identified in the vent communities, their respective metabolic traits, ecosystem functions and mediated biogeochemical processes have still to be resolved for estimating consequences of potential environmental disturbances by future mining activities.

KEYWORDS

16S rRNA, geochemistry, hydrothermal vents, sediments, Indian Ridge, enrichment, hydrogen oxidation

Introduction

Mid-Ocean Ridges, which are formed at spreading centers of tectonic plate boundaries, are the most common setting for the presence and formation of deep-sea hydrothermal vent systems. In these systems, geothermally heated and reduced fluids are emitted through fissures of the ocean floor. By mixing with the cold ambient seawater, minerals precipitate from the hot fluids (reaching temperatures of 400°C or even more) forming the typically observed chimney structures, enriched in various metals (Kelley et al., 2002; Haase et al., 2007). With the aim to achieve a carbon-neutral sustainable economy in the next decades, several metals have become important for implementing the energy and digital transformation. Therefore, deep-sea mining activities have moved into focus (Petersen et al., 2016). Actively venting hydrothermal systems provide a multitude of inorganic electron donors and acceptors (the latter mostly originating from the mixing with ambient seawater), that enable primary biomass production of microorganisms fueling species-rich ecosystems in the deep-sea (Hügler and Sievert, 2011; Dick et al., 2013; Levin et al., 2016). Depending on the geological setting and the host-rocks that shape the chemical fluid compositions, the most abundant electron-donors are hydrogen (H_2) and/or hydrogen sulfide (H_2S) (e.g., Wetzel and Shock, 2000; Perner et al., 2007; Adam and Perner, 2018). The availability of the reduced compounds strongly depends on the degree of mixing processes, which result in steep thermal and chemical gradients, providing a dynamic habitat for the prevailing microorganisms (Adam and Perner, 2018 and reference therein).

Microbial communities and their potential roles in biogeochemical cycles and ecosystem functions have been studied at the majority of the known Mid-Ocean Ridges. However, compared to the Mid-Atlantic Ridge (MAR) and East-Pacific Rise (EPR), the Indian Ridge (IR) still remains underrepresented. Microbiological studies at the Indian Ridge have so far included the Kairei, Edmond, and the newly discovered Onnuri vent fields at the slow-spreading Central Indian Ridge (CIR) (Nakamura and Takai, 2015; Han et al., 2018; Adam et al., 2019; Namirimu et al., 2022), the Longqi, Tianzuo and recently identified Old City hydrothermal fields at the ultraslow-spreading South-West Indian Ridge (SWIR) (Li et al., 2016; Ding et al., 2017; Yang et al., 2019; Lecoeuvre et al., 2021) as well as the recently discovered Pelagia vent site along the intermediate-spreading South-East Indian Ridge (SEIR) (Han et al., 2018). Predominantly, these studies have focused on the compositions of the microbial communities based on 16S rRNA gene tags and the putative metabolic functions and environmental implications of the identified taxa.

Starting in 2015, the German Federal Institute for Geosciences and Natural Resources (BGR) launched a program (INDEX) for the exploration of massive sulfide occurrences (SMS) and environmental base line studies in a license area on the Indian Ridge, awarded to Germany by the International Seabed authority. Compared to the MAR, a knowledge deficiency is postulated for IR vent environments regarding the baseline categories required for the determination of mining impacts. This gap includes both the geological background and the microbial and macrofaunal ecosystem functions (Amon et al., 2022). A recent review summarized and analyzed the insights (with respect to putative mining impacts) on IR ecosystems gained so far, but focused almost exclusively on the studies and descriptions of macrofaunal communities, which are known to comprise several endemic species contributing to the need of protection of these ecosystems (van der Most et al., 2023). However, in active vent environments, microbes also fulfill essential ecosystem functions and services like primary production and detoxification of harmful compounds, but also represent a valuable genetic resource for biotechnological or even medical applications (Orcutt et al., 2020 and references therein). For various reasons (including technical and ecological issues) the mining of active hydrothermal vent systems has become unlikely, moving inactive vent sites deposits in the focus of putative mining activities (Koschinsky et al., 2018; Van Dover et al., 2018; Amon et al., 2022). While the role of microbial communities and the possible impacts of their removal from active vent environments are known, the impact and ecosystem services of microbes in inactive vent sites – including element cycling and primary production - are only poorly understood (Orcutt et al., 2020; Van Dover et al., 2020). Since macrofaunal populations are far less abundant in inactive compared to active vents, the understanding of all microbial ecosystem functions in inactive vent environments is an essential prerequisite for the assessment of possible mining effects of SMS deposits.

In the course of the INDEX program, we already performed microbiological studies with sample material from the Kairei and Pelagia vent fields, collected within the framework of the 2016 sampling campaign (Han et al., 2018; Adam et al., 2019, 2021). These studies have addressed the enrichment of autotrophic, hydrogen-oxidizing microorganisms, comparisons of microbial community structures of active and inactive chimneys and the characterization of sediment-inhabiting microbial communities along a hydrothermal gradient. Several distinct phylogenetic groups (e.g., members of *Campylobacterales*, *Nautiliales,* and *Aquificales*) were exclusively found in active chimney habitats, while others (e.g., *Desulfobulbales*, *Thiotrichales,* and *Oceanospirillales*) appeared to belong to the inactive chimney exclusive community (Han et al., 2018). The sediment communities in the Kairei region correlated with sediment depth and showed varying compositions along the hydrothermal transition zone. However, near the active vent, no typical vent-associated chemosynthetic microorganisms were observed in the hydrothermally influenced sediments (Adam et al., 2019).

The aim of the present study is to provide an assessment of the microbial communities and their putative metabolisms and functions in the ecosystems of distinct vent fields of the IR, thereby expanding the baseline knowledge of microbial ecosystems in putative mining areas. Here we report on microbial communities from sediments, massive sulfides, silica mounds and fluids of six different vent sites along the CIR and SEIR, as well as ambient water samples collected in the course of the INDEX2019 sampling campaign. For most of the sampled vent systems, no microbiological studies have been carried out before. Our analyses combine the assessment of the microbial community compositions based on 16S rRNA gene sequencing and enrichments of hydrogen-oxidizing Bacteria with correlation analyses related to geochemical parameters.

Materials and methods

Sampling sites and sampling collection

Hydrothermally influenced and reference samples were taken with the help of the remotely operated vehicle (ROV) ROPOS (for

technical description refer to https://www.ropos.com) during the INDEX2019 cruise based on the RV Sonne. The sampling sites span six different hydrothermal vent systems along the Central Indian Ridge (CIR) and South-East Indian Ridge (SEIR, see Figure 1 and Supplementary Figure S1). Fluid samples were retrieved by means of the BGR-owned Kiel Pumping System (KIPS, Enwave GmbH), attached to the ROV as previously described (Garbe-Schönberg et al., 2006). Geological sulfide and rock samples were directly collected from the seafloor or snapped from chimney structures. Bacterial mat material was sampled with a slurp gun. Reference water samples were taken in Niskin bottles attached to the ROV or with a conductivity, temperature and depth (CTD) sensor package equipped with a water sampling rosette. Sediment cores were taken with push core liners, operated by the ROV. Two sediment cores, each for microbiological and sediment/porewater analyses, were taken in close proximity to each other. Upon arrival on deck, fluid and water samples were concentrated on polycarbonate membrane filters (0.2 µm pore size; Merck Millipore, Burlington, MA, USA) for microbiological analyses in the home laboratory. Subsamples of fluids were stored at 4°C for later setups of enrichment cultures as described below. For rock and chimney samples, little pieces of rock were broken off using an ethanol-sterilized spatula. This was possible due to the porous and fragile texture of the samples. From the slurp gun sample, flock material was collected by pipetting, using sterile cut-off pipette tips. Using ethanol-sterilized tools, sediment cores were subsampled in 2 cm horizons. All samples for DNA/RNA extractions were frozen at −80°C.

Porewater sampling and analyses

Porewater was sampled using rhizons (CSS, 5 cm Rhizosphere Research Products B.V., Netherlands) in specially prepared push core liners with a spacing of 2 cm, as described in a previous study (Adam et al., 2019). Minor and trace element concentrations of diluted porewater samples was determined by high resolution ICP-SF-MS (Element XR, Thermo Scientific, Waltham, MA, USA). Details on the sample preparation and measurement procedures can be found in Garbe-Schönberg (1993) and Adam et al. (2019).

Mineralogy and geochemistry of sulfide, rock, and sediment samples

The suite of collected geological samples comprises massive sulfides, non-sulfidic hydrothermal precipitates and sediments. The samples were documented on board, cleaned and prepared for mineralogical and geochemical analyses. The sediments in the push cores were subsampled at fixed intervals of 2 cm. All whole-rock analyses were conducted at the Activation Laboratories (Actlabs)

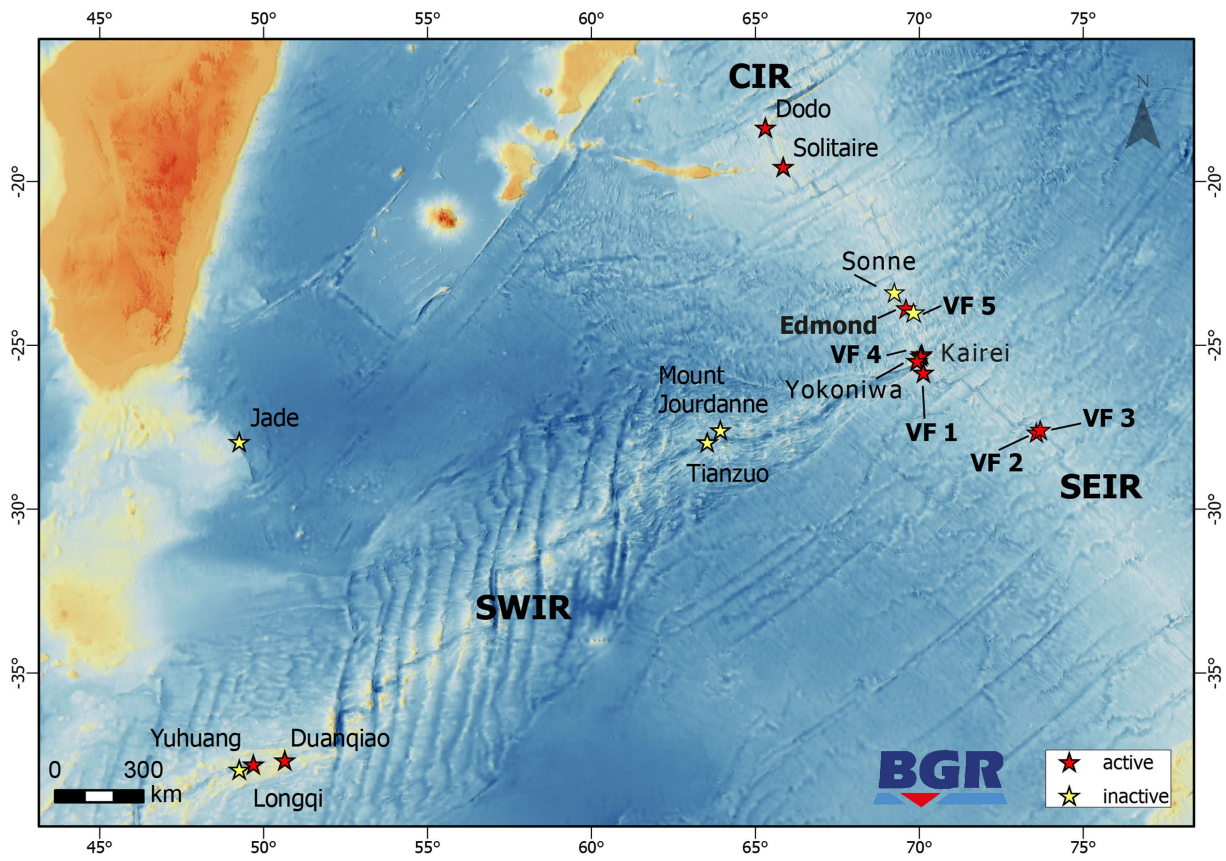

FIGURE 1
Map showing the locations of inactive and active hydrothermal vent sites along the CIR, SWIR, and SEIR. Locations marked in bold denote sites where microbiology studies have been performed in the framework of the INDEX2019 sampling campaign.

Ltd. in Ancaster, Canada that provide routine analytical service for the geology and mining sector worldwide. Measurements of the bulk concentrations of major, minor, trace and ultra-trace elements, as well as sulfur were addressed by a combination of analytical packages involving commonly applied techniques, such as ICP-MS, ICP-OES, neutron-activation and infrared spectroscopy. On the basis of geochemical compositions, the normative abundance endmember components were calculated for the sediment samples, reflecting the specific mineral assemblages and their different origins (e.g., pelagic, carbonates component or hydrothermal, sulfidic components). Polished, uncovered, epoxy-embedded thick sections were prepared from representative solid samples (e.g., chimneys) to further study their petrography and mineralogy. The thick sections were investigated using a LEICA DVM6 M digital microscope and a FEI F650 MLA-SEM (scanning-electron microscope equipped with a mineral liberation analyzer), both located at the Federal Institute for Geosciences and Natural Resources (BGR).

Fluid geochemistry

All hydrothermal fluids were collected using the remotely controlled inert flow-through fluid sampling system BGR-KIPS mounted underneath ROV ROPOS. Immediately after recovery, the fluids were homogenized in the samples flasks, and aliquots taken and filtered for (i) rapid on board analyses, and (ii) subsequent analyses in the home labs on shore. The *ex situ* pH (at 25°C), Eh, conductivity and H_2S content were measured with suitable electrodes (using a standard approach) in the ship's labs. The major and minor elements were analyzed with ICP-optical emission spectrometry (Spectro Ciros SOP, Amatek), and trace elements with a ICP-SF-MS (Element XR, Thermo Scientific) at the Institute of Geosciences at the CAU University Kiel. The instruments were calibrated as described in Garbe-Schönberg (1993) and Adam et al. (2019) and data validated using appropriate reference materials.

Microbial enrichment cultures

Directly after sampling, enrichment cultures were set up with fluid samples in 15 mL Hungate tubes, closed with butyl stoppers and screw-caps. From each fluid sample, 5 mL of fluid were added to 5 mL of organic-free MJ medium as previously described (Hansen and Perner, 2015). The enrichments contained H_2 as electron donor and $NaNO_3$ (5 mM), MnO_2 (powder), Fe(III) (5 mM, ferrihydrite), SO_4^{2-} (13.8 mM from MJ medium), or S^0 (powder) as electron acceptor. To all incubations, except the SO_4^{2-} reducing ones, 20 mM $NaMoO_4$ was added to inhibit sulfate reduction (Oremland and Capone, 1988). The ferrihydrite was synthesized according to Schwertmann and Cornell (2008). The headspace consisted of H_2/CO_2 (80/20) for anoxic incubations or $H_2/CO_2/O_2$ (79/20/1) for microoxic incubations. The incubations were done at room-temperature in the dark. All enrichments contained resazurin as redox indicator. The microoxic incubations were regularly flushed with $H_2/CO_2/O_2$ once the medium turned clear to re-supply oxygen. All enrichments were transferred several times and activity was confirmed by color change of the resazurin from blue to purple and clear.

To prove the H_2-consumption activity of the enrichments, we performed experiments where we measured H_2 in the headspace and respective electron-acceptor consumption or buildup of products from electron acceptor reduction in the medium. To increase the volume of the headspace, these experiments were performed in 100 ml serum vials with 45 ml medium and 5 mL inoculum. The headspace consisted of $H_2/N_2/CO_2$ (2/78/20) for anoxic enrichments and $H_2/N_2/CO_2/O_2$ (2/77/20/1) for microoxic enrichments. Measurements were done directly after inoculating the cultures and after the resazurin showed a color change. Sterile MJ with the respective headspace and electron acceptors added was used as controls. H_2 concentrations were measured with a Trace GC Ultra gas chromatograph (ThermoFisher Scientific, Waltham, MA, USA), using a ShinCarbon ST 100/120 column (Restek Corporation, Bellefonte, PA, USA) and a Pulsed Discharge Detector (Vici Valco Instruments, Houston, TX, USA) as described before (Hansen and Perner, 2015). Concentrations of NO_3- were measured according to Schnetger and Lehners (2014) on filtered samples. Sulfide was quantified with the cline assay (Cline, 1969) on samples fixed with 5% zinc acetate. Fe(II) and total Fe concentrations were determined spectrophotometrically with the ferrozine assay (Stookey, 1970) on samples acidified with HCl (1 M final concentration). For total Fe concentrations all Fe(III) was reduced to Fe(II) with hydroxylamine hydrochloride before the assay. Fe(III) was calculated from the difference between Fe(II) and total Fe concentrations. Dissolved Mn(II) was measured with the formaldoxime assay (Brewer and Spencer, 1971). All spectrophotometric assays were performed on 96 well plates with a plate reader (SPECTROstar Nano, BMG Labtech).

DNA extraction and 16S amplicon sequencing

DNA isolation and 16S amplicon sequencing were performed as previously described (Han et al., 2018; Adam et al., 2019). Briefly, *ca.* 500 mg of rock/chimney/mat material or half of a filter were used for DNA extractions with the Nucleospin DNA Soil Kit (Macherey Nagel, Düren, Germany) according to the manufacturer's instructions. Bacterial 16S rRNA gene amplicons (V3-V4 region) were generated with the Bact_341F/Bact_805R primer pair, while archaeal amplicons targeting the V4-V5 region were amplified with both the Arch_524F/Arch958R and Arch_519F/Arch_915R primer pairs. All primers contained the Illumina adaptor overhangs and sequencing libraries were prepared using the Nextera Index Kit (Illumina, St. Diego, USA) according to the manufacturer's recommendations. After a quality and concentration check, a sample pool with equimolar amounts of DNA was sequenced in a 2 × 300 bp paired-end sequencing run on Illumina's Mi-Seq platform (Adam et al., 2019).

Sequence data retrieval for comparative analyses

For comparative analyses, sequence raw reads of previous 16S amplicon studies from hydrothermally influenced environments of the Mid-Atlantic Ridge (MAR), CIR and SEIR (both sampled in the course of the INDEX2016 cruise) as well as the South-West Indian Ridge (SWIR) were retrieved from public databases. To ensure the

comparability of the datasets, only bacterial sequences of the V3-V4 region were included. Datasets of the following accession numbers and studies were used: SRP503162 (MAR fluids, Gonnella et al., 2016), SRP120106 (INDEX2016 chimney, water and fluid samples, Han et al., 2018), PRJNA474182 (INDEX2016 sediments, Adam et al., 2019) and PRJNA558519 (SWIR sediments, Yang et al., 2019).

Sequence processing and statistical analyses

Demultiplexed raw sequences from the Illumina MiSeq run as well as the downloaded bacterial raw sequences were quality-checked and processed using the Qiime2 environment (Bolyen et al., 2019). The sequence reads were filtered and merged using the dada2-plugin with default settings, removal of the primer sequences and a trimming of the single raw sequence read length to 260 nucleotides for bacterial sequences prior to merging (Callahan et al., 2016). Taxonomic assignments were performed using a pretrained classifier, based on SILVA database release 138 (Quast et al., 2013), which was trained with the respective primer pairs for Bacteria and Archaea (Pedregosa et al., 2011; Bokulich et al., 2018). The feature-classifier plugin (classify sklearn) was used for taxonomic assignments with default settings and the pre-trained SILVA classifier (Bokulich et al., 2018). After the taxonomic classification, any contaminating sequences were removed from the individual samples: eukaryotic and chloroplast sequences were removed from all datasets, as well as bacterial reads from the archaeal files and vice versa. Sequence alignments and phylogenetic trees were calculated using the "align-to-tree-mafft-fasttree" pipeline (Price et al., 2010). Principle Coordinate Analysis (PCoA) based on weighted and unweighted UniFrac distances and differential abundance analysis (RDA) were performed in R: A language and environment for statistical computing. R Foundation for Statistical Computing, Vienna, Austria. URL https://www.R-project.org/using the microeco package (Liu et al., 2021). Rarefication for PCoA analyses was performed with different subsample sizes: (i) with a sample size 14,000 for the 2019 bacterial sequences, (ii) with 200 subsamples for the 2019 archaeal sequences and (iii) with a sample size of 10,000 sequences for the comparison to sequence data of older studies. Clustering of samples was performed using a confidence level of 0.9. Porewater data used for RDA analyses can be found in Supplementary Table S1.

Results and discussion

Geological setting of the sampled vent sites

Samples have been retrieved from three vent fields at the CIR [Edmond, and the yet undescribed Vent Fields (VF) 5 and VF 4] and three fields from the SEIR (VF 1, VF 2 and VF 3; all of which have not been described yet) (see Figure 1 and Table 1). The active Edmond and the neighboring inactive VF 5 hydrothermal fields are both located off-axis and associated with prominent west-facing faults on the eastern flank of the CIR. The associated host rocks are basaltic in composition. The Edmond field comprises numerous active and inactive sulfide chimneys covering an area of more than hundred meters in length and in water depths of 3,330 to 3,250 m (Van Dover et al., 2001). The chlorine-rich, high-temperature fluids (Tmax = 382°C; Gallant and Von Damm, 2006) vent from black smoker chimneys ranging from only a few meters in height to about 35 m-tall, multi-spired structures. The presence of numerous old and disintegrated sulfide structures and abundant sulfide talus indicates long-lasting hydrothermal activity at this site (Van Dover et al., 2001). The inactive VF 5 consists of several mounds (each >200 m in diameter) with multiple standing and toppled chimney structures reaching up to 17 m in height (Müller et al., 2018). Mineralization occurs along a steep, west-facing fault, running parallel to the Edmond fault, at water depths between 3,070 and 3,200 m (Schwarz-Schampera, 2019; Fuchs et al., in prep.).

The large VF 4 vent field is located in a very different geotectonic setting. Here, hydrothermal activity occurs on a tectonic massif on the western flank of the CIR, close to the Rodriguez Triple Junction, and is associated with the exposure of mantle and lower crustal rocks (Schwarz-Schampera, 2019; Fuchs et al., in prep.). In contrast to the other studied vent fields, VF 4 is associated with mafic to ultramafic plutonic high rocks comprised of gabbros, harzburgithes and pyroxenites, which show an overall high degree of alteration/serpentinization. Black smoker venting of high-salinity fluids occurs at a number of active vent sites in water depths ranging from 2,625 to 3,020 m and reaches temperatures up to 328°C (Schwarz-Schampera, 2019; Fuchs et al., in prep.). Active and inactive vent sites are scattered along the sedimented, axis-facing slope of the tectonic massif.

The three hydrothermal vent fields sampled along the SEIR are all associated with mid-ocean ridge basaltic host rocks. VF 1 is the smallest of the fields and is associated with a small bounding fault on the western flank of the spreading center. Sulfide mineralization is documented only from a small area in water depths ranging from 2,910 to 2,940 m. Currently only low-temperature, diffuse (31°C) (Schwarz-Schampera, 2019; Fuchs et al., in prep.) fluid venting and associated faunal communities have been documented although the presence of sulfide talus and chimney debris indicates that higher temperatures have been present in the past.

The VF 2 and VF 3 hydrothermal fields are the largest vent fields sampled for this study. They are both associated with a large volcanic plateau on the eastern flank of the ridge axis that is cut by major ridge-parallel rift valley faults. Both hydrothermal fields stretch along large, axis-facing fault scarps with numerous active and inactive vent sites. At VF 3 sulfide mineralization has been documented along a strike length of 2.7 km. Hydrothermal mounds at VF 2 stretch over a long distance, however, individual mounds tend to be smaller than at VF 5. In contrast to the high-salinity fluids expelled at the two vent sites along the CIR (Kairei and VF 4), black smoker style venting at VF 2 and VF 3 is characterized by low-salinity fluids (Schwarz-Schampera, 2019; Fuchs et al., in prep.).

Mineralogy of rock samples

Four hydrothermally-derived sulfidic and non-sulfidic rock samples were collected in the scope of the current study to investigate the relationship between the presence of microbial communities and the rock substrate (Figure 2 and Table 2). The samples 083 ROPOS-F (R1) and 083 ROPOS-G (R2) were collected at the small active VF 1 that vents clear, shimmering fluid. Sample R1 is a large piece of

10.3389/fmicb.2023.1173613

TABLE 1 Overview of analyzed samples and parameters.

ID	Sample	Type	Vent site	Min. distance to vent (m)	Bac/ Shannon index	Arch/ Shannon index	PW chemistry	Fluid chemistry	Mineralogy
F2	083ROPOS-KIPS-A	Fluid	VF 1		+/6.96	+/4.74	–	+	–
R1	083ROPOS-F	Sulfide block	VF 1	9	+/6.26	+/5.3	–	–	+
R2	083ROPOS-G	Sulfide chimney	VF 1	3	+/8.15	+/1.76	–	–	+
S3	083ROPOS_PC2-1	Sediment horizon	VF 1	80	+/8.00	+/4.29	+ (PC3)	–	–
S4	083ROPOS_PC2-2	Sediment horizon	VF 1	80	–	+/n.a.	+ (PC3)	–	–
S5	083ROPOS_PC2-3	Sediment horizon	VF 1	80	+/8.52	+/4.09	+ (PC3)	–	–
S6	083ROPOS_PC2-4	Sediment horizon	VF 1	80	+/n.a.	+/n.a.	+ (PC3)	–	–
S7	083ROPOS_PC2-5	Sediment horizon	VF 1	80	+/6.7	+/3.37	+ (PC3)	–	–
S8	083ROPOS_PC2-6	Sediment horizon	VF 1	80	–	+/1.11	+ (PC3)	–	–
S9	083ROPOS_PC2-7	Sediment horizon	VF 1	80	–	+/1.59	+ (PC3)	–	–
F3	104ROPOS-KIPS-C/D	Fluid	VF 2		+/7.51	–	–	+	–
R3	104ROPOS-E	Silica	VF 2	36	+/n.a.	+/1.48	–	–	+
F4	106ROPOS-KIPS-B	Fluid	VF 2		+/8.37	+/3.23	–	+	–
R4	127ROPOS-D	Sulfide chimney	VF 3	3	+/6.8	+/5.66	–	–	+
S10	127ROPOS_PC3-6	Sediment horizon	VF 3	160	+/6.77	–	+(PC2)	–	–
M3	127ROPOS_SG1	Microbial mat	VF 3	14	+/8.18	+/4.81	–	–	–
M2	036SG6	Microbial mat	VF 4	52	+/8.19	+/4.12	–	–	–
F1	040ROPOS-KIPS-C	Fluid	VF 4		+/3.14	+/3.09	–	+	–
W2	031ROPOS N1	Ambient water IN-W	VF 5		+/7.06	–	–	–	–
S1	031ROPOS_PC2	Bulk sediment	VF 5	2,118	+/8.69	–	–	–	–
S2	031ROPOS_PC5-1	Sediment horizon	VF 5	1,147	+/9.46	–	+ (PC4)	–	–
W1	027ROPOS DNA_5	Ambient water IN-R	Edmond		+/n.a.	–	–	–	–
M1	027ROPOS DNA 6	Microbial mat	Edmond		+/8.35	–	–	–	–

Bac and Arch refer to the Amplicon sequencing of Bacteria and Archaea: +/– indicates if 16S rRNA gene tags are available, n.a. = Shannon index is not available for the respective sample. The ID denotes the designation of the (sub-) samples used for microbiological analyses. Porewater (PW) chemistry was determined for duplicate push cores, sampled adjacently to the microbiology cores and given in brackets in the respective column of the table.

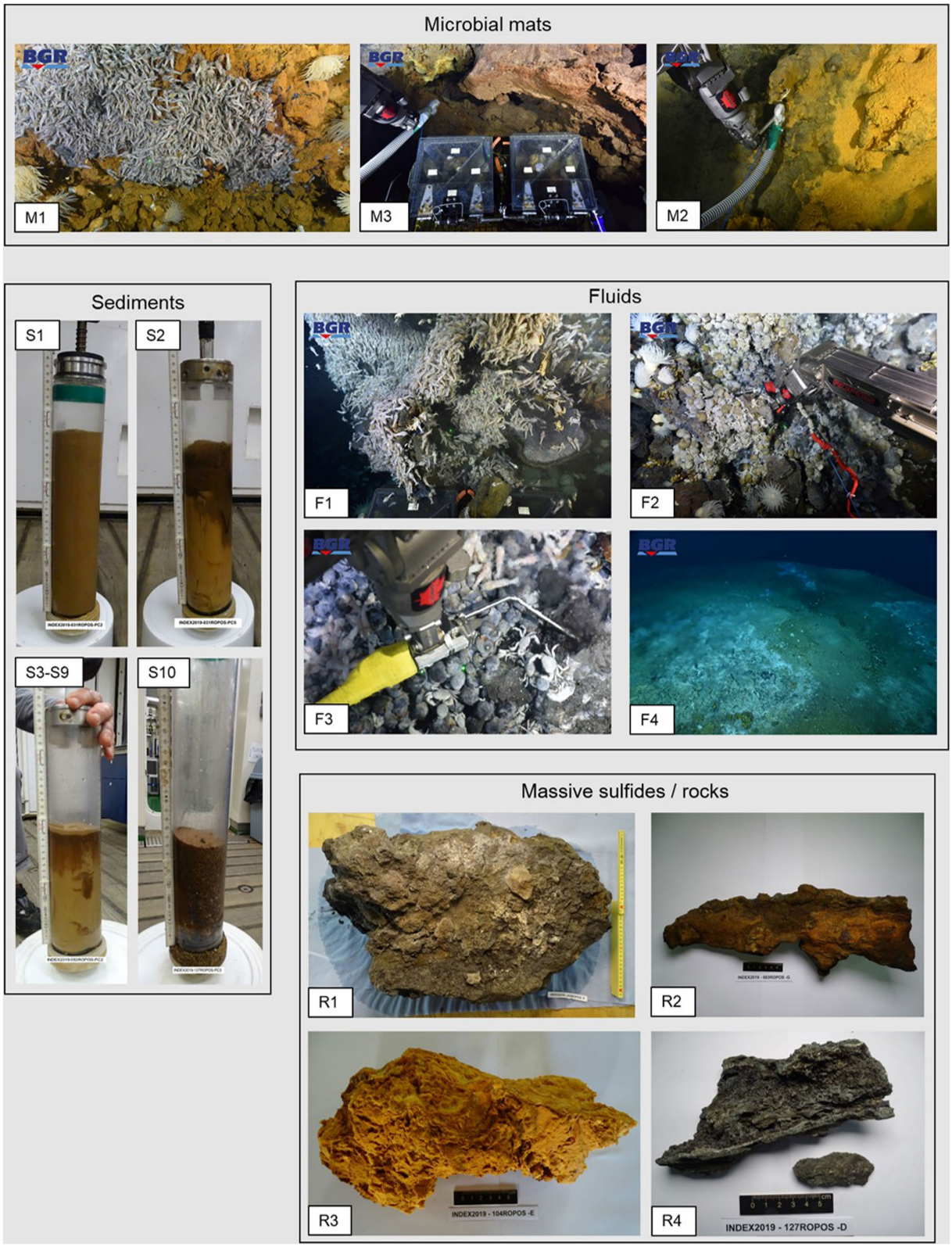

FIGURE 2
Photos of the sampled microbial mats, fluids, sediments, massive sulfides and rock material. Photos of microbial mats and fluids were taken *in situ* by means of ROPOS' cameras.

cemented silica, which very likely precipitated in form of sheets from these low-temperature fluids and incorporated abundant talus fragments of pyrite-rich sulfides, pieces of the basaltic host rocks and calcic fossils (e.g., shell fragments of bivalves and gastropods). The other specimen represents the tip of an old, clogged micro-chimney recovered in the vicinity of the active fluid exhaust. The mineralogical

TABLE 2 Mineral abundances and characteristics of massive sulfide samples.

ID	Sample	Associated vent field	Sample type	Sample characteristics	Mineral abundances									
					Cpy	*Icb*	*Po*	*Py/mc*	*Sl*	*Gn*	*Brn*	*Si*	*Ata*	*FeOOH*
R1	083ROPOS-F	VF 1	Massive sulfide block	Hydrothermal precipitate of pyrite and amorphous silica with enclosed lithoclasts and calcic (seashell) fragments	m	m	+	++	t	t		+++		m
R2	083ROPOS-G	VF 1	Massive sulfide chimney	Tip of a clogged sulfide micro-conduit from an active vent. Distinct temperature-depended mineral concentric zonation from the interior to the outside	++			+	m	t	m	++	t	
R3	104ROPOS-E	VF 2	Silica precipitate	White-to orange-colored solid precipitate of "sugary" silica. The sample contains thin alternating bands of more dense silica with glassy appearance. Minor oxidized Fe-bearing particles give distinct coloration.								+++		m
R4	127ROPOS-D	VF 3	Massive sulfide chimney	Wall-fragment of an active smoking chimney. The sample is characterized by numerous small fluid conduits and abundant pyrite and sphalerite.	m			+++	++			m		

ata, atacamite; cpy, chalcpyrite; brn, bornite; FeOx, Fe-oxyhydroxide-bearing minerals; gn, galena; icb, isocubanite; po, pyrrhotite; py/mc, pyrite/marcasite; si, silica; sl, sphalerite. Symbology: +++, dominant; ++, abundant; +, common; m, minor; t = traces.

study reveals the presence of predominant chalcopyrite and silica, pyrite and small volumes of sphalerite, galena and gold (Table 2). The characteristic concentric zonation of the mineral, with chalcopyrite in the interior, and pyrite, sphalerite and galena to the outside indicates the temperature-dependent sulfide precipitation from previously hot hydrothermal solutions. A white to orange-colored massive piece of silica precipitate (R3) has been recovered from VF 2. It is almost entirely composed of very fine-grained, agglomerated silica particles. More densely-packed silica particles occur in bands that alternate through the sample; minor amounts of very small grains of Fe-oxyhydroxide minerals within the silica are giving the characteristic coloration (Table 2). This specimen originates from Si-rich and metal-poor condensed vapor-phase fluids. A wall fragment of an active black smoker (R4) was collected from VF 3. It consists of numerous micro-sized fluid conduits and is composed of pyrite, marcasite and silica. Minor amounts of chalcopyrite and sphalerite were also observed (Table 2).

Mineralogy and porewater chemistry of sediments

Three push cores were analyzed for their porewater chemistry, and the geochemical and mineralogical composition of the sediments (Figure 3 and Supplementary Table S1). Sample 031ROPOS_PC4 (duplicate of microbiological core 031ROPOS_PC5), collected from VF 5, has a total length of about 15 cm. The uppermost layer is composed of almost 82% of red-colored oxidized and hydrated Fe-minerals of hydrothermal origin and almost 10% sulfides (Figure 3). The high volume of hydrothermal sediment correlated well

Vent field	Sample		Depth interval	Lithogenic component	Pelagic (carbonate) component	Hydrothermal (sulfidic) component	Hydrotherm. (Fe-and MnOOH)	Macroscopic description
			cm	*norm %*	*norm %*	*norm %*	*norm %*	
VF 5	031ROPOS PC4	duplicate of PC5	0-2	5.5	2.9	9.2	82.4	Red-colored Fe-stained sediment in the top layer and disturbed pelagic sediment with intermixed FeOOH phases in the bottom layer.
			2-4	5.5	6.5	9.6	78.3	
			4-6	10.4	10.4	9.5	69.8	
			6-8	24.5	33.9	4.9	36.6	
			8-10	10.5	65.3	4.0	20.2	
			10-12	9.4	54.4	4.0	32.3	
VF 1	083ROPOS PC3	duplicate of PC2	0-02	19.0	21.8	28.5	30.6	Thin top layer of red-colored Fe-stained sediment that grades into orange to grey-brown pelagic sediment.
			2-4	9.5	69.3	3.0	18.1	
			4-6	7.6	84.5	1.2	6.6	
			6-8	7.7	86.1	1.1	5.0	
			8-10	8.9	85.3	1.2	4.5	
			10-12	9.7	86.1	72.0	3.3	
			12-14	10.5	85.5	0.8	3.1	
			14-16	10.0	85.8	0.8	3.4	
			16-18	9.6	85.5	0.8	4.0	
VF 3	127ROPOS PC2	duplicate of PC3	0-2	1.5	1.7	47.0	49.8	Thick top layer of red-colored Fe-stained sediment that grades into red to grey-brown pelagic sediment. Some sulfide mineral are preserved.
			2-4	1.2	0.1	73.5	25.2	
			4-6	1.3	0.1	64.7	33.9	
			6-8	1.3	0.1	66.3	32.2	
			8-10	1.1	0.5	72.7	25.8	
			10-12	7.2	8.6	25.0	59.2	
			12-14	3.1	60.9	2.2	33.7	
			14-16	2.8	85.9	1.9	9.5	
			16-18	2.6	89.4	1.2	6.8	
			18-20	4.3	85.9	0.9	8.9	

FIGURE 3
Normative calculation of endmember fractions of sampled push core sediments based on the whole-rock chemistry. The endmembers reflect the abundance of the (i) lithogenic fraction (volcanic and plutonic rock material), (ii) the $CaCO_3$-rich pelagic fraction, and (iii) and (iv) the hydrothermal fractions. The latter are subdivided into sulfidic and Fe-/MnOOH mineral-bearing material.

with increased concentrations of Zn, Pb, Cr, Ni, Mo, and Mn in the porewater (Supplementary Table S1). The hydrothermal components grade into normal carbonate-rich pelagic sediment with increasing depth, that becomes dominant at depths of >8 cm. The push core sample 083ROPOS_PC3 (duplicate of microbiological core 083ROPOS_PC2) from VF1 is characterized by a sulfidic uppermost layer that grades into red-colored Fe-stained sediment, both accumulated during hydrothermal venting. At a depth of about 4 cm and greater, carbonate (background) sediments are predominant (Figure 3). This correlates in turn with a decrease of trace metals (e.g., Pb, Zn, Cu, Cd, Ni, Mn) in the porewater with increasing depth (Supplementary Table S1). The push core 127ROPOS_PC2 (duplicate of microbiological core 127ROPOS_PC-3), collected from the highly active VF 3, contains the highest volumes of sulfides in the top layers, reaching a maximum of 72.7% at a depth of 8 to 10 cm. The hydrothermally-derived Fe-oxyhydroxide and Mn-rich components occur mostly subordinate to the sulfide fraction. There is an abrupt decrease at a depth of 12–14 cm (and greater), where pelagic sediment becomes the predominant fraction (Figure 3).

Fluid geochemistry

In the scope of this study, we analyzed four low-temperature vent fluid samples from three vent fields. With the exception of 083ROPOS-KIPS-A (F2), the samples are not representing the main (commonly high-temperature) vent fluids (Table 3 and Supplementary Table S2). They are rather collected from slowly venting orifices in vicinity of the main vents, and characterized by low temperatures (max. 14°C) permitting ideal conditions for the settlement of microbial communities. However, fluid chemistry of our diffuse samples can be understood as diluted high-temperature fluid endmembers but all transitional metals needing higher temperatures for transport as dissolved species, e.g., Cu, Co, Ni removed during cooling and mixing with ambient seawater. More details of the corresponding high-temperature vent fluids can be found in Garbe-Schönberg and Schwarz-Schampera (submitted). The chemical analyses of the four hydrothermal samples analyzed in this study showed Mg concentrations, salinities and pH values close to those of normal bottom seawater (Table 3). Regression calculations to zero Mg, standard approach to calculate endmember compositions of the hydrothermal fluids, indeed exhibited a high fraction of seawater in all samples. The hydrothermal fractions in the samples of the slowly venting orifices F1, F3, and F4 contain a hydrothermal fraction of ≤6%; the sample F2 derived from the major vent of VF1 a hydrothermal fraction of 10%.

The sample F1 (040ROPOS-KIPS-C) was collected from a beehive structure at the ultramafic rock-hosted VF 4 vent field that vents a diffuse shimmering water of 14°C. This fluid still contained remarkable concentrations of Fe and Mn with 44.7 and 16.48 µM,

TABLE 3 Selected physical parameters and chemical compositions of hydrothermal fluid specimen.

ID	Sample	Vent field	Hydrothermal activity	T_{max}	pH	EM	Salinity	Eh	H_2S	Mg	Cl	Si	Fe	Mn	Cu	Zn
				°C	at 25°C	[%]	[‰]	mV	µM	mM	mM	mM	µM	µM	µM	µM
F1	040ROPOS-KIPS-C	VF 4	Diffuse shimmering water from beehive	14	7.33	4.96	32.9	−133	*< 10*	51.11	n.a.	0.94	44.70	16.48	*b.d.*	0.06
F2	083ROPOS-KIPS-A	VF 1	Diffuse, clear fluid	31	6.5	10.44	32.3	−251	60	48.16	498.97	1.91	9.44	8.31	*b.d.*	0.02
F3	104ROPOS-KIPS-C/D	VF 2	Diffuse, shimmering water	11,6	7.49	5.49	33.2	−150	23.5	50.83	514.02	0.28	1.29	0.34	0.004	0.01
F4	106ROPOS-KIPS-B	VF 2	Diffuse, shimmering water	< 10	7.27	6.01	33.8	−231	15	50.55	535.02	0.35	n.a.	0.44	*b.d.*	0.03
	Bottom seawater			1.8	7.74	0	31.1	27	0	53.60	532.08	0.01	<1.20	0.61	*<0.002*	0.02

It should be noted that hydrothermal fluids generally contain a significant amount of entrained seawater, as indicated by the hydrothermal endmember proportions (EM). Thus, the presented fluid data reflects compositions of hydrothermal fluid mixed with seawater.
b.d.: below the limit of detection, n.a., data not available.

respectively, in comparison to seawater. The fluid samples F3 and F4, both collected from small fissures exhausting the shimmering fluid, exhibited a similar chemical composition very close to seawater. The fluid F1 (083ROPOS-KIPS-A) was emitted at the vent field VF 1 from a small fissure on top of a basalt talus-covered mound that is characterized by sulfides formed under high-to lower fluid temperatures. The fluid yielded a maximum temperature of only 31°C, indicating the progressive cooling of the hydrothermal system (Schwarz-Schampera, 2019; Fuchs et al., in prep.). In comparison to seawater it contained elevated concentrations of 0.94 mM Si, 9.44 µM Fe and 8.31 µM Mn (Table 3). All of the four investigated fluids still exhibited low Eh values in the range of−133 and-255 mV, and (with the exception of F1) some dissolved H_2S (up to 60 µM). This provides an indication that reducing condition are maintained and reduced sulfur is still prevalent.

Taxonomic profiles of microbial communities

The taxonomic profiles of the sampled sediments, fluids, sulfides, rocks and microbial mats broadly resemble community compositions commonly found at deep-sea hydrothermal vent sites (e.g., Flores et al., 2011; Han et al., 2018; Adam et al., 2019). The diffuse fluids show high proportions (7–58%) of *Campylobacterales*, which are typical vent-inhabitants and often dominate microbial vent communities (Adam and Perner, 2018). Generally, the diffuse fluids, as well as rocks and massive sulfides, exhibited smaller proportions of "low abundant" Bacteria (<5% based on order level) than the sediment communities (12–42% compared to 47–72% in sediments). Furthermore, the observed diversities of archaeal communities were significantly lower than those of the bacterial communities, which is also generally reflected by the alpha diversity scores (for details see the section below).

Despite the differing geological settings and partially large distances between the sampled vent systems, no clearly geography-related differences in the taxonomic profiles were observed.

Rock communities and microbial mat compositions

Overall, the here analyzed massive sulfide and chimney samples were characterized by large proportions of uncultured and (below the class level) unspecified Bacteria (Table 4), hampering functional and metabolic predictions. Against our expectations, no distinct patterns of similarity between different microbial community compositions were observed with respect to the current hydrothermal activity associated with rock samples, i.e., between active or inactive chimney pieces. The respective bacterial communities of the massive sulfide block R1 (VF 1) and chimney sample R4 (VF 2) showed similar patterns both on the order level and when considering only the 10 most abundant genera with large proportions of Campilobacterota (Supplementary Figure S1A and Table 4), exceeding the relative campylobacterotal abundances previously observed for massive sulfides of the CIR and SEIR (Han et al., 2018). The highest genera-based abundances were observed for the typically vent-associated, chemoautotrophic, sulfur and hydrogen-oxidizing *Sulfurovum* genus (Inagaki et al., 2004; Mino et al., 2014) and the heterotrophic, typically sediment-inhabiting *Carboxylicivirga* genus (e.g., Wang et al., 2016; Table 4). The archaeal communities of R1 and R4 also showed the

TABLE 4 Most abundant bacterial genera of rock and microbial mat communities.

Sample	Sulfide block R1	Sulfide chimney R2	Silica sample R3	Sulfide R4	Microbial mat sample M3	Microbial mat sample M2	Microbial mat sample M1
Site	VF1	VF1	VF2	VF3	VF3	VF4	Edmond
Ten most abundant genera	*Campylobacter* (8%)	*Acidithiobacillaceae* clade 9 M32 (3%)	*Dehalococcoidia* clade SAR202 (8%)	*Campylobacter* (4%)	*Alteromonas* (4%)	*Aliikangiella* (3%)	*Colwellia* (3%)
	Candidatus Campbellbacteria (2%)	*Aquibacter* (3%)	NB1-j clade (4%)	*Candidatus* Moranbacteria (4%)	*Jejudonia* (2%)	*Mariprofundus* (20%)	*Mariprofundus* (4%)
	Carboxylicivirga (14%)	*Bythopirellula* (4%)	*Nitrosomonas* (5%)	*Carboxylicivirga* (11%)	*Marinobacter* (2%)	*Maritimimonas* (2%)	*Pseudofulvibacter* (3%)
	Ichthyobacterium (4%)	*Mariprofundus* (6%)	*Nitrospina* (8%)	*Desulfobulbus* (5%)	*Mariprofundus* (21%)	*Methylomonadaceae* clade pLW-20 (8%)	*Rubritalea* (2%)
	Nitratifractor (7%)	*Robiginitomaculum* (3%)	Phycisphaerae clade CCM11a (3%)	*Ichthyobacterium* (6%)	*Mesoflavibacter* (4%)	*Methylomonadaceae* marine methylotrophic group 2 (9%)	*Sulfurimonas* (12%)
	Oceanithermus (3%)	*Thiogranum* (6%)	*Pirellulaceae* Pir4 lineage (5%)	*Nitratifractor* (8%)	*Muricauda* (2%)	*Methyloprofundus* (3%)	*Thiohalomonas* (5%)
	Sulfurovum (11%)	*Thiohalophilus* (2%)	*Thermoanaerobaculaceae* Subgroup 10 (3%)	*Oceanithermus* (5%)	*Sulfitobacter* (4%)	*Nitrospina* (2%)	uncultured *Arenicellaceae* (3%)
	uncultured *Ardenticatenales* (2%)	uncultured Gammaproteobacteria (3%)	uncultured *Defluviicoccales* (7%)	*Sulfurovum* (17%)	uncultured *Planctomycetales* (3%)	Phycisphaerae clade CCM11a (2%)	uncultured *Cyclobacteriaceae* (4%)
	uncultured *Saprospiraceae* (2%)	uncultured *Planctomycetales* (3%)	uncultured *Kiloniellaceae* (7%)	uncultured *Saprospiraceae* (5%)	unspecified *Alteromonadaceae* (2%)	*Phycisphaeraceae* clade SM1A02 (2%)	uncultured *Thiotrichaceae* (9%)
	unspecified *Anaerolineaceae* (9%)	uncultured *Thiotrichaceae* (12%)	uncultured *Planctomycetales* (8%)	unspecified Bacteria (4%)	unspecified Gammaproteobacteria (2%)	Planctomycetota clade OM190 (5%)	unspecified *Flavobacteriaceae* (5%)

The ten most abundant genera per sample are displayed with their relative abundance given in brackets.

10.3389/fmicb.2023.1173613

highest diversities among all analyzed samples with large proportions of *Woesearchaeales* (Supplementary Figure S1B). In the clogged chimney sample R2 we observed large proportions of typically sulfur-oxidizing gammaproteobacterial genera, such as *Thiogranum*, *Thiohalophilus*, and uncultured *Thiotrichaceae* (Sorokin et al., 2007; Chernousova et al., 2009; Mori et al., 2015), adding up to 20% of all observed genera (Table 4 and Supplementary Figure S1). Based on the order level, the bacterial community composition of the clogged chimney piece R2 was similar to that of the VF 1 (surface) sediments (Supplementary Figure S1A), but additionally contained >5% of the deep-sea and hydrothermal vent associated, Fe-oxidizing *Mariprofundales* (Emerson et al., 2007). The archaeal community of R2 was characterized by the highest abundance of *Micrarchaeales* across all samples (Supplementary Figure S1B). Interestingly, no campylobacterotal Bacteria were identified in the silica mound sample from VF 2 (R3), which generally exhibited a quite diverse taxonomic profile. This involved orders frequently found in other sample types like *Planctomycetales*, but also high abundances of orders not found in any of the other samples analyzed in this study (Supplementary Figure S1A). Furthermore, the 10 most abundant genera in this sample were different from those of all other rock samples with large proportions of nitrifying *Nitrosomonas* and *Nitrospina* (e.g., Chain et al., 2003; Lücker et al., 2013), adding up to 13% (Table 4). The high bacterial diversity of the silica sample however, is not reflected in the respective archaeal community, consisting of 100% *Nitrosopumilales*.

Although the bacterial (and archaeal) communities of all sampled microbial mats exhibited clear similarities on the order level (Supplementary Figure S1), the 10 most abundant bacterial genera per sample differed almost completely. The only highly abundant genus shared between all microbial mats was the Fe-oxidizing *Mariprofundus*, contributing up to 21% of all genera (Table 4). At the Edmond vent field (M1), mesophilic campylobacterotal and gammaproteobacterial genera potentially involved in sulfur oxidation, i.e., *Sulfurimonas*, *Thiohalomonas*, and uncultured *Thiotrichaceae* (Chernousova et al., 2009; Han and Perner, 2015; Mori et al., 2015), were adding up to 26%. Interestingly, the as obligately psychrophilic described *Colwellia* genus (Techtmann et al., 2016) was also highly abundant in this sample (Table 4). Apart from *Mariprofundus* (20%), methanotrophic Bacteria of two different *Methylomonadaceae* groups and the *Methyloprofundus* genus (Bowman, 2005) constituted a major part of the bacterial community in microbial mat M2 (VF4).

Sediment communities

Due to the in most cases limited availability of sediment material and/or sequencing results of the sediments sampled within our study, a comparison of the taxonomic profiles of whole sediment cores of the different vent fields is not possible. However, we were able to identify some patterns in the distribution of certain genera.

The VF 1 sediments (S3–S9), sampled in a distance of *ca.* 80 m to an active vent, were characterized by community shifts with increasing sediment depth, especially regarding the bacterial communities. Apart from the high number of low abundant taxa, *Ectothiorhodospirales*, *Thiotrichales* (both Gammaproteobacteria), and *Pirellulales* (Planctomycetota) dominated the surface layer (0–2 cm) with proportions of more than 10% of Bacteria on the order level (Supplementary Figure S1). The deeper sediment horizons (4–10 cm) were characterized by a core community of *Dehalococcoidia* clade S085 Chloroflexi, Planctomycetota, *Steroidobacterales* and other Gammaproteobacteria in slightly varying percentages. The 6–8 cm horizon additionally contained higher proportions (>5%) of *Dehalococcoidia* clade SAR202 *Chloroflexi*, members of the NBj-1 group as well as members of the *Alphaproteobacteria* (Supplementary Figure S1A). These patterns were largely reflected in the ten most abundant genera (Table 5). However, a high abundance of the sulfate-reducing *Desulfatiglans* (Jochum et al., 2018) in the surface layer as well as increasing abundances of heterotrophic, ubiquitously distributed and sediment-associated *Woeseia* (Hoffmann et al., 2020) (Table 5). The respective archaeal communities showed a much lower diversity and the surface layers (0–4 cm) were characterized by high proportions of unassigned sequences and unspecified Archaea (Supplementary Figure S1B). Such a phenomenon was also observed for sediments of the Kairei vent field (Adam et al., 2019). The predominant archaeal members across all analyzed sediment depths at VF 1 were *Nitrosopumilales* (Nitrososphaera), contributing to up to 100% (in the 6–8 and 10–12 cm horizons, Supplementary Figure S1B). Other *Nitrososphaeria* and *Woesearchaeles* (Nanoarchaeia) contributed to up to 2 and 10%, respectively (Supplementary Figure S1B).

Unfortunately, and despite multiple attempts, only one sediment horizon of the core collected in VF 3 yielded bacterial 16S rRNA gene sequences of sufficient quality. This layer (10–12 cm) was characterized by the lowest proportion of low abundant Bacteria on the order level. The most abundant genera were the gammaproteobacterial, sulfur-oxidizing *Thiogranum* and uncultured *Thiotrichaceae* (19 and 21%, respectively, see Table 5). Furthermore, the highest abundances of sulfate-reducing Desulfobacterota were identified in this sediment horizon (*cf.* Supplementary Figure S1 and Table 5).

The two surface sediment samples at VF5 (S1 and S2) showed the highest proportions of low abundant Bacteria on the order level but otherwise differed completely in their community compositions (Supplementary Figure S1A). Interestingly, the bacterial community of bulk sediment sample S1 partially resembled those of deeper sediment horizons of the VF1 sample, exhibiting the highest proportion of *Woeseia* among all surface sediments (Table 5). Sample S2 showed the greatest differences to other sediment samples, sharing only the high abundance of *Pirellulales* with samples S3 and S10 (Supplementary Figure S1A). Also noticeable is the high percentage of unspecified Bacteria (17% of observed genera, see Table 5), which was not observed for any other sample.

Microbial communities of diffuse fluids and water samples

Three of the four sampled diffuse fluids (F2, F3, and F4) exhibited similar bacterial community compositions with a clear dominance of *Campylobacterales* (up to 58%, see Supplementary Figure S1A) and high abundances of the gammaproteobacterial *Thiomicrospirales* and *Thiotrichales,* all of which are involved in hydrogen and/or sulfur oxidation and frequently encountered at hydrothermal vents (e.g., Nakagawa and Takai, 2008; Hansen and Perner, 2016; Adam and Perner, 2018). Among these samples the campylobacterotal *Sulfurovum* displayed the most abundant genus with relative proportions between 29 and 42% (Table 6). The respective archaeal communities of fluids F3 and F4 (both from VF2) showed nearly identical compositions, mainly consisting of *Nitrosopumilales* (88–90%), Marine Benthic Group A (Nitrososphaeria, 1–3%) and

TABLE 5 Most abundant bacterial genera of sediment communities.

Sample	Bulk sediment S1	S2 (0–2 cm)	S3 (0–2 cm)	S5 (4–6 cm)	S6 (6–8 cm)	S7 (8–10 cm)	S10 (10–12 cm)
Site	Score	Score	Surya	Surya	Surya	Surya	Penumbra
Ten most abundant genera	Acidobacteriota subgroup 21 (3%)	*Candidatus* Omnitrophus (5%)	*Desulfatiglans* (5%)	Acidobacteriota Subgroup 22 (3%)	*Blastopirellula* (3%)	*Dehalococcoidia* clade S085 (6%)	*Alphanizomenon* NIES81 (2%)
	Dehalococcoidia clade S085 (3%)	*Ignavibacteriales* PHOS-HE36 group (3%)	Gammaproteobacteria clade B2M28 (6%)	*Dehalococcoidia* clade S085 (6%)	*Dehalococcoidia* clade S085 (6%)	NB1-j clade (4%)	*Candidatus* Thiobios (2%)
	Dehalococcoidia clade S202 (4%)	Nitrospinota P9X2b3D02 group (3%)	*Pirellulaceae* Pir4 lineage (4%)	*Dehalococcoidia* clade SAR202 (3%)	*Dehalococcoidia* clade SAR202 (5%)	*Phycisphaeraceae* Urania-1B-19 marine sediment group (3%)	*Desulfatiglans* (2%)
	NB1-j clade (4%)	Phycisphaerae clade CCM11a (2%)	*Thiogranum* (17%)	*Methylomirabilaceae* group wb1-A12 (3%)	*Methylomirabilaceae* group wb1-A12 (3%)	Planctomycetota clade OM190 (4%)	*Desulfosarcinaceae* Sva0081 sediment group (5%)
	Phycisphaeraceae Urania-1B-19 marine sediment group (3%)	*Pirellulaceae* Pir4 lineage (6%)	uncultured *Anaerolineaceae* (2%)	NB1-j clade (5%)	NB1-j clade (8%)	*Thiogranum* (3%)	*Gammaproteobacteria* clade B2M28 (10%)
	Planctomycetota clade OM190 (3%)	*Schekmanbacteria* (3%)	uncultured *Arenicellaceae* (2%)	*Nitrospira* (3%)	*Phycisphaeraceae* Urania-1B-19 marine sediment group (5%)	uncultured *Defluviicoccales* (4%)	*Thiogranum* (19%)
	uncultured *Arenicellaceae* (3%)	Sva0485 group (3%)	uncultured Gammaproteobacteria (2%)	uncultured *Defluviicoccales* (3%)	uncultured *Defluviicoccales* (6%)	uncultured *Gemmatimonadaceae* (3%)	uncultured *Arenicellaceae* (2%)
	uncultured *Defluviicoccales* (3%)	uncultured *Actinomarinales* (3%)	uncultured *Pirellulaceae* (3%)	uncultured *Kiloniellaceae* (3%)	uncultured *Magnetospiraceae* (5%)	uncultured *Magnetospiraceae* (3%)	uncultured *Chromatiaceae* (2%)
	uncultured *Planctomycetales* (2%)	uncultured *Cyclobacteriaceae* (2%)	uncultured *Thiotrichaceae* (11%)	uncultured *Magnetospiraceae* (4%)	uncultured *Vicinamibacterales* (4%)	uncultured *Planctomycetales* (3%)	uncultured *Pirellulaceae* (2%)
	Woeseia (10%)	unspecified Bacteria (17%)	unspecified *Aminicenantales* (3%)	*Woeseia* (7%)	*Woeseia* (6%)	*Woeseia* (10%)	uncultured *Thiotrichaceae* (21%)

The ten most abundant genera per sample are displayed with their relative abundance given in brackets.

10.3389/fmicb.2023.1173613

TABLE 6 Most abundant bacterial genera of fluid communities.

Sample	Diffuse fluid F2	Diffuse fluid F3	Diffuse fluid F4	Diffuse fluid F1	Ambient water W2	Ambient water W1
Site	VF1	VF2	VF2	VF4	VF5	Edmond
Ten most abundant genera	*Alcanivorax* (3%)	*Alcanivorax* (7%)	*Alteromonas* (5%)	*Alcanivorax* (56%)	*Alcanivorax* (3%)	*Alteromonas* (2%)
	Caminibacter (3%)	*Candidatus* Moranbacteria (2%)	*Dehalococcoidia* clade SAR202 (1%)	*Cocleimonas* (1%)	*Alteromonas* (5%)	*Cocleimonas* (13%)
	Nitratifractor (5%)	*Cocleimonas* (2%)	*Marinimicrobia* SAR406 clade (1%)	*Marinobacter* (1%)	*Dehalococcoidia* clade SAR202 (4%)	*Colwellia* (2%)
	Sulfurimonas (2%)	*Halomonas* (4%)	SAR324 clade (Marine group B, 1%)	*Mesoflavibacter* (2%)	*Marinimicrobia* SAR406 clade (3%)	JGI_00000069-P22 group (Gracilibacteria, 2%)
	Sulfurovum (42%)	JGI_00000069-P22 group (Gracilibacteria, 2%)	*Sulfurimonas* (14%)	*Pseudoalteromonas* (1%)	*Pseudoalteromonas* (10%)	*Pseudoalteromonas* (3%)
	Thiomicrospira (6%)	*Nitratifractor* (3%)	*Sulfurovum* (29%)	*Sulfurovum* (7%)	SAR324 clade (Marine group B, 3%)	*Psychromonas* (2%)
	Thioreductor (2%)	*Sulfurovum* (34%)	SUP05 cluster (4%)	*Thiomicrospira* (2%)	*Sulfurimonas* (5%)	*Sulfurimonas* (3%)
	uncultured *Thiotrichaceae* (2%)	uncultured Gammaproteobacteria (2%)	*Thiomicrospira* (8%)	uncultured *Cellvibrionaceae* (12%)	SUP05 cluster (16%)	*Sulfurovum* (50%)
	unspecified *Rhodobacteraceae* (3%)	unspecified *Rhodobacteraceae* (4%)	*Thioreductor* (2%)	uncultured *Micavibrionales* (3%)	unspecified *Alteromonadaceae* (3%)	SUP05 cluster (3%)
	unspecified *Thiotrichaceae* (3%)	unspecified *Sphingomanadaceae* (2%)	uncultured *Arcobacteraceae* (11%)	unspecified *Rhodobacteraceae* (12%)	unspecified *Rhodobacteraceae* (12%)	uncultured *Arcobacteraceae* (2%)

The ten most abundant genera per sample are displayed with their relative abundance given in brackets.

unassigned archaeal sequences (7–8%, see Supplementary Figure S1B). The archaeal community of F2 however, was characterized by a higher diversity and included high proportions (5%) of Marine Group II Thermoplasmata, which were not observed in any other analyzed sample and are mainly found in ocean surface waters (Rinke et al., 2019). Interestingly, in the ambient water sample retrieved in the realms of the Edmond vent field (W1), the typically vent-associated *Campylobacterales* also appear to dominate the bacterial community (Supplementary Figure S1A). The other major bacterial groups of this less diverse sample were also frequently found in the diffuse fluid samples (Table 6), indicating that a diffuse fluid flow occurred in the vicinity. In addition to the prevailing autotrophic sulfur oxidizers, a notably high abundance of the heterotrophic sulfur-oxidizing genus *Cocleimonas* (Tanaka et al., 2011) was observed in the W1 community (Table 6).

The diffuse fluid of the VF 4 vent system (F1) showed the lowest abundance of *Campylobacterales* and the least diverse bacterial community pattern among the sampled fluids, clearly dominated by the *Alcanivorax* genus (56%, see Supplementary Figure S1A and Table 6). Interestingly, the respective archaeal community broadly resembled those of the other fluids, but displayed the highest number of unassigned sequences observed in this study (Supplementary Figure S1B).

In both the diffuse fluid F1 (VF4) and the ambient water sample W2 (VF5), exceptionally high proportions of uncultured *Rhodospiraceae* (Alphaproteobacteria, 12% each) were observed (Table 6). On the order level, W2 exhibited the highest abundances of *Thiomicrospirales* (18%) and *Alteromonadales* (22%, both Gammaproteobacteria) in this study, but no "ambient-water exclusive" orders were identified (Supplementary Figure S1). The extraction of the 10 most abundant genera revealed an exceptionally high abundance of the gammaproteobacterial SUP05 cluster (16%), which has frequently been found in hydrothermal plume samples and was shown to be involved in sulfur and iron cycling (Hansen et al., 2022; Zhou et al., 2023). However, the typically vent-associated *Campylobacterales* were missing in this sample (Supplementary Figure S1 and Table 6).

Diversity of microbial communities

Overall, a much higher alpha diversity was observed in the bacterial communities compared to the archaeal ones (Supplementary Figure S1 and Table 1). The respective Shannon indices ranged from 3.1 to 9.5 for Bacteria, while they were limited to 1.1 to 5.7 for Archaea, reflecting the observations of the taxonomic profiles. Likewise, the highest Shannon diversity was observed for bacterial sediment communities (Table 1). Due to the limited number of successfully sequenced sediment samples, a clear zonation of the microbial diversity along the depth of the sediment core could not be detected. Site-specific differences in the Shannon indices could not be observed.

In order to assess the beta-diversity of the amplicon-derived microbial communities, we performed principle coordinates analyses (PCoA) with subsets of the bacterial and archaeal 16S gene tags of the 2019 INDEX cruise, using unweighted and weighted Unifrac distances. Due to the cut-off set for these analyses, samples R3, S6 and

W1 were excluded from the bacterial plots and samples R3, S4, S6, S8, and S9 from the archaeal plots. The ordination for bacterial communities showed a certain clustering according to the type of sample. This effect was more pronounced in the unweighted compared to the weighted analysis (*cf.* Figures 4A,B). Furthermore, the scattering directions differed slightly and the ordination of the samples along both coordinates occurred with smaller distances between the samples and clusters. This effect again is likely caused by the overall high numbers of low abundant Bacteria in our samples. In both analyses, the chimney sulfide R4 and the sulfide block R1 formed a distinct group, which exhibited a large distance to all other samples (Figures 4A,B). Yet, as these are only two samples they are not marked as a statistically relevant cluster in the plot. The bacterial sediment communities also clustered together quite closely. However, there were two outliers (the VF 1 surface sediment S3 and the 10–12 cm sediment layer S10) in the unweighted analysis, which were separated along

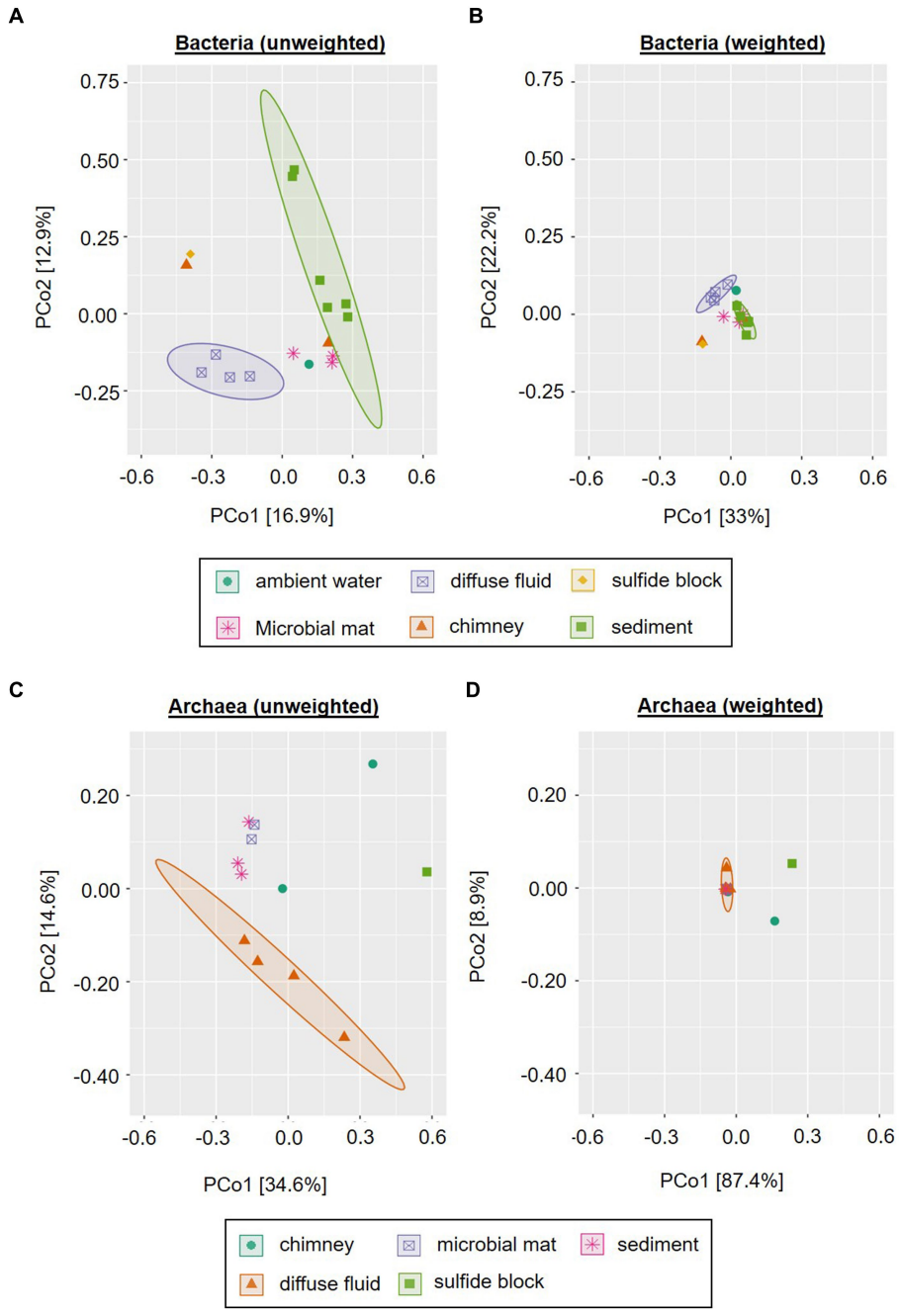

FIGURE 4
Principle Component Analysis of INDEX2019 samples. Unweighted **(A,C)** and weighted **(B,D)** Unifrac distances for Bacteria **(A,B)** and Archaea **(C,D)** are displayed. Ellipses show clusters based on a confidence level of 0.9 and $n > 3$ per parameter (i.e., sample type). Please note that for reasons of visibility, differing axe sizes were used for Bacteria and Archaea.

coordinate 2. Another cluster was composed of the four diffuse fluids, which was accompanied by the ambient water sample W2 (VF 5) in the weighted analysis (Figure 4 A and B). In the unweighted Unifrac analysis, the latter was positioned among the microbial mats and massive sulfide sample R2, forming a group between the sediment and fluid samples.

Similar to the bacterial communities, the archaeal communities also showed a sample type-specific clustering in the unweighted Unifrac analysis, albeit with differing cluster compositions (*cf.* Figures 4A–D). In contrast to the bacterial, the archaeal sediment sample S3 (surface horizon from VF 1) grouped closely together with microbial mat samples M2 and M3 along coordinate 2. Furthermore, a cluster containing the diffuse fluids extended along coordinate 1. Two samples were separated from the clusters and also showed diverging ordinations among each other: the sulfide block R1 and the sulfide chimney R4 (Figure 4C). In the weighted analyses, the majority of all samples formed a single cluster in the center of the plot (Figure 4D). The three distinctly different samples (diffuse fluid F3, sulfide rock R1 and sulfide chimney R4) however showed diverging ordinations: while F3 was only separated along coordinate 1 and appeared to belong to the cluster according to the applied statistics, R1 and R4 showed distinct ordinations along both axes. Thus, the greatest difference between archaeal communities was observed for the sulfide samples R1 and R4.

Furthermore, we compared the bacterial communities to those of a former INDEX cruise as well as fluids from the mid-Atlantic Ridge (MAR) and sediments from the South-West Indian Ridge (SWIR). In the unweighted Unifrac analysis the sediment samples of INDEX cruises clustered together with those of the SWIR, clearly separated from the remaining sample types (Figure 5A). The MAR fluids formed a small group within the computed fluid cluster, which still exhibited higher similarities to chimney and rock samples from the CIR and SEIR than to the majority of Indian Ridge (IR) fluids. The latter were closely arranged to ambient water, microbial mat, rock and plume samples (Figure 5A). When the abundance of the taxa is taken into account, the sediment communities of the SWIR formed a distinct cluster separated at a great distance from the other samples along coordinate 2 (Figure 5B). The MAR fluids took another outlier position, while the remaining (IR) samples clustered in the center of the ordination plot with smaller sample type-specific differences. Thus, in the weighted analysis, "Ridge-specific" differences in the beta diversity of bacterial communities dominated (Figure 5B).

Enrichments of hydrogen-oxidizing microorganisms from diffuse fluids

In hydrothermal vent environments reduced sulfur species (mainly hydrogen sulfide) and molecular hydrogen represent the most favorable electron donors for autotrophic growth of microorganisms (Adam and Perner, 2018). Given the high hydrogen concentrations measured in fluids from the Kairei vent field located on the CIR and

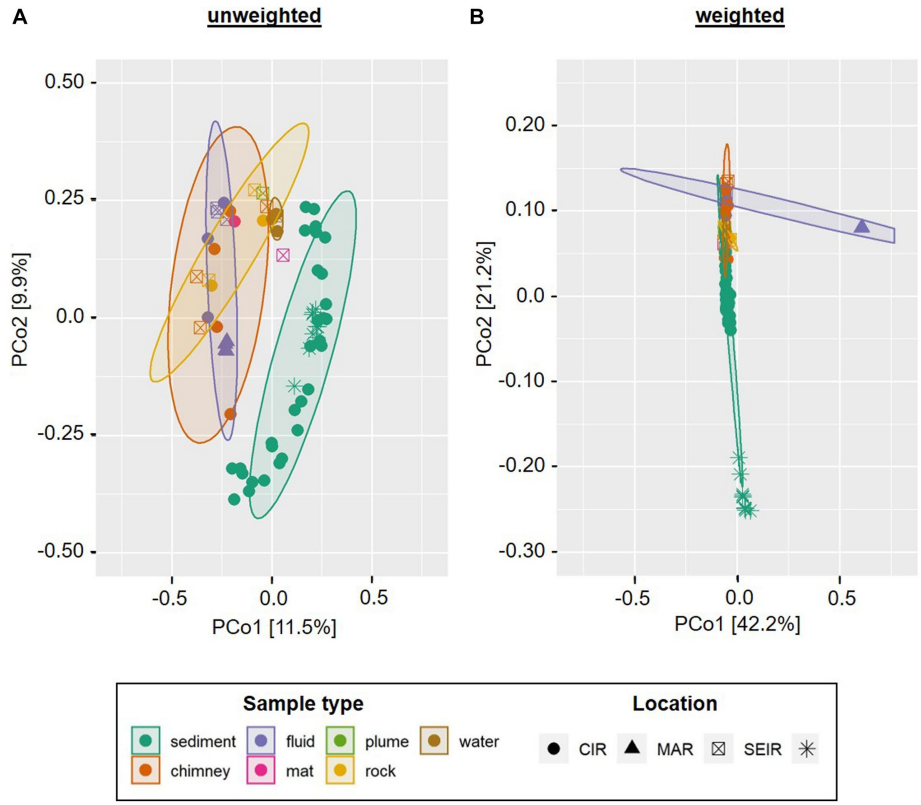

FIGURE 5
Principle Component Analysis of INDEX2019 samples in comparison with INDEX2016, SWIR sediments and MAR fluids. Unweighted **(A)** and weighted **(B)** Unifrac distances are displayed for bacterial communities only. Ellipses show clusters based on a confidence level of 0.9 and $n > 3$ per parameter (i.e., sample type). Please note that for reasons of visibility, differing axe sizes were used for the weighted and unweighted analyses.

previous isolations of hydrogen oxidizers from the CIR (Kumagai et al., 2008; Adam et al., 2021), we attempted to explore the hydrogen oxidation potential and electron-acceptor use of autotrophic microbial communities from three diffuse fluids (F2, F3, and F4) sampled within this study. After 1 year of consecutive transfers in organic-free artificial seawater medium with hydrogen as electron donor [H_2/CO_2 (80/20) atmosphere in the head space] and incubation at room-temperature, the five most abundant species of each culture constituted >80% of all species (including Archaea) observed in the respective communities (Figure 6G). In most cases, these species did not exhibit high abundances in the respective original fluids, likely resulting from the current inability to culture the microbial majority (Lloyd et al., 2018). Nevertheless, we were able to observe some sample-specific differences in consumption rates and compositions of the enrichments.

The highest hydrogen consumption rates of up to 83 nmol H_2*d^{-1}*ml^{-1} were observed for fluids F2 and F3 with oxygen or sulfate as electron donors (Figure 6). Still, these were in the lower range of rates previously measured in incubation experiments with hydrothermal fluids from the Mid-Atlantic Ridge (Perner et al., 2011). Overall, the enrichments of fluid F1 exhibited the lowest hydrogen consumption rates and with sulfate and Fe(III) as electron-acceptor, no growth and substrate consumption could be detected at all (Figure 6). This observation fits to the low abundance of typical chemoautotrophs in the bacterial communities of the original sample (*cf.* Supplementary Figure S1 and Table 6).

The use of oxygen as electron acceptor resulted in the dominance of *Hydrogenovibrio* and *Thiomicrospira* species in all enrichments (Figure 6G). In the past, *Thiomicrospira* species were mainly associated with sulfur oxidation. However, recent reclassifications placed several *Thiomicrospira* species into the *Hydrogenovibrio* genus and studies have shown the oxygen-coupled hydrogen oxidation ability of these organisms (Hansen and Perner, 2016; Gonnella et al., 2019). The nitrate-amended enrichments of F3 and F1 were also characterized by high proportions of *Hydrogenovibrio* members, accompanied by uncultured *Hydrogenimonas*. Members of this genus were also highly abundant in the corresponding F2 enrichment, and are known as nitrate-reducing hydrogen-oxidizers and have been isolated from vent environments (Takai et al., 2004). Surprisingly, the Mn(IV)- and Fe(III)-incubations did not result in the enrichment of typical dissimilatory metal-reducing hydrogen oxidizers (Figure 6G). Instead, we observed large proportion of heterotrophic Alphaproteobacteria (e.g., *Thalassospira* and *Parvibaculum*) (Rosario-Passapera et al., 2012; Liu et al., 2016) as well as *Hydrogenovibrio*, *Sulfuriomonas,* and *Pseudomonas* members in these enrichments. To our knowledge, none of the observed autotrophic hydrogen oxidizers (*Hydrogenovibrio* and *Sulfurimonas*) have so far been reported to use Mn(IV) or Fe(III) as electron acceptor. However, this may explain the comparably low hydrogen consumption rates of these incubations (Figure 6C,D). Despite the highest Fe-concentrations in the F1 fluid (Table 3), no Fe(III)-reducing culture could be enriched (Figure 6D). However, the comparably high manganese concentrations in F1 are reflected in the highest Mn(IV)-reduction rates among the enrichment cultures (*cf.* Table 3 and Figure 6C). Both sulfate-reducing incubations were dominated by the uncultured SEEP-SRB4 group. Although no cultured representative is available, these microbes are commonly associated with hydrocarbon-oxidation coupled to sulfate-reduction in hydrocarbon seeps and mud-volcanoes (Kleindienst et al., 2012). Thus, it is unlikely that they constitute the key hydrogen oxidizers in this incubation. Instead, we assume that this metabolism is carried out by members of the *Sulfurospirillum* genus, which constitute up to 16% and cultured representatives have been shown to couple hydrogen oxidation to sulfur reduction (Kodama et al., 2007). Still puzzling is the high abundance of *Hydrogenovibrio* members in these incubations (up to 42%), as they have not been reported to be involved in dissimilatory sulfate reduction. So far, only genes for the assimilatory reduction of sulfate have been detected in *Hydrogenovibrio* genomes (Jiang et al., 2017). One possible explanation for the presence of *Hydrogenovibrio* in these incubations is that the reduced sulfur compounds released by members of the highly abundant SEEP-SRB4 serve as an alternative energy source for *Hydrogenovibrio*. Elemental sulfur as electron acceptor led to the lowest hydrogen consumption rates of all incubations (Figure 6F). In the F2 and F3 incubations unspecified *Thiomicrospira* species dominated with proportions of 83% of all observed species (Figure 6G). Given the - for *Thiomicrospira* species - uncommonly low hydrogen consumption rates and their sulfur-oxidation ability, it could be assumed that these members used sulfur oxidation instead of hydrogen oxidation to support their growth. The same hypothesis could be postulated for the respective F1 incubation with regard to the dominance of the hydrogen-and sulfur-oxidizing *Sulfurimonas* genus. However, it was recently shown that several *Sulfurimonas* strains can couple the oxidation of hydrogen to the reduction of elemental sulfur (Wang et al., 2021).

Correlations of microbial communities with environmental parameters and levels of hydrothermal activity

Due to the in most cases limited numbers of individual samples per sample type, statistically relevant correlations of microbial communities with environmental parameters could only be computed for the sediment samples of the INDEX2019 sampling campaign. For this purpose, we performed redundancy analyses of the bacterial taxonomies with the porewater data. In the corresponding ordination plot (Figure 7) 68% (RDA1) and 23% (RDA2) of the variation was explained by the first two axes. Strong negative correlations were observed between the sediment depth and the abundance of Bacteria belonging to the SAR202 clade, S085 and NB1-j groups, *Woeseia* genus and the Pir4-lineage (Figure 7). Except for the Pir4-lineage, these groups and genera also showed a weak correlation with sodium. Nitrate concentrations correlated positively with *Candidatus* Omnitrophus, while a negative correlation was observed with the Pir4-lineage. For *Candidatus* Omnitrophus various metabolic traits have been inferred from metagenomic analyses, including heterotrophy, autotrophy, methane oxidation, and also nitrate reduction (Rinke et al., 2013; Momper et al., 2017). Given the correlations and relative bacterial abundances of up to 5% for *Candidatus* Omnitrophus, nitrate reduction may play a significant role in the VF 5 surface sediments (S1 and S2) and the 4–8 cm horizons of VF 1 sediments (S5 and S6). Furthermore, members of the metabolically diverse Sva0081 sediment group, B2M28 group and *Thiogranum* genera showed a rather weak positive correlation with sediment depth. Strong positive correlations with pH and SAC254 were observed for the *Desulfatiglans* genus (Figure 7). SAC254 displays a parameter indicating the presence and concentration of certain organic substances (above all aromatic compounds and humic acids).

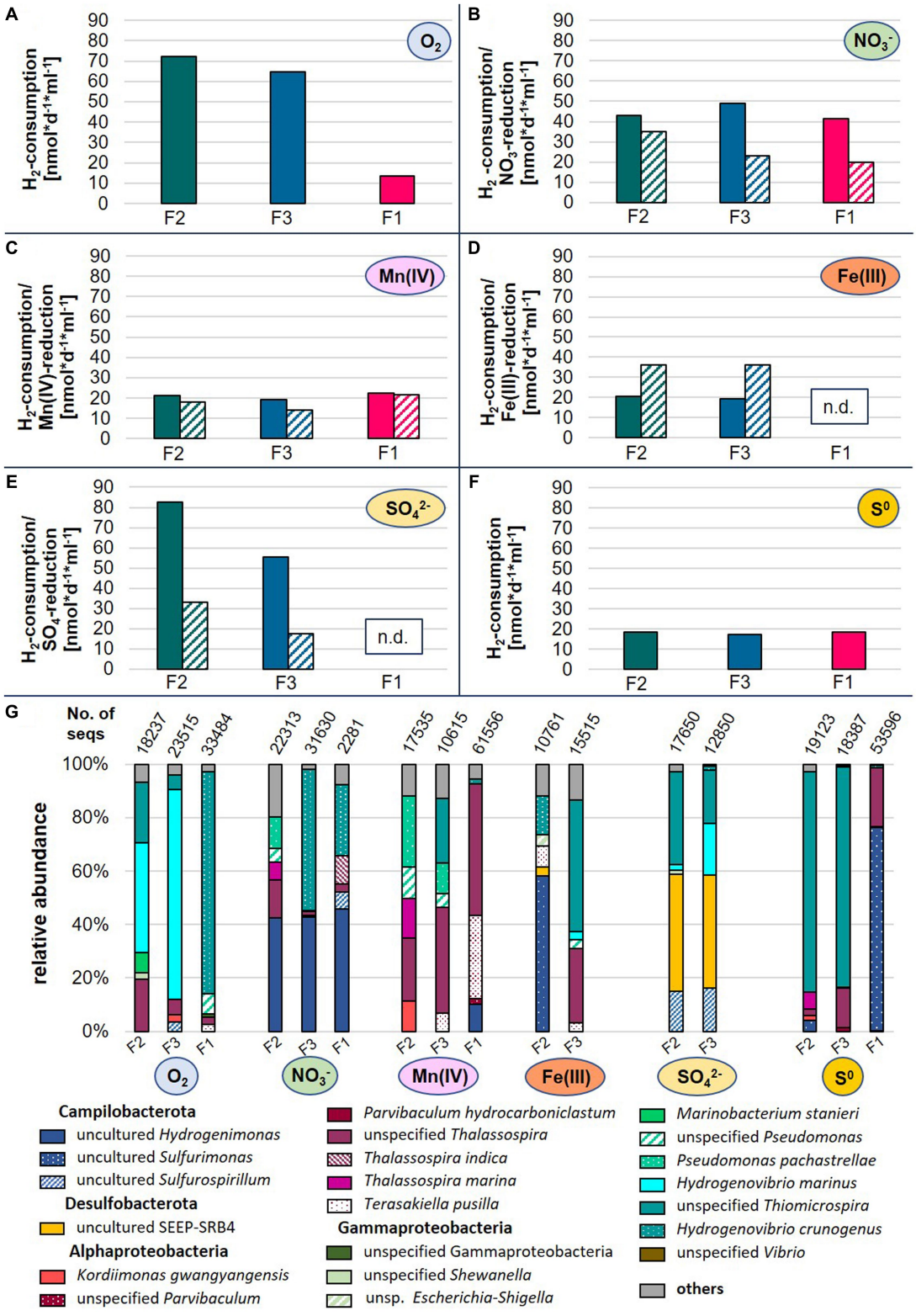

FIGURE 6
Hydrogen consumption rates **(A–F)** and microbial species abundances **(G)** of enrichment cultures inoculated with diffuse fluids. Hydrogen (filled bars) and electron-acceptor consumptions (dashed bars) are displayed as rates in nmol*d^{-1}*ml^{-1} based on three technical replicates. For oxygen and elemental sulfur, no consumption rates are available. N.d., not detectable, No. of seqs denotes the number of merged sequences used for the calculation of relative abundances.

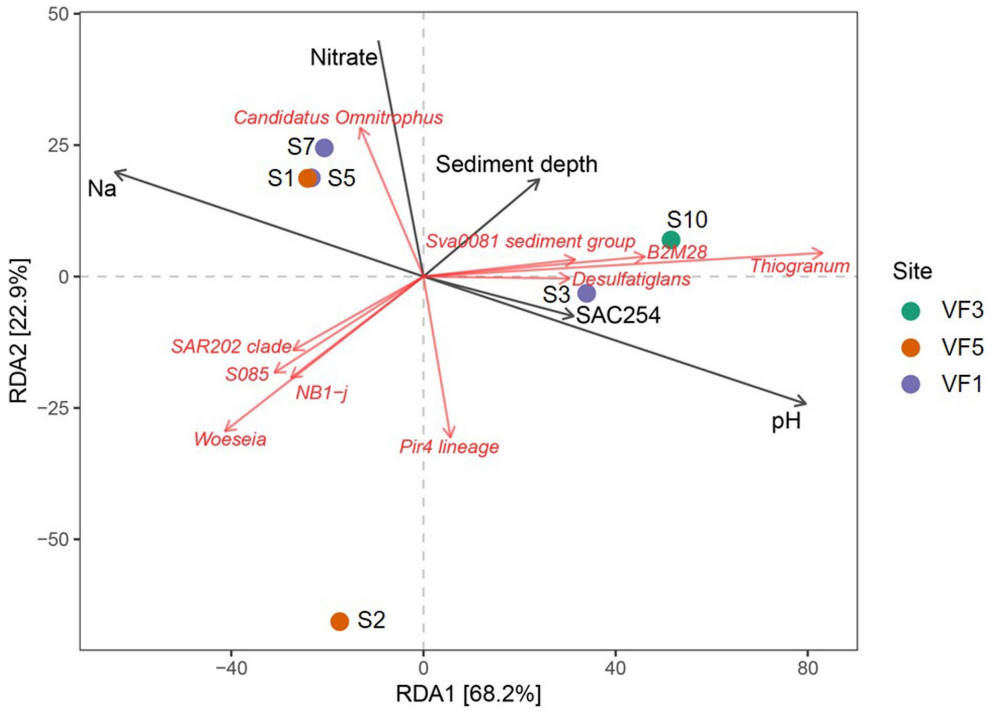

FIGURE 7
RDA plots showing correlations of environmental parameters with abundances of microbial taxa.

The genetic potential for the utilization of aromatic compounds found in some *Desulfatiglans* strains might explain this correlation (Jochum et al., 2018). In contrast to our observations from the INDEX2016 sampling campaign of Kairei sediments (Adam et al., 2019), in our current study no correlations between metal concentrations and bacterial communities or individual taxa was observed.

When considering whole bacterial communities of the sediment cores, correlations with sodium and nitrate were visible for two sediment horizons of VF 1 as well as the bulk sediment sample from the VF 5 vent site. Interestingly, the surface sediment horizon from VF 1 showed correlations with SAC254 and pH, rather than sodium and nitrate, matching the outlier position of this sediment horizon in the PCoA-plots (*cf.* Figures 4A,B,7). The 10–12 cm sediment horizon from VF 3 harbored the only bacterial community correlating with sediment depth, shaped by the above-mentioned correlating lineages. The greatest distance to other communities and environmental factors in the RDA-plots was observed for the surface sediment S2 from the VF 5 vent site (Figure 7). Against our expectations, no correlations with the distance to the next active venting site were observed, indicating that the geochemical parameters shaping the sediment communities are not directly linked to the current hydrothermal activities. This hypothesis is also supported by the lack of typically vent-associated chemoautotrophs in the studied sediment communities, even though the respective geochemical analyses identified hydrothermal sediment input at least in the surface horizons of the sampled sediments.

The comparably low bacterial diversity and predominant absence of chemosynthetic Bacteria, especially from the *Campylobacterales* order, in the diffuse fluid from VF 4 (F1) cannot be fully explained by the respective fluid geochemistry. However, the absence of sulfide species (below detection limit, Table 3) indicates that an important electron-donor for microbial vent communities (Perner et al., 2007; Amend et al., 2011) is missing in this habitat. The comparably low hydrogen oxidation potential in the corresponding enrichment cultures and absence of typical hydrogen oxidizers in the original communities further suggest that the hydrogen concentrations in fluid sample F1 are not sufficient to support a rich chemosynthetic community. Apart from this, the mixing with ambient seawater, characteristic for diffuse fluids, may also entrain seawater communities to the diffuse fluids (e.g., Anderson et al., 2013). The exceptionally high abundance of the *Alcanivorax* genus in this sample may indicate the presence of volcanic activity related hydrocarbon leakage in the vicinity of the fluid emission as recently hypothesized for *Alconivorax*-dominated hydrothermal plumes in the South-Pacific Ocean (Dede et al., 2023). Further indication for such a leakage may arise from the high abundance of methylotrophic taxa in the microbial mat sampled at VF 4. Although we unfortunately have no data on hydrocarbon concentrations in the sampled fluids, it can be assumed that fluid F1 contained higher fractions of H_2 and methane (CH_4). As vent field VF 4 is placed in an ultramafic rock-hosted setting, the associated serpentinization most likely led to high H_2 concentrations. The excess of H_2 can in turn produce CH_4 and other hydrocarbons (e.g., by Fischer-Tropsch reactions). Similar processes have been observed before in the Rainbow vent field at the MAR (Charlou et al., 2002). In the vicinity of the sampling site of diffuse fluid F1, high-temperature fluid emissions were also observed. Given the – compared to seawater – high heavy metal concentrations in this fluid (Table 3), elevated concentrations of lead, cadmium, zinc, manganese and iron can also be expected to prevail in the resulting plume and surroundings. This might further contribute to the high abundances of the *Alcanivorax* genus, which previously demonstrated the ability

for the detoxification of heavy metals in polluted sediments (Zhong et al., 2020).

Corresponding to the predominantly low Fe-contents in the sampled fluids, no Fe-oxidizing Bacteria and Archaea were detected in the respective communities. The occurrence of common Fe-oxidizing microbes (i.e., *Mariprofundus* species) was limited to the microbial mat samples M1-M3 (Edmond vent field, VF3 and VF4) as well as the clogged sulfide chimney R2 (VF1), indicative of previous Fe-rich venting at the respective sites. Since its first description in 2007, the *Mariprofundus* genus has frequently been identified in iron-rich hydrothermal vent environments and microbial mats, also from the SWIR, and are hypothesized to play an important role in the formation of Fe-oxyhydroxides in vent environments (Emerson et al., 2007; Singer et al., 2011; Li et al., 2013; Zhong et al., 2022). However, we did not observe higher abundances (i.e., >5%) of *Mariprofundales* in the microbial mat and sulfide samples of the Kairei and Pelagia vent fields in our previous study (Han et al., 2018). Unfortunately, we do not have any mineralogical or geochemical data on the host rocks of our microbial mat samples, but visual inspections of the sampling sites (Figure 2) already suggested the presence of Fe-oxides. Hence, Fe-oxidation appears to play a major role for energy conservation in the respective microbial mats. The mineralogical profile of the Fe-encrusted clogged sulfide chimney R2 was characterized by the highest concentrations of chalcopyrite across all samples of our 2019 sampling campaign, which may serve as a rich, biologically available Fe-, H_2S, and S-source and results in the high abundances of *Mariprofundales* and sulfur-oxidizing Gammaproteobacteria as described above.

The distinct geochemical characteristics of VF 2, i.e., the presence of silica mounds and granules with minor proportions of pyrite as well as the occurrence of Fe-depleted fluids coincides with exceptionally high abundances of uncultured genera, which in part were only found in the microbial community of the sampled precipitates. These included bacterial groups associated with nitrogen and carbon cycles, such as uncultured, putatively nitrifying *Nitrospina* and *Nitrosomonas* species (Koops and Pommerening-Röser, 2001; Lücker et al., 2013), uncultured chemoheterotrophic SAR202 Chloroflexi (Mehrshad et al., 2018) as well as putatively denitrifying, uncultured members of the *Kiloniellales* (Wiese et al., 2020). Some of these "VF 2-exclusive" were also identified in sediments from the Kairei vent field and already showed significant correlations with the silicate phases of the respective sediments (Adam et al., 2019), which gives further indications for the ecological importance in the silica-rich VF 2.

Putative ecosystem functions and impacts of mining scenarios

In addition to common heterotrophs, autotrophic microbial taxa and groups were observed in all sample and habitat types (*cf.* Supplementary Figure S1 and Tables 4–6). Given the relative abundances of these bacterial and archaeal autotrophs in the specific habitats (Supplementary Figure S1), the expected primary biomass production is generally higher in the actively venting environments compared to those currently missing hydrothermal activity and especially the sampled sediments. This microbial primary production serves as the basis for the rich fauna at active venting sites and thus contributed significantly to the demands for the protection of active hydrothermal vents (e.g., van der Most et al., 2023). However, the microbial mats, sampled from non-venting sites of different vent fields, with their noticeable high numbers of autotrophic *Mariprofundales* (Table 4; Singer et al., 2011) suggest that the microbial potential for CO_2-fixation and primary biomass production in non-venting habitats should not be neglected when assessing the possible ecological impacts of SMS mining. Given the fact that all our samples were taken from vent fields that still harbor at least a few actively venting sites, the microbial community compositions and primary production potential of fully extinct deep-sea hydrothermal vent sites may differ considerably. The microbial communities of the sampled massive sulfides, rocks and microbial mats also appear to be involved in various biogeochemical cycles, especially the nitrogen and sulfur cycles as discussed above. As we observed before in the 2016 sampling campaign, the high numbers of uncultured or unspecified microbes make it difficult to assess the impacts of the removal as well as the resilience of the respective communities and/or habitats (Han et al., 2018).

Apart from the putative removal of ecologically relevant microbial communities, deep-sea mining may also impact the environments by sediment/waste plumes generated in the mining process and expected to be emitted close to the seabed (Amon et al., 2022). Depending on the plume composition and deposition site of the sedimentary freight, different effects can be expected: if hydrothermal input accumulated on the sediments sampled during our 2019 campaign, a community shift with the enrichment of typically vent-associated microbes may occur. How persistent such a shift would be is questionable, since a constant hydrothermal fluid input is missing. In case of a high (heavy) metal load, toxic effects may also alter the benthic microbial populations and their respective biogeochemical cycling capacities, favoring the enrichment of putatively detoxifying (metal-reducing or-precipitating) species such as *Alcanivorax* (Zhong et al., 2020), which was highly abundant in one of our fluid samples (Table 6). However, an overall loss of microbial biodiversity on the seafloor habitats sampled within this study cannot be excluded as a possible effect of such a mining plume (*cf.* Jones et al., 2018; Amon et al., 2022).

Conclusion

As the interest in the mining of SMS deposits and the development of respective mining technologies are continuously increasing, the environmental impact assessment of mining activities is of fundamental relevance to develop mitigation strategies and foster a resilient ocean. With this study we expand the baseline knowledge about microbial communities as an integral part of ecosystems from Indian Ridge venting environments, including exceptional hydrothermal vent systems like VF 4. Given the overall high numbers of uncultured and unspecified microbes and the lack of typical community distribution patterns (e.g., zonation along distances to the active vents) in these venting environments, forecasting of mining impacts and the resilience of microbial communities remains difficult. Thus, continuous efforts in the study of microbial ecosystem functions in hydrothermal vent environments and SMS deposits are of eminent importance and must precede any disturbances of these ecosystems.

Data availability statement

The datasets presented in this study can be found in online repositories. The names of the repository/repositories and accession number(s) can be found at: https://www.ncbi.nlm.nih.gov/bioproject; PRJNA951358.

Author contributions

MP and AS planned the study. MP and NA-B assessed the compiled data and prepared the manuscript outline. NA-B wrote the manuscript with contributions and approval of all authors. DG-S performed fluid sampling and geochemical analyses of hydrothermal fluids. SF was responsible for mineralogy and geochemistry. SP contributed to the evaluation of geological data. KL-M collected samples for microbiological analyses, set up microbial enrichment cultures, measured consumption rates, extracted DNA and prepared 16S amplicons. DI performed the Illumina Sequencing. NA-B and KL-M maintained the enrichment cultures, performed bioinformatic and statistical analyses and evaluated the data. All authors contributed to the article and approved the submitted version.

Funding

The samples were recovered during a cruise within the exploration program INDEX by BGR. Thanks are due to BGR for funding of this study.

Acknowledgments

We thank the captain and crews of R/V Sonne as well as the ROV ROPOS for the excellent help with the retrieval of our deep-sea vent samples. DG-S thanks Karen Bremer and Ulrike Westernströer for help with analytical lab work. We are indebted to Thomas Kuhn for critical remarks during manuscript preparation.

Conflict of interest

The authors declare that the research was conducted in the absence of any commercial or financial relationships that could be construed as a potential conflict of interest.

Publisher's note

All claims expressed in this article are solely those of the authors and do not necessarily represent those of their affiliated organizations, or those of the publisher, the editors and the reviewers. Any product that may be evaluated in this article, or claim that may be made by its manufacturer, is not guaranteed or endorsed by the publisher.

Supplementary material

The Supplementary material for this article can be found online at: https://www.frontiersin.org/articles/10.3389/fmicb.2023.1173613/full#supplementary-material

References

Adam, N., Han, Y., Laufer-Meiser, K., Bährle, R., Schwarz-Schampera, U., Schippers, A., et al. (2021). Deltaproteobacterium strain KaireiS1, a mesophilic, hydrogen-oxidizing and sulfate-reducing bacterium from an inactive Deep-Sea hydrothermal chimney. *Front. Microbiol.* 12:686276. doi: 10.3389/fmicb.2021.686276

Adam, N., Kriete, C., Garbe-Schönberg, D., Gonnella, G., Krause, S., Schippers, A., et al. (2019). Microbial community compositions and geochemistry of sediments with increasing distance to the hydrothermal vent outlet in the Kairei field. *Geomicrobiol J.* 37, 242–254. doi: 10.1080/01490451.2019.1694107

Adam, N., and Perner, M. (2018). Microbially mediated hydrogen cycling in deep-sea hydrothermal vents. *Front. Microbiol.* 9:2873. doi: 10.3389/fmicb.2018.02873

Amend, J. P., McCollom, T. M., Hentscher, M., and Bach, W. (2011). Catabolic and anabolic energy for chemolithoautotrophs in deep-sea hydrothermal systems hosted in different rock types. *Geochim Cosmochim* 75, 5736–5748. doi: 10.1016/j.gca.2011.07.041

Amon, D. J., Gollner, S., Morato, T., Smith, C. R., Chen, C., Christiansen, S., et al. (2022). Assessment of scientific gaps related to the effective environmental management of deep-seabed mining. *Mar Pol* 138:105006. doi: 10.1016/j.marpol.2022.105006

Anderson, R. E., Beltran, M. T., Hallam, S. J., and Baross, J. A. (2013). Microbial community structure across fluid gradients in the Juan de Fuca ridge hydrothermal system. *FEMS Microbiol. Ecol.* 83, 324–339. doi: 10.1111/j.1574-6941.2012.01478.x

Bokulich, N. A., Kaehler, B. D., Rideout, J. R., Dillon, M., Bolyen, E., Knight, R., et al. (2018). Optimizing taxonomic classification of marker-gene amplicon sequences with QIIME 2's q2-feature-classifier plugin. *Microbiome* 6:90. doi: 10.1186/s40168-018-0470-z

Bolyen, E., Rideout, J. R., Dillon, M. R., Bokulich, N. A., Abnet, C. C., Al-Ghalith, G. A., et al. (2019). Reproducible, interactive, scalable and extensible microbiome data science using QIIME 2. *Nat. Biotechnol.* 37, 852–857. doi: 10.1038/s41587-019-0209-9

Bowman, J. P. (2005). "Methylococcales Ord. Nov" in *Bergey's manual of systematic bacteriology*. ed. D. J. E. A. Brenner (Boston, MA: Springer), 248–270.

Brewer, P. G., and Spencer, D. W. (1971). Colorimetric determination of manganese in anoxic waters. *Limnol. Oceanogr.* 16, 107–110. doi: 10.4319/lo.1971.16.1.0107

Callahan, B. J., McMurdie, P. J., Rosen, M. J., Han, A. W., Johnson, A. J., and Holmes, S. P. (2016). DADA2: high-resolution sample inference from Illumina amplicon data. *Nat. Methods* 13, 581–583. doi: 10.1038/nmeth.3869

Chain, P., Lamerdin, J., Larimer, F., Regala, W., Lao, V., Land, M., et al. (2003). Complete genome sequence of the ammonia-oxidizing bacterium and obligate chemolithoautotroph *Nitrosomonas europaea*. *J. Bacteriol.* 185, 2759–2773. doi: 10.1128/JB.185.9.2759-2773.2003

Charlou, J. L., Donval, J. P., Fouquet, Y., Jean-Baptiste, P., and Holm, N. (2002). Geochemistry of high H_2 and CH_4 vent fluids issuing from ultramafic rocks at the rainbow hydrothermal field (36°14′N, MAR). *Chem. Geol.* 191, 345–359. doi: 10.1016/S0009-2541(02)00134-1

Chernousova, E., Gridneva, E., Grabovich, M., Dubinina, G., Akimov, V., Rossetti, S., et al. (2009). *Thiothrix caldifontis* sp. nov. and *Thiothrix lacustris* sp. nov., gammaproteobacteria isolated from sulfide springs. *Int. J. Syst. Evol. Microbiol.* 59, 3128–3135. doi: 10.1099/ijs.0.009456-0

Cline, J. D. (1969). Spectrophotometric determination of hydrogen sulfide in natural waters. *Limnol. Oceanogr.* 14, 454–458. doi: 10.4319/lo.1969.14.3.0454

Dede, B., Priest, T., Bach, W., Walter, M., Amann, R., and Meyerdierks, A. (2023). High abundance of hydrocarbon-degrading Alcanivorax in plumes of hydrothermally active volcanoes in the South Pacific Ocean. *ISME J.* 17, 600–610. doi: 10.1038/s41396-023-01366-4

Dick, G. J., Anantharaman, K., Baker, B. J., Li, M., Reed, D. C., and Sheik, C. S. (2013). The microbiology of deep-sea hydrothermal vent plumes: ecological and biogeographic linkages to seafloor and water column habitats. *Front. Microbiol.* 4:124. doi: 10.3389/fmicb.2013.00124

Ding, J., Zhang, Y., Wang, H., Jian, H., Leng, H., and Xiao, X. (2017). Microbial community structure of deep-sea hydrothermal vents on the ultraslow spreading southwest Indian ridge. *Front. Microbiol.* 8:1012. doi: 10.3389/fmicb.2017.01012

Emerson, D., Rentz, J. A., Lilburn, T. G., Davis, R. E., Aldrich, H., Chan, C., et al. (2007). A novel lineage of Proteobacteria involved in formation of marine Fe-oxidizing microbial mat communities. *PLoS One* 2:e667. doi: 10.1371/journal.pone.0000667

Flores, G. E., Campbell, J. H., Kirshtein, J. D., Meneghin, J., Podar, M., Steinberg, J. I., et al. (2011). Microbial community structure of hydrothermal deposits from geochemically different vent fields along the mid-Atlantic ridge. *Environ. Microbiol.* 13, 2158–2171. doi: 10.1111/j.1462-2920.2011.02463.x

Fuchs, S., et al. (in prep.) *The discovery of 12 new hydrothermal vent fields and associated polymetallic sulfide occurences in the Central Indian Ocean*.

Gallant, R. M., and Von Damm, K. L. (2006). Geochemical controls on hydrothermal fluids from the Kairei and Edmond vent fields, 23°–25°S, Central Indian Ridge. *Geochem. Geophys.* 7:Q06018. doi: 10.1029/2005GC001067

Garbe-Schönberg, D. (1993). Simultaneous determination of thirty-seven trace elements in twenty-eight international rock standards by ICP-MS. *Geostand. Geoanal. Res.* 17, 81–97. doi: 10.1111/j.1751-908X.1993.tb00122.x

Garbe-Schönberg, D., Koschinsky, A., Ratmeyer, V., Jähmlich, H., and Westernströer, U. (2006). KIPS-A new multiport valve-based all-Teflon fluid sampling system for ROVs. *Geophys. Res. Abstr.* 8:7032. doi: 1607-7962/gra/EGU06-A-07032

Garbe-Schönberg, D., and Schwarz-Schampera, U. (submitted). "Geochemistry of hydrothermal fluids from the INDEX contract area" in *exploration of marine minerals-first results from the INDEX Camapign on polymetallic massive sulfides*. ed. U. Schwarz-Schampera (Springer New York, NY: Springer)

Gonnella, G., Adam, N., and Perner, M. (2019). Horizontal acquisition of hydrogen conversion ability and other habitat adaptations in the Hydrogenovibrio strains SP-41 and XCL-2. *BMC Genomics* 20:339. doi: 10.1186/s12864-019-5710-5

Gonnella, G., Böhnke, S., Indenbirken, D., Garbe-Schönberg, D., Seifert, R., Mertens, C., et al. (2016). Endemic hydrothermal vent species identified in the open ocean seed bank. *Nat. Microbiol.* 1:16086. doi: 10.1038/nmicrobiol.2016.86

Haase, K. M., Petersen, S., Koschinsky, A., Seifert, R., Devey, C. W., Keir, R., et al. (2007). Young volcanism and related hydrothermal activity at 5°S on the slow-spreading southern mid-Atlantic ridge. *Geochem Geophys* 8:Q11002. doi: 10.1029/2006gc001509

Han, Y., Gonnella, G., Adam, N., Schippers, A., Burkhardt, L., Kurtz, S., et al. (2018). Hydrothermal chimneys host habitat-specific microbial communities: analogues for studying the possible impact of mining seafloor massive sulfide deposits. *Sci. Rep.* 8:10386. doi: 10.1038/s41598-018-28613-5

Han, Y., and Perner, M. (2015). The globally widespread genus Sulfurimonas: versatile energy metabolisms and adaptations to redox clines. *Front. Microbiol.* 6:989. doi: 10.3389/fmicb.2015.00989

Hansen, C. T., Kleint, C., Bohnke, S., Klose, L., Adam-Beyer, N., Sass, K., et al. (2022). Impact of high Fe-concentrations on microbial community structure and dissolved organics in hydrothermal plumes: an experimental study. *Sci. Rep.* 12:20723. doi: 10.1038/s41598-022-25320-0

Hansen, M., and Perner, M. (2015). A novel hydrogen oxidizer amidst the sulfur-oxidizing Thiomicrospira lineage. *ISME J.* 9, 696–707. doi: 10.1038/ismej.2014.173

Hansen, M., and Perner, M. (2016). Hydrogenase gene distribution and H_2 consumption ability within the Thiomicrospira lineage. *Front. Microbiol.* 7:99. doi: 10.3389/fmicb.2016.00099

Hoffmann, K., Bienhold, C., Buttigieg, P. L., Knittel, K., Laso-Perez, R., Rapp, J. Z., et al. (2020). Diversity and metabolism of Woeseiales bacteria, global members of marine sediment communities. *ISME J.* 14, 1042–1056. doi: 10.1038/s41396-020-0588-4

Hügler, M., and Sievert, S. M. (2011). Beyond the Calvin cycle: autotrophic carbon fixation in the ocean. *Annu. Rev. Mar. Sci.* 3, 261–289. doi: 10.1146/annurev-marine-120709-142712

Inagaki, F., Takai, K., Nealson, K. H., and Horikoshi, K. (2004). *Sulfurovum lithotrophicum* gen. Nov., sp. nov., a novel sulfur-oxidizing chemolithoautotroph within the epsilon-Proteobacteria isolated from Okinawa trough hydrothermal sediments. *Int. J. Syst. Evol. Microbiol.* 54, 1477–1482. doi: 10.1099/ijs.0.03042-0

Jiang, L., Lyu, J., and Shao, Z. (2017). Sulfur metabolism of Hydrogenovibrio thermophilus strain S5 and its adaptations to Deep-Sea hydrothermal vent environment. *Front. Microbiol.* 8:2513. doi: 10.3389/fmicb.2017.02513

Jochum, L. M., Schreiber, L., Marshall, I. P. G., Jorgensen, B. B., Schramm, A., and Kjeldsen, K. U. (2018). Single-cell genomics reveals a diverse metabolic potential of uncultivated Desulfatiglans-related Deltaproteobacteria widely distributed in marine sediment. *Front. Microbiol.* 9:2038. doi: 10.3389/fmicb.2018.02038

Jones, D. O. B., Amon, D. J., and Chapman, A. S. A. (2018). Mining Deep-Ocean mineral deposits: what are the ecological risks? *Elements* 14, 325–330. doi: 10.2138/gselements.14.5.325

Kelley, D. S., Baross, J. A., and Delaney, J. R. (2002). Volcanoes, fluids, and life at mid-ocean ridge spreading centers. *Annu. Rev. Earth Planet. Sci.* 30, 385–491. doi: 10.1146/annurev.earth.30.091201.141331

Kleindienst, S., Ramette, A., Amann, R., and Knittel, K. (2012). Distribution and in situ abundance of sulfate-reducing bacteria in diverse marine hydrocarbon seep sediments. *Environ. Microbiol.* 14, 2689–2710. doi: 10.1111/j.1462-2920.2012.02832.x

Kodama, Y., Ha, L. T., and Watanabe, K. (2007). *Sulfurospirillum cavolei* sp. nov., a facultatively anaerobic sulfur-reducing bacterium isolated from an underground crude oil storage cavity. *Int. J. Syst. Evol. Microbiol.* 57, 827–831. doi: 10.1099/ijs.0.64823-0

Koops, H.-P., and Pommerening-Röser, A. (2001). Distribution and ecophysiology of the nitrifying bacteria emphasizing cultured species. *FEMS Microbiol. Ecol.* 37, 1–9. doi: 10.1111/j.1574-6941.2001.tb00847.x

Koschinsky, A., Heinrich, L., Boehnke, K., Cohrs, J. C., Markus, T., Shani, M., et al. (2018). Deep-sea mining: interdisciplinary research on potential environmental, legal, economic, and societal implications. *Integr. Environ. Assess. Manag.* 14, 672–691. doi: 10.1002/ieam.4071

Kumagai, H., Nakamura, K., Toki, T., Morishita, T., Okino, K., Ishibashi, J. I., et al. (2008). Geological background of the Kairei and Edmond hydrothermal fields along the central Indian ridge: implications of their vent fluids' distinct chemistry. *Geofluids* 8, 239–251. doi: 10.1111/j.1468-8123.2008.00223.x

Lecoeuvre, A., Menez, B., Cannat, M., Chavagnac, V., and Gerard, E. (2021). Microbial ecology of the newly discovered serpentinite-hosted Old City hydrothermal field (southwest Indian ridge). *ISME J.* 15, 818–832. doi: 10.1038/s41396-020-00816-7

Levin, L. A., Baco, A. R., Bowden, D. A., Colaco, A., Cordes, E. E., Cunha, M. R., et al. (2016). Hydrothermal vents and methane seeps: rethinking the sphere of influence. *Front. Mar. Sci.* 3:72. doi: 10.3389/fmars.2016.00072

Li, J., Peng, X., Zhou, H., Li, J., and Sun, Z. (2013). Molecular evidence for microorganisms participating in Fe, Mn, and S biogeochemical cycling in two low-temperature hydrothermal fields at the southwest Indian ridge. *J. Geophys. Res. Biogeosci.* 118, 665–679. doi: 10.1002/jgrg.20057

Li, J., Zhou, H., Fang, J., Wu, Z., and Peng, X. (2016). Microbial distribution in a hydrothermal plume of the southwest Indian ridge. *Geomicrobiol J.* 33, 401–415. doi: 10.1080/01490451.2015.1048393

Liu, C., Cui, Y., Li, X., and Yao, M. (2021). Microeco: an R package for data mining in microbial community ecology. *FEMS Microbiol. Ecol.* 97:fiaa255. doi: 10.1093/femsec/fiaa255

Liu, Y., Lai, Q., Du, J., Sun, F., and Shao, Z. (2016). *Thalassospira indica* sp. nov., isolated from deep seawater. *Int. J. Syst. Evol. Microbiol.* 66, 4942–4946. doi: 10.1099/ijsem.0.001449

Lloyd, K. G., Steen, A. D., Ladau, J., Yin, J., and Crosby, L. (2018). Phylogenetically novel uncultured microbial cells dominate earth microbiomes. *mSystems* 3, e00055–e00018. doi: 10.1128/mSystems.00055-18

Lücker, S., Nowka, B., Rattei, T., Spieck, E., and Daims, H. (2013). The genome of *Nitrospina gracilis* illuminates the metabolism and evolution of the major marine nitrite oxidizer. *Front. Microbiol.* 4:27. doi: 10.3389/fmicb.2013.00027

Mehrshad, M., Rodriguez-Valera, F., Amoozegar, M. A., Lopez-Garcia, P., and Ghai, R. (2018). The enigmatic SAR202 cluster up close: shedding light on a globally distributed dark ocean lineage involved in sulfur cycling. *ISME J.* 12, 655–668. doi: 10.1038/s41396-017-0009-5

Mino, S., Kudo, H., Arai, T., Sawabe, T., Takai, K., and Nakagawa, S. (2014). *Sulfurovum aggregans* sp. nov., a hydrogen-oxidizing, thiosulfate-reducing chemolithoautotroph within the *Epsilonproteobacteria* isolated from a deep-sea hydrothermal vent chimney, and an emended description of the genus *Sulfurovum*. *Int. J. Syst. Evol. Microbiol.* 64, 3195–3201. doi: 10.1099/ijs.0.065094-0

Momper, L., Jungbluth, S. P., Lee, M. D., and Amend, J. P. (2017). Energy and carbon metabolisms in a deep terrestrial subsurface fluid microbial community. *ISME J.* 11, 2319–2333. doi: 10.1038/ismej.2017.94

Mori, K., Suzuki, K. I., Yamaguchi, K., Urabe, T., and Hanada, S. (2015). *Thiogranum longum* gen. Nov., sp. nov., an obligately chemolithoautotrophic, sulfur-oxidizing bacterium of the family Ectothiorhodospiraceae isolated from a deep-sea hydrothermal field, and an emended description of the genus *Thiohalomonas*. *Int. J. Syst. Evol. Microbiol.* 65, 235–241. doi: 10.1099/ijs.0.070599-0

Müller, H., Schwalenberg, K., Reeck, K., Barckhausen, U., Schwarz-Schampera, U., Hilgenfeldt, C., et al. (2018). Mapping seafloor massive sulfides with the Golden eye frequency-domain EM profiler. *First Break* 36, 61–67. doi: 10.3997/1365-2397.n0127

Nakagawa, S., and Takai, K. (2008). Deep-sea vent chemoautotrophs: diversity, biochemistry and ecological significance. *FEMS Microbiol. Ecol.* 65, 1–14. doi: 10.1111/j.1574-6941.2008.00502.x

Nakamura, K., and Takai, K. (2015). "Indian Ocean hydrothermal systems: seafloor hydrothermal activities, physical and chemical characteristics of hydrothermal fluids, and vent-associated biological communities" in *Subseafloor biosphere linked to hydrothermal systems*. eds. J. Ishibashi, K. Okino and M. Sunamura (Tokyo: Springer), 147–161.

Namirimu, T., Kim, Y. J., Park, M.-J., Lim, D., Lee, J.-H., and Kwon, K. K. (2022). Microbial community structure and functional potential of Deep-Sea sediments on low activity hydrothermal area in the central Indian ridge. *Front. Mar. Sci.* 9:784807. doi: 10.3389/fmars.2022.784807

Orcutt, B. N., Bradley, J. A., Brazelton, W. J., Estes, E. R., Goordial, J. M., Huber, J. A., et al. (2020). Impacts of deep-sea mining on microbial ecosystem services. *Limnol. Oceanogr.* 65, 1489–1510. doi: 10.1002/lno.11403

Oremland, R. S., and Capone, D. G. (1988). "Use of "specific" inhibitors in Biogeochmeistry and microbial ecology" in *Advances in microbial ecology*. ed. K. C. Marshall (Boston, MA: Springer)

Pedregosa, F., Vraoquaux, G., Gramfort, A., Michel, V., Thirion, B., Grisel, O., et al. (2011). Scikit-learn: machine learning in Python. *JMLR* 12, 2825–2830.

Perner, M., Hentscher, M., Rychlik, N., Seifert, R., Strauss, H., and Bach, W. (2011). Driving forces behind the biotope structures in two low-temperature hydrothermal venting sites on the southern mid-Atlantic ridge. *Environ. Microbiol. Rep.* 3, 727–737. doi: 10.1111/j.1758-2229.2011.00291.x

Perner, M., Seifert, R., Weber, S., Koschinsky, A., Schmidt, K., Strauss, H., et al. (2007). Microbial CO_2 fixation and sulfur cycling associated with low-temperature emissions at the Lilliput hydrothermal field, southern mid-Atlantic ridge (9°S). *Environ. Microbiol.* 9, 1186–1201. doi: 10.1111/j.1462-2920.2007.01241.x

Petersen, S., Krätschell, A., Augustin, N., Jamieson, J., Hein, J. R., and Hannington, M. D. (2016). News from the seabed – geological characteristics and resource potential of deep-sea mineral resources. *Mar Pol* 70, 175–187. doi: 10.1016/j.marpol.2016.03.012

Price, M. N., Dehal, P. S., and Arkin, A. P. (2010). FastTree 2--approximately maximum-likelihood trees for large alignments. *PLoS One* 5:e9490. doi: 10.1371/journal.pone.0009490

Quast, C., Pruesse, E., Yilmaz, P., Gerken, J., Schweer, T., Yarza, P., et al. (2013). The SILVA ribosomal RNA gene database project: improved data processing and web-based tools. *Nucleic Acids Res.* 41, D590–D596. doi: 10.1093/nar/gks1219

Rinke, C., Rubino, F., Messer, L. F., Youssef, N., Parks, D. H., Chuvochina, M., et al. (2019). A phylogenomic and ecological analysis of the globally abundant marine group II archaea (ca. Poseidoniales Ord. Nov.). *ISME J.* 13, 663–675. doi: 10.1038/s41396-018-0282-y

Rinke, C., Schwientek, P., Sczyrba, A., Ivanova, N. N., Anderson, I. J., Cheng, J. F., et al. (2013). Insights into the phylogeny and coding potential of microbial dark matter. *Nature* 499, 431–437. doi: 10.1038/nature12352

Rosario-Passapera, R., Keddis, R., Wong, R., Lutz, R. A., Starovoytov, V., and Vetriani, C. (2012). *Parvibaculum hydrocarboniclasticum* sp. nov., a mesophilic, alkane-oxidizing alphaproteobacterium isolated from a deep-sea hydrothermal vent on the East Pacific rise. *Int. J. Syst. Evol. Microbiol.* 62, 2921–2926. doi: 10.1099/ijs.0.039594-0

Schnetger, B., and Lehners, C. (2014). Determination of nitrate plus nitrite in small volume marine water samples using vanadium(III)chloride as a reduction agent. *Mar. Chem.* 160, 91–98. doi: 10.1016/j.marchem.2014.01.010

Schwarz-Schampera, U. (2019) *Short cruise report SONNE cruise SO271/1 (INDEX2019)*. Hamburg, Germany: Leitstelle Deutsche Forschungsschiffe, Institute of Geology, Universität Hamburg.

Schwertmann, U., and Cornell, R. M. (2008). "Ferrihydrite" in *Iron oxides in the Labaroty: Preparation and characterization*. eds. U. Schwertmann and R. M. Cornell (Weinheim, Germany, Wiley-VCH: John Wiley and Sons), 103–112.

Singer, E., Emerson, D., Webb, E. A., Barco, R. A., Kuenen, J. G., Nelson, W. C., et al. (2011). *Mariprofundus ferrooxydans* PV-1 the first genome of a marine Fe(II) oxidizing Zetaproteobacterium. *PLoS One* 6:e25386. doi: 10.1371/journal.pone.0025386

Sorokin, D. Y., Tourova, T. P., Bezsoudnova, E. Y., Pol, A., and Muyzer, G. (2007). Denitrification in a binary culture and thiocyanate metabolism in *Thiohalophilus thiocyanoxidans* gen. Nov. sp. nov. - a moderately halophilic chemolithoautotrophic sulfur-oxidizing *Gammaproteobacterium* from hypersaline lakes. *Arch. Microbiol.* 187, 441–450. doi: 10.1007/s00203-006-0208-3

Stookey, L. L. (1970). Ferrozine – a new spectrophotometric reagent for Iron. *Anal. Chem.* 42, 779–781. doi: 10.1021/ac60289a016

Takai, K., Nealson, K. H., and Horikoshi, K. (2004). *Hydrogenimonas thermophila* gen. Nov., sp. nov., a novel thermophilic, hydrogen-oxidizing chemolithoautotroph within the ε-Proteobacteria, isolated from a black smoker in a central Indian ridge hydrothermal field. *Int. J. Syst. Evol. Microbiol.* 54, 25–32. doi: 10.1099/ijs.0.02787-0

Tanaka, N., Romanenko, L. A., Iino, T., Frolova, G. M., and Mikhailov, V. V. (2011). *Cocleimonas flava* gen. Nov., sp. nov., a gammaproteobacterium isolated from sand snail (*Umbonium costatum*). *Int. J. Syst. Evol. Microbiol.* 61, 412–416. doi: 10.1099/ijs.0.020263-0

Techtmann, S. M., Fitzgerald, K. S., Stelling, S. C., Joyner, D. C., Uttukar, S. M., Harris, A. P., et al. (2016). *Colwellia psychrerythraea* strains from distant Deep Sea basins show adaptation to local conditions. *Front. Environ. Sci.* 4:33. doi: 10.3389/fenvs.2016.00033

van der Most, N., Qian, P.-Y., Gao, Y., and Gollner, S. (2023). Active hydrothermal vent ecosystems in the Indian Ocean are in need of protection. *Front. Mar. Sci.* 9:1067912. doi: 10.3389/fmars.2022.1067912

Van Dover, C. L., Arnaud-Haond, S., Gianni, M., Helmreich, S., Huber, J. A., Jaeckel, A. L., et al. (2018). Scientific rationale and international obligations for protection of active hydrothermal vent ecosystems from deep-sea mining. *Mar. Pol.* 90, 20–28. doi: 10.1016/j.marpol.2018.01.020

Van Dover, C. L., Colaço, A., Collins, P. C., Croot, P., Metaxas, A., Murton, B. J., et al. (2020). Research is needed to inform environmental management of hydrothermally inactive and extinct polymetallic sulfide (PMS) deposits. *Mar Pol* 121:104183. doi: 10.1016/j.marpol.2020.104183

Van Dover, C. L., Humphris, S. E., Fornari, D., Cavanaugh, C. M., Collier, R., Goffredi, S. K., et al. (2001). Biogeography and ecological setting of Indian Ocean hydrothermal vents. *Science* 294, 818–823. doi: 10.1126/science.1064574

Wang, S., Jiang, L., Hu, Q., Liu, X., Yang, S., and Shao, Z. (2021). Elemental sulfur reduction by a deep-sea hydrothermal vent Campylobacterium Sulfurimonas sp. NW10. *Environ. Microbiol.* 23, 965–979. doi: 10.1111/1462-2920.15247

Wang, H., Qi, C., Chen, W., Dong, W., Tang, H., and Hu, X. (2016). Carboxylicivirga flava sp. nov., isolated from marine surface sediment. *Int. J. Syst. Evol. Microbiol.* 66, 5412–5416. doi: 10.1099/ijsem.0.001533

Wetzel, L. R., and Shock, E. L. (2000). Distinguishing ultramafic-from basalt-hosted submarine hydrothermal systems by comparing calculated vent fluid compositions. *J Geophys Solid Earth* 105, 8319–8340.

Wiese, J., Imhoff, J. F., Horn, H., Borchert, E., Kyrpides, N. C., Goker, M., et al. (2020). Genome analysis of the marine bacterium *Kiloniella laminariae* and first insights into comparative genomics with related *Kiloniella* species. *Arch. Microbiol.* 202, 815–824. doi: 10.1007/s00203-019-01791-0

Yang, Z., Xiao, X., and Zhang, Y. (2019). Microbial diversity of sediments from an inactive hydrothermal vent field, southwest Indian ridge. *Mar. Life Sci. Technol.* 2, 73–86. doi: 10.1007/s42995-019-00007-0

Zhong, Y. W., Zhou, P., Cheng, H., Zhou, Y. D., Pan, J., Xu, L., et al. (2022). Metagenomic features characterized with microbial Iron Oxidoreduction and mineral interaction in southwest Indian ridge. *Microbiol. Spec.* 10:e0061422. doi: 10.1128/spectrum.00614-22

Zhou, Z., Tran, P. Q., Adams, A. M., Kieft, K., Breier, J. A., Fortunato, C. S., et al. (2023). Sulfur cycling connects microbiomes and biogeochemistry in deep-sea hydrothermal plumes. *ISME J.* 17, 1194–1207. doi: 10.1038/s41396-023-01421-0

Zhong, Y. W., Zhou, P., Cheng, H., Zhou, Y. D., Pan, J., Xu, L., et al. (2020). Degradation of hydrocarbons and heavy metal reduction by marine Bacteria in highly contaminated sediments. *Microorganisms* 8:1402. doi: 10.3390/microorganisms8091402

Frontiers in Microbiology

Explores the habitable world and the potential of microbial life

The largest and most cited microbiology journal which advances our understanding of the role microbes play in addressing global challenges such as healthcare, food security, and climate change.

Discover the latest Research Topics

See more →

Frontiers

Avenue du Tribunal-Fédéral 34
1005 Lausanne, Switzerland
frontiersin.org

Contact us

+41 (0)21 510 17 00
frontiersin.org/about/contact